ISSN 0042-8469
e-ISSN 2217-4753
УДК 623 + 355/359

Вол. 73, бр. 1
2025

НАУЧНИ ЧАСОПИС МИНИСТАРСТВА ОДБРАНЕ И ВОЈСКЕ СРБИЈЕ

ВОЈНОТЕХНИЧКИ ГЛАСНИК

1 2025 ВОЈНОТЕХНИЧКИ ГЛАСНИК

ВТГ.МО.УПР.СРБ

www.vtg.mod.gov.rs

ISSN 0042-8469
e-ISSN 2217-4753
УДК 623 + 355/359

Том 73, № 1
2025

НАУЧНЫЙ ЖУРНАЛ МИНИСТЕРСТВА ОБОРОНЫ
И ВООРУЖЕННЫХ СИЛ РЕСПУБЛИКИ СЕРБИЯ

ВОЕННО-ТЕХНИЧЕСКИЙ ВЕСТНИК

ВОЕННО-ТЕХНИЧЕСКИЙ ВЕСТНИК
1 2025

ВТГ.МО.УПР.СРБ
www.vtg.mod.gov.rs

ISSN 0042-8469
e-ISSN 2217-4753
UDC 623 + 355/359

Vol. 73, Issue 1
2025

MTC

SCIENTIFIC JOURNAL OF THE MINISTRY OF DEFENCE AND THE SERBIAN ARMED FORCES

MILITARY TECHNICAL COURIER

MILITARY TECHNICAL COURIER
1 2025

ВТГ.МО.УПР.СРБ
www.vtg.mod.gov.rs

ISSN 0042-8469
e-ISSN 2217-4753
UDC 623 + 355/359

НАУЧНИ ЧАСОПИС МИНИСТАРСТВА ОДБРАНЕ И ВОЈСКЕ СРБИЈЕ

ВОЈНОТЕХНИЧКИ ГЛАСНИК

ВОЛУМЕН 73•БРОЈ 1• ЈАНУАР – МАРТ 2025.

NAUČNI ČASOPIS MINISTARSTVA ODBRANE I VOJSKE SRBIJE

VOJNOTEHNIČKI GLASNIK

VOLUMEN 73•BROJ 1•JANUAR – MART 2025.

втг.мо.упр.срб
www.vtg.mod.gov.rs
COBISS.SR-ID 4423938
DOI: 10.5937/VojnotehnickiGlasnik

ISSN 0042-8469
e-ISSN 2217-4753
UDC 623 + 355/359

НАУЧНЫЙ ЖУРНАЛ МИНИСТЕРСТВА ОБОРОНЫ И ВООРУЖЁННЫХ СИЛ РЕСПУБЛИКИ СЕРБИЯ

ВОЕННО-ТЕХНИЧЕСКИЙ ВЕСТНИК

ТОМ 73•НОМЕР ВЫПУСКА 1•ЯНВАРЬ – МАРТ 2025.

SCIENTIFIC JOURNAL OF THE MINISTRY OF DEFENCE AND SERBIAN ARMED FORCES

MILITARY TECHNICAL COURIER

VOLUME 73•ISSUE 1•JANUARY – MARCH 2025

втг.мо.упр.срб
www.vtg.mod.gov.rs
COBISS.SR-ID 4423938
DOI: 10.5937/VojnotehnickiGlasnik

ВЛАСНИЦИ:
Министарство одбране и Војска Србије

ИЗДАВАЧ:
Универзитет одбране у Београду, Војна академија

СОБСТВЕННИКИ: Министерство обороны и Вооружённые силы Республики Сербия
ИЗДАТЕЛЬСТВО: Университет обороны в г. Белград, Военная академия

OWNERS:
Ministry of Defence and Serbian Armed Forces
PUBLISHER:
University of Defence in Belgrade, Military Academy

С А Д Р Ж А Ј

ОРИГИНАЛНИ НАУЧНИ РАДОВИ

С О Д Е Р Ж А Н И Е

ОРИГИНАЛЬНЫЕ НАУЧНЫЕ СТАТЬИ

C O N T E N T S

ORIGINAL SCIENTIFIC PAPERS

ORIGINAL SCIENTIFIC PAPERS

Multi-valued mappings on Pompeiu-Hausdorff fuzzy b-metric spaces and a common fixed point result

Noreddine Makran[a], *Stojan* N. Radenović[b]

[a] University Mohammed Premier, Faculty of Sciences, Department of Mathematics, Oujda, Kingdom of Morocco, e-mail: makranmakran83@gmail.com, **corresponding author**, ORCID iD: https://orcid.org/0000-0001-8131-6733

[b] University of Belgrade, Faculty of Mechanical Engineering, Belgrade, Republic of Serbia, e-mail: radens@beotel.rs, ORCID iD: https://orcid.org/0000-0001-8254-6688

https://doi.org/10.5937/vojtehg73-51489

FIELD: mathematics, computer sciences
ARTICLE TYPE: original scientific paper

Abstract:

Introduction/purpose: The study of the theory of fuzzy sets was prompted by the presence of uncertainty as an essential part of real-world problems, leading Zadeh to address the problem of indeterminacy. The notion of fuzzy logic was introduced by Zadeh. Unlike traditional logic theory, where an element either belongs to the set or does not, in fuzzy logic, the affiliation of the element to the set is expressed as a number from the interval $[0, 1]$.

Methods: The theory of a fixed point in fuzzy metric spaces can be viewed in different ways, one of which involves the use of fuzzy logic. Fuzzy metric spaces, which are specific types of topological spaces with pleasing "geometric" characteristics, possess a number of appealing properties and are commonly used in both pure and applied sciences. Metric spaces and their various generalizations frequently occur in computer science applications. For this reason, a new space called a Pompeiu-Hausdorff fuzzy b*-metric space is constructed in this paper.*

Results: In this space, some new fixed point results are also formulated and proven. Additionally, a general common fixed point theorem for a pair of multi-valued mappings in Pompeiu-Hausdorff fuzzy b*-metric spaces is investigated. The findings obtained in fuzzy metric spaces,*

such as those discussed in the article of Shen, Y. et al. (2012. Fixed point theorems in fuzzy metric spaces. Applied Mathematics Letters, 25, pp.138-141), are generalized by the results in this paper, and additional specific findings are produced and supported by examples.

Conclusions: The study of denotational semantics and their applications in control theory using fuzzy b-metric spaces and Pompeiu-Hausdorff fuzzy b-metric spaces will be an important next step.

Key words: fuzzy metric space, fuzzy b-metric space, t-norm, fixed point, implicit relation.

Introduction and preliminaries

In 1975, Kramosil and Michalek (Kramosil & Michalek, 1975) proposed the idea of a fuzzy distance between two elements of a nonempty set, using the concepts of a fuzzy set and a t-norm.

A binary operation $T : [0,1] \times [0,1] \to [0,1]$ is a continuous t-norm if it satisfies the following conditions: T is continuous, associative, and commutative, $T(a,1) = a$ for all $a \in [0,1]$ and for all $a, b, c, d \in [0,1]$ if $a \leq c$ and $b \leq d$ then $T(a,b) \leq T(c,d)$.

The study of fixed point theory in metric spaces has a variety of applications in mathematics, particularly in solving differential equations. Many authors have studied the new class of generalized metric spaces, known as a b-metric space, introduced by Bakhtin (Bakhtin, 1989). For example, see (Aghajani et al., 2014; Aydi et al., 2012; Bota et al., 2011; Czerwik, 1993; Došenović et al., 2023; George & Veeramani, 1997; Makran et al., 2023; Rakić et al., 2020).

The relationship between b-metric and fuzzy metric spaces is considered in (Hassanzadeh & Sedghi, 2018). Conversely, (Sedghi & Shobe, 2012) introduced the concept of a fuzzy b-metric space, substituting the triangle inequality with a weaker one.

In this paper, a general common fixed point theorem for a pair of multivalued mappings in Pompeiu-Hausdorff fuzzy b-metric spaces is of interest to be proven.

DEFINITION 1. *(Sedghi & Shobe, 2012) A 3-tuple (X, M, T) is called a fuzzy $b-$metric space if X is an arbitrary nonempty set, T is a continuous t-norm, and M is a fuzzy set on $X \times X \times (0, \infty)$ satisfying the conditions for all $x, y, z \in X$, $t, u > 0$ and a given real number $s \geq 1$:*

(b_1) $M(x, y, t) > 0$,

(b_2) $M(x,y,t) = 1$ *if and only if* $x = y$,

(b_3) $M(x,y,t) = M(y,x,t)$,

(b_4) $M\left(x,z,s(t+u)\right) \geq T\left(M\left(x,y,t\right), M(y,z,u)\right)$,

(b_5) $M(x,y,.) : (0,\infty) \to [0,1]$ *is continuous.*

REMARK 1. In this paper we will further use a fuzzy b-metric space in the sense of Definition 1 with the additional condition $\lim\limits_{t\to\infty} M(x,y,t) = 1$.

Note that every fuzzy metric space is a fuzzy $b-$metric space with $s = 1$. But the converse need not be true as is shown in the following example.

EXAMPLE 1. (Dahhouch et al., 2024) Let $M(x,y,t) = e^{-\frac{|x-y|^p}{t}}$, where $p > 1$ is a real number, and $T(a,b) = a.b$ for all $a, b \in [0,1]$. Then (X,M,T) is a fuzzy b-metric space with $s = 2^{p-1}$.

DEFINITION 2. *(Sedghi & Shobe, 2012, 2014)*
Let (X,M,T) be a fuzzy b-metric space.

(i) A sequence (x_n) converges to x if $M(x_n,x,t) \to 1$ as $n \to \infty$ for each $t > 0$. In this case, we write $\lim\limits_{n\to\infty} x_n = x$.

(ii) A sequence (x_n) is called a Cauchy sequence if for all $\varepsilon \in (0,1)$ and $t > 0$, there exists $n_0 \in \mathbb{N}$ such that $M(x_n,x_m,t) > 1-\varepsilon$ for all $n,m \geq n_0$.

(iii) The fuzzy b-metric space (X,M,T) is said to be complete if every Cauchy sequence is convergent.

(iv) A subset $A \subset X$ is said to be closed if every sequence $x_n \in A$ such that $x_n \longrightarrow x$ we have $x \in A$.

(v) A subset $A \subset X$ is said to be compact if every sequence $x_n \in A$ has a convergent subsequence.

LEMMA 1. *(Sedghi & Shobe, 2012, 2014)*
In a fuzzy $b-$metric space (X,M,T)

(i) If a sequence (x_n) in X converges to x, then x is unique.

(ii) If a sequence (x_n) in X converges to x, then it is a Cauchy sequence.

Main results

In this section, a new space called a Pompeiu-Hausdorff fuzzy b-metric space was constructed. Several examples were presented to illustrate the properties of this space. In this framework, some new common fixed point results were formulated and proven. The following was introduced as the starting point:

Throughout this paper, $C(X)$ will denote the family of nonempty compact subsets of X, and $CL(X)$ will denote the family of nonempty closed subsets of X. For all $A, B \in C(X)$ and for all $t > 0$, we define a function on $C(X) \times C(X) \times (0, \infty)$ by

$$H_M(A, B, t) = \min\left\{\inf_{a\in A} M(a, B, t), \inf_{b\in B} M(A, b, t)\right\},$$

$$\text{where } M(C, y, t) = \sup_{z\in C} M(z, y, t).$$

Then H_M is called the Pompeiu-Hausdorff fuzzy b-metric induced by the fuzzy b-metric M. The triplet $(C(X), H_M, T)$ is called a Pompeiu-Hausdorff fuzzy b-metric space.

We define also $\delta_M(A, B, t)$ by

$$\delta_M(A, B, t) = \inf\{M(a, b, t), \quad a \in A \quad b \in B\}, \quad t > 0,$$

and it follows immediately from the definition of δ_M that

$$\delta_M(A, B, t) = 1 \iff A = B = \{.\} \text{ and}$$

$$M(a, b, t) \geq \delta_M(A, B, t) \quad \forall a \in A \quad \forall b \in B, \quad t > 0.$$

Indeed: If $A = B = \{.\}$, then $\delta_M(A, B, t) = \delta_M(\{a\}, \{a\}, t) = M(a, a, t) = 1$.

Now, if $\delta_M(A, B, t) = 1$, $\forall t > 0$, then $\forall a \in A$, $b \in B$, $\quad M(a, b, t) \geq \delta_M(A, B, t) = 1$.

So, $A = B = \{a\} = \{b\} = \{.\}$.

LEMMA 2. *Let (X, M, T) be a fuzzy b-metric space with the constant s. Then H_M is a fuzzy set on $C(X) \times C(X) \times (0, \infty)$ satisfying the conditions for all $A, B, C \in C(X)$, $t, u > 0$:*

(H_1) $H_M(A, B, t) > 0$,

(H_2) $H_M(A,B,t)=1$ *if and only if* $A=B$,

(H_3) $H_M\left(A,C,s(t+u)\right)\geq T\left(H_M\left(A,B,t\right),H_M(B,C,u)\right)$,

(H_4) $H_M(A,B,.):(0,\infty)\to[0,1]$ *is continuous.*

(H_5) $\lim\limits_{t\to\infty}H_M(A,B,t)=1$ *if and only if* $\lim\limits_{t\to\infty}M(x,y,t)=1$.

Proof

(H_1) Let $A,B\in C(X)$, and show that $H_M(A,B,t)>0,\quad \forall t>0$, one obtains

$$\begin{aligned}H_M(A,B,t) &= \min\left\{\inf_{a\in A}M(a,B,t),\inf_{b\in B}M(A,b,t)\right\},\\ &= \min\left\{\inf_{a\in A}\sup_{b\in B}M(a,b,t),\inf_{b\in B}\sup_{a\in A}M(a,b,t)\right\}.\end{aligned}$$

Suppose that $H_M(A,B,t)=\inf\limits_{a\in A}\sup\limits_{b\in B}M(a,b,t)$, according to the characterization of $\inf$ and $\sup$, there exist $a_n\in A,b_n\in B$ such that $\lim\limits_{n\to\infty}M(a_n,b_n,t)=H_M(A,B,t),\quad \forall t>0$.

Since A,B two compact, then $(a_n),(b_n)$ admit respectively two subsequences also noted $(a_n),(b_n)$ such that $a_n\to a\in A$ and $b_n\to b\in B$ $(n\to\infty)$.

By Definition 1 (b_4), one gets

$$\begin{aligned}M(a_n,b_n,t) &\geq T\left(M\left(a_n,a,\frac{t}{2s}\right),M\left(a,b_n,\frac{t}{2s}\right)\right)\\ &\geq T\left(M\left(a_n,a,\frac{t}{2s}\right),T\left(M\left(a,b,\frac{t}{4s^2}\right),M\left(b,b_n,\frac{t}{4s^2}\right)\right)\right),\end{aligned}$$

letting $n\to\infty$ one obtains

$$\begin{aligned}H_M(A,B,t) &\geq T\left(1,T\left(M\left(a,b,\frac{t}{4s^2}\right),1\right)\right)\\ &= M\left(a,b,\frac{t}{4s^2}\right)>0,\quad \forall t>0.\end{aligned}$$

Similarly, if $H_M(A,B,t)=\inf\limits_{b\in B}\sup\limits_{a\in A}M(a,b,t)$, then $H_M(A,B,t)>0$, $\forall t>0$.

(H_2) Let $A,B\in C(X)$, $t>0$ and show that $H_M(A,B,t)=1,\Leftrightarrow A=B$.

If $A=B$, there exists $H_M(A,B,t)=H_M(A,A,t)=\inf\limits_{a\in A}M(a,A,t)$.

According to the characterization of $\inf$, there exists $a_n \in A$, such that $\lim_{n\to\infty} M(a_n, A, t) = H_M(A, A, t)$. Since A is a compact, then (a_n) admits a subsequence also noted (a_n), such that $a_n \to a \in A$. On the other hand, there is

$$M(a_n, A, t) = \sup_{x\in A} M(a_n, x, t) \geq M(a_n, a, t),$$

letting $n \to \infty$ one obtains

$$H_M(A, A, t) = \lim_{n\to\infty} M(a_n, A, t) \geq \lim_{n\to\infty} M(a_n, a, t) = 1.$$

So, $H_M(A, A, t) = 1$.

Now, if $H_M(A, B, t) = 1$, then

$$\begin{aligned}
&\inf_{a\in A} M(a, B, t) = 1 \text{ and } \inf_{b\in B} M(A, b, t) = 1\\
\Rightarrow\quad &\forall\, a \in A,\ M(a, B, t) = 1 \text{ and } \forall\, b \in B,\ M(A, b, t) = 1,\\
\Rightarrow\quad &\forall\, a \in A,\ \sup_{b\in B} M(a, b, t) = 1 \text{ and } \forall\, b \in B,\ \sup_{a\in A} M(a, b, t) = 1,\\
\Rightarrow\quad &\forall\, a \in A,\ \exists b_n \in B : \lim_{n\to\infty} M(a, b_n, t) = 1\\
\text{and}\quad &\forall\, b \in B,\ \exists a_n \in A : \lim_{n\to\infty} M(a_n, b, t) = 1,\\
\Rightarrow\quad &\forall\, a \in A,\ \exists b_n \in B :\ b_n \to a \in B \text{ and } \forall\, b \in B,\ \exists a_n \in A :\ a_n \to b \in A,\\
\Rightarrow\quad &A = B.
\end{aligned}$$

(H_3) Let $A, B, C \in C(X),\ t, u > 0$ and $s \geq 1$, show that

$$H_M\left(A, C, s(t+u)\right) \geq T\left(H_M\left(A, B, t\right), H_M(B, C, u)\right).$$

Suppose that $H_M\left(A, C, s(t+u)\right) = \inf_{a\in A} M\left(a, C, s(t+u)\right)$. First one proves that $\forall a \in A,\ \forall b \in B$, one has

$$M\left(a, C, s(t+u)\right) \geq T(M(a, b, t), M(b, C, u)).$$

Indeed, there is $M(b, C, u) = \sup_{c\in C} M(b, c, u)$, then there exists $c_n \in C$ such that:
$\lim_{n\to\infty} M(b, c_n, u) = M(b, C, u)$. By Definition 1 (b_4) one gets

$$M(a, c_n, s(t+u)) \geq T(M(a, b, t), M(b, c_n, u)),$$

letting $n \to \infty$ one has

$$\begin{aligned} M(a,C,s(t+u)) &\geq \lim_{n\to\infty} M(a,c_n,s(t+u)) \\ &\geq \lim_{n\to\infty} T(M(a,b,t),M(b,c_n,u)) \\ &= T(M(a,b,t),\lim_{n\to\infty} M(b,c_n,u)) \\ &= T(M(a,b,t),M(b,C,u)). \end{aligned}$$

So,

$$M\left(a,C,s(t+u)\right) \geq T(M(a,b,t),M(b,C,u)). \tag{1}$$

Now, by (1), one has

$$\begin{aligned} M\left(a,C,s(t+u)\right) &\geq T(M(a,b,t),M(b,C,u)), \\ &\geq T(M(a,b,t),\inf_{b\in B} M(b,C,u)), \quad \forall b\in B. \end{aligned}$$

Then

$$\begin{aligned} M\left(a,C,s(t+u)\right) &\geq T(\sup_{b\in B} M(a,b,t),\inf_{b\in B} M(b,C,u)), \\ &= T(M(a,B,t),\inf_{b\in B} M(b,C,u)), \quad \forall a\in A. \end{aligned}$$

This implies

$$\begin{aligned} H_M\left(A,C,s(t+u)\right) &= \inf_{a\in A} M\left(a,C,s(t+u)\right) \\ &\geq T(\inf_{a\in A} M(a,B,t),\inf_{b\in B} M(b,C,u)) \\ &\geq T(H_M(A,B,t),H_M(B,C,u)). \end{aligned}$$

Because $(\inf_{a\in A} M(a,B,t) \geq H_M(A,B,t)$ and $\inf_{b\in B} M(b,C,u) \geq H_M(B,C,u))$.

Similarly, if $H_M\left(A,C,s(t+u)\right) = \inf_{c\in C} M\left(A,c,s(t+u)\right)$, then

$$H_M\left(A,C,s(t+u)\right) \geq T(H_M(A,B,t),H_M(B,C,u)).$$

(H_4) Let $A,B\in C(X)$, show that $H_M(A,B,.):(0,\infty)\to[0,1]$ is continuous, let (t_n) a sequence of elements in $(0,\infty)$ which converges to t, then one proves $\lim_{n\to\infty} H_M(A,B,t_n) = H_M(A,B,t)$.

By Definition 1 (b_5), for all $(a,b) \in A \times B$, one gets

$$\lim_{n\to\infty} M(a,b,t_n) = M(a,b,t), \text{ i.e.,}$$

$\forall \varepsilon > 0 \quad \exists n_0 \in \mathbb{N} \quad \forall n > n_0 :$

$$\begin{aligned} & M(a,b,t) - \varepsilon \le M(a,b,t_n) \le M(a,b,t) + \varepsilon, \\ \Rightarrow \quad & \sup_{b\in B} M(a,b,t) - \varepsilon \le \sup_{b\in B} M(a,b,t_n) \le \sup_{b\in B} M(a,b,t) + \varepsilon, \\ \Rightarrow \quad & M(a,B,t) - \varepsilon \le M(a,B,t_n) \le M(a,B,t) + \varepsilon, \end{aligned}$$

$$\Rightarrow \quad \inf_{a\in A} M(a,B,t) - \varepsilon \le \inf_{a\in A} M(a,B,t_n) \le \inf_{a\in A} M(a,B,t) + \varepsilon. \quad (2)$$

Similarly, one finds

$$\inf_{b\in B} M(A,b,t) - \varepsilon \le \inf_{b\in B} M(A,b,t_n) \le \inf_{b\in B} M(A,b,t) + \varepsilon. \quad (3)$$

Thus, by (2) and (3), one can deduce

$$H_M(A,B,t) - \varepsilon \le H_M(A,B,t_n) \le H_M(A,B,t) + \varepsilon.$$

So, $\lim_{n\to\infty} H_M(A,B,t_n) = H_M(A,B,t)$.

(H_5) Let $A, B \in C(X),\ t > 0$ show that $\lim_{t\to\infty} H_M(A,B,t) = 1$ if and only if $\lim_{t\to\infty} M(x,y,t) = 1$.

If $A = \{x\}$ and $B = \{y\}$, one has

$$\begin{aligned} \lim_{t\to\infty} H_M(A,B,t) = 1 \quad & \Rightarrow \quad \lim_{t\to\infty} H_M(\{x\},\{y\},t) = 1 \\ & \Rightarrow \quad \lim_{t\to\infty} M(x,y,t) = 1. \end{aligned}$$

Now, if $\lim_{t\to\infty} M(x,y,t) = 1$. Suppose that $H_M(A,B,t) = \inf_{a\in A} \sup_{b\in B} M(a,b,t)$, according to the characterization of $\inf$ and $\sup$, there exist $a_n \in A, b_n \in B$ such that $\lim_{n\to\infty} M(a_n,b_n,t) = H_M(A,B,t), \quad \forall t > 0$. Thus

$$\begin{aligned} \lim_{t\to\infty} H_M(A,B,t) &= \lim_{t\to\infty} \left(\lim_{n\to\infty} M(a_n,b_n,t) \right) \\ &= \lim_{n\to\infty} \left(\lim_{t\to\infty} M(a_n,b_n,t) \right) = 1. \end{aligned}$$

Similarly, if $H_M(A,B,t) = \inf_{b\in B} \sup_{a\in A} M(a,b,t)$, then $\lim_{t\to\infty} H_M(A,B,t) = 1$.

DEFINITION 3. *Let Ψ be the set of all continuous functions $\psi(t_1,t_2,t_3,t_4):[0,1]^4\longrightarrow\mathbb{R}$ such that:*
(ψ_0) : *ψ is nonincreasing in variable t_1 and nondecreasing in variables t_2,t_3,t_4.*
(ψ_1) : $\forall u,v\in[0,1]\quad \psi(u,v,v,u)\leq 0$ *or* $\psi(u,v,u,v)\leq 0\Longrightarrow v<u$.
(ψ_2) : $\forall u\in[0,1]\quad \psi(u,u,1,1)\leq 0\Longrightarrow u=1$.

EXAMPLE 2. $\psi(t_1,t_2,t_3,t_4)=\frac{1}{p}ln\,(t_2)-ln\,(t_1)$, with $p>1$.

EXAMPLE 3. $\psi(t_1,t_2,t_3,t_4)=\dfrac{1}{1+t_1}-\dfrac{t_1}{2}-\lambda\left(\dfrac{1}{1+t_2}-\dfrac{t_2}{2}\right),\ 0<\lambda<1.$

EXAMPLE 4. $\psi(t_1,t_2,t_3,t_4)=\beta(t_1)-\lambda\beta(t_2)$, with $\beta:(0,1]\to[0,\infty)$ and $\beta(1)=0$ is a continuous function strictly decreasing, $0<\lambda<1$.

EXAMPLE 5. $\psi(t_1,t_2,t_3,t_4)=\beta(t_1)-\lambda\beta(\frac{t_2+t_3}{4}+\frac{t_4}{2})$, with $\beta:(0,1]\to[0,\infty)$ and $\beta(1)=0$ is a continuous function strictly decreasing, $0<\lambda<1$.

EXAMPLE 6. $\psi(t_1,t_2,t_3,t_4)=\gamma(t_1)-k(t)\gamma(t_2)$, with $\gamma:(0,1]\to[0,\infty)$, $\gamma(1)=0$ is a continuous function strictly decreasing and k is a function from $(0,\infty)$ into $(0,1)$.

DEFINITION 4. *A function $\Im:X\longrightarrow CL(X)$, where (X,M,T) is a fuzzy b-metric space, called closed if for all sequences (x_n) and (y_n) of elements from X and $x,y\in X$ such that $\lim\limits_{n\to\infty}x_n=x$, $\lim\limits_{n\to\infty}y_n=y$ and $y_n\in\Im(x_n)$ for every $n\in\mathbb{N}$, one has $y\in\Im(x)$.*

THEOREM 1. *Let (X,M,T) be a complete fuzzy b-metric space with constant s, it can be supposed that M is continuous with respect to one of its variables. Let $\Im,\Re:X\longrightarrow C(X)$ be two closed maps and $\psi\in\Psi$ such that*

$$\psi\left(\ H_M\left(\Im(x),\Re(y),t\right),M\left(x,y,t\right),M\left(\Im(x),x,t\right),M\left(\Re(y),y,t\right)\ \right)\leq 0. \quad (4)$$

Then $\Im$ and $\Re$ have a common fixed point $x\in X$.

Moreover, if x is absolutely fixed for $\Im$ and $\Re$ (which means that $\Im(x)=\{x\}$ and $\Re(x)=\{x\}$), then the fixed point is unique.

For the proof of this theorem one needs two lemmas.

LEMMA 3. *In a fuzzy b-metric space (X, M, T), if the function M is continuous with respect to one of its variable, then it is continuous with respect to the other.*

Proof

Suppose that M is continuous with respect to the first variable, and let (y_n) be a sequence of the elements of X such that (y_n) is b-convergent to $y \in X$. Then since M is symmetric one has for all $x \in X$:

$$\lim_{n\to\infty} M(x, y_n, t) = \lim_{n\to\infty} M(y_n, x, t) = M(y, x, t) = M(x, y, t), \quad t > 0.$$

LEMMA 4. *Let (X, M, T) be a fuzzy b-metric space and let $A \in C(X)$. If M is continuous with respect to one of its variables, then for all $x \in X$, there exists $y_0 \in A$ such that*

$$M(x, A, t) = \sup_{y\in A} M(x, y, t) = M(x, y_0, t), \quad t > 0.$$

Proof

One has $M(x, A, t) = \sup_{y\in A} M(x, y, t)$, so for every $n \in \mathbb{N}^*$, $t > 0$, there exists $x_n \in A$ such that

$$M(x, A, t) - \frac{1}{n} < M(x, x_n, t) \leq M(x, A, t) < M(x, A, t) + \frac{1}{n}.$$

Since A is compact, (x_n) has a subsequence, also noted (x_n), which is b-convergent to $y_0 \in A$. Therefore:

$$|M(x, x_n, t) - M(x, A, t)| < \frac{1}{n} \longrightarrow 0 \quad \text{when} \quad n \longrightarrow \infty.$$

from where $\lim_{n\to\infty} M(x, x_n, t) = M(x, A, t)$, so since M is continuous, one deduces that

$$\lim_{n\to\infty} M(x, x_n, t) = M(x, y_0, t),$$

hence from the uniqueness of the limit in a fuzzy b-metric space, one has $M(x, y_0, t) = M(x, A, t), \quad t > 0.$

Proof of the Theorem

Let $x_0 \in X$, and $x_1 \in \Im x_0$. Since $x_1 \in \Im x_0$, one has

$$H_M(\Im x_0, \Re x_1, t) = \min\left\{\inf_{x\in\Im x_0} M(x, \Re x_1, t), \inf_{y\in\Re x_1} M(\Im x_0, y, t)\right\}$$

$$\leq \inf_{x\in\Im x_0} M(x,\Re x_1,t)$$
$$\leq M(x_1,\Re x_1,t)=\sup_{y\in\Re x_1} M(x_1,y,t).$$

$\Re x_1$ is compact and M is continuous with respect to one of its variables, so, according to Lemma 4, there exists $x_2\in\Re x_1$ such that

$$H_M\left(\Im x_0,\Re x_1,t\right)\leq M(x_1,x_2,t),\quad t>0.$$

In the same manner, since $x_2\in\Re x_1$, one gets

$$H_M\left(\Im x_2,\Re x_1,t\right)\leq M(\Im x_2,x_2,t)=\sup_{x\in\Im x_2} M(x,x_2,t).$$

$\Im x_2$ is compact and M is continuous with respect to one of its variables, so, according to Lemma 4, there exists $x_3\in\Im x_2$ such that

$$H_M\left(\Im x_2,\Re x_1,t\right)\leq M(x_2,x_3,t),\quad t>0.$$

In the same way, there exists $x_4\in\Re x_3$ such that

$$H_M\left(\Im x_2,\Re x_3,t\right)\leq M(x_3,x_4,t),\quad t>0.$$

By recurrence, we construct a sequence (x_n) such that $x_{2n+1}\in\Im x_{2n}$, and $x_{2n+2}\in\Re x_{2n+1}$ which satisfies:

$$H_M\left(\Im x_{2n},\Re x_{2n-1},t\right)\leq M(x_{2n+1},x_{2n},t), \tag{5}$$

and

$$H_M\left(\Im x_{2n},\Re x_{2n+1},t\right)\leq M(x_{2n+1},x_{2n+2},t). \tag{6}$$

According to (4), with $x=x_{2n}$ and $y=x_{2n-1}$ one has

$$\psi\left(\begin{array}{c} H_M\left(\Im x_{2n},\Re x_{2n-1},t\right),M\left(x_{2n},x_{2n-1},t\right),M\left(\Im x_{2n},x_{2n},t\right), \\ M\left(\Re x_{2n-1},x_{2n-1},t\right)\end{array}\right)\leq 0.$$

Since $x_{2n+1}\in\Im x_{2n}$, and $x_{2n}\in\Re x_{2n-1}$, then

$$M\left(\Im x_{2n},x_{2n},t\right)\geq M\left(x_{2n+1},x_{2n},t\right), \tag{7}$$

and

$$M\left(\Re x_{2n-1},x_{2n-1},t\right)\geq M\left(x_{2n},x_{2n-1},t\right). \tag{8}$$

By (5), (7), (8) and (ψ_0) one has

$$\psi\left(\begin{array}{c} M\left(x_{2n+1},x_{2n},t\right),M\left(x_{2n},x_{2n-1},t\right),M\left(x_{2n+1},x_{2n},t\right), \\ M\left(x_{2n},x_{2n-1},t\right) \end{array}\right)\leq 0.$$

By (ψ_1), one has

$$M\left(x_{2n},x_{2n+1},t\right)<M\left(x_{2n-1},x_{2n},t\right),\qquad n\in\mathbb{N},\ t>0. \tag{9}$$

In the same way, by (4) with $x=x_{2n}$ and $y=x_{2n+1}$, one gets

$$\psi\left(\begin{array}{c} H_M\left(\Im x_{2n},\Re x_{2n+1},t\right),M\left(x_{2n},x_{2n+1},t\right),M\left(\Im x_{2n},x_{2n},t\right), \\ M\left(\Re x_{2n+1},x_{2n+1},t\right) \end{array}\right)\leq 0.$$

Since $x_{2n+2}\in\Re x_{2n+1}$, then

$$M\left(\Re x_{2n+1},x_{2n+1},t\right)\geq M\left(x_{2n+2},x_{2n+1},t\right). \tag{10}$$

By (6), (7), (10) and (ψ_0) one has

$$\psi\left(\begin{array}{c} M\left(x_{2n+1},x_{2n+2},t\right),M\left(x_{2n},x_{2n+1},t\right),M\left(x_{2n+1},x_{2n},t\right), \\ M\left(x_{2n+2},x_{2n+1},t\right) \end{array}\right)\leq 0.$$

By (ψ_1), one has

$$M\left(x_{2n},x_{2n+1},t\right)<M\left(x_{2n+1},x_{2n+2},t\right),\qquad n\in\mathbb{N},\ t>0. \tag{11}$$

According to (9) and (11), one has:

$$M\left(x_{n-1},x_n,t\right)<M\left(x_n,x_{n+1},t\right),\qquad n\in\mathbb{N}^*,\ t>0. \tag{12}$$

Therefore, $(M\left(x_n,x_{n+1},t\right))$ is a strictly increasing sequence of positive real numbers in $[0,1]$.

One puts $M_n(t)=M\left(x_n,x_{n+1},t\right)$. Then, $(M_n(t))$ is a strictly increasing sequence.

So, there exists $M(t)$ such that $\lim\limits_{n\to\infty}M_n(t)=M(t),\ t>0$.

Suppose that $0 < M(t) < 1$. According to (4), with $x = x_{2n}$ and $y = x_{2n+1}$ one has

$$\psi\left(\begin{array}{c} H_M\left(\Im x_{2n}, \Re x_{2n+1}, t\right), M\left(x_{2n}, x_{2n+1}, t\right), M\left(\Im x_{2n}, x_{2n}, t\right), \\ M\left(\Re x_{2n+1}, x_{2n+1}, t\right) \end{array}\right) \leq 0.$$

By (6), (7), (10) and (ψ_0), one has

$$\begin{aligned} & \psi\left(\begin{array}{c} M\left(x_{2n+1}, x_{2n+2}, t\right), M\left(x_{2n}, x_{2n+1}, t\right), M\left(x_{2n+1}, x_{2n}, t\right), \\ M\left(x_{2n+2}, x_{2n+1}, t\right) \end{array}\right) \leq 0, \\ \Rightarrow \quad & \psi\left(\ M_{2n+1}(t), M_{2n}(t), M_{2n}(t), M_{2n+1}(t)\ \right) \leq 0. \end{aligned}$$

Since ψ is continuous function, letting $n \to \infty$ one obtains

$$\psi\left(\ M(t), M(t), M(t), M(t)\ \right) \leq 0.$$

By (ψ_1), one gets $M(t) < M(t)$, a contradiction. Then $M(t) = 1$. Now, we will prove that (x_n) is a Cauchy squence. Suppose that (x_n) is not a Cauchy sequence, then for all $0 < \varepsilon < 1$, there exist two sub-sequences $(x_{n(i)})$ and $(x_{m(i)})$ such that for each $i \in \mathbb{N}$, let $n(i), m(i) \in \mathbb{N}$ satisfying $n(i) > m(i) \geq i$, such that

$$M\left(x_{2n(i)}, x_{2m(i)+1}, t\right) \leq 1 - \varepsilon. \tag{13}$$

Now, we choose $2n(i)$ corresponding to $2m(i)+1$ such that it is the smallest even integer with $n(i) > m(i)$ and satisfies Inequality (13). Hence,

$$M\left(x_{2n(i)-1}, x_{2m(i)+1}, t\right) > 1 - \varepsilon \tag{14}$$

By (13), we get

$$\begin{aligned} 1 - \varepsilon \quad & \geq \quad M\left(x_{2n(i)}, x_{2m(i)+1}, t\right) \\ & \geq \quad T\left(M\left(x_{2n(i)}, x_{2n(i)-1}, \frac{t}{2s}\right), M\left(x_{2n(i)-1}, x_{2m(i)+1}, \frac{t}{2s}\right)\right). \end{aligned}$$

By (14), we have

$$1 - \varepsilon \geq M\left(x_{2n(i)}, x_{2m(i)+1}, t\right) \quad \geq \quad T\left(M\left(x_{2n(i)}, x_{2n(i)-1}, \frac{t}{2s}\right), 1 - \varepsilon\right)$$

$$= T\left(M_{2n(i)-1}\left(\frac{t}{2s}\right), 1-\varepsilon\right)$$

letting $i \to \infty$ we obtain

$$1-\varepsilon \geq \lim_{i\to\infty} M\left(x_{2n(i)}, x_{2m(i)+1}, t\right) \geq T\left(1, 1-\varepsilon\right) = 1-\varepsilon.$$

So

$$\lim_{i\to\infty} M\left(x_{2n(i)}, x_{2m(i)+1}, t\right) = 1-\varepsilon.$$

By (4), with $x = x_{2m(i)}$ and $y = x_{2n(i)-1}$, we get

$$\psi\left(\begin{array}{c} H_M\left(\Im x_{2m(i)}, \Re x_{2n(i)-1}, t\right), M\left(x_{2m(i)}, x_{2n(i)-1}, t\right), \\ M\left(\Im x_{2m(i)}, x_{2m(i)}, t\right), M\left(\Re x_{2n(i)-1}, x_{2n(i)-1}, t\right) \end{array}\right) \leq 0.$$

Since $x_{2m(i)+1} \in \Im x_{2m(i)}$, and $x_{2n(i)} \in \Re x_{2n(i)-1}$, then

$$M\left(\Im x_{2m(i)}, x_{2m(i)}, t\right) \geq M\left(x_{2m(i)+1}, x_{2m(i)}, t\right), \tag{15}$$

and

$$M\left(\Re x_{2n(i)-1}, x_{2n(i)-1}, t\right) \geq M\left(x_{2n(i)}, x_{2n(i)-1}, t\right). \tag{16}$$

By (15), (16) and (ψ_0), we have

$$\psi\left(\begin{array}{c} H_M\left(\Im x_{2m(i)}, \Re x_{2n(i)-1}, t\right), M\left(x_{2m(i)}, x_{2n(i)-1}, t\right), \\ M\left(x_{2m(i)+1}, x_{2m(i)}, t\right), M\left(x_{2n(i)}, x_{2n(i)-1}, t\right) \end{array}\right) \leq 0.$$

Since $x_{2m(i)+1} \in \Im x_{2m(i)}$ and $x_{2n(i)} \in \Re x_{2n(i)-1}$, then

$$\begin{aligned} H_M\left(\Im x_{2m(i)}, \Re x_{2n(i)-1}, t\right) &\leq M\left(x_{2m(i)+1}, \Re x_{2n(i)-1}, t\right) \\ &= T\left(M\left(x_{2m(i)+1}, \Re x_{2n(i)-1}, t\right), 1\right) \\ &= T\left(\begin{array}{c} M\left(x_{2m(i)+1}, \Re x_{2n(i)-1}, t\right), \\ M\left(x_{2n(i)}, \Re x_{2n(i)-1}, t\right) \end{array}\right) \\ &\leq M\left(x_{2m(i)+1}, x_{2n(i)}, 2ts\right). \end{aligned}$$

So

$$H_M\left(\Im x_{2m(i)}, \Re x_{2n(i)-1}, t\right) \leq M\left(x_{2m(i)+1}, x_{2n(i)}, 2ts\right). \tag{17}$$

By (17) and (ψ_0), we get

$$\psi\left(\begin{array}{c} M\left(x_{2n(i)}, x_{2m(i)+1}, 2st\right), \\ T\left(M_{2m(i)}\left(\frac{t}{2s}\right), M\left(x_{2m(i)+1}, x_{2n(i)-1}, \frac{t}{2s}\right)\right), \\ M_{2m(i)}\left(t\right), M_{2n(i)-1}\left(t\right) \end{array}\right) \leq 0$$

$$\Rightarrow \quad \psi\left(\begin{array}{c} M\left(x_{2n(i)}, x_{2m(i)+1}, 2st\right), T\left(M_{2m(i)}\left(\frac{t}{2s}\right), 1-\varepsilon\right), \\ M_{2m(i)}(t), M_{2n(i)-1}(t) \end{array}\right) \leq 0.$$

letting $i \to \infty$, we obtain

$$\begin{aligned} & \psi\left(\ 1-\varepsilon, T(1,1-\varepsilon), 1, 1\ \right) \leq 0 \\ \Rightarrow \quad & \psi\left(\ 1-\varepsilon, 1-\varepsilon, 1, 1\ \right) \leq 0. \end{aligned}$$

By (ψ_2), we get $1-\varepsilon = 1$, which is a contradiction.

Hence, (x_n) is a Cauchy sequence in a complete fuzzy b-metric space. So, there exists $x \in X$ such that $\lim_{n\to\infty} M(x_n, x, t) = 1$. Next, we show that $x \in \Im x \cap \Re x$, indeed, we have $x_{2n} \in \Re x_{2n-1}$ and $x_{2n+1} \in \Im x_{2n}, \quad n \in \mathbb{N}$.

Since $\lim_{n\to\infty} x_{2n-1} = \lim_{n\to\infty} x_{2n} = \lim_{n\to\infty} x_{2n+1} = x$, $\Im$ and $\Re$ are closed, then $x \in \Im x \cap \Re x$.

Unicity. Suppose that $\Im x = \{x\}$ and that there exists $y \in X$ is another common fixed point of $\Im$ and $\Re$, such that $\Re y = \{y\}$. Then by (4), we have

$$\begin{aligned} & \psi\left(\begin{array}{c} H_M(\Im x, \Re y, t), M(x, y, t), M(\Im x, x, t), \\ M(\Re y, y, t) \end{array}\right) \leq 0 \\ \Rightarrow \quad & \psi\left(\begin{array}{c} M(x, y, t), M(x, y, t), M(x, x, t), \\ M(y, y, t) \end{array}\right) \leq 0 \\ \Rightarrow \quad & \psi\left(\ M(x, y, t), M(x, y, t), 1, 1\ \right) \leq 0. \end{aligned}$$

By (ψ_2) we get $M(x, y, t) = 1$, then $x = y$.

THEOREM 2. *Let (X, M, T) be a complete fuzzy b-metric space with the constant s. Let $\Im : X \longrightarrow CL(X)$ be a closed maps and $\psi \in \Psi$ such that*

$$\psi\left(\ \delta_M(\Im(x), \Im(y), t), M(x, y, t), M(\Im(x), x, t), M(\Im(y), y, t)\ \right) \leq 0. \quad (18)$$

Then $\Im$ has a unique fixed point $x \in X$.

Proof Let $x_0 \in X$, define the sequence (x_n) of the elements from X such that: $x_{n+1} \in \Im x_n$ for every $n \in \mathbb{N}$.

According to (18), with $x = x_{n-1}$ and $y = x_n$ we have

$$\psi\left(\ \delta_M(\Im x_{n-1}, \Im x_n, t), M(x_{n-1}, x_n, t), M(\Im x_{n-1}, x_{n-1}, t), M(\Im x_n, x_n, t)\ \right) \leq 0.$$

Since $x_n \in \Im x_{n-1}$ and $x_{n+1} \in \Im x_n$ we get

$$M(\Im x_{n-1}, x_{n-1}, t) \geq M(x_n, x_{n-1}, t), \quad M(\Im x_n, x_n, t) \geq M(x_{n+1}, x_n, t)$$

and $\delta_M\left(\Im x_{n-1}, \Im x_n, t\right) \leq M\left(x_n, x_{n+1}, t\right)$.

By (ψ_0), we have

$$\psi\left(\ M\left(x_n, x_{n+1}, t\right), M\left(x_{n-1}, x_n, t\right), M\left(x_n, x_{n-1}, t\right), M\left(x_{n+1}, x_n, t\right)\ \right) \leq 0.$$

By (ψ_1), we have

$$M\left(x_{n-1}, x_n, t\right) < M\left(x_n, x_{n+1}, t\right), \qquad n \in \mathbb{N}^*,\ t > 0.$$

So, using the same argument as in Theorem 1, we deduce that x_n is a Cauchy sequence and converges to $x \in X$, the fixed point of $\Im$.

Unicity. Suppose that there exists $y \in X$ is another fixed point of $\Im$. Then by (18), we have

$$\psi\left(\begin{array}{c} \delta_M\left(\Im x, \Im y, t\right), M\left(x, y, t\right), M\left(\Im x, x, t\right), \\ M\left(\Im y, y, t\right) \end{array}\right) \leq 0$$

by (ψ_0), we have

$$\begin{array}{rl} & \psi\left(\begin{array}{c} M\left(x, y, t\right), M\left(x, y, t\right), M\left(x, x, t\right), \\ M\left(y, y, t\right) \end{array}\right) \leq 0 \\ \Rightarrow & \psi\left(\ M\left(x, y, t\right), M\left(x, y, t\right), 1, 1\ \right) \leq 0. \end{array}$$

By (ψ_2) we get $M\left(x, y, t\right) = 1$, then $x = y$.

As a consequence of Theorem 2, if $\Im = f$ is single-valued mapping, then we obtain the following:

COROLLARY 1. *Let (X, M, T) be a complete fuzzy b-metric space with the constant s. Let $f : X \longrightarrow X$ be a continuous mapping and $\psi \in \Psi$ such that*

$$\psi\left(\ M\left(fx, fy, t\right), M\left(x, y, t\right), M\left(fx, x, t\right), M\left(fy, y, t\right)\ \right) \leq 0.$$

Then f has a unique fixed point $x \in X$.

EXAMPLE 7. Let X be the subset of $\mathbb{R}^3$ defined by $X = \{A, B, C, D\}$, where $A = (1, 0, 0),\ B = (0, 1, 0),\ C = (0, 0, 1)$ and $D = (2, 2, 2)$. $T(c, d) = c.d$ for all $c, d \in [0, 1]$ and (X, M, T) is a complete fuzzy $b-$metric space such that:

$$M(x, y, t) = e^{\frac{-d(x,y)}{t}}, \quad x, y \in X,\ t > 0,$$

where $d(x, y)$ denotes the Euclidean distance of $\mathbb{R}^3$.

Let $\Im : X \to X$ be given by $\Im(A) = \Im(B) = \Im(C) = A, \Im(D) = B$.
Show that for all $x, y \in X$

$$\psi\left(M\left(\Im x, \Im y, t\right), M\left(x, y, t\right), M\left(\Im x, x, t\right), M\left(\Im y, y, t\right) \right) \leq 0.$$

with ψ as in Example 4, and $\beta(t) = -ln(t)$.

Indeed: If $x, y \in \{A, B, C\}$ we have $M\left(\Im x, \Im y, t\right) = M\left(A, A, t\right) = 1$.
So $\beta(M\left(\Im x, \Im y, t\right)) = 0 \leq \lambda\beta(M\left(x, y, t\right)),\ \lambda \in (0, 1)$.
If $x \in \{A, B, C\}$ and $y = D$, we find

$$M\left(\Im x, \Im y, t\right) = e^{\frac{-\sqrt{2}}{t}} \text{ and } M\left(x, y, t\right) = e^{\frac{-3}{t}}.$$

So, $\beta(M\left(\Im x, \Im y, t\right)) \leq \lambda\beta(M\left(x, y, t\right)),\ \lambda \in (\frac{\sqrt{2}}{3}, 1)$.

Now, all the hypotheses of Corollary 1 are satisfied and thus $\Im$ has a unique fixed point, which is $x = A$.

REMARK 2. From Corollary 1 and Example 6 we obtain Theorem 3.1 (Shen et al., 2012) Let $(X, M, *)$ be an M-complete fuzzy metric space and T a self-map of X and suppose that $\varphi : [0, 1] \longrightarrow [0, 1]$ satisfies the foregoing properties $(P1)$ and $(P2)$. Furthermore, let k be a function from $(0, \infty) \longrightarrow (0, 1)$. If for any $t > 0$, T satisfies the following condition: $\varphi(M(Tx, Ty, t)) \leq k(t)\varphi(M(x, y, t))$, where $x, y \in X$ and $x \neq y$, then T has a unique fixed point.

Conclusion

In this paper, a new space called a Pompeiu-Hausdorff fuzzy b-metric space is constructed. Some examples in this space are presented. Additionally, some new fixed-point results in this space are formulated and proven, which extends the results of (Shen et al., 2012), and the existence and uniqueness of the common fixed point in such a space are demonstrated.

The approach proposed may pave the way for new developments in generalized metrical structures and fixed-point theory.

References

Aghajani, A., Abbas, M. & Roshan, J.R. 2014. Common fixed point of generalized weak contractive mappings in partially ordered b-metric spaces. *Mathematica Slovaca*, 64, pp. 941–960. Available at: https://doi.org/10.2478/s12175-014-0250-6.

Aydi, H., Bota, M., Karapinar, E. & Mitrović, S. 2012. A fixed point theorem for set-valued quasi-contractions in b-metric spaces. *Fixed Point Theory and Applications*, 2012, art.number:88. Available at: https://doi.org/10.1186/1687-1812-2012-88.

Bakhtin, I. 1989. The contraction mapping principle in quasimetric spaces. *Func. An., Gos. Ped. Inst. Unianowsk*, 30, pp. 26–37.

Bota, M., Molnár, A. & Varga, C. 2011. On Ekeland's Variational Principle in b-Metric Spaces. *Fixed Point Theory*, 12(1), pp. 21–28 [online]. Available at: https://www.math.ubbcluj.ro/~nodeacj/vol__12(2011)_no_1.php [Accessed: 5 June 2024].

Czerwik, S. 1993. Contraction mappings in b-metric spaces. *Acta Mathematica et Informatica Universitatis Ostraviensis*, 1(1), pp. 5–11 [online]. Available at: https://dml.cz/handle/10338.dmlcz/120469 [Accessed: 5 June 2024].

Dahhouch, M., Makran, N. & Marzouki, B. 2024. A generalized fixed point theorem in fuzzy b-metric spaces and applications. *Boletim da Sociedade Paranaense de Matemática*, 42, pp. 1–7 [online]. Available at: https://doi.org/10.5269/bspm.63276.

Došenović, T., Rakić, D., Radenović, S. & Carić, B. 2023. Ćirić type nonunique fixed point theorems in the frame of fuzzy metric spaces. *AIMS Mathematics*, 8(1), pp. 2154–2167. Available at: https://doi.org/10.3934/math.2023111.

George, A. & Veeramani, P. 1997. On some results of analysis for fuzzy metric spaces. *Fuzzy Sets and Systems*, 90(3), pp. 365–368. Available at: https://doi.org/10.1016/S0165-0114(96)00207-2.

Hassanzadeh, Z. & Sedghi, S. 2018. Relation between b-metric and fuzzy metric spaces. *Mathematica Moravica*, 22(1), pp. 55–63. Available at: https://doi.org/10.5937/MatMor1801055H.

Kramosil, I. & Michalek, J. 1975. Fuzzy Metrics and Statistical Metric Spaces. *Kybernetica*, 11(5), pp. 326–334 [online]. Available at: https://www.kybernetika.cz/content/1975/5/336/paper.pdf [Accessed: 5 June 2024].

Makran, N., El Haddouchi, A. & Marzouki, B. 2023. A generalized common fixed point of multi-valued maps in b-metric space. *Boletim da Sociedade Paranaense de Matemática*, 41, pp. 1–9. Available at: https://doi.org/10.5269/bspm.51655.

Rakić, D., Mukheimer, A., Došenović, T., Mitrović, Z. & Radenović, S. 2020. On some new fixed point results in fuzzy b-metric spaces. *Journal of Inequalities and Applications*, 2020, art.number:99. Available at: https://doi.org/10.1186/s13660-020-02371-3.

Sedghi, S. & Shobe, N. 2012. Common fixed point theorem in b-fuzzy metric space. *Nonlinear Functional Analysis and Applications (NFAA)*, 17(3), pp. 349–359 [online]. Available at: http://nfaa.kyungnam.ac.kr/journal-nfaa/index.php/NFAA/article/view/38 [Accessed: 5 June 2024].

Sedghi, S. & Shobe, N. 2014. Common fixed point theorem for R-weakly commuting maps in b-fuzzy metric space. *Nonlinear Functional Analysis and Applications (NFAA)*, 19(2), pp. 285–295 [online]. Available at: http://nfaa.kyungnam.ac.kr/journal-nfaa/index.php/NFAA/article/view/238 [Accessed: 5 June 2024].

Shen, Y., Qiu, D. & Chen, W. 2012. Fixed point theorems in fuzzy metric spaces. *Applied Mathematics Letters*, 25(2), pp. 138–141. Available at: https://doi.org/10.1016/j.aml.2011.08.002.

Aplicaciones multivaluadas en espacios b-métricos difusos de Pompeiu-Hausdorff y un resultado de punto fijo común

Noreddine Makran[a], *Stojan* N. Radenović[b]

[a] Universidad Mohammed Premier, Facultad de Ciencias, Departamento de Matemáticas, Oujda, Reino de Marruecos, **autor de correspondencia**

[b] Universidad de Belgrado, Facultad de Ingeniería Mecánica, Belgrado, República de Serbia

CAMPO: matemáticas, ciencias computacionales

TIPO DE ARTÍCULO: artículo científico original

Resumen:

Introducción/objetivo: El estudio de la teoría de conjuntos difusos surgió a partir de la presencia de la incertidumbre como parte esencial de los problemas del mundo real, lo que llevó a Zadeh a abordar el problema de la indeterminación. Zadeh introdujo el concepto de lógica difusa. A diferencia de la teoría lógica tradicional, en la que un elemento pertenece o no al conjunto, en la lógica difusa la afiliación del elemento al conjunto se expresa como un número del intervalo $[0, 1]$.

Métodos: La teoría de un punto fijo en espacios métricos difusos puede verse de diferentes maneras, una de las cuales implica el uso de la lógica difusa. Los espacios métricos difusos, que son tipos específicos de espacios topológicos con características "geométricas" agradables, poseen una serie de propiedades atractivas y se utilizan comúnmente tanto en ciencias puras como aplicadas. Los espacios métricos y sus diversas generalizaciones ocurren con frecuencia en aplicaciones de ciencias de la computación. Por esta razón, en este artículo se construye un nuevo espacio llamado espacio b-métrico difuso de Pompeiu-Hausdorff.

Resultados: En este espacio, también se formulan y prueban algunos nuevos resultados de punto fijo. Además, se investiga un teorema de punto fijo común general para un par de aplicaciones multivaluadas en espacios b-métricos difusos de Pompeiu-Hausdorff. Los hallazgos obtenidos en espacios métricos difusos, como los discutidos en el artículo de Shen, Y. et al. (2012. Fixed point theorems in fuzzy metric spaces. Applied Mathematics Letters, 25, pp.138-141), se generalizan a partir de los resultados de este documento, y se producen hallazgos específicos adicionales que se respaldan con ejemplos.

Conclusión: El estudio de la semántica denotacional y sus aplicaciones en la teoría de control utilizando espacios b-métricos difusos y espacios b-métricos difusos de Pompeiu-Hausdorff será un siguiente paso importante.

Palabras claves: espacio métrico difuso, espacio b-métrico difuso, norma t, punto fijo, relación implícita.

Многозначные отображения в нечетких b-метрических пространствах типа Помпею-Хаусдорфа и результат с общей неподвижной точкой

Нуреддин Макран[а], *Стоян* Н. Раденович[б]

[а] Университет Мохаммеда Премьера, факультет естественных наук, кафедра математики, г. Уджда, Королевство Марокко, **корреспондент**

[б] Белградский университет, машиностроительный факультет, г. Белград, Республика Сербия

РУБРИКА ГРНТИ: 27.25.17 Метрическая теория функций
ВИД СТАТЬИ: оригинальная научная статья

Резюме:

Введение/цель: Изучению теории нечетких множеств способствовало наличие неопределенности как неотъемлемой части реальных проблем, что привело Заде к решению проблемы неопределенности. Именно он ввел понятие нечеткой логики. В отличие от традиционной логической теории, где элемент либо принадлежит множеству, либо нет, в нечеткой логике принадлежность элемента к множеству выражается числом из интервала $[0, 1]$.

Методы: Теорию неподвижной точки в нечетких метрических пространствах можно рассматривать по-разному.

Один из подходов предполагает использование нечеткой логики. Нечеткие метрические пространства как специфические типы топологических пространств с приятными "геометрическими" характеристиками обладают рядом привлекательных свойств и широко используются как в чистой, так и в прикладной науке. Метрические пространства и их различные обобщения часто встречаются в приложениях вычислительных наук. В связи с вышеизложенным в данной работе сформировано новое пространство, называемое нечетким b-метрическим пространством Помпею-Хаусдорфа.

Результаты: В этом пространстве также сформулированы и доказаны некоторые новые результаты о неподвижной точке. Помимо того, исследована теорема об общей неподвижной точке для пары многозначных отображений в нечетких b-метрических пространствах типа Помпею-Хаусдорфа. Результаты, полученные в нечетких метрических пространствах, как, например, те, которые обсуждались в статье Шена и др. (Shen, Y. et al. 2012. Fixed point theorems in fuzzy metric spaces. Applied Mathematics Letters, 25, pp.138-141), обобщаются результатами данного исследования, а в дополнение приводятся конкретные выводы, подкрепленные примерами.

Выводы: Следующим важным шагом станет изучение денотационной семантики и ее применения в теории управления с использованием нечетких b-метрических пространств и нечетких b-метрических пространств Помпею-Хаусдорфа.

Ключевые слова: нечеткое метрическое пространство, нечеткое b-метрическое пространство, t-норма, фиксированная точка, неявное отношение.

Вишезначна пресликавања расплинутих б-метричких простора типа Помпеју-Хауздорф и резултат заједничке непокретне тачке

Нуредин Макран[а], *Стојан* Н. Раденовић[б]

[а] Универзитет „Мухамед Премијер",
Природно-математички факултет, Одсек за математику,
Оујда, Краљевина Мароко, **аутор за преписку**

[б] Универзитет у Београду, Машински факултет,
Београд, Република Србија

ОБЛАСТ: математика
КАТЕГОРИЈА (ТИП) ЧЛАНКА: оригинални научни рад

Сажетак:

Увод/циљ: Проучавање теорије расплинутих скупова подстакнуто је несигурношћу као суштинском цртом проблема у реалном свету, што је навело Задеа да се позабави проблемом неодређености и уведе појам расплинуте логике. За разлику од традиционалне теорије логике, у којој један елемент припада или не припада неком скупу , у расплинутој логици припадност елемента неком скупу изражава се бројем из интервала $[0, 1]$.

Методе: Теорија непокретне тачке у расплинутим метричким просторима може се посматрати на различите начине, од којих један подразумева коришћење расплинуте логике. Расплинути метрички простори, као специфични типови тополошких простора са пријатним „геометријским" карактеристикама, имају много интересантних карактеристика и обично се користе и у чистим и у примењеним наукама. Метрички простори и њихове различите генерализације често се срећу у применама рачунарских наука. Зато је у овом раду конструисан нови простор назван расплинути б-метрички простор типа Помпеју-Хауздорф.

Резултати: У овом простору формулисани су и доказани неки нови резултати непокретне тачаке. При томе је испитана општа теорема заједничке непокретне тачке за пар вишезначног пресликавања у расплинутим б-метричким просторима типа Помпеју-Хауздорф. Налази добијени у расплинутим метричким просторима, као што су они наведени у чланку Шена и сарадника (Shen, Y. et al. 2012. Fixed point theorems in fuzzy metric spaces. Applied Mathematics Letters, 25, pp.138-141), генерализовани су резултатима овог рада који презентује и додатне специфичне налазе поткрепљене примерима.

Закључак: Следећи важан корак биће проучавање денотационе семантике и њене примене у теорији управљања помоћу расплинутих б-метичких простора и расплинутих б-метричких простора типа Помпеју-Хауздорф.

Кључне речи: расплинути метрички простор, расплинути б-метрички простор, т-норма, непокретна тачка, имплицитна релација.

Paper received on: 07.06.2024.
Manuscript corrections submitted on: 30.01.2025.
Paper accepted for publishing on: 31.01.2025.

Application of the AHP and PROMETHEE II individual decision-making methods and the Condorcet group decision-making method in the selection of a multipurpose armored wheeled combat vehicle

Miša D. Živković[a], *Darko* I. Božanić[b],
Milija M. Suknović[c], *Boris* V. Delibašić[d]

[a] University of Defence in Belgrade, Military Academy, Department of Tactics with Weapon Systems, Belgrade, Republic of Serbia,
e-mail: zivkovic.misa@yahoo.com, **corresponding author**,
ORCID iD: https://orcid.org/0009-0007-1918-4259

[b] University of Defence in Belgrade, Military Academy, Department of Tactics with Weapon Systems, Belgrade, Republic of Serbia,
e-mail: dbozanic@yahoo.com,
ORCID iD: https://orcid.org/0000-0002-9657-0889

[c] University of Belgrade, Faculty of Organizational Sciences, Department of Business Systems Organization,
Belgrade, Republic of Serbia,
e-mail: milija.suknovic@fon.bg.ac.rs,
ORCID iD: https://orcid.org/0009-0003-0449-5258

[d] University of Belgrade, Faculty of Organizational Sciences, Department of Business Systems Organization,
Belgrade, Republic of Serbia,
e-mail: boris.delibasic@fon.bg.ac.rs,
ORCID iD: https://orcid.org/0000-0002-6153-5119

https://doi.org/10.5937/vojtehg73-54049

FIELD: decision science, military sciences
ARTICLE TYPE: original scientific paper

Abstract:

Introduction/purpose: Wheeled armored combat vehicles are combat systems that are increasingly present in modern armed conflicts, especially in operations against asymmetric threats. The global wheeled armored vehicle market is constantly growing, which reflects their application in a wide range of missions and tasks of armed forces. The existence of numerous models of these vehicles with different technical and exploitation characteristics, along with the possibility of adaptation to specific needs, further complicates the choice of the most suitable alternative. The paper presents the case of solving the problem of selecting the most suitable multi-purpose medium-class wheeled armored vehicle with a 4x4 drive formula when choosing one of the four alternatives, using individual and group multi-criteria decision-making methods.

Methods: In the paper, the methods of multi-criteria decision making were applied to solve problems in the field of complex combat systems selection. Experts from the field of tactics with weapon systems have ranked the alternatives following the defined criteria using the AHP (Analytic Hierarchy Process) and the PROMETHEE II (Preference Ranking Organization Method for Enrichment Evaluations II) methods. The results obtained by individual decision making were subjected to the Condorcet method of group decision making to make a final decision.

Result: Selection of the most suitable vehicle by the defined criteria.

Conclusion: Solving the problem involves taking into account the views of military experts regarding the optimization of multiple criteria to provide the best performance vehicle suitable for use in various missions. The choice of a multi-purpose wheeled armored combat vehicle is a complex process influenced by numerous factors that cannot be analyzed objectively without the application of adequate mathematical models.

Keywords: armored combat vehicles, multi-criteria decision making, AHP, PROMETHEE II, Condorcet method.

Introduction

Armored combat vehicles are special motor vehicles considered for performing various tasks in the operations of armed forces. Their basic characteristics are mobility, protection, and firepower (the ability to transport personnel and cargo).

Today, there is a tendency for wheeled armored vehicles of all types to dominate in equipping armed forces in the world, compared to tanks and tracked infantry fighting vehicles, which are significantly more expensive and more demanding in terms of maintenance. In support of this, the constant growth of the world market of wheeled armored vehicles, especially those belonging to the light and medium class, is evidenced, with estimates that this trend will continue (Kurtay, 2024). Multi-purpose armored combat vehicles with a 4x4 wheel drive formula are suitable for carrying out various tasks, such as reconnaissance, territory control, transport and support of infantry units, and fire support, but also for command and control and medevac.

The choice of a wheeled armored combat vehicle is a challenge even for experts in that field and requires a certain level of compromise in requirements and respect for the specific needs of military or police units, as well as for the spectrum of threats to which the vehicle and its users may be exposed.

The paper presents one of possible models for the application of various multi-criteria decision-making methods to provide support to

decision makers in the preliminary selection of a 4x4 wheel drive armored combat vehicle. For this purpose, two individual decision-making methods are described and practically applied - AHP and PROMETHEE II and the Condorcet group decision-making method. It was noted that choosing between vehicles with similar performance is complex when there are conflicting criteria to consider.

The mentioned methods were applied in the case of solving a specific problem - ranking and choosing the most optimal variant among the four offered models of armored combat vehicle wheel drive 4x4: BOV M16 Miloš-2, Despot, Tatra 815-7 Patriot II and Zetor-Gerlach. The mentioned vehicles were chosen for two basic reasons: the availability of data on technical and exploitation characteristics and similarity in essential characteristics, whereby there is no intention of the author to single out a specific vehicle as the absolute best. The offered vehicles belong to the middle class of armored vehicles from 10 to 20 t and in certain aspects have similar performance, which can make the choice even more difficult for experts.

For the purposes of this research, military experts were hired. The use of expert evaluation in the development of a multi-criteria decision-making model proved to be necessary (Kizielewicz & Sałabun, 2024; Puška et al, 2018). In this case, the experts defined three main criteria, namely: mobility, protection, and the ability to transport personnel and cargo (payload capacity), while firepower and command and control criteria were omitted, bearing in mind that with all four offered alternatives there are numerous options for equipping with different combat and other systems depending on the need, which exceeds the scope of this research. Also, the problem is viewed from the aspect of combat vehicle capabilities, without considering the value aspect (purchase price, maintenance, etc.). The ranking of the alternatives based on the defined criteria, which are explained below, was carried out based on the subjective opinion of four military experts in the field of tactics with weapons systems. Considering the medium level of complexity of the problem and the chosen decision-making methods, a model of the participation of a smaller number of experts was chosen. In this research, performing a high level of expertise in the field of wheeled armored unit tactics was essential for valid individual decision making. The interview was conducted with a total of 12 Infantry branch officers, and four of them met the set criteria regarding the necessary professional experience and knowledge in wheeled armored vehicles.

The first two experts performed the ranking using the AHP method, while the third and the fourth applied the AHP-PROMETHEE II model. The

results obtained by the individual decision making of four experts were subjected to the Condorcet method of group decision making, to make a final decision.

The AHP method was chosen because it requires the active participation of military experts for adequate comparison by pairs and determining the weight of the criteria, and because it provides good results for the given number of criteria. Also, based on the analyzed literature, the AHP method is useful for structuring the problem of choosing vehicles and combat systems. On the other hand, the PROMETHEE II method is very easy to use by experts and provides additional precision by defining the preference parameters on each criterion. The Condorcet method was chosen because it is more representative than models of simple majority voting in group decision making, as it takes into account all possible comparisons of the ranks of alternatives obtained by experts through individual decision making.

The analysis of the literature leads to the conclusion that multi-criteria decision-making methods have been applied in many areas of military activity, individually or in a variant of the combination of two or more methods, to make the best use of their capabilities in support of finding an optimal solution to the problem. In the field of combat system selection, there is a large number of scientific works in which the subject methods were used: Kurtay (2024) applies the Fuzzy EDAS method for the selection of an armored vehicle; Genc (2015) applies the ELECTRE III and PROMETHE II methods, while Gazibey et al. (2015) apply the DEMATEL method for criteria analysis and tank selection; Radovanović et al. (2023) ranks Unmanned Combat Air Vehicle for military needs using multiple methods (DIBR, FUCOM, LMAW, and EDAS); Starčević et al. (2019) apply the AHP-DEA model to the selection of military vehicles for use in multinational operations; Tešić & Marinković (2023) perform the selection of complex combat systems using several methods and aggregators; Jokic et al. (2024) apply the DEX method to select the optimal caliber for an automatic rifle; Radovanović et al. (2019) apply the AHP method, and Pamučar & Dimitrijević (2021) the TOPSIS and MABAC methods for the selection of anti-armor missile systems; Santos et al. (2021) apply the AHP method in the selection of a warship; Sun et al. (2013) apply the Fuzzy-AHP method, and Furch & Švásta (2022) integrate a number of multi-criteria decision-making methods for the selection of unmanned ground platforms; Radovanović et al. (2024) select an assault rifle using the LMAW - gray EDAS hybrid model. In the study of the UN working group, the AHP method was used to rank the importance of the capabilities of

armored personnel carriers and wheeled and tracked vehicles (UN Department of Operational Support, 2023).

The analyzed literature unequivocally indicates that the authors are interested in the application of various mathematical methods when choosing complex combat systems.

The work is conceived in several parts. In the next part, a description of armored combat vehicles was given. Furthermore, the methods used in the creation of the model were presented, in order to finally give a detailed description of the criteria and a presentation of the results obtained through the application of the model.

Basic characteristics of armored vehicles

The development of armored combat vehicles took place following the reached level of technological progress in the world and changes in the physiognomy of armed conflicts, constantly adapting to new threats. The first armored vehicles were used during the First World War in the form of transporters with light armor protection and were intended for the transport of infantry units to support tanks on the battlefield (Radetić, 2001). Regarding the vehicle type, originally half-tracked combat vehicles were used while later tracked vehicles were dominant, and wheeled vehicles were rarely used. After the Second World War, the intensive development of infantry fighting vehicles began to ensure a higher speed of maneuver of infantry units, at the same time providing better armor protection and firepower. After the period of the Cold War, a more intensive development of wheeled armored combat vehicles of all types began, under new - asymmetric threats and in the conditions of increasingly frequent conflicts in the urban environment (Kurtay, 2024). Such a situation required the use of vehicles of smaller dimensions and high maneuverability, but also with adequate protection, suitable for carrying out tasks such as reconnaissance, territory control, operations of special military and police forces, and for conflicts of lower intensity.

The key capabilities of armored vehicles are traditionally contained in the so-called "iron triangle" which implies mobility, protection, and firepower (Dean, 2024). In addition to the mentioned universal characteristics, for wheeled armored combat vehicles that are essentially intended to carry out the transport of combat formations and assets to the desired location, the ability to transport personnel and cargo, i.e. the vehicle's carrying capacity, is very important, and the efficiency of this type of vehicle is often considered through three main characteristics: mobility, protection and payload capacity (Giurgiu et al, 2023).

In a 2023 United Nations task force study, an expanded list of criteria for the classification of armored fighting vehicles (APVs) was proposed and included protection, mobility, firepower, payload capacity, and command and control systems. Also, the necessity of considering new capabilities by the requirements of the modern combat environment, such as survivability, adaptability, connectivity, surveillance, threat detection, identification in combat, etc., has been increasingly discussed recently (Giurgiu et al, 2023). The essence of such tendencies is to ensure a high degree of situational awareness on the battlefield to quickly react in terms of eliminating or avoiding the threat.

Mobility is very important for the efficiency of vehicle use in different terrain conditions, but also from the aspect of force protection, thanks to the reduced exposure of the vehicle to potential threats. Mobility largely depends on the combat weight of the vehicle, because it affects the acceleration, i.e., the agility of the vehicle in combat, as well as the power of the engine and the suspension system (Muždeka, 2012). As the mass of the vehicle directly affects the maneuverability of the vehicle, there must be a balance concerning armored protection and transport capacity (Kamel, 2017). On the other hand, the number of crew members and the mass of additional cargo are related to the self-protection capability. Namely, the greater mass with which it is possible to load the vehicle is an indicator of the possibility of implementing different weapons systems - greater firepower and for acting on different targets (anti-armor means, for acting on targets in the airspace, etc.), but also a larger number of combat-formation members, which protects the vehicle itself in battle, among other things. Also, in terms of additional protection, the greater carrying capacity of the vehicle provides the possibility of using various modular elements for the protection of the vehicle for protection against light anti-armor systems of less penetration (Dean & Cazalet, 2024).

In terms of firepower, modern wheeled armored combat vehicles are not far behind other combat vehicles and can be equipped with different combat stations with light and heavy machine guns, cannons of caliber up to 30 mm, but also with secondary weapons such as anti-armor systems, grenade launchers, light anti-aircraft systems, etc.

From the above, it can be concluded that there is a high degree of interdependence among the characteristics, and it is necessary to have an adequate balance to achieve greater efficiency in combat. This is especially important in terms of the use of multi-purpose vehicles. In order to choose the most optimal variant of the vehicle, it is necessary to first decompose the main criteria into an optimal number of sub-criteria, and

then carry out their evaluation to ensure a compromise in the level of the vehicle's capabilities, according to the specific requirements of use.

Description of the methods

The work used the AHP and PROMETHEE II methods of individual multi-criteria decision making and the Condorcet method of group multi-criteria decision making. The presentation of the model is given in Figure 1. As it can be seen from the figure, the model has four phases. In the first phase, criteria and sub-criteria specific to the presented problem are defined. Through the second phase, the experts compare the criteria, and after that, the weight coefficients of the criteria are calculated for each expert. The obtained values represent the input to the third phase of the model where the ranking of the alternatives is performed using the AHP and PROMETHEE II methods. Finally, in the fourth stage, the final values for the ranking of the alternatives are obtained by applying the Condorcet method. A brief description of the applied methods in the model is given in the following sections.

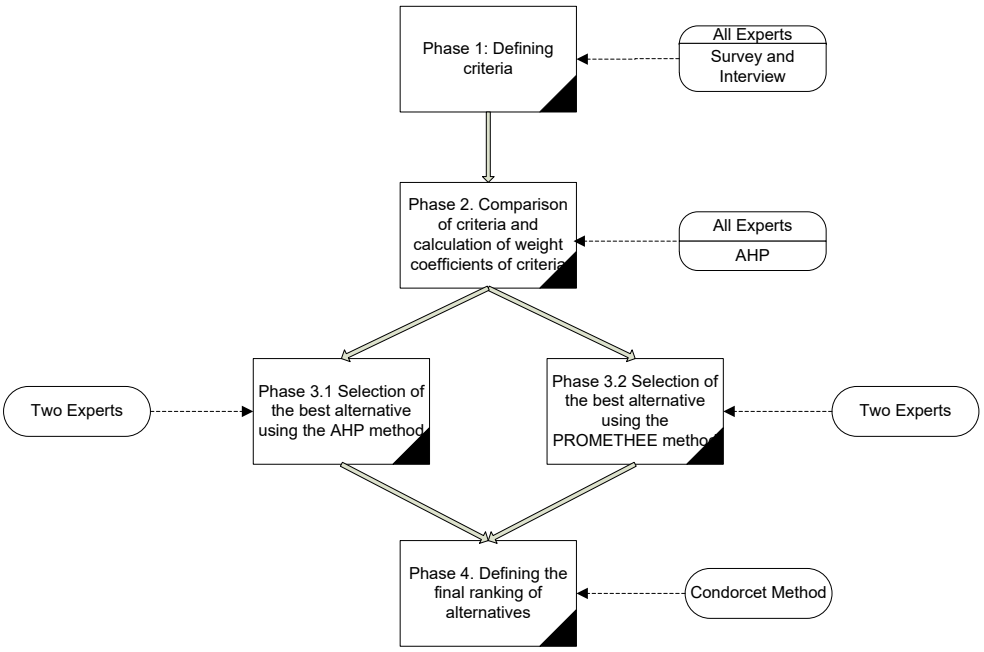

Figure 1 – Flowchart of the AHP - PROMETHEE - Condorcet model

Description of the Analytic Hierarchy Process (AHP) Method

The Analytical Hierarchical Process Method was developed by Saaty (1980) and it is based on a pairwise comparison of decision elements (criteria, sub-criteria, and alternatives). For pairwise comparisons, the values given in the scale of mutual importance in Table 1 are applied.

Table 1 – Saaty's scale of relative importance (Saaty, 2008)

Definition	**Intensity of Importance**
Equal importance	1
Moderate importance	3
Strong importance	5
Very strong importance	7
Extreme importance	9
Intermediate values	2, 4, 6, 8
Reciprocal values of the above numbers	1/2, 1/3, ... 1/9
If the activities are very close	1.1 – 1.9

The basic features of the AHP method are the ability to work with numerical and non-numerical data (Elraaid et al, 2024), the ability to determine the weights of the criteria, and the assessment of consistency, i.e., checking the quality of the given assessments.

The procedure for applying the AHP method includes several steps. The first step involves defining the problem that needs to be solved and presenting it through the structuring of the hierarchy of goals, criteria, sub-criteria, and possible alternatives (Saaty, 2008). This step is the most demanding for experts, but it is also the most creative (Kovačević et al, 2024; Biswas et al, 2025). In addition to the knowledge about the problem being investigated, experts must also be familiar with the way of applying the Saaty scale when making comparisons.

The second step of the method is the formation of a set of matrices for the mutual comparison of all criteria (sub-criteria) by pairs and defining their weights.

The next step is to calculate the consistency ratio (CR), the value of which must be less than 0.1 to be acceptable. The consistency ratio is calculated according to the formula:

$$CR = \frac{CI}{RI} \qquad (1)$$

where CI is the consistency index and RI is the randomness index (Random Index - RI).

The random index (RI) is determined empirically and depends on the number of criteria, i.e., on the dimensions of the assessment matrix - n (Table 2).

Table 2 – Random indices according to Saaty (Saaty, 1988)

n	**1**	**2**	**3**	**4**	**5**	**6**	**7**	**8**	**9**	**10**
RI	0	0	0.58	0.9	1.12	1.24	1.32	1.41	1.45	1.49

The consistency index is calculated according to the formula:

$$CI = \frac{\lambda_{max} - n}{n-1} \qquad (2)$$

λ_{max} is the eigenvalue calculated for each criterion by the formula:

$$\lambda_{max} = \frac{Aw * w}{w * w} \qquad (3)$$

where A is the criteria comparison matrix, and w is the eigenvector for the criteria, i.e., the degree of confidence in the criteria (weight of the criteria).

The comparison matrix A is multiplied by a vector by multiplying w (corresponding to a particular criterion) by the value of each cell in the same row, and the resulting products are summed. The procedure is repeated for all rows in the matrix. Finally, if the obtained CR consistency ratio is less than 0.1, the matrix is consistent, and the alternatives are compared according to each criterion. A ratio value greater than 0.1 indicates that the criteria comparison matrix is inconsistent and that it is necessary for the participants to correct their assessments in solving a specific problem or to structure the hierarchy of the problem in another way (or formulate questions differently when comparing elements).

Then the weighted sum is calculated, which is obtained by multiplying the matrix of alternatives with the eigenvector w. By comparing them, a conclusion is reached about the most favorable variant and it is possible to rank them. A higher value of the difficult sum for a certain alternative indicates that it is more favorable.

Description of the PROMETHEE II method

The PROMETHEE method is a prominent multi-criteria decision-making method that evaluates alternatives depending on the preferences of decision makers (Brans & Mareschal, 2005; Oubahman & Duleba, 2021). Many authors highlight the simplicity of its application as the main

advantage of this method compared to others, as well as the possibility of solving complex problems in conditions where the criteria are mutually opposed (Oubahman & Duleba, 2021; Taherdoost & Madanchian, 2023). The PROMETHEE I method was created in 1984 (Brans et al, 1984), while the PROMETHEE II method was first presented in the work of Brans & Vicke (1985), and since then it has been used in a large number of research related decision making cases. Also, later, new modifications of the PROMETHE method - PROMETHEE III, IV, V, as well as the GAIA graphic representation of the optimal solution were developed.

Here, a brief overview of the PROMETHEE II method will be given, bearing in mind that it provides a complete comparison and ranking of alternatives, unlike PROMETHEE I which allows only a partial comparison of alternatives. It can be used for single-criteria and multi-criteria decision analysis.

This method requires defining a preference function for the mutual comparison of alternatives, as well as the parameters of that function. The parameters of the preference function are the indifference parameter (m) which indicates up to which limit of the difference between two alternatives according to a certain criterion there is no preference, and the preference parameter (n) which indicates that above a certain difference in value between the two alternatives there are certain preferences (Suknović et al, 2021). Thus, the preference function identifies the existence and then describes the value of the difference between the two alternatives, which goes from 0 to 1 for each criterion.

Six general types of preference functions can be used to express a preference, namely: simple type; "U" type, "V" type, stepped type, linear type, and Gaussian type (Brans et al, 1986). Which of the mentioned functions will be used primarily depends on the characteristics of each of the criteria (Oubahman & Duleba, 2021). The linear type of preference is general and is most often applied in practice because it can cover the largest number of problems (Suknović et al, 2021). Table 3 describes the types of functions that will be applied in the paper.

The first step in the application of the PROMETHEE method is the calculation of preferences by pairs for all criteria, using the appropriate preference function and the type of extremization (minimization/maximization). Previously, by applying some of the methods, weights are determined for each criterion because PROMETHEE does not have a mechanism for determining weights.

The second step involves multiplying the received preferences of the pairs of alternatives with the corresponding weights of the criteria while in the third step the weighted sum of preferences is calculated.

Table 3 – Description of the PROMETHEE method function types (Brans et al, 1986; Brans & Mareschal, 2005)

Graph function	Definition	Parameters
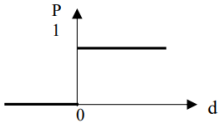	*I type (ordinary):* p(*d*) = 1, $d > 0$ (strict preference) p(*d*) = 0, $d \leq 0$ (indifference)	-
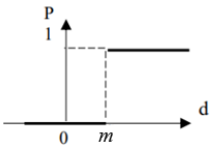	*II type („U“):* p(*d*) = 1, $d > m$ (strict preference) p(*d*) = 0, $d \leq 0$ (indifference)	*m*
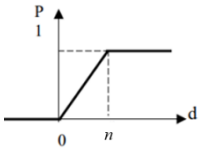	*III type („V“):* p(*d*) = 1, *d* ≥ *n* (strict preference) p(*d*) = *d*/*n*, 0 < *d* < *n* (weak preference) p(*d*) =0, *d* ≤ 0 (indindifference)	*n*
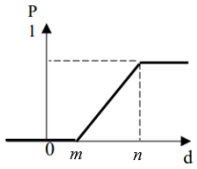	*V type (linear):* p(*d*) = 1, $d \geq n$ (strict preference) p(*d*) = (*d*-*m*)/(*n*-*m*), $m < d < n$ (weak preference) p(*d*) = 0, $d \leq m$ (indifference)	*m, n*

In the fourth step, the positive, negative, and net flow of alternatives are determined (Suknović et al, 2021). A positive flow indicates how preferred an alternative is on average compared to other alternatives, while a negative flow indicates how preferred other alternatives are compared to the observed one. A net flow (T) can be represented mathematically as the difference between the positive flow (T^+) and the negative flow (T^-): $T = T^+ - T^-$.

The overall ranking of alternatives is based on the highest net flow value.

Description of the Condorcet method

The Condorcet method is among the most prominent and oldest methods of group decision making. In practice, it was most often applied in the political election process, but also in other areas, such as product procurement. It is specific in that it requires mutual comparison of alternatives by pairs to determine how many times a certain alternative was ranked better than the others (Suknović et al, 2021). By applying that

simple rule, the Condorcet method ensures that the choice of a certain alternative is based on the opinion of the majority of people participating in the decision. It can be applied in its original form or in combination with the Borda method (Herrero & Villar, 2021) and other methods (Green-Armytage, 2011; Brandt et al, 2021).

The procedure for applying this method implies the formation of a matrix of the order of alternatives. Alternatives are compared in pairs and the number of times one alternative dominates over the other among all decision makers is entered in the appropriate cell of the matrix. Then the value of the vector W is calculated by adding all the dominances in one row of the matrix for the first alternative and then for the others. The most acceptable alternative is the one that has the highest value of the vector W.

However, the Condorcet method also has its limitations, i.e., it does not always allow to determine the best alternative. This situation in which alternatives are offered in the same rank is called the "Condorcet paradox" (Suknović et al, 2021). One of possible solutions implies that one of the decision makers reconsiders and changes the order of alternatives, but in that case the equality of decision-making participants is violated (Tomczak et al, 2019).

In this case, group decision making will be carried out based on the decisions of four military experts, which were made independently, without influencing each other.

Description of the alternatives and the criteria

The process of multi-criteria decision making using the presented model was carried out in the case of a preliminary selection of one of four alternatives according to three main criteria and several sub-criteria within them.

For alternatives, four models of multi-purpose armored wheel drive 4x4 models were selected: (A1) BOV M16 Miloš 2; (A2) Despot; (A3) Tatra 815-7 Patriot II and (A4) ATV Zetor Gerlach, between which the optimal solution was chosen. For that purpose, data on technical and operational characteristics, available on the official websites of their manufacturers (Table 4), were collected.

All the listed alternatives (Figure 2) have a similar purpose, ie., they are suitable for carrying out military and police tasks, such as reconnaissance, territory control, transportation and support of special units, command, fire support, medical evacuation, etc.

Table 4 – Basic technical and operational characteristics of the vehicles

Data type	Vehicle model - Alternatives			
	Miloš-2	*Despot*	*Patriot II*	*Zetor Gerlach*
Maximum engine power (kW)	252	240	300	240
Vehicle specific power (kW/t)	14	17.1	16.7	16.5
Maximum speed (km/h)	100	120	110	117
Maximum climb (%)	60	50	45	60
Maximum side slope (%)	30	30	32	57
Vertical obstacle (m)	0.5	0.5	0.5	0.5
Trench width (m)	0.8	0.8	0.9	1
Water obstacle depth (m)	0.9	1.1	1.2	1.2
Total mass (t)	18	14	18	14.5
Load capacity (t)	2.5	3	4.5	2.3
Number of crew members	2+8	2+8	2+6	2+4
Autonomy of movement (km)	600	700	700	600
Ballistic protection level (STANAG 4569)	3	2	2	3
Mine protection level (STANAG 4569)	2a/2б	2a/2б	2a/2б	3a/3б

Figure 2 – Alternatives: a. Miloš-2 (Yugoimport, 2024), b. Despot (TRB, 2024), c. Patriot II (Excaliburarmy, 2024), d. Zetor Gerlach (Zetorengineering, 2024)

Based on the relevant scientific and professional literature and the views of experts in the field of construction and use of wheeled armored combat vehicles, and by the available data on the vehicles, the following basic criteria were defined based on which the alternatives will be ranked:

Criterion 1 (K1): Mobility - represents the vehicle's ability to move and maneuver in different terrain conditions. In this paper, it will be considered through the following sub-criteria: vehicle specific power (K_{11}), autonomy of movement (K_{12}), and passability (K_{13}). The specific power of the vehicle is the ratio of engine power to the total mass of the armored combat vehicle and is expressed in kW/t. The value of this criterion directly indicates the performance of the vehicle such as acceleration, maximum speed, and agility, which is very important from the aspect of quick reaction in various combat situations (Muždeka, 2012). Autonomy of movement implies the maximum distance that the vehicle can move with one filling of the fuel tank and is important from the point of view of the so-called operational mobility, i.e., planning logistical needs in operations. The vehicle's passability implies the ability of an armored vehicle to overcome a space with different characteristics (slope of the terrain), as well as certain obstacles. Different parameters describe the vehicle's passability, and in this case, it will be considered through the ability to overcome the front and side slopes, vertical obstacles, trenches of a certain width, as well as water obstacles of a certain depth (without prior preparation).

Criterion 2 (K2): Protection - refers to the resistance of the armored vehicle to the effects of various types of weapons and the explosion of mines and the possibility of protecting people and key equipment and systems in the vehicle, and is expressed by a certain level of ballistic (K_{21}) and anti-mine protection (K_{22}), most often according to the NATO standard STANAG 4569. The level of protection for which the vehicle is certified indicates specifically the type and caliber of the projectile/amount of explosives that the vehicle's armor can withstand, as well as the type of weapon/tools, the distance, and the angle at which the projectile was fired.

Criterion 3 (K3): Transport of people and cargo (payload capacity) - represents the total number of people - members of military or police units with complete combat equipment, for which adequate space is provided in the front and rear part of the vehicle, as well as the mass of useful cargo that can be loaded or additionally equip the vehicle with certain systems.

Ranking results

The first decision maker (DM1) will rank the combat vehicles using the AHP method based on the hierarchy of criteria presented in Table 5.

Table 5 – Criteria and sub-criteria

Goal	Criteria		Sub-criteria			
The selection of a multipurpose armored combat vehicle 4x4	K_1	Mobility	K_{11}	Specific power		
			K_{12}	Cruising range		
			K_{13}	Obstacle crossing capabilities	K_{131}	Overcoming front gradient
					K_{132}	Side slope overcoming
					K_{133}	Overcoming vertical obstacle/Trench/Fording capability
	K_2	Protection	K_{21}	Ballistic protection		
			K_{22}	Antimine protection		
	K_3	Payload capacity	K_{31}	Number of crew members		
			K_{32}	Mass of additional cargo		

By applying Saaty's scale (Table 1), DM1 performed a comparison of the criteria/sub-criteria by branches of the hierarchy, whereby a total of 5 matrices were formed (Tables 6-10, under a), and then the matrices were normalized and the value of the vector w was determined (Tables 6 -10, under b).

Table 6 – Ranking of the main criteria in relation to the set goal

a)	K_1	K_2	K_3
K_1	1	1.2	1.4
K_2	0.83	1	1.1
K_3	0.71	0.91	1
Σ	2.55	3.11	3.50

б)	K_1	K_2	K_3	**w**	CR
K_1	0.393	0.386	0.400	**0.393**	0
K_2	0.327	0.322	0.314	**0.321**	
K_3	0.280	0.292	0.286	**0.286**	
Σ				1	

Table 7 – Ranking of the sub-criteria concerning vehicle mobility

a)	K_{11}	K_{12}	K_{13}
K_{11}	1	3	1
K_{12}	0.33	1	0.33
K_{13}	1	3	1
Σ	2.33	7	2.33

б)	K_{11}	K_{12}	K_{13}	**w**	CR
K_{11}	0.429	0.429	0.429	**0.429**	0
K_{12}	0.143	0.143	0.143	**0.143**	
K_{13}	0.429	0.429	0.429	**0.429**	
Σ				1	

Table 8 – Ranking of the sub-criteria concerning vehicle passability

a)	K_{131}	K_{132}	K_{133}
K_{131}	1	1	1.5
K_{132}	1	1	1.5
K_{133}	0.67	0.67	1
Σ	2.67	2.67	4

б)	K_{131}	K_{132}	K_{133}	**w**	CR
K_{131}	0.375	0.375	0.375	**0.375**	0
K_{132}	0.375	0.375	0.375	**0.375**	
K_{133}	0.250	0.250	0.250	**0.250**	
Σ				1	

Table 9 – Ranking of the sub-criteria concerning the level of vehicle protection

a)	K_{21}	K_{22}
K_{21}	1	1.4
K_{22}	0.71	1
Σ	1.71	2.40

б)	K_{21}	K_{22}	w	CR
K_{21}	0.583	0.583	**0.583**	0
K_{22}	0.417	0.417	**0.417**	
Σ			1	

Table 10 – Ranking of the sub-criteria concerning the payload capacities

a)	K_{31}	K_{32}
K_{31}	1	2
K_{32}	0.5	1
Σ	1.5	3

б)	K_{31}	K_{32}	**w**	CR
K_{31}	0.667	0.667	**0.667**	0
K_{32}	0.333	0.333	**0.333**	
Σ			1	

The matrix consistency check (Tables 6, 7, 8, 9, and 10) was performed using formulas (1), (2), and (3) and it was found that all values of the CR consistency index are less than 0.1, i.e., the matrices are consistent.

In this way, the relative weight values of the criteria and sub-criteria were obtained, based on which the absolute weight values are calculated by multiplying the relative weight of each sub-criterion with the weight value of all super-criteria in the displayed hierarchy. The absolute values of the weights for the subcriteria of the leaves of the tree hierarchy are shown in Figure 3 (bold numbers in shaded boxes).

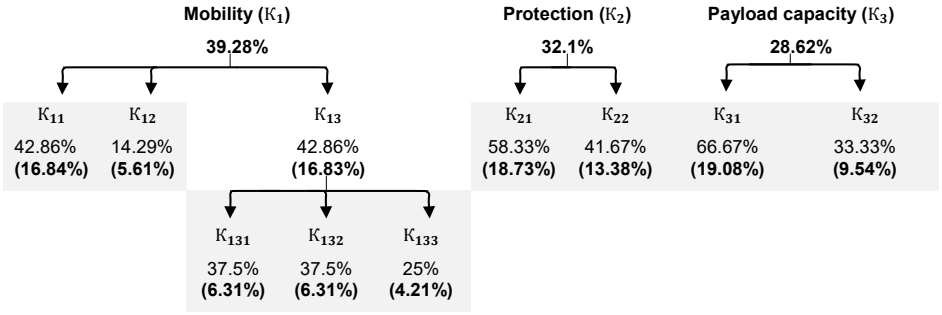

Figure 3 – Relative and absolute weights (in bold) of the criteria and sub-criteria

The results of the comparison of the alternatives according to each criterion of the hierarchy tree leaf (the criteria and sub-criteria which are the last in the hierarchy tree) are shown in Tables 11-19.

Table 11 – Comparison of the alternatives according to the specific power

K_1	A1	A2	A3	A4	Average
A1	1	0.20	0.25	0.25	0.071
A2	5	1	1.5	1.6	0.393
A3	4	0.67	1	1.20	0.282
A4	4	0.63	0.83	1	0.254
Σ	14	2.49	3.58	4.05	1

Table 12 – Comparison of the alternatives according to the autonomy of movement

K_2	A1	A2	A3	A4	Average
A1	1	0.2	0.2	1	0.083
A2	5	1	1	5	0.417
A3	5	1	1	5	0.417
A4	1	0.2	0.2	1	0.083
Σ	12	2.40	2.40	12	**1**

Table 13 – Comparison of the alternatives according to overcoming the climb

K_{131}	A1	A2	A3	A4	Average
A1	1	5	7	1	0.421
A2	0.2	1	3	0.2	0.106
A3	0.14	0.33	1	0.14	0.052
A4	1	5	7	1	0.421
Σ	2.34	11.33	18	2.34	1

Table 14 – Comparison of the alternatives according to overcoming the side slope

K_{132}	A1	A2	A3	A4	Average
A1	1	1	0.83	0.13	0.087
A2	1	1	0.83	0.13	0.087
A3	1.2	1.2	1	0.13	0.100
A4	8	8	8	1	0.726
Σ	11.2	11.2	10.67	1.38	1

Table 15 – Comparison of the alternatives according to the obstacles overcoming

K_{133}	A1	A2	A3	A4	Average
A1	1	0.50	0.25	0.20	0.082
A2	2	1	0.50	0.33	0.156
A3	4	2	1	0.67	0.313
A4	5	3	1.50	1	0.449
Σ	12	6.50	3.25	2.20	1

Table 16 – Comparison of the alternatives according to the ballistic protection level

K_{21}	A1	A2	A3	A4	Average
A1	1	7	7	1	0.437
A2	0.14	1	1	0.14	0.062
A3	0.14	1	1	0.14	0.062
A4	1	7	7	1	0.438
Σ	2.29	16	16	2.29	1

Table 17 – Comparison of the alternatives according to the mine protection level

K_{22}	A1	A2	A3	A4	Average
A1	1	1	1	0.14	0.100
A2	1	1	1	0.14	0.100
A3	1	1	1	0.14	0.100
A4	7	7	7	1	0.700
Σ	10	10	10	1.43	1

Table 18 – Comparison of alternatives according to the number of crew members

K_{31}	A1	A2	A3	A4	Average
A1	1	1	5	7	0.413
A2	1	1	5	7	0.413
A3	0.20	0.20	1	5	0.128
A4	0.14	0.14	0.2	1	0.047
Σ	2.34	2.34	11.2	20	1

Table 19 – Comparison of the alternatives according to the mass of additional cargo

K_{32}	A1	A2	A3	A4	Average
A1	1	0.50	0.14	1.20	0.090
A2	2	1	0.20	3	0.178
A3	7	5	1	7	0.656
A4	0.83	0.33	0.14	1	0.076
Σ	10.83	6.83	1.49	12.2	1

Finally, by inserting the mean values from the normalized matrices for all alternatives according to each criterion of the hierarchy list (from Tables 11-19 under b) into the new matrix (Table 20) and multiplying with the absolute weights, the weighted sum value and the final ranking of the alternatives are obtained (Table 21).

Table 20 – Normalized decision-making table

	K_{11}	K_{12}	K_{131}	K_{132}	K_{133}	K_{21}	K_{22}	K_{31}	K_{32}
A1	0.071	0.083	0.421	0.087	0.082	0.437	0.100	0.413	0.090
A2	0.393	0.417	0.106	0.087	0.156	0.062	0.100	0.413	0.178
A3	0.282	0.417	0.052	0.100	0.313	0.062	0.100	0.128	0.656
A4	0.254	0.083	0.421	0.726	0.449	0.438	0.700	0.047	0.076
w	**0.168**	**0.056**	**0.063**	**0.063**	**0.042**	**0.187**	**0.134**	**0.191**	**0.095**

Table 21 – Ranking of the alternatives

Alternatives	Weighted sum	**Rank**
A1	0.2347	**2**
A2	0.2291	**3**
A3	0.2056	**4**
A4	0.3306	**1**

Based on the analysis performed by DM1, the following ranking of the alternatives was obtained: A4, A1, A2, and A3. The most favorable alternative is A4, and the least favorable is A3, with alternatives A1 and A2 having similar values of the weighted sum.

The second decision maker (DM2) applies the AHP method, in the same way as DM1, whereby the value of the absolute weights of the main criteria is obtained as follows: mobility 35.29%, protection 35.29%, and carrying capacity 29.41%. Table 22 shows the normalized decision matrix, and Table 23 shows the ranking of the alternatives.

Table 22 – Normalized decision-making table

	K_{11}	K_{12}	K_{131}	K_{132}	K_{133}	K_{21}	K_{22}	K_{31}	K_{32}
A1	0.071	0.083	0.421	0.087	0.082	0.437	0.100	0.413	0.090
A2	0.393	0.417	0.106	0.087	0.156	0.062	0.100	0.413	0.178
A3	0.282	0.417	0.052	0.100	0.313	0.062	0.100	0.128	0.656
A4	0.254	0.083	0.421	0.726	0.449	0.438	0.700	0.047	0.076
w	**0.137**	**0.060**	**0.055**	**0.055**	**0.046**	**0.206**	**0.147**	**0.166**	**0.128**

Table 23 – Ranking of the alternatives

Alternatives	Weighted sum	**Rank**
A1	0.2313	**2**
A2	0.2155	**4**
A3	0.2190	**3**
A4	0.3343	**1**

The decision maker (DM2) received the following ranking of the alternatives: A4, A1, A3, and A2, where it is evident that in this case the alternatives A1, A2 and A3 have close values of the difficult sum.

The third decision-maker (DM3) applies the AHP method to determine the weights of the criteria and in that procedure the following values of the absolute weights of the main criteria were obtained: mobility 36.45%, protection 33.24%, and carrying capacity 30.31%. It then applies the PROMETHEE II method in the final ranking of the alternatives. The decision maker fills in Table 24, based on the available data on the vehicles, in which he evaluates the value of the subcriterion K_{133} based on the width of the trench and the depth of the water obstacle that the vehicle can overcome, and the value of the anti-mine protection level is expressed by a unique number, bearing in mind that the values a and b do not differ (the level of explosion protection under the center of the armored body and under the wheels of the combat vehicle is the same).

Table 24 – Data for vehicle selection

	K_{11}	K_{12}	K_{131}	K_{132}	K_{133}	K_{21}	K_{22}	K_{31}	K_{32}
A1	14	600	60	30	0.8/0.9	3	2а/2б	10	2.5
A2	17.1	700	50	30	0.8/1.1	2	2а/2б	10	3
A3	16.7	700	45	32	0.9/1.2	2	2а/2б	8	4.5
A4	16.5	600	60	57	1/1.2	3	3а/3б	6	2.3

Then, for each criterion, the appropriate type of the preference function (chosen from Table 3), the parameters of preference and indifference, and the type of extremization were determined (Table 25). The type of extremization is the same for all criteria because a higher value is preferred.

After calculating the difference in the value of the criteria for all mutual pairwise comparisons (Table 26), the preferences of the pairs of the alternatives were obtained by applying the defined functions (Table 27).

Table 25 – Weights and the parameters of the preference functions

	K_{11}	K_{12}	K_{131}	K_{132}	K_{133}	K_{21}	K_{22}	K_{31}	K_{32}
w	0.158	0.063	0.051	0.051	0.042	0.205	0.128	0.227	0.076
Tip f-je	lin.	lin.	lin.	lin.	lin.	lin.	lin.	simpl.	lin.
m	0.25	25	4	3	0.1	0.5	0.5	0	0.3
n	0.75	70	8	6	0.2	1	1	0	0.8
min/max					max				

Table 26 – Differences in the value of criteria by all pairs of the alternatives

	K_{11}	K_{12}	K_{131}	K_{132}	K_{133}	K_{21}	K_{22}	K_{31}	K_{32}
A1A2	-3.1	-100	10	0	-0.1	1	0	0	-0.5
A1A3	-2.7	-100	15	-2	-0.2	1	0	2	-2
A1A4	-2.5	0	0	-27	-0.25	0	-1	4	0.2
A2A1	3.1	100	-10	0	0.1	-1	0	0	0.5
A2A3	0.4	0	5	-2	-0.1	0	0	2	-1.5
A2A4	0.6	100	-10	-27	-0.15	-1	-1	4	0.7
A3A1	2.7	100	-15	2	0.2	-1	0	-2	2
A3A2	-0.4	0	-5	2	0.1	0	0	-2	1.5
A3A4	0.2	100	-15	-25	-0.05	-1	-1	2	2.2
A4A1	2.5	0	0	27	0.25	0	1	-4	-0.2
A4A2	-0.6	-100	10	27	0.15	1	1	-4	-0.7
A4A3	-0.2	-100	15	25	0.05	1	1	-2	-2.2

Table 27 – Preferences of the pairs of the alternatives according to all criteria

	K_{11}	K_{12}	K_{131}	K_{132}	K_{133}	K_{21}	K_{22}	K_{31}	K_{32}
A1A2	0	0	1	0	0	1	0	0	0
A1A3	0	0	1	0	0	1	0	1	0
A1A4	0	0	0	0	0	0	0	1	0
A2A1	1	1	0	0	0	0	0	0	1
A2A3	0.3	0	0	0	0	0	0	1	0
A2A4	0.7	1	0	0	0	0	0	1	1
A3A1	1	1	0	0	1	0	0	0	1
A3A2	0	0	0	0	0	0	0	0	1
A3A4	0	1	0	0	0	0	0	1	1
A4A1	1	0	0	1	1	0	1	0	0
A4A2	0	0	1	1	0.5	1	1	0	0
A4A3	0	0	1	1	0	1	1	0	0

By multiplying the preferences in Table 27 with the weights of the criteria w, the so-called "weighted preferences" were obtained for each pair of comparisons (A1A2, A1A3...), which are then entered into a weighted preference matrix to calculate positive, negative and net flows (Table 28).

Table 28 – Matrix of the weighted preferences of the alternatives with the positive and negative flow values

	A1	A2	A3	A4	T^+	T	Rank
A1	*	0.2555	0.4828	0.2273	0.322	-0.016	**3**
A2	0.2959	*	0.2746	0.4759	0.349	0.087	**1**
A3	0.3384	0.0758	*	0.3656	0.260	-0.137	**4**
A4	0.3789	0.4555	0.4343	*	0.423	0.067	**2**
T^-	0.3380	0.2620	0.3970	0.3560		0.001	

Based on the value of the net flow, DM3 established the following order of alternatives: A2, A4, A1, and A3, where it is noticeable that the difference between the value of the net flows of the first-ranked alternative A2 and the second-ranked alternative A4 is insignificant. Therefore, the alternatives A2 and A4 are almost equally good in this case.

The fourth decision maker (DM4) applies the same model as the previous one. When evaluating the criteria using the AHP method, the following weight values of the main criteria were obtained: mobility - 36.29%, protection 27.85%, and transport of people and cargo - 35.86%, which indicates that DM4 favors the mobility and transport capabilities of vehicles, in relation to protection. By applying the PROMETHEE II method, DM4 performs the final ranking of alternatives. Due to the limitations of this work and the procedure already described, the tables with the values of the criteria weights, the parameters and the types of the preference function are presented as well as the matrix of the weighted preferences with the flow values (Tables 29 and 30).

Table 29 – Weights and the parameters of the preference functions

	K_{11}	K_{12}	K_{131}	K_{132}	K_{133}	K_{21}	K_{22}	K_{31}	K_{32}
w	0.141	0.062	0.061	0.047	0.053	0.162	0.116	0.239	0.120
function	lin.	lin.	lin.	lin.	lin.	„U“	„U“	„U“	lin.
m	1	40	6	4	0.1	0.5	0.5	1	0.2
n	2	80	12	8	0.2	0	0	0	0.7
min/max					max				

Table 30 – Matrix of the weighted preferences of the alternatives with the positive and negative flow values

	A1	A2	A3	A4	T^+	T	**Rank**
A1	*	0.2031	0.4624	0.2390	0.302	-0.033	**3**
A2	0.2739	*	0.2390	0.4202	0.311	0.073	**1**
A3	0.3750	0.1195	*	0.4202	0.305	-0.057	**4**
A4	0.3564	0.3923	0.3860	*	0.378	0.018	**2**
T^-	0.3350	0.2380	0.3620	0.3600		0.001	

Based on the analysis performed by DM4, the same ranking of the alternatives was obtained as in the previous case.

Application of the Condorcet method

The ranking results obtained by individual decision-making methods by four decision makers are entered in Table 31 in order to determine the optimal solution using the Condorcet method under the conditions of group decision making.

Table 31 – Result of the group decision making

Ranking of alternatives by each decision maker					Matrix					Vektor w
Rank	DM1	DM2	DM3	DM4	Alternatives	A1	A2	A3	A4	Σ
1	A4	A4	A2	A2	A1	*	2	4	0	**6**
2	A1	A1	A4	A4	A2	2	*	3	2	**7**
3	A2	A3	A1	A1	A3	0	1	*	0	**1**
4	A3	A2	A3	A3	A4	4	2	4	*	**10**

In the table, a matrix was formed for the purpose of mutual comparison of the alternatives by pairs and determining how much one alternative dominated in all individual rankings in relation to the other. Then the value of the vector W is calculated by adding the values of all dominances in one row of the matrix, for the alternative A1, and then for the others.

By applying the Condorcet method, it was found that the most acceptable alternative is A4 (the highest value of the vector W=10), and the most unfavorable is A3 (the lowest value of the vector W=1). The alternatives A1 and A2 are of similar value.

Conclusion

The application of multi-criteria decision-making methods is indispensable when deciding between a number of alternatives and when the entire spectrum of characteristics of a complex combat system is taken into account. This is especially pronounced when striving to achieve a balance between the criteria that belong to the so-called "iron triangle" of the multipurpose combat armored vehicle. The paper presents a model of the application of the AHP and PROMETHEE II methods on the specific case of ranking four alternatives according to nine criteria/sub-criteria, in two cases using the AHP method and in two cases using the AHP-PROMETHEE II model. Group decision making aimed at the final selection of the most favorable alternative was carried out using the Condorcet method.

In the results of the evaluation of the criteria by military experts, uniformity is evident in determining the weights of the main criteria, whereby in three cases priority was given to vehicle performance, i.e., vehicle mobility, and in one case the mobility and protection criteria were equal. In the first two cases, in which priority was clearly expressed on the criteria of mobility and force protection, the first ranked alternative was A4, i.e., the Zetor Gerlach vehicle. In the third case, in which the value of the transport capacity criterion was slightly lower compared to the mobility criterion, and in the fourth case, in which the highest degree of uniformity of all three criteria was present, a different result was obtained, the first-ranked alternative was A2, i.e., the Despot vehicle. Finally, by applying the Condorcet method, it was found that the most favorable alternative is A4.

The obtained results indicate that the final ranking of the alternatives depends significantly on the experts' clear vision of the solution to the problem, expressed primarily through the evaluation of criteria using the AHP method. Bearing in mind that the subsequent comparison depends a lot on specific, clearly measurable differences in characteristics from alternative to alternative. This certainly supports the claim that for the purposes of use in modern combat operations, high-performance vehicles are needed in terms of agility, the ability to maneuver in a limited space and passability. The subject methods can be effectively applied for the ranking of armored vehicles by defining different scenarios that can be presented through an adequate ratio of the values of the key criteria.

The defined criteria can serve as one of the models for the preliminary ranking of vehicles of this type because they require data that is generally available. Normally, the value aspect has an important influence on the final decision and therefore there must be an adequate balance between

capabilities, procurement price, and costs throughout the vehicle's entire lifecycle.

Proper hierarchical structuring of problems on multiple levels ensures simpler evaluation of elements and helps experts to achieve consistency, i.e., to be consistent in grading. In order to express small differences between the elements of the comparison, the experts used very small values of relative importance from the Saaty scale.

Multi-criteria individual and group decision-making methods are an effective tool that can contribute to making objective decisions when choosing a specific combat system; therefore, it is necessary to know the possibilities of each of the methods in order to fully exploit their possibilities.

Further research steps should be focused on incorporating the consideration of value aspects and the application of Fuzzy logic into the selection of wheeled armored vehicles in the conditions of uncertainties and various scenarios.

References

Brandt, F., Hofbauer, J. & Strobel, M. 2021. Exploring the No-Show Paradox for Condorcet Extensions. In: Diss, M. & Merlin, V. (Eds.) *Evaluating Voting Systems with Probability Models. Studies in Choice and Welfare*, pp.251-273. Cham: Springer. Available at: https://doi.org/10.1007/978-3-030-48598-6_11.

Brans, J.P. & Mareschal, B. 2005. Promethee Methods. In: *Multiple Criteria Decision Analysis: State of the Art Surveys. International Series in Operations Research & Management Science*, 78. New York, NY: Springer. Available at: https://doi.org/10.1007/0-387-23081-5_5.

Brans, J.P., Mareschal, B. & Vincke, P. 1984. PROMETHEE: A new family of outranking methods in MCDM. *Operational Research*, 84, pp.477-490.

Brans J.P. & Vincke, Ph. 1985. Note—A Preference Ranking Organisation Method (The PROMETHEE Method for Multiple Criteria Decision-Making). *Management Science*, 31(6), pp.647-656. Available at: https://doi.org/10.1287/mnsc.31.6.647.

Brans, J.P., Vincke, Ph. & Mareschal, B. 1986. How to select and how to rank projects: The Promethee method. *European Journal of Operational Research*, 24(2), pp.228-238. Available at: https://doi.org/10.1016/0377-2217(86)90044-5.

Biswas, A., Gazi, K.H., Sankar, P.M. & Ghosh, A. 2025. A Decision-Making Framework for Sustainable Highway Restaurant Site Selection: AHP-TOPSIS Approach based on the Fuzzy Numbers. *Spectrum of Operational Research*, 2(1), pp.1-26. Available at: https://doi.org/10.31181/sor2120256.

Dean, S.E. 2024. 4×4 armoured fighting vehicles: recent developments. *European Security & Defence*, 6/2024(June), pp.24-31 [online]. Available at:

https://euro-sd.com/wp-content/uploads/2024/06/ESD_6_2024-1.pdf [Accessed: 13 July 2024].

Dean, S.E. & Cazalet, M. 2024. Add-on armour systems. *European Security & Defence*, 1/2024(January), pp.42-45 [online]. Available at: https://euro-sd.com/wp-content/uploads/2024/01/ESD_1_2024.pdf [Accessed: 13 July 2024].

Elraaid, U., Badi, I. & Bouraima, M.B. 2024. Identifying and Addressing Obstacles to Project Management Office Success in Construction Projects: An AHP Approach. *Spectrum of Decision Making and Applications*, 1(1), pp.33-45. Available at: https://doi.org/10.31181/sdmap1120242.

-Excaliburarmy. 2024. *Armoured personnel carriers and infantry fighting vehicles* [online]. Available at: https://www.excaliburarmy.cz/download/product/7/ea-apc-ifv-program.pdf [Accessed: 13 July 2024].

Furch, J. & Švásta, A. 2022. Use of Multicriteria Analysis in Unmanned Ground Vehicle Selection. *Challenges to national defence in contemporary geopolitical situation*, 2022(1), pp.17-25. Available at: https://doi.org/10.47459/cndcgs.2022.2.

Gazibey, Y., Kantemir, O. & Demirel, A. 2015. Interaction among the Criteria Affecting Main Battle Tank Selection: An Analysis with DEMATEL Method. *Defence Science Journal*, 65(5), pp.345-355. Available at: https://doi.org/10.14429/dsj.65.8924.

Genc, T. 2015. Application of ELECTRE III and PROMETHEE II in evaluating the military tanks. *International Journal of Procurement Management (IJPM)*, 8(4), pp.457-475. Available at: https://doi.org/10.1504/IJPM.2015.070743.

Giurgiu, T., Virca, I., Grigoraș, C. & Năstăsescu, V. 2023. Trends in Development of Military Vehicles Capabilities Based on Advanced Technologies. In: *International conference KNOWLEDGE-BASED ORGANIZATION*, 29(3), pp.15-22. Available at: https://doi.org/10.2478/kbo-2023-0070.

Green-Armytage, J. 2011. Four Condorcet-Hare Hybrid Methods for Single-Winner Elections. *Voting Matters*, 29, pp.1-14 [online]. Available at: https://www.votingmatters.org.uk/ISSUE29/ISSUE29.pdf [Accessed: 09 October 2024].

Herrero, C. & Villar, A. 2021. Group decisions from individual rankings: The Borda-Condorcet rule. *European Journal of Operational Research*, 291(2), pp.757-765. Available at: https://doi.org/10.1016/j.ejor.2020.09.043.

Jokic, Z., Delibasic, B. & Randjelovic, A. 2024. Selection of Rifle Caliber in Rearming Process of the Serbian Army. *Management: Journal of Sustainable Business and Management Solutions in Emerging Economies*, 29(1), pp.41-52. Available at: https://doi.org/10.7595/management.fon.2021.0011.

Kamel, H. 2017. Studying the Trade-Off Between Protection and Mobility of Armored Vehicles. In: *Proceedings of the ASME 2017 International Mechanical Engineering Congress and Exposition*, Tampa, FL, USA, Volume 12: Transportation Systems, Paper No: IMECE2017-72531, V012T16A008, November 3–9. Available at: https://doi.org/10.1115/IMECE2017-72531.

Kizielewicz, B. & Sałabun, W. 2024. SITW Method: A New Approach to Re-identifying Multi-criteria Weights in Complex Decision Analysis. *Spectrum of Mechanical Engineering and Operational Research*, 1(1), pp.215-226. Available at: https://doi.org/10.31181/smeor11202419.

Kovačević, I., Pantelić, O. & Anđelković-Labrović, J. 2024. Predictors of employees' voluntary turnover intentions: Analytic hierarchy process approach. *Yugoslav Journal Of Operations Research*, 34(3), pp.587-602. Available at: https://doi.org/10.2298/YJOR231215002K.

Kurtay, K.G. 2024. Selection of Military Armored Vehicle Using Fuzzy EDAS method. *Computer and Decision Making: An International Journal*, 1, pp.134-150. Available at: https://doi.org/10.59543/comdem.v1i.10413.

Muždeka, S. 2012. *Osnovi borbenih vozila*. Belgrade, Serbia: Medija centar „Odbrana" (in Serbian). ISBN: 978-86-335-0369-3.

Oubahman, L. & Duleba, S. 2021. Review of PROMETHEE method in transportation. *Production Engineering Archives*, 27(1), pp.69-74. Available at: https://doi.org/10.30657/pea.2021.27.9.

Pamučar, D.S. & Dimitrijević, S.R. 2021. Multiple-criteria model for optimal Anti Tank Ground missile weapon system procurement. *Vojnotehnički glasnik/Military Technical Courier*, 69(4), pp.792-827. Available at: https://doi.org/10.5937/vojtehg69-32117.

Puška, A., Beganović, A. & Šadić, S. 2018. Model for investment decision making by applying the multi-criteria analysis method. *Serbian Journal of Management*, 13(1), pp.7-28. Available at: https://doi.org/10.5937/sjm13-12436.

Radetić, M. 2001. Pravci daljeg razvoja borbenih vozila pešadije. *Vojnotehnički glasnik/Military Technical Courier*, 49(1), pp.83-100 (in Serbian). Available at: https://doi.org/10.5937/vojtehg0101083R.

Radovanović, M., Božanić, D., Tešić, D., Puška, A., Hezam, I.M. & Jana, C. 2023. Application of hybrid DIBR-FUCOM-LMAW-Bonferroni-Grey-EDAS model in multicriteria decision-making. *Facta Universitatis, Series: Mechanical Engineering,* 21(3), pp.387-403. Available at: https://doi.org/10.22190/FUME230824036R.

Radovanović, M., Petrovski, A., Cirkin, E., Behlić, A., Jokić, Ž., Chemezov, D., Hashimov, E.G., Bouraima, M.B. & Jana, C. 2024. Application of the new hybrid model LMAW-G-EDAS multi-criteria decision-making when choosing an assault rifle for the needs of the army. *Journal of Decision Analytics and Intelligent Computing*, 4(1), pp.16-31. Available at: https://doi.org/10.31181/jdaic10021012024r.

Radovanović, M., Ranđelović, A. & Milić, A. 2019. Komparativna analiza protivoklopnih sistema korišćenjem AHP metode. *Vojno delo*, 71(7), pp.234-250 (in Serbian). Available at: https://doi.org/10.5937/vojdelo1907234R.

Saaty, T.L. 1980. *The Analytic Hierarchy Process: Planning, Priority Setting, Resource Allocation*. New York, NY: McGraw Hill. ISBN: 0070543712.

Saaty, T.L. 1988. What is the Analytic Hierarchy Process? In: Mitra, G., Greenberg, H.J., Lootsma, F.A., Rijkaert, M.J. & Zimmermann, H.J. (Eds.) *Mathematical Models for Decision Support. NATO ASI Series*, 48, pp.109-121.

Berlin, Heidelberg: Springer. Available at: https://doi.org/10.1007/978-3-642-83555-1_5.

Saaty, T.L. 2008. Decision making with the analytic hierarchy process. *International Journal of Services Sciences (IJSSCI)*, 1(1), pp.83-98. Available at: https://doi.org/10.1504/IJSSCI.2008.017590.

Santos, M. dos, Costa, I.P. de A., & Gomes, C.F.S. 2021. Multicriteria Decision-Making In the Selection of Warships: A New Approach To the AHP Method. *International Journal of the Analytic Hierarchy Process*, 13(1), pp.147-169. Available at: https://doi.org/10.13033/ijahp.v13i1.833.

Starčević, S., Bojović, N., Junevičius, R. & Skrickij, V. 2019. Analytical hierarchy process method and data envelopment analysis application in terrain vehicle selection. *Transport*, 34(5), pp.600-616. Available at: https://doi.org/10.3846/transport.2019.11710.

Suknović, M., Delibašić, B., Jovanović, M., Vukićević, M. & Radovanović, S. 2021. *Odlučivanje, sedmo prerađeno i dopunjeno izdanje*. Belgrade: University of Belgrade, Faculty of Organizational Sciences [online]. Available at: https://id.fon.bg.ac.rs/uploads/documents/empire_plugin/A0032%20Odlucivanje.pdf (in Serbian). ISBN: 978-86-7680-370-5 [Accessed: 09 October 2024].

Sun, Y., Tao, G., Xiong, G. & Chen, H. 2013. The Fuzzy-AHP Evaluation Method for Unmanned Ground Vehicles. *Applied Mathematics & Information Sciences*, 7(2), pp.653-658. Available at: https://doi.org/10.12785/amis/070232.

Taherdoost, H. & Madanchian, M. 2023. Using PROMETHEE Method for Multi-Criteria Decision Making: Applications and Procedures. *Iris Journal of Economics & Business Management - IJEBM*, 1(1), pp.1-7. Available at: https://doi.org/10.33552/IJEBM.2023.01.000502.

Tešić, D. & Marinković, D. 2023. Application of fermatean fuzzy weight operators and MCDM model DIBR-DIBR II-NWBM-BM for efficiency-based selection of a complex combat system. *Journal of Decision Analytics and Intelligent Computing*, 3(1), pp.243-256. Available at: https://doi.org/10.31181/10002122023t.

Tomczak, M., Biruk, S. & Jaskowski, P. 2019. Selection of Construction Products Suppliers According to the Condorcet Criterion. *IOP Conference Series: Materials Science and Engineering*, 471(11), art.number:112068. Available at: https://doi.org/10.1088/1757-899X/471/11/112068.

-TRB. 2024. *Despot 4x4 armoured multi-purpose vehicle* [online]. Available at: https://trb.ba/wp-content/uploads/2021/11/Despot_presentation.pdf [Accessed: 13 July 2024].

-UN Department of Operational Support. 2023. *COE Working Group - Secretariat Issue Paper: Classification of Armored Personnel Carriers Based on Capability Instead of Value* [online]. Available at: https://operationalsupport.un.org/sites/default/files/secretariat_issue_paper_1_-_mandated_study_-_classification_of_armored_personnel_carriers_based_on_capability_instead_of_value.pdf [Accessed: 11 August 2024].

-Yugoimport. 2024. *Miloš 2 višenamensko oklopno borbeno vozilo 4x4* [online]. Available at: https://www.yugoimport.com/sites/default/files/documents/2024-01/Milo%C5%A1%202%20srp..pdf (in Serbian) [Accessed: 12 July 2024].

-Zetorengineering. 2024. *ATV Zetor Gerlach 4x4* [online]. Available at: https://www.zetorengineering.sk/wp-content/uploads/2021/05/ATM-novy-vynatok-final-verzia-ANG.pdf [Accessed: 12 July 2024].

Aplicación de los métodos de decisión individual AHP y PROMETHEE II y del método de decisión grupal Condorcet en la selección de un vehículo blindado de combate polivalente sobre ruedas

Miša D. Živković[a], **autor de correspondencia**, *Darko* I. Božanić[a], *Milija* M. Suknović[b], *Boris* V. Delibašić[b]

[a] Universidad de Defensa de Belgrado, Academia Militar, Departamento de Tácticas con Sistemas de Armas, Belgrado, República de Serbia

[b] Universidad de Belgrado, Facultad de Ciencias Organizacionales, Departamento de Organización de Sistemas Empresariales, Belgrado, República de Serbia

CAMPO: ciencia de la decisión, ciencias militares
TIPO DE ARTÍCULO: artículo científico original

Resumen:

Introducción/objetivo: Los vehículos blindados de combate sobre ruedas son sistemas de combate cada vez más presentes en los conflictos armados modernos, especialmente en operaciones contra amenazas asimétricas. El mercado mundial de vehículos blindados sobre ruedas está en constante crecimiento, lo que refleja su aplicación en una amplia gama de misiones y tareas de las fuerzas armadas. La existencia de numerosos modelos de estos vehículos con diferentes características técnicas y de rendimiento, junto con la posibilidad de adaptación a necesidades específicas, complica aún más la elección de la alternativa más adecuada. El artículo presenta el caso de solución del problema de selección del vehículo blindado sobre ruedas de clase media polivalente más adecuado con una fórmula de tracción 4x4 al elegir una de las cuatro alternativas, utilizando métodos de toma de decisiones multicriterio individuales y grupales.

Métodos: En el presente trabajo se han aplicado los métodos de toma de decisiones multicriterio para resolver problemas en el ámbito de la selección de sistemas de combate complejos. Expertos en el campo táctico con sistemas de armas han clasificado las alternativas siguiendo los criterios definidos utilizando los métodos AHP (Analytic Hierarchy Process) y PROMETHEE II (Preference Ranking Organization Method for

Enrichment Evaluations II). Los resultados obtenidos mediante la toma de decisiones individual se sometieron al método Condorcet de toma de decisiones grupal para tomar una decisión final.

Resultados: Selección del vehículo más adecuado según los criterios definidos.

Conclusión: Solucionar el problema involucra tomar en consideracionn las opiniones de los expertos militares en cuanto a la optimización de múltiples criterios para ofrecer el vehículo de mejor rendimiento adecuado para su uso en diversas misiones. La elección de un vehículo blindado de combate sobre ruedas polivalente es un proceso complejo en el que influyen numerosos factores que no pueden analizarse objetivamente sin la aplicación de modelos matemáticos adecuados.

Palabras claves: vehículos blindados de combate, toma de decisiones multicriterio, AHP, PROMETHEE II, método Condorcet.

Применение индивидуальных методов принятия решений AHP и PROMETHEE II, а также группового метода принятия решений Condorcet при выборе многоцелевого боевого колесного бронетранспортера

Миша Д. Живкович[а], **корреспондент**, *Дарко* И. Божанич[б], *Милия* М. Сукнович[б], *Борис* В. Делибашич[б]

[а] Университет обороны в г. Белград, Военная академия, кафедра тактики с системами вооружия, г. Белград, Республика Сербия

[б] Белградский университет, факультет организационных наук, кафедра организации бизнес-систем, г. Белград, Республика Сербия

РУБРИКА ГРНТИ: 27.47.19 Исследование операций,
28.17.31 Моделирование процессов управления,
73.47.12 Организация управления и автоматизированные системы управления транспортом,
78.21.53 Исследования и разработки в области эффективности, надежности и боевого использования вооружения и военной техники

ВИД СТАТЬИ: оригинальная научная статья

Резюме:

Введение/цель: Боевые колесные бронетранспортеры − это боевые системы, которые все чаще используются в современных вооруженных конфликтах, особенно в операциях против асимметричных угроз. Мировой рынок колесных бронированных машин постоянно растет, что отражается на их применении в широком спектре миссий и задач вооруженных сил. Существование многочисленных моделей этих транспортных средств с различными техническими и

эксплуатационными характеристиками наряду с возможностью адаптации к конкретным потребностям усложняет выбор наиболее соответствующей альтернативы. В данной статье представлен пример решения задачи выбора наиболее подходящей многоцелевой колесной бронированной машины среднего класса с формулой привода 4x4 при выборе одной из четырех альтернатив с использованием индивидуальных и групповых многокритериальных методов принятия решений.

Методы: В данной статье применялись методы многокритериального принятия решений в решении задач в области выбора сложных боевых систем. Эксперты в области тактики и систем вооружения оценивали альтернативы в соответствии с определенными критериями, используя методы AHP (Analytic Hierarchy Process) и PROMETHEE II (Preference Ranking Organization Method for Enrichment Evaluations II). Результаты, полученные в ходе индивидуального принятия решений, были обработаны методом группового принятия решений Condorcet для принятия окончательного решения.

Результаты: Был сделан выбор наиболее подходящего транспортного средства по утвержденным критериям.

Вывод: Решение проблемы предполагает учет мнений военных экспертов относительно оптимизации множества критериев для обеспечения наилучших характеристик транспортного средства, используемого в различных миссиях. Выбор многоцелевой колесной бронированной боевой машины является сложным процессом, на который влияют многочисленные факторы, не поддающиеся объективному анализу без применения подходящих математических моделей.

Ключевые слова: боевые бронетранспортеры, многокритериальное принятие решений, AHP, PROMETHEE II, метод Condorcet.

Примена метода индивидуалног одлучивања АН и PROMETHEE II и методе групног одлучивања Condorcet при избору вишенаменског оклопног борбеног возила точкаша

Миша Д. Живковић[а], **аутор за преписку**, *Дарко* И. Божанић[б], *Милија* М. Сукновић[б], *Борис* В. Делибашић[б]

[а] Универзитет одбране у Београду, Војна академија, Катедра тактике са системима наоружања, Београд, Република Србија

[б] Универзитет у Београду, Факултет организационих наука, Катедра за организацију пословних система, Београд, Република Србија

ОБЛАСТ: операциона истраживања, војне науке
КАТЕГОРИЈА (ТИП) ЧЛАНКА: оригинални научни рад

Сажетак:

Увод/циљ: Оклопна борбена возила точкаши су све присутнији у савременим оружаним сукобима, нарочито у операцијама против асиметричних претњи. Тржиште ових возила је у константном порасту у свету, што је одраз њихове примене у широком спектру мисија и задатака оружаних снага. Постојање бројних модела оклопних возила точкаша различитих техничких и експлоатационих карактеристика, са могућношћу прилагођавања специфичним потребама, додатно отежава избор најпогоднијe алтернативе. У раду је представљен случај решавања проблема избора најпогоднијег вишенаменског оклопног возила точкаша средње класе и формуле погона 4x4. Изабрана је једна од четири понуђене алтернативе, применом метода индивидуалног и групног вишекритеријумског одлучивања.

Методе: Примењене су методе вишекритеријумског одлучивања при решавању проблема из области сложених борбених система. Експерти из области тактике са системима наоружања су применом метода AHP (Analytic Hierarchy Process) и PROMETHEE II (Preference Ranking Organization Method for Enrichment Evaluations II) извршили рангирање алтернатива у складу са дефинисаним критеријумима. Резултати добијени индивидуалним одлучивањем подвргнути су методи групног одлучивања Condorcet ради доношења коначне одлуке о оптималном решењу.

Резултати: Изабрано је најопогодније возило у складу са дефинисаним критеријумима.

Закључак: Решење проблема подразумева узимање у обзир ставова војних експерата у погледу оптимизације више критеријума ради обезбеђења возила најбољих перформанси погодног за употребу у различитим мисијама. Избор вишенаменског оклопног борбеног возила точкаша је комплексан процес на који утичу бројни фактори које није могуће анализирати објективно без примене адекватних математичких модела.

Кључне речи: оклопна борбена возила, вишекритеријумско одлучивање, AHP, PROMETHEE II, метод Condorcet.

Paper received on: 10.10.2024.
Manuscript corrections submitted on: 27.01.2025.
Paper accepted for publishing on: 28.01.2025.

Effects of shrinkage, temperature and the degree of connection (N/N_f) on the behavior of steel-concrete composite beams

Halima Aouad[a], *Nacer* Rahal[b], *Houda* Beghdad[c], *Mohamed* Sadoun[d], *Abdelaziz* Souici[e], *Sara* Zatir[f], *Khaled* Benmahdi[g]

[a] Mustapha Stambouli University, Department of Civil Engineering, Mascara, People's Democratic Republic of Algeria, e-mail: aouadhal@gmail.com, **corresponding author**, ORCID iD: https://orcid.org/0009-0004-1999-1489

[b] Mustapha Stambouli University, Department of Civil Engineering, Mascara, People's Democratic Republic of Algeria + University of Sciences and Technology, Laboratory of Mechanical Structure and Construction Stability, Oran, People's Democratic Republic of Algeria, e-mail: n.rahal@univ-mascara.dz, ORCID iD: https://orcid.org/0009-0002-0400-8360

[c] Mustapha Stambouli University, Department of Civil Engineering, Mascara, People's Democratic Republic of Algeria, e-mail: houda.beghdad@univ-mascara.dz, ORCID iD: https://orcid.org/0009-0001-3548-5138

[d] Mustapha Stambouli University, Department of Civil Engineering, Mascara, People's Democratic Republic of Algeria, e-mail: m.sadoun@univ-mascara.dz, ORCID iD: https://orcid.org/0009-0008-2314-9402

[e] Mustapha Stambouli University, Department of Civil Engineering, Mascaral, People's Democratic Republic of Algeria + University of Sciences and Technology, Laboratory of Mechanical Structure and Construction Stability, Oran, People's Democratic Republic of Algeria, e-mail: a.souici@univ-mascara.dz, ORCID iD: https://orcid.org/0009-0004-3845-7409

[f] University Tahri Mohamed of Bechar, Architecture and Urban Department, Bechar, People's Democratic Republic of Algeria, e-mail: zatir.sara@univ-bechar.dz, ORCID iD: https://orcid.org/0000-0002-6187-3441

[g] Mustapha Stambouli University, Department of Civil Engineering, Mascara, People's Democratic Republic of Algeria, e-mail: k.benmahdi@univ-mascara.dz, ORCID iD: https://orcid.org/0000-0002-8244-5817

https://doi.org/10.5937/vojtehg73-50812

FIELD: mechanics
ARTICLE TYPE: original scientific paper

Abstract:

Introduction/purpose: Temperature and time-dependent effects such as concrete shrinkage and creep significantly affect the behavior of steel-concrete composite beams. Hence, taking into account the demands brought by these additional effects is necessary. This necessity has resulted in various theoretical and numerical research studies. This article proposes an analytical tool capable of predicting a new redistribution of stresses brought by the combined action of temperature and concrete shrinkage in composite steel-concrete beams in partial shear connection. In this work, the partial shear connection at the steel-concrete interface is taken into account according to the degree of connection (N/N_f).

Methods: This involves reformulating the model proposed in 2024 by Rahal et al analyzing the behavior of composite steel-concrete beams in full shear connection under the effect of temperature and concrete shrinkage. In this present study, the main contribution is the introduction of the effect of the connection degree (N/N_f) at the steel-concrete interface, thus leading to an analytical model capable of predicting additional stresses brought by shrinkage and temperature in composite steel-concrete beams in partial shear connection.

Results: When referred to the model proposed in 2024 by Rahal et al, the results from this current approach are satisfactory. They clearly show that the degree of connection significantly affects the forces brought about by the combined action of concrete shrinkage and temperature.

Conclusion: The results of the present approach and those of the existing model developed by Rahal et al are in good agreement. They clearly show the effect of concrete shrinkage and temperature as a function of the connection degree N/N_f on the behavior of composite steel-concrete beams.

Key words: degree of connection (N/N_f), shrinkage, time, steel-concrete interface.

Introduction

A composite steel-concrete beam consists of a steel beam on which a reinforced concrete slab rests. The connection at the steel-concrete interface is guaranteed by metallic elements called shear connectors (Dias & Karam, 2021). They are usually headed studs.

The advantages presented by this structural system such as: good seismic performance, speed and ease of construction, lightness, reduced construction cost and better ductility allow it to be widely used in civil

engineering (Bradford & Gilbert, 1992; Nie & Cai, 2003; Dias & Karam, 2021).

The behavior of steel-concrete composite beams is influenced by various factors, in particular the cracking of concrete under negative moment (Fan et al, 2010a, 2010b), the deformation capacity of shear connectors (Bradford & Gilbert, 1991; Al-deen et al, 2011a, 2011b) as well as the shrinkage and creep of the concrete slab (Amadio & Fragiacomo, 1997; Xiang et al, 2015). To this end, the justification of the resistance of this type of beam requires a precise prediction as a function of time to avoid possible cracking of concrete or exaggerated deflection (Kwak & Seo, 2000).

The time-dependent analysis of the behavior of composite steel-concrete beams has been the subject of much research. The first studies carried out began in the early 1970s (Roll, 1971). In the case of full shear connection at the steel-concrete interface, which ignores the relative slip between the two materials, several calculation approaches have been proposed (Souici et al, 2015; Partov & Kantchev, 2009, 2011, 2012, 2014; Tehami & Ramdane, 2009; Rahal et al, 2012). In this type of assembly, the long-term deflection will be obtained by analyzes of the cross section (Gilbert, 1989). Actually, partial shear connection, for which the relative slip at the steel-concrete interface must be taken into account, is widely applied (Wen et al, 2024). This relative sliding reduces the resistance of composite beams and considerably affects their behavior over time (Wen et al, 2024).

In the case of the partial shear connection at the steel-concrete interface, which takes into account the relative slip between the two materials, several calculation approaches have been proposed (Gara et al, 2010; Ranzi & Bradford, 2006; Sakr & Sakla, 2008; Newmark et al, 1951; Faella et al, 2010; Beghdad et al, 2017; Tarantino & Dezi, 1992).

Fire is a dangerous phenomenon for the safety of human lives because the mechanical properties of a composite beam deteriorate when exposed to a possible fire and consequently there may be the collapse of the construction or one of its components (Dias & Karam, 2021). In order to protect human lives, checking the resistance of a composite steel-concrete beam in a fire situation has become a necessity.

In the absence of external mechanical stress, concrete drying causes progressive shortening over time; this is called concrete shrinkage (Rahal et al, 2024). In addition, and due to a thermal gradient or temperature variations, a statically determinate composite beam undergoes deformations and displacements without the appearance of internal forces (Rahal et al, 2024). Concrete shrinkage and temperature produce stresses

that vary over time. Predicting the behavior of composite steel-concrete beams under the simultaneous effect of shrinkage and concrete temperature is extremely complex.

The calculation and design codes for composite steel-concrete beams do not provide methods for accurately estimating deformations caused by a shrinkage-temperature combination (Mark et al, 2010).

Due to the lack of dedicated analytical methods for justifying the strength of steel-concrete composite beams taking both concrete shrinkage and temperature, the calculation and design codes for steel-concrete composite beams do not provide methods to estimate accurately the deformations caused by the shrinkage-temperature combination (Mark et al, 2010). Therefore, very simplified approaches based on approximate values of shrinkage and thermal effect are leading to unreliable results (Rahal et al, 2024). Faced with this insufficiency, the development and implementation of new calculation procedures leading to good approaches to correctly predict the effects of shrinkage and temperature has become necessary.

In this context, we seek through this article to propose an analytical, precise and simple approach in practical applications to predict the behavior of composite steel-concrete beams. In this new proposal, we will analyze the behavior of composite beams in partial shear connection at the steel-concrete interface under the shrinkage-temperature combination. This current contribution consists of enriching and expanding the model proposed by Rahal et al. (2024) in which full shear connection was used. In this approach the relative slip between the steel and the concrete was taken into account according to the degree of connection (N/Nf) defined by the European code Eurocode 4 (Hendy & Johnson, 2006). According to Eurocode 4 (Hendy & Johnson, 2006), if full shear connection is used, the connection degree is $N/N_f = 1$. On the other hand, in the case of partial shear connection, the connection degree is given as: $0.40 \leq N/N_f < 1$.

Theoretical bases

The total strain ε(t) that develops in an uncracked, axially loaded concrete element is composed of four elementary strains (Kumar Mehta & Monteiro, 2005; Gilbert, 1989; Gilbert & Ranzi, 2011; Favre et al, 1996). It is evaluated as follows:

$$\varepsilon(t) = \varepsilon_{sh}(t) + \varepsilon_e(t) + \varepsilon_{cr}(t) + \varepsilon_T(t) \quad (1)$$

$\varepsilon_e(t)$: the instantaneous strain,
$\varepsilon_{cr}(t)$: the strain of creep,
$\varepsilon_{sh}(t)$: the deformation of shrinkage, and
$\varepsilon_T(t)$: the thermal expansion.

In accordance with the irreversible theory of concrete (the rate of creep theory), the total deformation of an uncracked and axially loaded concrete specimen can be obtained by the expression below (Kumar Mehta & Monteiro, 2005; Gilbert, 1989; Gilbert & Ranzi, 2011; Favre et al, 1996):

$$\frac{d\,\varepsilon(t,\tau)}{d\,\varphi}=\frac{1}{E_c(\tau_1)}\frac{d\,\sigma_c(t)}{d\,\varphi}+\frac{\sigma_c(t)}{E_c(\tau_1)}+\frac{\varepsilon_{sh}(\infty)}{\varphi(\infty)} \tag{2}$$

φ: the shrinkage coefficient,
E_c: the elastic modulus of concrete,
σ_c: the stress applying to the concrete slab,
τ_1: the application time of the constraint, and
t: the calculation moment.

Formulation of the proposed method

This study applies to the analysis of the elastic behavior of simply supported steel-concrete composite beams including both the shrinkage of concrete, the temperature and the degree of connection (N/N_f) at the steel-concrete interface.

In order to formulate the present analytical approach, we introduce the degree of connection (N/N_f) at the steel-concrete interface into the model proposed by Rahal et al. (2024). In this work, the figure (Figure 1) shows different forces loading the mixed steel-concrete cross section.

These forces are:
ΔT: the thermal gradient = T_0-T_1,
N_0: the normal force applied externally, and
M_0: the externally applied bending moment.

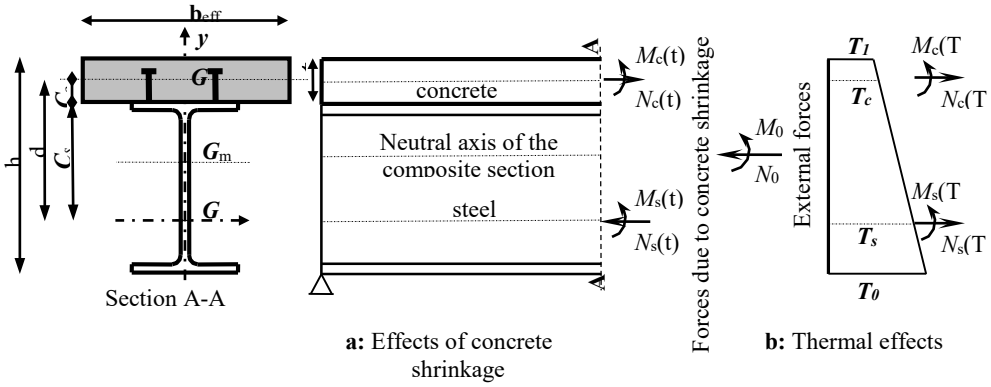

Figure 1 – Internal forces in a composite steel-concrete beam subjected to shrinkage and temperature (Rahal et al, 2024)

Thermal actions

Thermal actions can cause significant geometric changes in large buildings. These loadings can be: elongation when the structure is exposed to temperature or shortening when it is cooled (Gerhard, 1998; Beer, 2010). When a beam is exposed to thermal changes ΔT, it generates:

- thermal strains: $\varepsilon_T = \alpha\, \Delta T$ and
- thermal elongations: $\Delta_{LT} = \varepsilon_T\, L = \alpha\, \Delta T\, L$,

where α is the coefficient of thermal expansion ($°C^{-1}$), (= 1.2×10^{-5} for steel and 1.0×10^{-5} for concrete),
L is the initial length of the bar, and
ΔT is the temperature variation (° C).

When a beam is subjected to thermal effects, the temperature gradient ΔT develops a curvature and an axial deformation calculated respectively by the following relationships (Eqs. 3 and 4) (Gerhard, 1998; Beer, 2010):

$$\chi_T = \alpha_T \frac{\Delta T}{h} \tag{3}$$

$$\varepsilon_T = \alpha_T\, \Delta T \frac{d}{h} \tag{4}$$

In a composite steel-concrete beam, the bending moment acting on the cross section is the result of the four elementary forces ($M_s(t)$, $M_c(t)$, $N_s(t)$ and $N_c(t)$) applying the steel beam and the concrete slab individually. Hence, four equations are necessary to determine these four unknowns (Szabó, 2006). These four equations are obtained by kinematic analysis (two equations) and static analysis (two equations).

Static and kinematic study

From Figure 1, the static study will provide the following two equations

$$N_s(t) = -\alpha_s t_s - \left(\alpha_c t_c + N_c(t)\right)\left[\left(\frac{A_s}{A_m} - \frac{A_c C_c^2}{I_m}\right)\left(1 - \frac{N}{N_f}\right) - 1\right] \tag{5}$$

$$M_s(t) = -\Delta T\left(\frac{\alpha_s}{h_s} + \frac{\alpha_c}{t_c}\right) - M_c(t) + \left[N_c(t) + \alpha_c t_c\right] a\left(1 - k\right) \tag{6}$$

with:

$$K = \left[\left(\frac{A_s}{A_m} - \frac{A_c C_c^2}{I_m}\right)\left(1 - \frac{N}{N_f}\right)\right]$$

$M_c(t)$: bending moment in the concrete slab due to creep,
$M_s(t)$: bending moment in the steel beam,
N: number of shear connectors in partial shear connection,
$N_c(t)$: normal force in the concrete slab due to creep,
N_f: number of shear connectors in full shear connection,
$N_s(t)$: normal effort in the steel section,
N/N_f: rate of shear connection in (%),
t_c: thickness of the slab,
A_c: area of the concrete slab,
A_m: area of the composite beam,
A_s: area of the steel beam,
I_m: moment of inertia of the composite beam,
α_c: thermal expansion coefficient of concrete, and
α_s: thermal expansion coefficient of steel.

Kinematic analysis

In composite steel-concrete beams, the kinematic analysis results in the condition at the steel-concrete interface (Tehami & Ramdane, 2009; Partov & Kantchev, 2009, 2011, 2012, 2014; Rahal et al, 2012; Souici et al, 2015; Beghdad et al, 2017; Rahal et al, 2024). According to this characteristic, we can write the following two compatibility equations in curvature (Eq. 7) and in deformation (Eq. 8):

$$\chi(t)=\frac{M_c(t)}{E_c I_c}=\frac{M_s(t)}{E_s I_s} \tag{7}$$

$$\varepsilon_c(t)=\frac{N_c(t)}{E_c\ A_c}+\frac{M_c(t)}{E_c\ I_c}C_c=\frac{N_s(t)}{E_s\ A_s}+\frac{M_s(t)}{E_s\ I_s}C_s \tag{8}$$

I_s: moment of inertia of the steel beam, and
I_c: moment of inertia of the concrete slab.

Curvature

In accordance with the irreversible law of concrete (the rate of creep theory), the first condition (Eq.7) can be transformed into a differential equation of the type of relation (Eq.2), so one can write:

$$\chi(t)=\frac{1}{E_c I_c}\left[dM_c(t)+M_c(t).d\varphi\right]=\frac{M_s(t)}{E_s I_s} \tag{9}$$

$$\chi(t)=\frac{1}{E_c I_c}\left[dM_c(t)+M_c(t).d\varphi\right]=-\frac{\Delta T}{E_s I_s}\left(\frac{\alpha_s}{h_s}+\frac{\alpha_c}{t_c}\right)+ \tag{10}$$

$$\frac{1}{E_s I_s}\left[N_c(t)+\alpha_c t_c\right]a(1-k)-\frac{1}{E_s I_s}M_c(t)$$

$$\chi(t)=\frac{1}{E_cI_c}\left[\frac{dM_c(t)}{d\varphi}(1-k)+\Delta T\frac{\alpha_c}{t_c}+M_c(t)(1-k)+\Delta T\frac{\alpha_c}{t_c}\right]+$$

$$\frac{1}{E_sI_s}\Delta T\frac{\alpha_s}{h_s}+\frac{1}{E_sI_s}\Delta T\frac{\alpha_c}{t_c}+\frac{1}{E_sI_s}\frac{dM_c(t)}{d\varphi}(1-k)- \qquad 11)$$

$$\frac{1}{E_sI_s}\frac{dN_c(t)}{d\varphi}a(1-k)-\frac{1}{E_sI_s}\alpha_c t_c=0$$

$$\chi(t)=\left(\frac{1}{E_cI_c}+\frac{1}{E_sI_s}\right)(1-k)\frac{dM_c(t)}{d\varphi}+\left(\frac{1}{E_cI_c}+\frac{1}{E_sI_s}\right)\Delta T\frac{\alpha_c}{t_c}-$$

$$\frac{1}{E_sI_s}\frac{dN_c(t)}{d\varphi}a(1-k)-\frac{1}{E_sI_s}\alpha_c t_c+\frac{1}{E_cI_c}M_c(t)(1-k)+ \qquad (12)$$

$$\frac{1}{E_cI_c}\Delta T\frac{\alpha_c}{t_c}+\frac{1}{E_sI_s}\Delta T\frac{\alpha_s}{h_s}=0$$

$$\chi(t)=\left(1+\frac{I_c}{nI_s}\right)(1-k)\frac{dM_c(t)}{d\varphi}+\left(1+\frac{I_c}{nI_s}\right)\Delta T\frac{\alpha_c}{t_c}-$$

$$\frac{I_c}{nI_s}a(1-k)\frac{dN_c(t)}{d\varphi}-\frac{I_c}{nI_s}\alpha_c t_c+M_c(t)(1-k)+ \qquad (13)$$

$$\Delta T\frac{\alpha_c}{t_c}+\frac{I_c}{nI_s}\Delta T\frac{\alpha_s}{h_s}=0$$

α_c: steel-concrete equivalence coefficient ($n=E_s/E_c$).

Deformation

In accordance with the irreversible law of concrete (the rate of creep theory), the second condition (Eq.8) can be transformed into differential equations of the type of relation (Eq.2), so one can write:

$$\varepsilon(t)=\frac{1}{E_c A_c}\left[dN_c(t)+N_c(t).d\varphi\right]+\frac{C_c}{E_c I_c}\left[dM_c(t)+M_c(t).d\varphi\right] \tag{14}$$

$$-d\varepsilon_{sh}(t)=\frac{N_s(t)}{E_s A_s}-\frac{M_s(t)}{E_s I_s}C_s$$

$$\varepsilon(t)=\frac{1}{E_c A_c}\frac{dN_c(t)}{d\varphi}(k-1)+\frac{\alpha_c t_c}{E_c A_c}+\frac{1}{E_c A_c}N_c(t)(k-1)+$$

$$\frac{\alpha_c t_c}{E_c A_c}+\frac{C_c}{E_c I_c}(1-k)\frac{dM_c(t)}{d\varphi}+\frac{C_c}{E_c I_c}\Delta T\frac{\alpha_c}{t_c}+$$

$$\frac{C_c}{E_c I_c}(1-k)M_c(t)+\frac{C_c}{E_c I_c}\Delta T\frac{\alpha_c}{t_c}-\frac{d\varepsilon_{sh}(t)}{d\varphi}=-\frac{\alpha_s t_s}{E_s A_s}- \tag{15}$$

$$\frac{\alpha_c t_c}{E_s A_s}-\frac{1}{E_s A_s}\frac{dN_c(t)}{d\varphi}(k-1)+\frac{C_s}{E_s I_s}\Delta T\frac{\alpha_s}{h_s}+\frac{C_s}{E_s I_s}\Delta T\frac{\alpha_c}{t_c}+$$

$$\frac{C_s}{E_s I_s}(1-k)\frac{dM_c(t)}{d\varphi}-\frac{C_s}{E_s I_s}a(1-k)\frac{dN_c(t)}{d\varphi}-\frac{C_s}{E_s I_s}\alpha_c t_c$$

$$\varepsilon(t)=\left(\frac{C_c}{E_cI_c}-\frac{C_s}{E_sI_s}\right)(1-k)\frac{dM_c(t)}{d\varphi}+\left(\frac{C_c}{E_cI_c}-\frac{C_s}{E_sI_s}\right)\Delta T\frac{\alpha_c}{t_c}+$$

$$\left(\frac{1}{E_cA_c}+\frac{1}{E_sA_s}+\frac{C_sa}{E_sI_s}\right)(k-1)\frac{dN_c(t)}{d\varphi}+\left(\frac{1}{E_cA_c}+\frac{1}{E_sA_s}+\frac{C_sa}{E_sI_s}\right)\alpha_ct_c+$$

$$\frac{C_c}{E_cI_c}(1-k)M_c(t)+\frac{C_c}{E_cI_c}\Delta T\frac{\alpha_c}{t_c}+\frac{1}{E_cA_c}(k-1)N_c(t)+\frac{1}{E_cA_c}\alpha_ct_c= \tag{16}$$

$$\frac{d\varepsilon_{sh}(t)}{d\varphi}-\frac{\alpha_st_s}{E_sA_s}+\frac{C_s}{E_sI_s}\Delta T\frac{\alpha_s}{h_s}$$

$$\varepsilon(t)=\frac{1}{E_cA_c}\frac{dN_c(t)}{d\varphi}(k-1)+\frac{\alpha_ct_c}{E_cA_c}+\frac{1}{E_cA_c}N_c(t)(k-1)+\frac{\alpha_ct_c}{E_cA_c}+$$

$$\frac{C_c}{E_cI_c}(1-k)\frac{dM_c(t)}{d\varphi}+\frac{C_c}{E_cI_c}\Delta T\frac{\alpha_c}{t_c}+\frac{C_c}{E_cI_c}(1-k)M_c(t)+\frac{C_c}{E_cI_c}\Delta T\frac{\alpha_c}{t_c} \tag{17}$$

$$-\frac{d\varepsilon_{sh}(t)}{d\varphi}=-\frac{\alpha_st_s}{E_sA_s}-\frac{\alpha_ct_c}{E_sA_s}-\frac{1}{E_sA_s}\frac{dN_c(t)}{d\varphi}(k-1)+\frac{C_s}{E_sI_s}\Delta T\frac{\alpha_s}{h_s}+$$

$$\frac{C_s}{E_sI_s}\Delta T\frac{\alpha_c}{t_c}+\frac{C_s}{E_sI_s}(1-k)\frac{dM_c(t)}{d\varphi}-\frac{C_s}{E_sI_s}\frac{dN_c(t)}{d\varphi}a(1-k)-\frac{C_s}{E_sI_s}\alpha_ct$$

The two equations (Eqs. 13 and 17) can be rewritten in the following simplified form:

$$A_1\frac{dM_c(t)}{d\varphi}+A_2\frac{dN_c(t)}{d\varphi}+M_c(t)=-K_1 \tag{18}$$

$$A_3 \frac{dM_c(t)}{d\varphi} + A_4 \frac{dN_c(t)}{d\varphi} + A_5 M_c(t) + A_6 N_c(t) = E_c \frac{\varepsilon_{sh}(\infty)}{\varphi_\infty} - K_2 \qquad (19)$$

Additional forces

The general solution of the two differential equations (Eqs. 18 and 19) will give the expressions we are looking for to estimate the additional stresses brought about by the combined effect of concrete shrinkage and temperature. They are of the following form:

$$N_c(t) = C_1.a_{1(\lambda_1)}.e^{\lambda_1.\phi} + C_2.a_{2(\lambda_2)}e^{\lambda_2\phi} + K_1 \qquad (20)$$

$$M_c(t) = C_1.a_{1(\lambda_1)}.e^{\lambda_1.\varphi} + C_2.a_{2(\lambda_2)}e^{\lambda_2\varphi} + K_2 \qquad (21)$$

In the equations (Eqs. 18, 19, 20 and 21), the constants A_1 to A_6 K_1 and K_2 are calculated according to: the geometric and physical characteristics of the mixed cross section, the thermal expansion coefficient of steel and concrete, the degree of connection (N/N_f) and the temperatures T_0 and T_1. On the other hand, the two constants C_1 and C_2 are obtained using the boundary conditions.

Model validation

Our present formulation is validated by examining the composite beam treated in Eurocode 4 (Hendy & Johnson, 2006).

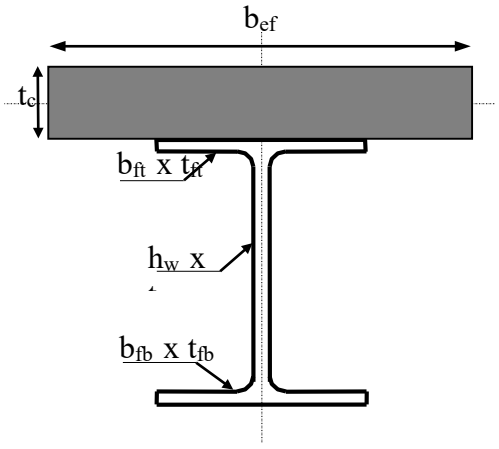

Figure 2 – Cross section characteristics

This example was also used by Rahal et al. (2024) to validate their model in the full shear connection. In this study, the shrinkage parameters are calculated according to Eurocode 2 (European Standard, 2004). The data to use is as follows:

b_{eff} = 3100 mm, t_c = 250 mm, b_{ft} = 400 mm, t_{ft} = 20 mm, b_{fb} = 400 mm, t_{fb} = 30 mm, h_w = 1175 mm, t_w = 12.5 mm. In this example, our beam is supposed to be subjected at time t = 420 days to a flame such that: T_0 = 140 °C and T_1 = 100 °C.

Results

The graphs of the figures (Figures 3 to 8) show the evolution as a function of time and the degree of connection (N/N_f) of the additional forces brought by the shrinkage of the concrete and the temperature and which request a mixed section steel-concrete in partial shear connection.

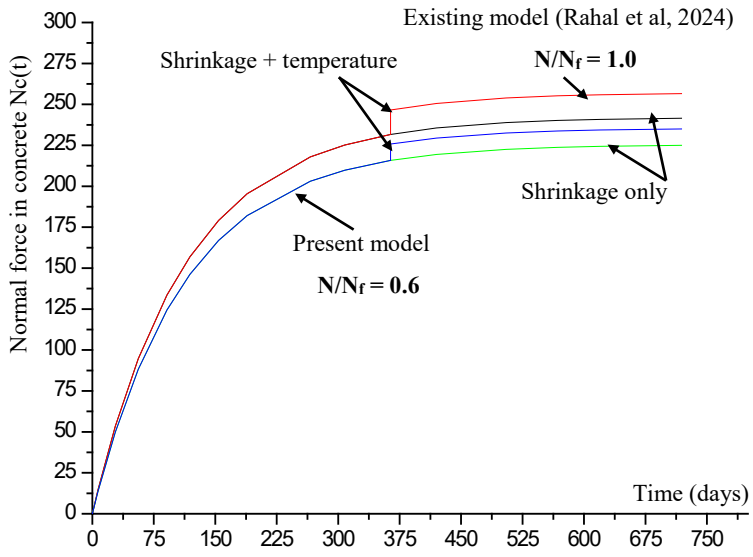

Figure 3 – Evolution in time of the normal force $N_c(t)$ in the concrete slab

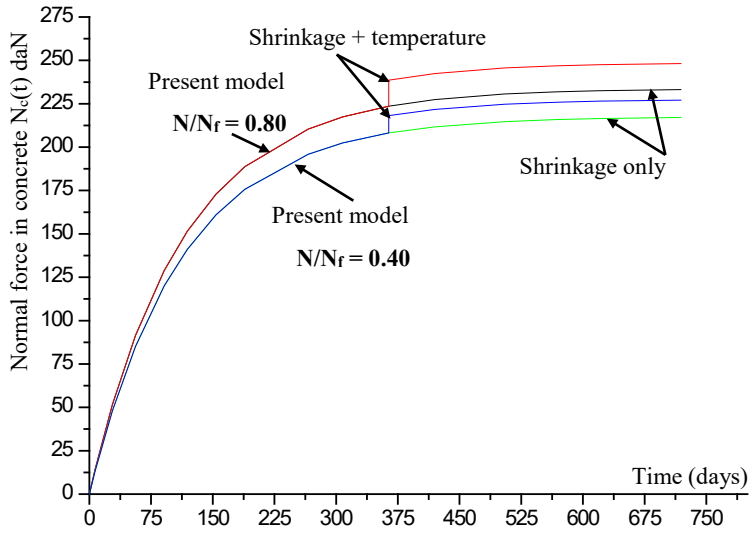

Figure 4 – Evolution in time of the normal force $N_c(t)$ in the concrete slab

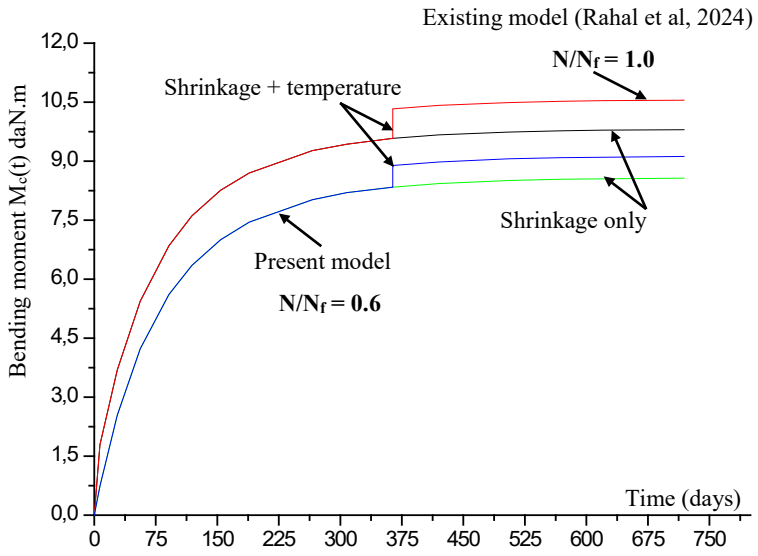

Figure 5 – Evolution in time of the bending moment $M_c(t)$ in the concrete slab

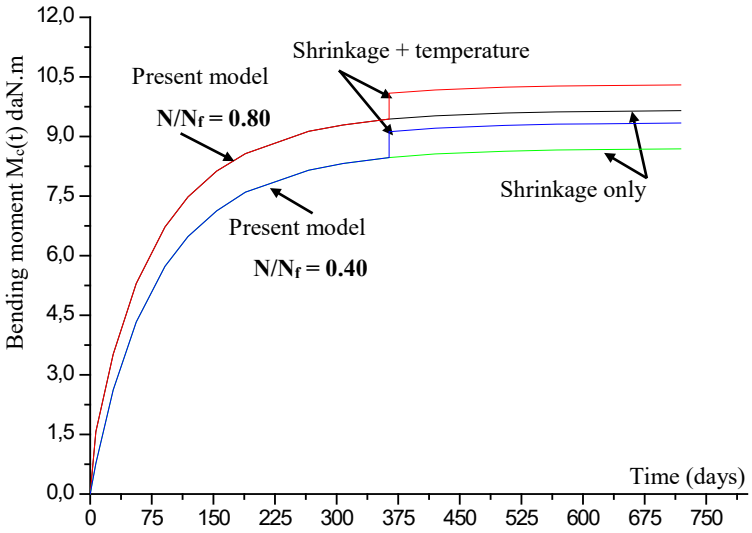

Figure 6 – Evolution in time of the bending moment $M_c(t)$ in the concrete slab

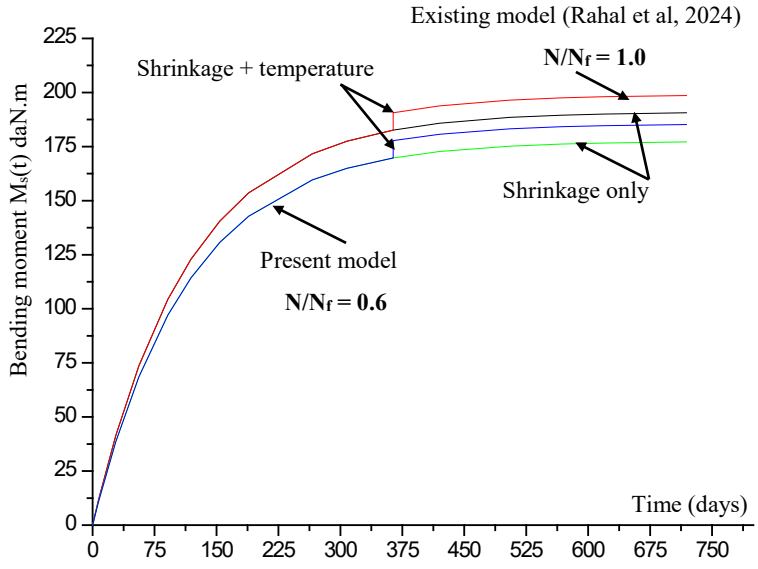

Figure 7 – Evolution in time of the bending moment $M_s(t)$ in the steel beam

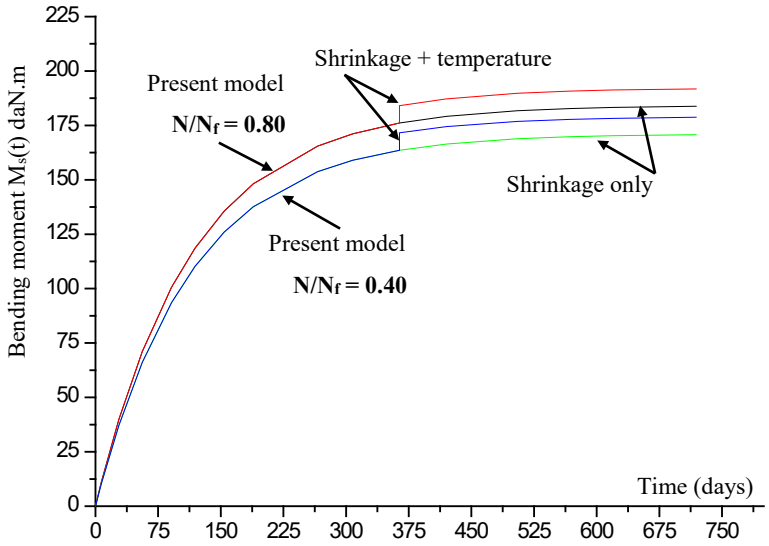

Figure 8 – Evolution in time of the bending moment $M_s(t)$ in the steel beam

Conclusion

The present study focuses on the analysis of the effect of concrete shrinkage on the behavior of composite steel-concrete beams in partial shear connection exposed to temperature.

In this article, the main contribution lies in taking into account the effect of the connection degree (N/N_f) at the steel-concrete interface. This allows us to arrive at an analytical model capable of predicting the additional stresses brought by shrinkage and temperature in composite steel-concrete beams in partial shear connection. The present work is a continuation of that proposed by Rahal et al. (2024). The interest of this approach is to evaluate the new redistribution of constraints according to the degree of connection (N/N_f).

Previous studies clearly show that the bending stiffness of composite steel-concrete beams is reduced in the presence of sliding at the steel-concrete interface. The results obtained by our present approach (Figures 3 to 8) are clearly consistent with this conclusion because the introduction of sliding considerably changes the forces applying the steel beam and the concrete slab under the combined action of concrete shrinkage and temperature.

This research provides a simple and effective tool allowing the estimation, at any instant, of the forces ($N_c(t)$, $N_s(t)$, $M_c(t)$ and $M_s(t)$) which develop on the steel beam and the concrete slab and consequently the knowledge of the new redistribution of local stresses. If the beam is exposed to cooling, the values of temperatures T_0 and T_1 must be negative.

In perspective, future studies will be carried out on composite beams including, at the same time, the effects of concrete creep and temperature.

References

Al-deen, S., Ranzi, G. & Vrcelj, Z. 2011a. Full-scale long-term experiments of simply supported composite beams with solid slabs. *Journal of Constructional Steel Research*, 67(3), pp.308-321. Available at: https://doi.org/10.1016/j.jcsr.2010.11.001.

Al-deen, S., Ranzi, G & Vrcelj, Z. 2011b. Full-scale long-term and ultimate experiments of simply-supported composite beams with steel deck. *Journal of Constructional Steel Research*, 67(10), pp.1658-1676. Available at: https://doi.org/10.1016/j.jcsr.2011.04.010.

Amadio, C. & Fragiacomo, M. 1997. Simplified Approach to Evaluate Creep and Shrinkage Effects in Steel-Concrete Composite Beams. *Journal of Structural Engineering*, 123(9), pp.1153-1162. Available at: https://doi.org/10.1061/(ASCE)0733-9445(1997)123:9(1153).

Beer, G. 2010. *Baustatik: Von den Grundlagen bis zur Computerstatik (Textbook Series TU Graz)*. Verlag d. Technischen Universität Graz. ISBN: 978-3851251210.

Beghdad, H., Tehami, M. & Rahal, N. 2017. Shrinkage behaviour modelling of steel-concrete composite beams with varying degree of connection. *Asian Journal of Civil Engineering (BHRC)*, 18(8), pp.1271-1285 [online]. Available at: https://ajce.bhrc.ac.ir/Volumes-Issues/agentType/View/PropertyID/9500 [Accessed: 02 May 2024].

Bradford, M.A. & Gilbert, R.I. 1991. Time-dependent behaviour of simply-supported steel-concrete composite beams. *Magazine of Concrete Research*, 43(157), pp.265-274. Available at: https://doi.org/10.1680/macr.1991.43.157.265.

Bradford, M.A. & Gilbert, R.I. 1992. Composite Beams with Partial Interaction under Sustained Loads. *Journal of Structural Engineering*, 118(7), pp.1871-1883. Available at: https://doi.org/10.1061/(ASCE)0733-9445(1992)118:7(1871).

Dias, M.S.F. & Karam, V.J. 2021. Thermal analysis of steel and concrete composite beams cross sections in fire situations. *IBRACON Structures and Materials Journal,* 14(5), e14509. Available at: https://doi.org/10.1590/S1983-41952021000500009.

-European Standard. 2004. *EN 1992-1-1: Eurocode 2: Design of concrete structures - Part 1-1 : General rules and rules for buildings* [online]. Available at:

https://www.phd.eng.br/wp-content/uploads/2015/12/en.1992.1.1.2004.pdf [Accessed: 02 May 2024].

Faella, C., Martinelli, E. & Nigro, E. 2010. Steel-concrete composite beams in partial interaction: Closed-form ‘‘exact” expression of the stiffness matrix and the vector of equivalent nodal forces. *Engineering Structures*, 32(9), pp.2744-2754. Available at: https://doi.org/10.1016/j.engstruct.2010.04.044.

Fan, J., Nie, J., Li, Q. & Wang, H. 2010a. Long-Term Behavior of Composite Beams under Positive and Negative Bending. I: Experimental Study. *Journal of Structural Engineering*, 136(7), pp.849-857. Available at: https://doi.org/10.1061/(ASCE)ST.1943-541X.0000175.

Fan, J., Nie, X., Li, Quan & Li, Quanwang. 2010b. Long-Term Behavior of Composite Beams under Positive and Negative Bending. II: Analytical Study. *Journal of Structural Engineering*, 136(7), pp.858-865. Available at: https://doi.org/10.1061/(ASCE)ST.1943-541X.0000176.

Favre, R., Jaccourd, J.-P., Burdet, O. & Charif, H. 1996. *Dimensionnement des structures en béton : aptitude au service et éléments de structures*. Presses Polytechniques et Universitaires Romandes (PPUR). ISBN: 978-2-88074-330-7.

Gara, F., Ranzi, G. & Leoni, G. 2010. Short- and long-term analytical solutions for composite beams with partial interaction and shear-lag effects. *International Journal of Steel Structures*, 10(4), pp.359-372. Available at: https://doi.org/10.1007/BF03215844.

Gerhard, E. 1998. *Praktische Baustatik, Teil 2*. Vieweg+Teubner Verlag Wiesbaden. Available at: https://doi.org/10.1007/978-3-663-11118-4.

Gilbert, R.I. 1989. Time-Dependent Analysis of Composite Steel-Concrete Sections. *Journal of Structural Engineering*, 115(11), pp.2687-2705. Available at: https://doi.org/10.1061/(ASCE)0733-9445(1989)115:11(2687).

Gilbert. R.I. & Ranzi, G. 2011. *Time Dependent Behaviour of Concrete Structures, 1st Edition*. CRC Press. Available at: https://doi.org/10.1201/9781482288711.

Hendy, C.R. & Johnson, R.P. 2006. *Designers' guide to EN 1994-2 Eurocode 4 : design of composite steel and concrete structures. Part 2, General rules and rules for bridges.* London, UK: Thomas Telford Ltd. ISBN: 978-0727731616.

Kumar Mehta, P. & Monteiro, P.J.M. 2005. *Concrete: Microstructure, Properties and Materials, Third Edition*. McGraw-Hill Professional . ISBN: 978-0071462891.

Kwak, H.-G & Seo, Y.-J. 2000. Long-term behavior of composite girder bridges. *Computer Structures*, 74(5), pp.583-599. Available at: https://doi.org/10.1016/S0045-7949(99)00064-4.

Newmark, N.M, Siess, C.P. & Viest, I.M. 1951. Tests and analysis of composite beams with incomplete interaction. *Proceedings of the Society for Experimental Stress Analysis,* 9(1), pp.75-92.

Nie, J. & Cai, C.S. 2003. Steel–Concrete Composite Beams Considering Shear Slip Effects. *Journal of Structural Engineering*, 129(4), pp.495-506. Available at: https://doi.org/10.1061/(ASCE)0733-9445(2003)129:4(495).

Partov, D. & Kantchev, V. 2009. Time-dependent analysis of composite steel-concrete beams using integral equation of Volterra, according Eurocode 4. *Engineering Mechanics*, 16(5), pp.367-392 [online]. Available at: https://web.archive.org/web/20200321071535id_/http://www.engineeringmechanics.cz/pdf/16_5_367.pdf [Accessed: 02 May 2024].

Partov, D. & Kantchev, V. 2011. Level of creep sensitivity in composite steel-concrete beams according to ACI 209R-92 model, comparison with Eurocode-4 (CEB MC90-99). *Engineering Mechanics*, 18(2), p. 91-116 [online]. Available at: http://147.229.35.49/pdf/18_2_091.pdf [Accessed: 02 May 2024].

Partov, D. & Kantchev, V. 2012. Gardner&Lockman Model (2000) and its Application in Numerical Analysis of Composite Beams. *Procedia Engineering*, 40, pp.357-362. Available at: https://doi.org/10.1016/j.proeng.2012.07.108.

Partov, D. & Kantchev, V. 2014. Gardner and Lockman Model in Creep Analysis of Composite Steel-Concrete Sections. *ACI Structural Journal*, 111(1), pp.59-70. Available at: https://doi.org/10.14359/51686430.

Rahal, N., Souici, A., Beghdad, H., Tehami, M., Djaffari, D., Sadoun, M. & Benmahdi, K. 2024. Effects of shrinkage in composite steel-concrete beam subjected to fire. *Steel and Composite Structures*, 50(4), pp.375-382. Available at: https://doi.org/10.12989/scs.2024.50.4.375.

Rahal, N., Tehami, M., Souici, A. & Beghdad, H. 2012. Applying of Integral Equation of Volterra for Determining the Section Forces in Composite Beam, Regarding Shrinkage of Concrete. *Key Engineering Materials*, 498, pp.173-186. Available at: https://doi.org/10.4028/www.scientific.net/KEM.498.173.

Ranzi, G. & Bradford, M.A. 2006. Analytical solutions for the time dependent behavior of composite beams with partial interaction. *International Journal of Solid and Structures*, 43(13), pp.3770-3793. Available at: https://doi.org/10.1016/j.ijsolstr.2005.03.032.

Roll, F. 1971. Effects of Differential Shrinkage and Creep on a Composite Steel-Concrete Structure. *ACI Symposium Publication*, 27, pp.187-214 [online]. Available at: https://www.concrete.org/publications/internationalconcreteabstractsportal/m/details/id/17182 [Accessed: 02 May 2024].

Sakr, M.A. & Sakla, S.S.S. 2008. Long-term deflection of cracked composite beams with nonlinear partial shear interaction: I — Finite element modeling. *Journal of Constructional Steel Research*, 64(12), pp.1446-1455. Available at: https://doi.org/10.1016/j.jcsr.2008.01.003.

Souici, A., Tehami, M., Rahal, N., Bekkouche, M.S. & Berthet. J.F. 2015. Creep effect on composite beam with perfect steel-concrete connection. *International Journal of Steel Structures*, 15(2), pp.433-445. Available at: https://doi.org/10.1007/s13296-015-6013-6.

Szabó, B. 2006. *Influence of shear connectors on the elastic behaviour of composite girders*. PhD thesis. Otaniemi, Espoo: Helsinki University of Technology [online]. Available at: https://aaltodoc.aalto.fi/items/5856e568-6ec5-4a9e-8232-f2fd69723786 [Accessed: 02 May 2024].

Tarantino, A.M. & Dezi, L. 1992. Creep Effects in Composite Beams with Flexible Shear Connectors. *Journal of Structural Engineering*, 118(8), pp.2063-2080. Available at: https://doi.org/10.1061/(ASCE)0733-9445(1992)118:8(2063).

Tehami, M. & Ramdane, K.-E. 2009. Creep behaviour modelling of a composite steel-concrete section. *Journal of Constructional Steel Research*, 65(5), pp.1029-1033. Available at: https://doi.org/10.1016/j.jcsr.2009.01.001.

Wen, C., Lin, Z., Xu, Z., Xu, C., Liu, X. & Yang, G. 2024. Time-dependent response of continuous steel-concrete composite beams under sustained loading. *Journal of Constructional Steel Research*, 213, art.number: 108339. Available at: https://doi.org/10.1016/j.jcsr.2023.108339.

Xiang, T., Yang, C. & Zhao, G. 2015. Stochastic Creep and Shrinkage Effect of Steel-Concrete Composite Beam. *Advances in Structural Engineering*, 18(8), pp.1129-1140. Available at: https://doi.org/10.1260/1369-4332.18.8.1129.

Efectos de la contracción, la temperatura y el grado de conexión (N/N_f) sobre el comportamiento de vigas mixtas acero-hormigón

Halima Aouad[a], **autor de correspondencia**, *Nacer* Rahal[ab], *Houda* Beghdad[a], *Mohamed* Sadoun[a], *Abdelaziz* Souici[ab], *Sara* Zatir[c], *Khaled* Benmahdi[a]

[a] Universidad Mustapha Stambouli, Departamento de Ingeniería Civil, Mascara, República Argelina Democrática y Popular

[b] Universidad de Ciencias y Tecnología, Laboratorio de Estructura Mecánica y Estabilidad de la Construcción, Orán, República Argelina Democrática y Popular

[c] Universidad Tahri Mohamed de Bechar, Departamento de Arquitectura y Urbanismo, Bechar, República Argelina Democrática y Popular

CAMPO: mecánica
TIPO DE ARTÍCULO: artículo científico original

Resumen:

Introducción/objetivo: Los efectos dependientes de la temperatura y el tiempo, como la contracción y la fluencia del concreto, afectan significativamente el comportamiento de las vigas compuestas de acero y concreto. Por lo tanto, es necesario tener en cuenta las demandas que plantean estos efectos adicionales. Esta necesidad ha dado lugar a diversos estudios de investigación teóricos y numéricos. Este artículo propone una herramienta analítica capaz de predecir una nueva redistribución de tensiones provocada por la acción combinada de la temperatura y la contracción del hormigón en vigas compuestas de acero y hormigón en conexión de corte parcial. En este trabajo se tiene en cuenta la conexión de corte parcial en la interfaz acero-hormigón según el grado de conexión (N/N_f).

Métodos: Se trata de reformular el modelo propuesto en 2024 por Rahal et al analizando el comportamiento de vigas compuestas de acero y hormigón en conexión de corte total bajo el efecto de la temperatura y la contracción del hormigón. En este presente estudio, la principal contribución es la introducción del efecto del grado de conexión (N/N_f) en la interfaz acero-hormigón, lo que lleva a un modelo analítico capaz de predecir tensiones adicionales provocadas por la contracción y la temperatura en vigas compuestas de acero y hormigón en conexión de corte parcialResultados: Cuando se hace referencia al modelo propuesto en 2024 por Rahal et al, los resultados de este enfoque actual son satisfactorios. Muestran claramente que el grado de conexión afecta significativamente las fuerzas provocadas por la acción combinada de la contracción del hormigón y la temperatura.

Conclusión: Los resultados del presente enfoque y los del modelo existente desarrollado por Rahal et al concuerdan bien. Muestran claramente el efecto de la contracción del hormigón y la temperatura en función del grado de conexión N/N_f sobre el comportamiento de vigas mixtas de acero y hormigón.

Palabras claves: grado de conexión (N/N_f), retracción, tiempo, interfaz acero-hormigón

---

Влияние усадки, температуры и степени сцепления (N/N_f) на характеристики сталебетонных композитных балок

Халима Авед[а], **корреспондент**, *Насер* Рахал[аб], *Хауда* Бегдад[а], *Мухамед* Садун[а], *Абдулазиз* Соици[аб], *Сара* Затар[в], *Халед* Бенмахди[а]

[а] Университет Туши Мустафы Стамбули, строительный факультет, г. Маскара, Алжирская Народная Демократическая Республика

[б] Университет естественных наук и технологий, Лаборатория машиностроения и прочности конструкций, г. Оран, Алжирская Народная Демократическая Республика

[в] Университет Тахри Мохаммед Бешар, департамент архитектуры и урбанизма, г. Бешар, Алжирская Народная Демократическая Республика

РУБРИКА ГРНТИ: 67.09.33 Бетоны. Железобетон. Строительные растворы, смеси, составы

ВИД СТАТЬИ: оригинальная научная статья

Резюме:

Введение/цель: Эффекты, зависящие от температуры и времени, такие как усадка бетона и ползучесть, существенно влияют на поведение сталебетонных композитных балок. Следовательно, необходимо учитывать требования, связанные с этими дополнительными эффектами, которые являются

предметом многих теоретических и численных исследований. В данной статье представлен аналитический инструментарий, обеспечивающий возможность прогнозирования нового перераспределения нагрузок, вызванных совместным действием температуры и усадки бетона в композитных сталебетонных балках при частичном сдвиговом соединении. В исследовании учитывается частичное сдвиговое соединение в интерфейсе сталь-бетон в зависимости от степени сцепления (N/N_f).

Методы: В связи с вышеизложенным необходимо откорректировать модель, предложенную в 2024 году Рахалом и соавторами для анализа поведения композитных сталебетонных балок при полном сдвиговом соединении под воздействием температуры и усадки бетона. Главный вклад данного исследования заключается в учете влияния степени сцепления (N/N_f) в интерфейсе сталь-бетон, что позволяет создать аналитическую модель, способную прогнозировать дополнительные нагрузки, возникающие в результате усадки и температуры в композитных сталебетонных балках при частичном сдвиговом соединении.

Результаты: Данный подход дал лучшие результаты по сравнению с моделью, предложенной в 2024 году Рахалом и соавторами. Они недвусмысленно показывают, что степень сцепления существенно влияет на усилия, вызываемые совместным действием усадки бетона и температуры.

Вывод: Результаты настоящего подхода и результаты существующей модели, разработанной Рахалом и соавторами, не противоречат друг другу. Они наглядно показывают влияние усадки бетона и температуры в зависимости от степени сцепления N/N_f на поведение композитных сталебетонных балок.

Ключевые слова: степень сцепления (N/N_f), усадка, время, интерфейс сталь-бетон.

Утицај скупљања, температуре и степена спрезања (N/N_f) на понашање спрегнутог челично-бетонског носача

Халима Авед[а], **аутор за преписку**, *Насер* Рахал[аб], *Хауда* Бегдад[а], *Мухамед* Садун[а], *Абделазиз* Соици[аб], *Сара* Затар[в], *Калед* Бенмахди[а]

[а] Универзитет „Мустафа Стамболи”, Одсек за грађевинарство, Маскара, Народна Демократска Република Алжир

[б] Универзитет природних наука и технологије, Лабораторија за машинске структуре и стабилност конструкције, Оран, Народна Демократска Република Алжир

[в] Универзитет „Тахри Мохамед Бешар”, Одељење за архитектуру и урбанизам, Бешар, Народна Демократска Република Алжир

ОБЛАСТ: механика
КАТЕГОРИЈА (ТИП) ЧЛАНКА: оригинални научни рад

Сажетак:

Увод/циљ: Температура и ефекти зависни од времена, као што су течење и скупљање бетона, знатно утичу на понашање спрегнутих носача од челика и бетона. Стога је неопходно узети у обзир захтеве ових додатних ефеката који су предмет различитих теоријских и нумеричких истраживања. У овој студији предлаже се аналитички алат способан да предвиди нову прерасподелу напона проузроковану комбинованим деловањем температуре и скупљања бетона у спрегнутим челично-бетонским носачима у парцијалном смичућем споју. Такође, узима се у обзир парцијални смичући спој на интерфејсу челик-бетон према степену спрезања (N/N_f).

Методе: Преформулисан је модел који су Рахал и сарадници предложили 2024. године анализирајући понашање спрегнутих челично-бетонских носача у пуном спрезању под утицајем температуре и скупљања бетона. Главни допринос ове студије представља увођење утицаја степена спрезања (N/N_f) на интерфејсу челик-бетон. Тиме се долази до аналитичког модела способног да предвиди додатна напрезања услед скупљања и температуре у спрегнутим челично-бетонским гредама у парцијалном смичућем споју.

Резултати: У односу на модел који су Рахал и сарадници предложили 2024. године, испоставило се да су резултати приступа из студије задовољавајући. Они јасно показују да степен спрезања значајно утиче на силе настале комбинованим деловањем скупљања бетона и температуре.

Закључак: Резултати наведеног приступа добро се слажу са резултатима постојећег модела који су развили Рахал и сарадници. Јасно се показује утицај скупљања бетона и температуре у функцији степена спрезања (N/N_f) на понашање спрегнутих челично-бетонских носача.

Кључне речи: степен спрезања (N/N_f), скупљање, време, интерфејс челик-бетон.

Paper received on: 02.05.2024.
Manuscript corrections submitted on: 27.01.2025.
Paper accepted for publishing on: 28.01.2025.

Electrogastrogram-based detection of cybersickness with the application of wavelet transformation and machine learning: a case study

Ilija V. Tanasković[a], *Nenad* B. Popović[b], *Jaka* J. Sodnik[c], *Sašo* J. Tomažič[d], *Nadica* S. Miljković[e]

[a]University of Belgrade, School of Electrical Engineering, Belgrade, Republic of Serbia +
The Institute for Artificial Intelligence Research and Development of Serbia, Novi Sad, Republic of Serbia,
e-mail: ilija.tanaskovic@ivi.ac.rs, **corresponding author**,
ORCID iD: https://orcid.org/0000-0002-6488-4074

[b] University of Belgrade, School of Electrical Engineering, Belgrade, Republic of Serbia,
e-mail: nenad.pop92@gmail.com,
ORCID iD: https://orcid.org/0000-0002-5221-1446

[c] University of Ljubljana, Faculty of Electrical Engineering, Ljubljana, Republic of Slovenia,
e-mail: jaka.sodnik@fe.uni-lj.si,
ORCID iD: https://orcid.org/0000-0002-8915-9493

[d] University of Ljubljana, Faculty of Electrical Engineering, Ljubljana, Republic of Slovenia,
e-mail: saso.tomazic@fe.uni-lj.si,
ORCID iD: https://orcid.org/0000-0002-2968-8879

[e] University of Belgrade, School of Electrical Engineering, Belgrade, Republic of Serbia +
University of Ljubljana, Faculty of Electrical Engineering, Ljubljana, Republic of Slovenia,
e-mail: nadica.miljkovic@etf.bg.ac.rs,
ORCID iD: https://orcid.org/0000-0002-3933-6076

https://doi.org/10.5937/vojtehg73-51577

FIELD: electronics, information technology
ARTICLE TYPE: original scientific paper

Abstract:

Introduction/purpose: The application of virtual reality (VR) and simulation technologies in military training offers cost-effective and versa-

ACKNOWLEDGMENT: This research was partially funded by the Slovenian Research Agency within the research program ICT4QoL–Information and Communications Technologies for Quality of Life, grant number P2-0246. Nadica Miljković was partly supported by the Ministry of Science, Technological Development and Innovation of the Republic of Serbia [Grant No. 451-03-65/2024-03/200103].

tile approach to training enhancement. However, prevalence of cybersickness (CS), characterized by symptoms such as nausea, limits their widespread use.

Methods: This study introduces objective parameters for the detection of CS using three-channel electrogastrogram (EGG) recording from one specific subject and assesses the independence and linear correlation for appropriate channel selection. The paper employs a 3-level discrete wavelet transformation (DWT) on the chosen channel to identify key parameters indicative of gastric disturbances. Furthermore, the paper investigates recovery from CS following VR and examines the application of unsupervised machine learning (ML) for segmenting EGG into baseline and CS, utilizing significant features previously identified.

Results and discussion: The analysis reveals no significant differences across EGG channels and moderate to low linear correlation between channel pairs. The feature selection demonstrates that the root mean square of the amplitude as well as the maximum and mean values of the power spectral density (PSD) calculated on all DWT coefficients, are effective for CS detection while the dominant EGG scale could not indicate CS for any level of decomposition. Furthermore, recovery signs appear approximately 8 minutes after the first VR experience supporting the idea of conducting multiple sessions the same day i.e., intensive VR-based training.

Conclusions: The unsupervised ML shows potential in identifying CS-affected EGG signal segments with feature extraction based on DWT, offering a novel approach for enhancing the prevention of CS occurrence in VR-based military training and other VR-related environments.

Keywords: cybersickness, discrete wavelet transform, electrogastrography (EGG), feature selection, machine learning, military training, power spectral density, virtual reality.

Introduction

The application of simulation technologies in the training of military personnel has been around since the 1950s. In recent years due to the rapid development of graphics, the application of virtual reality (VR) has emerged as a promising approach in the army (Bruzzone & Massei, 2017; Tecknotrove. 2023). The application of simulators in the military offers a cost-effective, rapid, and versatile method for preparing personnel for a wide range of scenarios including psychomotor training (*e.g.*, shortening reaction time), cognitive learning (*e.g.*, solving tactical problems), and affective learning (*e.g.*, adapting the training process to the students' abilities

and interests) (Bruzzone & Massei, 2017; Vlačić et al., 2020). However, the widespread applicability of these advanced training tools is limited to the prevalence of cybersickness (CS). The mismatch between visual and vestibular sensors is commonly assumed to cause CS, while CS is characterized by symptoms similar to motion sickness (MS), including nausea, disorientation, and headache. Therefore, CS emerges as a significant barrier to an immersive experience provided by simulation and VR technologies (Dennison et al., 2016; LaViola, 2000; Miljković et al., 2019; Gruden et al., 2021). Moreover, CS symptoms can manifest during or after exposure to virtual environments, posing a particular concern for VR-based training adoption. The recognition and mitigation of CS are of paramount importance, especially in contexts where the physical and cognitive readiness of military personnel is non-negotiable (NATO Science and Technology Office. 2021).

Traditional methods for investigating CS have predominantly relied on subjective reporting of symptoms through questionnaires (Tian et al., 2023; Dennison et al., 2016; Gruden et al., 2021). Such a qualitative approach, while providing insights, is fraught with limitations, including the potential for subjectivity and bias (Dennison et al., 2016). Given that many CS symptoms, such as nausea, are associated with the smooth muscles of the stomach, the electrogastrogram (EGG) emerges as a promising objective measure (Dennison et al., 2016; Tian et al., 2023; Miljković et al., 2019; Popović, 2021). EGG, capable of capturing changes in gastric myoelectrical activity, offers a direct link to the physiological underpinnings of CS, bypassing the subjectivity of self-reported measures and as a supplementary objective measure to commonly used questionnaires. (Miljković & Sodnik, 2023).

The exploration of EGG as a diagnostic tool for CS started a few decades ago, with a growing potential. Traditional EGG analysis is focused on changes in the EGG amplitude in both time and frequency domains. Additionally, frequency shifts in power spectral density (PSD) towards specific frequency bands indicative of gastric distress, such as bradygastria (slow gastric waves) and tachygastria (rapid gastric waves) could be used as CS indicators (Popović, 2021; Dennison et al., 2016). These features have laid the groundwork for understanding the physiological responses associated with CS, yet the complexity of EGG signals calls for more sophisticated analytical techniques to capture their assessment potential fully.

Recent advances have introduced machine learning (ML) models as a complement to the traditional statistical approaches for assessing the changes in the EGG dynamics. Despite this, literature shows that investigations focusing exclusively on the EGG features for CS detection through ML are sparse (Yang et al., 2022). A few studies have experimented with integrating ML models with the EGG features, but only in combination with the features derived from multiple physiological and behavioral measurements (*e.g.*, EEG, electrocardiogram – ECG, posture, electrodermal activity – EDA, etc.) to estimate the levels of CS during the simulation or the Simulator Sickness Questionnaire (SSQ) scores (Dennison et al., 2016, 2019; Keshavarz et al., 2022). However, these studies (Dennison et al., 2016, 2019; Keshavarz et al., 2022) found that using the EGG features alone did not yield significant results, highlighting a notable gap in the research and showing a promising opportunity for future investigations with demonstrated the potential of the EGG features. Jakus et al. (2022) successfully employed ML models to detect the occurrence of nausea, one of the primary symptoms of CS. This emerging evidence indicates that, although the application of ML to EGG data for CS detection is still in its early stages, it could be a promising approach to pair ML with innovative feature engineering for extracting information of interest. The significant challenge in applying ML to detect the onset of CS is due to the lack of reliable real-time labels required for supervised learning. Labeling is predominantly conducted using questionnaires, which poses limitations for real-time analysis. The SSQ, widely used as a gold standard for assessing CS, is administered only before and after a VR experience (Miljković & Sodnik, 2023; Merchant & Kirollos, 2022; Tian & Boulic, 2024). While effective in determining whether CS occurred, the SSQ lacks the temporal resolution required for training supervised models. To address this, the Fast Motion Sickness Scale (FMS) has been introduced, as a good substitution due to the high correlation to the SSQ (Keshavarz & Hecht, 2011), involving participants self-reporting their CS levels at regular intervals, typically every minute (Tian & Boulic, 2024; Merchant & Kirollos, 2022; Dennison et al., 2016, 2019). Despite its higher temporal resolution, the FMS is subjective and susceptible to bias, as participants may underreport symptoms to appear resilient or may delay acknowledging discomfort (Tian & Boulic, 2024; Merchant & Kirollos, 2022). Considering these challenges, unsupervised ML emerges as a promising approach for CS detection using the EGG sig-

nals. By not relying on potentially unreliable or biased labels, unsupervised methods can detect intrinsic patterns and variations in the data, providing a more objective and accurate analysis of CS-related changes in gastric activity (Miljković & Sodnik, 2023; Tian & Boulic, 2024). Moreover, an objective method for assessing CS is crucial for enhancing the widespread adoption of VR technologies, particularly in military training, where it enables personnel to gain experience in controlled environments that closely simulate realistic scenarios (Kuhl et al., 1995; Miljković & Sodnik, 2023).

This paper proposes the use of discrete wavelet transformation (DWT), a method well-suited for analyzing non-stationary signals with the ability to analyze changes in both time and frequency without the necessity of compromise imposed by the short-time Fourier transform (STFT) including a fixed window size leading to a trade-off between time and frequency resolution, poorer localization for non-stationary signals, and less effective handling of rapid signal changes. Wavelet-based features have already shown promise in identifying disturbances in gastric activity in diabetic patients by allowing for the decomposition of the EGG signal into components that can be analyzed with great precision (Tokmakçi, 2007; Kara et al., 2005). To our knowledge, this is the first paper dealing with CS detection using wavelet transformation. Through this approach, we seek to contribute to the fields of defense sciences and VR technologies, offering insights that could enhance the efficacy and safety of VR-based military training programs, as well as other VR applications.

Aim of the study

This paper is an extension of the previous research (Popović, 2021; Miljković et al., 2019; Miljković & Sodnik, 2023) which investigated the application of the EGG signals for CS detection. The focus of the paper is on the EGG analysis from a single subject who experienced severe symptoms of nausea which led to the cessation of VR experience. The novelty of the proposed method lies in the adoption of wavelet-based features, which have already been utilized in the detection of disturbances in EGG signals in subjects with diabetes (Tokmakçi, 2007; Kara et al., 2005). Also, our methodology explores the indication of recovery from CS with EGG (hereinafter stomach recovery) after VR experience and the possible application of unsupervised ML models to segment signals into two groups (baseline and CS). In this study, the following research questions are presented:

1. Can we use wavelet-based features to detect the CS segments of the EGG recording?
2. Concerning the fact that the three-channel EGG is available for recording, can we use automatic detection of the most suitable channel?
3. Given the features observed in EGG, can a subject achieve recovery following VR exposures in a relatively short break (10 minutes) as proposed by Popović (2021) after experiencing CS?
4. Can an unsupervised ML model be used for the recognition of EGG recording to the baseline and CS segments in the time domain?

Methods and materials

The summary of the proposed methodology is shown using a block diagram in Figure 1. The proposed pipeline begins with a statistical comparison of the EGG channels to assess independence and linear correlation. This is followed by the extraction of features which are subsequently analyzed to identify reliable indicators of CS segments and recovery segments by applying appropriate methods for feature extraction and selection. In the final step, unsupervised segmentation is utilized to divide the signal into two distinct clusters (CS and recovery), facilitating a clearer understanding of the data. The feature extraction step is implemented using MATLAB 2023b (The Mathworks Inc., Natick, USA), while the remaining steps (including channel comparison, feature selection, CS recovery, and unsupervised ML segmentation) are implemented in Python 3.9 (Van Rossum & Drake, 1995) using libraries numpy (Harris et al., 2020) and pandas (McKinney, 2010) for data manipulation; matplotlib for visualization (Hunter, 2007); scipy for signal filtering and statistic tests (Virtanen et al., 2020); statsmodels (Seabold & Perktold, 2010) for the correction of p-value for multiple comparisons, and scikit-learn for unsupervised ML (Pedregosa et al., 2011).

Dataset and preprocessing

This case study is focused on one female subject who experienced severe CS symptoms during VR exposure. The subject signed the Informed Consent in accordance with the Declaration of Helsinki. The study is performed in compliance with the Code of Ethics for researchers and the Guidelines for ethical conduct in research involving people issued by

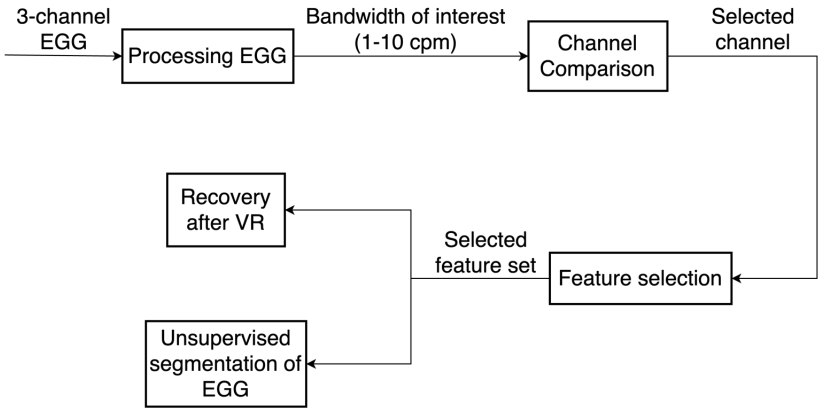

Figure 1 – Block diagram of the proposed methodology. cpm – cycle per minute

the University of Ljubljana. A detailed description of hardware and software setup that is used in VR-related study is provided by (Miljković et al., 2019). The sampling frequency of the recorded signal is set to 2 Hz and the gain is set to 1000. The recording process was segmented based on the participant's engagement with the VR equipment, encompassing a pre-VR baseline segment of 8 minutes (B1), the first VR exposure of 4 minutes (VR1), a 10-minute pause (B2), a second VR session (VR2) planned for 6 minutes and 20 seconds but terminated after 2 minutes due to the emergence of severe CS symptoms, and a final 8-minute post-VR baseline (B3). VR1 contains Rock Falls VR with an included roller coaster session lasting 4 min while VR2 contains a T-Rex Kingdom VR roller coaster session lasting 6 min and 20 s. (Miljković et al., 2019; Popović, 2021; Meta. 2024)

These segments are delineated solely based on the timing of VR equipment usage, which does not exclude the possibility of CS effects manifesting outside VR periods. The signal is filtered using one 5^{th} order bandpass Butterworth filter to roughly extract the bandwidth of interest for the EGG signal between 1 and 10 cpm (cycles per minute) respectively (Dennison et al., 2016; Miljković et al., 2019). The filtering is conducted in both forward and backward directions to achieve zero-phase filtering.

Channel comparison

The EGG is captured using three channels, as outlined in (Miljković et al., 2019; Popović, 2021; Gruden et al., 2021). The electrode for channel

(ch) 1 is located above the stomach's lesser curvature, an area characterized by a lower density of Cajal interstitial cells compared to the pacemaker region adjacent to the greater curvature, where the electrode for ch3 is positioned. A common electrode is affixed along the line connecting the navel to the sternum, 8 cm above the navel. Ch2 electrode is strategically placed equidistant from ch1 and ch3, ensuring the angles between them are identical. To prevent potential breathing-induced artifacts, all three electrodes are positioned 8-9 cm from the common electrode, carefully avoiding placement over the ribs. The reference electrode is secured to the electrically inactive tissue atop the iliac bone. (Popović, 2021)

Initially, a Friedman chi-square test is conducted to assess the comparability of samples across the three channels. In case the Friedman test rejects the null hypothesis, a post-hoc analysis is performed utilizing the Wilcoxon signed-rank test for pairwise signal comparisons. The calculated *p*-values are adjusted for multiple comparisons using Bonferroni's correction method to mitigate the risk of Type I errors setting the threshold of adjusted *p*-value on 0.05. Furthermore, to investigate the information that each channel may provide, the correlation between channel pairs is explored using Pearson's coefficient and scatterplots, aiming to deepen our understanding of the inter-channel relationships in the presence of CS.

Feature selection

Our methodology adopts amplitude- and frequency-based features proposed by the literature (Gruden et al., 2021; Miljković et al., 2019; Tian et al., 2023; Dennison et al., 2016), but instead of extracting frequency bands using classical filtering or STFT, the use of DWT is proposed. The detailed description of the features is provided in the subsection on Feature extraction. This substitution is particularly advantageous for its ability to provide variable resolution across multiple scales, a feature not available with the STFT which uses a fixed window size or with classical frequency band filtering that lacks temporal resolution. This adaptive resolution of DWT allows for smaller windows at higher frequencies to capture rapid changes, and larger windows at lower frequencies to better resolve slower waves. These capabilities make DWT highly suitable for the complex, non-stationary characteristics of EGG signals in CS detection, offering a more nuanced analysis by adapting to the varying dynamics of the signal. (Tokmakçi, 2007; Kara et al., 2005)

Discrete wavelet transformation

DWT is a mathematical tool utilized for the decomposition of signals into a hierarchical structure of frequency bands, enabling detailed analysis with localization in both time and frequency domains. It operates by iteratively applying low-pass and high-pass filters to the samples, thereby extracting its detail coefficients (from the highpass filter) and approximation coefficients (from the lowpass filter) at each level of decomposition. The decomposition process is visualized in Figure 2 where 2↓ stands for downsampling with factor 2 and *cd1* stands for the detail coefficient of the first level decomposition.

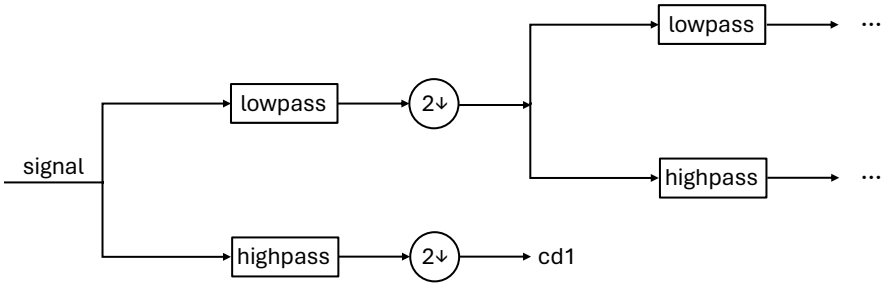

Figure 2 – Block diagram of discrete wavelet transform

The reason for downsampling the signal is to fulfill the sampling theorem—which mandates that the sampling frequency should be at least twice the highest frequency in the signal to prevent aliasing and since half of the samples are removed, the effective sampling rate is reduced in half. The process continues as many times as the levels of decomposition are needed. The remaining coefficients, after the j number of decomposition, are called approximation coefficients and their length as well as the length of the last detail coefficients are $2j$ times the length of the original signal. The adaptability of the DWT coefficients, facilitated by the choice of wavelet basis functions, allows for the optimization of signal representation, making it particularly effective for analyzing signals with transient or non-stationary characteristics. (Akansu & Haddad, 2001; Percival & Walden, 2006; Valens, 1999)

Feature extraction

Our study is focused on one subject and in order to conduct appropriate feature selection we augment our dataset by employing feature extraction on multiple consecutive windows with a length of 60 s and 50% overlap creating one data interval per window to capture the nuances and characteristics on more stationary parts of the signal. This resulted in 59 data intervals for the entire signal. The EGG signal is decomposed using the 'db3' Daubechies wavelet with three levels of decomposition which results in three detailed coefficients (cd) and one approximation coefficient (ca) (Tokmakçi, 2007). Based on the literature review, four types of features have been identified as appropriate for the analysis:

- root means square (RMS) of the amplitude (Gruden et al., 2021; Popović et al., 2019b),
- maximum of PSD (Gruden et al., 2021; Jakus et al., 2022),
- mean of PSD (Tokmakçi, 2007), and
- dominant scale.

The RMS is a standard metric for quantification of amplitude variations in biomedical signals (Cacioppo et al., 2007). Studies (Popović, 2021; Gruden et al., 2021; Jakus et al., 2022) have demonstrated that the onset of CS is associated with increased gastric activity, characterized by an elevated amplitude. The RMS is employed to quantify this amplitude increase, facilitating the detection of CS onset. Additionally, it is used to monitor the recovery of the amplitude to the baseline level, serving as an indicator of the recovery. The maximum of PSD also referred to as the dominant power, identifies the highest power concentrated at a specific rhythm (Popović, 2021; Gruden et al., 2021). An increase in the signal amplitude and the RMS during CS periods is expected to correspond with an increase in the maximum of PSD, making it a good indicator in distinguishing between normal and disturbed gastric rhythms. Similarly, the changes in PSD can be effectively captured by calculating the mean of PSD. CS is associated with rapid and unstable gastric rhythms (tachygastria) where the stomach becomes atonic and lacks frequency stability (Kara et al., 2005). Consequently, the PSD spectrum may become more dispersed, lacking a single dominant peak (Gruden et al., 2021; Dennison et al., 2016; Popović et al., 2019b). Therefore, an increase in overall spectral power should be expected, not just an increase in the dominant power. This highlights the

complementary nature of the mean PSD to the maximum PSD. As features of PSD, both the maximum and the mean PSD are anticipated to reflect elevated power with the onset of CS and a return to nominal levels as indicators of recovery, while the mean is more sensitive to changes in PSD. In addition to magnitude-based measures, the dominant scale is proposed as a feature in the assessment of EGG recordings. The dominant scale, defined as the scale at which the power PSD of the wavelet coefficients reaches its maximum, is proposed as the DWT counterpart to the dominant frequency obtained using the STFT analysis. This feature aims to locate the primary oscillation of smooth muscle cells by identifying the argument of the maximum PSD at each level of decomposition, effectively pinpointing the dominant rhythm on the subband. Since the dominant frequency has established itself as a standard feature for detecting the onset of CS, with stomach activity shifting from normal gastric rhythms to tachygastric bands (Popović, 2021; Gruden et al., 2021; Kim et al., 2005; Tian et al., 2023), the dominant scale is hypothesized to show similar potential. It is expected to increase with the onset of CS and return to normal levels upon recovery.

These features are extracted from the preprocessed signal and all four coefficients (three cds and one ca) resulting in a total of 20 features. By incorporating DWT in the feature extraction process, the emphasis is placed on its inherent filter bank properties. This approach allows for the decomposition of the original EGG signal into multiple frequency bands and enables the tracking of changes indicative of CS. The PSD-based features are calculated using MATLAB *pwelch* function with a 10-sample long Kaiser window with a 50% overlap and parameter beta of 2.5 which indicate stronger attenuation of the side lobes. The flexible Kaiser window function is selected as it can be adjusted to provide different transition widths (*i.e.*, sharpness) by choosing the appropriate parameter (beta) to set the trade-off between the main lobe width and the peak side lobe level (Kaiser & Schafer, 1980; Oppenheim, 2008; Lee & Kuo, 2001). Since a majority of other EGG-related studies used the von Hann window function (Kara et al., 2005; Tian et al., 2023; Tokmakçi, 2007), we compared the results for the application of both the Kaiser and von Hann window. The MATLAB function *pwelch* is used to estimate the PSD in the proposed implementation. The scaling factor inherent in DWT is accounted for by adjusting the signal sampling rate at each level of decomposition. Starting from the original signal rate, the

sampling rate is halved at each successive level: beginning at 2 Hz, then 1 Hz for the first level of decomposition, 0.5 Hz for the second level, and 0.25 Hz for the third level. This downsampling is a critical step in utilizing DWT, as described by Percival & Walden (2006) and Valens (1999). The dominant scale is determined as the argument of the maximum value of PSD, reflecting the peak position within the spectral content. Adjusting the sampling rate at each level ensures that the concept of scale is linked to the frequency bands of the decomposed signal, effectively bridging these two key aspects of wavelet analysis (Percival & Walden, 2006; Valens, 1999).

Identifying features appropriate for the detection of CS segments

In this phase of our research, the features from the EGG recordings that could be indicative of CS are identified. The structure of our case study data collection alternated between the baseline and VR segments, comprising three baselines and two VR segments in total. Given the uncertainty regarding the subject's recovery from the initial VR exposure (which will be investigated later), our analysis for CS detection is deliberately confined to B1 and VR1 segments. According to the timeline detailed in a protocol proposed by Popović (2021), the initial baseline segment spanned 8 minutes, followed by a 4-minute VR session. The feature extraction methodology involved using overlapping windows to generate a single data interval, which is then categorized into the corresponding segment (baseline or VR) based on the majority of the windows duration.

To discern features that significantly differentiate between the B1 and VR1 segments, the non-parametric Mann-Whitney U test is employed. Given the nature of the problem, which involves comparing data intervals before and after an event (the start of VR1), a statistical test designed for repeated measurements would be more suitable. However, because the number of data intervals in the two groups is not equal, the Mann-Whitney test was initially used. To confirm these findings, the analysis also utilizes the Wilcoxon signed-rank test, which is appropriate for repeated measures (McKnight & Najab, 2010; Woolson, 2005), and equalizes the number of samples by excluding the first few data intervals from B1 to match the number of intervals in VR1. This approach allowed us to validate the robustness of our feature selection while addressing the constraints of unequal sample sizes. The Bonferroni correction is applied to adjust the p-values to avoid Type I error and set a threshold for adjusted (adjusted) p-values at

0.05. This statistical rigor ensures the reliability of our findings, highlighting features with a genuine association with CS, thereby advancing our understanding of its detection through EGG signals. Further steps of the proposed pipeline are conducted using only statistically significant features determined in this step.

EGG recovery after the VR experience

A notable methodological variation introduced by Popović (2021) in the study design was the scheduling of both VR sessions on the same day, diverging from the approaches of Miljković et al. (2019) and Tian et al. (2023), which spaced the multiple with at least one day apart. Despite incorporating a 10-minute pause between the VR sessions, this adjustment prompts an inquiry into whether the stomach smooth muscles fully recovered and whether the data interval distribution during B2 mirrors that of B1. The comparative analysis is conducted by assessing each data interval from B2. This involved assessing whether each feature fell within the 5^{th} and 95^{th} quantiles of the distribution observed in B1. For a data interval to be considered as part of a distribution B1, it is determined that at least two-thirds of its features must reside within the specified quantile range. Such an analysis is pivotal for validating the consistency of the subject's response across sessions and for reinforcing the reliability of the data collected after VR1.

Unsupervised segmentation of the EGG signal

This step in our methodology employs unsupervised ML for the segmentation of data intervals into two clusters: baseline and VR. Due to the study retrospective nature and the absence of real-time CS labels, unsupervised learning was selected as an appropriate approach. This application aims to complement the statistical analysis provided in the previous step where the degree of recovery of each data interval is tested. Employing ML aims to explore whether data intervals across the three baseline segments naturally group together and whether the data intervals from both VR sessions exhibit similar patterns, potentially clustering them into a single, unified group.

For this task, the KMeans model is selected, known for simplicity and efficiency while assigning data in two clusters. The model decides based

on the predefined number of centroids (in our case two: baseline and VR) and iteratively assigning each interval to a specific centroid to minimize the inertia, which is defined as the mean squared distance between each sample and its closest centroid. One of the drawbacks of the KMeans is the sensitivity in the initialization of centroids, which is overcome using multiple initializations (setting *n_init* to a default value of 10) (Géron, 2022; Pedregosa et al., 2011). This ensures that the algorithm is independently initialized 10 times, with each run starting from a different set of initial centroids. The final model is automatically selected based on the inertia, with the KMeans class retaining the model with the lowest inertia after all 10 runs. (Géron, 2022; Pedregosa et al., 2011)

Results

The Friedman's chi-square test reveals a significant difference between the samples originating from three channels, yielding a chi-square value of 9.30 and a *p*-value of approximately 0.01. The subsequent post-hoc analysis, detailed in Table 1 and conducted using the Wilcoxon signed-rank test indicates no significant differences between the samples across multiple channels.

Table 1 – Results of the post-hoc test (Wilcoxon signed rank test) are conducted after the Friedman test. The table shows the p-value, the adjusted p-value, and whether the null hypothesis is rejected

Pairs of channels (ch)	*p*-value	adjusted *p*-value	Rejected null hypothesis
ch1 vs. ch2	0.076	0.229	False
ch2 vs. ch3	0.767	1.000	False
ch1 vs. ch3	0.888	1.000	False

The relationship between the channels is further investigated using the Pearson correlation coefficient and scatter plots of pairs of signals. The Pearson correlation coefficients between channels are 0.63, 0.33, and 0.13 for ch1 vs. ch2, ch2 vs. ch3, and ch1 vs. ch3, respectively. The scatterplots of pairs of signals are presented in Figure 3.

A crucial aspect of our methodology involves identifying features that effectively distinguish between B1 and VR1 segments. The feature selection process is conducted in two scenarios. The first scenario used only the features from ch1 due to its position, which is least prone to noise, as suggested by Miljković et al. (2019) and Popović et al. (2019b). In the sec-

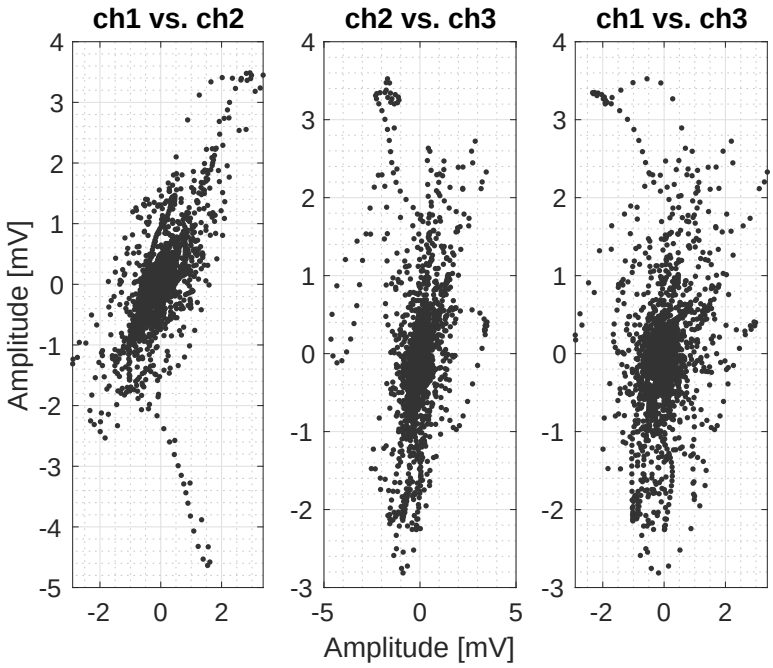

Figure 3 – Scatter plot of the pairs of the signal channels

ond scenario, combined features from ch1 and ch3 are used because ch3 has a low correlation with ch1 (0.13), indicating potential and additional valuable information, even though the analysis using the Wilcoxon signed-rank test showed no significant differences between the samples across multiple channels. To achieve this, the Mann-Whitney test is employed for feature selection, with the outcomes of this evaluation presented in Table 2. Additionally, the statistical analysis is performed on the features from both ch1 and ch3 and the results are presented in Table 3. The features demonstrating statistical significance, indicated by an adjusted *p*-value of less than 0.05, are highlighted in bold. Moreover, the results of feature selection using the Wilcoxon signed-rank test, conducted on the features from ch1 alone, as well as the combination of ch1 and ch3, confirm the findings of the Mann-Whitney test, with all features, except the features based on the dominant scale, showing statistically significant differences between B1 and VR1. Consequently, based on the results from Table 2 and Table 3, which indicate no significant difference in the selected features distinguishing between B1 and VR1 using either only features from ch1 or the

combined use of ch1 and ch3, a further analysis was carried out using only the features from ch1, as proposed by Miljković et al. (2019) and Popović et al. (2019b).

Table 2 – Results of feature selection using statistical tests conducted on channel 1. The Table shows the feature name, the p-value, and the adjusted p-value. The statistically significant features that could be used to discriminate between baseline and VR are marked in bold.

Feature	Decomposition level	*p*-value	Adjusted *p*-value
RMS amplitude value	processed signal	<0.001	**0.007**
	cd1	<0.001	**0.002**
	cd2	<0.001	**0.002**
	cd3	<0.001	**0.004**
	ca3	<0.001	**0.010**
Max value of PSD	processed signal	<0.001	**0.007**
	cd1	<0.001	**0.001**
	cd2	<0.001	**<0.001**
	cd3	<0.001	**<0.001**
	ca3	<0.001	**0.002**
Mean value of PSD	processed signal	<0.001	**0.007**
	cd1	<0.001	**0.001**
	cd2	<0.001	**<0.001**
	cd3	<0.001	**<0.001**
	ca3	<0.001	**0.002**
Dominant Scale of PSD	processed signal	1.000	1.000
	cd1	0.138	1.000
	cd2	0.098	1.000
	cd3	0.176	1.000
	ca3	0.532	1.000

Through the analysis comparing each of the 19 data intervals from B2 against the distribution derived from B1, it is determined that only 5 data intervals from B2 could be considered recovered. The recovery process after VR1 is visually represented in Figure 4, where the data intervals with recovered muscle cells are indicated with the orange color. Specifically, the 6^{th}, 7^{th}, 17^{th}, 18^{th}, and 19^{th} intervals from B2 show similarity with the distribution of B1. Based on Figure 4, the 6^{th} and 7^{th} data intervals correspond to time between 2 minutes and 30 s and 3 minutes and 30 s after VR1 stopped. However, since the 6^{th} and 7^{th} intervals are followed by intervals that do not meet the recovery criteria (i.e. show similarity with the distribution of B1) then the 6^{th} and 7^{th} intervals are considered transient or outliers and are thus not indicative of a stable state. The 17^{th} interval could be considered the first which resembles the distribution of B1 and from the

Table 3 – The results of feature selection using statistical tests conducted on features integrated from channels 1 and 3. The Table shows the feature name, p-value, and adjusted p-value. The statistically significant features that could be used to discriminate between baseline and VR are marked in bold.

Feature	Decomposition level	*p*-value	Adjusted *p*-value
RMS amplitude value	processed signal	<0.001	**<0.001**
	cd1	<0.001	**<0.001**
	cd2	<0.001	**<0.001**
	cd3	<0.001	**<0.001**
	ca3	<0.001	**<0.001**
Max value of PSD	processed signal	<0.001	**<0.001**
	cd1	<0.001	**<0.001**
	cd2	<0.001	**<0.001**
	cd3	<0.001	**<0.001**
	ca3	<0.001	**<0.001**
Mean value of PSD	processed signal	<0.001	**<0.001**
	cd1	<0.001	**<0.001**
	cd2	<0.001	**<0.001**
	cd3	<0.001	**<0.001**
	ca3	<0.001	**<0.001**
Dominant Scale of PSD	processed signal	1.000	1.000
	cd1	0.072	1.000
	cd2	0.035	0.713
	cd3	0.095	1.000
	ca3	0.472	1.000

17th to the 19th data intervals it can be assumed that the muscle cells of the stomach are recovered. Based on this finding, as well on Figure 4, it is assumed that the recovery is completed 8 minutes after VR1 stopped.

The last step in our pipeline is unsupervised segmentation of the EGG signal. The overlapped windows for the extraction of features resulted in 59 data intervals. The models divide 47 intervals in the first cluster and 12 intervals in the second cluster. The visual representation of the clustering results is shown in Figure 5 using different colors. The majority cluster, containing 47 data intervals, is not marked with color, while the intervals that belong to the minority cluster are colored in orange. Since overlapping windows are used, in cases where two consecutive and overlapped windows are clustered in two different groups, it is considered to be the transition between the states and that part of the signal is colored in wheat (light orange). According to the clusterization results, 25% of VR1 are categorized under the VR segment, while 50% of data intervals originating from VR2 are grouped as VR segments. Based on Figure 5, during VR1 the initial

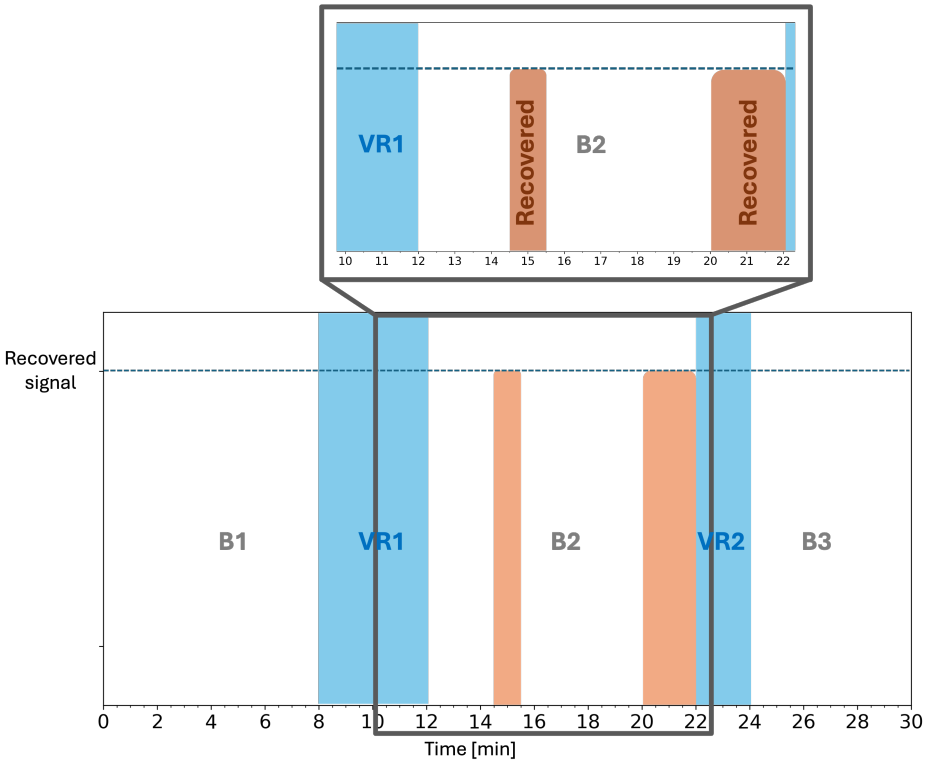

Figure 4 – Visual representation of the recovery process after the first VR experience. The light brown color indicates the recovered data intervals, while the blue color indicates the VR experience.

cluster identified as CS is likely due to movement artifacts from mounting the VR headset or to the emotional response to VR (Cacioppo et al., 2007), which were captured by the EGG signals and misclassified by the model. Notably, the latter part of VR1 did not form a distinct CS cluster, possibly because the CS symptoms were milder compared to the severe symptoms experienced during VR2 that led to the session termination. These observations highlight the models sensitivity to both physiological artifacts, emotional response and varying intensities of CS symptoms. These clusters were identified through unsupervised learning applied to the EGG signals, with no real-time feedback from the participants. The model segmented the data solely based on the distribution within the feature set, uncovering intrinsic patterns potentially associated with CS.

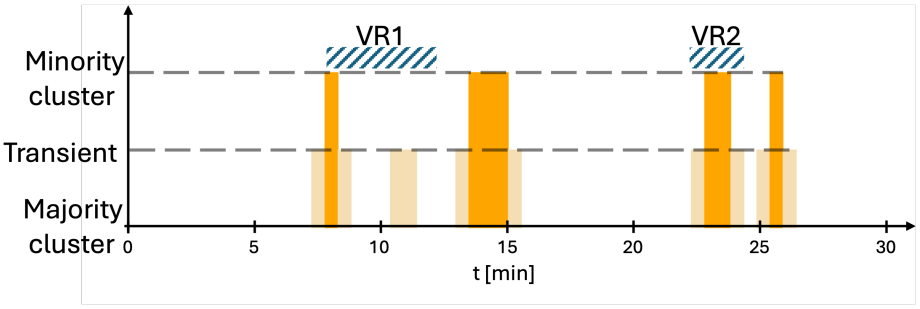

Figure 5 – Visual representation of the results of clustering using the KMeans model with appropriate segments. The data intervals belonging to the window associated with the majority cluster are not colored, while the data intervals associated with the minority cluster are colored in orange. The part of the signal with transitions between two states is colored in wheat (light orange).

The results of the proposed methodology are compared between the features extracted using both the Kaiser window, with its adjustable beta parameter allowing for tailored transition widths, and the commonly used von Hann window (Kara et al., 2005; Tian et al., 2023; Tokmakçi, 2007). The comparative analysis demonstrated that the choice of windowing method did not affect any of the study results or contributions. Specifically, there were no differences in the number of significant features identified, the recovery time following the VR exposure, or the clustering outcomes of the data intervals using ML, regardless of which windowing method was employed.

Discussion

The channel comparison analysis is important for subsequent steps in methodology as statistically significant differences between the channels suggest that each can offer unique and additive information apart from the already used time delay between array recordings of the EGG signal (O'Grady et al., 2010, 2018; Miljković et al., 2023). Conversely, if no significant differences are found, it may be possible to conduct the recording process by reducing the number of channels used, thereby minimizing the complexity of the setup through fewer wires and electrodes. Certainly, this approach relies on dedicated protocols and signal processing. For instance: to compare dominant frequencies in post-prandial and fasting states one channel carries information of interest (Popović et al., 2019a;

Popović, 2021). However, to the best of our knowledge, this is the first time to explore channel information content in terms of CS detection from EGG signals. From the analysis of the results provided in Table 1, it can be seen that even though the Friedman test shows a difference between channels the post-hoc shows no significant difference during pairwise comparison. It can also be remarked that the lowest adjusted *p*-value (0.23) is calculated by comparing ch1 and ch2, while for the other two comparisons, the *p*-value shows a maximum value (1.00). Recording multiple channels does not always provide new information, but investigating the linear relationship between channels seems more interesting. The strongest linear correlation observed between ch1 and ch2 (0.63) points out to some level of linear relationship, whereas the correlations between ch2 and ch3, and ch1 and ch3, suggest minimum to no linear relationship. Contrary to these numerical findings, the visual analysis presented in Figure 3 does not highlight such pronounced differences between channel pairs as suggested by the Pearson coefficients. Also, it can be noticed that all three coefficients are positive which is explained by the direction of the recording vectors described by (Popović, 2021; Miljković et al., 2019). Our analysis, which primarily utilized ch1 for assessing CS, aligns with the support found in the relevant literature (Miljković et al., 2019). However, our examination of statistical tests reveals no significant difference between the channels, suggesting they may derive from the same distribution and thus not necessitate additional processing. Despite this, ch1 has shown promising results (Miljković et al., 2019), affirming its retention for further analysis. Meanwhile, ch2, because of its moderate correlation with ch1 (0.63), does not emerge as a strong candidate due to its similarity. On the contrary, ch3, displaying a low correlation with ch1 (0.13), indicates a divergence that could be beneficial. Thus, the feature selection is also performed on the features combined from both ch1 and ch3 and presented in Table 3 and it could be observed that the combined use of these channels not only supports but also strengthens the outcomes achieved using ch1 alone. Since the results of the test for independent measurements (Mann-Whitney) are shown in Table 3, the analysis is repeated using the test for repeated measurements (Wilcoxon signed-rank). As no difference in the selected features is found when combining features derived from ch1 and ch3, further analysis is conducted using only ch1, as suggested by Miljković et al. (2019). Although there is no unanimous recommendation for the selection of EGG channels,

guided visual observation and manual corrections remain the gold standard for evaluating EGG recordings (Jakus et al., 2022; Gruden et al., 2021; Popović et al., 2019b). While multiple channels can enhance reliability and provide additional information, selecting a single channel offers simplicity in both hardware and processing pipelines. Therefore, ch1 is selected for further analysis to align with previous research (Miljković et al., 2019). A more in-depth analysis of channel selection for CS detection, similar to that proposed by Popović et al. (2019), should be considered in future studies.

During the identification of the features effective for CS detection, our analysis exclusively compares data from B1 and VR1. This comparison strategy ensures that the B1 features are free from any influence of previous VR sessions, confirming that the stomach smooth muscles are in a completely recovered state. It also guarantees that the responses observed during the initial VR exposure are solely due to that particular VR experience, without interference from past exposures. The use of an amplitude seems a good choice as based on the literature the amplitude variations could be used as a short-term indicator of CS (Gruden et al., 2021) and the use of RMS on all decomposition levels proves to be a suitable CS marker. Likewise, in the frequency domain, the normal electrical rhythm of stomach smooth muscles, typically ranging between 2 cpm and 4 cpm, provides a baseline against which deviations can be measured. Disruptions in this rhythm manifest as either slow gastric waves - bradygastria (1-2 cpm) or rapid gastric waves - tachygastria (4-10 cpm), with each offering distinct markers for CS. The published literature confirms that extracting PSD on frequency bands that correspond to bradygastria and tachygastria and monitoring their changes in time could be used to detect changes in EGG that originated from the onset of CS (Miljković et al., 2019; Tian et al., 2023; Dennison et al., 2016). However, statistical analysis reveals that all features extracted from PSD, except the dominant scale, across all wavelet coefficients, serve as a reliable indicator for CS in our study. This finding diverges from the existing literature (Gruden et al., 2021; Miljković et al., 2019; Tian et al., 2023; Popović et al., 2019b), where the dominant frequency is strongly correlated with CS. Since the dominant scale is inspired by this well-established metric, it is expected to be a strong indicator of CS onset, showing that further research is necessary. Conversely, all other examined features demonstrate significant statistical differences (p-value < 0.010) between the B1 and VR1 samples. This uniform significance

across all wavelet coefficients for the remaining features suggests that exploring more decomposition levels could be a promising direction for future research. Consequently, the features related to the dominant scale are excluded from subsequent analyses, with the focus shifting to those features that show statistical significance.

As explained in both methodology and the discussion regarding feature selection, the changes in the protocol which included multiple VR experiences on the same day raise a question of whether the smooth muscles of the stomach had enough time to recover from CS and not corrupt further experiment. The results indicate that 5 data intervals of B2 meet the conditions and can be considered to be the part of B1 distribution. The majority of the B2 segment is considered to be still corrupted by the disturbances and it can be only assumed that the stomach recovery was completed approximation 8 minutes after VR1 cessation. This also indicates a good assumption when conducting feature selection only on B1 and VR1 and that selection involving remaining segments could compromise findings. Although these findings suggest that there is a necessity for longer pauses than 10 minutes to assess if recovery is indeed completed after 8 minutes or if it is mandatory to have longer pauses as proposed by Miljković et al. (2019) and Tian et al. (2023) further research on a larger group of subjects with the same protocol is required, including multiple VR experiences in the same day, but longer pauses within to confirm our claims.

The final step in our methodology is the development of an ML model to discern between two predefined clusters (baseline and VR), due to the absence of labels. Considering that accurately labeling CS symptoms in real-time is challenging due to the lack of reliable methods for real-time detection, unsupervised learning is advocated as a step toward objective estimation of CS symptoms. Assessments typically rely on pre- and post-experience questionnaires like the SSQ, which do not provide the temporal resolution necessary for precise labeling during EGG recording (Tian & Boulic, 2024; Merchant & Kirollos, 2022). While self-reporting scales such as the Fast Motion Sickness Scale (FMS) have been proposed (Dennison et al., 2016, 2019; Merchant & Kirollos, 2022; Tian & Boulic, 2024), these methods are subjective and can introduce bias, as frequent interruptions may disrupt participants' concentration and potentially influence the onset of CS. Considering these limitations, the potential of unsupervised ML emerges as a significant advantage. Unsupervised approaches can

detect intrinsic patterns and variations in EGG signals without relying on potentially unreliable or biased labels, offering a more objective and accurate analysis of CS-related changes in gastric activity. The KMeans model is used to group data intervals in two clusters. From Figure 5 it can be seen that the VR1 segment is considered to be baseline or transient where only one data interval at the beginning of VR1 is grouped as actual VR. In the case of VR2, it can be observed that data intervals belong to VR with transient and CS intervals. The weak link observed between the clusters and VR segments can be attributed to initial assumptions regarding the relationship between CS and VR exposure that require reevaluation. Firstly, it is assumed that the data intervals extracted from the EGG signals would naturally cluster into two distinct groups: baseline and CS. However, our findings suggest that CS manifests in a more nuanced and gradual manner, lacking clear-cut boundaries the states. Future research should explore the possibility of using more than two clusters with the idea of extracting multiple levels of CS or the utilization of different unsupervised models (such as Density-Based Spatial Clustering of Applications with Noise - DBSCAN) which does not predefine the number of clusters (Géron, 2022). Secondly, it is assumed that CS symptoms would be confined to the duration of VR exposure. Contrary to this assumption, studies have shown that CS symptoms can take several minutes to develop after the onset of VR exposure (e.g., approximately 3 minutes during video-watching tasks) and can persist long after the VR experience has ended, sometimes lasting up to several days depending on the individual's susceptibility (Isu et al., 2014; Tian et al., 2023). In our study, it is observed that the feature set distribution from B2 began to resemble B1 only eight minutes after the VR1 session concluded. This delay underscores the extended impact of CS beyond the VR session itself, suggesting that CS is not strictly bounded by VR experience. Nevertheless, this step shows promising and interesting results regarding stomach recovery and automatic CS detection in EGG signals.

In examining the MLs role in CS detection, the literature review highlights two approaches: the utilization of EEG features as a sole indicator, and the multimodal approach consisting of a combination of features extracted from physiological and behavioral signals including ECG, EGG, posture, EDA, etc. (Yang et al., 2022; Keshavarz et al., 2022). A common objective in these studies is the prediction of CS severity, typically determined through the SSQ (before and/or after the simulation) or ver-

bal estimations of symptoms during the simulation. While EGG features have not been widely recognized as standalone indicators for CS or nausea, recent studies integrating EGG in multimodal ML models have yielded substantial accuracy. Keshavarz et al. (2022) developed a multimodal ML model for real-time estimation of visually induced MS (which is a synonym for CS) and the classification of subjects whether they experience sickness or not during the simulation. This approach uses EGG features as an indicator but concludes that EGG features alone showed only a weak link with the majority of CS measurements. Similarly, Dennison et al. (2019) shows that a model based only on EGG achieved an accuracy of 48% for multiclass classification of symptoms during the simulation, but in combination with different features achieved an accuracy of 95%. In our opinion, nausea as one of the most specific symptoms of CS is inherently linked to the smooth muscles of the stomach, which EGG directly captures. This connection underpins our hypothesis that EGG data harbors valuable insights into nausea and CS manifestations. Supporting this notion is the study conducted by Jakus et al. (2022), which reports an 88% accuracy rate in nausea detection, proving the premise that with innovative and creative feature engineering, EGG can indeed serve as a reliable source of information for CS assessment. All available ML-based research reports used label information about CS and trained their model in a supervised manner with reliable evaluation metrics. Conversely, an unsupervised ML approach is employed for segmentation and the direct comparison with the established literature could not be performed due to the lack of evaluation metrics. Future research should not only expand the participant pool but also enable a robust comparative analysis with our work and validate the findings.

Contribution of the study

Our study, which focuses on a single participant and employed an innovative protocol using EGG recordings to explore CS during VR sessions, yields insights into the initial research questions:

1. It is found that traditional and wavelet-based features effectively indicate CS segments within the signal. However, features related to the dominant scale do not demonstrate significant differences, neither in the signal nor in the wavelet coefficients.

2. Statistical tests reveal no significant differences across channels. Additionally, the Pearson correlation coefficients indicate a medium linear correlation between ch1 and ch2, while the remaining two coefficients achieve low to no linear correlation.
3. The unsupervised ML model shows promising results in detecting the segments of the signal affected by the CS.

An additional contribution of our study is the finding that the choice between the Kaiser and von Hann window functions did not significantly impact the identification of significant features, the recovery patterns following VR1, or the segmentation outcomes in CS detection using machine learning methods.

Limitations of the study

We recognize the following limitations and propose directions for future research:

1. Although this study offers valuable preliminary findings, it is based on a single case study which may limit the generalizability of our findings due to potential individual differences in anatomical, physiological, or psychological characteristics. Future research with a larger study group is necessary to confirm these findings, enabling robust statistical analyses that can clarify trends and minimize the possibility of misleading results caused by individual variability.
2. Wavelet-based features are proved to be important parameters in the detection of CS and further exploration of different wavelets apart from Daubechies and different levels of decomposition may be considered for future research.
3. This paper only investigates linear correlations between different channels of EGG, but appropriate analysis to reveal potential nonlinear relations could be explored in the future.
4. The extension of the feature set (*e.g.*, entropy, crest factor as well as max, mean, and min values of each DWT coefficient) Miljković et al. (2019); Jakus et al. (2022); Tokmakçi (2007) could be investigated for CS detection.
5. The weak link between the clusters and VR segments (25% for VR1 and 50% for VR2) suggests that data intervals could not be naturally clustered into two distinct groups (baseline and CS), as well as

that CS symptoms would be confined to the duration of VR exposure, highlighting the need for improved evaluation of clustering and determination of cluster number in future research.

6. The more compelling comparative analysis of unsupervised models, including ones without the predefined number of clusters such as DBSCAN, could be included in future work as well as different appropriate metrics for clusterization analysis.
7. The duration of the segments used in this study is relatively short. It should be noted that for EGG measurements it is typically recommended to measure 15 minutes or more (Stern et al., 1987; Parkman et al., 2003). On the other hand, our approach enables quasi-real-time analysis, which is not feasible with protocols that involve relatively long signal measurements. In support of our approach, the detection of sickness onset can be performed almost immediately with the application of amplitude threshold in the time domain (Gruden et al., 2021).
8. This research only explored two window functions (Kaiser and von Hann), and future studies should expand the investigation by examining how different window function selections influence the feature extraction process in EGG signal analysis.

Conclusion

Our investigation into CS through EGG recordings during VR sessions, despite being conducted with a single participant and employing a non-traditional protocol, has yielded significant insights. The statistical analyses reveal no significant differences between channels, suggesting uniformity in the EGG signal response to CS across different recordings. Meanwhile, the correlation analysis reveals a moderate linear correlation (0.63) between ch1 and ch2, whereas the other two pairs exhibit low to negligible linear correlation. It is found that the RMS of the EGG amplitude, the maximum value of PSD, and the mean value of PSD across all DWT coefficients could be used for the detection of CS resulting in 15 significant features. The observations of stomach recovery are evident 8 minutes after the VR experience confirming no necessity for longer pauses between VR experiences. Lastly, the application of an unsupervised ML model demonstrates potential in identifying CS-affected signal segments, indicating a fruitful di-

rection for future research involving a broader exploration of unsupervised ML techniques in this context.

Statement

During the preparation of this work, the author(s) used GPT4 (ChatGPT) in order to improve readability and language. After using this tool/service, the author(s) reviewed and edited the content as needed and take(s) full responsibility for the content of the publication.

References

Akansu, A.N. & Haddad, R.A. 2001. *Multiresolution signal decomposition: Transforms, subbands, and wavelets, 2nd Edition*. San Diego: Academic Press. ISBN 978-0-12-047141-6.

Bruzzone, A.G. & Massei, M. 2017. Simulation-Based Military Training. In: *Mittal, S., Durak, U. & Ören, T. (Eds.) Guide to Simulation-Based Disciplines. Simulation Foundations, Methods and Applications.* pp. 315–361. Cham: Springer. Available at: https://doi.org/10.1007/978-3-319-61264-5_14.

Cacioppo, J.T., Tassinary, L.G. & Berntson, G. 2007. *Handbook of psychophysiology*. Cambridge University Press. ISBN 9781139461931.

Dennison, M.S., D'Zmura, M., Harrison, A.V., Lee, M. & Raglin, A.J. 2019. Improving motion sickness severity classification through multi-modal data fusion. In: *Pham, T. (Eds.) Proceedings Artificial Intelligence and Machine Learning for Multi-Domain Operations Applications*. Vol. 11006, art.number:110060T. Available at: https://doi.org/10.1117/12.2519085.

Dennison, M.S., Zachary Wisti, A. & D'Zmura, M. 2016. Use of physiological signals to predict cybersickness. *Displays*, 44, pp. 42–52. Available at: https://doi.org/10.1016/j.displa.2016.07.002.

Gruden, T., Popović, N.B., Stojmenova, K., Jakus, G., Miljković, N., Tomažič, S. & Sodnik, J. 2021. Electrogastrography in Autonomous Vehicles—An Objective Method for Assessment of Motion Sickness in Simulated Driving Environments. *Sensors*, 21(2), art.number:550. Available at: https://doi.org/10.3390/s21020550.

Géron, A. 2022. *Hands-On Machine Learning with Scikit-Learn, Keras, and TensorFlow (3rd ed)*. Sebastopol, California: O'Reilly Media, Inc. ISBN 9781098122478.

Harris, C.R., Millman, K.J., Van Der Walt, S.J., Gommers, R., Virtanen, P., Cournapeau, D., Wieser, E., Taylor, J., Berg, S., Smith, N.J., Kern, R., Picus, M., Hoyer, S., Van Kerkwijk, M.H., Brett, M., Haldane, A., Del Río, J.F., Wiebe, M., Peterson, P., Gérard-Marchant, P., Sheppard, K., Reddy, T., Weckesser, W.,

Abbasi, H., Gohlke, C. & Oliphant, T.E. 2020. Array programming with NumPy. *Nature*, 585, pp. 357–362. Available at: https://doi.org/10.1038/s41586-020-2649-2.

Hunter, J.D. 2007. Matplotlib: A 2D Graphics Environment. *Computing in Science & Engineering*, 9(3), pp. 90–95. Available at: https://doi.org/10.1109/MCSE.2007.55.

Isu, N., Hasegawa, T., Takeuchi, I. & Morimoto, A. 2014. Quantitative analysis of time-course development of motion sickness caused by in-vehicle video watching. *Displays*, 35(2), pp. 90–97. Available at: https://doi.org/10.1016/j.displa.2014.01.003.

Jakus, G., Sodnik, J. & Miljković, N. 2022. Electrogastrogram-Derived Features for Automated Sickness Detection in Driving Simulator. *Sensors*, 22(22), art.number:8616. Available at: https://doi.org/10.3390/s22228616.

Kaiser, J. & Schafer, R. 1980. On the use of the I0-sinh window for spectrum analysis. *IEEE Transactions on Acoustics, Speech, and Signal Processing*, 28(1), pp. 105–107. Available at: https://doi.org/10.1109/TASSP.1980.1163349.

Kara, S., Dirgenali, F. & Okkesim, S. 2005. Estimating Gastric Rhythm Differences Using a Wavelet Method from the Electrogastrograms of Normal and Diabetic Subjects. *Instrumentation Science & Technology*, 33(5), pp. 519–532. Available at: https://doi.org/10.1080/10739140500222907.

Keshavarz, B. & Hecht, H. 2011. Validating an Efficient Method to Quantify Motion Sickness. *Human Factors: The Journal of the Human Factors and Ergonomics Society*, 53(4), pp. 415–426. Available at: https://doi.org/10.1177/0018720811403736.

Keshavarz, B., Peck, K., Rezaei, S. & Taati, B. 2022. Detecting and predicting visually induced motion sickness with physiological measures in combination with machine learning techniques. *International Journal of Psychophysiology*, 176, pp. 14–26. Available at: https://doi.org/10.1016/j.ijpsycho.2022.03.006.

Kim, Y.Y., Kim, H.J., Kim, E.N., Ko, H.D. & Kim, H.T. 2005. Characteristic changes in the physiological components of cybersickness. *Psychophysiology*, 42(5), pp. 616–625. Available at: https://doi.org/10.1111/j.1469-8986.2005.00349.x.

Kuhl, J., Evans, D., Papelis, Y., Romano, R. & Watson, G. 1995. The Iowa Driving Simulator: an immersive research environment. *Computer*, 28(7), pp. 35–41. Available at: https://doi.org/10.1109/2.391039.

LaViola, J.J. 2000. A discussion of cybersickness in virtual environments. *ACM SIGCHI Bulletin*, 32(1), pp. 47–56. Available at: https://doi.org/10.1145/333329.333344.

Lee, B.H. & Kuo, S. 2001. *Real-Time Digital Signal Processing: Implementaions, Applications and Experiements with the TMS320C55X.* Wiley Hoboken, NJ, USA. ISBN 1-280-55452-5.

McKinney, W. 2010. Data Structures for Statistical Computing in Python. In: *Van der Walt, S. & Millman, J. (Eds.) Proceedings of the 9th Python in Science Conference*. Austin, Texas, pp.56-61, June 28 - July 3. Available at: https://doi.org/10.25080/Majora-92bf1922-00a.

McKnight, P.E. & Najab, J. 2010. Mann-Whitney U Test. *The Corsini Encyclopedia of Psychology*. 30 January. Available at: https://doi.org/10.1002/9780470479216.corpsy0524.

Merchant, W. & Kirollos, R. 2022. An Overview of Cybersickness Self-Report Measures for use in Defence Research and Development Canada Experiments, Reference Document DRDC-RDDC-2022-D063. *Defence Research and Development Canada*. [online]. Available at: https://cradpdf.drdc-rddc.gc.ca/PDFS/unc392/p814963_A1b.pdf [Accessed: 10 June 2024].

Meta. 2024. *Epic Roller Coasters* [online]. Available at: https://www.meta.com/experiences/pcvr/epic-roller-coasters/1477883658957255/#reviews [Accessed: 10 June 2024].

Miljković, N., Popović, N.B., Prodanov, M. & Sodnik, J. 2019. Assessment of sickness in virtual environments. In: *Konjović, Z., Zdravković, M. & Trajanović, M. (Eds.) Proceedings of the 9th International Conference on Information Society and Technology (ICIST 2019)*. Kopaonik, Serbia, pp.76-81, March 10-13 [online]. Available at: https://www.eventiotic.com/eventiotic/files/Papers/URL/f412a358-82d8-46aa-b0c9-6ad30de5890d.pdf [Accessed: 10 June 2024] ISBN: 978-86-85525-24-7.

Miljković, N., Popović, N.B. & Sodnik, J. 2023. Electrogastrogram Signal Processing: Techniques and Challenges with Application for Simulator Sickness Assessment. In: *Biomedical Signal Processing, 1st Edition*, pp.62-89. CRC Press [online]. Available at: https://www.taylorfrancis.com/chapters/edit/10.1201/9781003201137-4/electrogastrogram-signal-processing-nadica-miljkovi%C4%87-nenad-popovi%C4%87-jaka-sodnik [Accessed: 10 June 2024] ISBN: 9781003201137.

Miljković, N. & Sodnik, J. 2023. Towards Objective Assessment of Driving Simulation Sickness: Pros and Cons of Stomach Electrical Activity. In: *Kemeny, A., Chardonnet, J.-R. & Colombet, F. (Eds.) Proceedings of the Driving Simulation Conference 2023 Europe VR*. Antibes Juan-les-Pins, France, pp.81-88, September 6-8 [online]. Available at: https://proceedings.driving-simulation.org/proceeding/dsc-2023/towards-objective-assessment-of-driving-simulation-sickness-pros-and-cons-of-stomach-electrical-activity/ [Accessed: 10 June 2024] ISBN: 978-2-9573777-3-2.

NATO Science and Technology Office. 2021. *Guidelines for Mitigating Cybersickness in Virtual Reality Systems. Peer-reviewed Final Report of the Human Factors and Medicine Panel/Modeling and Simulations Group, Activity Number 323 (NATO STO-TR-HFM-MSG-323)* [online]. Available at: https://apps.dtic.mil/sti/pdfs/AD1183673.pdf [Accessed: 10 June 2024].

O'Grady, G., Angeli, T.R., Paskaranandavadivel, N., Erickson, J.C., Wells, C.I., Gharibans, A.A., Cheng, L.K. & Du, P. 2018. Methods for High-Resolution Electrical Mapping in the Gastrointestinal Tract. *IEEE Reviews in Biomedical Engineering*, 12, pp. 287–302. Available at: https://doi.org/10.1109/RBME.2018.2867555.

O'Grady, G., Du, P., Cheng, L.K., Egbuji, J.U., Lammers, W.J.E.P., Windsor, J.A. & Pullan, A.J. 2010. Origin and propagation of human gastric slow-wave activity defined by high-resolution mapping. *American Journal of Physiology-Gastrointestinal and Liver Physiology*, 299(3), pp. G585–G592. Available at: https://doi.org/10.1152/ajpgi.00125.2010.

Oppenheim, A.V. 2008. *Discrete-time Signal Processing, 2nd Edition*. Pearson Education. ISBN 9788131704929.

Parkman, H.P., Hasler, W.L., Barnett, J. & Eaker, E. 2003. Electrogastrography: a document prepared by the gastric section of the American Motility Society Clinical GI Motility Testing Task Force. *Neurogastroenterology & Motility*, 15(2), pp. 89–102. Available at: https://doi.org/10.1046/j.1365-2982.2003.00396.x.

Pedregosa, F., Varoquaux, G., Gramfort, A., Michel, V., Thirion, B., Grisel, O., Blondel, M., Prettenhofer, P., Weiss, R., Dubourg, V., Vanderplas, J., Passos, A., Cournapeau, D., Brucher, M., Perrot, M. & Duchesnay, E. 2011. Scikit-learn: Machine Learning in Python. *Journal of Machine Learning Research*, 12, pp. 2825–2830 [online]. Available at: https://www.jmlr.org/papers/volume12/pedregosa11a/pedregosa11a.pdf [Accessed: 10 June 2024].

Percival, D.B. & Walden, A.T. 2006. *Wavelet Methods for Time Series Analysis (Cambridge Series in Statistical and Probabilistic Mathematics, Series Number 4)*. Cambridge University Press. ISBN 9780521685085.

Popović, N.B. 2021. *Methods for assessment of electrical activity of smooth muscles*. Phd thesis, Belgrade, Serbia: University of Belgrade, School of Electrical Engineering. [online]. Available at: https://nardus.mpn.gov.rs/handle/123456789/18615 [Accessed: 10 June 2024].

Popović, N.B., Miljković, N. & Popović, M.B. 2019a. Simple gastric motility assessment method with a single-channel electrogastrogram. *Biomedical Engineering/Biomedizinische Technik*, 64(2), pp. 177–185. Available at: https://doi.org/10.1515/bmt-2017-0218.

Popović, N.B., Miljković, N., Stojmenova, K., Jakus, G., Prodanov, M. & Sodnik, J. 2019b. Lessons Learned: Gastric Motility Assessment During Driving Simulation. *Sensors*, 19(14), art.number:3175. Available at: https://doi.org/10.3390/s19143175.

Seabold, S. & Perktold, J. 2010. Statsmodels: Econometric and Statistical Modeling with Python. In: *Van der Walt, S. & Millman, J. (Eds.) Proceedings of the 9th Python in Science Conference*. Austin, Texas, pp.92-96, June 28-July 3. Available at: https://doi.org/10.25080/Majora-92bf1922-011.

Stern, R.M., Koch, K.L., Stewart, W.R. & Lindblad, I.M. 1987. Spectral analysis of tachygastria recorded during motion sickness. *Gastroenterology*, 92(1), pp. 92–97. Available at: https://doi.org/10.1016/0016-5085(87)90843-2.

Tecknotrove. 2023. Role of defense simulator training in enhancing national security. *Tecknotrove.com*, 26 September [online]. Available at: https://tecknotrove.com/role-of-defence-simulator-training-in-national-security/ [Accessed: 10 June 2024].

Tian, N., Achache, K.H., Ben Mustapha, A.R. & Boulic, R. 2023. EGG Objective characterization of cybersickness symptoms towards navigation axis. In: *2023 IEEE Conference on Virtual Reality and 3D User Interfaces Abstracts and Workshops (VRW)*. Shanghai, China, pp.289-297, March 25-28. Available at: https://doi.org/10.1109/VRW58643.2023.00068.

Tian, N. & Boulic, R. 2024. Who says you are so sick? An investigation on individual susceptibility to cybersickness triggers using EEG, EGG and ECG. *IEEE Transactions on Visualization and Computer Graphics*, 30(5), pp. 2379–2389. Available at: https://doi.org/10.1109/TVCG.2024.3372066.

Tokmakçi, M. 2007. Analysis of the Electrogastrogram Using Discrete Wavelet Transform and Statistical Methods to Detect Gastric Dysrhythmia. *Journal of Medical Systems*, 31(4), pp. 295–302. Available at: https://doi.org/10.1007/s10916-007-9069-9.

Valens, C. 1999. *A really friendly guide to wavelets*. [online]. Available at: https://www.cs.unm.edu/~williams/cs530/arfgtw.pdf [Accessed: 10 June 2024].

Van Rossum, G. & Drake, F.L. 1995. *Python reference manual, Release 2.1.1.* Amsterdam, The Netherlands: Stichting Mathematisch Centrum. ISBN 1441412697.

Virtanen, P., Gommers, R., Oliphant, T.E., Haberland, M., Reddy, T., Cournapeau, D., Burovski, E., Peterson, P., Weckesser, W., Bright, J., van der Walt, S.J., Brett, M., Wilson, J., Millman, K.J., Mayorov, N., Nelson, A.R.J., Jones, E., Kern, R., Larson, E., Carey, C.J., Polat, I., Feng, Y., Moore, E.W., VanderPlas, J. & SciPy1.0Contributors. 2020. SciPy 1.0: fundamental algorithms for scientific computing in Python. *Nature methods*, 17, pp. 261–272. Available at: https://doi.org/10.1038/s41592-019-0686-2.

Vlačić, S.I., Knežević, A.Z., Mandal, S., Rođenkov, S. & Vitsas, P. 2020. Improving the pilot selection process by using eye-tracking tools. *Journal of Eye Movement Research*, 12(3). Available at: https://doi.org/10.16910/jemr.12.3.4.

Woolson, R.F. 2005. Wilcoxon Signed-Rank Test. In: *Encyclopedia of Biostatistics*. 15 July. Available at: https://doi.org/10.1002/0470011815.b2a15177.

Yang, A.H.X., Kasabov, N. & Cakmak, Y.O. 2022. Machine learning methods for the study of cybersickness: a systematic review. *Brain Informatics*, 9, art.number:24. Available at: https://doi.org/10.1186/s40708-022-00172-6.

Electrogastrograma-detección de la ciberenfermedad mediante la aplicación de la transformación wavelet y el aprendizaje automático: estudio de caso

Ilija V. Tanasković[a,b], **autor de correspondencia**, *Nenad* B. Popović[a], *Jaka* J. Sodnik[c], *Sašo* J. Tomažič[c], *Nadica* S. Miljković[a,c]

[a] Universidad de Belgrado, Facultad de Ingeniería Eléctrica, Belgrado, República de Serbia

[b] Instituto de Investigación y Desarrollo de Inteligencia Artificial de Serbia, Novi Sad, República de Serbia

[c] Universidad de Liubliana, Facultad de Ingeniería Eléctrica, Liubliana, República de Eslovenia

CAMPO: electrónica, tecnologías de información

TIPO DE ARTÍCULO: artículo científico original

Resumen:

Introducción/objetivo: La aplicación de tecnologías de realidad virtual (RV) y simulación en el entrenamiento militar ofrece un enfoque rentable y versátil para mejorar el entrenamiento. Sin embargo, la prevalencia de la ciberenfermedad (CS), caracterizada por síntomas como náuseas, limita su uso generalizado.

Métodos: Este estudio introduce parámetros objetivos para la detección de CS utilizando el registro de electrogastrograma (EGG) de tres canales de un sujeto específico y evalúa la independencia y correlación lineal para la selección apropiada del canal. El artículo emplea una transformación wavelet discreta de 3 niveles (DWT) en el canal elegido para identificar parámetros clave indicativos de trastornos gástricos. Además, el artículo investiga la recuperación de CS después de VR y examina la aplicación de aprendizaje automático (ML) no supervisado para segmentar EGG en línea base y CS, utilizando características significativas identificadas previamente.

Resultados: El análisis no revela diferencias significativas entre los canales EGG y una correlación lineal moderada a baja entre pares de canales. La selección de características demuestra que la raíz cuadrada media de la amplitud, así como los valores máximos y medios de la densidad espectral de potencia (PSD) calculados en todos los coeficientes DWT son efectivos para la detección de CS, mientras que la escala EGG dominante no pudo indicar CS para ningún nivel de descomposición. Además, los signos de recuperación aparecen aproximadamente 8 minutos después de la primera experiencia de VR, lo que respalda

la idea de realizar múltiples sesiones el mismo día, es decir, un entrenamiento intensivo basado en VR.

Conclusión: El ML no supervisado muestra potencial en la identificación de segmentos de señales EGG afectados por CS con extracción de características basada en DWT, ofreciendo un enfoque novedoso para mejorar la prevención de la aparición de CS en el entrenamiento militar basado en VR y otros entornos relacionados con VR.

Palabras claves: ciberenfermedad, transformada wavelet discreta, electrogastrografía (EGG), selección de características, aprendizaje automático, entrenamiento militar, densidad espectral de potencia, realidad virtual.

Обнаружение симптомов киберболезни на основании электрогастрограммы с применением вейвлет-преобразования и машинного обучения: целевое исследование

Илья В. Танаскович[а,б], **корреспондент**, *Ненад* Б. Попович[а], *Яка* Й. Содник[в], *Сашо* Й. Томажич[в], *Надица* С. Милькович[а,в]

[а] Белградский университет, электротехнический факультет, г. Белград, Республика Сербия

[б] Институт исследований и разработок в области искусственного интеллекта Сербии, г. Нови-Сад, Республика Сербия

[в] Люблянский университет, факультет электротехники, г. Любляна, Республика Словения

РУБРИКА ГРНТИ: 28.17.33 Компьютерное моделирование реальности. Виртуальная реальность

ВИД СТАТЬИ: оригинальная научная статья

Резюме:

Введение/цель: Применение виртуальной реальности (ВР) и симуляторов обеспечивает экономичный и интуитивно понятный подход к боевой подготовке. Однако из-за тошноты, возникающей в процессе учений на симуляторе (симптомы тошноты – СТ), ограничивает их в более широком применении.

Методы: В данном исследовании представлены объективные параметры обнаружения СТ с использованием трехканальной электрогастрограммы (ЭГГ), записанной у одного

респондента, а также оценена независимость и линейная корреляция для соответствующего выбора одного канала. В статье к выбранному каналу ЭГГ применялось дискретное вейвлет-преобразование (ДВП) с тремя уровнями с целью выявления ключевых особенностей, указывающих на дисфункцию желудка. Помимо того, в ходе исследования оценивалось восстановление после СМ, вызванных использованием ВР, и анализировалось применение неконтролируемого машинного обучения (МО) для сегментации ЭГГ на базовый сегмент и сегмент во время СТ, используя важные особенности, выявленные ранее.

Результаты: Проведенный анализ не выявил существенных различий между тремя каналами ЭГГ. Однако была выявлена линейная корреляция (от умеренной к низкой) между парами каналов. Выбор признаков демонстрирует, что среднеквадратичное значение амплитуды, а также максимальное и среднее значения спектральной плотности мощности (СПМ), рассчитанные по всем коэффициентам ДВП, эффективны для обнаружения СТ, в то время как доминирующая шкала ЭГГ не может указывать СТ ни на одном уровне декомпозиции. Помимо того, признаки восстановления проявляются примерно через 8 минут после первого использования виртуальной реальности, что подтверждает идею о проведении нескольких сеансов обучения в один и тот же день, т.е. интенсивные учения в среде виртуальной реальности возможны.

Выводы: Применение неконтролируемого МО может идентифицировать сегменты ЭГГ во время СТ с извлечением функций на основании ДВП, предлагая новый подход к предотвращению СТ в боевой подготовке в среде виртуальной реальности, а также в других средах, связанных с технологией ВР.

Ключевые слова: киберболезнь, дискретное вейвлет-преобразование, электрогастрография (ЭГГ), выбор признаков, машинное обучение, военная подготовка, спектральная плотность мощности, виртуальная реальность.

Детекција симптома изазваних коришћењем симулатора заснована на електрогастрографском сигналу уз примену дискретне трансформације таласићима и машинског учења: студија случаја

Илија В. Танасковић[а,б], **аутор за преписку**, *Ненад* Б. Поповић[а], *Јака* Ј. Содник[в], *Сашо* Ј. Томажич[в], *Надица* С. Миљковић[а,в]

[а] Универзитет у Београду, Електротехнички факултет, Београд, Република Србија

[б] Истраживачко-развојни институт за вештачку интелигенцију, Нови Сад, Република Србија

[в] Универзитет у Љубљани, Електротехнички факултет, Љубљана, Република Словенија

ОБЛАСТ: електроника, информационе технологије
КАТЕГОРИЈА (ТИП) ЧЛАНКА: оригинални научни рад

Сажетак:

Увод/циљ: Примена виртуелне реалности (ВР) и симулатора пружа исплатив и интуитиван приступ војној обуци. Међутим, могућност појаве мучнине, која је изазвана коришћењем симулатора (симптома мучнине – СМ), ограничава њихову ширу примену.

Методе: Ово истраживање уводи објективне параметре за детекцију СМ, коришћењем троканалног електрогастрограма (ЕГГ) снимљеног на једном испитанику, и процењује независност и линеарну корелацију за одговарајући избор једног канала. Примењена је дискретна трансформација таласићима (ДТТ) са три нивоа на изабрани ЕГГ канал, како би се идентификовала кључна обележја која указују на поремећај рада желуца. Поред тога, евалуиран је опоравак након СМ, настао услед коришћења ВР, а анализирана је и примена машинског учења (МУ) без надгледања за сегментацију ЕГГ на основни сегмент и сегмент током СМ, коришћењем претходно идентификованих обележја од значаја.

Резултати и дискусија: Анализа показује да нема значајних разлика између три ЕГГ канала, као и умерену до ниску линеарну корелацију између парова канала. Избор обележја сугерише да се применом средње квадратне вредности амплитуде, као и максималне и просечне вредности спектралне густине снаге (СГС), израчунате на свим ДТТ коефицијентима, успешно детектује СМ, док примена доми-

Tanasković, I. et al., Electrogastrogram-based detection of cybersickness with the application of wavelet transformation and..., pp.79–114

нантне скале ЕГГ није указала на присуство СМ ни за један ниво декомпозиције. Поред тога, показано је да се знаци опоравка појављују приближно 8 минута након првог ВР искуства, што указује на то да се више ВР сесија може спровести истог дана, односно да је интензивна ВР обука могућа.

Закључак: Примена МУ без надгледања има потенцијал у идентификацији ЕГГ сегмената током СМ уз издвајање обележја заснованих на ДТТ, нудећи нови приступ у превенцији појаве СМ у војној обуци заснованој на ВР, као и другим областима повезаним са ВР технологијом.

Кључне речи: симптоми мучнине, дискретна трансформација таласићима, електрогастрографија, одабир обележја, машинско учење, војна обука, спектрална густина снаге, виртуелна реалност.

Paper received on: 11.06.2024.
Manuscript corrections submitted on: 27.01.2025.
Paper accepted for publishing on: 28.01.2025.

A comparative study of turbulence models for predicting the aerodynamic drag of a spin-stabilized projectile

Quang Tuan Nguyen

Le Quy Don Technical University, Faculty of Special Equipment,
Hanoi, Socialist Republic of Vietnam,
e-mail: tuannguyenmta28@gmail.com,
ORCID iD: https://orcid.org/0000-0002-7741-8232

https://doi.org/10.5937/vojtehg73-54634

FIELD: mechanical engineering, fluid dynamics, exterior ballistics
ARTICLE TYPE: original scientific paper

Abstract:

Introduction/purpose: In this research, the influence of different turbulence models on the aerodynamic drag prediction of a generic spin-stabilized projectile was analyzed. The turbulence models chosen for investigation were one-equation Spalart-Allmaras, two-equation models Standard k-ε, Realizable k-ε, Standard k-ω and SST k-ω. The special sniper projectile M118 was selected for the study.

Methods: The flows around the projectile were numerically simulated using RANS equations intergrated into ANSYS Fluent software with different turbulence models. The numerical simulation was carried out at various Mach numbers to study the effect of turbulence models on the projectile aerodynamic drag prediction. The computational results were compared to the available experimental data to evaluate the ability of the turbulence models.

Results: The research results have shown that the turbulence models significantly affect the numerical simulation results. The Spalart-Allmaras turbulence model performs better than other models in the subsonic flow regime. The Standard k-ε, Realizable k-ε and SST k-ω models perform better than other models in the supersonic flow regime.

Conclusion: Computational Fluid Dynamics is a powerful tool to analyze the aerodynamics of flying bodies. By appropriately selecting turbulence models, the flow around flying bodies can be accurately investigated. In the case of generic ogive-cylinder-boattail projectiles, on the one hand, the Spalart-Allmaras model is suitable for subsonic flow, and the Standard k-ε, Realizable k-ε and SST k-ω models are recommended for the supersonic flight regime, on the other hand.

Key words: turbulence models, Ansys Fluent, spin-stabilized projectiles, subsonic flow, supersonic flight regime.

Introduction

RANS equations have been widely used in aerospace and defense industry for years. They are solved together with a turbulence model describing the turbulence behavior of the flow. Selecting an appropriate turbulence model is crucial in aerodynamic analysis of flying bodies.

Generally speaking, aerodynamics has provided various models to describe the turbulent behavior of the flow around a body. Each model has its own strengths and shortcomings and has been proven to be effective in different applications. No turbulence model is universally suitable for all turbulent flows. Researchers have selected turbulence models based on their own knowledge and experience.

In the field of weapon design, various turbulence models have been successfully used so far to analyze flows around projectiles. Xu et al. (2022) adopted the Spalart-Allmaras turbulence model to investigate the aerodynamic characteristics of a 57mm projectile with a drag controlling device. Demir et al. (2024) analyzed the drag reduction of modified bullets using the Spalart-Allmaras turbulence model. The Standard k-ε turbulence model was applied by Silton at the Army Research Laboratory to conduct Navier-Stokes computations for a 0.50 cal. projectile (Silton, 2002). Many other authors have also implemented the Standard k-ε turbulence model to study flows around various flying bodies (Muthukumaran et al, 2013; Gholap et al, 2022; Bui et al, 2024; Nguyen et al, 2024). Hao et al. (2024) used the Realizable k-ε turbulence model to carry out the aerodynamic characterization of bullet heads with different arcuate curves. Ferfouri et al. (2023) adopted the Realizable k-ε turbulence model for predicting the aerodynamic drag coefficient of the M107 155mm projectile. The Realizable k-ε turbulence model was also applied by Silton to perform numerical computation for spinning projectiles from subsonic to supersonic speeds (Silton, 2005, 2011). Meanwhile, Hamel & Gagnon (2011) implemented the Standard k-ω turbulence model for a parametric study on a 155mm artillery shell equipped with a roll-decoupled course correction fuze. The SST k-ω model has also been used in multiple research studies. Luo et al. (2024) adopted the SST k-ω model to study the aerodynamic characteristics of a tail-stabilized projectile with the asymmetrical diversion groove. The SST k-ω turbulence model was applied by Jiajan et al. (2015) to investigate the effect of boattail junction shaping on the aerodynamic drag and stability of supersonic spin-stabilized rounds. Sertkaya et al. (2022) used the SST k-ω turbulence model for computing the aerodynamic coefficients of 155 mm ammunition.

In order to select an appropriate turbulence model for a specific flow, one has to know the performance characteristics of each model. A comparative study on the prediction of the aerodynamic characteristics of four aircraft with different turbulence models performed by Jang et al. (2018) has shown that the skin friction drag predicted with the SST k-ε is the smallest, while the k- ε model predicts the largest skin friction drag for all configurations. Somashekar & Immanuel Selwyn Raj investigated the effect of six turbulence models, namely, the Spalart-Allmaras, the Standard k-ε, the k-ε RNG, the Realizable k-ε, the Standard k-ω, and the SST k-ω, on the prediction of the aerodynamic characteristics of a mini-unmanned aerial vehicle. They have drawn a conclusion that these six turbulence models have the same general behavior with some differences in the coefficients of lift and drag, and the Spalart-Allmaras model is the most efficient model to describe the turbulence of the subsonic flow around a mini-UAV in terms of the deviation of the coefficients of lift and drag values and the calculation time (Somashekar & Immanuel Selwyn Raj, 2021). Julian et al. (2023) carried out a study on the effect of the Spalart - Allmaras, the Standard k-ε and the Standard k-ω turbulence models on the aerodynamic performance of the NACA 4415 airfoil. However, in the field of projectile design, to the best of the author's knowledge, there is still no published work dedicated to the comparative analysis of the performance of different turbulence models in studying flows around a spin-stabilized projectile.

Therefore, inspired by the above literature review conclusion, the main objective of this research is to study the comparative performance of five widely used turbulence models, namely, the Spalart-Allmaras, the Standard k-ε, the Realizable k-ε, the Standard k-ω and Menter's SST k-ω turbulence models, in prediction of the aerodynamic drag coefficient of a spin-stabilized projectile for better understanding the turbulence models' ability to predict the drag acting on a generic projectile stabilized by spinning. The M118 projectile is chosen for the present study because its aerodynamic data obtained experimentally has been published in the open literature and can be used for validating the simulation results.

Mathematical model

Governing equations

The continuous flow around a projectile is described by the 3D Navier-Stokes conservation equations as follows:

The conservation of the mass:

$$\frac{\partial \rho}{\partial t}+\frac{\partial(\rho u_i)}{\partial x_i}=0 \tag{1}$$

The conservation of the momentum:

$$\frac{\partial(\rho u_i)}{\partial t}+\frac{\partial(\rho u_i u_j)}{\partial x_j}=-\frac{\partial p}{\partial x_i}+\frac{\partial \tau_{ij}}{\partial x_j}+\rho f_i \tag{2}$$

The conservation of the energy:

$$\frac{\partial}{\partial t}\rho\left(e+\frac{1}{2}u_i u_i\right)+\frac{\partial}{\partial x_j}\left[\rho u_j\left(h+\frac{1}{2}u_i u_i\right)\right]=\frac{\partial}{\partial x_j}\left(\sigma_{ij}u_i\right)-\frac{\partial q_j}{\partial x_j} \tag{3}$$

where ρ is the air density, u_i is the i-th component of the velocity vector, x_i is the i-th component of the position vector, p is the air pressure, e is the specific internal energy, and h is the specific enthalpy, q_j is the j-th component of the heat flux vector, and σ_{ij} is the stress tensor.

The Navier-Stokes equations are resolved using the RANS method coupled with one of the following turbulence models.

Spalart–Allmaras model

The one-equation Spalart-Allmaras turbulence model was originally presented in 1992 and has been widely used in aerospace and defence industry (Spalart & Allmaras, 1992). Its transport equation is as follows:

$$\begin{aligned}&\frac{\partial}{\partial t}\left(\rho\tilde{\nu}\right)+\frac{\partial}{\partial x_i}\left(\rho\tilde{\nu}u_i\right)=\\&=G_\nu+\frac{1}{\sigma_{\tilde{\nu}}}\left\{\frac{\partial}{\partial x_j}\left[\left(\mu_t+\rho\tilde{\nu}\right)\frac{\partial\tilde{\nu}}{\partial x_j}\right]+C_{b2}\rho\left(\frac{\partial\tilde{\nu}}{\partial x_j}\right)^2\right\}-Y_\nu+S_{\tilde{\nu}}\end{aligned} \tag{4}$$

where $\tilde{\nu}$ is the eddy viscosity, μ_t is the turbulent viscosity coefficient, C_{b2} is a constant, G_ν is the production term, Y_ν is the destruction term, and $S_{\tilde{\nu}}$ is the user-defined source term.

The turbulent viscosity coefficient μ_t is determined as follows:

$$\mu_t=\rho\tilde{\nu}f_{\nu 1},\ f_{\nu 1}=\frac{\chi^3}{\chi^3+c_{\nu 1}^3},\ \chi=\frac{\tilde{\nu}}{\nu}\ , \tag{5}$$

The production term G_ν is given by:

$$G_v = C_{b1}\rho\tilde{S}\tilde{v}\ ,\ \tilde{S} = S + \frac{\tilde{v}}{\kappa^2 d^2} f_{v2}\ ,\ f_{v2} = 1 - \frac{\chi}{1+\chi f_{v1}} \tag{6}$$

where C_{b1} and κ are constants, *d* is the distance from the wall, f_{v1} and f_{v2} are damping functions, and *S* is a scalar measure of the deformation tensor and is determined as follows:

$$S = \sqrt{2\Omega_{ij}\Omega_{ij}}\ ,\ \Omega_{ij} = \frac{1}{2}\left(\frac{\partial u_i}{\partial x_i} - \frac{\partial u_j}{\partial x_j}\right) \tag{7}$$

The destruction term is calculated as follows:

$$Y_v = C_{\omega 1}\rho f_\omega \left(\frac{\tilde{v}}{d}\right)^2\ ,\ f_\omega = g\left(\frac{1+C_{\omega 3}^6}{g+C_{\omega 3}^6}\right)^{1/6} \tag{8}$$

where $g = r + C_{\omega 2}\left(r^6 - r\right)$, $r = \frac{\tilde{v}}{\tilde{S}\kappa^2 d^2}$, and (9)

$C_{\omega 1}$, $C_{\omega 2}$ and $C_{\omega 3}$ are constants. The values of the model constants were provided by Spalart and Allmaras (Spalart & Allmaras, 1992).

Standard k-ε model

The *k-ε* turbulence model was proposed by Launder & Spalding (1974). It enables to take into account turbulent eddy viscosity using kinetic energy *k* and dissipation rate *ε*. These parameters are defined by:

$$\frac{\partial(\rho k)}{\partial t} + u\frac{\partial(\rho k)}{\partial x} + v\frac{\partial(\rho k)}{\partial y} + w\frac{\partial(\rho k)}{\partial z} = \frac{\partial}{\partial x}\left[\left(\mu + \frac{\mu_t}{\sigma_k}\right)\frac{\partial k}{\partial x}\right] + \tag{10}$$
$$= \frac{\partial}{\partial y}\left[\left(\mu + \frac{\mu_t}{\sigma_k}\right)\frac{\partial k}{\partial y}\right] + \frac{\partial}{\partial z}\left[\left(\mu + \frac{\mu_t}{\sigma_k}\right)\frac{\partial k}{\partial z}\right] + P_k - \rho\varepsilon,$$

$$\frac{\partial(\rho\varepsilon)}{\partial t} + u\frac{\partial(\rho\varepsilon)}{\partial x} + v\frac{\partial(\rho\varepsilon)}{\partial y} + w\frac{\partial(\rho\varepsilon)}{\partial z} = \frac{\partial}{\partial x}\left[\left(\mu + \frac{\mu_t}{\sigma_k}\right)\frac{\partial \varepsilon}{\partial x}\right] + \tag{11}$$
$$= \frac{\partial}{\partial y}\left[\left(\mu + \frac{\mu_t}{\sigma_k}\right)\frac{\partial \varepsilon}{\partial y}\right] + \frac{\partial}{\partial z}\left[\left(\mu + \frac{\mu_t}{\sigma_k}\right)\frac{\partial \varepsilon}{\partial z}\right] + P_k C_{1\varepsilon}\frac{\varepsilon}{k} - \rho C_{2\varepsilon}\frac{\varepsilon^2}{k}$$

where the function P_k is defined as:

$$P_k = \tau_{xx}\frac{\partial u}{\partial x} + \tau_{xy}\frac{\partial u}{\partial y} + \tau_{xz}\frac{\partial u}{\partial z} + \tau_{yx}\frac{\partial v}{\partial x} + \tau_{yy}\frac{\partial v}{\partial y} + \tau_{yz}\frac{\partial v}{\partial z} + \\ + \tau_{zx}\frac{\partial w}{\partial x} + \tau_{zy}\frac{\partial w}{\partial y} + \tau_{zz}\frac{\partial w}{\partial z}, \quad (12)$$

where k is the kinetic energy, ε is the dissipation rate, E_{ij} represents the component of the rate of deformation, and μ_t represents the eddy viscosity. $C_{1\varepsilon}$, $C_{2\varepsilon}$, σ_k and σ_ε are constant numbers: $C_{1\varepsilon}$ = 1.44, $C_{2\varepsilon}$ = 1.92, σ_k =1.00 and σ_ε = 1.30.

The turbulent viscosity coefficient μ_t is calculated using the equation below:

$$\mu_t = \rho C_\mu \frac{k^2}{\varepsilon}, \quad (13)$$

where the parameter C_μ is a constant number, C_μ = 0.0845.

Realizable k-ε model

The Realizable k-ε is a modification to the Standard k-ε turbulence model to enhance its performance. It was first presented by Shih et al. (1994). The transport equations for k and ε of this model are given as follows:

$$\frac{\partial}{\partial t}(\rho k) + \frac{\partial}{\partial x_j}(\rho k u_j) = \\ = \frac{\partial}{\partial x_j}\left[\left(\mu + \frac{\mu_t}{\sigma_k}\right)\frac{\partial k}{\partial x_j}\right] + G_k + G_b - \rho\varepsilon - Y_M + S_k \quad (14)$$

$$\frac{\partial}{\partial t}(\rho\varepsilon) + \frac{\partial}{\partial x_j}(\rho\varepsilon u_j) = \\ = \frac{\partial}{\partial x_j}\left[\left(\mu + \frac{\mu_t}{\sigma_\varepsilon}\right)\frac{\partial \varepsilon}{\partial x_j}\right] + \rho C_1 S\varepsilon - \rho C_2 \frac{\varepsilon^2}{k + \sqrt{\upsilon\varepsilon}} + C_{1\varepsilon}\frac{\varepsilon}{k}C_{3\varepsilon}G_b + S_\varepsilon \quad (15)$$

where $C_1 = max\left[0.43, \frac{n}{n+5}\right]$, $n = S\frac{k}{\varepsilon}$, $S = \sqrt{2S_{ij}S_{ij}}$; G_k is the turbulence kinetic energy due to the mean velocity gradients; G_b is the turbulence kinetic energy due to the buoyancy; Y_M is the contribution of the fluctuating

dilatation on compressible turbulence to the overall dissipation rate; S_k and S_ε are the user-defined source terms; and C_2, $C_{1\varepsilon}$, and $C_{3\varepsilon}$ are constants of the model (Shih et al, 1994).

Standard k-ω model

The Standard k-ω model is a two-equation turbulence model developed by Wilcox and first introduced in 1998 (Wilcox, 1998). It is based on the turbulent kinetic energy *k* and the specific dissipation rate *ω*. The transport equations for *k* and *ω* are as follows:

$$\frac{\partial}{\partial t}(\rho k)+\frac{\partial}{\partial x_i}(\rho k u_i)=\frac{\partial}{\partial x_j}\left(\Gamma_k \frac{\partial k}{\partial x_j}\right)+G_k-Y_k+S_k \tag{16}$$

$$\frac{\partial}{\partial t}(\rho \omega)+\frac{\partial}{\partial x_i}(\rho \omega u_i)=\frac{\partial}{\partial x_j}\left(\Gamma_\omega \frac{\partial \omega}{\partial x_j}\right)+G_\omega-Y_\omega+S_\omega \tag{17}$$

where G_k is the turbulence kinetic energy due to the mean velocity gradients; G_ω is the generation of *ω*; Γ_k and Γ_ω are respectively the effective diffusivity of *k* and *ω*; Y_k and Y_ω are respectively the dissipations of *k* and ω due to the turbulence; and S_k and S_ω are the user-defined source terms.

Γ_k and Γ_ω are defined as follows:

$$\Gamma_k=\mu+\frac{\mu_t}{\sigma_k},\ \Gamma_\omega=\mu+\frac{\mu_t}{\sigma_\omega} \tag{18}$$

where σ_k and σ_ω are respectively the turbulent Prandtl numbers for *k* and *ω*, and the turbulent viscosity is determined through the following expression:

$$\mu_t=\alpha^*\frac{\rho k}{\omega} \tag{19}$$

The turbulence kinetic energy G_k is calculated as:

$$G_k=-\rho\overline{u_i' u_j'}\frac{\partial u_j}{\partial x_i} \tag{20}$$

The quantity G_ω is defined as:

$$G_\omega = \alpha \frac{\omega}{k} G_k \tag{21}$$

where α and α^* are the closure coefficients of the model (Wilcox, 1998).

The dissipations Y_k and Y_ω are determined as follows:

$$Y_k = \rho\beta^* f_{\beta^*} k\omega,\ Y_\omega = \rho\beta^* f_{\beta^*} \omega^2 \tag{22}$$

The values of the model constants are: $\sigma_{k,1}$ = 1.176, $\sigma_{\omega,1}$ = 2.0, $\sigma_{k,2}$ = 1.0, $\sigma_{\omega,2}$ = 1.168, $\beta_{i,1}$ = 0.075, $\beta_{i,2}$ = 0.0828, β^* = 0.09, k = 0.41.

Shear Stress Transport (SST) k-ω model

The SST k-ω turbulence model was introduced by Menter (1994). It is a two-equation eddy-viscosity model which has been used for a wide variety of aerodynamic applications. This turbulence model blends the k-ε and the k-ω models to combine their advantages. The two transport equations are defined as follows:

$$\frac{\partial}{\partial t}(\rho k) + \frac{\partial}{\partial x_i}(\rho k u_i) = \frac{\partial}{\partial x_j}\left(\Gamma_k \frac{\partial k}{\partial x_j}\right) + G_k - Y_k + S_k \tag{23}$$

$$\frac{\partial}{\partial t}(\rho \omega) + \frac{\partial}{\partial x_i}(\rho \omega u_i) = \frac{\partial}{\partial x_j}\left(\Gamma_\omega \frac{\partial \omega}{\partial x_j}\right) + G_\omega - Y_\omega + D_\omega + S_\omega \tag{24}$$

Here D_ω is the the cross-diffusion term.

The turbulent viscosity coefficient μ_t is computed as follows:

$$\mu_t = \frac{\rho k \alpha_1}{\max\left[\alpha_1 \omega,\ SF_2\right]}, \tag{25}$$

where α_1 is a constant of the turbulence model, S is the strain rate magnitude, and F_2 is a blending function.

In the SST k-ω model, the turbulent Prandtl numbers σ_k and σ_ω are defined as:

$$\sigma_k = \frac{1}{\frac{F_1}{\sigma_{k,1}} + \frac{1-F_1}{\sigma_{k,2}}},\ \sigma_\omega = \frac{1}{\frac{F_1}{\sigma_{\omega,1}} + \frac{1-F_1}{\sigma_{\omega,2}}} \tag{26}$$

where F_1 is a blending function and $\sigma_{k,1}$, $\sigma_{k,2}$, $\sigma_{\omega,1}$, and $\sigma_{\omega,2}$ are constants.

The parameters G_k and G_ω are defined as:

$$G_k = min\left(G_k, 10\rho\beta^* k\omega\right),\ G_\omega = \frac{\alpha}{\upsilon_t} G_k, \tag{27}$$

where β^* is a constant the value of which is 0.09, $\upsilon_t = k / \omega$.

The cross-diffusion term D_ω is determined as follows:

$$D_\omega = 2\left(1 - F_1\right)\rho\sigma_{\omega,2}\frac{1}{\omega}\frac{\partial k}{\partial x_j}\frac{\partial \omega}{\partial x_j} \tag{28}$$

The values of the constants in the SST k-ω model are as the same as of the constants in the Standard k-ω model.

Projectile geometry

The 7.62mm M118 sniper projectile has been widely used and its aerodynamics has been studied experimentally (McCoy, 1988). Therefore, this projectile will be used for the evaluation of the turbulence models. The M118 projectile configuration reproduced from published work (McCoy, 1988) is presented in Figure 1 (all measurements are in mm). The total length of the bullet is 32.76mm. The bullet bearing cylinder diameter is 7.82mm. The bullet secant ogive nose is 16.89mm in length with a 55mm radius. Additionally, the 9.30-degree filleted boattail is 5.78mm of length and the meplat diameter is 1.40mm. The projectile 3D model created using Inventor 2021 software (Figure 2) is imported into Ansys Fluent for the subsequent numerical simulation.

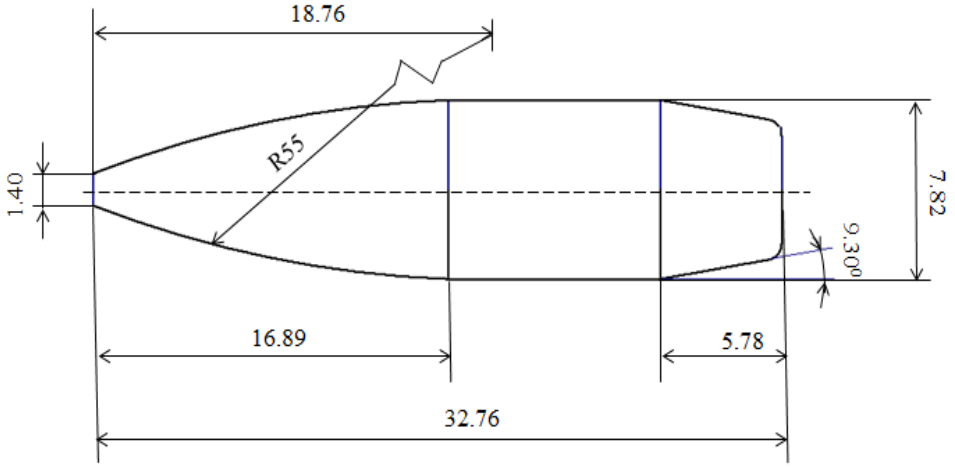

Figure 1 – M118 projectile dimensions (in mm)

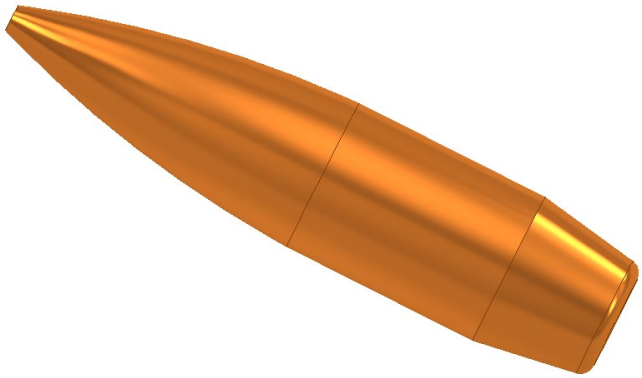

Figure 2 – 3D geometry model of the M118 projectile

Computational approach

Computational domain

The numerical simulation of the flow around the projectile was performed using the Ansys Fluent package (Matsson, 2023). A rectangular computational domain is adopted in this research as illustrated in Figure 3. The computational domain has to be large enough to capture the complex features of the flow around the projectile. Hence, in this study, the dimensions of the computational domain are set to a length of 50L, a height of 10L, and a width of 10L. Here L is the total length of the projectile (L = 32.76mm).

Solver setup and boundary conditions

The simulation employed the pressure-based solver and the finite volume method with the second order of accuracy for pressure, density, momentum, and turbulent kinetic energy. The Coupled algorithm was adopted in this study. The air is considered the ideal gas. The air viscosity model is the three component Sutherland model. The computational domain was set with the following boundary conditions: inlet, outlet, and wall. For the inlet flow, static pressure, static temperature and velocity were defined. The static pressure was set for the outlet flow. The wall was established as non-slip. The atmosphere parameters were set as follows: p_0 = 101325*Pa* and T_0 = 288,16*K.* The convergence criterion was set to 10^{-3} to the residuals of the solution.

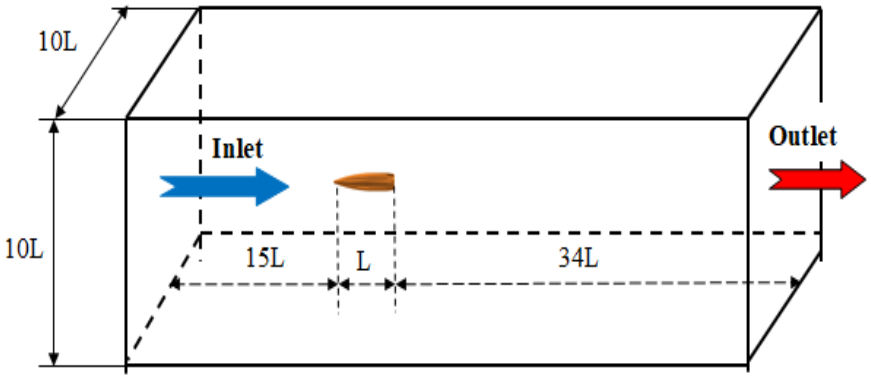

Figure 3 – Computational domain

Results and discussion

The numerical determination of the aerodynamic drag coefficient of the M118 projectile was performed at subsonic and supersonic speeds using five different turbulence models, namely, the Spalart-Allmaras, the Standard k-ε, the Realizable k-ε, the Standard k-ω and the SST k-ω turbulence models to investigate their ability to describe the flows around a generic spin-stabilized projectile.

Comparative performance of the turbulence models at subsonic flow

To evaluate the performance of different turbulence models at the subsonic flow, the aerodynamic zero-yaw drag coefficient was computed at the Mach number of 0.8 using the five abovementioned turbulence models. First, a mesh independence study was conducted to ensure that the simulation result is not affected by the mesh size. In the process of mesh generation, the dimensionless distance y+ was set below 1 for the Spalart-Allmaras, the Standard k-ω, and the SST k-ω turbulence models to better resolve the turbulent boudary layer. In the case of the Standard k-ε and the Realizable k-ε models, the y+ value was maintained at around 30 for better wall treatment with wall functions. The mesh size was then gradually increased by adjusting the size of elements on the projectile surface and in the computation domain to get better resolution. The computation results of the zero-yaw aerodynamic drag coefficient (C_d) of the M118 projectile for different turbulence models and mesh sizes are presented in Table 1.

Table 1 – Computational drag coefficients obtained with different turbulence models and mesh sizes at Mach 0.8

Turbulence models	Mesh size (Million elements)	C_d
Spalart-Allmaras	0.326	0.168
	2.514	0.131
	3.653	**0.128**
	5.273	0.128
Standard k-ω	0.326	0.175
	2.514	0.127
	3.653	**0.113**
	5.273	0.113
SST k-ω	0.326	0.158
	2.514	0.119
	3.653	**0.114**
	5.273	0.114
Standard k-ε	0.309	0.167
	2.392	0.125
	3.266	**0.118**
	4.886	0.118
Realizable k-ε	0.309	0.163
	2.392	0.116
	3.266	**0.110**
	4.886	0.110

It can be seen from Table 1 that for the Spalart-Allmaras, the Standard k-ω and the SST k-ω turbulence models, from the mesh size of 3.653 million elements, the drag coefficients remain unchanged with the subsequent increase of the mesh size. Meanwhile, for the Standard k-ε and the Realizable k-ε models, from the mesh size of 3.266 million elements, the drag coefficients also remain unchanged with the subsequent increase of the mesh size. Consequently, the drag coefficients with the mesh sizes of 3.653 and 3.266 million elements can be taken as computational drag coefficients for the respective investigated turbulence models. The drag coefficient of the M118 projectile obtained experimentally is 0.132 (McCoy, 1988). The comparison of the drag

coefficients obtained computationally against the experimental data is presented in Table 2.

Table 2 – Comparison of the computational drag coefficients with different turbulence models against the experimental data at Mach 0.8

Turbulence models	Computational C_d	Experimental C_d	Difference
Spalart-Allmaras	0.128	0.132	3.0%
Standard k-ω	0.113		14.4%
SST k-ω	0.114		13.6%
Standard k-ε	0.118		10.6%
Realizable k-ε	0.110		16.6%

Obviously, the drag coefficient obtained with the Spalart-Allmaras model is the closest to the experimental value (the discrepancy is only 3.0%), while the differences between the drag coefficients obtained with four remaining turbulence models and the experimental value are greater than 10%. Additionally, the Realizable k-ε has shown the lowest prediction of the drag coefficient. The Standard k-ω and the SST k-ω turbulence models have given similar values of aerodynamic drag coefficients. Except the Spalart-Allmaras model, the remaining models have a significantly underpredicted aerodynamic drag coefficient. Overall, it can be concluded that the Spalart-Allmaras is the most adequate turbulence model to predict the aerodynamic drag of a spin-stabilized projectile at subsonic speed.

Comparative performance of the turbulence models at supersonic flow

In this section, the aerodynamic zero-yaw drag coefficient of the M118 projectile was obtained using CFD simulation at the Mach number of 1.8 with five turbulence models of interest and compared against experimental data to assess the capability of each turbulence model at the supersonic flow regime. The research strategy used previously for the subsonic flow is also adopted for the supersonic flow here. In the end, the simulation results of the aerodynamic drag coefficients with different turbulence models and mesh sizes are presented in Table 3.

Clearly, the mesh independence study has indicated that from the mesh sizes of 3.653 million elements for the Spalart-Allmaras, the Standard k-ω and the SST k-ω models and of 3.344 million elements for the Standard k-ε and the Realizable k-ε models, the subsequent additional

mesh refinements will not change the simulation results. Therefore, the aerodynamic drag coefficients obtained with these mesh sizes can be accepted as the computational drag coefficients for the respective turbulence models.

Table 3 – Computational drag coefficients obtained with different turbulence models and mesh sizes at Mach 1.8

Turbulence models	**Mesh size (Million elements)**	**C_d**
Spalart-Allmaras	0.326	0.389
	2.522	0.377
	3.653	**0.374**
	5.273	0.374
Standard k-ω	0.326	0.370
	2.522	0.345
	3.653	**0.328**
	5.273	0.328
SST k-ω	0.326	0.369
	2.522	0.351
	3.653	**0.348**
	5.273	0.348
Standard k-ε	0.311	0.382
	2.436	0.352
	3.344	**0.348**
	4.963	0.348
Realizable k-ε	0.311	0.380
	2.436	0.338
	3.344	**0.335**
	4.963	0.335

To assess the performance of the turbulence models, the computational aerodynamic drag coefficients are compared to the experimental data (McCoy, 1988) as presented in Table 4.

It is evident that the drag coefficients obtained using the SST k-ω, the Standard k-ε and the Realizable k-ε models are the closest to the

experimental value with the discrepancies of 2.0%, 2.0% and 1.8%, respectively. The Spalart-Allmaras model has significantly overpredicted the aerodynamic drag with the discrepancy of nearly 10%, meanwhile the Standard k-ω has slightly underpredicted the aerodynamic drag with the discrepancy of 3.8%. Therefore, these observations lead to the conclusion that it is appropriate to apply the SST k-ω, the Standard k-ε or the Realizable k-ε turbulence model in predicting the aerodynamic drag of a spin-stabilized projectile flying at supersonic speed.

Table 4 – Comparison of the computational drag coefficients with different turbulence models against the experimental data at Mach 1.8

Turbulence models	**Computational C_d**	**Experimental C_d**	**Difference**
Spalart-Allmaras	0.374	0.341	9.7%
Standard k-ω	0.328		3.8%
SST k-ω	0.348		2.0%
Standard k-ε	0.348		2.0%
Realizable k-ε	0.335		1.8%

Conclusion

In this study, the comparative performance of five distinct turbulence models in predicting the aerodynamic drag coefficient of the M118 projectile at subsonic and supersonic flows was numerically investigated. In summary, the following conclusions can be drawn from the study:

Firstly, CFD is a powerful numerical tool to study the flow around projectiles as well as to predict their aerodynamic characteristics. The obtained simulation results have shown a good agreement with the experimental data measured from spark range firings.

Secondly, the turbulence models perform differently at different flow regimes. In general, the Spalart-Allmaras is the most suitable turbulence model for the subsonic flow, meanwhile the Standard k-ε, the Realizable k-ε and the SST k-ω turbulence models are recommended for the supersonic flow regime.

The findings in this study provide necessary guidance for the selection of an appropriate turbulence model to predict and analyze the aerodynamic characteristics of a spin-stabilized projectile. The comparative result obtained in the present research is a significant contribution to the field of computational aerodynamics for better

understanding the capability of the available turbulence models in the RANS approach.

Future work

Although the presented study has shed light on some questions regarding the performance of five most widely used turbulence models on the aerodynamic drag coefficient prediction, further work needs to be done to establish whether each of the turbulence models is suitable for predicting dynamic aerodynamic coefficients, such as roll-damping moment coefficient, pitch-damping moment coefficient, Magnus force and moment coefficients of a spin-stabilized projectile. Therefore, further analysis of dynamic aerodynamic coefficients would be recommended for a deeper understanding of the ability of the existing turbulence models.

References

Bui, X.S., Nguyen, Q. T., Nguyen, H. M. & Doan, V.D. 2024. Theoretical study on the sabot separation process of a sub-caliber projectile fired from rifled guns. *Defense and Security Studies*, 5, pp.29-45. Available at: https://doi.org/10.37868/dss.v5.id264.

Demir, H., Cimen, M., Yilman, O. & Tekin, E. 2024. Computational Fluid Dynamics Analysis of Drag Reduction in Bullet via Geometric Modifications. *Bayburt University Journal of Science*, 7(1), pp.47-56. Available at: https://doi.org/10.55117/bufbd.1493857.

Ferfouri, A., Allouche, T., Jerković, D.D., Hristov, N., Vučković, M. & Benmeddah, A. 2023. Prediction of drag aerodynamic coefficient of the 155 mm projectile under axisymmetric flow using different approaches. *Journal of the Serbian Society for Computational Mechanics*, 17(2), pp.69-86. Available at: https://doi.org/10.24874/jsscm.2023.17.02.06.

Gholap, T.B., Salokhe, R.V., Ghadage, G.V., Mane, S.V. & Sahoo, D. 2022. Aerodynamic analysis of an AK-47 bullet moving at Mach 2.0 in close proximity to the ground. *FME Transactions*, 50(2), pp.369-381. Available at: https://doi.org/10.5937/fme2201369G.

Hamel, N. & Gagnon, E. 2011. CFD and Parametric Study on a 155 mm Artillery Shell Equipped with a Roll-Decoupled Course Correction Fuze. In: *29th AIAA Applied Aerodynamics Conference*, Honolulu, Hawaii, June 27-30. Available at: https://doi.org/10.2514/6.2011-3027.

Hao, B., Jiang, Q., Xu, C. & Liu, L. 2024. Aerodynamic Characterization of Bullet Heads with Different Arcuate Curves. *Journal of Applied Fluid Mechanics*, 17(5), pp.1015-1026. Available at: https://doi.org/10.47176/jafm.17.05.2333.

Jang, Y., Huh, J., Lee, N., Lee, S. & Park, Y. 2018. Comparative Study on the Prediction of Aerodynamic Characteristics of Aircraft with Turbulence Models.

International Journal of Aeronautical & Space Sciences, 19, pp.13-23. Available at: https://doi.org/10.1007/s42405-018-0022-6.

Jiajan, W., Chue, R.S.M, Nguyen, T. & Yu, S.C.M. 2015. Boattail juncture shaping for spin-stabilized rounds in supersonic flight. *Shock Waves*, 25, pp.189-204. Available at: https://doi.org/10.1007/s00193-015-0550-y.

Julian, J., Iskandar, W. & Wahyuni, F. 2023. Effect of Mesh Shape and Turbulence Model on Aerodynamic Performance at NACA 4415. *Journal of Applied Fluid Mechanics*, 16(12), pp.2504-2517. Available at: https://doi.org/10.47176/jafm.16.12.1983.

Launder, B.E. & Spalding, D.B. 1974. The numerical computation of turbulent flows. *Computer Methods in Applied Mechanics and Engineering*, 3(2), pp.269-289. Available at: https://doi.org/10.1016/0045-7825(74)90029-2.

Luo, A.A., Xiao, Q.K., Liu, X., Guo, J.C. & Zhang, Y.H. 2024. Numerical Study on Aerodynamic Characteristics of Tail-stabilized Projectile with Asymmetrical Diversion Groove. *Journal of Applied Fluid Mechanics*, 17(1), pp.116-135. Available at: https://doi.org/10.47176/jafm.17.1.2062.

Matsson, J.E. 2023. *An Introduction to Ansys Fluent 2023*. Mission, KS, USA: SDC Publications. ISBN: 978-1-63057-648-6.

McCoy, R.L. 1988. *The aerodynamic characteristics of 7.62mm match bullets*. Defense Technical Information Center: U.S. Army Laboratory Command, Ballistic Research Laboratory, Aberdeen Proving Ground, Maryland [online]. Available at: https://apps.dtic.mil/sti/tr/pdf/ADA205633.pdf [Accessed: 07 November 2024].

Menter, F.R. 1994. Two-equation eddy-viscosity turbulence models for engineering applications. *AIAA Journal*, 32(8), pp.1598-1605. Available at: https://doi.org/10.2514/3.12149.

Muthukumaran, C.K., Rajesh, G. & Kim, H.D. 2013. Launch Dynamics of Supersonic Projectiles. *Journal of Spacecraft and Rockets*, 50(6), pp.1150-1162. Available at: https://doi.org/10.2514/1.A32466.

Nguyen, Q.T., Nguyen, H.M. & Son, B.X. 2024. Numerical investigation on the supersonic flow around a saboted bullet. *Vojnotehnički glasnik/Military Technical Courier*, 72(2), pp.676-694. Available at: https://doi.org/10.5937/vojtehg72-48837.

Sertkaya, A.A., Caliskan, C. & Neseli, S. 2022. Comparison of Real and Simulation Aerodynamic Coefficients for 155 mm Ammunition Using Open-Source Code SU2 Software. *Journal of Polytechnic*, 25(4), pp.1835-1845. Available at: https://doi.org/10.2339/politeknik.1133519.

Shih, T.-H., Liou, W.W., Shabbir, A., Yang, Z. & Zhu, J. 1994. A new k-ε eddy viscosity model for high Reynolds number turbulent flows. *Computers & Fluids*, 24(3), pp.227-238. Available at: https://doi.org/10.1016/0045-7930(94)00032-T.

Silton, S.I. 2002. *Navier-Stokes Computations for a Spinning Projectile From Subsonic to Supersonic Speeds*. Defense Technical Information Center: Army Research Laboratory, Aberdeen Proving Ground, Maryland [online]. Available at: https://apps.dtic.mil/sti/pdfs/ADA407616.pdf [Accessed: 07 November 2024].

Silton, S.I. 2005. Navier-Stokes Computations for a Spinning Projectile from Subsonic to Supersonic Speeds. *Journal of Spacecraft and Rockets*, 42(2), pp.223-231. Available at: https://doi.org/10.2514/1.4175.

Silton, S.I. 2011. Navier-Stokes Predictions of Aerodynamic Coefficients and Dynamic Derivatives of a 0.50-cal Projectile. In: *29th AIAA Applied Aerodynamics Conference*, Honolulu, Hawaii, June 27-3. Available at: https://doi.org/10.2514/6.2011-3030.

Somashekar, V. & Immanuel Selwyn Raj, A. 2021. Comparative Study on the Prediction of Aerodynamic Characteristics of Mini - Unmanned Aerial Vehicle with Turbulence Models. *International Journal of Aviation, Aeronautics, and Aerospace*, 8(1), art.number:7. Available at: https://doi.org/10.15394/ijaaa.2021.1559.

Spalart, P. & Allmaras, S. 1992. A one-equation turbulence model for aerodynamic flows. In: *30th Aerospace Sciences Meeting and Exhibit*, Reno, NV, USA, January 06-09. Available at: https://doi.org/10.2514/6.1992-439.

Wilcox, D.C. 1998. *Turbulence Modeling for CFD, 2nd Edition.* DCW industries La Canada.

Xu, Y., Dong, F. & Zheng, N. 2022. Ballistic and Aerodynamic Characteristics Simulation for Trajectory Correction Projectile. *Mechanika*, 28(3), pp.230-236. Available at: https://doi.org/10.5755/j02.mech.31431.

Un estudio comparativo de modelos de turbulencia para predecir la resistencia aerodinámica de un proyectil estabilizado por giro

Quang Tuan Nguyen

Universidad Técnica Le Quy Don, Facultad de Equipos Especiales, Hanói, República Socialista de Vietnam

CAMPO: ingeniería mecánica, dinámica de fluidos, balística exterior
TIPO DE ARTÍCULO: artículo científico original

Resumen:

Introducción/objetivo: En esta investigación, se analizó la influencia de diferentes modelos de turbulencia en la predicción de la resistencia aerodinámica de un proyectil genérico estabilizado por giro. Los modelos de turbulencia elegidos para la investigación fueron Spalart-Allmaras de una ecuación, los modelos de dos ecuaciones Standard k-ε, Realizable k-ε, Standard k-ω y SST k-ω. El proyectil especial de francotirador M118 se seleccionó para el estudio.

Métodos: Los flujos alrededor del proyectil se simularon numéricamente utilizando ecuaciones RANS integradas en el software ANSYS Fluent con diferentes modelos de turbulencia. La simulación numérica se llevó a cabo a varios números de Mach para estudiar el efecto de los modelos de turbulencia en la predicción de la resistencia aerodinámica del proyectil. Los resultados computacionales se compararon con los datos

experimentales disponibles para evaluar la capacidad de los modelos de turbulencia.

Resultados: Los resultados de la investigación han demostrado que los modelos de turbulencia afectan significativamente los resultados de la simulación numérica. El modelo de turbulencia de Spalart-Allmaras funciona mejor que otros modelos en el régimen de flujo subsónico. Los modelos Standard k-ε, Realizable k-ε y SST k-ω funcionan mejor que otros modelos en el régimen de flujo supersónico.

Conclusión: La dinámica computacional de fluidos es una herramienta poderosa para analizar la aerodinámica de cuerpos voladores. Al seleccionar adecuadamente los modelos de turbulencia, se puede investigar con precisión el flujo alrededor de los cuerpos voladores. En el caso de proyectiles genéricos de ojiva-cilindro-cola de barco, por un lado, el modelo de Spalart-Allmaras es adecuado para el flujo subsónico, y por otro lado, se recomiendan los modelos Standard k-ε, Realizable k-ε y SST k-ω para el régimen de vuelo supersónico.

Palabras claves: modelos de turbulencia, Ansys Fluent, proyectiles estabilizados por giro, flujo subsónico, régimen de vuelo supersónico.

Сравнительное исследование моделей турбулентности для прогнозирования аэродинамического сопротивления снаряда стабилизируемого вращением

Куанг Туан Нгуен

Государственный технический университет им. Ле Куй Дона,
факультет специального машиностроения,
г. Ханой, Социалистическая Республика Вьетнам

РУБРИКА ГРНТИ: 30.17.33 Газовая динамика,
30.17.53 Прикладная аэродинамика
ВИД СТАТЬИ: оригинальная научная статья

Резюме:

Введение/цель: В данной статье исследовано влияние различных моделей турбулентности на прогнозирование аэродинамического сопротивления снаряда, стабилизируемого вращением вокруг продольной оси. Для проведения исследования были выбраны следующие модели турбулентности: модель Спаларта-Аллмараса с одним уравнением, модель Standard k-ε с двумя уравнениями, Realizable k-ε, Standard k-ω и SST k-ω. В качестве снаряда был выбран специальный снайперский патрон M118.

Методы: Потоки вокруг снарядов были численно проанализированы с использованием уравнений RANS, интегрированных в программное обеспечение ANSYS Fluent с

различными моделями турбулентности. Численное моделирование было проведено при различных числах Маха с целью изучения влияния моделей турбулентности на прогнозирование аэродинамического сопротивления снарядов. Для проверки моделирования результаты вычислений были сравнены с имеющимися экспериментальными данными.

Результаты: Результаты исследований показали, что модели турбулентности оказывают существенное влияние на результаты численного моделирования. Модель турбулентности Спаларта-Аллмараса работает лучше других моделей при дозвуковом режиме течения. Модели Realizable k-ε и SST k-ω показали лучшие результаты при сверхзвуковом режиме течения.

Выводы: Вычислительная гидродинамика является эффективным инструментом для анализа аэродинамики летящих тел. Путем соответствующего выбора моделей турбулентности на разных скоростях можно с точностью испытать поток вокруг летящих тел. С одной стороны, для случаев типовых снарядов, таких как оживально-цилиндрическо-конический (boat tail), модель Спаларта-Аллмараса подходит для дозвукового режима течения. С другой стороны, модели Standard k-ω, Realizable k-ε и SST k-ω рекомендуются для сверхзвукового режима течения.

Ключевые слова: модели турбулентности, Ansys Fluent, стабилизируемые вращением снаряды, дозвуковой поток, сверхзвуковой режим полета.

Компаративна студија модела турбуленције за предвиђање аеродинамичког отпора код пројектила стабилизованог ротацијом око уздужне осе

Кван Туан Нуиен

Државни технички универзитет „Ле Куи Дон”,
Факултет специјалног машинства,
Ханој, Социјалистичка Република Вијетнам

ОБЛАСТ: машинство, динамика флуида, спољна балистика
КАТЕГОРИЈА (ТИП) ЧЛАНКА: оригинални научни рад

Сажетак:

Увод/циљ: У овом истраживању анализиран је утицај различитих модела турбуленције на предвиђање аеродинамичког отпора генеричког пројектила стабилизованог ротацијом око уздужне осе. Модели турбуленције који су одабрани за истраживање били су Spalart-Allmaras-ов модел са једном једначином, као и модели са две

једначине: Standard к-ε, Realizable к-ε, Standard к-ω и SST к-ω. За студију је одабран специјални снајперски метак М118.

Методе: Урађена је нумеричка симулација струјања око пројектила помоћу RANS једначина интегрисаних у софтверу ANSYS Fluent са различитим моделима турбуленције. Нумеричка симулација је изведена за различите бројеве Маха ради проучавања утицаја модела турбуленције на предвиђање аеродинамичког отпора пројектила. Резултати прорачуна упоређени су са доступним експерименталним подацима ради процене модела турбуленције.

Резултати: Показано је да модели турбуленције имају значајан утицај на резултате нумеричке симулације. Spalart-Allmaras-ов модел турбуленције показао се бољи од других модела у режиму подзвучног струјања, док су модели Realizable к-ε и SST к-ω ефикаснијиод других модела у режиму суперсоничног струјања.

Закључак: Рачунарска динамика флуида је моћан алат за анализу аеродинамике тела у лету. Струјање око тела у лету може се прецизно испитати помоћу одговарајућег избора модела турбуленције. Код типова генеричких пројектила, са оживално-цилиндричним и делимично конусним задњим делом (boat tail), модел Spalart-Allmaras је погодан за подзвучни режим струјања, док су, с друге стране, модели Standard k-ω, Realizable к-ε и SST к-ω погоднији за режим надзвучног струјања.

Кључне речи: модели турбуленције, Ansys Fluent, пројектили стабилизовани ротацијом око уздужне осе, подзвучно струјање, режим надзвучног лета.

Paper received on: 07.11.2024.
Manuscript corrections submitted on: 27.01.2025.
Paper accepted for publishing on: 28.01.2025.

Numerical optimization by the PFEMCT - SIF method of the crack propagation of a linear elastic material

Mohammed Bentahar[a], *Noureddine* Mahmoudi[b], *Youcef* Moulai Arbi[c]

[a] University of Saida Dr. Moulay Tahar, Faculty of Technology, Department of Civil Engineering and Hydraulics, Saida, People's Democratic Republic of Algeria, e-mail: bentahae@yahoo.fr, ORCID ID: https://orcid.org/0000-0002-2166-678X

[b] University of Saida Dr. Moulay Tahar, Faculty of Technology, Department of Civil Engineering and Hydraulics, Saida, People's Democratic Republic of Algeria, e-mail: mahmoudi.noureddine@yahoo.fr, ORCID ID: https://orcid.org/0000-0002-9740-0857

[c] Mustapha Stambouli University, Laboratory of Quantum Physics of Matter and Mathematical Modeling (LPQ3M), Mascara, People's Democratic Republic of Algeria, e-mail: youcef.moulaiarbi@univ-mascara.dz, **corresponding author**, ORCID ID: https://orcid.org/0000-0002-6534-8820

https://doi.org/10.5937/vojtehg73-52739

FIELD: mechanics
ARTICLE TYPE: original scientific paper

Abstract:

Introduction/purpose: This study investigates the influence of contour numbers surrounding the crack tip on stress intensity factors (SIFs) using the Propagation Finite Element Method Crack Tip Stress Intensity Factor (PFEMCT-SIF) approach. It also compares the maximum circumferential stress criterion (MCSC) and the Richard criterion for crack propagation prediction.

Methods: A finite element code written in Visual Fortran was developed to model crack tips with 3, 5, 10, 15 and 20 contours using 4-node quadratic CPE4 elements. Abaqus software was utilized to calculate SIFs and crack orientation angles. Horizontal and inclined cracks were analyzed in a steel plate under tensile loading. The results were validated against analytical solutions and previous numerical studies.

Results: The 10-contour model showed the best agreement with analytical SIF values. Increasing contour numbers improved SIF accuracy for horizontal cracks, but excessive refinement led to divergence for inclined cracks. The MCSC and the Richard criterion produced comparable crack trajectories, with the MCSC demonstrating slightly higher precision.

Conclusions: The PFEMCT-SIF method effectively evaluates SIFs and predicts crack propagation paths. A 10-contour crack tip model balances accuracy and computational efficiency. The study highlights the importance of optimizing crack tip mesh refinement in fracture mechanics simulations.

Key words: crack tip, crack propagation, SFEMCT-SIF method, MCSC and Richard criterion, contours.

Introduction

In fracture mechanics, crack propagation modeling by different numerical methods plays a beneficial role in solving various problems.

It is significantly used in fracture mechanics, structures calculation, materials fatigue and damage, etc. It also makes it possible to treat certain thermal, energetic and electromagnetic fatigue problems. Precise prediction of the fatigue life of components or structures creates a great interest in modeling and mechanical engineering applications. In this regard, there is now an increasing need to be able to accurately simulate initial cracks in structures. To solve various problems in fracture mechanics, application of numerical methods proves to be useful. Therefore, numerical methods have been widely developed in recent years, and remain among the most used methods and offer solutions for a very large number of applications.

Alshoaibi (2015) characterized the singularity and the stress intensity factors around the crack tip; he also used the motion extrapolation method to simulate crack propagation in 2D by the finite element method of a linear elastic plate.

Rao & Rahman (2000) used the EFGM method to eliminate the Lagrange multipliers drawbacks, typically used in the Galerkin formulations without elements. Boulenouar et al. (2014) used the displacement extrapolation technique to obtain the SIF at the crack front. Zaleha et al. (2007) evaluated the displacement extrapolation technique (DET) for the prediction of stress intensity factors. Cho (2015) evaluated the Petrov-Galerkin natural elements method (PG-NE), and proposed mixed modes to calculate the stress intensity factors of a two-dimensional inclined crack. (Boulenouar et al, 2016b) presented a study based on numerical examples demonstrating the efficiency, the robustness and the precision of the calculation algorithm allowing to predict the crack propagation path. Yaylaci (2016) proposed a comparative study between the finite element method (FEM) and the analytical method of a composite material with planar layers containing a perpendicular internal crack. However, Hamdi et al. (2007) used the strain energy density criterion on

filled rubber materials to predict the initial orientation of a central crack in the case of large strains. Thus, this criterion was validated in the two cases of fragile and ductile materials: fragile materials by Theocaris (1984), Boulenouar et al. (2013, 2016a), Ayatollahi & Sedighiani (2012), Pegorin et al. (2012), Choi et al. (2006) and ductile materials (Komori, 2005; Chow & Jilin, 1985; Carpinteri, 1984).

Another study proposed by Boulenouar & Bendida (2019) is based on the implementation of the displacement correlation technique (DCT) and the maximum circumferential stress (MCS) theory in a finite element code by the use of the Ansys Parametric Design Language (APDL).

A comparative study between the finite element method (FEM) and the analytical method was proposed by Yaylaci (2016) to solve a plane problem of a laminated composite material containing an internal perpendicular crack using Ansys software in elements finished for 2D analysis. On the other hand, a crack propagation study was presented by Bentahar & Benzaama (2023) and Bentahar et al. (2024) to evaluate the stress intensity factor by the FEM method.

For a precise estimation of stress intensity factors in mode I, II and the mixed mode, Sajith et al. (2018) proposed a simple and effective technique based on finite elements which uses nodal displacements of crack faces for a precise estimation of the stress intensity factors in mode I, II and in the mixed mode.

Malekan et al. (2018) presented a work based on the XFEM method to model nucleation and crack propagation in structures made of linear or non-linear materials. In addition, different energies were evaluated by Bentahar et al. (2021a) and by Bentahar (2023a, 2023b) using the XFEM method.

To obtain the stress intensity factors at the crack front, Benamara et al. (2017) proposed a study for homogeneous materials based on the displacement extrapolation technique (DET).

Using a Fortran program, Alshoaibi (2018) presented a numerical simulation-based study of crack growth, using the extrapolation technique of displacement to obtain singular stresses in the crack front and the values of the stress intensity factors. In addition, this method is used to find out the crack direction by the maximum circumferential stress criterion.

The aim of this study is to model the effect of the number of contours at the crack tip on the stress intensity factor by the (SFEMCT-SIF) method using the maximum circumferential stress criterion (MCSC) and the Richard criterion for 3, 5, 10, 15, and 20 contours around the crack tip region. In addition, this work uses Fortran to program correctly and control evenly the number of contours around the crack tip.

Law of fatigue crack propagation in 2D

To estimate the growth rate of fatigue cracks, Paris & Erdogan (1963) used the most common model, that of a crack stressed in pure mode I, with an applied load; the direction in this case is compatible.

It propagates depending on the material parameter and the environment. The value ΔKseuil lower than the amplitude of the stress intensity factor for a loading cycle $\Delta K_I = K_{Imax} - K_{Imin}$. (Figure 1) shows the three propagation regimes.

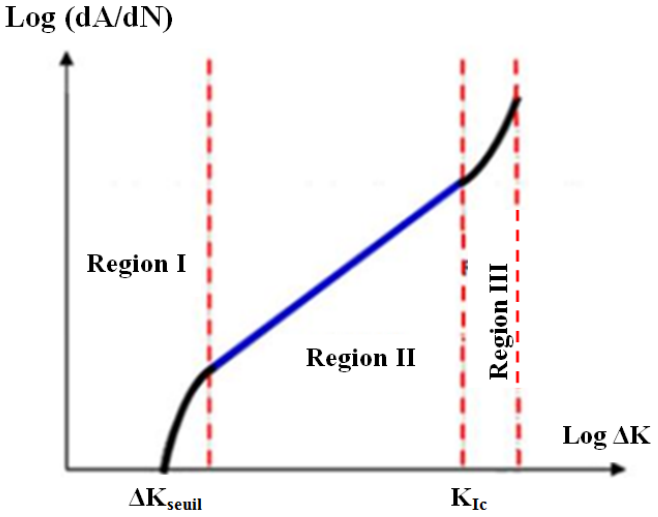

Figure 1 – Explanatory diagram of the three crack propagation regions in case of mode I

• In region I, the cracking rates in this regime are very low.

We observe the coalescence of microcracks and the formation of one or more macrocracks; for this, the value of ΔK is greater than ΔK_{seuil}.

• In region II, the cracking rate is linear. In this regime on the log − log diagram, the Paris law, defined by equation (1), establishes a linear relationship between log(da) and log(ΔK) – this is a so-called stable propagation regime

$$\frac{d_a}{d_N} = C\left(\Delta K\right)^m \tag{1}$$

where ΔK is the variation of the stress intensity factor during a cycle that induces an advance da of the crack, and C and m are two parameters of the material defining respectively the position and the slope of the Paris line.

Bentahar, M. et al, Numerical optimization by the PFEMCT -SIF method of the crack propagation of a linear elastic material, pp.136-161

• In region III, there is a so-called unstable propagation regime. It is characterized by a strong acceleration of the crack and ΔK tends towards the toughness of the material K_{Ic} which is experimentally observed during the rupture of the part.

The propagation speed is here higher than that expected in the Paris regime (region II).

Crack propagation criteria

In order to simulate crack propagation under the linear elastic condition, the crack path direction must be determined. There are several methods used to predict the direction of the crack trajectory such as the maximum normal stress theory (or the maximum circumferential stress theory (Erdogan & Sih, 1963) and the minimum strain energy density theory criteria (Sih, 1974).

Maximum circumferential stress criterion (MCSC)

The maximum circumferential stress criterion (MCSC) is a criterion that requires the calculation of the stress intensity factors K_I and K_{II} to determine this bending angle, on the one hand, and, on the other hand, it indicates that the crack always propagates in the direction of the maximum σθθ. This is because the direction of crack growth is directly determined by the local stress field along a small circle of the radius r centered at the crack tip:

$$tan\frac{\theta}{2} = \left[\frac{1}{4}\frac{K_I}{K_{II}} \pm \sqrt{\left(\frac{K_I}{K_{II}}\right)^2 + 8}\right] \tag{2}$$

where K_I and K_{II} are, respectively, the stress intensity factors corresponding to mode I and II loading.

Criterion of Richard 2D

This criterion was developed empirically by Richard (1985) and Rossmanith (1984). Here, the comparative stress intensity factor Kv is defined by equation (3):

$$\mathrm{K_v} = \frac{K_I}{2} + \frac{1}{2}\sqrt{\mathrm{K_I^2}} + 5.366\mathrm{K_{II}^2} = \mathrm{K_{Ic}} \tag{3}$$

KV is based on the stress intensity factors K_I and K_{II}, and the fracture toughness K_{IC} is related to K_V and crack growth is discontinuous when K_V is greater than K_{IC}. This criterion provides an excellent approximation of the fracture limit surface of the maximum tangential stress criterion of Erdogan & Sih (1963). The crack pucker angle θ can be determined by equation (4):

$$\theta = \mp\left[140^{\circ}\frac{|K_{II}|}{|K_I|+|K_{II}|} - 70^{\circ}\left(\frac{|K_{II}|}{|K_I|+|K_{II}|}\right)^2\right] \quad (4)$$

when the bending angle is θ< 0, K_{II} > 0, on the one hand, and, on the other hand, K_I always > 0.

Influence of the number of singularity area contours

Crack origin

The CT point is the crack front center and the starting point for creating the other nodes by this method. The coordinates of this point are given by equation (5):

$$\begin{Bmatrix}\mathrm{X(CT)} = a\\ \mathrm{Y(CT)} = 0\end{Bmatrix} \quad (5)$$

where
(a) is the crack length, and
(CT) is the crack tip designation.

Singularity zone

The singularity zone is found in the crack front zone (plasticization zone) where the stresses gradients and deformations are the most important; there, singular elements were used.

For the Abaqus simulation, the CPE4 type elements were chosen. This element type is used for 2D models, quadrilateral with four nodes, and it is well suited for simulation. Thus, singular elements are used around the crack front. These singular types "quarter point" elements are collapsed quadratic elements.

These elements are obtained by following different stages:

1. Move the knots from the side connecting the middle to the crack front "quarter-point" (L/4) closer to the crack front, making from this mode the singularity effect reproduction 1/√r.

2. Collapse one of the sides (2D) or one of the faces (3D) belonging to the crack front so that these nodes collapsed on this side or this face will have the same coordinates. The reason for this transformation from a quadrilateral or a quadrangular prism to a triangle or a triangular prism is that the first only shows a singular behavior around the singular point of the crack while the second reproduces singularity in its whole domain.

3. Restrict the coincident nodes on the collapsed side or face for a joint movement, i.e., completely united, which allows the reproduction of the singularity $1/\sqrt{r}$ - an elastic-linear behavior characteristic.

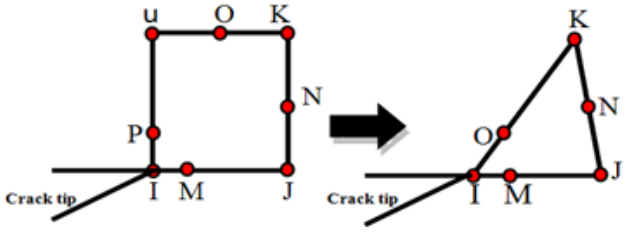

Figure 2 – Illustration of a quadrilateral element reduced to obtain a triangular element, (Bentahar et al, 2021b)

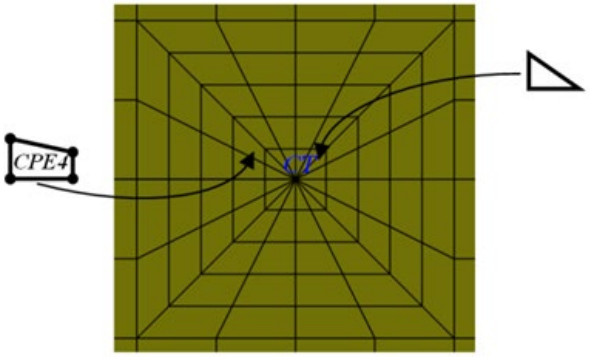

Figure 3 – Element types chosen for modeling.

Singularity zone outlines

From the point node (CT) of the crack point, the singular elements created by equation (6):

$$\begin{cases} x_i = X(CT) - j\dfrac{L}{t}\cos\big((i-1)\theta\big) \\ y_i = Y(CT) - j\dfrac{L}{t}\sin(i\theta) \end{cases} \tag{6}$$

i = 1.16 (number of elements in each contour);
j = 1, t (contour number); and
θ = π/16 (angle division).

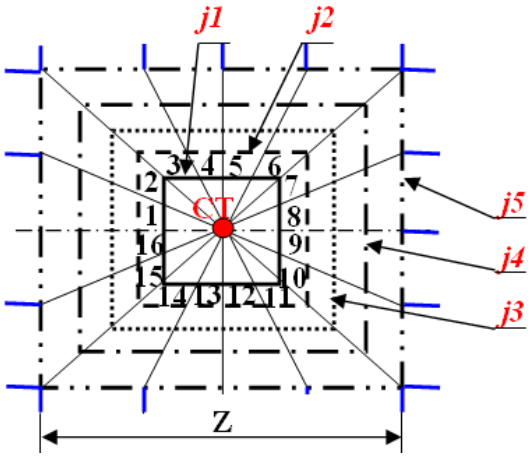

Figure 4 – Singularity zone with its contours and its elements - illustration.

Stress field in the crack front vicinity

Figure 4 illustrates the stress field near a crack point with the polar coordinates (r, θ) in the crack tip (CT) by equation (7).

$$\sigma_{i,j}^{I,II}(r,\theta) = \frac{K_{I,II}}{\sqrt{2\pi r}} f_{ij}(\theta) \tag{7}$$

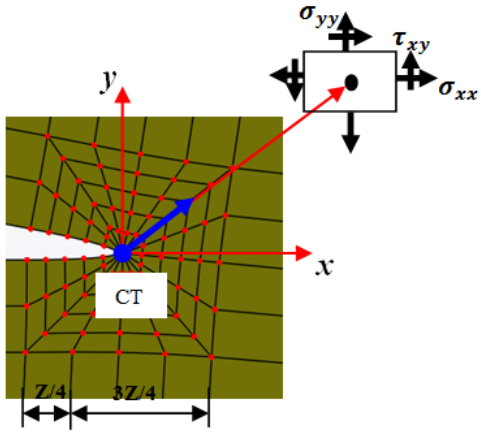

Figure 4 – Stress field in the crack tip (CT) - properties

Bentahar, M. et al, Numerical optimization by the PFEMCT -SIF method of the crack propagation of a linear elastic material, pp.136-161

The position of the stress field in the polar coordinates (r, θ) for an isotropic linear elastic material at the crack tip is determined by equation (8):

$$\sigma_{xx} = \frac{K_I}{\sqrt{2\pi r}}\cos\frac{\theta}{2}\left(1-\sin\frac{\theta}{2}\sin\frac{3\theta}{2}\right)$$
$$\sigma_{yy} = \frac{K_I}{\sqrt{2\pi r}}\cos\frac{\theta}{2}\left(1+\sin\frac{\theta}{2}\sin\frac{3\theta}{2}\right) \quad (8)$$
$$\tau_{xy} = \frac{K_I}{\sqrt{2\pi r}}\sin\frac{\theta}{2}\cos\frac{\theta}{2}\cos\frac{3\theta}{2}$$

Tada et al. (2000) proposed a general equation to describe the stress field in 2D in the crack front vicinity; the latter is defined by the stress intensity factor K.

Stress intensity factor

The stress intensity factor K is the only important parameter that allows to know the state of stress and deformation at any crack point, Fiordalisi (2014). For the crack in the opening position, the relationship between the distal stress perpendicular to the crack axis σ and the stress intensity factor K_I, is given analytically by equation (9) proposed by Ewalds & Wanhill (1984) and the correction factor (F) is given by equation (10):

$$K_I = F\sigma\sqrt{a\pi} \quad (9)$$

where F is the correction factor given by:

$$F = 1.12 - 0.23\left(\frac{a}{W}\right) + 10.6\left(\frac{a}{W}\right)^2 - 21.7\left(\frac{a}{W}\right)^3 + 30.4\left(\frac{a}{W}\right)^4 \quad (10)$$

where the stress intensity factor K_{II} is calculated by the relation:

$$K_I sin\theta + K_{II}(3cos\theta - 1) \quad (11)$$

Numerical model and simulation

Horizontal crack propagation

The structure considered has a length B of 12 mm and a width W of 10 mm. The horizontal crack length a is 3.5 mm and the length of the front Z is 1.5 mm. The parametric mesh consists of 478 square CPE4 type elements with four nodes. The total number of degrees of freedom is equal

to 1016. The Fortran program for creating the mesh that will be analyzed by the Abaqus finite element code has been applied. The steel structure with E = 210 GPa and v = 0.3 is subjected to a uniform tensile stress σ = 120 MPa. To study and characterize the stress field in the crack tip vicinity, a several front contour numbers are proposed for the optimization of this area and therefore, the stress intensity factor in the mixed mode is calculated. The mesh including the numbers of 3, 5, 10, 15, and 20 contours is analyzed while keeping the same type of CPE4 elements at 4 nodes.

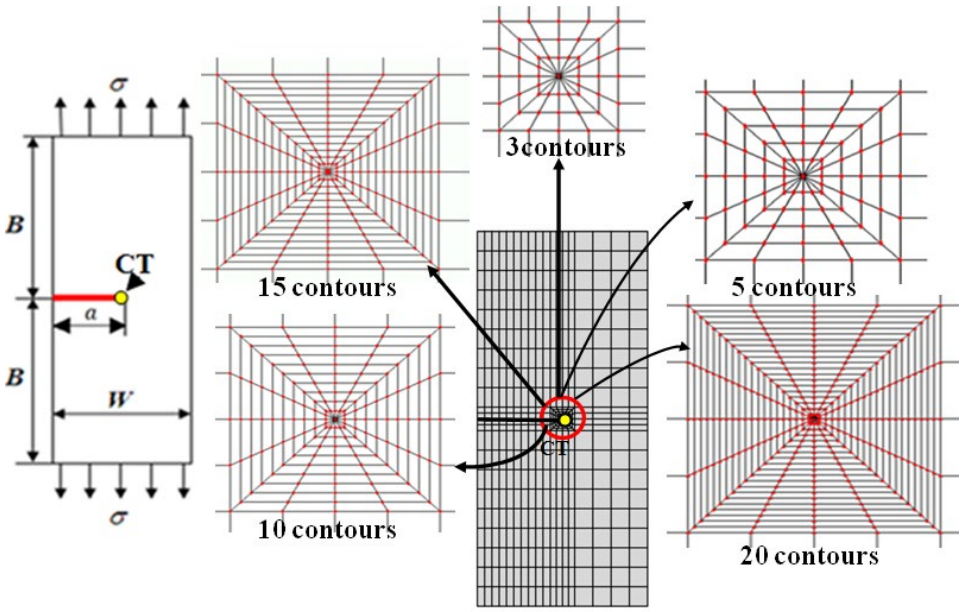

Figure 5 – a) Geometry model with boundary conditions and the proposed structure dimensions for a horizontal crack of the length a and b) PFEMCT-SIF model with different numbers of contours for the singularity zone

Figures 6a, b, and c illustrate a very long horizontal crack with different crack tip shapes used by Alshoaibi & Ariffin (2008), FRANC2D and the PFEMCT-SIF method. On the other hand, numerically, Figure 7 shows the three comparison methods presented by a) Phongthanapanich & Dechaumphai (2004), b) Rao & Rahman (2000) and c) PFEMCT-SIF method, in the case of a horizontal crack with an angle α = 0º and a = 3.5 mm. In addition, this study has different contours numbers (3, 5, 10, 15, and 20 contours). Table 1 below presents the comparison between the results obtained by the method (EFGM) proposed by Rao & Rahman (2000) and the results obtained by the PFEMCT-SIF method.

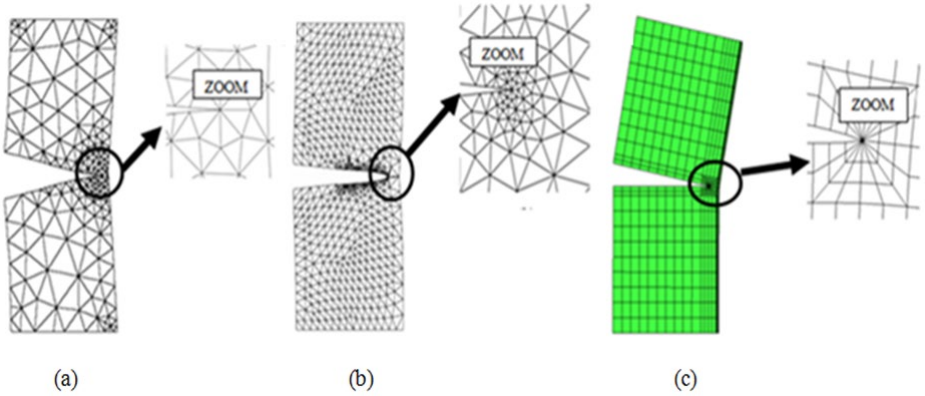

Figure 6 – Crack tip model: a) Alshoaibi & Ariffin (2008), b) FRANC2D, and c) PFEMCT-SIF method

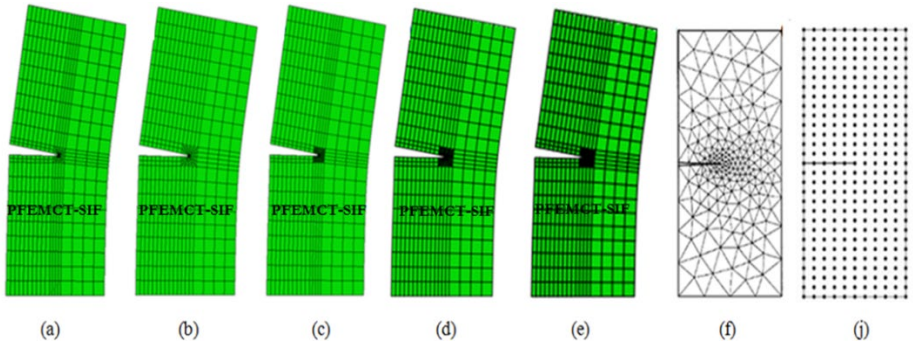

Figure 7 – Crack propagation in the case of α = 0°: a) 3 contours, b) 5 contours, c) 10 contours, d) 15 contours, and e) 20 contours, (f) Phongthanapanich & Dechaumphai (2004), and (j) Rao & Rahamen (2000)

Table 1 – Comparison of the results obtained by the PFEMCT-SIF method and the method proposed by Rao & Rahman (2000) concerning the stress intensity factors K_I and K_{II} in the case of different numbers of contours (3, 5, 10, 15, and 20 contours).

PFEMCT-SIF method										(Rao & Rahman, 2000)	
3 contours		5 contours		10 contours		15 contours		20 contours			
K_I	K_{II}	K_I	K_{II}	K_I	K_{II}	K_I	K_{II}	K_I	K_{II}	K_I	K_{II}
30.32	4.099	30.73	4.128	31.05	4.151	30.32	4.099	30.73	4.128	31.05	4.151
32.66	4.408	33.03	4.427	33.30	4.440	32.66	4.408	33.03	4.427	33.30	4.440
32.92	4.453	33.31	4.475	33.60	4.492	32.92	4.453	33.31	4.475	33.60	4.492
32.62	4.465	33.36	4.482	33.65	4.499	32.62	4.465	33.36	4.482	33.65	4.499
32.78	4.471	33.37	4.484	33.67	4.500	32.78	4.471	33.37	4.484	33.67	4.500
32.78	4.471	33.37	4.484	33.67	4.500	32.78	4.471	33.37	4.484	33.67	4.500

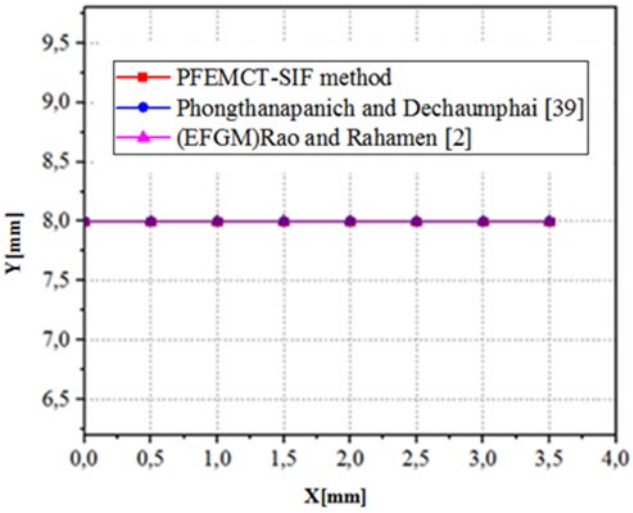

(a)

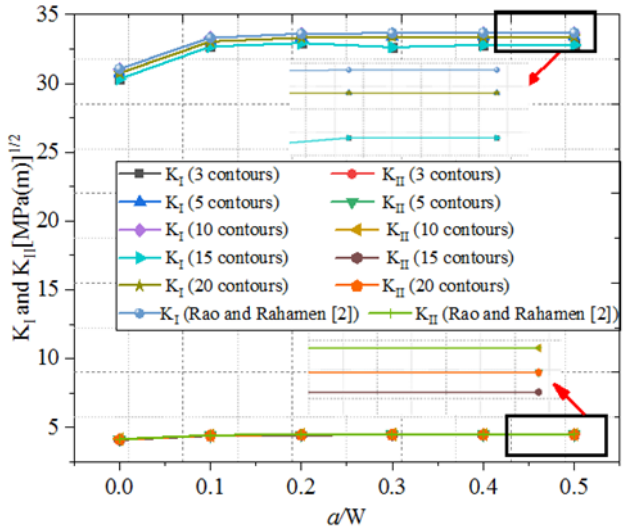

(b)

Figure 8 – (a) Crack trajectory obtained by the three methods and (b) comparison between the results obtained by the method proposed by Rao & Rahman (2000) and the the PFEMCT-SIF for different numbers of contours.

Figure 8 shows the comparison of the crack propagation in mode I, of the length a = 3.5mm between the three methods (EFGM) proposed by Rao & Rahman (2000), Adaptive Delaunay triangulation proposed by

Phongthanapanich & Dechaumphai (2004) and the PFEMCT-SIF method presented for different numbers of contours (3, 5, 10, 15, and 20 contours). In the case of α = 0º, the crack trajectory remains very comparable.

Figure 8b shows the evaluation of the SIF between the PFEMCT-SIF method presented for different numbers of contours and the method proposed by Rao & Rahman (2000); it can be noted that the comparison between these results allows to conclude that the numerical model used correctly describes the stress and strain field near the crack tip (CT) in the conditions of pure mode I. The comparison was made in the cases of the ratios a/w = 0.1, 0.2, 0.3, 0.4 and 0.5. It can be noted that the results obtained are the best.

Inclined horizontal crack propagation

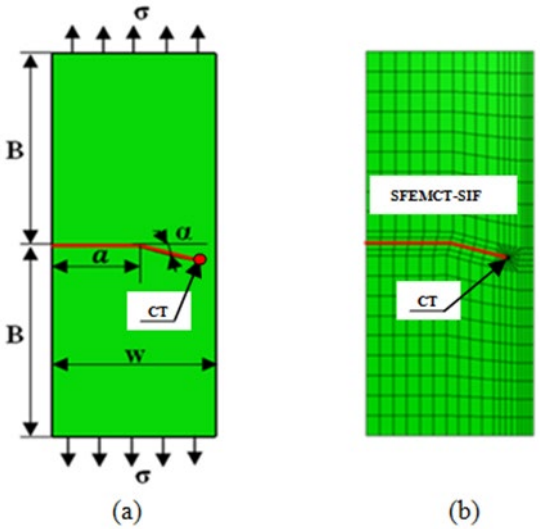

Figure 9 – a) Inclined horizontal crack proposed model geometry of the length a and the inclination angle α for five propagations, and b) inclined horizontal crack PFEMCT-SIF model

Figure 10 illustrates the crack propagation trajectory concerning the angle of crack α= -15.60º with 3, 5, 10, 15, and 20 contours, by the PFEMCT-SIF method in the first propagation.

Figure 11 presents the crack trajectory comparison in modes I and II in the case of a = 6.8 mm between the three methods: the EFGM proposed by Rao & Rahman (2000), the adaptive Delaunay triangulation method proposed by Phongthanapanich and Dechaumphai (2004) and the

PFEMCT-SIF method presented in this study for different numbers of contours (3, 5, 10, 15, and 20 contours).

Figure 12 shows the comparison of the crack trajectory between the study presented by Phongthanapanich & Dechaumphai (2004) and Rao & Rahman (2000) and the PFEMCT-SIF method. First of all, the angle α varies between 0º and 2.533º (Figure 9), i.e., the crack propagates horizontally along the opening mode (modes I and II), as shown in Figure 11.

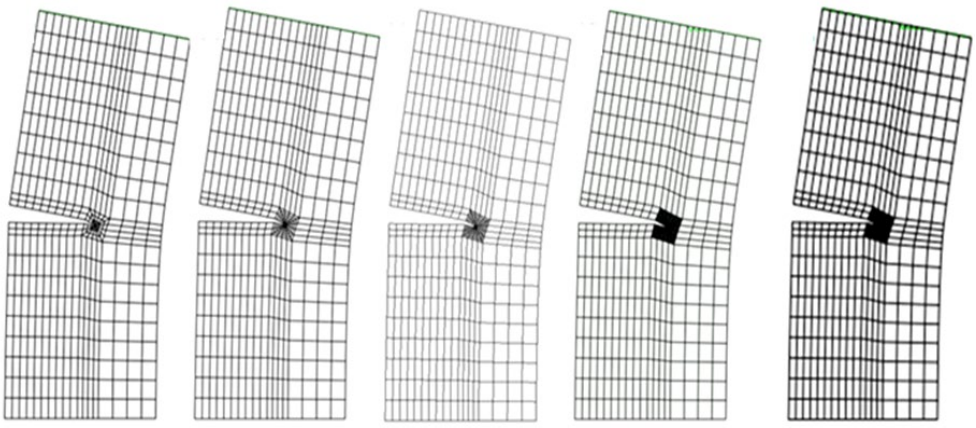

Figure 10 – Crack propagation trajectory α = -15.60º: a) 3 contours, b) 5 contours, c) 10 contours, d) 15 contours, and e) 20 contours, by the PFEMCT-SIF method in the first propagation

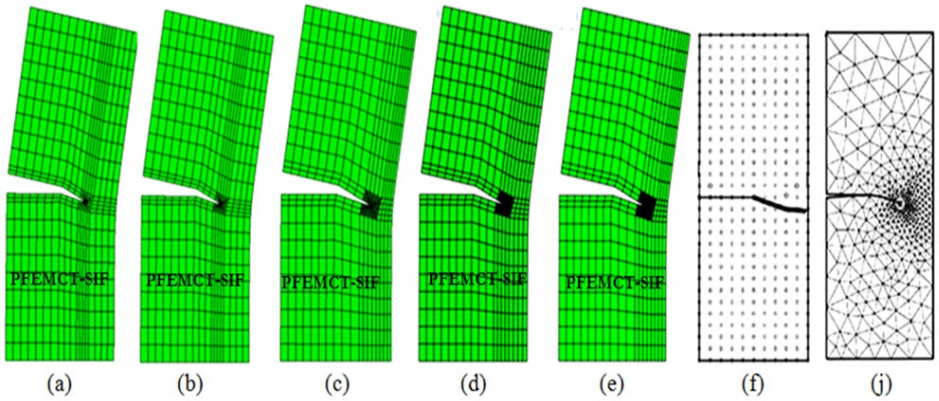

Figure 11 – Crack propagation trajectory by the PFEMCT-SIF method: a) 3 contours, b) 5 contours, c) 10 contours, d) 15 contours, and e) 20 contours, (f) Phongthanapanich & Dechaumphai (2004) and (j) Rao & Rahman (2000)

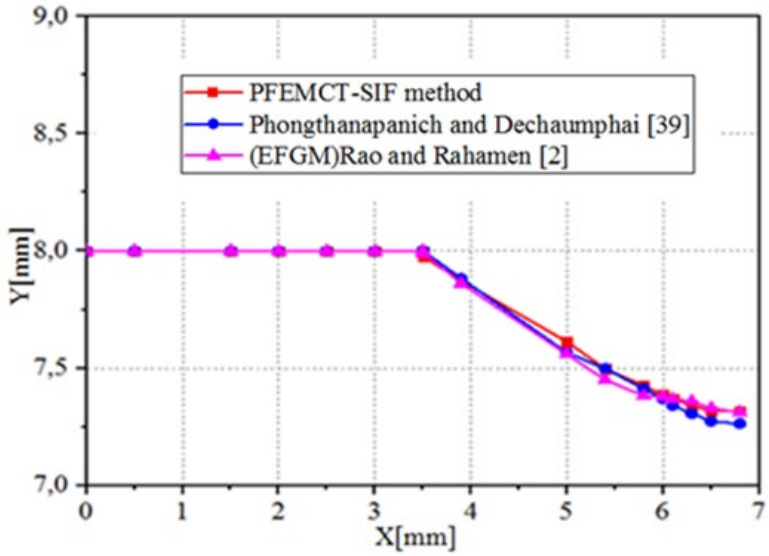

Figure 12 – Comparison of the results between the three methods: Rao & Rahman (2000), Phongthanapanich & Dechaumphai (2004), and the PFEMCT-SIF method

The comparison in Figure 12 shows a good correlation between the three methods, especially in mode I up to a slit length of (a= 3.5) mm. The calculations of Y are based on equation (5). Moreover, the results of the comparison between the analytical method and the PFEMCT-SIF method are shown in Tables 2 and 3, respectively.

Table 2 – Comparison of the results obtained by the PFEMCT-SIF method and the analytical method for the stress intensity factors K_I for different numbers of contours (3, 5, 10, 15, and 20 contours)

K_I [MPa.(m)$^{1/2}$] PFEMCT-SIF method					Analytical method	
3 contours	5 contours	10 contours	15 contours	20 contours	K_I	α[°]
32.92	33.03	33.60	33.66	33.75	33.4	-15.60
42.63	43.20	43.63	43.58	43.87	42.9	-0.8237
55.51	56.38	57.03	56.93	57.47	56.95	0.9473
75.88	77.31	78.41	78.16	79.25	75.68	1.691
112.2	114.9	115.3	116.4	118.9	114.51	2.533

Table 3 – Comparison of the results obtained by the PFEMCT-SIF method and the analytical method for the stress intensity factors K_{II} for different numbers of contours (3, 5, 10, 15, and 20 contours)

K_{II} [MPa.(m)$^{1/2}$] PFEMCT-SIF method					Analytical method	
3contours	5 contours	10 contours	15 contours	20 contours	K_{II}	α[◦]
4.453	4.475	4.492	4.483	4.499	4.324	-15.60
0.2590	0.2419	0.2278	0.2359	0.2094	0.2404	-0.8237
-0.3796	-0.4120	-0.4385	-0.4267	-0.4807	-0.4006	0.9473
-1.017	-1.071	-1.113	-1.095	-1.187	-1.056	1.691
-1.975	-2.067	-2.000	-2.111	-2.283	-2.038	2.533

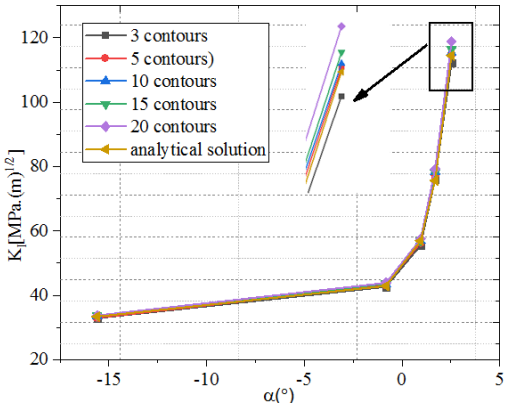

(a)

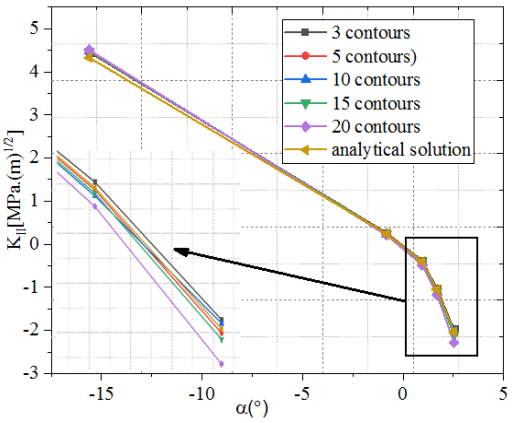

(b)

Figure 13 – Comparison of the stress intensity factors between the PFEMCT-SIF method and the analytical method proposed by Ewalds & Wanhill (1984): a) K_I and b) K_{II}

In Figures 13a and 13b, it can be noted that the results of the crack length effect on the stress intensity factor K_I (Figure 13a) and on K_{II} (Figure 13b) clearly illustrate the proportionality between the results of the study presented and the analytical method for equations (9), (10) and (11) proposed by Ewalds & Wanhill (1984). The results agree well in the case of the ten-contour model; regarding the case of K_I and K_{II}, they are somewhat distant in the case of the 20-contour model. This is due to the fact that whenever the crack is in a tilting state, the crack tip contours are affected and a divergence from the reference values occurs.

This comparison is made in the case of the length from 3.5mm to 5.5mm. In addition, the K_I values increase with increasing the crack length and the K_{II} values decrease. These forms of the results were obtained by Boulenouar et al (2014), Alshoaibi & Ariffin (2008) in different cases of crack propagation for both modes I and II.

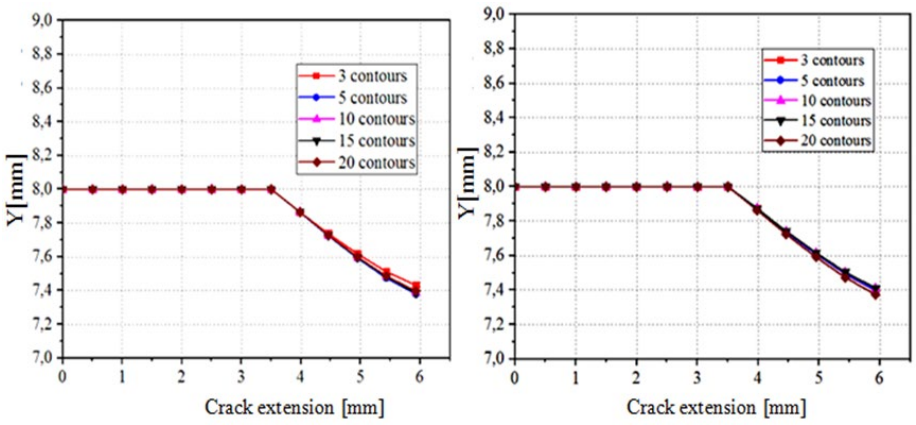

Figure 14 – Crack propagation path PFEMCT-SIF method by: a) Richard criterion and b) MCS criterion

Figure 14 illustrates the crack propagation trajectory by two criteria of crack propagation: Figure 14a presents the results obtained by the Richard criterion, and Figure 14b shows the results obtained by the MCS criterion. It is important to predict the evolution of the crack trajectory during the propagation by the two criteria. The numbers of 5, 10, 15, and 20 contours give very proportional results between them. A slight difference is obtained in the case of 3 contours by the Richard criterion, on the one hand, while, on the other hand, 5, 10, and 15 contours of the crack tip give a good correlation between them. However, a slight difference is obtained in the case of 20 contours in the MCS criterion; in this context, the results obtained by Bouchard (2000) and Bouchard et al. (2003) found that the MCS criterion gives good results compared to other crack propagation criteria.

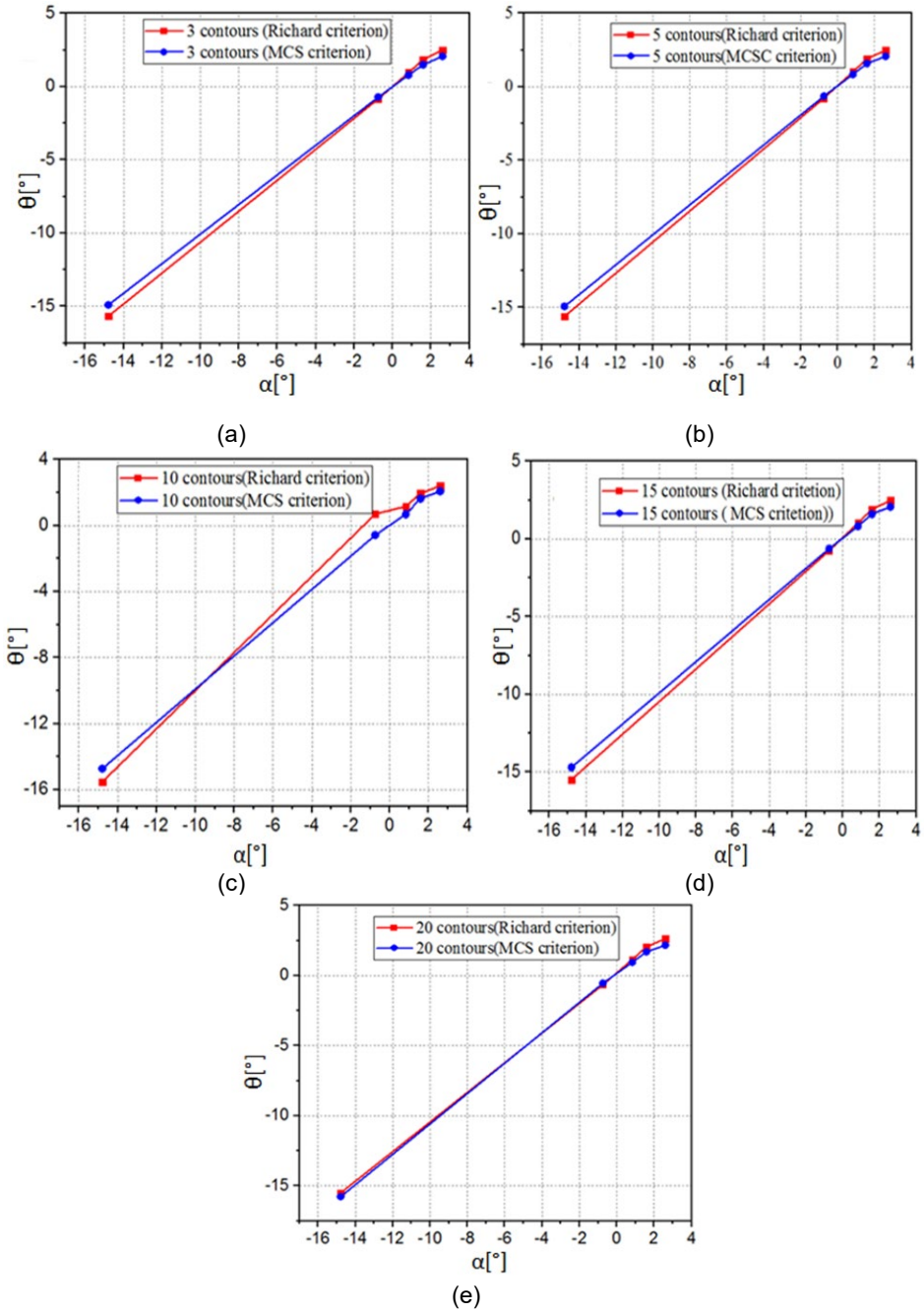

Figure 15 – Comparison between the MCS and the Richard criterion by the PFEMCT-SIF; a) 3 contours, b) 5 contours, c) 10 contours, d) 15 contours, and e) 20 contours

Figure 15 illustrates the inclination angle variation (α) according to the twist angle (θ) and calculated by the Richard criterion and the MCS criterion. Equations (2) and (4) are used and estimated at each crack length. The results obtained by the PFEMCT-SIF are comparable between the two criteria, (Richard's and that of the maximum tangential stress). We have chosen the criterion of the maximum circumferential stress (MCS). The use of the MCS criterion gives a crack propagation trajectory very close to that obtained using the Richard criterion, as shown in Figures 15a, b, c, d, and e which have presented the comparison for different numbers of the contours - 3,5,10,15, and 20 contours, respectively.

Conclusion

It can be noted that:

This study had two important parts to compare. The first one is based on the comparison in terms of crack trajectory - it can be seen that the results obtained from this comparison are very consistent with the studies presented by Phongthanapanich & Dechaumphai (2004) and Rao & Rahman (2000). The second part of this study is based on the evaluation of the stress intensity factor and compared by the work of Rao & Rahman (2000). Two cases have been considered, a crack with a horizontal angle α = 0º and a crack with a horizontal angle α ranging from -15.60º to 2.533º. In fact, this study is based on the effect of the number of contours around the crack point (CT) on the stress intensity factor (SIF).

Singular quarter-point elements proposed by Barsoum (1976) are used to numerically model the singularity of the stress and strain fields in the vicinity of the crack tip to calculate the SIF by the PFEMCT-SIF method. The MCS criterion presents more precise results than that of Richard's criterion, in which, for K_{II}> 0, of the angle θ <0 and vice versa, while K_I always> 0.

In general, the stress intensity factor K_I is increased with the increase in the crack length (a). However, the stress intensity factor K_{II} is decreased with increasing the crack length (a).

This study was very useful in terms of Fortran programming, and it is not easy to program a structure that contains a square end of a crack that contains several numbers of contours, by using the PFEMCT-SIF method to evaluate the stress intensity factor SIF.

As the crack begins to extend and tilt at an angle α, the crack tip elements become interconnected with each other.

Moreover, it can be seen that in the first case where α = 0, it is found that the more refined the crack front, the better the proportionality with the validation method proposed by Rao & Rahman (2000).

In the second case, when the angle α, is inclined, the best and closest number of contours around the crack front with the validation method proposed by Rao & Rahman (2000) is 10 contours. Therefore, we can say that this is the average case between the cases used and it helps to evaluate and find acceptable values for the stress intensity factor (SIF) by the PFEMCT-SIF method.

References

Alshoaibi, A. 2018. A two dimensional Simulation of crack propagation using Adaptive Finite Element Analysis. *Journal of Computational Applied Mechanics,* 49(2)**,** pp.335-341. Available at: https://doi.org/10.22059/JCAMECH.2018.264698.319.

Alshoaibi, A.M. 2015. Finite Element Modelling of Mixed Mode Crack Propagation. *International Journal of Soft Computing and Engineering (IJSCE),* 5(5)**,** pp.61-66 [online]. Available at: https://www.ijsce.org/portfolio-item/e2745115515 [Accessed: 12 August 2024].

Alshoaibi, A.M. & Ariffin, A.K. 2008. Fatigue life and crack path prediction in 2D structural components using an adaptive finite element strategy. *International Journal of Mechanical and Materials Engineering (IJMME),* 3(1)**,** pp.97-104.

Ayatollahi, M.R. & Sedighiani, K. 2012. Mode I fracture initiation in limestone by strain energy density criterion. *Theoretical and Applied Fracture Mechanics,* 57(1)**,** pp.14-18. Available at: https://doi.org/10.1016/j.tafmec.2011.12.003.

Barsoum, R.S. 1976. On the use of isoparametric finite elements in linear fracture mechanics. *International Journal for Numerical Methods in Engineering,* 10**,** pp.25-37. Available at: https://doi.org/10.1002/nme.1620100103.

Benamara, N., Boulenouar, A., Aminallah, M. & Benseddiq, N. 2017. On the mixed-mode crack propagation in FGMs plates: comparison of different criteria. *Structural Engineering and Mechanics,* 61(3)**,** pp.371-379. Available at: https://doi.org/10.12989/sem.2017.61.3.371.

Bentahar, M. 2023a. ALLDMD Dissipation Energy Analysis by the Method Extended Finite Elements of a 2D Cracked Structure of an Elastic Linear Isotropic Homogeneous Material. *Journal of Electronics, Computer Networking and Applied Mathematics (JECNAM),* 3(02)**,** pp.1-8. Available at: https://doi.org/10.55529/jecnam.32.1.8.

Bentahar, M. 2023b. Fatigue Analysis of an Inclined Crack Propagation Problem by the X-FEM Method. *International Journal of Applied and Structural Mechanics (IJASM),* 3(04)**,** pp.23-31. Available at: https://doi.org/10.55529/ijasm.34.23.31.

Bentahar, M. & Benzaama, H. 2023. Numerical Simulation of the Synthetic Strain Energy and Crack Characterization Parameters Using the Fem Method of a Two-Dimensional Multi-Position Model. *Selcuk University Journal of Engineering Sciences*, 22(03), pp.100-109 [online]. Available at: https://hdl.handle.net/20.500.12395/52415 [Accessed: 12 August 2024].

Bentahar, M., Benzaama, H. & Mahmoudi, N. 2021a. Numerical Modeling of the Evolution of the Strain Energy ALLSE of the Crack Propagation by The X-FEM Method. *Revue des matériaux et énergies renouvelables,* 5(2)**,** pp.24-31 [online]. Available at: https://www.asjp.cerist.dz/en/article/167392 [Accessed: 12 August 2024].

Bentahar, M., Benzaama, H. & Mahmoudi, N. 2021b. Numerical modeling of the contact effect on the parameters of cracking in a 2D Fatigue Fretting Model. *Fracture and Structural Integrity,* 15(57)**,** pp.182-194. Available at: https://doi.org/10.3221/IGF-ESIS.57.15.

Bentahar, M., Moulai Arbi, Y. & Mahmoudi, N. 2024. Finite element analysis of characterization parameters the double cracks in linear elastic DCFEM. *Studies in Engineering and Exact Sciences,* 5(2)**,** e5929. Available at: https://doi.org/10.54021/seesv5n2-039.

Bouchard, P.-O. 2000. *Contribution à la Modélisation Numérique en Mécanique de la Rupture et Structures Multimatériaux*. PhD thesis. École Nationale Supérieure des Mines de Paris [online]. Available at: https://pastel.archives-ouvertes.fr/tel-00480372 [Accessed: 12 August 2024].

Bouchard, P.-O., Bay, F. & Chastel, Y. 2003. Numerical modelling of crack propagation: automatic remeshing and comparison of different criteria. *Computer Methods in Applied Mechanics and Engineering,* 192(35-36)**,** pp.3887-3908. Available at: https://doi.org/10.1016/S0045-7825(03)00391-8.

Boulenouar, A. & Bendida, N. 2019. Crack growth path simulation in a cement mantle of THR using crack box technique. *Journal of Theoretical and Applied Mechanics,* 57(2), pp.317-329. Available at: https://doi.org/10.15632/jtam-pl/104512.

Boulenouar, A., Benouis, A. & Benseddiq, N. 2016a. Numerical Modelling of Crack Propagation in Cement PMMA: Comparison of Different Criteria. *Materials Research,* 19(4)**,** pp.846-855. Available at: https://doi.org/10.1590/1980-5373-MR-2015-0784.

Boulenouar, A., Benseddiq, N. & Mazari, M. 2013. Strain energy density prediction of crack propagation for 2D linear elastic materials. *Theoretical and Applied Fracture Mechanics,* 67-68**,** pp.29-37. Available at: https://doi.org/10.1016/j.tafmec.2013.11.001.

Boulenouar, A., Benseddiq, N., Mazari, M. & Benamara, N. 2014. FE model for linear-elastic mixed mode loading: estimation of SIFs and crack propagation. *Journal of Theoretical and Applied Mechanics,* 52(2)**,** pp.373-383 [online]. Available at: http://jtam.pl/FE-model-for-linear-elastic-mixed-mode-loading-estimation-of-SIFs-and-crack-propagation,102170,0,2.html [Accessed: 12 August 2024].

Boulenouar, A., Benseddiq, N., Merzoug, M., Benamara, N. & Mazari, M. 2016b. A strain energy density theory for mixed mode crack propagation in rubber-like materials. *Journal of Theoretical and Applied Mechanics,* 54(4), pp.1417-1431. Available at: https://doi.org/10.15632/jtam-pl.54.4.1417.

Carpinteri, A. 1984. Size effects in material strength due to crack growth and material non-linearity. *Theoretical and applied fracture mechanics,* 2(1)**,** pp.39-45. Available at: https://doi.org/10.1016/0167-8442(84)90038-7.

Cho, J.-R. 2015. Computation of 2-D mixed-mode stress intensity factors by Petrov-Galerkin natural element method. *Structural Engineering and Mechanics,* 56(4)**,** pp.589-603. Available at: https://doi.org/10.12989/sem.2015.56.4.589.

Choi, D.H., Choi, H.Y. & Lee, D. 2006. Fatigue life prediction of in-plane gusset welded joints using strain energy density factor approach. *Theoretical and Applied Fracture Mechanics,* 45(2)**,** pp.108-116. Available at: https://doi.org/10.1016/j.tafmec.2006.02.003.

Chow, C.L. & Jilin, X. 1985. Application of the strain energy density criterion to ductile fracture. *Theoretical and Applied Fracture Mechanics,* 3(3)**,** pp.185-191. Available at: https://doi.org/10.1016/0167-8442(85)90029-1.

Erdogan, F. & Sih, G.C 1963. On the Crack Extension in Plates Under Plane Loading and Transverse Shear. *Journal of Basic Engineering*, 85(4), pp.519-525. Available at: https://doi.org/10.1115/1.3656897.

Ewalds, H.L. & Wanhill, R.J.H. 1984. *Fracture Mechanics*. Oxford, UK: Butterworth-Heinemann LtdI. SBN: 978-0713135152.

Fiordalisi, S. 2014. *Modélisation tridimensionelle de la fermeture induite par plasticité lors de la propagation d'une fissure de fatigue dans l'acier 304L.* PhD thesis. Poitiers, France: École doctorale Sciences et ingénierie des matériaux, mécanique, énergétique et aéronautique [online]. Available at: https://theses.fr/2014ESMA0018 [Accessed: 12 August 2024].

Hamdi, A., Aït Hocine, N., Nait Abdelaziz, M. & Benseddiq, N. 2007. Fracture of elastomers under static mixed mode: the strain-energy-density factor. *International Journal of Fracture,* 144**,** pp.65-75. Available at: https://doi.org/10.1007/s10704-007-9080-7.

Komori, K. 2005. Ductile fracture criteria for simulating shear by node separation method. *Theoretical and Applied Fracture Mechanics,* 43(1)**,** pp.101-114. Available at: https://doi.org/10.1016/j.tafmec.2004.12.006.

Malekan, M., Silva, L.L., Barros, F.B., Pitangueira, R.L.S. & Penna, S.S. 2018. Two-dimensional fracture modeling with the generalized/extended finite element method: An object-oriented programming approach. *Advances in Engineering Software,* 115**,** pp.168-193. Available at: https://doi.org/10.1016/j.advengsoft.2017.09.005.

Paris, P. & Erdogan, F. 1963. A Critical Analysis of Crack Propagation Laws. *Journal of Basic Engineering*, 85(4), pp.528-533. Available at: https://doi.org/10.1115/1.3656900.

Pegorin, F., Kotousov, A., Berto, F., Swain, M.V. & Sornsuwan, T. 2012. Strain energy density approach for failure evaluation of occlusal loaded ceramic tooth crowns. *Theoretical and Applied Fracture Mechanics,* 58(1)**,** pp.44-50. Available at: https://doi.org/10.1016/j.tafmec.2012.02.006.

Phongthanapanich, S. & Dechaumphai, P. 2004. Adaptive Delaunay triangulation with object-oriented programming for crack propagation analysis. *Finite Elements in Analysis and Design,* 40(13-14)**,** pp.1753-1771. Available at: https://doi.org/10.1016/j.finel.2004.01.002.

Rao, B.N. & Rahman, S. 2000. An efficient meshless method for fracture analysis of cracks. *Computational Mechanics,* 26**,** pp.398-408. Available at: https://doi.org/10.1007/s004660000189.

Richard, H.A. 1985. *Bruchvorhersagen bei überlagerter Normal- und Schubbeanspruchung von Rissen.* Düsseldorf: VDI-Verl. ISBN: 3188506317.

Rossmanith, H. 1984. *Structural Failure, Product Liability and Technical Insurance*. North-Holland. ISBN: 978-0444868695.

Sajith, S., Murthy, K.S.R.K & Robi, P.S. 2018. A simple technique for estimation of mixed mode (I/II) stress intensity factors. *Journal of Mechanics of Materials and Structures,* 13(2)**,** pp.141-154. Available at: https://doi.org/10.2140/jomms.2018.13.141.

Sih, G.C. 1974. Strain-energy-density factor applied to mixed mode crack problems. *International Journal of Fracture,* 10**,** pp.305-321. Available at: https://doi.org/10.1007/BF00035493.

Tada, H., Paris, P.C. & Irwin, G.R. 2000. *The Stress Analysis of Cracks Handbook, Third Edition.* ASME Press. Available at: https://doi.org/10.1115/1.801535.

Theocaris, P.S. 1984. A higher-order approximation for the T-criterion of fracture in biaxial fields. *Engineering Fracture Mechanics,* 19(6)**,** pp.975-991. Available at: https://doi.org/10.1016/0013-7944(84)90144-9.

Yaylaci, M. 2016. The investigation crack problem through numerical analysis. *Structural Engineering and Mechanics,* 57(6)**,** pp.1143-1156. Available at: https://doi.org/10.12989/sem.2016.57.6.1143.

Zaleha, M., Ariffin, A.K. & Muchtar, A. A. 2007. Prediction of Crack Propagation Direction for Holes Under Quasi-Static Loadingg. *Computational & Experimental Mechanics,* pp.141-151 [online]. Available at: https://core.ac.uk/download/17049988.pdf [Accessed: 12 August 2024].

Optimización numérica por el método PFEMCT-SIF de la propagación de grietas en un material elástico lineal

Mohammed Bentahar[a], *Noureddine* Mahmoudi[a], *Youcef* Moulai Arbi[b]

[a] Universidad de Saida Dr. Moulay Tahar, Facultad de Tecnología, Departamento de Ingeniería Civil e Hidráulica, Saida, República Argelina Democrática y Popular

[b] Universidad de Mustapha Stambouli, Laboratorio de Física Cuántica de Materia y Modelamiento Matemático (LPQ3M), Mascara, República Argelina Democrática y Popular, **autor de correspondencia**

CAMPO: ingeniería mecánica
TIPO DE ARTÍCULO: artículo científico original

Resumen:

Introducción/objetivo: Este estudio investiga la influencia de los números de contorno que rodean la punta de la grieta en los factores de intensidad de tensión (SIF) utilizando el enfoque del factor de intensidad de tensión de

la punta de la grieta del método de elementos finitos de propagación (PFEMCT-SIF). También compara el criterio de tensión circunferencial máxima (MCSC) y el criterio de Richard para la predicción de la propagación de grietas.

Métodos: Se desarrolló un código de elementos finitos escrito en Visual Fortran para modelar puntas de grietas con 3, 5, 10, 15 y 20 contornos utilizando elementos CPE4 cuadráticos de 4 nodos. Se utilizó el software Abaqus para calcular los SIF y los ángulos de orientación de las grietas. Se analizaron grietas horizontales e inclinadas en una placa de acero sometida a carga de tracción. Los resultados se validaron frente a soluciones analíticas y estudios numéricos previos.

Resultados: El modelo de 10 contornos mostró la mejor concordancia con los valores analíticos de SIF. El aumento de los números de contorno mejoró la precisión de SIF para grietas horizontales, pero el refinamiento excesivo provocó divergencia para grietas inclinadas. El MCSC y el criterio de Richard produjeron trayectorias de grietas comparables, y el MCSC demostró una precisión ligeramente superior.

Conclusión: El método PFEMCT-SIF evalúa eficazmente las SIF y predice las trayectorias de propagación de grietas. Un modelo de punta de grieta de 10 contornos equilibra la precisión y la eficiencia computacional. El estudio destaca la importancia de optimizar el refinamiento de la malla de la punta de la grieta en las simulaciones de mecánica de fracturas.

Palabras claves: punta de grieta, propagación de grietas, método SFEMCT-SIF, MCSC y criterio de Richard, contornos.

Численная оптимизация распространения трещины в линейно-упругом материале методом PFEMCT-SIF

Мухаммед Бентахар[а], *Нуредин* Мамуди[а], *Юсуф* Мулаи Арби[б]

[а] Университет Саиды Мулай Тахар, технологический факультет, кафедра гражданского строительства и гидравлики, Саида, Алжирская Народная Демократическая Республика

[б] Университет Туши Мустафы Стамбули, лаборатория квантовой физики материи и математического моделирования (LPQ3M), Маскара, Алжирская Народная Демократическая Республика, **корреспондент**

РУБРИКА ГРНТИ: 30.19.00 Механика деформируемого твердого тела
ВИД СТАТЬИ: оригинальная научная статья

Резюме:

Введение/цель: В данной статье исследуется влияние числа контуров, окружающих вершину трещины, на коэффициенты интенсивности напряжений (SIFS) с использованием метода конечных элементов распространения коэффициента интенсивности напряжений в вершине трещины (PFEMCT-SIF).

В статье также сравниваются критерий максимального окружного напряжения (MCSC) и критерий по Ричарду для прогнозирования распространения трещин.

Методы: В ходе исследования был разработан конечно-элементный код, написанный в Visual Fortran, для моделирования вершин трещин с 3, 5, 10, 15 и 20 контурами и с использованием 4-узловых четырехугольных элементов CPE4. Программное обеспечение Abaqus использовалось для расчета размеров трещин и углов ориентации трещин. Были проанализированы горизонтальные и наклонные трещины в стальном листе, подвергнутом растягивающей нагрузке. Результаты были подтверждены аналитическими решениями и предыдущими численными исследованиями.

Результаты: В результате исследования 10-контурная модель показала наилучшее соответствие с аналитическими значениями SIF. Увеличение числа контуров улучшило точность SIF у горизонтальных трещин, в то время как чрезмерная плотность сетки привела к расхождению в наклонных трещинах. Критерий MCSC и критерий Ричарда дали сопоставимые траектории трещин, причем MCSC оказался более точным.

Выводы: Метод PFEMCT-SIF эффективно оценивает параметры SIF и прогнозирует пути распространения трещин. Также выявлено, что 10-контурная модель вершины трещины обеспечивает баланс между точностью и вычислительной эффективностью. В исследовании подчеркивается значимость оптимизации плотности сетки вершин трещин при моделировании механики разрушения.

Ключевые слова: вершина трещины, распространение трещины, метод SFEMCT-SIF, критерий MCSC и критерий Ричарда, контуры.

Нумеричка оптимизација ширења прслине у линеарном еластичном материјалу помоћу метода PFEMCT-SIF

Мухамед Бентахар[б], *Нуредин* Мамуди[а], *Јусуф* Мулаи Арби[б]

[а] Универзитет у Саиди „Др Мулаи Тахар”, Технолошки факултет, Департман за грађевинарство и хидраулику, Саида, Народна Демократска Република Алжир

[б] Универзитет „Мустафа Стамболи”, Лабораторија за квантну физику материје и математичко моделирање (LPQ3M), Маскара, Народна Демократска Република Алжир, **аутор за преписку**

ОБЛАСТ: механика
КАТЕГОРИЈА (ТИП) ЧЛАНКА: оригинални научни рад

Сажетак:

Увод/циљ: У овој студији испитује се утицај броја контура које окружују врх прслине на факторе интензитета напона (stress intensity factor - SIF) коришћењем приступа PFEMCT-SIF (Propagation Finite Element Method Crack Tip Stress Intensity Factor). Такође, пореде се критеријум максималног ободног напрезања (maximum circumferential stress criterion – MCSC) и критеријум по Richard-у за предвиђање ширења прслине.

Методе: Код коначних елемената, написан у Visual Fortran-у, развијен је за моделовање врхова прслина са 3, 5, 10, 15 и 20 контура помоћу квадратних елемената чистог оптерећења са 4 чвора (CPE4). Софтвер Abaqus коришћен је за израчунавање фактора интензитета напона и углова оријентације прслина. Анализиране су хоризонталне и нагнуте прслине на челичној плочи при напону на затезање. Резултати су потврђени поређењем са аналитичким решењима и претходним нумеричким студијама.

Резултати: Модел са 10 контура показао је најбоље слагање са аналитичким вредностима фактора интензитета напона. Повећање броја контура побољшало је прецизност фактора интензитета напона код хоризонталних прслина, док је превелика густина мреже довела до дивергенције код нагнутих прслина. Оба критеријума (MCSC и Richard) дала су упоредиве путање прслине, при чему је критеријум максималног ободног напрезања показао нешто већу прецизност.

Закључак: Метода PFEMCT-SIF ефикасно процењује факторе интензитета напона и предвиђа путеве ширења прслина. Модел врха прслине са 10 контура представља баланс између прецизности и рачунарске ефикасности. Истакнута је важност оптимизације густине мреже врха прслине у симулацијама механике лома.

Кључне речи: врх прслине, ширење прслине, метода SFEMCT-SIF, критеријум MCSC и критеријум по Richard-у, контуре.

Paper received on: 13.08.2024.
Manuscript corrections submitted on: 28.01.2025.
Paper accepted for publishing on: 29.01.2025.

VOJNOTEHNIČKI GLASNIK / MILITARY TECHNICAL COURIER, 2025, Vol. 73, Issue 1

Impact of concrete compressive strength on the reliability and the plastic moment of steel-concrete composite beams

Nabil Daanoune[a], *Nassim* Kernou[b]

University of Bejaia, Faculty of Technology,
Laboratory of Construction Engineering and Architecture (LGCA),
Bejaia, People's Democratic Republic of Algeria

[a] e-mail: nabil.daanoune@univ-bejaia.dz, **corresponding author**,
ORCID iD: https://orcid.org/0009-0002-8815-3185

[b] e-mail: nassim.kernou@univ-bejaia.dz,
ORCID iD: https://orcid.org/0000-0002-5334-0231

https://doi.org/10.5937/vojtehg73-53935

FIELD: mechanical engineering, civil engineering
ARTICLE TYPE: original scientific paper

Abstract:

Introduction/purpose: This study investigated the influence of concrete compressive strength on the reliability and the plastic resistance moment of steel-concrete composite beams. The objective was to evaluate the impact of concrete strength variations on structural performance, with a particular attention to the plastic resistance moment which is critical to the safety and compliance of the composite beam.

Methods: To model the nonlinear behavior of concrete, Abaqus created a three-dimensional numerical model including a concrete damage plasticity (CDP) model. Reliability analysis was performed, and the failure probability was assessed using Monte Carlo simulations (MCS) and first-order (FORM) and second-order (SORM) reliability methods. The limit state function was determined according to Eurocode 4 criteria considering the concrete compressive strength of 25 to 80 MPA.

Results: As a result, it was found that the compressive strength of concrete significantly affects the plastic resistance moment and the reliability index of the composite beam. The high strength of concrete improves the plastic resistance moment, and the reliability index varies depending on the geometric and material property of the composite section and loading conditions.

Conclusion: The compressive strength of concrete is an important parameter that determines the structural characteristics and safety of steel-concrete composite beams. This highlighted the need to consider the variability of concrete strength when designing and evaluating composite structures to ensure compliance with reliability standards.

Key words: composite beam, nonlinear modelling, plastic resistance moment, reliability analysis, finite element analysis, failure probability.

Introduction

Due to the combination of concrete compressive strength and steel tensile strength, steel-concrete composite beams are frequently utilized in moderne construction to create reliable and efficient systems. The behavior of these beams is strongly influenced by concrete compressive strength which also affects their plastic resistance moment and reliability. The purpose of this study is to examine how these two crucial factors are affected by the compressive strength of concrete.

Many researchers use a limit state function based on Eurocode 4 criteria (CEN, 1994) to study the reliability of steel-concrete composite beams. The goal of this strategy is to offer more precise insights into the behavior of the system under study. Using a case study as validation, Mamuda et al. (2018) examined the four failure modes of bending, shearing, deflection, and shear connector capacity when analyzing the reliability of beams. The impact of various parameter variations on reliability was evaluated. Chaves et al. (2010) examined the design specifications for the steel-concrete composite beam. The study of the structural reliability of the timber concrete composite beam is evaluated by Daanoune et al. (2024). This evaluation is carried out by the MCS, the FORM and the SORM methods for three failure modes in concrete, timber and at the connectors. Another research where the limit state function is based on the resistance criteria according to Eurocode 4 was carried out by Lydia & Nassim (2022). This study focuses on the evaluation of the reliability of square composite columns under axial compression and the results show that steel tubular columns filled with high performance concrete (HPCFTC) are more reliable than those filled with ordinary concrete (OCFSTC).

In this context, the study provides a comprehensive analysis using numerical simulations to investigate the influence of concrete tensile strength. A 3D finite element model has been developed in Abaqus to simulate the behavior of composite beams to account for the nonlinear behavior of concrete in tension and compression through Concrete Damage Plasticity - CDP (Dassault Systèmes, 2016; CEN, 2004). The reliability analysis is performed using the Monte Carlo simulation (MCS) and the first-order (FORM) and the second-order (SORM) reliability methods, as developed by Rackwitz (2001), which include the treatment of uncertainties in the parameters affecting the system behavior. The applied limit state functions are designed to verify the plastic resistance moment of the composite beam in bending, in accordance with Eurocode 4 standards (CEN, 1994). The study considers a range of concrete

compressive strengths from 25 to 80 MPa. The results demonstrate a significant influence of concrete compressive strength on reliability and plastic moment capacity. This study provides valuable insights into the design and analysis of steel-concrete composite beams, enabling the optimization of their performance and safety, and proposes a clear approach to the use of safety factors to adjust the reliability level of the system, thereby ensuring the proper functioning of the composite beam.

Methodology

Plastic resistance moment of the composite cross section to bending

The calculation of the neutral axis depth Z_{pl} and the determination of the plastic neutral axis (PNA) position according to Eurocode 4 (CEN, 1994; Johnson, 2018; Liang, 2018) allows for the calculation of the plastic resistance moment $M_{pl,Rd}$ of the composite section. This procedure is performed using the following equations.

If the neutral axis is located in the concrete slab

$$Z_{pl} = \frac{N_{pla}}{b_{eff} \times 0.85 \times f_{cd}} \quad (1)$$

$$M_{pl,Rd} = N_{pla}\left(\frac{h_a}{2} + h_c - \frac{Z_{pl}}{2}\right) \quad (2)$$

where:

$$N_{pla} = A_a \times \frac{f_y}{\gamma_a} \quad (3)$$

$$f_{cd} = \frac{f_c}{\gamma_c} \quad (4)$$

b_{eff}: effective width of the concrete flange,
γ_a: safety factors of steel,
γ_c: safety factors of concrete,
f_y: yield strength of the steel section,
f_c: compressive strength of the concrete,
h_a: height of the steel section,
h_c: height of the concrete flange,
A_a: area of the steel section, and
if the neutral axis is located in the steel flange

$$Z_{pl} = \frac{N_{pla} - N_{cf}}{2b_f \times f_y} \times \gamma_a + hc \quad (5)$$

$$M_{pl,Rd} = N_{pla}\left(\frac{h_a}{2} + \frac{h_c}{2}\right) - \left(N_{pla} - N_{cf}\right)\frac{Z_{pl}}{2} \quad (6)$$

where:

$$N_{cf} = \frac{0.85.f_c}{\gamma_c} \times h_c \times b_{eff} \quad \text{.....(7)}$$

b_f: width of the steel flange.

Composite cross section design

For the study of the flexural behavior of steel-concrete composite beams, four types of composite steel-concrete beams were tested by Du et al. (2021), each with a different class of concrete: C25, C45, C65, and C80 with a compressive strength of 24.5 MPa; 45.9 MPa; 63.1 MPa and 78.3 MPa, respectively. Figure 1 illustrates the layout and the transverse and longitudinal dimensions of the steel-concrete composite beam with the stud connection. The beam is subjected to four-point bending, with one end pinned and the other end on a roller.

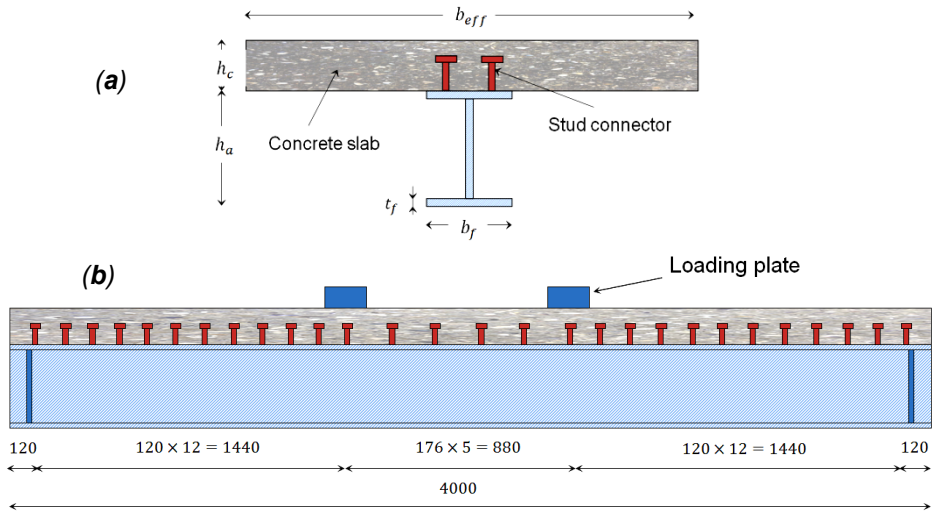

*Figure 1 – Cross-sectional dimensions of composite beams: (**a**) cross-section; (**b**) longitudinal section*

Finite element analysis (FEA) setup and parameters

These samples are modeled using a 3D finite element (FE) model with Abaqus software (Dassault Systèmes, 2016). In the FE models, damage plasticity was used to simulate the mecanical behavior of concrete. Cracking or crushing of concrete results in a reduction of its elastic modulus. The tensile behavior of concrete was assumed to be linear up to the uniaxial tensile strength $f_t = \frac{f_c}{10}$ according to Eurocode 2 (CEN, 2004). The uniaxial stress-strain relationship in compression for

concrete can be identified by the following formula of Hognestad Model (Hognestad, 1951):

$\sigma_c = f'_c \times \frac{\varepsilon}{\varepsilon_0} \times \left(2 - \frac{\varepsilon}{\varepsilon_0}\right)$ for $\varepsilon \leq \varepsilon_0$.....(8)

$\sigma_c = f'_c \times \left[1 - 0.15\left(\frac{\varepsilon - \varepsilon_0}{\varepsilon_{cu} - \varepsilon_0}\right)\right]$ for $\varepsilon > \varepsilon_0$ .....(9)

where $\varepsilon_{cu}$is the ultimate compressive strain and $\varepsilon_0 = \frac{2 \times f'c}{E}$ is the strain at the ultimate stress according to Hognestad Model, see (Hognestad, 1951). This model has been used and mentioned in the papers of several authors such as Guo et al. (2020) and Rezaie et al. (2022).

$E_{cm}\,[MPa] = 22000 \times \left(\frac{fcm}{10} MPa\right)^{0.3}$: the elasticity modulus of concrete given by Eurocode 2, Table 3.1 (CEN, 2004).

f'_c: the ultimate concrete compressive stress.

The steel material properties of the steel beam and the screw stud connectors were defined as isotropic elastoplastic behavior (Dassault Systèmes, 2016). The yield strength and ultimate tensile strength of the studs were 350 MPa and 480 MPa and the yield strength and the ultimate tensile strength of the steel beam were 495.4 MPa and 572 MPa (Du et al, 2021).

Probabilistic methods for the reliability analysis

Three different methods were employed: the Monte Carlo method, the FORM, and the SORM.

The Monte Carlo simulation is practical and accurately represents the real phenomenon during a sample test. The principle of this method involves generating a large number of simulations, typically in the order of 10^n(Haldar & Mahadevan, 1999) to calculate the failure probability $P_f$using the equation:

$$P_f = \frac{Nf}{N} \quad \text{.....(10)}$$

where Nf is the number of times the system fails, and N is the total number of simulations. In our study, à MATLAB command was used to generate à number N of simulations with a given mean and standard deviation.

The FORM Method: This method is a first-order Taylor series expansion of the limit state function $G(x)$ around a point P^*, called the design point. It involves determining the reliability index β, which is the shortest distance between the origin O and the point P^* in the centered standard space. The reliability index β then provides access to an approximate failure probability P_f (Grandhi & Wang, 1999). The reliability index was calculated using the Hasofer-Lind-Rackwitz-Fiessler algorithm:

$$\beta = \min_{g(u)=0} \sqrt{\sum_{i=1}^{n} u_i^2} \text{.....(11)}$$

$$P_{f,FORM} = \Phi(-\beta) \text{.....(12)}$$

where Φ is the cumulative distribution function - CDF (Grandhi & Wang, 1999), see Appendix 1.

The SORM Method: This method is a second-order Taylor series expansion of the limit state function $G(x)$ and corrects the failure probability obtained by the FORM. For this method, we used the Breitung formula to calculate P_f (Haldar & Mahadevan, 1999):

$$P_{f,SORM} \approx \Phi(-\beta) \prod_{j=1}^{n-1} \frac{1}{\sqrt{1+\beta k_j}} \text{.....(13)}$$

We define the principal curvatures k_j as the eigenvalues of the matrix A , where its elements a_{ij} are defined by:

$$a_{ij} = \frac{(RDR^{'})_{ij}}{|\nabla G(U^*)|} i,j = 1,2,3,\dots,n-1 \text{ ..... (14)}$$

Here, D is the Hessian matrix $(n \times n)$ of the limit state function in the reduced centered normal space evaluated at the design point. R is the rotation matrix obtained by the Gram-Schmidt transformation (Haldar& Mahadevan, 1999), see Appendix 6.

Mechano-reliability coupling

The mechano-reliability coupling of Abaqus-MATLAB is used to evaluate the flexural failure mode of composite beams according to Eurocode 4 (CEN, 1994) Abaqus simulates the behavior of the mechanism related to material interaction and nonlinearity, while MATLAB does reliability analysis, focusing on the flexural over the failure mode of the limit state functions. This approach takes into account the uncertainties in the properties of certain geometric and material parameters, determining the probability of reaching the moment of plastic resistance and guaranteeing compliance with the safety criteria.

In our reliability study, we distinguish two limit state functions according to the position of the neutral axis

$$G_1(x) = N_{pla}\left(\frac{h_a}{2} + h_c - \frac{Z_{pl}}{2}\right) - M_{sd} \text{.....(15)}$$

$$G_2(x) = N_{pla}\left(\frac{h_a}{2} + \frac{h_c}{2}\right) - \left(N_{pla} - N_{cf}\right)\frac{Z_{pl}}{2} - M_{sd} \text{.....(16)}$$

Table 1 – Random variables chosen from the limit state function

Properties	Variables	Mean	COV	Distribution	Ref.
Material	f_y	$495.4\ \mathrm{N/mm^2}$	6%	Lognormal	Bartlett et al. (2003)
	f_c	$24.5\ \mathrm{N/mm^2}$	6%	Lognormal	Bartlett et al. (2003)
Geometric	h_a	$250\ \mathrm{mm}$	5%	normal	Ellingwood et al. (1982)
	h_c	$100\ \mathrm{mm}$	5%	normal	Ellingwood et al. (1982)
Loading	M_{sd}	$355.68\ \mathrm{KN.m}$	5%	normal	Du et al. (2021)

The following flowchart explains the Abaqus-MATLAB coupling steps:

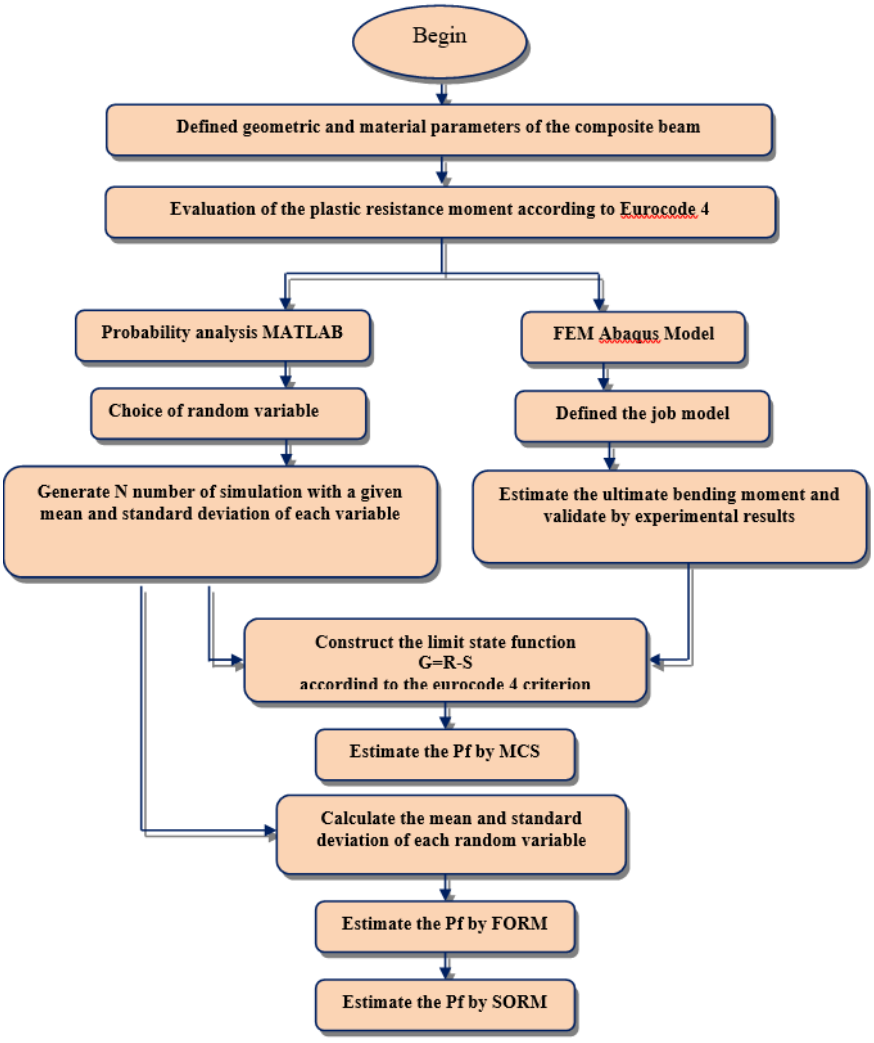

Figure 2 – Abaqus-MATLAB mechanical-reliability coupling flowchart

Results and discussion

Abaqus and the reliability results

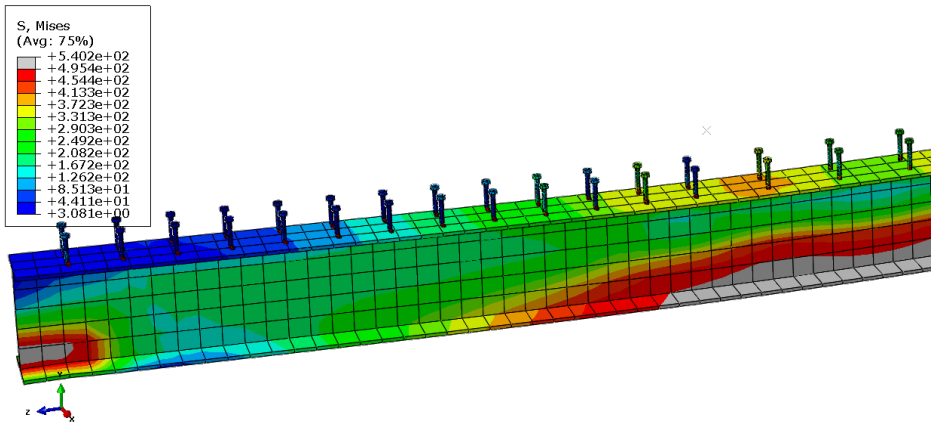

Figure 3 –Stress distributions in the connection at the maximum load

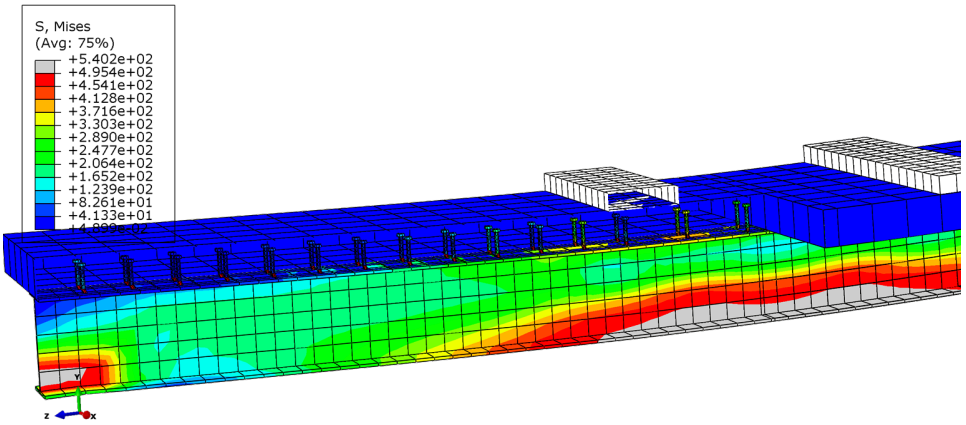

Figure 4 – Stress distributions in the composite beam with a 3D cut view

Figures 3 and 4 illustrate the stress distribution within the composite beam under the maximum load. Across the four types of beams studied, it was observed that the neutral axis is consistently located near or within the thickness of the concrete slab. This suggests that the bottom fiber of

the steel beam is yielded before the concrete reaches its maximum compressive strength. This prediction is confirmed by the Abaqus results of the finite element analysis, Figures 3 and 4 (in gray), which show that the bottom fiber in the middle of the steel beam has reached its maximum strength of 495.4 MPa.

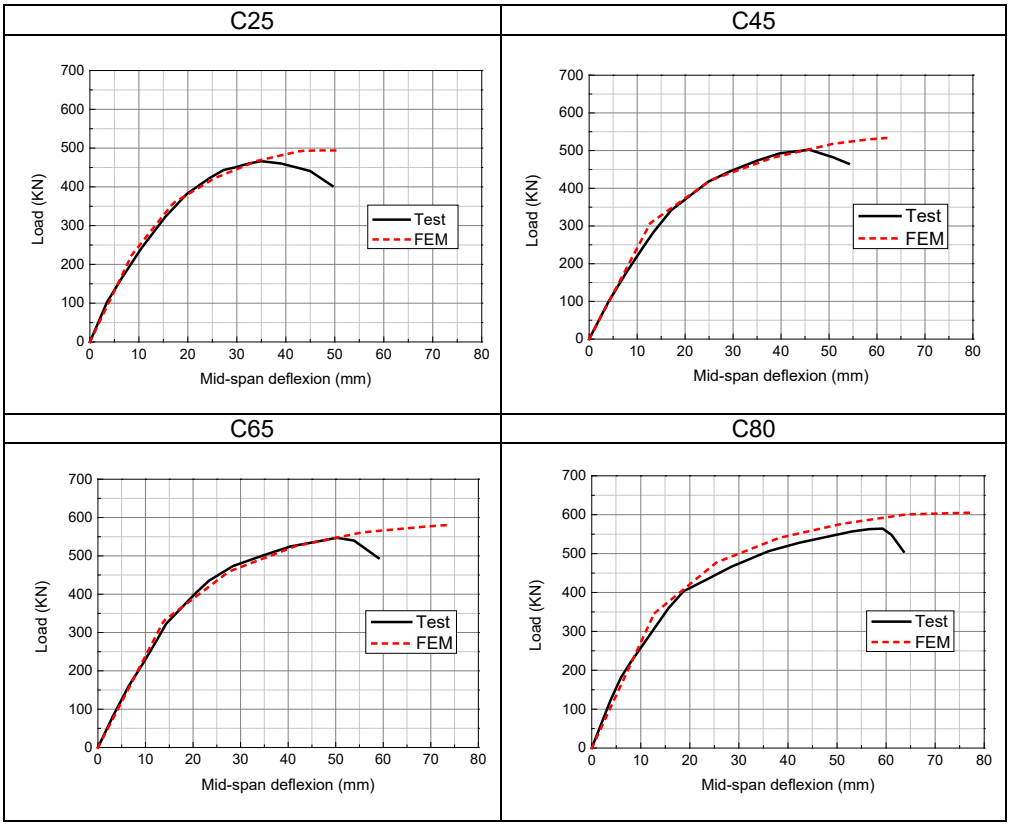

Figure 5 – Load-deflexion curve with different concrete classes of the composite beam

Figure 5 compares the mid-span load-deflection curves of the beam obtained by a nonlinear method and the experimental results given by Du et al. (2021). In all four composite beam samples, the finite element simulation (FEM) accurately estimated the curve of the experimental part and thus provided a globally consistent estimate of the composite beam behavior under load. It offers the possibility to thoroughly analyze the different stages of structural deformation and to visualize the behavior up to the ultimate loading phase, which is difficult to accomplish by

experimental tests alone. However, the slight overestimation of ductility observed in the FEM simulation results compared to the experimental data can be explained by the use of simplified elastoplastic laws to represent the behavior of steel. The force-deflection curves of steel-concrete composite beams in nonlinear analysis do not have a descending branch in this study due to the ductility of steel and the application of an elastoplastic or bilinear constitutive law, which influences the curve by delaying the formation of a decreasing branch. Steel can reach its plastic domain without immediately losing its strength. Indeed, once the steel enters its plastic phase, the stiffness of the beam decreases, and the force-deflection curve tends to stabilize or become horizontal. This type of curve is observed by Chiorean & Buru (2017) and Benyahi et al. (2021) and by Luo et al. (2012) which confirms the results obtained in the FEM model studied.

Table 2 – Plastic resistance moments for each concrete class

Specimen	Plastic resistance moment (kN.m)M_{plRd}		Ultimate Abaqus moment (kN.m)	Ultimate experimental moment (kN.m)	$\frac{M_{abaqus}}{M_{exp}}$
	for γ_c=1	for γ_c=1.5			
C25	365.87	332.0336	355.68	341.3	1.04
C45	422.79	388.9604	392.41	378.8	1.03
C65	441.23	416.6237	423.68	408.8	1.04
C80	450.785	430.9544	432.45	423.8	1.02

Table 3 – Reliability indices and probabilities of failure

Specimen	Abaqus		
	MCS	FORM	SORM
C25	$P_f = 0.3509$	$\beta = 0.3443$ $P_f = 0.3653$	$P_f = 0.3571$
C45	$P_f = 0.0043$	$\beta = 2.6184$ $P_f = 0.0044$	$P_f = 0.0043$
C65	$P_f = 1.1700e-04$	$\beta = 3.7918$ $P_f = 7.4775e-05$	$P_f = 7.2567e-05$
C80	$P_f = 4.0000e-06$	$\beta = 4.4518$ $P_f = 4.2580e-06$	$P_f = 4.1438e-06$

Table 2 presents a comparison between the ultimate moment obtained by theory and the test. The results demonstrate a good agreement between the experimental ultimate moments and those calculated with Abaqus, which confirms the used simulation method. The observed ratios $\mathrm{M_{abaqus}/M_{exp}}$ are relatively low and fluctuate between 1.02 and 1.04, which is generally acceptable compared to 1.01 found by Du et al. (2021) and Mans et al. (2001), as well as between 0.95 and 1.05 for Nie et al. (2009) and 1.03 for Youn et al. (2011). According to the results of Table 3, it is evident that the reliability of steel-concrete composite structures varies considerably depending on the quality of the concrete used. For concrete class C25, the probability of failure is high $P_f = 0.3509$, indicating low structural reliability. Increasing the concrete class C45, C65, C80 results in a decrease in the probability of failure $P_f = 0.0043$, $1.1700e-04$, $4.0000e-06$, while the reliability index β increases $\beta = 0.3443, 2.6184$, 3.7918 , 4.4518, indicating increased strength and safety. Consistent results are obtained using different techniques, the MCS, the FORM and the SORM, confirming that composite beams with high-quality concrete slabs C65 and C80 are more reliable than those with low-quality concrete slabs C25. In summary, the choice of high-quality concrete, such as C65 and C80, ensures strong structural performance and increased reliability, making these composite beams ideal for supporting high loads and meeting strict safety requirements. The reliability results obtained by the FORM, the SORM and the MCS also show that when the limit state functions are nonlinear, the SORM method provides a better approximation than the FORM. Indeed, the SORM considers the limit state surface as a curve shape (hyperboloid), while the FORM simplifies it into a tangent plane. This more realistic approach allows the SORM to obtain results very close to those of the Monte Carlo method known for its high accuracy. The studies of Yu et al. (2017) and Morse et al. (2017) corroborate these results.

According to Eurocode 2 and many international codes and regulations (fib, 2013; The Government of the Hong Kong Special Administrative Region: Buildings Department, 2020; ACI Committee 318, 2019) the safety factor $\gamma c = 1.5$ is used in structural calculations to ensure a certain level of reliability by reducing the characteristic strength of concrete. This explains the inherent uncertainties due to the design and measurement during construction. In this study, we used the actual mean values of the geometric and material parameters for the reliability analysis, while taking into account the uncertainties by integrating the standard deviation of these parameters. The results of the reliability analysis (Figure

7) and the plastic resistance moments (Figure 6) for $\gamma c = 1$ and $\gamma c = 1.5$ were compared to evaluate the safety margins provided in the calculations according to Eurocode 4.

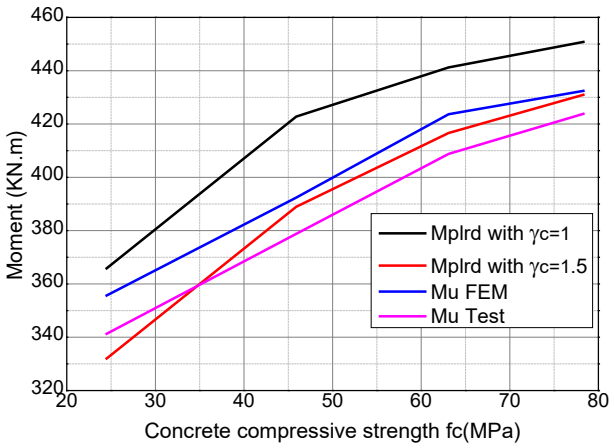

Figure 6 – Moment variation as a function of the concrete compressive strength

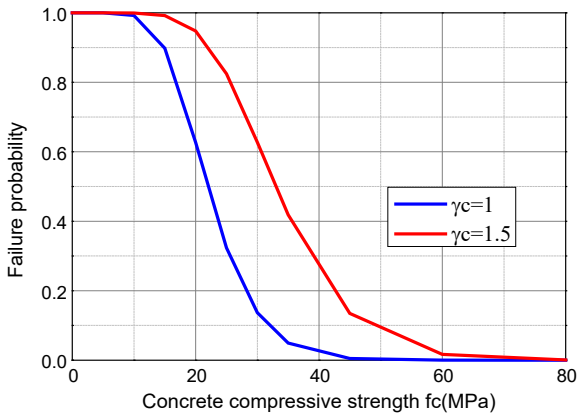

Figure 7 – Variation in failure probability as a function of the concrete compressive strength

As shown in the curve in Figure 7, the safety factor has a significant impact on the reliability index, which is based on the concrete compressive strength. When $\gamma c = 1$, the initial reliability index is high, but it decreases

as the concrete strength decreases, indicating a decrease in structural safety margins and an increased probability of failure when the concrete compressive strength is low. This decrease is particularly noticeable when f_c values are around 20 MPa. In contrast, when $\gamma c = 1.5$, the reliability index remains higher overall f_c, indicating a more robust design with higher safety margins. Even at higher concrete strengths, where the index $\gamma c = 1$ becomes critical, $\gamma c = 1.5$ ensures significantly higher reliability. According to Eurocode standards, the results demonstrate the importance of using an appropriate safety factor to ensure good structural reliability.

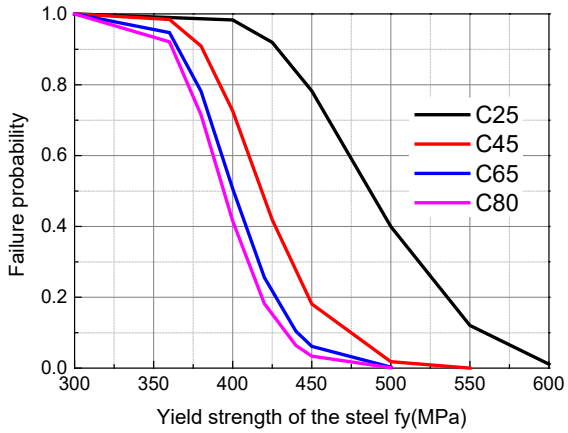

Figure 8 – Variation in failure probability as a function of the yield strength of steel

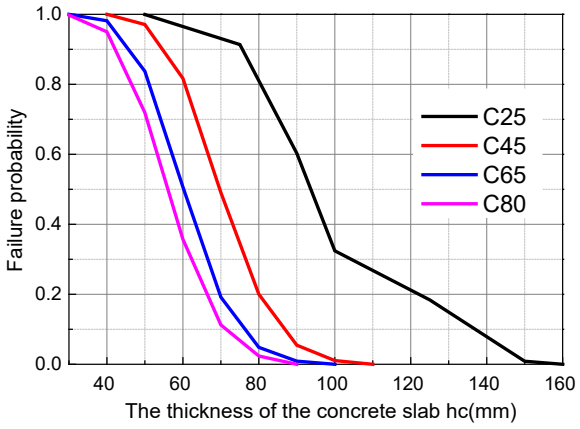

Figure 9 – Variation in failure probability as a function of the concrete slab thickness

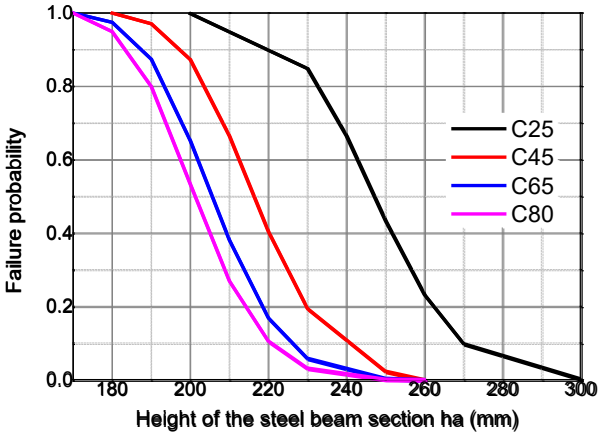

Figure 10 – Variation in failure probability as a function of the steel beam height

The results of the three last Figures (8, 9 and 10) show that several factors influence the probability of failure P_f of the steel concrete composite beam. First, an increase in the steel beam strength generally leads to a decrease in failure probability (Figure 8) because stronger steel increases the structural performance. This decrease is even more pronounced when the concrete has a high strength C45, C65 or C80, because stronger concrete requires stronger adhesives to maximize its potential. In parallel, a higher section height of the composite section, whether concrete (Figure 9) or steel (Figure 10) reduces failure probability while improving the stiffness of the beam. The probability of failure decreases with increasing height for all types of concrete, with a stronger effect for high-strength concrete, which exhibits superior performance even at lower section heights. Therefore, increasing the overall height of the composite section and improving the strength of the steel beam significantly reduces the probability of failure of the composite system, with benefits that are particularly evident when the concrete is high strength.

Conclusion

The evaluation of steel-concrete composite beams reveals several essential insights into their structural reliability and performance. The finite element method (FEM) has demonstrated high accuracy in predicting the behavior of composite beams under load, by closely aligning with experimental results. The FEM remains a valuable tool to analyze structural deformation steps and predict failure outcomes.

The comparison between the original values and the experiments confirms the simulations using the FEM and maintains a good conformational system. Notably, the failure probability P_f is a sign that the high-strength concrete is used. The concrete classes C45, C65 and C80 have a safer and more reliable system than the concrete C25. This trend relieves the import of high-strength concrete to increase the structure performance and safety.

Furthermore, the results highlight that increasing the section height of both concrete and steel components reduces the failure probability P_f, thereby improving beam stiffness and overall reliability. The benefits of these design adjustments are more pronounced with high-strength concrete, which retains its performance advantages even at smaller section heights.

The results highlight the importance of selecting high-strength materials and optimizing section dimensions to improve the safety and reliability of composite beams, aligning with Eurocode standards and ensuring robust structural performance.

References

-ACI Committee 318. 2019. *ACI CODE-318-19(22): Building Code Requirements for Structural Concrete and Commentary (Reapproved 2022)* [online]. Availble at: https://www.concrete.org/store/productdetail.aspx?ItemID=318U19 [Accessed: 14 November 2024]

Bartlett, F.M., Dexter, R.J., Graeser, M.D., Jelinek, J.J., Schmidt, B.J. & Galambos, T.V. 2003. Updating Standard Shape Material Properties Database for Design and Reliability. *Engineering Journal*, 40(1), pp.2-14. Available at: https://doi.org/10.62913/engj.v40i1.800.

Benyahi, K., Bouafia, Y., Oudjene, M., Barboura, S. & Kachi, M.S. 2021. Numerical Procedure for the Three-Dimensional Nonlinear Modelling of Composite Steel–Concrete Beams. *International Journal of Steel Structures*, 21(3), pp.1063-1081. Available at: https://doi.org/10.1007/s13296-021-00490-1.

-CEN (The European Committee for Standardization). 1994. *CEN ENV 1994-1-2:1994(MAIN) Eurocode 4: Design of composite steel and concrete structures - Part 1-2: General rules - Structural fire design* [online]. Available at: https://standards.iteh.ai/catalog/standards/cen/6476197f-10f8-435d-8813-683bbdbd497e/env-1994-1-2-1994 [Accessed: 14 November 2024].

-CEN (The European Committee for Standardization). 2004. *CEN EN 1992-1-2:2004(MAIN) Eurocode 2: Design of concrete structures - Part 1-2: General rules - Structural fire design* [online]. Available at: https://standards.iteh.ai/catalog/standards/cen/597bff7e-4f49-446f-ac9b-69829a09d098/en-1992-1-2-2004 [Accessed: 14 November 2024].

Chaves, I.A., Beck, A.T. & Malite, M. 2010. Reliability-based evaluation of design guidelines for cold-formed steel-concrete composite beams. *Journal of the Brazilian Society of Mechanical Sciences and Engineering*, 32(5), pp.442-449. Available at: https://doi.org/10.1590/S1678-58782010000500003.

Chiorean, C.G. & Buru, S.M. 2017. Practical nonlinear inelastic analysis method of composite steel-concrete beams with partial composite action. *Engineering Structures*, 134, pp.74-106. Available at: https://doi.org/10.1016/j.engstruct.2016.12.017.

Daanoune, N., Kernou, N., Fellah, M. & El-Hiti, G.A. 2024. Reliability and mechanical performance of timber-concrete composite beams in the non-linear domain. *Građevinar,* 76(11), pp.993-1003. Available at: https://doi.org/10.14256/JCE.4055.2024.

-Dassault Systèmes. 2016. *Abaqus analysis user's guide*. Dassault Systèmes, SIMULIA.

Du, H., Hu, X., Shi, D. & Xue, W. 2021. Flexural Performance of Composite Beams Using High-Strength Steel and High-Strength Concrete. *International Journal of Steel Structures,* 22, pp.27-41. Available at: https://doi.org/10.1007/s13296-021-00558-y.

Ellingwood, B., MacGregor, J.G., Galambos, T.V. & Cornell, C.A. 1982. Probability Based Load Criteria: Load Factors and Load Combinations. *Journal of the Structural Division*, 108(5), pp.978-997. Available at: https://doi.org/10.1061/JSDEAG.0005959.

-fib (The International Federation for Structural Concrete). 2013. *fib Model Code for Concrete Structures 2010*. International Federation for Structural Concrete (fib). Available at: https://doi.org/10.1002/9783433604090.

Grandhi, R.V. & Wang, L. 1999. *Structural Reliability Analysis and Optimization: Use of Approximations.* NASA/CR-1999-209154. Document ID:19990049421 [online]. Available at: https://ntrs.nasa.gov/citations/19990049421 [Accessed: 14 November 2024].

Guo, Y.-T., Chen, J., Nie, X., Tao, M.-X., Wang, J.-J. & Fan, J.-S. 2020. Investigation of the shear resistances of steel–concrete–steel composite structures with bidirectional webs. *Journal of Constructional Steel Research*, 164, art.number:105846. Available at: https://doi.org/10.1016/j.jcsr.2019.105846.

Haldar, A. & Mahadevan, S. 1999. *Probability, Reliability, and Statistical Methods in Engineering Design*. Wiley. ISBN: 978-0-471-33119-3.

Hognestad, E. 1951. *A study of combined bending and axial load in reinforced concrete members*. University of Illinois Engineering Experiment Station: Bulletin Series No. 399.

Johnson, R.P. 2018. *Composite Structures of Steel and Concrete: Beams, Slabs, Columns and Frames for Buildings*. Wiley. Available at: https://doi.org/10.1002/9781119401353.

Liang, Q.Q. 2018. *Analysis and design of steel and composite structures, 1st Edition*. CRC Press. Available at: https://doi.org/10.1201/9781315274843.

Luo, Y., Li, A. & Kang, Z. 2012. Parametric study of bonded steel–concrete composite beams by using finite element analysis. *Engineering Structures*, 34, pp.40-51. Available at: https://doi.org/10.1016/j.engstruct.2011.08.036.

Lydia, M. & Nassim, K. 2022. Reliability Analysis and Comparative Study of Ordinary Concrete and High Performance Concrete Filled with Steel Tube under Axial Compression. *International Journal of Engineering Research in Africa*, 61, pp.245-261. Available at: https://doi.org/10.4028/p-9h1zq6.

Mamuda, A., Abubakar, I. & Samson, D. 2018. Reliability-Based Structural Safety Evaluation of Concrete-Steel Composite Beams According to Euro Code 4. *Engineering Physics*, 2(2), pp.32-40 [online]. Available at: https://www.sciencepublishinggroup.com/article/10.11648/j.ep.20180202.11 [Accessed: 14 November 2024].

Mans, P., Yakel, A.J. & Azizinamini, A. 2001. Full-Scale Testing of Composite Plate Girders Constructed Using 485-MPa High-Performance Steel. *Journal of Bridge Engineering*, 6(6), pp.598-604. Available at: https://doi.org/10.1061/(ASCE)1084-0702(2001)6:6(598).

Morse, L., Khodaei, Z.S. & Aliabadi, M.H. 2017. Multi-Fidelity Modeling-Based Structural Reliability Analysis with the Boundary Element Method. *Journal of Multiscale Modelling*, 8(03n04), art.number:1740001. Available at: https://doi.org/10.1142/S1756973717400017.

Nie, J., Li, H. & Tang, L. 2009. Experimental study on HSS-concrete composite beams. *Journal of Building Structures*, 30(02), pp.64-69 [online]. Available at: http://www.jzjgxb.com/EN/Y2009/V30/I02/64 [Accessed: 14 November 2024].

Rackwitz, R. 2001. Reliability analysis—a review and some perspectives. *Structural Safety*, 23(4), pp.365-395. Available at: https://doi.org/10.1016/S0167-4730(02)00009-7.

Rezaie, F., Farnam, S.M. & Pour Bahar, S. 2022. Numerical Analysis of Reinforced Concrete Beam-Column Joints without Transverse Reinforcement. *Numerical Methods in Civil Engineering*, 7(2), pp.50-60. Available at: https://doi.org/10.52547/nmce.2022.238.

-The Government of the Hong Kong Special Administrative Region: Buildings Department. 2020. *Code of Practice for Structural Use of Concrete 2013 (2020 Edition).* The Government of the Hong Kong Special Administrative Region: Buildings Department [online]. Available at: https://www.bd.gov.hk/doc/en/resources/codes-and-references/code-and-design-manuals/CoP_SUC2013e.pdf [Accessed: 14 November 2024].

Youn, S.-G., Bae, D. & Kim, Y.-J. 2011. Ultimate Flexural Strength of Hybrid Composite Girders Using High-Performance Steel of HSB600 at Sagging Bending. In: *Composite Construction in Steel and Concrete VI,* pp.680-690. Available at: https://doi.org/10.1061/41142(396)56.

Yu, B., Ning, C.-L. & Li, B. 2017. Probabilistic durability assessment of concrete structures in marine environments: Reliability and sensitivity analysis. *China Ocean Engineering*, 31(1), pp.63-73. Available at: https://doi.org/10.1007/s13344-017-0008-3.

Efecto de la resistencia a la compresión del hormigón sobre la fiabilidad y el momento plástico de vigas mixtas de acero y hormigón

Nabil Daanoune, **autor de correspondencia**, *Nassim* Kernou

Universidad de Bejaia, Facultad de Tecnología,
Laboratorio de Ingeniería de la Construcción y Arquitectura (LGCA),
Bejaia, República Argelina Democrática y Popular

CAMPO: ingeniería mecánica, ingeniería civil
TIPO DE ARTÍCULO: artículo científico original

Resumen:

Introducción/objetivo: Este estudio investigó la influencia de la resistencia a la compresión del hormigón en la confiabilidad y el momento de resistencia plástica de las vigas compuestas de acero y hormigón. El objetivo fue evaluar el impacto de las variaciones de la resistencia del hormigón en el desempeño estructural, con especial atención al momento de resistencia plástica, que es crítico para la seguridad y la conformidad de la viga compuesta.

Métodos: Para modelar el comportamiento no lineal del hormigón, Abaqus creó un modelo numérico tridimensional que incluye un modelo de plasticidad del daño del hormigón (CDP). Se realizó un análisis de confiabilidad y se evaluó la probabilidad de falla utilizando simulaciones de Monte Carlo (MCS) y métodos de confiabilidad de primer orden (FORM) y segundo orden (SORM). La función de estado límite se determinó de acuerdo con los criterios del Eurocódigo 4 considerando la resistencia a la compresión del hormigón de 25 a 80 MPA.

Resultados: Como resultado, se encontró que la resistencia a la compresión del hormigón afecta significativamente el momento de resistencia plástica y el índice de confiabilidad de la viga compuesta. La alta resistencia del hormigón mejora el momento de resistencia plástica y el índice de confiabilidad varía según la propiedad geométrica y del material de la sección compuesta y las condiciones de carga.

Conclusión: La resistencia a la compresión del hormigón es un parámetro importante que determina las características estructurales y la seguridad de las vigas mixtas de acero y hormigón. Esto puso de relieve la necesidad de considerar la variabilidad de la resistencia del hormigón al diseñar y evaluar estructuras mixtas para garantizar el cumplimiento de los estándares de confiabilidad.

Palabras claves: viga compuesta, modelado no lineal, momento resistente plástico, análisis de confiabilidad, análisis de elementos finitos, probabilidad de falla.

Влияние прочности бетона при сжатии на надежность и момент пластического сопротивления сталебетонных композитных балок

Набиль Даанун, **корреспондент**, *Нассим* Керноу

Университет Беджая, технологический факультет,
Лаборатория строительной инженерии и архитектуры (LGCA),
г. Беджая, Алжирская Народная Демократическая Республика

РУБРИКА ГРНТИ: 67.09.33 Бетоны. Железобетон. Строительные растворы, смеси, составы
ВИД СТАТЬИ: оригинальная научная статья

Резюме:

Введение/цель: В данном исследовании изучалось влияние прочности бетона при сжатии на надежность и момент пластического сопротивления сталебетонных композитных балок. Цель исследования заключалась в оценке влияния изменений прочности бетона на эксплуатационные характеристики конструкции. Особое внимание уделялось моменту пластического сопротивления, который имеет решающее значение для безопасности и прочности композитной балки.

Методы: Для моделирования нелинейного поведения бетона компания «Abaqus» создала трехмерную численную модель, включающую модель пластичности бетона при повреждении (CDP). Был проведен анализ надежности и оценка вероятности отказа с использованием моделирования по методу Монте-Карло (MCS) и методам определения надежности первого порядка (FORM) и второго порядка (SORM). Функция предельного состояния была определена в соответствии с критериями Еврокода 4 с учетом прочности бетона на сжатие от 25 до 80 МПа.

Результаты: Результаты исследования показали, что прочность бетона на сжатие существенно влияет на момент пластического сопротивления и показатель надежности композитной балки. Высокая прочность бетона повышает пластическое сопротивление, а показатель надежности варьируется в зависимости от геометрических параметров, свойств композитных материалов и условий нагружения.

Вывод: Прочность бетона на сжатие является важным параметром, определяющим конструктивные характеристики и безопасность сталебетонных композитных балок. Этот факт подчеркивает необходимость учета изменений прочности бетона при проектировании и оценке композитных конструкций для обеспечения соответствия стандартам надежности.

Ключевые слова: композитная балка, нелинейное моделирование, момент пластического сопротивления, анализ надежности, конечно-элементный анализ, вероятность отказа.

Утицај чврстоће бетона при притиску на поузданост и моменат пластичности спрегнутих челично-бетонских носача

Набил Данун, **аутор за преписку**, *Насим* Керну

Универзитет у Беџаји, Технолошки факултет,
Лабораторија за грађевинско инжењерство и архитектуру (ЛГЦА),
Беџаја, Народна Демократска Република Алжир

ОБЛАСТ: машинство, грађевинарство
КАТЕГОРИЈА (ТИП) ЧЛАНКА: оригинални научни рад

Сажетак:

Увод/циљ: У овој студији испитан је утицај чврстоће бетона при притиску на поузданост и пластични отпорни моменат спрегнутих носача од челика и бетона. Циљ је био да се процени утицај различитих чврстоћа бетона на понашање конструкције, с посебним нагласком на пластични отпорни моменат који је критичан за сигурност и испуњавање захтева за спрегнути носач.

Методе: За моделирање нелинераног понашања бетона, Абакус је креирао тродимензионални нумерички модел који обухвата модел оштећења бетона услед пластичности (Concrete Damage Plasticity –CDP model). Анализирана је поузданост, а вероватноћа отказа је процењена помоћу симулација Монте Карло (MCS), као и помоћу метода поузданости првог (FORM) и другог реда (SORM). Функција граничног стања одређена је према критеријумима Еврокода 4 узимајући у обзир чврстоћу бетона при притиску од 25 до 80 MPA.

Резултати: Показано је да чврстоћа бетона при притиску знатно утиче на пластични отпорни моменат и индекс поузданости спрегнутог носача. Висока чврстоћа бетона побољшава пластични отпорни моменат, док индекс поузданости варира зависно од својстава материјала, геометрије спрегнутог пресека, као и услова оптерећења.

Закључак: Чврстоћа бетона при притиску важан је параметар који одређује структурне карактеристике и сигурност спрегнутих носача од челика и бетона. Зато је при пројектовању и процени спрегнутих конструкција неопходно да се варијабилност чврстоће бетона узме у обзир како би се осигурало поштовање стандарда поузданости.

Кључне речи: спрегнути носач, нелинеарно моделирање, пластични отпорни моменат, анализа поузданости, анализа коначних елемената, вероватноћа отказа.

Paper received on: 04.10.2024.
Manuscript corrections submitted on: 28.01.2025.
Paper accepted for publishing on: 29.01.2025.

Application of different hardware and software in the concept of digital pilot training and selection

Aleksandar Z. Knežević[a], *Aleksandar* G. Bukvić[b], *Branimir* B. Krstić[c]

University of Defense in Belgrade, Military Academy, Belgrade, Republic of Serbia

[a] Department of Air Force,
e-mail: aleksandar.knezevic@va.mod.gov.rs, **corresponding author**,
ORCID iD: https://orcid.org/0000-0001-6786-4530

[b] Department of Military Mechanical Engineering,
e-mail: aleksandar.bukvic@mod.gov.rs, corresponding author,
ORCID iD: https://orcid.org/0000-0002-3025-8446

[a] Department of Military Mechanical Engineering,
e-mail: branimirkrstic@yahoo.com,
ORCID iD: https://orcid.org/0000-0002-9612-6104

https://doi.org/10.5937/vojtehg73-54803

FIELD: mechanical engineering
ARTICLE TYPE: original scientific paper

Abstract:

Introduction/purpose: In many military air forces and civil aviation organizations that use or own training aircraft equipped with a digital cockpit, training tools such as trainers and simulators are understood to a varying extent. Special attention is paid to the ratio of hours spent training on the real aircraft to the number of hours spent on the simulator. This approach in training professional circles and the public is called Live virtual constructive. For all other teaching aids used for preparation for training, neither the methodology nor the extent of their use has been specifically investigated. The research aims to develop instruments that will measure and evaluate the success and qualitative progress in pilot training achieved by using the digital cabin space, based on which a decision can be made about further training for a specific aircraft type.

Methods: In conjunction with a PC-based aviation training device and advanced statistical analyses, an eye movement tracking device will help arrive at a reference pattern of instrument observation to train pilots and select pilot candidates.

ACKNOWLEDGMENT: The authors are grateful for the financial support through three projects from the Ministry of Defense of the Republic of Serbia (project name: VA-TT/5/13-15 „Application of digital cabin space in pilot training" and VA-TT-2/19-21 „Investigation of perceptual and motor characteristics of pilot cadets in instrument flying on piston and jet aircraft", VA-TT/2/24-26 "Application of concept of digital training and pilot's selection").

Results: The proposed concept's research includes detailed descriptions of the application of trainers and teaching aids with different profiles, which significantly impact the quality of the implementation of the digital cabin space in the training of cadet pilots.

Conclusion: Given that the Military Academy educates cadet pilots who continue their training in the operational flying units of the Serbian Armed Forces (SAF), it is essential that during the period spent at the Military Academy, their quality theoretical preparation be carried out.

Keywords: flight training, simulation, hardware, software, eye tracking.

Introduction

Flight simulation systems come in various forms and provide varying assistance in the training of candidate pilots and trained pilots. Flight simulators and trainers which are known today can be classified into the following groups:

- Full Flight Simulator,
- Flight Training Device,
- Flight and Navigation Procedures Trainer, and
- Basic Instrument Training Device.

The flight simulation and training device can be any of the above simulator/trainer types. All types of simulators and trainers have a common name: Flight Simulation Training Device.

For each of the mentioned types of devices for flight simulation and training, there is a more detailed division according to the EASA (European Aviation Safety Agency), which goes along with the corresponding characteristics that each device must meet (EASA, 2018). The breakdown is given in Table 1.

At the end of the 20th century, a device based on the PCATD (PCATD- Personal Computer-Based Aviation Training Device) became available to pilot candidates and their instructors for training on the ground. These devices consist of a display console, a PC monitor that houses the instruments of the aircraft being flown and a controller used for control.

At the beginning of the 21st century, there was an increased emphasis on using PCATD personal computers in flight training. Today's computers can realistically represent high-quality situations and instruments on board an airplane in life-size. Current technology has also succeeded in providing aerodynamic models and near-realistic flight controllers used by the pilot in flight and having the same high accuracy

as the devices intended for training a particular type of aircraft. The U.S. Federal Aviation Administration (FAA) has approved using these devices in training as the equivalent of real flight time, but only for a specific type of flight and a certain number of hours defined by the FAA (FAA, 1997).

Table 1 – Distribution of types of flight simulation and training devices according to the EASA

(Flight Navigation and Procedures Trainer - FNTP)
• EASA FNTP Level I
• EASA FNTP Level II
• EASA FNTP Level III
• MCC (multi crew cooperation). Not a true "level" of qualification, but an add-on that allows any level of FNTP to be used for multi crew cooperation training.
Flight Training Devices (FTD)
• EASA FTD Level 1
• EASA FTD Level 2
• EASA FTD Level 3 (Helicopter only)
Full Flight Simulators (FFS)
• EASA FFS Level A
• EASA FFS Level B
• EASA FFS Level C
• EASA FFS Level D

Personal computers must have special software for simulating flights, and the most suitable for use on the market is "Microsoft Flight Simulator," as an amateur and gaming software for flight simulators. Pilots can practice procedures for the types of aircraft they are trained in. The PCATD provides capabilities and functions for practicing instrument and instrument flying tasks. Deviations are observed in exercises for flight in instrument flight conditions (IFR) which cannot be performed as well as in other simulators or, of course, in real aircraft.

This paper concerns the concept of digital training and the selection of cadet pilots at the Military Academy. The technical solution implemented has introduced and applied the concept of pilot training for digital cabin space, which, in addition to trainers and simulators, envisages other methods and synthetic means of different profiles.

The optimal pilot training profile was created according to the needs of the Air Force and Air Defense. This model can be modified and adapted to the needs of civil aviation organizations in training pilots who use aircraft equipped with digital cockpits.

The Air Force Command has issued a certificate of use of the Trainer for the aircraft of the Serbian Armed Forces.

Research methods have been developed to evaluate the success and progress of cadet pilot training achieved by applying digital cabin space. On this basis, a decision can be made on the further education of each candidate for a particular aircraft type. This technical solution was developed in two projects funded by the Ministry of Defense, namely:

1. VA-TT/5/13-15 "Application of Digital Cabin Space in Pilot Training" Decision of the Senate of the University of Defense, No. 9/11 of 15 November 2012.
2. VA-TT-2/19-21 "Research of Perceptual and Motor Characteristics of Cadet Pilots in Instrument Flying on Piston and Jet Airplanes" Decision of the Senate of the University of Defense, No. 3/82 of 5 December 2018.

Methodology

Materials

Interactive learning materials

To master theoretical knowledge in aviation, cadet pilots use CAE Oxford Aviation Academy interactive materials in compliance with the EASA. The materials are interactive books and multimedia (CBT Computer Based Training). Each lesson is accompanied by clear and precise narrations that guide the cadet-pilot through the material. During the many years of implementation of CBT, cadet pilots have shown better results in preparations for practical flights on the Lasta aircraft. The Lasta training plane features a cockpit built by the American company Garmin. At the Military Academy, Garmin software and a hardware simulator for the Garmin 500/600 are used, Figure 1. Cadet pilots learn to navigate Garmin systems using Flight Plan pages and GPS direct-to-head courses. Generations who have used these training tools have shown better results in the initial stages of basic flight training.

Figure 1 – Garmin 500, the instrument found in the Lasta aircraft (left), and a desktop trainer with Garmin software used to train cadet pilots

PCATD (Flight Simulator based on commercial software)

Simulators imitate parts of the aircraft and components with which the pilot has direct contact: the cockpit with the control units, instruments, the environment in which the use is carried out, and more. The use of simulators achieves significant savings because it avoids the consumption of aircraft resources, fuel, and ordnance (if it is combat training), does not pollute the environment, reduces the risk of any injuries or accidents, and it is possible to practice emergency procedures that are difficult or risky to carry out in reality. Simulator training cannot fully recreate all the effects and conditions that occur in reality, and that must be practiced on actual aircraft.

The Lasta aircraft trainer is a tool used to train cadet pilots in visual and instrumental flying using commercially available hardware and software developed at the Military Academy within the project "Application of Digital Cabin Space in Pilot Training." The original software add-on (Figure 2), which is the result of the work of the research team of the Military Academy, has the following characteristics:

1. High precision in geometry,
2. A large number of polygons (63813), and
3. High-resolution external textures (4K 3480 x 1280 pixels).

The virtual cabin space has the following characteristics:

1. High precision in geometry,
2. A large number of polygons (49490),
3. High-resolution textures (4K 3480 x 1280),
4. Fully "clickable",
5. Equipped with the appropriate avionics, and
6. Brightness and intensity in line with reality.

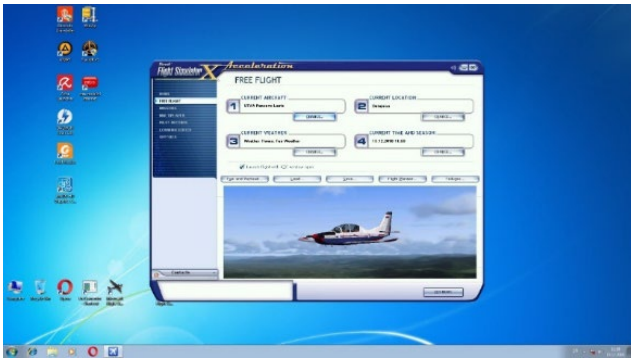

Figure 2 – Software add-on for the Lasta aircraft in Flight Simulator 10

For the Flight Simulator 10 software programming environment, a simulator containing a simulation model of the Lasta aircraft has been created. This simulator is classified as a "Personal Computer-Based Aviation Training Device (PCATD)". It is based on the computer platform for flight simulation "Microsoft Flight Simulator X," with a field of view of 90 degrees (Figure 3) and a field of view of 270 degrees (Figure 4). This configuration allows for the exact visualization as in a real aircraft. All the characteristics of the flight dynamics of the aircraft are defined through the "XML" code that is implemented on the computer platform.

Figure 3 – PCATD trainer for the Lasta aircraft with a 90° field of view

Figure 4 – PCATD trainer for the Lasta aircraft with a field of view of 270°

The flight controls used on this trainer are identical in shape, color and function to the controls in a real aircraft (Figure 5).

Figure 5 – Controls in the cockpit of a Lasta aircraft (left) and in the physical setup of the PCATD trainer (right)

This way, adapting to the cabin space and creating a mental image of the working environment is faster, easier, and cheaper. Adding the Martin Baker seat, built into the flight simulator, creates an additional positive impression of the working space in the aircraft (Figure 3).

The control surfaces include a joystick, a rudder control, and a throttle control with a USB input for a computer. These components are intended to control the aircraft around the longitudinal, lateral, and vertical axes, as well as the engine control (power and pitch), on which additional switches are used to control the landing gear and flaps. Before the flight, meteorological conditions can be defined, as well as failures and the time of occurrence of failures during the flight. Speed, altitude, course, time, and positions on the map can be read at the end of the flight.

A trainer of this type is not of the highest technological complexity. Still, it provides training in instrument flying procedures, the use of devices and instruments, and regular and emergency procedures.

The flight simulator with software add-on for the Lasta aircraft consists of three high-resolution (HD) projectors (Figure 6 position 10) which project their image onto three projection screens (Figure 6 position 11), and one high-resolution (HD) monitor. The projectors are positioned at an angle to capture a field of view of 90° x 60° and thus give an overall image of 3480 x 1280 pixels. The software add-on allows them to spherically rotate the image they display on the canvases with the help of an IR sensor to track head movements.

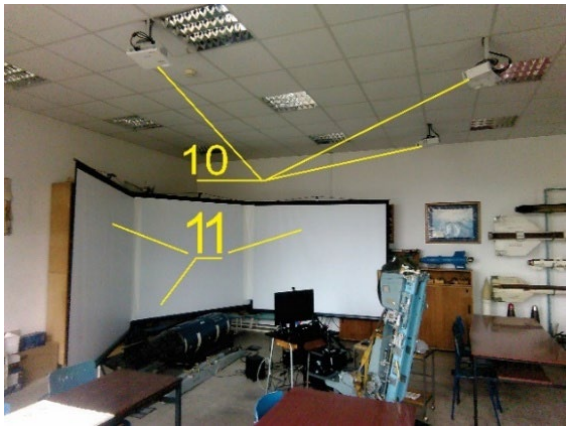

Figure 6 – Arrangement of the projection surfaces and the projectors on the PCATD simulator

A view of the cabin area is given on a single touchscreen which presents the pilot with only the instrument panel. The left and right consoles with switches found in a real aircraft are absent.

With the modernization of the Lasta aircraft trainer, the field of view has been expanded. It is provided by three 4K resolution projectors (short throw projectors) for projecting images from a short distance and a cylindrical screen measuring 270° x 60° (Figure 7).

Figure 7 – Modernized PCATD trainer for the Lasta aircraft and the position of the short-throw projectors (rounded positions)

This improvement has eliminated the use of IR sensors which existed in the previous variant of the trainer, and increased the angle to which it is possible to see the aircraft surroundings up to 270°. This is important for the training of fighter pilots, where the dynamics of the movement of the gaze is far more intense and where it is insisted that the relations between the projection of the wings and the orientation on the ground (visual orientation) are compared. This is due to the possibility of a 270° field of view (Figure 8). The Lasta aircraft trainer exceeds the criteria defined for the width of the field of view on the category D FFS simulator (180°x60°) and the category 3 FTD trainer (150°x60°) as defined by the EASA (European Union Aviation Safety Agency (EASA, 2018).

Figure 8 – Extension of the field of view to the PCATD trainer for the Lasta aircraft

An eye-tracking device was demonstrated as part of this trainer (Figure 9, position 6). The schedule of attention distribution (shifting view from instrument to instrument) in the glass cockpit configuration was recorded and compared with the established observation scheme of analog instruments. The experiment was conducted with cadet pilots as well as experienced pilots.

Figure 9 – Eye-tracking device

The concept of digital training and the selection of pilots for training purposes has been extended to the needs of training helicopter pilots. A version of the PCATD trainer has been created, which has the width of the field of view of the FTD trainer of the third category (150°x60°), a projection screen in the form of a spherical section, and a pilot seat on which the pilot controls for the helicopter are installed (the so-called cyclic and collective stick) (Figure 10).

Figure 10 – PCATD trainer for the Gazelle helicopter with analog instruments and with a projection surface in the form of a spherical section measuring 150° x 60°

The characteristic cockpit view of the helicopter in Figure 10 satisfies the required projection width in contrast to the aircraft training needs. Analog instruments found on older types of helicopters are especially characteristic.

The simulator allows the flight to be recorded and later analyzed by incorporating the FS recorder plug-in, an add-on to the basic software. Flight parameter data and footage can then be reproduced as a separate flight or within a next-flight scenario. This option is used when analyzing flights with cadet pilots, although it is not part of the standard simulation software.

The main advantage of this solution is the multifunctionality of the trainers' applications depending on the need, whether it is the training of cadet pilots, fighter pilots or psychological and medical selection from the aspect of checking future pilots.

Virtual reality (VR) devices

In 2021, the EASA announced that it had approved a virtual reality training solution for a helicopter (EASA, 2021), which is a big step for this method of training.

The VR environment is simple and easy to implement on a PCATD. High-reliability sensors in VR devices play a significant role in their success. Virtual interaction itself increases the interest of cadet pilots. The Military Academy uses Oculus Rift VR device glasses. Implementing the existing software add-on for the Lasta aircraft, which is used in the VR environment, includes the software that bridges the connection between the Oculus Rift VR device and the Microsoft Flight Simulator X.

During the training at the Military Academy, adverse effects were observed when using VR glasses, which were not mentioned in previous research and impacted the training itself. Sponges on VR glasses, which make the device comfortable, when used at high temperatures in the room, interfere with the user and affect the result of training and the execution of tasks because the glasses fog up from sweat. An additional problem arises if users wear glasses because VR glasses cannot be adapted to different diopters. In the paper entitled "A Model for the Adoption of Virtual Reality Technology for Dynamic Learning (Fussell & Troung, 2022) some interesting facts were presented about the difficulties of using VR glasses. Figure 11 shows the use of the PCATD with the VR environment, which is used at the Military Academy for the initial training of cadets.

Figure 11 – PCATD with the VR environment, the Lasta aircraft accessory

Other hardware and software used in pilot training

Sky Demon is one of the most well-known flight planning and tracking software. This software is also known as Electronic Flight Bag Software. It allows you to plan your flight as well as GPS navigation during the flight. Its unique options allow you to update aeronautical data in real time. Within its unique features, Sky Demon also has an internal simulator called X-plane. When the simulation mode of this software is started, it can be networked with the Microsoft Flight Simulator X software with the help of a

smaller software called FSX2Sky Demon located on the Google Play platform. The software takes data from the simulation currently running on the computer and plots the flight path on Google Maps (Figure 12). At the same time, it transmits speed and course data to Sky Demon. It receives feedback from Sky Demon in the form of winds that are obtained from weather stations in real time and has an impact on the flight of the model in the simulation once recorded and saved in the Google Map extension, .gpx. It can be subsequently analyzed in 3D and 2D mode (Figure 13).

Figure 12 – Using the SKY Demon software (bottom left part of the image) with the addition of the FSX2 Sky Demon app (upper left part of the image)

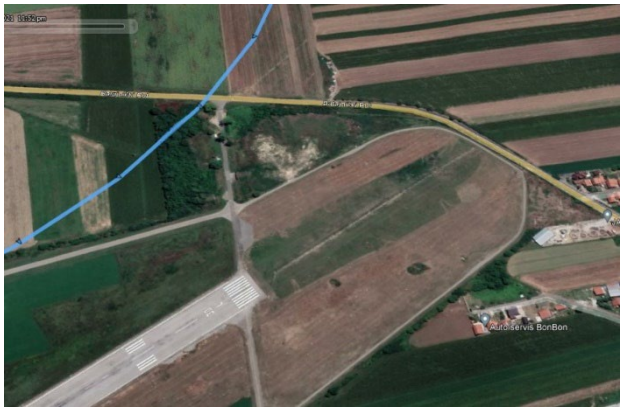

Figure 13 – Recorded trajectory from a simulated flight in the SKY Demon app and the FSX add-on for the Lasta aircraft. The trajectory is recorded in the Google Map extension .gpx

Methods

Analysis of the flight parameter data and the eye movement recording obtained from the simulator

This chapter presents an experiment conducted with cadet pilots of the Military Academy in flights in simulators with different visual environments or fidelity. The task is to spot any differences in the flight performance and presentation data in the best way. This and similar studies have been carried out using free software for these purposes. One group of cadets practiced taking off and landing with the Lasta aircraft on the school circuit in a conventional simulated environment that involved projecting the environment of the aircraft on the projection screens and the aircraft cabin on a monitor in front of the eyes of the examinees. This group of cadets served as a control group in the trial. The second group of cadets practiced taking off and landing with the Lasta aircraft on a simulator with a virtual cabin space and the aircraft surroundings. This group served as an experimental group. The first and last control flights were flown in a conventional simulated environment to examine the effect of changing the simulated environment on the flight performance and instrument observation strategies. The experiment was designed to determine whether there is a transfer of skills from one simulation environment to another.

For the experiment in which the flight parameters were compared (project number VA-TT/2/24-26), the PC flight simulator used in earlier research (projects numbered VA-TT/5/13-15 and VA-TT-2/19-21) by researchers from the Military Academy and described in the study (Vlačić et al, 2020) has been specially upgraded with Simpit Technologies' Centurion 270 PRO cylindrical 270° vision system to increase its fidelity in the field of view. The experiment used an add-on for the Lasta aircraft, a military pilot training aircraft, which falls into the category of technologically advanced aircraft due to its integrated electronic instruments (EFIS).

A new hardware configuration of the computer commercially available during the experiment allowed for a better multi-frame operation and a curved projection of an external scenario with a resolution of 3080 x 1024 pixels. Figure 14 shows the trainer with the settings from the experiment and a device that records eye movements in the background.

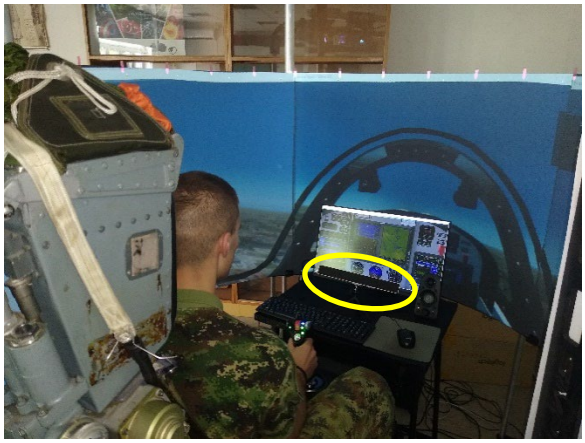

Figure 14 – Lasta aircraft trainer with 270° field of view and the eye tracking device (rounded position)

The Microsoft FSX software add-on for the Lasta aircraft has been enhanced with additional software called FlyInside FSX by FlyInside Inc. 2018. This made it possible to set up a model of the Last aircraft in virtual reality with the help of an Oculus Rift Virtual Reality headset. The Flyinside software uses the features of the Microsoft Flight Simulator and adds an interface to the VR environment. The flight dynamics and features of the original software remain the same. Figure 11 shows the exterior of the VR flight simulator, while Figure 15 shows both the flight scenery and the VR simulation presentation in the cockpit.

Figure 15 – View from the cockpit of the VR flight simulator for the Lasta aircraft

During the flight, a demonstration of the traffic pattern typically used in training to practice take-off and landing on the Lasta aircraft was used for testing. The subjects who participated in a comparison of the flight performance and instrument eye scanning strategies on the simulators of different fidelity practiced the same traffic pattern.

Matthias Neusinger (2007-2010) created the FS Recorder module to record flight performance data from the simulator used in the study by Vlačić et al. (2020). FS Recorder is free software that adds flight recording and playback functions to the core software. This software records flight data parameters during all flights in a conventional simulated environment and VR. It can record and reproduce flights of almost unlimited length. It stores data in its own frc data format. In addition, the FS Recorder converter created by Matthias Neusinger (2007-2010) was used to convert the FS Recorder frc files into text files. After conversion, the actual flight data is formatted into rows and columns, where each row contains a single set of parameters (from now on referred to as sample data), and each column represents a specific parameter. The lines represent a single sample of data and consist of a series of values separated by space (tabs or spaces). These values must correspond to the definitions of the columns (i.e., latitude, longitude, altitude, pitch, heading, flap position, instrument airspeed (IAS). Indicated Airspeed, Actual Airspeed (TAS), and True Airspeed). The most important column for synchronizing eye-tracking and flight performance footage is the "timestamp" column, which records the time interval in seconds from the start of the recording for each parameter that makes up that row of data (i.e., latitude, longitude, altitude, pitch). In this way, it is possible to compare the events in the simulation with a timer that measures time within the eye-tracking software, as they start working almost instantly.

Collection of the flight data parameters

To enter as much data as possible about the flight parameters in specific flight segments in the studio, the Proračun function was created in the R programming language. In this function, the flight performance data by segments of the traffic pattern is extracted and analyzed based on the pre-inserted part of the pilot's knowledge and experience. One part evaluates the performance of the flight in the traffic pattern, and the other part evaluates the grade according to the size of the standards that are evaluated and compared according to the official methodological manuals for training. In this study, a very important detail is the number of flights given for training as a norm defined by methodological manuals. It

represents a series of knowledge transferred and practiced from flight to flight.

Each traffic pattern flight practice contains six flights with six take-offs and landings. After the csv files for one of the respondents are imported into the R environment, to begin with; it is essential to set aside the time frame in which each traffic pattern takes place. This is achieved by filtering based on a variable that contains a value of 0 if the aircraft is in the air or 1 if the aircraft is on the ground. Since the aircraft is on the ground for a short time, filtering it based on a value of 1 is more convenient. The final value of the column is obtained - a timestamp, between which there is an interrupted time series that represents the beginning or end of a school circle. The function filters this variable and writes the data to the Times table, which has a separate appendix for each cadet pilot and each of his flights.

After that, certain required segments are reached based on filtering by several set criteria for the given time frames in which the traffic pattern takes place. The example below shows how the mean square deviation from the flight course of a given value in the segment of the school circle from the first turn to the second turn (Crosswind) is calculated.

```
if (l=="crosswind") {
        p2<- abs(cww$heading- 32)#daje promenljivoj p vrednost razlike kursa i zadanog kursa#
    prenos2<- data.frame(p2)
                rms_crs_head<-sqrt(mean(prenos2$p2^2))
        Zapis_crosswind$head_second_circle<<- prenos2$p2
                Zapis_crosswind$rms[2]<<-rms_crs_head
                print("rms_crs_head")
                print(rms_crs_head)
```

Collection of the data obtained from an eye-tracking recorder

Gaze transition strategies are defined as eye movements that an individual can perform and that are relevant to flying an airplane. Specifically, the two relevant eye movements are fixations (i.e., the time that elapses while one's gaze is focused on one particular location or the number of glances at that same point) and saccade (i.e., the rapid movement of the eyes from one point of fixation to another) (Ziv, 2016). In practice, at least when it comes to aviation, the point at which the number of views is measured is defined as an area of interest (AOI).

A sequence of gaze movements can start from any other AOI and is a return scan path or "revisit" with any other AOI. A study by Lefrancois et al. (2016) provides research results between visual patterns and flight performance with experienced pilots. It explains how they did not divide efficiently their visual attention compared to the reference crew. They assume that prerecorded experts' visual pattern could help novice pilots to adopt appropriate gaze strategies.

A study by Ayala et al. (2023) provides the results of the influence of the difficulty of the flight task on the instrument observation strategy of pilots with less flight experience. This study performed an entropy-based analysis at 10 AOI in a simulated landing scenario. A series of fixation locations were then generated for each flight. The necessary codes are written in Python to calculate the Static Gaze Entropy (SGE) and the Gaze Transition Entropy (GTE). The SGE is a measure of a view's dispersion calculated over a given viewing period. The more evenly distributed the fixations across the AOI (i.e., the wider the dispersion of the gaze), the higher the entropy. The view transition entropy (GTE) examines the complexity of a fixation sequence through the analysis of gaze transition matrices.

A similar approach to the measure of the entropy of the transition of gaze was developed by Mandal & Kang (2018) in their study. A network eye movement analysis was applied for dynamic tasks, where different AOIs were represented as network vertices (nodes), and the transition of views between them was represented by directed paths between the vertices of the network. The development of grid-based visualization and other similar attempts are an effort to replace traditional measures of transition views such as the number and duration of fixations, which did not provide a sufficiently reliable indication of the difference in observation strategies, to be more reliable.

Grid-based visualization and measurement of gaze transition requires first creating an AOI transition matrix, which is a tabular representation of the eye fixation transitions that occur between different AOI pairs (Table 2). The information about the transition matrix is used to develop a web presentation which visualizes the visual scanning strategy of the respondent.

Table 2 – Gaze transition matrix between AOIs in horizontal flight (an example)

	TO AOI			
FROM AOI	AST	AVST	EI	OC
AST	0	1	2	6
AVST	1	0	1	8
EI	1	0	0	3
OC	7	8	2	0

A way of presenting data for a static network as in Mandal et al. (2016) with some adjustments was used in the paper of Vlačić et al. (2020). The proposed four AOIs on the simulated cockpit of the Lasta aircraft for this study can be seen in Figure 16.

Figure 16 – Appearance of the cockpit of the Lasta aircraft in the Microsoft Flight Simulator and 4 AOIs for which the instrument scanning schedule was recorded in the paper Vlačić et al. (2020)

Eye movement recording was performed using the GP3 Desktop Eye Tracker from Gazepoint (Figure 9) with a sampling rate of 60 Hz and an angular accuracy of 0.5° —1°. When the simulation and the FS Recorder software are started, the recording function in the Gazepoint Analysis software is also started so that the timeline of recording flight parameters and view transition can be compared. It is interesting to note that the difference between the number of AOIs in the example from the Ayala et al. (2023) study (where there were 10) comes from the fact that the cockpit of the Lasta aircraft is equipped with electronic instruments that combine the display of several parameters in one space, which is exactly what was

stated in the introduction as the need to conduct research. This study used an igraph package (Csardi & Nepusz, 2005) in the R programming language to convert AOI transition matrices (Table 1) into diagrams. There is a difference in the proposed color of the knots compared to the proposed principle in Mandal et al. (2016). Based on the RGB palette of the RColorBrewer package in the R programming language, it has been defined that: red means a low fixation duration, orange means a longer fixation duration, and yellow means the longest fixation duration, as shown in Figure 17.

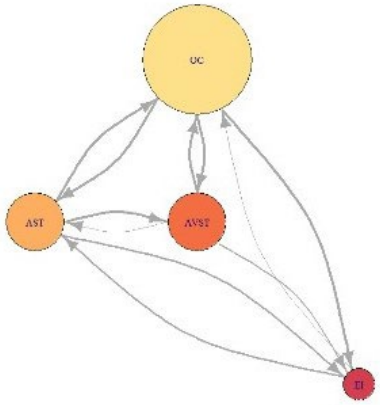

Figure 17 – Visualization of the instrument observation strategies using the network method (an example for participant No. 5)

To statistically check the different strategies visualized in this way, calculations of the centrality of the nodes within the diagram were carried out using the Igraph package in the R programming language. These measurements inherent in diagrams determine the relative importance of the node in relation to the diagram. In this study, these were measures of the degree of centrality (Indegree), centrality by closeness (Closeness), and Relational Centrality (Betweenness). In addition, these measures have been normalized to determine how far each of these measures is from the maximum recorded value within a given time interval, or in this case the flight phase.

Results

The data obtained from the recordings from the flight recorder files in conventional and virtual environments reveal a distinct and characteristic progress of the group that rehearsed the traffic pattern in the virtual environment. Better results from this group were recorded even when they

were returned for testing on a conventional simulator together with the control group after practice, as was envisaged by the experiment setup. An example of a more precise runway alignment in the direction of landing, i.e., a more minor deviation from the ideal trajectory of the given course in the final approach for each of the subjects, is given in Figure 18. The trend of progression and differences in the mean square deviation from the ideal trajectory of the final view for the groups of subjects is shown in Figure 19. The graphical representation is given using the functions of the ggplot package and the RColorBrewer package in the R programming language.

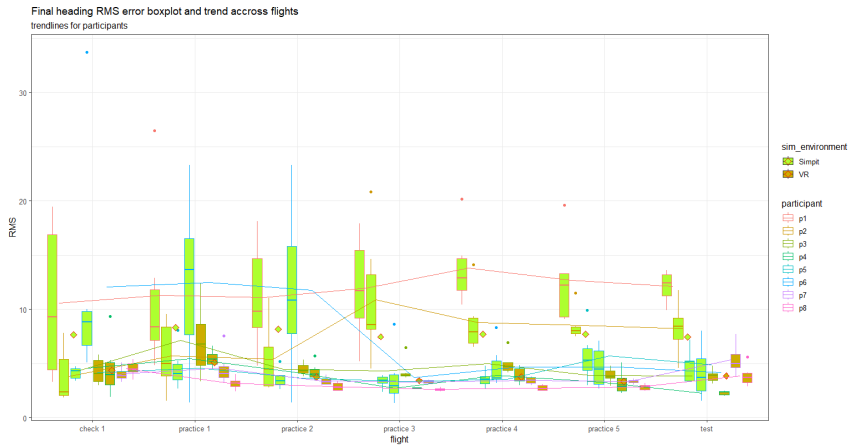

Figure 18 – Summary statistics for the mean squared deviation from the final approach course for the experimental group (VR)- and the control group (Simpit)-, with a trendline by flight

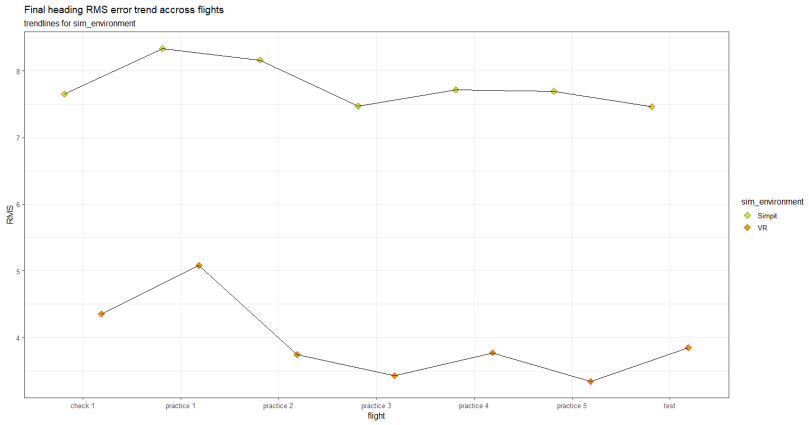

Figure 19 – Size and trend of the mean square deviation from the final approach heading for the experimental group (VR)-down and the control group (Simpit)-up, with the trendline by flight

The analysis of the eye movement imaging device results revealed that the control group had a weaker strategy for observing the instruments than the experimental group. When looking at traditional measures for assessing eye movement, the number and duration of fixations, it was observed that the control group had acquired a habit of observing more instruments that show inclination, angle of climb, and velocity (Bank AOI, Pitch AOI, IAS AOI-, shown in Figure 20).

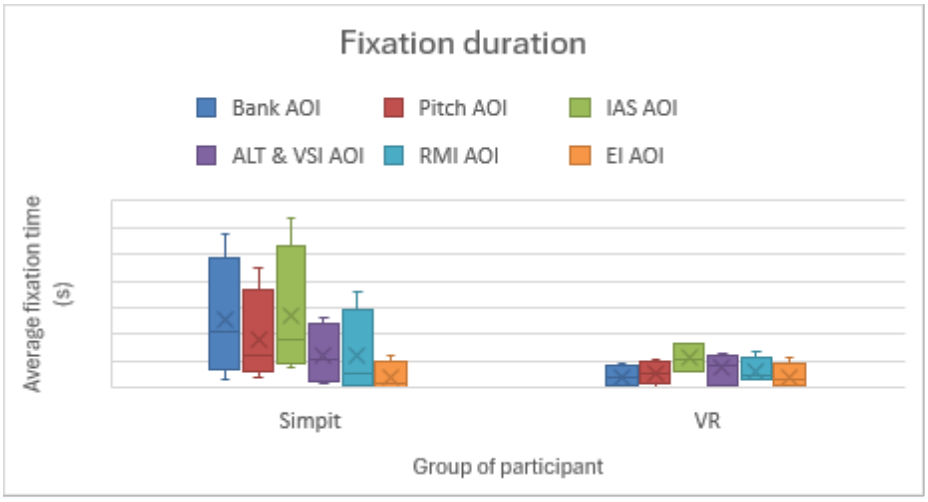

Figure 20 – Summary statistics of the average fixation time in the phase of the final approach across the school circle (Final) in each group of participants for all defined AOI

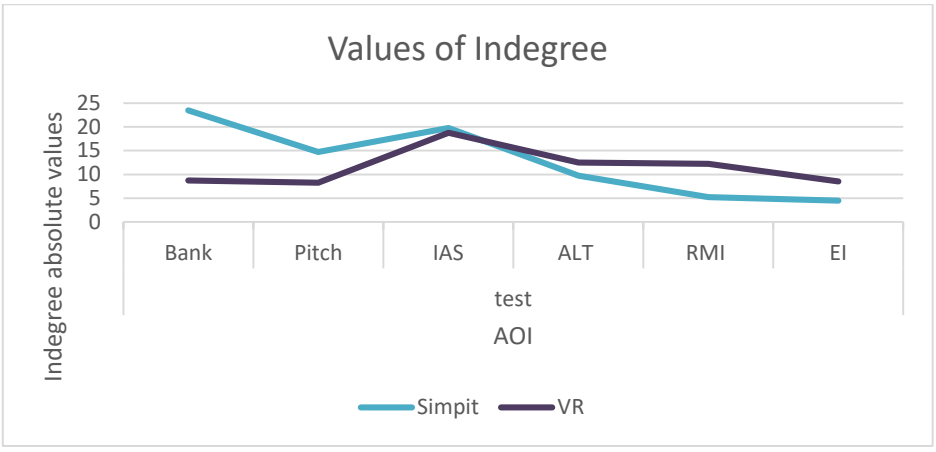

Figure 21 – Display of the absolute values and the trend of the Indegree measure for the final approach phase for each of the AOIs by groups of subjects

Also, the measures of the centrality of nodes within the diagram using the Igraph package in the R programming language showed that subjects in the conventional simulation environment had higher centrality values for the same AOI as in traditional measures (Bank AOI, Pitch AOI, IAS AOI-, Figure 21).

In contrast, the subjects who flew in the VR environment had a higher degree of centrality for the areas of interest in height, Altitude AOI, RMI AOi, and the AOI engine (Figure 21), which proves that these two groups of subjects have developed different strategies for observing instruments.

Conclusion

Basic flight training is considered the most crucial stage of pilot training and the basis for a successful process of producing future pilots. This training phase has undergone significant changes with the introduction of the Lasta aircraft which belongs to the category of technically advanced aircraft. This aircraft is characterized by a high degree of digitalization of the cockpit and other systems. Due to these characteristics, paying close attention to flight safety and training is necessary. To do this, attention must be paid to the theoretical training stage with synthetic means.

The aircraft manufacturer Lasta did not provide funding for training and simulators. The Military Academy's research team has acquired and developed many training tools to make the training process more efficient. The concept of digital training includes a series of digital devices designed to enhance flight training.

The assessment of flight instructors and examiners from the Military Academy after flights with cadet pilots of the first generation of pilots-cadets who began flight training after practicing on these trainers is that the results in training, especially in the early stages of basic training, are better. The simulators and trainers based on COTS components are the core of these devices.

VR offered opportunities to improve the flight training process—cadets learn faster and more efficiently, and their memory of flight tasks is better.

The GP3 Desktop Eye Tracker proved to be a valuable tool for evaluating results in a simulated environment. It is also fully applicable as an additional tool for selecting piles.

With its packages and functions, open-source software, such as the R environment, allows you to work with large amounts of data, such as logs from flight parameter recorders, either from a real aircraft or a

simulator. In the foreground comes the possibility of detailed statistical processing of data, which can prove a hypothesis or compare groups of respondents. In this way, so-called quick tools can be created to contribute to decision making regarding how experiments should be continued. On the other hand, the possibility of graphical representations and simulations of processes can serve to understand better the progress of complete processes for those who need to become users of data processing services.

Although digital training is not mandatory in the current pilot training model at the Military Academy, it is successfully implemented. Its potential is significant and can, to some extent, affect the very nature of the basic training process.

References

Ayala, N., Zafar, A., Kearns, S., Irving, E., Cao, S. & Niechwiej-Szwedo, E. 2023. The effects of task difficulty on gaze behavior during landing with visual flight rules in low-time pilots. *Journal of Eye Movement Research,* 16(1). Available at: https://doi.org/10.16910/jemr.16.1.3.

Csardi, G. & Nepusz, T. 2005. The igraph software package for complex network research. *ResearchGate,* November [online]. Available at: https://www.researchgate.net/publication/221995787_The_Igraph_Software_Package_for_Complex_Network_Research#fullTextFileContent [Accessed: 16 November 2024].

-EASA. 2021. EASA approves the first Virtual Reality (VR) based Flight Simulation Training Device*. EASA (European Union Aviation Safety Agency),* 26 April [online]. Available at: https://www.easa.europa.eu/en/newsroom-and-events/press-releases/easa-approves-first-virtual-reality-vr-based-flight-simulation [Accessed: 16 November 2024].

-EASA. 2018. CS-FSTD(A) Issue 2*. EASA (European Union Aviation Safety Agency),* 03 May [online]. Available at: https://www.easa.europa.eu/document-library/certification-specifications/cs-fstda-issue-2#group-read-more [Accessed: 16 November 2024].

-FAA. 1997. *Approval of flight simulators and flight training devices.* Washington, DC: United States Department of Transportation, Federal Aviation Administration.

Fussell, S.G. & Troung, D. 2022. Using virtual reality for dynamic learning: an extended technology acceptance model. *Virtual Reality,* 26, pp.249-267. Available at: https://doi.org/10.1007/s10055-021-00554-x.

Lefrancois, O., Matton, N., Gourinat, Y., Peysakhovich, V. & Causse, M. 2016. The role of Pilots' monitoring strategies in flight performance. In: *European Association for Aviation Psychology Conference EAAP32*, Cascais, Portugal, ffhal-01405262, September 26-30 [online]. Available at: https://enac.hal.science/hal-01405262v1 [Accessed: 16 November 2024].

Mandal, S. & Kang, Z. 2018. Using Eye Movement Data Visualization to Enhance Training of Air Traffic Controllers: A Dynamic Network Approach. *Journal of Eye Movement Research,* 11(4). Available at: https://doi.org/10.16910/jemr.11.4.1.

Mandal, S., Kang, Z. & Millan, A. 2016. Data Visualization of Complex Eye Movements Using Directed Weighted Networks: A Case Study on a Multi-Element Target Tracking Task. *Proceedings of the Human Factors and Ergonomics Society Annual Meeting*, 60(1), pp.106-110. Available at: https://doi.org/10.1177/1541931213601024.

Vlačić, S.I., Knežević, A.Z., Mandal, S., Rođenkov, S. & Vitsas, P. 2020. Improving the pilot selection process by using eye-tracking tools. *Journal of Eye Movement Research*, 12(3). Available at: https://doi.org/10.16910/jemr.12.3.4.

Ziv, G. 2016. Gaze behavior and visual attention: A review of eye tracking studies in aviation. *The International Journal of Aviation Psychology,* 26(3-4), pp.75-104. Available at. https://doi.org/10.1080/10508414.2017.1313096.

Aplicación de distintos equipos y programas informáticos en el concepto de formación y selección de pilotos digitales

Aleksandar Z. Knežević[a], *Aleksandar* G. Bukvić[b], *Branimir* B. Krstić[b]

Universidad de Defensa de Belgrado, Academia Militar,
Belgrado, República de Serbia

[a] Departamento de la Fuerza Aérea, **autor de correspondencia**

[b] Departamento de Ingeniería Mecánica Militar

CAMPO: ingeniería mecánica
TIPO DE ARTÍCULO: artículo científico original

Resumen:

Introducción/objetivo: En muchas fuerzas aéreas militares y organizaciones de aviación civil que utilizan o poseen aviones de entrenamiento equipados con una cabina digital, las herramientas de entrenamiento como entrenadores y simuladores se entienden en mayor o menor medida. Se presta especial atención a la proporción de horas de entrenamiento en el avión real con respecto al número de horas de entrenamiento en el simulador. Este enfoque en la formación de los círculos profesionales y del público se denomina en directo virtuales constructivas. Para todos los demás medios didácticos utilizados en la preparación para la formación, no se ha investigado específicamente ni la metodología ni el alcance de su uso. La investigación tiene como objetivo desarrollar instrumentos que midan y evalúen el éxito y el progreso cualitativo en la formación de pilotos logrados mediante el uso del espacio de cabina digital, en función de los cuales se pueda tomar una decisión sobre la formación adicional para un tipo de avión específico.

Métodos: Junto con un dispositivo de entrenamiento de aviación basado en PC y análisis estadísticos avanzados, un dispositivo de seguimiento del movimiento ocular ayudará a llegar a un patrón de referencia de observación de instrumentos para capacitar a los pilotos y seleccionar candidatos a piloto.

Resultados: La investigación del concepto propuesto incluye descripciones detalladas de la aplicación de entrenadores y medios didácticos con diferentes perfiles, que impactan significativamente en la calidad de la implementación del espacio de cabina digital en la formación de pilotos cadetes.

Conclusión: Dado que la Academia Militar forma pilotos cadetes que continúan su formación en las unidades operativas de vuelo de las Fuerzas Armadas de Serbia (SAF), es fundamental que durante el período de estancia en la Academia Militar se lleve a cabo su preparación teórica de calidad.

Palabras claves: entrenamiento de vuelo, simulación, hardware, software, seguimiento ocular.

Применение различных аппаратных и программных средств в концепции цифрового обучения и отбора пилотов

Александар З. Кнежевич[а], *Александар* Г. Буквич[б], *Бранимир* Б. Крстич[б]

Университет обороны в г. Белград, Военная академия,
г. Белград, Республика Сербия

[а] кафедра военной авиации, **корреспондент**

[б] департамент военного механического инжиниринга

РУБРИКА ГРНТИ: 78.25.13 Военная авиационная техника и вооружение
ВИД СТАТЬИ: оригинальная научная статья

Резюме:

Введение/цель: В военной авиации и организациях гражданской авиации, которые пользуются или владеют учебно-тренеровочными самолетами, оснащенными цифровой кабиной пилота, средства обучения, такие как тренажеры и симуляторы, используются в разной степени. Особое внимание уделяется соотношению часов, затраченных на обучение на настоящем воздушном судне, с количеством часов, проведенных на тренажере. Такой подход в профессиональной среде принято называть конструктивным моделированием в режиме реального времени. Однако методология и степень использования других учебных средств для подготовки к учениям отдельно не изучались.

Методы: Использование устройств отслеживания движения глаз в сочетании с высокоточным пилотажным тренажером

было исследовано с помощью расширенного статистического анализа с целью разработки эталонной модели осмотра приборов для обучения курсантов и отбора кандидатов в пилоты.

Результаты: Исследование предлагаемой концепции включает в себя подробное описание применения тренажеров и учебных средств различного профиля, которые существенно влияют на качество внедрения цифрового пространства кабины при обучении будущих пилотов.

Вывод: Учитывая тот факт, что Военная академия готовит военных летчиков, которые продолжат свое обучение в оперативных летных подразделениях Вооруженных сил Сербии (ВСС), необходимо провести качественную теоретическую подготовку в течение обучения в Военной академии.

Ключевые слова: летная подготовка, имитационное моделирование, аппаратное обеспечение, программное обеспечение, отслеживание глаз.

Примена различитог хардвера и софтвера у концепту дигиталне обуке и селекције пилота

Александар З. Кнежевић[а], *Александар* Г. Буквић[б], *Бранимир* Б. Крстић[б]

Универзитет одбране у Београду, Војна академија,
Београд, Република Србија

[а] Катедра војног ваздухопловства, **аутор за преписку**

[б] Катедра војномашинског инжењерства

ОБЛАСТ: машинство
КАТЕГОРИЈА (ТИП) ЧЛАНКА: оригинални научни рад

Сажетак:

Увод/циљ: У многим војним ваздухопловствима, као и цивилним ваздухопловним организацијама које користе или поседују школске авионе опремљене дигиталним кабинским простором, подразумева се употреба средстава за обуку као што су тренажери и сумулатори различитог профила. Посебна пажња придаје се односу броја часова проведених у обуци на авиону и броја часова на симулатору. Овај приступ у обуци у стручним круговима и јавности познат је као Жива виртуелна конструктивна. За сва остала наставна средства која се користе у сврху припреме за обуку није посебно истражена методологија нити обим њихове употребе.

Методе: Употреба уређаја за праћење покрета ока у спрези са тренажером одређеног степена верности истражена је помоћу напредних статистичких анализа како би се дошло до референтног

шаблона осматрања инструмената који би служио за обуку пилота и селекцију кандидата за пилоте.

Резултати: У оквиру истраживања предложеног концепта детаљно је описана примена тренажера и наставних средстава различитог профила, која имају значајан утицај на квалитет имплементације дигиталног кабинског простора у обуци кадета-пилота.

Закључак: С обзиром на то да се на Војној академији образују кадети-пилоти који своју обуку настављају у летачким јединицама Војске Србије (ВС), врло је важно да се у току периода проведеног на школовању изврши њихова квалитетна теоријска припрема.

Кључне речи: летачка обука, симулација, хардвер, софтвер, праћење покрета ока.

EDITORIAL NOTE: The third author of this article, *Branimir* Krstić, is a current member of the Editorial Board of the *Military Technical Courier*. Therefore, the Editorial Team has ensured that the double blind reviewing process was even more transparent and more rigorous. The Team made additional effort to maintain the integrity of the review and to minimize any bias by having another associate editor handle the review procedure independently of the editor – author in a completely transparent process. The Editorial Team has taken special care that the referee did not recognize the author's identity, thus avoiding the conflict of interest.

Paper received on: 16.07.2024.
Manuscript corrections submitted on: 29.01.2025.
Paper accepted for publishing on: 30.01.2025.

Influence of sediment additions on the mechanical behavior of fiber-reinforced concrete in aggressive environments

Louafi Goudih[a], *Hamid* Sellaf[b],
Benamar Balegh[c], *Ali* Meksi[d],
Adda Hadj Mostefa[e], *Mohamed Elamine* Dahamni[f]

[a] Mustapha Stambouli University, Department of Civil Engineering,
Laboratory for the Study of Structures and Mechanics of Materials,
Mascara, People's Democratic Republic of Algeria,
e-mail: louafi.goudih@univ-mascara.dz,
ORCID iD: https://orcid.org/0009-0004-2793-1654

[b] University of Saida, Department of Civil Engineering and Hydraulics,
Saida, People's Democratic Republic of Algeria +
Civil Engineering and Environmental Laboratory,
Sidi Bel Abbes, People's Democratic Republic of Algeria,
e-mail: hamid.sellaf@univ-saida.dz,
ORCID iD: https://orcid.org/0009-0006-3943-3024

[c] University of Ahmed Draia Adrar, Department of Civil Engineering,
Adrar, People's Democratic Republic of Algeria +
Civil Engineering and Environmental Laboratory,
Sidi Bel Abbes, People's Democratic Republic of Algeria,
e-mail: ben.balegh@univ-adrar.edu.dz,
ORCID iD: https://orcid.org/0000-0002-8529-7063

[d] Mustapha Stambouli University, Department of Civil Engineering,
Laboratory for the Study of Structures and Mechanics of Materials,
Mascara, People's Democratic Republic of Algeria,
e-mail: a.meksi@univ-mascara.dz,
ORCID iD: https://orcid.org/0009-0009-0320-3704

[e] University of Relizane, Department of Civil Engineering and Public Works,
Innovative Materials and Renewable Energies Laboratory,
Relizane, People's Democratic Republic of Algeria,
e-mail: addahadjmostefa@yahoo.fr,
ORCID iD: https://orcid.org/0009-0004-0086-9280

[f] University Oran 1 - Ahmed Ben Bella,
Condensed Matter Science Laboratory (LSMC),
Oran 1, People's Democratic Republic of Algeria,
e-mail: dahamnimohamedelamine@gmail.com,
corresponding author,
ORCID iD: https://orcid.org/0000-0001-5920-1198

https://doi.org/10.5937/vojtehg73-50424

ACKNOWLEDGMENT: This work was supported by PRFU project code A01L02UN010120200004 and the Civil Engineering and Environmental Laboratory of the University of Sidi Bel Abbes, Algeria.

FIELD: materials
ARTICLE TYPE: original scientific paper

Abstract:

Introduction/purpose: The use of supplementary cementitious materials (SCM) in construction has gained popularity due to their ability to improve the mechanical properties and environmental sustainability of concrete. This study aimed to investigate the potential of utilizing waste materials, specifically marble powder (MP) and dam sediment (DS), as partial replacements for cement in self-compacting concrete (SCC). The primary objectives were to recycle these waste materials and assess the durability and strength of SCC exposed to aggressive chemical environments.

Methods: In this study, cement was partially replaced with 40% MP, 40% DS, and a combination of 20% MP and 20% DS. The performance of such concrete was evaluated through compressive strength tests conducted for 28 days. Durability was assessed by exposing the concrete to chemical attacks from hydrochloric acid (HCl), sulfuric acid (H_2SO_4), and sodium sulfate (Na_2SO_4) solutions. Mass loss due to these chemical attacks was also measured.

Results: The concrete incorporating MP demonstrated compressive strengths similar to that of the control concrete, achieving 37.61 MPa at 28 days. The concrete with DS exhibited lower strength (31.81 MPa) and showed higher resistance to HCl (ML = 38.78%) compared to the MP concrete (ML = 40.74%). Additionally, all concrete samples exhibited good resistance to sulfuric acid due to the formation of expansive ettringite which protected the concrete from further degradation.

Conclusions: The results indicated that both marble powder and dam sediment are viable supplementary materials for improving the mechanical properties and durability of SCC. The concrete with marble powder showed superior strength, while dam sediment contributed to enhanced acid resistance. The combination of these materials offers a sustainable solution for concrete exposed to aggressive environments.

Key terms: concrete (SCC), sediment, marble powder, fiber, mass loss, mechanical, aggressive environment.

Introduction

The process of dredging dam sediments is necessary to ensure water storage capacity. This process generates over 600 million cubic meters of dredged sediment yearly, while less than 1% is currently recycled. Sediment storage can significantly impact the development of ecosystems and coastlines downstream of major river systems (Sellaf et al, 2023). Sediments generally consist of soil residues, organic minerals, and other

natural elements resulting from coastal erosion. These can be classified as organic and inorganic pollutants (heavy metals such as lead, chromium, mercury, salts, etc.). On the other hand, there is a growing demand for materials used in construction.

However, major obstacles and problems have been discovered in the sediment beneficiation process due to major differences in material properties and the quantities of salts and organic matter they contain, which can lead to high permeability and corrosion of reinforcement (Labiod-Aloui et al, 2014).

The deterioration of concrete elements exposed to aggressive sulfuric acid environments is a major durability issue affecting critical civil infrastructure's life-cycle performance and maintenance costs. Sulfuric acid present in groundwater or chemical waste or generated by the oxidation of sulfur compounds (e.g., pyrite) in backfill can attack the substructure protecting concrete elements (Bassuoni & Nehdi, 2007). Furthermore, concrete structures in industrial areas are vulnerable to deterioration due to acid rain, of which sulfuric acid is a major component (Thunuguntla & Gunneswara Rao, 2018).

Muhedin & Ibrahim (2023) studied the characteristics of concrete that used waste glass powder (WGP) in place of cement and sand. The results of laboratory tests were used to determine the compressive strength and separate tensile strength of concrete with 0%, 5%, 10%, 15%, and 20% partial replacement of sand and cement separately by WGP. The concrete compressive strength could be improved significantly at 7, 28, 60, and 90 days when using WGP as a partial replacement of cement at 5%, 10%, and 15% which can be considered a reasonable ratio.

Ranatunga et al. (2023) used coconut shell ash as a partial replacement for cement to reduce environmental impact while achieving the previously specified structural performance of concrete. The replacement percentage varies from 15% to 30% of the total content, and the optimum content for partial replacement is reached at 20% to achieve the targeted average compressive strength of 25 MPa.

Scherer et al. (2023) concluded that using rice hull ash and rock powders as a partial cement replacement could help investigate concrete durability in aggressive environments. The concrete containing these mineral admixtures showed better durability and less mass loss than the reference concrete. Concrete containing mineral admixtures showed better resistance to acid corrosion than Portland cement concrete.

Materials and methods

Materials used

The sediment used in this study was recovered in the discharge area of the Fergoug dam, located in theMohamadia region of Mascara (west Algeria). This dam was the first dredged dam in Algeria from 1986 to 1989, and it had over 10 million m3 of dredged sediment (Hammadi et al, 2011). This dredging was carried out with floating suction dredge extruders. Sediment (vases) are sucked into the dredge and discharged through a pipeline consisting of a floating and a fixed part of several hundred meters in length (Hammadi et al, 2011).

The thermal method was used to prepare the sediment following standard XP P94-047. After calcination in an oven at 450 °C, organic matter was removed. As a result, the dam sediments contain an organic percentage of 6.25%.

Marble powder was prepared from the remains of marble stones from workshops and quarries by placing it in a micro-diffusion device, crushing it, and then sieving it through a 2 mm sieve. These two specimens were subject to several laboratory identification tests using standard procedures adopted by the AFNOR and ISO standards NF P94-068 (AFNOR, 1998b), NF P94-057 (AFNOR, 1992), NF 94-056 (AFNOR, 1996), NF P94-054 (AFNOR, 1991) and NF P94-051 (AFNOR, 1993).

The chemical analysis of the specimens was carried out in accordance with NF EN 1744 (AFNOR, 1998a), and the results are presented in Table 1.

Gravel is traditional and commonly used on building sites. These aggregates were washed and then sieved to obtain 03 fractions 3/8, 8/15. The characteristics were determined according to standards, and we obtained the following: absolute density (2.62 g cm-3) and apparent density (1.40 g cm-3).

The cement used in this research is ordinary Portland cement (OPC) prepared from 76% clinker, 18% lime, and 6% gypsum. The chemical analysis of the cement is presented in Table 2. The densities of cement, sediment, and marble powder are approximately 3.2, 2.46, and 2.75 g cm-3, respectively.

In our experimental study, we used a crushed sand fraction (0/3) from the Tizi quarry in the southwest region of Mascara. Before use, the sand is washed to reduce impurities. The absolute density value has been estimated at 2500 kg m-3 le and a fineness coefficient of 2.78, with a water absorption capacity of around 2.4% and a cleanliness level of 78%. A 5% solution of sulfuric acid, hydrochloric acid, and sodium sulfate was chosen

for the mix. Formal tests are carried out and prepared to test the concrete resistance to chemical attack.

In this study, all mixes were made with a water/cement ratio (w/c) set at 0.55. The sand/cement (S/C) ratio was 1:3 for all samples. Plasticizers were added to the mix to achieve similar workability. The plasticizer content ranged from 2% to 2.5% by weight of the binder.

Table 1 – Some properties of the investigated materials (Sellaf et al, 2023)

	Dam Sediment	Marble powder	Sand
Liquid limit (%)	32.28	35	20
Plastic limit (%)	15.09	13	Nul
Plasticity index (%)	17.19	22	Nul
Volume of blue VB (g cm-3)	4.5	5.2	0.39
Specific gravity	2,46	2.63	2.75
Apparent density (g cm-3)	1.26	1.45	1.53
Fineness modulus	1.2	1.35	2.78
Organic content (%)	6.25	0.05	Nul

Table 2 – Chemical compositions of the soils used in the study (Sellaf & Balegh, 2023)

Property	Dam sediment	Marble powder	Crushed sand	Cement
SiO_2 (%)	61.75	60,5	56,82	21,23
Al_2O_3 (%)	8.39	4,85	5,12	5,23
Fe_2O_3 (%)	0.71	11,85	0,16	2,34
CaO (%)	12.51	9,45	13,4	63,25
MgO (%)	0.37	1,22	10,38	2,01
NaOH (%)	Nul	0,08	0,07	0,15
CL (%)	Nul	0,05	0,05	0,01
$P.F_2$ (%)	16.27	12	14	5,78

Concrete mix-design

Our formulation study consists of formulating vibrated concrete and self-compacting concrete based on marble powder and/or Fergoug sediment as additions. The introduction of mineral additions leads to a modification of the porosity of cementitious matrix and influences the concrete mechanical and self-compacting characteristics.

The fluidity of self-compacting concrete is obtained by adding superplasticizers. This admixture must not be too high (close to saturation dosage). Otherwise, the concrete sensitivity to variations in water content will be increased, leading to problems of segregation and bleeding.

The formulation method used to design the self-compacting concrete compositions tested in this experimental study is an empirical method based on four points:

The self-compacting concrete formulation meets the mechanical strength criteria (fixed or desired) chosen from Bolomey's formula, see equation 1 (Denis, 2008):

$$\mathrm{F}'_{\mathrm{c}} = R_C\ G\ \left[\frac{L_{Equi}}{E_{eff} + Air} - 5\right] \ldots\ldots\ldots\ldots\ldots\ldots\ldots\ldots\ldots\ldots\ldots\ldots (1)$$

where

F'_C: compressive strength of concrete in (MPa),
R_C: compressive strength of cement in (MPa),
L_{Equiv}: cement + k. mineral additions (in kg),
Eeff: effective water quantity,
Air: air volume (in liter), and
G: granular coefficient.

Admixture dosage is calculated to limit segregation and bleeding. The superplasticizer dosage is determined experimentally from tests on fresh concrete, for which the spread must be between 60 and 70 cm.

The composition of the skeleton is optimized to reduce segregation and promote flow. To achieve this, the granulometric analysis of the concrete must fit into granular spindles (Figure1).

As regards the formulation of the corresponding vibrated concretes, their compositions were either obtained from those of the SCC, maintaining identical cement quantities and granular proportions, or from the Dreux-Gorisse method (high-performance vibrated concrete).

All the compositions studied during this research project are presented in Table 3. Aggregate quantities regarding soaked material mass (saturated aggregates on a dry surface) and admixture dosages for liquid product mass are given.

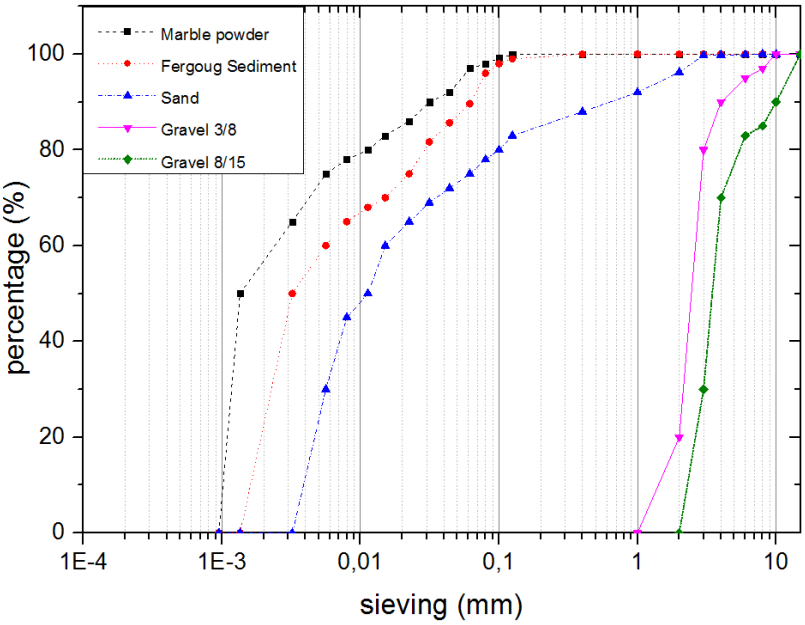

Figure1 – Aggregates grading curves

Table 3 – Composition of various concretes (kgm^{-3})

Composition (kg/m3)	Self-Compacting Concrete (SCC)			
	VC	SCCMP	SCCDS	SCCDSMP
Cement CEM I 42.5	350	210	210	210
Quartz powder	50	--	--	--
Marble powder (MP)	--	140	--	70
Dam sediment (DS)	--	--	140	70
Sand 0/3	962	962	962	962
Gravel 3/8	221	221	221	221
Gravel 8/15	636	636	636	636
water	192.5	192.5	192.5	192.5
superplasticizers	17.5	17.5	17.5	17.5

The self-compacting concrete (SCC) mix was designed following ACI-237R-07 (ACI Committee 237, 2007). Table 3 shows the different mix designs, taking additive contents into account. The mixing and production process for self-placing concrete is illustrated in Figure 2, as proposed by Pająk & Ponikiewski (2013). First, quarry sand, coarse aggregate, and fine aggregate were added and mixed for ten minutes, followed by the addition and mixing of cement, marble powder (MP), and dam sediment (DS) for another ten minutes. The next step was to add 60% of the mixed water to the dose of superplasticizer and then leave it to mix for three minutes. Mixing was stopped, and the mixed materials were left to stand and settle for a while. Mixing was then resumed for two minutes with the addition of the remaining water. The shapes of various cast specimens in accordance with the tests envisaged were as follows:

- Cylinders of 11.22 cm in size for compressive strength, 3 specimens for each age, and cubes of 7 .7.7cm for durability tests (acid attack).

After pouring, the samples are covered with a plastic film to prevent water evaporation.

Figure 2 – 7.7.7 cm cubes for durability tests and 11.22 cm cylinders for compressive strength tests

Results and discussion

Characteristics of fresh and cured formulations

Abrams cone slump test

According to NF EN 12350-2 (AFNOR, 2019) of the Abrams cone device, fresh concrete slump values ranging between 640 mm to 720 mm must be obtained, given by measuring the diameter of the concrete, which is more representative than the slump value (see Figure 3).

Figure 3 – Abrams cone slump/spread test

The L-box flow test

The vertical part of the L-box is filled with concrete at one time, NF EN 12350-10 (AFNOR, 2010a). After opening the trapdoor, the concrete flows through standard reinforcement (39 mm between 3 bars φ14), corresponding to heavily reinforced structures,but can be lightened if necessary (58 mm clearance between 2 bars).

For SCC to be accepted, the filling ratio of the L-shaped box (H2/H1 height ratio (see Figure 4) must be greater than 0.8.

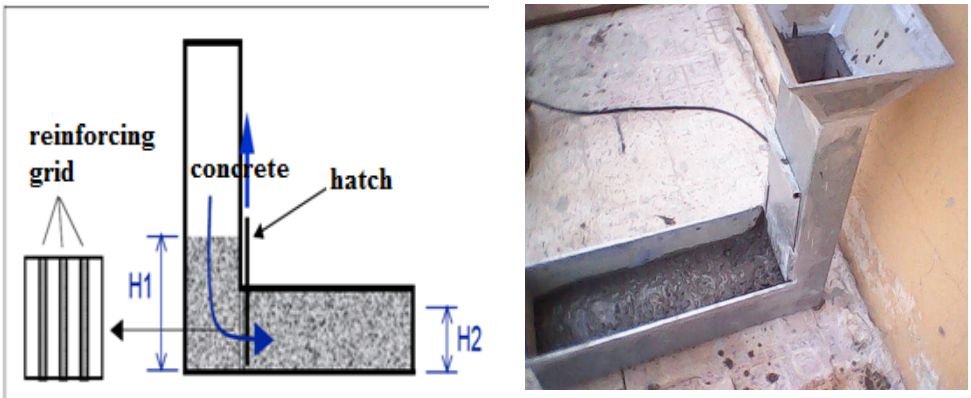

Figure 4 – The L-box test

Flow times can also be measured to assess concrete viscosity. For the first test, this is the time required to reach a spreading diameter of 50 cm, noted t50. For the second one, the time measured (tL) is between the opening of the trapdoor and the moment when the concrete reaches the bottom of the L-box.

The segregation test

Another way of testing the static segregation of SCC is to observe one (or two) specimen(s) of hardened concrete in the direction of casting and observe the distribution of aggregates over the height of the specimen, NF EN 12350-11 (AFNOR, 2010b).

These photographs clearly illustrate that the two concrete formulations presented here are not subject to static segregation. The aggregates are evenly distributed over the entire height of the sawn specimens (cast vertically from the top). This repeated observation for all the SCC compositions studied led to the same conclusion.

Table 4 – Fresh and hardened properties of various formulations

	Settling/ Spreading (cm)	Segregation (%)	L-Box	Theoretical density (kg m-3)	Actual density (kg m-3)	Hardened density (kg m-3)
VC	8,5	--	0.85	2300	2250	2370
SCCMP	68	12.5	0.89	2350	2400	2380
SCCDS	70	13.20	0.88	2320	2350	2385
SCCDSMP	69	12.80	0.86	2330	2345	2382

- Static segregation of SCC: the sieve stability test calculates a segregation rate and deduces whether or not the concrete tested has satisfactory stability. All SCCs have a segregation rate of less than 15%, synonymous with sufficient stability.

- On the dynamic segregation of SCC: the L-box test is used to determine the filling ratio (the height of concrete at the bottom to that at the beginning of the box), which should, in principle, be greater than 0.8.

- Regarding the consistency of vibrated concrete, no conditions had been set beforehand.

SCCDSMP showed the best performance compared with SCCMP and SCCDS. This is due to the physical nature of sediment fillers and marble powder which control compressive strength through a denser matrix and a better dispersion of cement grains (Bonavetti et al, 2001; Diederich et al, 2013).

Determination of uniaxial compressive strength

The specimens used to determine the compressive strength of the various concretes studied were cylindrical test specimens measuring 11cm in diameter and 22cm in height. After demolding, they were stored in a room at 20°C and 95 ± 5% relative humidity until the specified time (7, 14, 21, 28 days).

The press used has a maximum capacity of 3000 kN (Figure 5). Compressive strength was assessed in accordance with standard NF EN 206-1 (AFNOR, 2004): tests were carried out on the most appropriate force scale (600 or 1500 kN), with a loading speed of 0.5 $MPas^{-1}$.

Figure 5 – Press used

Compression tests

The influence of the type of addition on the compressive strengths of concrete at different times is illustrated in Figure 6.

The analysis of the results illustrated in Figure 6 shows the evolution of compressive strength as a function of age for concrete containing different percentages of marble powder and dam sediment preserved in lime-saturated water for 7, 14, 21, and 28 days. It can be seen that the compressive strength of all concretes increases steadily with age and shows no drop.

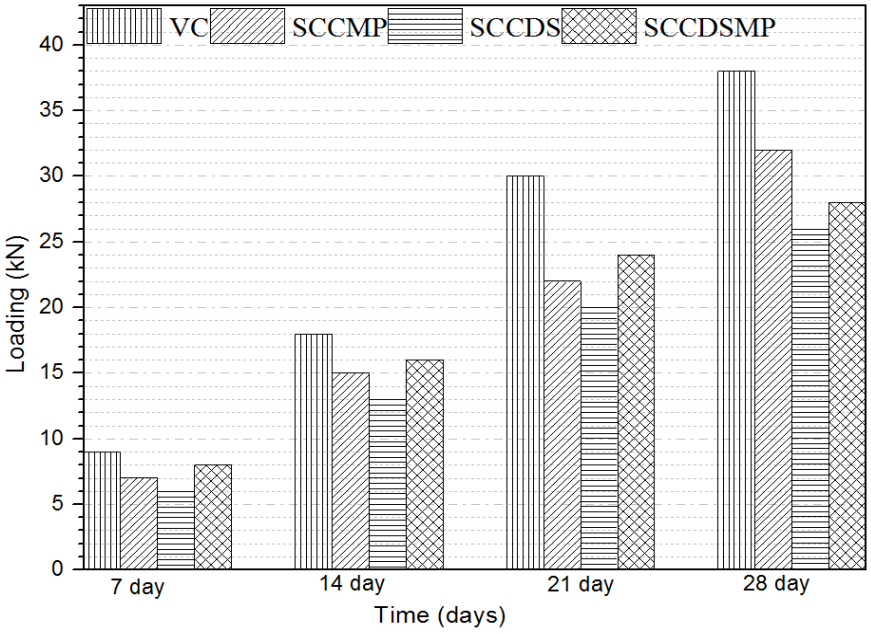

Figure 6 – Influence of the type of addition on the compressive strengths of concretes at different maturities

Figure 6 clearly shows the significant influence of marble powder on compressive strength. The various maturities elaborated with low marble powder show strengths close to those of the control concrete at 7, 14, 21, and 28 days. On the other hand, the concrete made from SCCDS dam sediments had compressive strengths around 15% lower than those of the concrete containing SCCMP marble powder. In comparison, the concrete made from SCCDS dam sediments had compressive strengths around 20% lower than those of SCCMP.

It can be concluded that substituting part of the cement with treated dam sediment provides acceptable compressive strength but lower than the strength given by marble powder, with percentages close to those of the control concrete (without addition). From Figure 6, it can be concluded that the differences between the 28-day strengths and those given for the control concrete are as follows: 30% for dam sediment and 20% for marble powder, Table 5.

Table 5 – Evolution of the ratio of compressive strength to measured strength

Age (days)	VC		SCCMP		SCCDS		SCCDSMP	
i	σi	σi /σ28	σi	σi /σ28	σi	σi /σ28	σi	σi /σ28
7	11	0.25	9.50	0.25	8.00	0.25	11.5	0.27
14	20.60	0.47	16.20	0.43	14.50	0.45	18	0.45
21	31	0.71	24	0.63	22	0.69	26	0.64
28	43.46	1.00	37.61	1.00	31.81	1.00	40.11	1.00

To better visualize all the variations in the rate of evolution of compressive strengths, we study the ratio:

- D_i / D_{28} : (i = 7 - 28 days), Table 5.

For a 7-day duration, we observed an evolution of between 25% for SCCMP and SCCDS, which is equal to that of VC vibrated concrete, but we observed an evolution of 30% for SCCDS, see Figure 6.

At 14 days, an increase of around 47% is obtained for VC vibrated concrete, while SCCMP and SCCDS self-compacting concretes show an increase of around 43% to 45%.

At 14 to 28 days, the difference is more significant, with VC vibrated concrete showing an increase in strength of 53%, while SCCMP and SCCDS self-placing concretes show increases ranging from 55 to 57%.

Self-compacting concrete containing dam sediment develops strength comparable to self-compacting concrete containing marble powder at 21 days without any noticeable reduction.

SCCMP self-compacting concrete develops strength comparable to VC vibrated concrete at 28 days.

The properties of the aggregates used to make concrete mixes are presented in Table 1 and Figure 1. Much sediment was supplied from the Fergoug dam site in northwest Algeria. It was prepared using two processes: the first involves extracting it from the dam and placing it in a kiln at 450°C to remove impurities and organic matter, while the second process involves crushing and sieving under a two-millimeter sieve. Its dimensions vary from 1 mm to 2 mm (Figure 1).

Testing the durability of concretes in acid solutions

To evaluate the durability of hardened concretes exposed to acid solutions and to highlight the influence of acids on different compositions

of different concretes, we monitored the variation in the mass of the cubic test specimens (70. 70. 70) mm^3 in the following solutions: 5% hydrochloric acid (HCl); 5% sulfuric acid (H_2SO_4);5% sodium sulfate (Na_2SO_4).

Mass variation was monitored on the test tubes immersed in various acid solutions (Figures 7 and 8) in accordance with ASTM C267, using a 0.01 g precision balance (Figure 9).

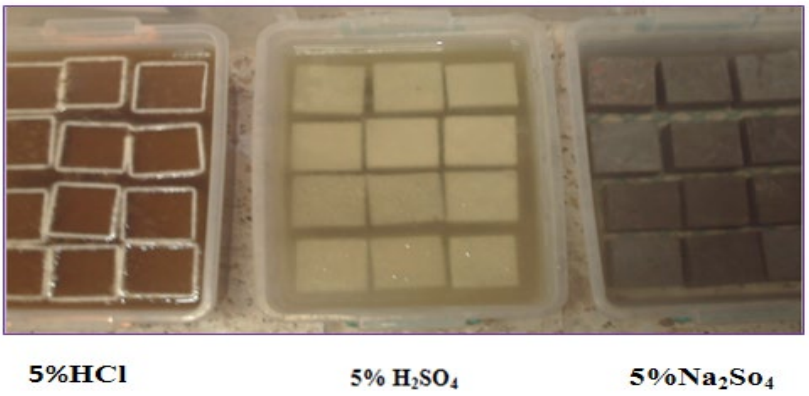

Figure 7 – Cubic test tubes immersed in acid solutions

Once the test tubes have been removed from their storage medium, they are cleaned 3 times with fresh water and left to dry for 30 min.

In order to better characterize the progress of the degradation of concretes with different additions by the attack of acid solutions and sulfate, we opted to quantify the loss of the mass of these concretes over time for a period of 1 to 28 days.

Figure 8 – Condition of the cubic specimens after acid etching

Figure 9 – Precision balance test

Influence of hydrochloric acid solution (5% HCl)

After 24 hours of immersion in a hydrochloric acid solution, VC vibrated concrete, SCCMP, and SCCDS self-placing concretes show the same strength levels (ML = 1.59 to 1.77%), see Figure 10. From 7 days onwards, the attack progresses over time, particularly in the case of vibrated concrete VC, with a mass loss of 49.36% at 28 days. At 28 days of attack, the mass losses recorded are significant, amounting to 40.74% for SCCMP marble powder concrete and 38.78% for SCCDS dam sediment concrete.

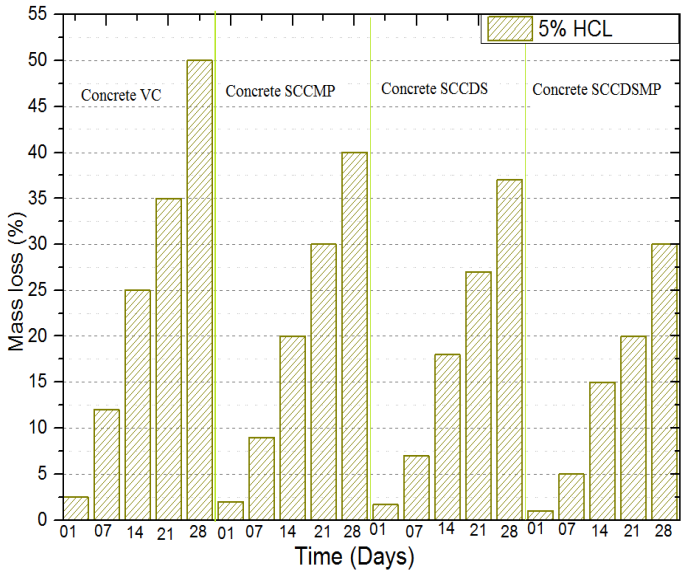

Figure 10 – Influence of the acid solution HCL on the mass loss of concrete from different additions at different times

Influence of the sulfuric acid solution (5% H_2SO_4)

The self-placing concretes of the two additions (marble powder, dam sediment) show very good resistance to attack by the sulfuric acid solution after 24 hours since mass losses do not exceed 0.11% (Figure 11). This resistance tends to weaken over time, giving rise to mass losses of 1.30% for SCCMP marble powder concretes, 0.29% for SCCDS dam sediment concretes, and 0.25% after 7 days, while the rates recorded at 21 days are 3.91% and 1.09%, respectively. After a 28-day attack, the SCCDS sediment dam concretes showed better strength (ML = 1.11%) than the SCCMP marble powder concretes (ML = 5.34%), with high mass loss rates for the VC vibrated concretes of 17.50% at 28 days. (ML: mass loss).

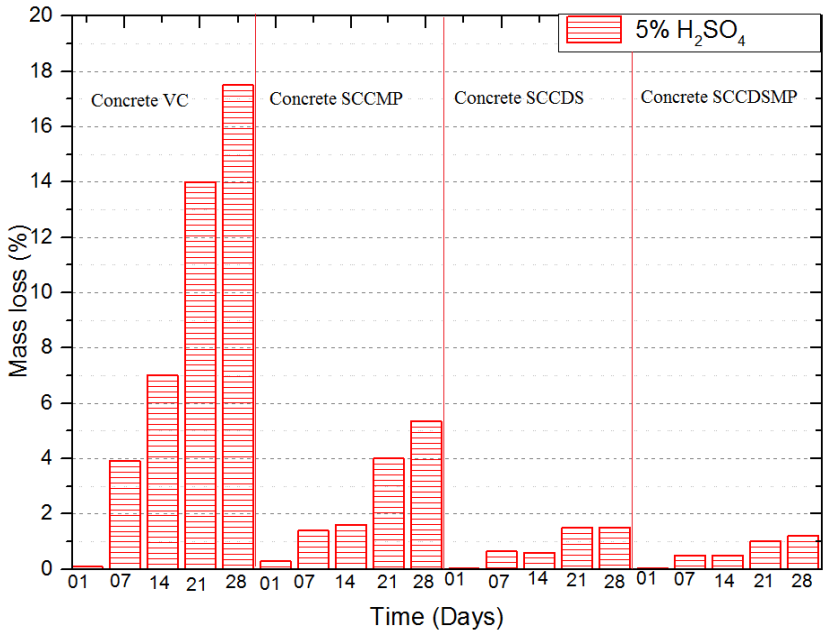

Figure 11 – Influence of the acid solution H_2SO_4 on the mass loss of concrete from different additions at different times

Influence of the sodium sulfate solution (5% Na_2SO_4)

Generally speaking, concretes with 3 additions (SCCMP and SCCDS) show almost the same resistance to attack by the sodium sulfate solution at each maturity. The mass losses recorded are very close at each maturity and are effectively (- 0.09 to - 0.1%) at 1 day, (0.65 to 0.77%) at 7 days, (1.96 to 2.46%) at 21 days and (2.60 to 3.20%) at 28 days (Figure 12).

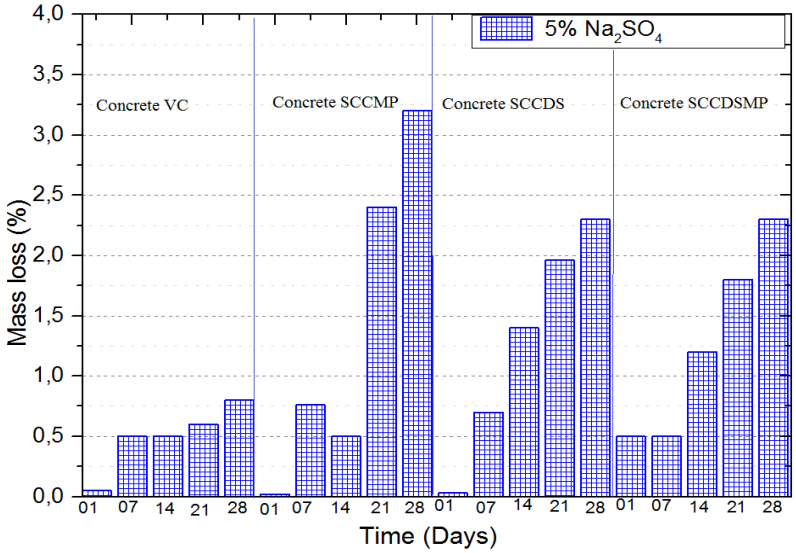

Figure 12 – Influence of the sodium sulfate solution Na_2SO_4 on the mass loss of concrete from different additions at different times

At 28 days of immersion in the sulfate solution, the VC vibrated concrete showed less mass loss than the self-placing concretes with the 3 additions (marble powder and dammed sediment). This phenomenon is probably attributed to the filling of vacant voids in the pores of vibrated concrete exposed to the sulfate solution by secondary gypsum and ettringite, resulting in lower mass loss than the other concrete.

The mass losses of concretes made with various additions are more or less affected by the nature of the acid solution, with the most aggressive being (HCl), followed by (H_2SO_4), and finally (Na_2SO_4).

Concrete is more resistant to sulfuric acid attacks but shows no signs of resistance to hydrochloric acid solutions. This difference in resistance may be due to the high proportion of $CaCO_3$ and CaO in the gaskets and C_3S in the cement (47.15%), which, after hydration, gives rise to a large quantity of portlandite. The latter, in turn, reacts with acid (HCl) to form large amounts of calcium chloride salt. Given the solubility of this salt, porosity tends to increase, facilitating the penetration of the aggressive medium into the cementitious matrix and consequent weakness in strength.

Concretes made with different additives are more or less affected by sulfate (Na_2SO_4). By comparison, concrete made without admixtures shows good resistance to the sulfatic acid solution, compared with the

attack of other solutions. This resistance can be attributed to the formation of expansive secondary ettringite, which covers the surface layer of the cementitious matrix and thus limits the inward progress of acidic degradation.

Visual examination

Figure 13 shows the condition of the cubes of different concretes at the age of 28 days and after 28 days of immersion in lime-saturated water. Visual examination reveals no signs of degradation.

The photos shown in Figure 13 concern the SCCDSMP concrete sample formed from dam sediments, marble powder and cement, and submerged in the solutions over a period of 28 days.

Visual analysis was carried out to assess the obvious signs of external deterioration of the concrete specimens, such as weathering, cracking, and softening, following storage in different media.

Figure 13 – Condition of the cubic specimens of SCCDSMP concrete after etching at 28 days

Figure 13 shows the results of changes and deformations in the concrete formed from dam deposits, marble powder, and cement in the following ratios: 30 %, 20 %, and 50 %. The concrete samples immersed in HCl acid and H_2SO_4 acid showed considerable deformation; a thin layer of yellowish rust on the surface differed from the initial color of the cementitious matrix and appeared to be due to the presence of weakly crystalline Fe_2O_3 iron hydroxide.

The surface of the concrete is thoroughly cleaned, with a significant loosening of the sand grains. The solubility of the salt formed, $Ca(NO_3)_2.2H_2O$, after the reaction of HCl with the portlandite $Ca(OH)_2$ released during cement hydration and its extensive external filtration with

progressive decalcification of the C-S-H, led to significant mass losses. The samples immersed in Na_2SO_4 acid appear to have no effect or change.

In HCl, a significant reduction in the volume of concrete samples was observed. As a general rule, concrete surfaces undergo more pronounced deterioration in HCl than in H_2SO_4. HCl is more aggressive than H_2SO_4. The results of mass loss tests confirmed these observations.

Conclusions

The experimental results of this study which consisted of monitoring the evolution of the mechanical strengths (compression) of concrete made with cement and mineral additions (marble powder, Fergoug dam sediment), quantified by the chemical attack of acid solutions (hydrochloric, sulfuric, and sulfatic with a concentration of 5%), and the relative mass variations or mass losses, lead to the following conclusions:

The various maturities produced with marble powder have strengths close to those of the control concrete at 28 days (R_C28= 37.61 MPa). On the other hand, the concrete made with SCCFS dam sediment has a compressive strength 15% lower (R_C28= 31.81 MPa) than that of the concrete made with SCCMP marble powder, which is 20% lower (R_C28= 30.09 MPa). This difference in strength may be due to the high proportion of marble powder contained in the concrete, which is due to the consumption of Portlandite (CH) produced as a result of cement hydration. This reaction produces additional C-S-H gels that contribute to the improved strength of marble concretes. On the other hand, the strength of concrete based on dam sediments is always lower than that of the control concrete, which can be explained by the activity and percentages of fines contained in these mineral additions.

The mass losses of concretes made with various additions are more or less affected by the nature of the acid solution, with the most aggressive HCl, followed by H_2SO_4, and finally Na_2SO_4.

SCCDS dam sediment concretes are more resistant (ML = 38.78%) to attack by the hydrochloric acid solution than marble powder concretes (ML = 40.74%);

Concrete made without additives shows good resistance to the sulfuric acid solution (ML = 0.9%). This resistance can be attributed to the formation of expansive secondary ettringite which covers the surface layer of the cementitious matrix and, therefore, limits the inward progress of acidic degradation.

Concrete made from marble powder and dam sediments (SCCDSMP) gave positive results, similar to those of concrete made from quartz powder (VC).

References

-ACI Committee 237. 2007. 237R-07: Self-Consolidating Concrete. *ACI American Concrete Institute*, January 4 [online]. Available at: https://www.concrete.org/publications/internationalconcreteabstractsportal/m/details/id/18605?gad_source=1&gclid=CjwKCAiA6aW6BhBqEiwA6KzDc9agd-Q_3KklxCQYzmj-flVB06rtwGVxavJ-pElLHf1cHJYAaPr6tRoCdCAQAvD_BwE [Accessed: 12 April 2024].

-AFNOR Association française de normalisation. 1991. *NF P94-054: Sols : reconnaissances et essais - Détermination de la masse volumique des particules solides des sols - Méthode du pycnomètre à eau* [online]. Available at: https://www.boutique.afnor.org/fr-fr/norme/nf-p94054/sols-reconnaissance-et-essais-determination-de-la-masse-volumique-des-parti/fa020767/11077 [Accessed: 12 April 2024].

-AFNOR Association française de normalisation. 1992. *NF P94-057: Sols : reconnaissance et essais - Analyse granulométrique des sols - Méthode par sédimentation* [online]. Available at: https://www.boutique.afnor.org/fr-fr/norme/nf-p94057/sols-reconnaissance-et-essais-analyse-granulometrique-des-sols-methode-par-/fa020768/11074 [Accessed: 12 April 2024].

-AFNOR Association française de normalisation. 1993. *NF P94-051: Sols : reconnaissance et essais - Détermination des limites d'Atterberg - Limite de liquidité à la coupelle - Limite de plasticité au rouleau* [online]. Available at: https://www.boutique.afnor.org/fr-fr/norme/nf-p94051/sols-reconnaissance-et-essais-determination-des-limites-datterberg-limite-d/fa020765/11080 [Accessed: 12 April 2024].

-AFNOR Association française de normalisation. 1996. *NF P94-056: Sols : reconnaissance et essais - Analyse granulométrique - Méthode par tamisage à sec après lavage* [online]. Available at: https://www.boutique.afnor.org/fr-fr/norme/nf-p94056/sols-reconnaissance-et-essais-analyse-granulometrique-methode-par-tamisage-/fa026936/11075 [Accessed: 12 April 2024].

-AFNOR Association française de normalisation. 1998a. *NF EN 1744-1: Essais pour déterminer les propriétés chimiques des granulats - Partie 1 : analyse chimique* [online]. Available at: https://www.boutique.afnor.org/fr-fr/norme/nf-en-17441/essais-pour-determiner-les-proprietes-chimiques-des-granulats-partie-1-anal/fa039721/62422 [Accessed: 12 April 2024].

-AFNOR Association française de normalisation. 1998b. *NF P94-068: Sols : reconnaissance et essais - Mesure de la capacité d'adsorption de bleu de méthylène d'un sol ou d'un matériau rocheux - Détermination de la valeur de bleu de méthylène d'un sol ou d'un matériau rocheux par l'essai à la tache* [online]. Available at: https://www.boutique.afnor.org/fr-fr/norme/nf-p94068/sols-reconnaissance-et-essais-mesure-de-la-capacite-dadsorption-de-bleu-de-/fa043689/394 [Accessed: 29 March 2024].

-AFNOR Association française de normalisation. 2004. *NF EN 206-1: Concrete - Part 1 : specification, performance, production and conformity* [online]. Available at: https://www.boutique.afnor.org/en-gb/standard/nf-en-2061/concrete-

part-1-specification-performance-production-and-conformity/fa125184/22922 [Accessed: 12 April 2024].

-AFNOR Association française de normalisation. 2010a. *NF EN 12350-10: Essai pour béton frais - Partie 10 : béton auto-plaçant - Essai à la boîte en L* [online]. Available at: https://www.boutique.afnor.org/fr-fr/norme/nf-en-1235010/essai-pour-beton-frais-partie-10-beton-autoplacant-essai-a-la-boite-en-l/fa165666/36401 [Accessed: 12 April 2024].

-AFNOR Association française de normalisation. 2010b. *NF EN 12350-11: Essai pour béton frais - Partie 11 : béton auto-plaçant - Essai de stabilité au tamis* [online]. Available at: https://www.boutique.afnor.org/fr-fr/norme/nf-en-1235011/essai-pour-beton-frais-partie-11-beton-autoplacant-essai-de-stabilite-au-ta/fa165665/36326 [Accessed: 12 April 2024].

-AFNOR Association française de normalisation. 2019. *NF EN 12350-2: Essais pour béton frais - Partie 2 : essai d'affaissement* [online]. Available at: https://www.boutique.afnor.org/fr-fr/norme/nf-en-123502/essais-pour-beton-frais-partie-2-essai-daffaissement/fa190558/83431 [Accessed: 12 April 2024].

Bassuoni, M.T. & Nehdi, M.L. 2007. Resistance of self-consolidating concrete to sulfuric acid attack with consecutive pH reduction. *Cement and Concrete Research*, 37(7), pp.1070-1084. Available at: https://doi.org/10.1016/j.cemconres.2007.04.014.

Bonavetti, V.L., Rahhal, V.F. & Irassar, E.F. 2001. Studies on the carboaluminate formation in limestone filler-blended cements. *Cement and Concrete Research*, 31(6), pp.853-859. Available at: https://doi.org/10.1016/S0008-8846(01)00491-4.

Denis, P.E. 2008. *Optimisation du béton autoplaçant : mise en place en laboratoire et sur chantier*. Master's Final Project. Leeds: École des Mines de Saint-Étienne.

Diederich, P., Mouret, M. & Ponchon, F. 2013. Simple tools for achieving self-compacting ability of concrete according to the nature of the limestone filler. *Construction and Building Materials*, 48, pp.840-852. Available at: https://doi.org/10.1016/j.conbuildmat.2013.07.071.

Hammadi, L., Ponton, A. & Belhadri, M. 2011. Rheological study and valorization of waste sludge from wastewater treatment plants in the dredging operation of hydraulic dams. *Energy Procedia*, 6, pp.302-309. Available at: https://doi.org/10.1016/j.egypro.2011.05.034.

Labiod-Aloui, Z., Trouzine, H., Ghembaza, M.S., Nouioua, T. & Sebaibi, Y. 2014. Experimental investigation of mixtures of bentonite and dredged sediments from Chorfa dam in Algeria. *Turkish Journal of Earth Sciences*, 23(3), pp.330-338. Available at: https://doi.org/10.3906/yer-1302-13.

Muhedin, D.A. & Ibrahim, R.K. 2023. Effect of waste glass powder as partial replacement of cement & sand in concrete. *Case Studies in Construction Materials*, 19, e02512. Available at: https://doi.org/10.1016/j.cscm.2023.e02512.

Pająk, M. & Ponikiewski, T. 2013. Flexural behavior of self-compacting concrete reinforced with different types of steel fibers. *Construction and Building*

Materials, 47, pp.397-408. Available at: https://doi.org/10.1016/j.conbuildmat.2013.05.072.

Ranatunga, K.S., del Rey Castillo, E. & Toma, C.L. 2023. Evaluation of the optimal concrete mix design with coconut shell ash as a partial cement replacement. *Construction and Building Materials*, 401, art.number:132978. Available at: https://doi.org/10.1016/j.conbuildmat.2023.132978.

Scherer, C., de Lima, L.F. & Zorzi, J.E. 2023. Effect of partial replacement of cement by fine powders on the corrosion resistance of concrete. *Construction and Building Materials*, 401, art.number:132982. Available at: https://doi.org/10.1016/j.conbuildmat.2023.132982.

Sellaf, H. & Balegh, B. 2023. Effect Of Waste Marble Powder On The Properties Of White Mortar Made From Tuff. *Journal of New Technology and Materials*, 13(1), pp.25-32 [online]. Available at: https://www.asjp.cerist.dz/index.php/en/article/227651 [Accessed: 17 October 2024].

Sellaf, H., Balegh, B. & Bkhiti, M. 2023. The Assessment and Treatment of Dredged Sediments and Limestone Tuff Using Waste Ceramic with Low-Cement. *Advanced Engineering Forum*, 48, pp.45-58. Available at: https://doi.org/10.4028/p-2j4d93.

Thunuguntla, C.S. & Gunneswara Rao, T.D. 2018. Effect of mix design parameters on mechanical and durability properties of alkali activated slag concrete. *Construction and Building Materials*, 193, pp.173-188. Available at: https://doi.org/10.1016/j.conbuildmat.2018.10.189.

Influencia de la adición de sedimentos en el comportamiento mecánico del hormigón reforzado con fibras en ambientes agresivos

Louafi Goudih[a], *Hamid* Sellaf[b], *Benamar* Balegh[c], *Ali* Meksi[a], *Adda* Hadj Mostefa[d], *Mohamed Elamine* Dahamni[e]

[a] Universidad Mustapha Stambouli, Departamento de Ingeniería Civil, Laboratorio de Estudios de Estructuras y Mecánica de Materiales, Mascara, República Argelina Democrática y Popular

[b] Universidad de Saida, Departamento de Ingeniería Civil e Hidráulica, Saida, República Argelina Democrática y Popular + Laboratorio de Ingeniería Civil y Medio Ambiente, Sidi Bel Abbes, República Argelina Democrática y Popular

[c] Universidad de Ahmed Draia Adrar, Departamento de Ingeniería Civil, Adrar, República Argelina Democrática y Popular + Laboratorio de Ingeniería Civil y Medio Ambiente, Sidi Bel Abbes, República Argelina Democrática y Popular

[d] Universidad de Relizane, Departamento de Ingeniería Civil y Obras Públicas, Laboratorio de Materiales Innovadores y Energías Renovables, Relizane, República Argelina Democrática y Popular

[e] Universidad de Orán 1 - Ahmed Ben Bella, Laboratorio de Ciencias de la Materia Condensada (LSMC), Orán 1, República Argelina Democrática y Popular, **autor de correspondencia**

CAMPO: materiales
TIPO DE ARTÍCULO: artículo científico original

Resumen:

Introducción/objetivo: El uso de materiales cementantes suplementarios (SCM) en la construcción ha ganado popularidad debido a su capacidad para mejorar las propiedades mecánicas y la sostenibilidad ambiental del hormigón. Este estudio tuvo como objetivo investigar el potencial de utilizar materiales de desecho, específicamente polvo de mármol (MP) y sedimento de presa (DS), como reemplazos parciales del cemento en el hormigón autocompactante (SCC). Los objetivos principales fueron reciclar estos materiales de desecho y evaluar la durabilidad y la resistencia del SCC expuesto a entornos químicos agresivos.

Métodos: En este estudio, el cemento fue reemplazado parcialmente por 40% MP, 40% DS y una combinación de 20% MP y 20% DS. El desempeño de dicho concreto fue evaluado a través de pruebas de resistencia a la compresión realizadas durante 28 días. La durabilidad fue evaluada exponiendo el concreto a ataques químicos de soluciones de ácido clorhídrico (HCl), ácido sulfúrico (H_2SO_4) y sulfato de sodio (Na_2SO_4). También se midió la pérdida de masa debido a estos ataques químicos.

Resultados: El hormigón que incorpora MP presentó resistencias a la compresión similares a las del hormigón control, alcanzando 37,61 MPa a los 28 días. El hormigón con DS exhibió menor resistencia (31,81 MPa) y mostró mayor resistencia al HCl (ML = 38,78%) en comparación con el hormigón MP (ML = 40,74%). Además, todas las muestras de hormigón exhibieron buena resistencia al ácido sulfúrico debido a la formación de etringita expansiva que protegió al hormigón de una mayor degradación.

Conclusión: Los resultados indicaron que tanto el polvo de mármol como el sedimento de presa son materiales complementarios viables para mejorar las propiedades mecánicas y la durabilidad del hormigón autocontenible. El hormigón con polvo de mármol mostró una resistencia superior, mientras que el sedimento de presa contribuyó a mejorar la resistencia a los ácidos. La combinación de estos materiales ofrece una solución sostenible para el hormigón expuesto a entornos agresivos.

Palabras claves: hormigón (SCC), sedimento, polvo de mármol, fibra, pérdida de masa, mecánico, ambiente agresivo.

Влияние добавок на седиментационную устойчивость и механические свойства фибробетона в агрессивных средах

Луафи Гудих[а], *Хамид* Селлаф[б], *Бенамар* Балег[в], *Али* Мекси[а], *Адда* Хадж Мостефа[г], *Мохаммед Эль-Амин* Дахамни[д]

[а] Университет Туши Мустафы Стамбули,
факультет гражданского строительства,
Лаборатория по изучению структур и механики материалов,
г. Маскара, Алжирская Народная Демократическая Республика

[б] Университет Саиды,
факультет гражданского строительства и гидротехники,
г. Саида, Алжирская Народная Демократическая Республика +
Лаборатория гражданского строительства и охраны окружающей среды,
г. Сиди-Бель-Аббес, Алжирская Народная Демократическая Республика

[в] Университет Ахмеда Дрейи в Адраре,
факультет гражданского строительства,
г. Адрар, Алжирская Народная Демократическая Республика +
Лаборатория гражданского строительства и охраны окружающей среды,
г. Сиди-Бель-Аббес, Алжирская Народная Демократическая Республика

[г] Университет в Релизане,
факультет гражданского строительства и общественных работ,
Лаборатория инновационных материалов и возобновляемых источников энергии, г. Релизан, Алжирская Народная Демократическая Республика

[д] Университет Ахмеда Бен Беллы в Оране 1,
Лаборатория конденсированных сред (LSMC),
г. Оран 1, Алжирская Народная Демократическая Республика,
корреспондент

РУБРИКА ГРНТИ: 81.09.00 Материаловедение
ВИД СТАТЬИ: оригинальная научная статья

Резюме:

Введение/цель: Использование заменителей цементных материалов (ЗЦМ) в строительстве приобрело популярность благодаря их способности улучшать механические свойства и экологическую устойчивость бетона. Целью данного исследования было изучение потенциала использования отходов, в частности, мраморной крошки (МР) и отложений плотины (ОП) в качестве частичной замены цемента в самоуплотняющемся бетоне (СУБ). Основными задачами были утилизация этих отходов и оценка долговечности и прочности ЗЦМ, подверженных воздействию агрессивных химических сред.

Методы: В данном исследовании цемент был частично заменен на 40% МК, 40% ОП и смеси из 20% МК и 20% ОП. Свойства полученного бетона испытаны на прочность при сжатии в течение 28 дней. Прочность бетона оценивалась путем воздействия растворов соляной кислоты (HCl), серной кислоты (H_2SO_4) и сульфата натрия (Na_2SO_4). Также была измерена потеря массы в результате этих химических воздействий.

Результаты: Бетон, содержащий МК, показал прочность на сжатие, аналогичную прочности контрольного бетона,

достигнув 37,61 МПа через 28 дней. Бетон с ОП обладал более низкой прочностью (31,81 МПа) и более высокой стойкостью к HCl (ML = 38,78%) по сравнению с бетоном с МК (ML = 40,74%). Помимо того, все образцы бетона показали высокую стойкость к воздействию серной кислоты благодаря образованию обширного эттрингита, защищавшего бетон от дальнейшего разрушения.

Вывод: Результаты показали, что как мраморная крошка, так и отложения плотины являются полезными материалами-заменителями для улучшения механических свойств и долговечности бетона. Бетон с мраморной крошкой показал превосходную прочность, а отложения плотины способствовали повышению кислотостойкости. Сочетание этих материалов обеспечивает надежное решение для бетона, подверженного воздействию агрессивных сред.

Ключевые слова: бетон (СУБ), добавки, мраморная крошка, волокно, потеря массы, механическая обработка, агрессивная среда.

Утицај седиментних адитива на механичко понашање бетона армираног влакнима у агресивним срединама

Луафи Гуди[а], *Хамид* Селаф[б], *Бенамар* Бали[в], *Али* Мекси[а], *Ада* Хаџ Мустифа[г], *Мухамед Еламин* Дахамни[д]

[а] Универзитет „Мустафа Стамболи”, Одсек за грађевинарство, Лабораторија за проучавање конструкција и механике материјала, Маскара, Народна Демократска Република Алжир

[б] Универзитет у Саиди, Одсек за грађевинарство и хидраулику, Саида, Народна Демократска Република Алжир + Лабораторија за грађевинарство и заштиту животне средине, Сиди Бел Абес, Народна Демократска Република Алжир

[в] Универзитет „Ахмед Драиа” у Адрару, Одсек за грађевинарство, Адрар, Народна Демократска Република Алжир + Лабораторија за грађевинарство и заштиту животне средине, Сиди Бел Абес, Народна Демократска Република Алжир

[г] Универзитет у Релизану, Департман за грађевинарство и јавне радове, Лабораторија за иновативне материјале и обновљиве енергије, Релизане, Народна Демократска Република Алжир

[д] Универзитет „Ахмед Бен Бела” у Орану 1, Лабораторија за науку о кондензованој материји (ЛСМЦ), Оран 1, Народна Демократска Република Алжир, **аутор за преписку**

ОБЛАСТ: материјали
КАТЕГОРИЈА (ТИП) ЧЛАНКА: оригинални научни рад

Сажетак:

Увод/циљ: Материјали који замењују цемент (Supplementary Cementitious Materials, SCM) све чешће се додају бетону у градитељству због своје способности да побољшавају механичка својства бетона, као и због одрживости животне средине. У овој студији испитане су могућности коришћења отпадних материјала – мермерног праха (МП) и седимената насталих при грађењу брана (ДС), као делимичне замене за цемент у самозбијајућем бетону (Self-compacting Concrete, SCC). Примарни циљеви били су рециклирање ових отпадних материјала и процена трајности и чврстоће самозбијајућег бетона изложеног хемијски агресивном окружењу.

Методе: У овом истраживању цемент је био делимично замењен са 40% МП, 40% ДС и комбинацијом 20% МП и 20% ДС. Перформансе бетона су испитане тестовима чврстоће при притиску током 28 дана. Трајност је испитивана излагањем бетона хемијској агресији раствора хлороводоничне киселине (HCl), сумпорне киселине (H_2SO_4) као и натријум сулфата (Na_2SO_4). Такође, вршено је мерење губитка масе услед овог излагања хемикалијама.

Резултати: Бетон са садржајем МП показао је чврстоћу при притиску сличну оној коју има контролни бетон, постижући 37,61 MPa за 28 дана, док је бетон са ДС имао мању чврстоћу (31,81 MPa), а већу отпорност на хлороводоничну киселину (ML=38,78%) у поређењу са бетоном са МП (ML=40,74%). При томе су сви узорци бетона имали добру отпорност на сумпорну киселину због формирања експанзивног етрингита који штити бетон од даље деградације.

Закључак: Резултати су указали да су и мермерни прах и седимент брана могући као допунски материјали за побољшавање механичких особина и трајности самозбијајућег бетона. Показано је да бетон са мермерним прахом има супериорну чврстоћу, док је седимент добијен грађењем брана допринео побољшању отпорности на киселине. Комбинација ових материјала нуди одрживо решење за бетоне изложене агресивним срединама.

Кључне речи: бетон (SCC), седимент, мермерни прах, влакно, губитак масе, механичка обрада, агресивна средина.

Paper received on: 13.04.2024.
Manuscript corrections submitted on: 29.01.2025.
Paper accepted for publishing on: 30.01.2025.

Effects of scrap rubber waste on the mechanical performance of mortar made of crushed sand and sediment

Adda Hadj Mostefa[a], *Benamar* Balegh[b], *Hamid* Sellaf[c], *Mohamed Elamine* Dahamni[d]

[a] University of Relizane, Department of Civil Engineering and Public Works, Innovative Materials and Renewable Energies Laboratory, Relizane, People's Democratic Republic of Algeria,
e-mail: addahadjmostefa@yahoo.fr,
ORCID iD: https://orcid.org/0009-0004-0086-9280

[b] University of Ahmed Draia Adrar, Department of Civil Engineering, Adrar, People's Democratic Republic of Algeria +
Civil Engineering and Environmental Laboratory, Sidi Bel Abbes, People's Democratic Republic of Algeria,
e-mail: ben.balegh@univ-adrar.edu.dz,
ORCID iD: https://orcid.org/0000-0002-8529-7063

[c] University of Saida, Department of Civil Engineering and Hydraulics, Saida, People's Democratic Republic of Algeria +
Civil Engineering and Environmental Laboratory, Sidi Bel Abbes, People's Democratic Republic of Algeria,
e-mail: hamid.sellaf@univ-saida.dz,
ORCID iD: https://orcid.org/0009-0006-3943-3024

[d] University Oran 1 - Ahmed Ben Bella, Condensed Matter Science Laboratory (LSMC), Oran 1, People's Democratic Republic of Algeria,
e-mail: dahamnimohamedelamine@gmail.com,
corresponding author,
ORCID iD: https://orcid.org/0000-0001-5920-1198

https://doi.org/10.5937/vojtehg73-50150

FIELD: materials, civil engineering
ARTICLE TYPE: original scientific paper

Abstract:

Introduction/purpose: The consumption of natural sand in Algeria is high due to its extensive use in mortar, while sediments and rubber waste pose significant environmental and societal challenges. This study investigates the effects of incorporating rubber waste content in mortars mixed with crushed sand and sediment. The primary goal is to valorize crushed sand particles through physical and mechanical tests, evaluating their potential as an alternative to natural sand in mortar mixtures.

ACKNOWLEDGMENT: This work was supported by the CNEPRU project with code A01L02UN010120200004 and the Civil Engineering and Environmental Laboratory of the University of Sidi Bel Abbes, Algeria.

Methods: Experimental work was carried out to study the impact of partially and fully replacing sediments with crushed sand particles in mortar mixes. Mortar mixtures were prepared using different sediment-to-crushed sand ratios (10%, 25%, 35%, 50%, and 100%) to observe their influence on physical and mechanical properties. Additionally, the effects of adding 2%, 4%, and 6% granulated rubber to the optimal mortar were analyzed. Various tests, including those tsting compressive strength, flexural strength, and ultrasonic pulse velocity, were performed to evaluate the performance of the mixtures.

Results: The results indicated that replacing sediment with crushed sand improved the strength properties of mortar, particularly due to better particle packing. The mortar containing 65 wt% sediments and 35 wt% crushed sand showed properties similar to the reference mortar. The addition of rubber waste increased compressibility but enhanced mechanical properties when used in moderation. Ultrasonic pulse velocity decreased with higher crushed sand content, and the porosity of the mixtures was reduced.

Conclusions: Crushed sand and sediment particles are effective fillers for mortar, ensuring good performance and improved strength. The efficiency of these materials depends on their morphology and genesis. The study demonstrates that crushed sand can be a viable alternative to natural sand, and rubber waste can be used as a reinforcing material in mortar, though its proportions should be carefully controlled to avoid negative effects on mechanical properties.

Key words: mortar, sediment, crushed sand, scrap rubber waste, compressive strength, tensile strength.

Introduction

The surge in demand for sand in Algeria over the past decade, driven by substantial development programs in construction, has resulted in a shortage of this essential material. For this reason, the use of alternative materials is essential, such as tuff (Cherrak et al, 2013), crushed sand (Srivastava & Singh, 2020), dune sand, fine limestone, natural pozzolans, and various wastes (Chouhan et al, 2020; Bederina et al, 2013). Moreover, reusing all concrete and mortar waste can effectively protect the environment and contribute to sustainable development (Benyamina et al, 2019). In addition, the quantities of limestone fines and crushed sand are very abundant in many quarries, which poses the problem of disposal and reuse in the manufacture of concrete (Chouhanet al, 2020).

The problem of sedimentation also affects dams and energy production; for example, the Fargoug dam, located in the northwest of

Algeria, about 20 km south of the city of Mohammedia (region of Mascara), is one of the many dams that suffer from this problem. Thus, dredging these sediments and reusing them as alternative materials is a solution to recycle and valorize them, given their physical, chemical, and biological properties and stabilizing capacity (Fonti et al, 2013). Also, one can reuse them in base layer locations for roadways (Sellaf et al, 2023).

Researchers have recently conducted numerous studies to explore using crushed sand in mortar and concrete. The strength properties of concrete using crushed sand are almost identical to traditional concrete. Furthermore, bottle chips are combined with crushed sand to partially replace the conventional sand used in the proposed concrete (Cepuritisa et al, 2016). The use of crushed sand also ensures the position of natural sand as an aggregate for concrete's durability and mechanical performance (Lam, 2020; Bédérina et al, 2005). It should be noted that sediment and crushed sand particles are nearly identical, owing to their physical nature and high flour content (Ma et al, 2022). Therefore, it is very appropriate to use sediment as an alternative material, and it serves as a filler in the cement slurry that reinforces the dense microstructure (Singh et al, 2015).

On the other hand, more than 26,000 tonnes of waste rubber tires are dumped annually in Algeria (Nakhaei et al, 2012). Waste tires mainly comprise synthetic rubber, carbon black, silicone, and steel. There are many ways to dispose of rubber tires, including storage or landfills. Alternatively, there are various ways to recycle rubber waste, including using it for fencing and decorative elements (Khan et al, 2016; Trouzine et al, 2012; Khorrami et al, 2010) and in the field of filtration of landfill leachate.

This study is planned to develop the consistency limit properties, bulk density, compressive and tensile strength, and ultrasonic pulse velocity of mortar composed of crushed sand particles and sediments with different mixing ratios and to find out the effect of its different percentage addition on some important physical-mechanical properties of such mortar. Then, the optimal mortar sample was obtained with rubber scraps in different proportions to improve the mechanical strength. The importance of this research lies in examining the effectiveness of the combined use of sediments, crushed sand, and rubber scraps as partial substitutes for sand in mortar mixtures. Also, this study aims to eliminate rubber waste, sediments, and aggregate grinding waste and recycle them as substitutes for aggregates used in mortars, thus protecting the environment.

Experimental procedures

Materials and preparation methods

Sediment

Sediment specimens are dam sediment of the region of Fergoug in the south of Mascara in the northwest of Algeria, and they are generally cohesive brown and grey soils. The specific gravity of the sediment was 2.55.

The particle size distribution for the soils is shown in Table 1.

Table 1 – Properties of the investigated materials

Property	Sediment	Reference sand	Particles of crushed sand
Liquid limit (%)	38	22	15
Plastic limit (%)	23	14	0.00
Plasticity index (%)	15	8	0.00
Volume of blue VB (cm^3)	5.5	0.75	0.39
Specific gravity	2,55	2.63	2.70
Visual sand equivalent (%)	0.00	70	45
Apparent density (g cm-3)	1.26	1.45	1.53
Fineness modulus	1.2	1.80	3.10
Organic content (%)	3.2	1	0.00

Specific gravity is the ratio of a material's density with that of water at 4 °C (where it is most dense and is taken to have the value 999.974 kg m^{-3}). It is therefore a relative quantity with no units.

The soil chemical analysis was conducted following the AFNOR standard NF EN 1744 (AFNOR, 1998a), and the results are presented in Table 2. The main constituent of the sediment is silica with 76.01 % where the ratio SiO_2/Al_2O_3 equals 19.02.

Table 2 – Chemical compositions of materials

Property	Soil S	Soil RS	Soil CS
SiO_2 (%)	64.18	76.010	6.39
SO_3 (%)	0.021	0.034	0.106
Al_2O_3 (%)	0.03	3.996	2.33
Fe_2O_3 (%)	0.84	1.551	0.807
CaO (%)	17.30	5.918	47.41
K_2O (%)	17.30	1.261	0.44
MgO (%)	0.27	1.365	1.49
NaOH (%)	0.00	0.221	0.079
CL (%)	0.00	0.006	0.00
P.A.F (%)	0.5	8.150	41.330
$CaCO_3$ (%)	22.73	12	67.00

The particle size analyses were conducted using the sieving and hydrometer methods (Amar et al, 2018). The grain size distribution curve indicates that the sediment is predominantly silt-sized, with 55.3% clay. Furthermore, the percentage of particles with a diameter less than 80 μm is approximately 82.90%. The limit liquid is about 38% (AFNOR, 1992, 1996), and the plasticity index is about 15%. The material from the Fergoug sediment is classified as inorganic silts. The organic matter content is determined using the ignition test at 450°C, following the standard NF EN 1744 (AFNOR, 1998a), which is about 3.2% for sediment samples. The specific gravity, determined through a pycnometer, is approximately 2.55. The maximal and minimal void ratios were theoretically calculated based on dry density and specific gravity. The void ratio values range from 1.53 to 1.95.

Particles of crushed sand

Two soils samples of different origins and physical properties were selected. The first sample, crushed sand, was obtained from the Tizi quarry site in Mascara, northwest Algeria. These two soil samples underwent various laboratory identification tests, following standard procedures established by AFNOR and ISO standards. The specific gravity of particles in crushed sand was 2.70, whereas that of the reference sand was 2.63. The particle size distribution for the materials is presented in Table 1. The results of the chemical analysis of the soils, shown in Table 2, are carried out according to the standard NF EN 1744 (AFNOR, 1998a).

The tests to determine the Atterberg limits and the density of solid particles were conducted following the standards NF P94-054 and NF P94-051 (AFNOR, 1991, 1993), and the specific surface area of the sand

was determined using the Methylene Blue test (AFNOR, 1998b). The specific surface area is approximately 115.5 $m^2 g^{-1}$, and the volume of Methylene Blue used is approximately $7cm^3$.

The materials used included (S), (CS), (RS), and (SCS), representing sediment, crushed sand, reference sand, and a soil mixture, respectively. The sediment (S) and crushed sand (CS) were utilized as fine aggregates, as depicted in Figure 1.

Figure 1 – Fine aggregates: sediment (S) and crushed sand (CS)

Figures 2a and 2b represent the main components of sediment (S) and crushed sand (CS) using X-ray diffraction.

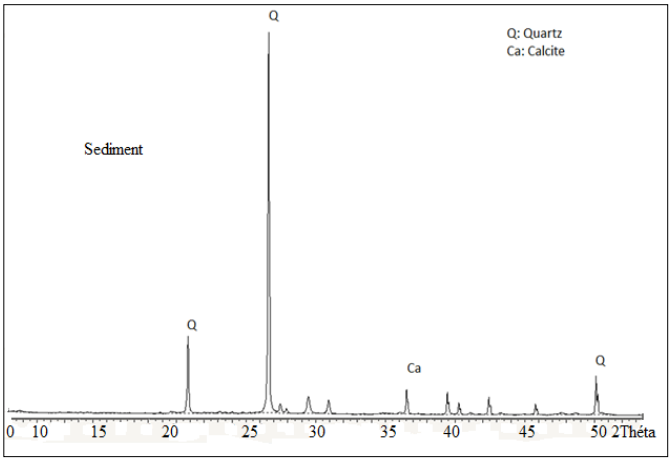

Figure 2a – X-ray diffraction of sediment

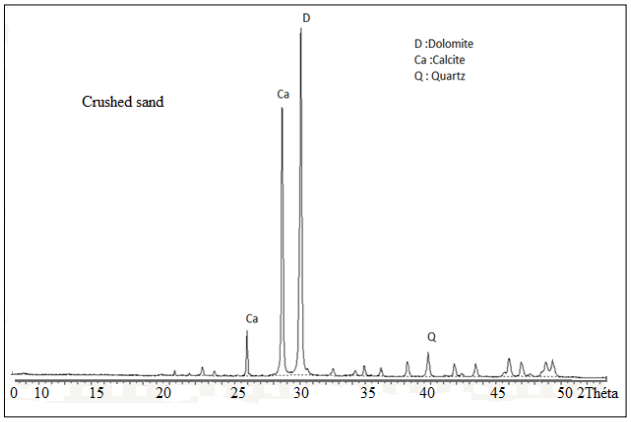

Figure 2b – X-ray diffraction of crushed sand.

Figure 3 shows the values of grain size distribution for the studied specimens. The grain size distribution decreases with the crushed sand content. For sediment (S), the fineness modulus was 1.2 for the sand samples. In contrast, the values for the composite samples with 10%, 25%, 35%, 50%, and 100% crushed sand content were 1.45, 1.65, 1.98, 2.55, and 2.55, respectively. When compared to the reference sand, the fineness modulus was observed to be equivalent to the SCS3 mixture.

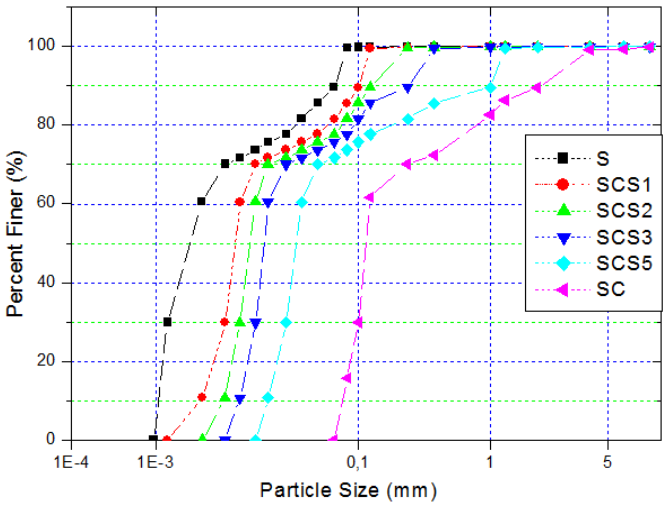

S: 100% sediment, RS: Reference sand, SCS1: 90% sediment and 10% crushed sand; SCS2: 75% sediment and 25% crushed sand; SCS3 65% sediment and 35% crushed sand, SCS5: 50% sediment and 50% crushed sand; SC: 100% crushed sand

Figure 3 – comparative grain size distribution in the investigated samples

Mortar-mix design

Five mortars are mixed with a constant water/cement (W/C) ratio and a variable sediment/crushed sand (S/CS) ratio. The main objective of using a variable S/CS ratio is to emphasize the sole effect of this addition on the physical and mechanical characteristics of the mortar, serving as a substitute for sand. Mortar compositions were prepared by integrating sediment with crushed sand in the following ratios: 100% sediment, 90% sediment with 10% crushed sand, 75% sediment with 25% crushed sand, 65% sediment with 35% crushed sand, 50% sediment with 50% crushed sand, and 100% crushed sand. A reference specimen was also produced, consisting of mortar with sediment, for comparison.

To facilitate the readings, the mixtures with the acronym MSCS refer to the mortar made from sediment to crushed sand, while the reference mortar is called MRS. For further investigation, a similar mortar containing a superplasticizer has been formulated. The polycarboxylate superplasticizer has been used in constant amounts, comprising 1.2 by weight of cement.

Table 3 – Cement chemical and mineralogical features and the water chemical analysis.

Chemical and mineralogical composition of cement (%)		Chemical analysis of water(mg/l)	
SiO_2	20.19	Cl	113,60
Al_2O_3	5.23	SO_4	65,46
Fe_2O_3	2.34	NO_3^-	12,22
CaO	56.90	NO_2	0,00
MgO	2.01	Na^+	0,00
NaOH	0.15	K^+	0,00
CL	0.01	Mg^{2+}	51,36
$P.F_2$	5.84	Ca^{2+}	32,86
Ins	4.26	CO_3^{2-}	0,00
Free CaO	1.01	HCO_3	368,44
C_3S	60	Fe	0,03
C_2S	16	Cl^-	113,60
C_3A	5	SO_4^-	65,46

The cement utilized in this investigation is ordinary Portland cement (CPJ), comprised of 76% clinker, 18% calcareous material, and 6% gypsum. The chemical analysis of the cement and mineral admixtures is presented in Table 3.

Scrap tires rubber

Scrap tire rubber fibers can be derived from tires using two primary processes: (i) ambient processing, where scrap tire rubber is ground or treated at or above regular room temperature, and (ii) cryogenic processing, which involves freezing waste rubber with liquid nitrogen and subsequently grinding frozen rubber into small particles using a mill (Caltrans, 2006). The tire rubber fiber constitutes an intricate blend of elastomers, encompassing polyisoprene, polybutadiene, and styrene-butadiene. The key components of rubber include stearic acid (1.2%), zinc oxide (1.9%), extender oil (1.9%), and carbon black (31.0%) (Akbulut et al, 2007). Table 4 presents some properties of scrap tire rubber.

Table 4 – Some properties of the scrap tire rubber fibre

Properties	Tire rubber
Density (mg m^{-3})	1.153-1.198
Tensile strength (MPa)	16-20
Elongation (%)	400-500

Sample preparation

The mortars were mixed, and prisms of 40 x 40 x 160 mm were prepared according to the standard NF EN 196-1 (AFNOR, 1990). The mortar samples were cured for 24 hours in the laboratory at 20 ± 2°C with a relative humidity of approximately 50%. The mixed design of mortars is detailed in Table 5. At the onset of the experiment, the mortar specimens were immersed in potable water, and the penetration time was measured at intervals of 4, 7, 14, 28, 56, and 90 days.

Table 5 – Compositions of mortar (kg m^{-3}).

Mixture code	MS	MCS	MRS	MSCS1	MSCS2	MSCS3	MSCS5
Cement	450	450	450	450	450	450	450
Water	225	225	225	225	225	225	225
Sediment	1350	-	-	1215	1012	878	675
Crushed sand	-	1350	-	135	338	472	675
Reference sand	-	9	1350	-	-	-	-
Superplasticizer	9		9	9	9	9	9

Results and discussion

Consistency limits

Atterberg limit tests were conducted to ascertain the consistency limit values of the sands and their mixtures following the reference standard NF P94-057 (AFNOR, 1992).

As shown in Figure 4, the consistency limits of the mixture of sediment and crushed sand decrease progressively with increasing the crushed sand particle content. The consistency limit of the mixture of 75% sediment with 25% crushed sand is close to the consistency limit of the reference sand.

As shown in Figure 4, for sediment, the plastic limit gradually decreases with an increased amount of crushed sand particles. The results of the Atterberg limit test indicate that sediment has a higher plasticity index value than crushed sand. The results of the plastic limit test indicate that crushed sand has a null value (sediment 23%, RS 14.00%, SCS1 14.02%, SCS2 12.50%, SCS3 12.03%, and SCS5 10.00%, SC: 0.00%).

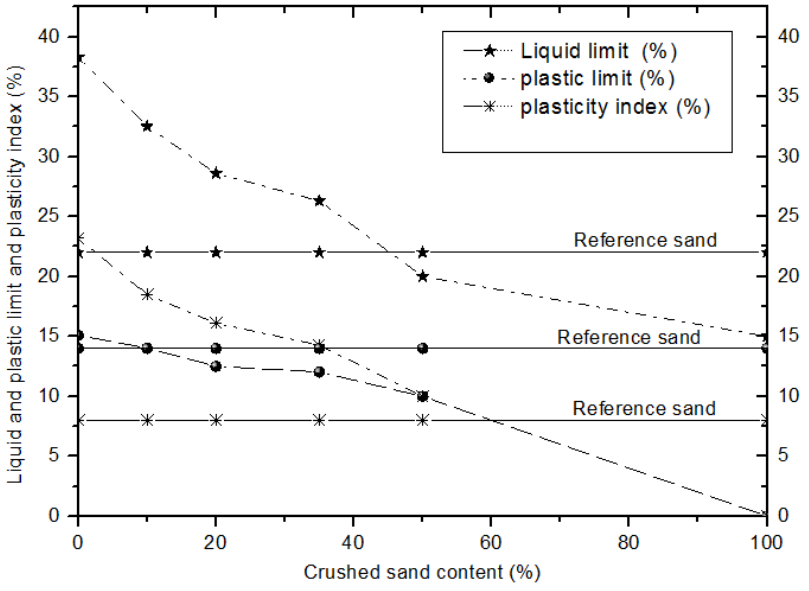

Figure 4 – Effect of the particles of the crushed sand content on the consistency limits of sediment

Changes in the consistency limits of the mixtures may result from factors such as the type of mixture, the exchange capacity of the clay (Cetin et al, 2006; Bell, 1993), and the proportion of clay minerals in the mixtures (Okagbue & Onyeobi, 1999). Notably, plastic limits were investigated for the mixtures of tire-cohesive clayey soil in the reference (Sivapullaiah et al, 2000). They initially remain stable, exhibit a subsequent decrease, and stabilize again. These findings are parallel to those observed in fine-grained cohesive soils with medium plasticity.

Bulk density

As shown in Figure 5, the bulk density shows a significant proportional increase with the percentage of incorporated fines. This phenomenon appears primarily attributable to the top density of crushed sand waste fines compared to regular sand, as measured during the experimental campaign. This result aligns with the findings in the reference material (Schmitz et al, 2004).

This test was conducted following the European Standard EN 1015-10 (NBN, 1999). Dry bulk density suddenly decreases in the mortar with crushed sand replacement and linearly decreases with increasing the proportion of crushed sand.

Unlike fresh mortar, hardened mortar MSCS 4 exhibited a higher dry bulk density than the reference mortar MRS. This seems to be due to the addition of crushed sand in the mixture induced by the reduction of air voids in the mortars (Arnould & Virlogeux, 1986). Thus, voids in the mortar that are not filled with sand due to the absence of sediment incorporation are instead filled with the latter.

On the other hand, mortar MSCS3, which incorporates twice as much sediment and includes crushed sand, exhibits the same dry bulk density as MRS, similar to that of the reference mortar.

As outlined in numerous studies, the primary concern with porous aggregates is their water absorption capability. This factor impacts the workability during casting and the material properties (Aoual-Benslafa et al, 2015). One portion of water facilitates the hydration of cement, while another portion is absorbed by the aggregates, contributing to the plasticity of the mixture. Pavia & Toomey (2008) substantiates this phenomenon in his research on mortars.

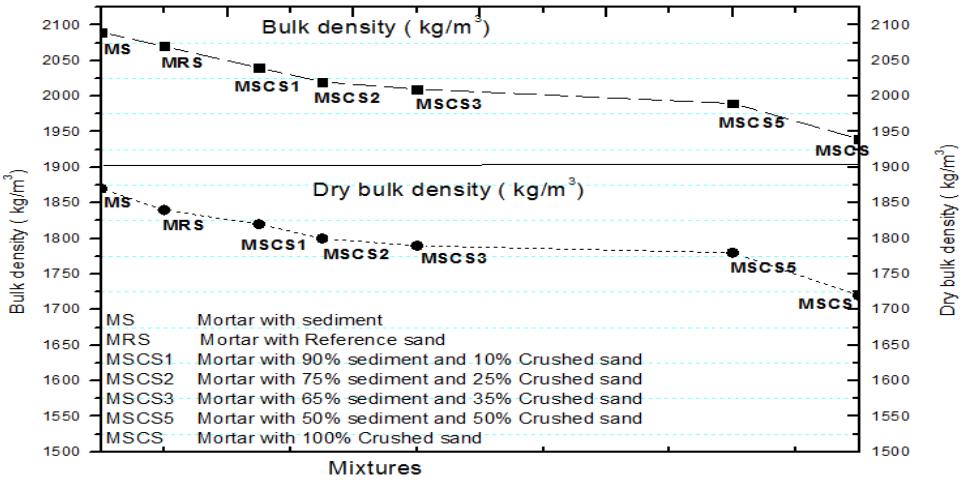

Figure 5 – Effect of crushed sand and sediment content on the bulk density of mortars

Tensile strength

To calculate the tensile strength of the specimen, beam specimens of size 40 · 40 · 160 mm are cast according to specifications. The flexural strength is determined by applying three-point loads (i.e., to achieve pure bending) on these specimens. For each type of mortar, a set of three specimens, previously subjected to curing periods of 4, 7, 14, 28, 56, and 90 days, was used, and the results are presented in Figures 6.

The compressive strength of all the mortars falls within the range of 2.16–6.25 MPa, 5.32–15.41 MPa, 10.11–25.23 MPa, 15.66–28.42 MPa, and 18.52–30.23 MPa at curing periods of 4, 7, 14, 28, 56, and 90 days. The compressive strength of all mortar mixtures increases with changing the curing period. The mortar with crushed sand exhibits lower compressive strength than the reference mortar at all test ages. Moreover, an increase in the replacement level of crushed sand results in an overall improvement in the compressive strength of the mortar.

Crushed sand, when used to replace river sand, improves the aggregate particle packing. Moreover, it can be observed from Figure 6 that at the replacement levels of 35% and 50%, the compressive strength of the mortar with crushed sand is higher by 10% and 25% during the curing periods of 4, 7, 14, and 28 days. Additionally, the compressive strength at 56 and 90 days for the mortar with crushed sand is only slightly higher by 1.66%, 1.57%, 1.20%, and 1.30% compared to the mortar with MRS.

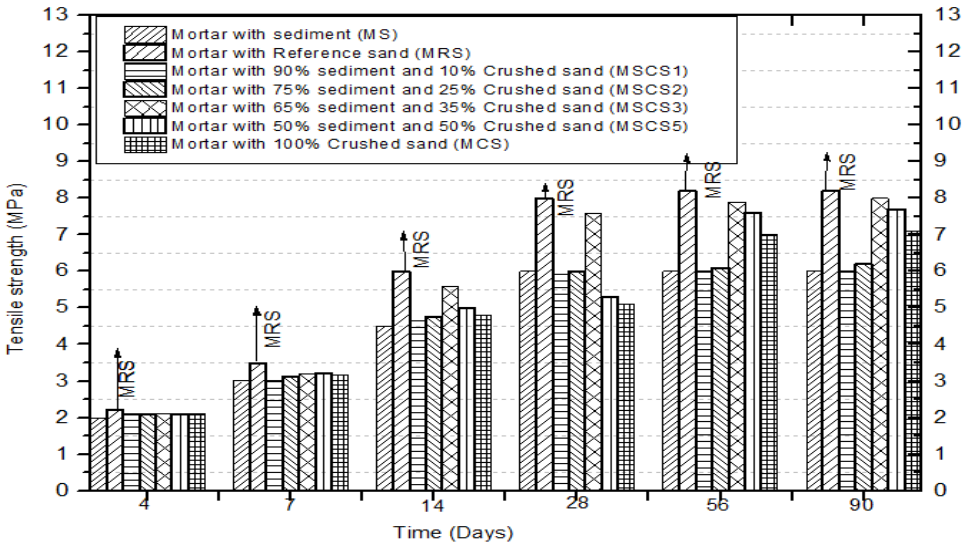

Figure 6 – Effect of crushed sand and sediment content on the tensile strength of mortars

Compressive strength

Compressive strength follows the same trend as the tensile strength obtained in the test, as shown in Figure 7. It is found that the maximum strength is observed at MRS (8.21 MPa), MSCS3 (8.02 MPa), MSCS5 (7.7 MPa), MSCS2 (6.24 MPa), and MSCS1 (6.08 MPa). Regarding mortar, the obtained values for MS (6.00 MPa) are lower than those for the reference mortar (MRS). Generally, the properties of hardened mortar are influenced by the characteristics of the granular constituents, which depend on the relative water absorption of aggregates. Consequently, the increase in resistance is subordinate to the rise in the water absorption capacity (Torres & García-Ruiz, 2009; Wang et al, 2013).

The increase in the replacement level of crushed sand results in an enhancement of the flexural strength of the mortar. The 28-day flexural strength of the mortar with crushed sand at 25%, 35%, and 50%, is measured at 6.00 MPa, 7.61 MPa, and 5.32 MPa, respectively. This represents an increase of 1.33%, 1.05%, and 1.51% compared to the corresponding reference mortar. A similar trend of increasing flexural strength with higher levels of crushed sand replacement is also observed in the mortar during the curing periods of 56 and 90 days.

These results align with the previous findings by Tommaso and Revecca, who utilized crushed sand and sediment as substitutes for reference sand aggregate in a reinforced mortar (D'Antino et al, 2019; Li & Liu, 2021). Corinaldesi (2012) attributed the observed detrimental effect of crushed sand to a high porosity of its particles, resulting in a decrease in severity. Lu et al. (2022) discovered an intriguing relationship between compressive strength and particle size, noting that this relationship is consistent across all specimens.

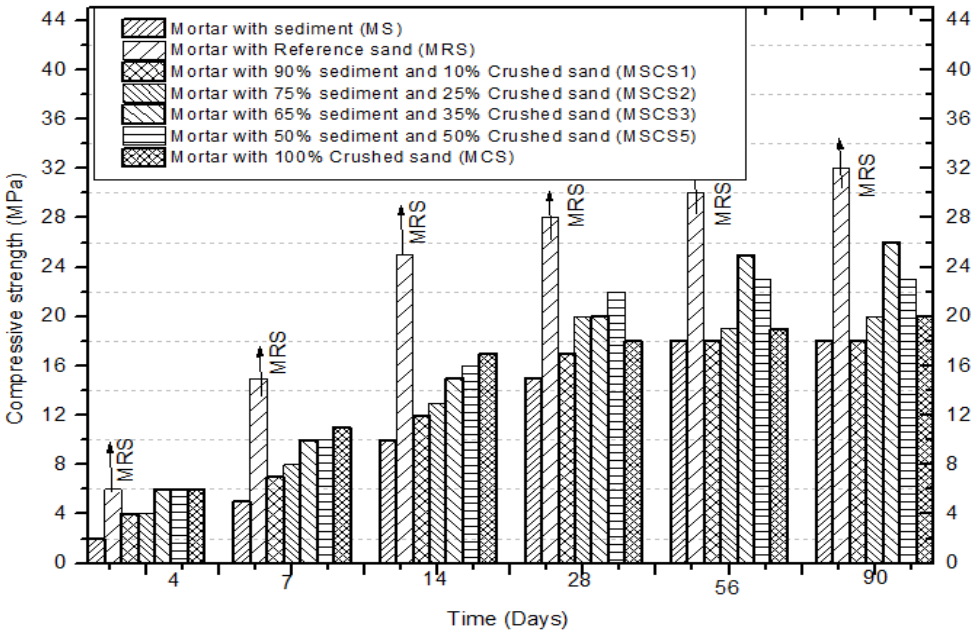

Figure 7 – Influence of crushed sand and sediment content on the compressive strength of mortars

Ultrasonic pulse velocity

The values obtained show that all the mortars made with crushed sand material obtained slightly lower results, around 6.6%- 14.8% concerning the reference sand.

Generally, the pulse velocity of mortars made with crushed sand was greater than that of mortars made with reference sand. As depicted in Figure 8, the 28-day ultrasonic pulse velocities for the mortar types MRS, MSCS3, MSCS5, MSCS2, MSCS1, MS, and MSC were 4120 m/s, 3850 m/s, 3760 m/s, 3740 m/s, 3680 m/s, 3620 m/s, and 3510 m/s, respectively. These values were lower than the 4120 m s^{-1} recorded for the control group.

Moreover, as depicted in Figure 8, it is evident that, at the 35% replacement level, ultrasonic pulse velocities of the mortar containing crushed sand are higher by 10%, 25%, and 50% at the curing periods of 28 days. The increased incorporation of crushed sand enhanced the velocity of mortar MSCS3, and all the produced mortars exhibited lower velocities than MRS. These results align with the findings reported by Corinaldesi in 2012 (Jiang et al, 2022).

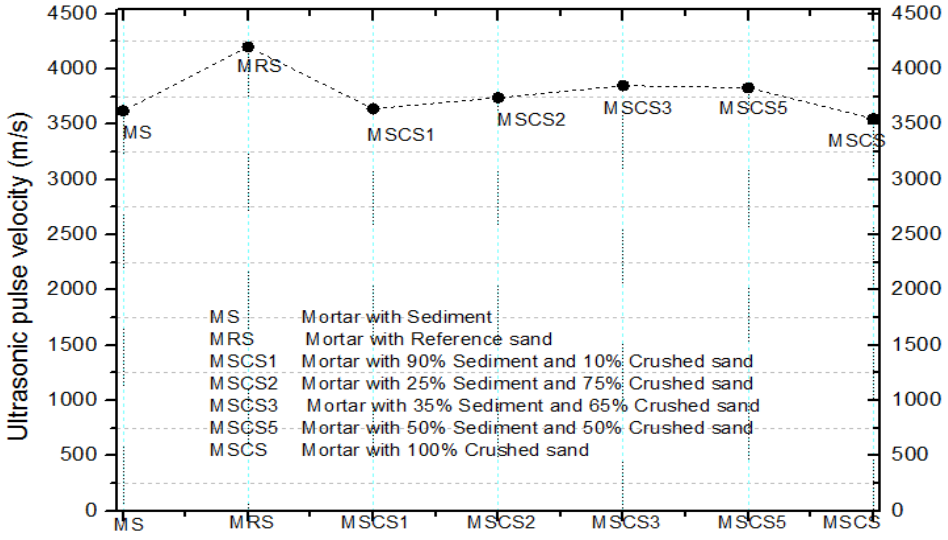

Figure 8 – Effect of crushed sand and sediment content on the ultrasonic pulse velocities of mortars

Reinforcement of mortar MSC35 with scrap tire rubber

The optimal mortar, MSC35opt, was treated with scrap tire rubber, as indicated in the studies by Jiang et al. (2022) and Su et al. (2022). The goal was to determine the best content of rubber powder. Jeon prepared a slurry with crumb rubber powder contents ranging from 0% to 15%, with 5% intervals, based on the volume of sand. Su et al. (2022) replaced the natural aggregates with four different volume percentages: 2%, 5%, 7.5%, and 10%, according to the differential contents of 2%, 4%, and 6%. Five specimens were prepared for each blend of mortars. The mixed mortar designs are detailed in Table 5. Samples of each composition were individually immersed in water. Before conducting the mechanical tests, the specimens were dried for three hours in the laboratory. Compressive strengths were determined at 14, 28, 56, and 84 days. The mixture code

includes a letter indicating the type of sand used. Further details about the mixtures can be found in Table 5.

Table 5 – Compositions of MSCS mortar containing scrap rubber (kg m^{-3}).

Mixture	MSCS	MSR2	MSR4	MSR6
Cement	450	450	450	450
Water	225	225	225	225
Sediment	877	864	838	824
Crushed sand	473	463	453	443
Scrap rubber	Nul	10	20	30
Superplasticizer	9	9	9	9

Compressive strength and tensile strength

When scrap rubber was added to partially substitute coarse aggregates, compressive strength decreased as rubber quantity increased. To calculate the flexural strength of the specimens, beam specimens with dimensions of 40 x 40 x 160 mm were prepared. Their flexural strengths were determined by applying three-point loads (to induce pure bending) on these specimens, as illustrated in Figure 9, following the standard NF EN 196-1 (AFNOR, 1995).

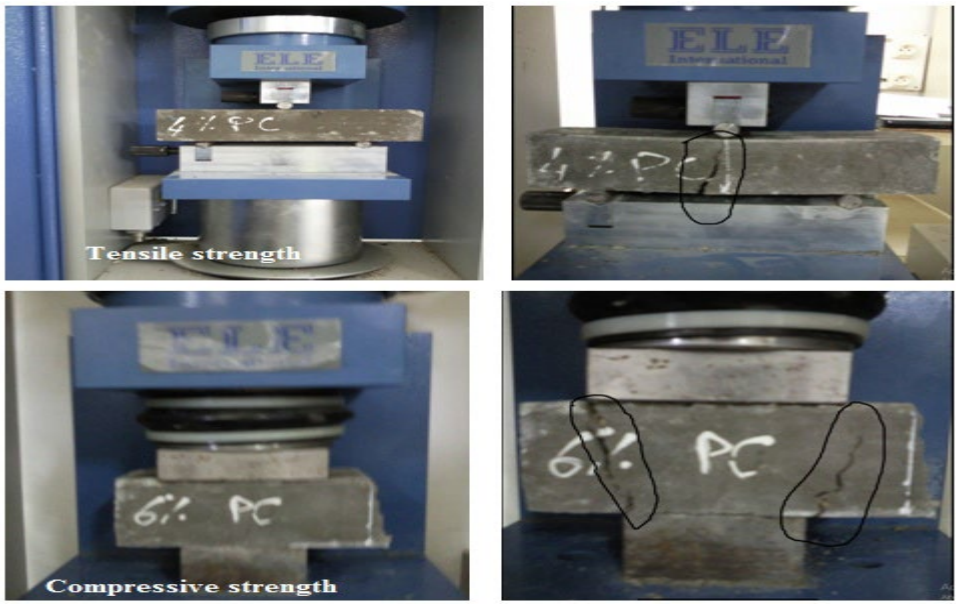

Figure 9 – Compression and tensile strength machines to test prisms 40 · 40 · 160 mm^3

The variation in flexural strength concerning the percentage increase in scrap rubber is notable. It is observed that the flexural strength of the specimens with rubber particles exhibits a decreasing trend as the quantity of rubber increases, as depicted in Figure 10.

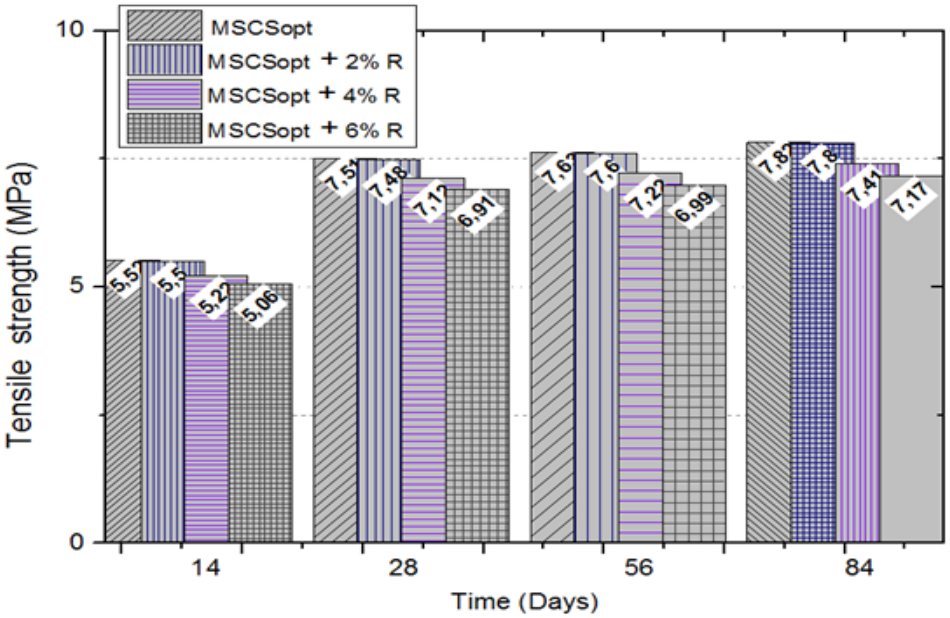

Figure 10 – Influence of scrap rubber addition rate on tensile strength.

Figure 11 illustrates that substituting rubber aggregate significantly diminishes the compressive strength of the composite at 14, 28, 56, and 84 days. This is the primary reason why the rubber aggregate substitution volume fraction was restricted to 6% (84-day compressive strength: MSCSopt = 26 MPa; compressive strength with 6% rubber granulate = 23.19 MPa). Specifically, it is evident that a 2% rubber aggregate substitution results in an almost imperceptible 0.8% drop in compressive strength and a 0.2% decrease in tensile strength. Meanwhile, the strength loss due to a 4% rubber aggregate substitution is approximately 8.5%. These findings are consistent with the previous studies. The study reveals that the observed impact of rubber aggregates on the high compressibility of the particles in the mixture induces local bonding stresses between the rubber and the cementitious matrix (Gupta et al, 2019).

Bin Kabit et al. (2021) concluded that a modified rubber mortar mixture has the potential to effectively reduce shrinkage in cement

mortars. Wei et al. (2021) found that tire rubber decreased the mortar's consistency, compressive strength, and flexural strength.

The decrease in Si-O-Si hybrid compounds, inhibited by the hydroxyl group during the hydrolyzation process, may be the cause of the poor bending strength observed in the mortar containing 6% rubber powder (Rattanaveeranon et al, 2019).

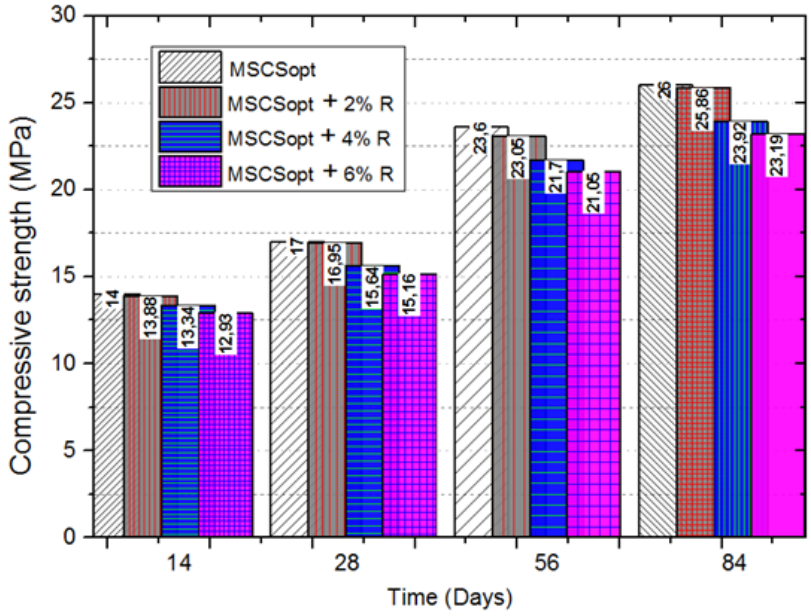

Figure 11 – Influence of scrap rubber addition rate on compressive strength

Conclusions

- Crushed sand and sediment particles are used as very effective fillers to mortar to ensure good performance, sufficient workability, and improved strength. The efficiency of particles depends on their morphology and genesis.
- The compressive strength and tensile strength of the resulting mortar depended on the fineness modulus of the aggregate and the plasticity index. In general, compressive strength was reduced with reduced fineness modulus of the aggregate and th eincreased sand plasticity index.
- Incorporating crushed sand particles in mortar enhances mechanical properties, successfully minimizing porosity through improved pore size distribution.

- Mortar modified with 65 wt% sediments and 35 wt% crushed sand particles demonstrated a significantly approximate resistance compared to the reference sand mortar.
- The bulk density of fresh mortar and the dry bulk density of hardened mortar for different mixes showed a significantly approximate match.
- Ultrasonic pulse velocity decreases with the increased quantity of crushed sand particles.
- Due to the high compressibility of used scrap rubber waste, the compression and recompression indices increase dramatically with the rubber content of used tire.
- Scrap rubber waste can be used as a reinforcing material in mortar mixes, but proportions should not be exceeded.

References

-AFNOR Association française de normalisation. 1991. *NF P94-054: Sols : reconnaissances et essais - Détermination de la masse volumique des particules solides des sols - Méthode du pycnomètre à eau* [online]. Available at: https://www.boutique.afnor.org/fr-fr/norme/nf-p94054/sols-reconnaissance-et-essais-determination-de-la-masse-volumique-des-parti/fa020767/11077 [Accessed: 29 March 2024].

-AFNOR Association française de normalisation. 1992. *NF P94-057: Sols : reconnaissance et essais - Analyse granulométrique des sols - Méthode par sédimentation* [online]. Available at: https://www.boutique.afnor.org/fr-fr/norme/nf-p94057/sols-reconnaissance-et-essais-analyse-granulometrique-des-sols-methode-par-/fa020768/11074 [Accessed: 29 March 2024].

-AFNOR Association française de normalisation. 1993. *NF P94-051: Sols : reconnaissance et essais - Détermination des limites d'Atterberg - Limite de liquidité à la coupelle - Limite de plasticité au rouleau* [online]. Available at: https://www.boutique.afnor.org/fr-fr/norme/nf-p94051/sols-reconnaissance-et-essais-determination-des-limites-datterberg-limite-d/fa020765/11080 [Accessed: 29 March 2024].

-AFNOR Association française de normalisation. 1990. *NF EN 196-1: Méthodes d'essais des ciments. Détermination des résistances mécaniques* [online]. Available at: https://www.boutique.afnor.org/fr-fr/norme/nf-en-1961/methodes-dessais-des-ciments-determination-des-resistances-mecaniques/fa020279/77168 [Accessed: 29 March 2024].

-AFNOR Association française de normalisation. 1996. *NF P94-056: Sols : reconnaissance et essais - Analyse granulométrique - Méthode par tamisage à sec après lavage* [online]. Available at: https://www.boutique.afnor.org/fr-fr/norme/nf-p94056/sols-reconnaissance-et-essais-analyse-granulometrique-methode-par-tamisage-/fa026936/11075 [Accessed: 29 March 2024].

-AFNOR Association française de normalisation. 1998a. *NF EN 1744-1: Essais pour déterminer les propriétés chimiques des granulats - Partie 1 : analyse chimique* [online]. Available at: https://www.boutique.afnor.org/fr-fr/norme/nf-en-17441/essais-pour-determiner-les-proprietes-chimiques-des-granulats-partie-1-anal/fa039721/62422 [Accessed: 29 March 2024].

-AFNOR Association française de normalisation. 1998b. *NF P94-068: Sols : reconnaissance et essais - Mesure de la capacité d'adsorption de bleu de méthylène d'un sol ou d'un matériau rocheux - Détermination de la valeur de bleu de méthylène d'un sol ou d'un matériau rocheux par l'essai à la tache* [online]. Available at: https://www.boutique.afnor.org/fr-fr/norme/nf-p94068/sols-reconnaissance-et-essais-mesure-de-la-capacite-dadsorption-de-bleu-de-/fa043689/394 [Accessed: 29 March 2024].

Akbulut, S., Arasan, S. & Kalkan E. 2007. Modification of clayey soils using scrap tire rubber and synthetic fibres. *Applied Clay Science*, 38(1-2), pp.23-32. Available at: https://doi.org/10.1016/j.clay.2007.02.001.

Amar, M., Benzerzour, M., Safhi, A.E.M. & Abriak, N.-E. 2018. Durability of a cementitious matrix based on treated sediments. *Case Studies in Construction Materials*, 8, pp.258-276. Available at: https://doi.org/10.1016/j.cscm.2018.01.007.

Aoual-Benslafa, F.K., Kerdal, D., Ameur, M., Mekerta, B. & Semcha, A. 2015. Durability of Mortars Made with Dredged Sediments. *Procedia Engineering*, 118, pp.240-250. Available at: https://doi.org/10.1016/j.proeng.2015.08.423.

Arnould, M. & Virlogeux, M. & 1986. *Granulats et bétons légers.* Champs-sur-Marne, France: Presses de l'école nationale des Ponts et Chaussées. ISBN: 978-2-85978-086-9.

Bédérina, M., Khenfer, M.M., Dheilly, R.M. & Quéneudec, M. 2005. Reuse of local sand: effect of limestone filler proportion on the rheological and mechanical properties of different sand concretes. *Cement and Concrete Research*, 35(6), pp.1172-1179. Available at: https://doi.org/10.1016/j.cemconres.2004.07.006.

Bederina, M., Makhloufi, Z., Bounoua, A., Bouziani, T. & Quéneudec, M. 2013. Effect of partial and total replacement of siliceous river sand with limestone crushed sand on the durability of mortars exposed to chemical solutions. *Construction and Building Materials*, 47, pp.146-158, Available at: https://doi.org/10.1016/j.conbuildmat.2013.05.037.

Bell, F.G. 1993. *Engineering Treatment of Soils*, *1st Edition*. London: CRC Press. Abailable at: https://doi.org/10.1201/9781482288971.

Benyamina, S., Menadi, B., Bernard, S. & Kenai S. 2019. Performance of self-compacting concrete with manufactured crushed sand. *Advances in concrete construction*, 7(2), pp.87-96, Available at: https://doi.org/10.12989/acc.2019.7.2.087.

Bin Kabit, M.R., Sarkawi, S.S.R., Mannan, M.D.A. & Adebayo, J.O. 2021. Effect of Silica Fume and Synthetic Fibre towards the Compressive Strength of Modified Crumb Rubber Cement Mortar. *Defect and Diffusion Forum*, 411, pp.135-142. Available at: https://doi.org/10.4028/www.scientific.net/DDF.411.135.

Cepuritisa, R., Jacobsena, S., Pedersenc, B. & Mørtsell, E. 2016. Crushed sand in concrete – Effect of particle shape in different fractions and filler properties on rheology. *Cement and Concrete Composites,* 74, pp.26-41. Available at: https://doi.org/10.1016/j.cemconcomp.2016.04.004.

Cetin, H., Fener, M. & Gunaydin, O. 2006. Geotechnical properties of tire-cohesive clayey soil mixtures as fill material. *Engineering Geology*, 88(1-2), pp.110-120. Available at: https://doi.org/10.1016/j.enggeo.2006.09.002.

Cherrak, M., Bali, A. & Silhadi, K. 2013. Concrete mix design containing calcareous tuffs as a partial sand substitution. *Construction and Building Materials*, 47, pp.318-323. Available at: https://doi.org/10.1016/j.conbuildmat.2013.05.051.

Chouhan, H.S., Kalla, P., Nagar, R., Gautam, P.K. & Arora, A.N. 2020. Investigating use of dimensional limestone slurry waste as fine aggregate in mortar. *Environment, Development and Sustainability,* 22, pp.2223-2245. Available at: https://doi.org/10.1007/s10668-018-0286-9.

Corinaldesi, V. 2012. Recycled-Aggregate Bedding Mortars for Repair of Historical Buildings. *Applied Mechanics and Materials*, 174-177, pp.1481-1488. Available at: https://doi.org/10.4028/www.scientific.net/AMM.174-177.1481.

D'Antino, T., Carozzi, F.G. & Poggi, C. 2019. Diagonal Compression of Masonry Walls Strengthened with Composite Reinforced Mortar. *Key Engineering Materials*, 817, pp.528-535. Available at: https://doi.org/10.4028/www.scientific.net/KEM.817.528.

Fonti, V., Dell'Anno, A. & Beolchini, F. 2013. Influence of biogeochemical interactions on metal bioleaching performance in contaminated marine sediment. *Water Research*, 47(14), pp.5139-5152, Available at: https://doi.org/10.1016/j.watres.2013.05.052.

Gupta, T., Siddique, S., Sharma, R.K. & Chaudhary, S. 2019. Behaviour of waste rubber powder and hybrid rubber concrete in aggressive environment. *Construction and Building Materials*, 217, pp.283-291. Available at: https://doi.org/10.1016/j.conbuildmat.2019.05.080.

Jiang, W., Zhu, H., Haruna, S.I., Shao, J., Yu, Y. & Wu, K. 2022. Mechanical properties and freeze–thaw resistance of polyurethane-based polymer mortar with crumb rubber powder. *Construction and Building Materials,* 352, art.number:129040. Available at: https://doi.org/10.1016/j.conbuildmat.2022.129040.

Khan, I.M., Kabir, S., Alhussain, M.A. & Almansoor, F.F. 2016. Asphalt Design Using Recycled Plastic and Crumb-rubber Waste for Sustainable Pavement Construction. *Procedia Engineering*,145, pp.1557-1564. Available at: https://doi.org/10.1016/j.proeng.2016.04.196.

Khorrami, M., Vafai, A., Khalilitabas, A.A., Desai, C.S. & Ardakani, M.H.M. 2010. Experimental Investigation on Mechanical Characteristics and Environmental Effects on Rubber Concrete. *International Journal of Concrete Structures and Materials*, 4(1), pp.17-23. Available at: https://doi.org/10.4334/IJCSM.2010.4.1.017.

Lam, N.N. 2020. A Study on Using Crushed Sand to Replace Natural Sand in High-Strength Self-compacting Concrete Towards Sustainable Development in Construction. In: *IOP Conference Series: Earth and Environmental Science; 6th International Conference on Environment and Renewable Energy*, Hanoi, Vietnam, 505, art.number:012003, February 24-26. Available at: https://doi.org/10.1088/1755-1315/505/1/012003.

Li, X. & Liu, J. 2021. One-dimensional compression feature and particle crushability behavior of dry calcareous sand considering fine-grained soil content and relative compaction. *Bulletin of Engineering Geology and the Environment*, 80, pp.4049-4065. Available at: https://doi.org/10.1007/s10064-021-02160-2.

Lu, L.L., Zhang, R. & Zhang, Y.B. 2022. Experimental Study of Cement Mortar on Compressive Strength and Wave Velocity Characteristics for Different Sand/Cement Ratio and Particle Sizes. *Key Engineering Materials,* 931, pp.199-204. Available at: https://doi.org/10.4028/p-dlhef1.

Ma, Z., Shen, J., Wang, C. & Wu, H. 2022. Characterization of sustainable mortar containing high-quality recycled manufactured sand crushed from recycled coarse aggregate. *Cement and Concrete Composites*, 132, art.number:104629. Available at: https://doi.org/10.1016/j.cemconcomp.2022.104629.

Nakhaei, A., Marandi, S.M., Sani Kermani, S. & Bagheripour, M.H. 2012. Dynamic properties of granular soils mixed with granulated rubber. *Soil Dynamics and Earthquake Engineering,* 43, pp.124-132. Available at: https://doi.org/10.1016/j.soildyn.2012.07.026.

-NBN Bureau of Normalization. 1999. *NBN EN 1015-10:1999: Méthodes d'essai des mortiers pour la maçonnerie - Partie 10: Détermination de la masse volumique apparente séche du mortier durci* [online]. Available at: https://app.nbn.be/data/r/platform/frontend/detail?p40_id=273242&p40_language_code=fr&p40_detail_id=101336&lang=fr [Accessed: 29 March 2024].

Okagbue, C.O. & Onyeobi, T.U.S. 1999. Potential of marble dust to stabilize red tropical soils for road construction. *Engineering Geology*, 53(3-4), pp.371-380. Available at: https://doi.org/10.1016/S0013-7952(99)00036-8.

Pavia, S. & Toomey, A.B. 2008. Influence of the aggregate quality on the physical properties of natural feebly-hydraulic lime mortars. *Materials and Structures*, 41, pp.559-569. Available at: https://doi.org/10.1617/s11527-007-9267-4.

Rattanaveeranon, S., Dumrongsil, S. & Jiamwattanapong, K. 2019. Effect of Latex Rubber and Rubber Powder as an Admixture on Bending Strength of Cement Mortar. *Applied Mechanics and Materials*, 891, pp.180-186. Available at: https://doi.org/10.4028/www.scientific.net/AMM.891.180.

Schmitz, R.M., Schreoder, C. & Charlier, R. 2004. Chemo-mechanical interactions in clay a correlation between clay mineralogy and Atterberg limits. *Applied Clay Science*, 26(1-4), pp.351-358. Available at: https://doi.org/10.1016/j.clay.2003.12.015.

Sellaf, H., Balegh, B. & Bkhiti, M. 2023. The Assessment and Treatment of Dredged Sediments and Limestone Tuff Using Waste Ceramic with Low-Cement.

Advanced Engineering Forum, 48, pp.45-58. Available at: https://doi.org/10.4028/p-2j4d93.

Singh, L.P., Goel, A., Bhattachharyya, S.K., Ahalawat, S., Sharma, U. & Mishra, G. 2015. Effect of Morphology and Dispersibility of Silica Nanoparticles on the Mechanical Behaviour of Cement Mortar. *International Journal of Concrete Structures and Materials,* 9(2), pp.207-217. Available at: https://doi.org/10.1007/s40069-015-0099-2.

Sivapullaiah, P.V., Sridharan, A. & Bhaskar Raju, K.V. 2000. Role of amount and type of clay in the lime stabilization of soils. *Proceedings of the Institution of Civil Engineers - Ground Improvement,* 4(1), pp.37-45. Available at: https://doi.org/10.1680/grim.2000.4.1.37.

Srivastava, A. & Singh, S.K. 2020. Utilization of alternative sand for preparation of sustainable mortar: A review. *Journal of Cleaner Production*, 253, art.number:119706, Available at: https://doi.org/10.1016/j.jclepro.2019.119706.

Su, P., Dai, Q., Li, M., Ma, Y. & Wang, J. 2022. Investigation of the mechanical and Shrinkage properties of plastic-rubber compound modified cement mortar with recycled tire steel fiber. *Construction and Building Materials,* 334, art.number:127391. Available at: https://doi.org/10.1016/j.conbuildmat.2022.127391.

Torres, M.L. & García-Ruiz, P.A. 2009. Lightweight pozzolanic materials used in mortars: Evaluation of their influence on density, mechanical strength and water absorption. *Cement and Concrete Composites*, 31(2), pp.114-119. Available at: https://doi.org/10.1016/j.cemconcomp.2008.11.003.

Trouzine, H., Bekhiti, M. & Asroun, A. 2012. No AccessEffects of scrap tyre rubber fibre on swelling behaviour of two clayey soils in Algeria. *Geosynthetics International*, 19(2), pp.124-132, Available at: https://doi.org/10.1680/gein.2012.19.2.124.

Wang, J.-J., Zhang, H.-P., Deng, D.-P. & Liu, M.-W. 2013. Effects of mudstone particle content on compaction behavior and particle crushing of a crushed sandstone–mudstone particle mixture. *Engineering Geology*, 167, pp.1-5. Available at: https://doi.org/10.1016/j.enggeo.2013.10.004.

Wei, C.B., Othman, R., Sheng, T.W., Jaya, R.P. & Al Bakri Abdullah, M.M. 2021. Properties of Mortar with Waste Tyre Rubber as Partial Sand Replacement. *Key Engineering Materials,* 879, pp.49-61. Available at: https://doi.org/10.4028/www.scientific.net/KEM.879.49.

Efectos de los desechos de caucho sobre el comportamiento mecánico de morteros de arena triturada y sedimentos

Adda Hadj Mostefa[a], *Benamar* Balegh[b], *Hamid* Sellaf[c], *Mohamed Elamine* Dahamni[d]

[a] Universidad de Relizane, Departamento de Ingeniería Civil y Obras Públicas, Laboratorio de Materiales Innovadores y Energías Renovables, Relizane, República Argelina Democrática y Popular

[b] Universidad de Ahmed Draia Adrar, Departamento de Ingeniería Civil,
Adrar, República Argelina Democrática y Popular +
Laboratorio de Ingeniería Civil y Medio Ambiente,
Sidi Bel Abbes, República Argelina Democrática y Popular

[c] Universidad de Saida, Departamento de Ingeniería Civil e Hidráulica,
Saida, República Argelina Democrática y Popular +
Laboratorio de Ingeniería Civil y Medio Ambiente,
Sidi Bel Abbes, República Argelina Democrática y Popular

[d] Universidad de Orán 1 - Ahmed Ben Bella,
Laboratorio de Ciencias de la Materia Condensada (LSMC),
Orán 1, República Argelina Democrática y Popular,
autor de correspondencia

CAMPO: materiales, ingeniería civil
TIPO DE ARTÍCULO: artículo científico original

Resumen:

Introducción/objetivo: El consumo de arena natural en Argelia es elevado debido a su uso extensivo en morteros, mientras que los sedimentos y los residuos de caucho plantean importantes desafíos ambientales y sociales. Este estudio investiga los efectos de la incorporación de residuos de caucho en morteros mezclados con arena triturada y sedimentos. El objetivo principal es valorizar las partículas de arena triturada mediante pruebas físicas y mecánicas, evaluando su potencial como alternativa a la arena natural en mezclas de morteros.

Métodos: Se realizó un trabajo experimental para estudiar el impacto de reemplazar parcial o totalmente los sedimentos con partículas de arena triturada en mezclas de mortero. Se prepararon mezclas de mortero utilizando diferentes proporciones de sedimento a arena triturada (10%, 25%, 35%, 50% y 100%) para observar su influencia en las propiedades físicas y mecánicas. Además, se analizaron los efectos de agregar 2%, 4% y 6% de caucho granulado al mortero óptimo. Se realizaron varias pruebas, incluidas las de resistencia a la compresión, resistencia a la flexión y velocidad del pulso ultrasónico, para evaluar el desempeño de las mezclas.

Resultados: Los resultados indicaron que la sustitución de sedimentos por arena triturada mejoró las propiedades de resistencia del mortero, en particular debido a una mejor compactación de las partículas. El mortero que contenía 65 % en peso de sedimentos y 35 % en peso de arena triturada mostró propiedades similares al mortero de referencia. La adición de desechos de caucho aumentó la compresibilidad, pero mejoró las propiedades mecánicas cuando se utilizó con moderación. La velocidad del pulso ultrasónico disminuyó con un mayor contenido de arena triturada y se redujo la porosidad de las mezclas.

Conclusión: La arena triturada y las partículas de sedimento son materiales de relleno eficaces para el mortero, garantizando un buen rendimiento y

una mayor resistencia. La eficiencia de estos materiales depende de su morfología y génesis. El estudio demuestra que la arena triturada puede ser una alternativa viable a la arena natural, y los residuos de caucho pueden utilizarse como material de refuerzo en el mortero, aunque sus proporciones deben controlarse cuidadosamente para evitar efectos negativos en las propiedades mecánicas.

Palabras claves: mortero, sedimento, arena triturada, desechos de caucho, resistencia a la compresión, resistencia a la tracción.

Влияние резиновой крошки на механические характеристики раствора, изготовленного из измельченного песка и отложений

Адда Хадж Мостефа[а], *Бенамар* Балег[б], *Хамид* Селлаф[в], *Мохаммед Эль-Амин* Дахамни[г]

[а] Университет в Релизане, факультет гражданского строительства и общественных работ, Лаборатория инновационных материалов и возобновляемых источников энергии, г. Релизан, Алжирская Народная Демократическая Республика

[б] Университет Ахмеда Дрейи в Адраре, факультет гражданского строительства, г. Адрар, Алжирская Народная Демократическая Республика + Лаборатория гражданского строительства и охраны окружающей среды, г. Сиди-Бель-Аббес, Алжирская Народная Демократическая Республика

[в] Университет Саиды, факультет гражданского строительства и гидротехники, г. Саида, Алжирская Народная Демократическая Республика + Лаборатория гражданского строительства и охраны окружающей среды, г. Сиди-Бель-Аббес, Алжирская Народная Демократическая Республика

[г] Университет Ахмеда Бен Беллы в Оране 1, Лаборатория конденсированных сред (LSMC), г. Оран 1, Алжирская Народная Демократическая Республика, **корреспондент**

РУБРИКА ГРНТИ: 81.09.00 Материаловедение
ВИД СТАТЬИ: оригинальная научная статья

Резюме:

Введение/цель: Природный песок в Алжире широко используется в строительных растворах, в то время как отложения и резиновые отходы создают серьезные экологические и социальные проблемы. В данном исследовании изучается влияние содержания резиновых отходов в строительных растворах, смешанных с измельченным песком и отложениями. Основная цель исследования заключалась в валоризации измельченных частиц песка путем физико-механических испытаний и оценка их потенциала для замены природного песка в строительных смесях.

Методы: В ходе исследования было экспериментально изучено влияние частичной и полной замены отложений измельченными частицами песка в растворных смесях. Раствор готовился в различном соотношении отложений и измельченного песка (10%, 25%, 35%, 50% и 100%) с целью изучения их влияния на физические и механические свойства. Также были проанализированы влияние добавок 2%, 4% и 6% резиновой крошки на оптимальный раствор. Для оценки характеристик смесей были проведены различные испытания, включая испытания на прочность, прочность на изгиб и испытания на скорость ультразвукового импульса.

Результаты: Результаты показали, что замена отложений измельченным песком улучшила прочностные свойства раствора, в частности, за счет лучшей утрамбовки частиц. Раствор, содержащий 65 мас.% отложений и 35 мас.% измельченного песка, показал свойства, аналогичные контрольному раствору. Добавление резиновой крошки повышает сжимаемость, но улучшает механические свойства при умеренном использовании. При увеличении содержания измельченного песка скорость ультразвукового импульса снижается, а пористость смесей уменьшается.

Вывод: Измельченный песок и частицы отложений являются эффективными связывающими элементами в строительных растворах. Они обеспечивают превосходные эксплуатационные характеристики и повышенную прочность. Эффективность этих материалов зависит от их морфологии и происхождения. Исследование показывает, что измельченный песок может быть жизнеспособной альтернативой природному песку, а резиновую крошку можно использовать в качестве армирующего материала в строительных растворах. Однако их пропорции следует тщательно контролировать во избежание негативного влияния на механические свойства.

Ключевые слова: строительный раствор, отложения, измельченный песок, резиновая крошка, прочность на сжатие, растяжение.

Утицај отпадног гуменог гранулата на механичке перформансе малтера од дробљеног песка и седимента

Ада Хаџ Мустифа[а], *Бенамар* Бали[б],
Хамид Селаф[в], *Мухамед Еламин* Дахамни[г]

[а] Универзитет у Релизану, Департман за грађевинарство и јавне радове, Лабораторија за иновативне материјале и обновљиве енергије, Релизане, Народна Демократска Република Алжир

[б] Универзитет „Ахмед Драиа” у Адрару, Одсек за грађевинарство, Адрар, Народна Демократска Република Алжир +
Лабораторија за грађевинарство и заштиту животне средине, Сиди Бел Абес, Народна Демократска Република Алжир

[в] Универзитет у Саиди, Одсек за грађевинарство и хидраулику, Саида, Народна Демократска Република Алжир +
Лабораторија за грађевинарство и заштиту животне средине, Сиди Бел Абес, Народна Демократска Република Алжир

[г] Универзитет „Ахмед Бен Бела” у Орану 1, Лабораторија за науку о кондензованој материји (ЛСМЦ), Оран 1, Народна Демократска Република Алжир,
аутор за преписку

ОБЛАСТ: материјали, грађевинарство
КАТЕГОРИЈА (ТИП) ЧЛАНКА: оригинални научни рад

Сажетак:

Увод/циљ: Потрошња природног песка у Алжиру је велика због његове широке употребе у малтерима, док седименти и гумени отпад представљају значајан еколошки и друштвени проблем. Ова студија истражује утицај коришћења гуменог отпада у малтерима помешаног са дробљеним песком и седиментима. Основни циљ био је да се изврши валоризација честица дробљеног песка путем физичког и механичког испитивања, као и да се процени њихов потенцијал да замене природни песак у мешавинама малтера.

Методе: Експерименталним путем проучаван је утицај делимичне и потпуне замене седимената честицама дробљеног песка у мешавинама малтера. Оне су припремљене у различитим односима седимента и дробљеног песка (10%, 25%, 35%, 50% и 100%) како би се испитао њихов утицај на физичка и механичка својства. Такође, анализирани су ефекти додавања 2%, 4% и 6% гуменог гранулата оптималном малтеру. Извршена су различита испитивања, укључујући тестирања чврстоће, чврстоће на савијање и брзине ултразвучног импулса ради процене перформанси мешавина.

Резултати: Показано је да замена седимента дробљеним песком побољшава својства чврстоће малтера, нарочито због бољег паковања честица. Малтер са 65 теж% седимента и 35 теж% дробљеног песка испољио је својства слична референтном малтеру. Додавање гуменог отпада повећало је стишљивост, али и побољшало механичка својства када се користио умерено. Брзина ултразвучног импулса опала је са већим садржајем дробљеног песка, а порозност мешавина се смањила.

Закључак: Честице дробљеног песка и седимената су ефекасна везива за малтер која обезбеђују добре перформансе и побољшавају чврстоћу. Ефикасност ових материјала зависи од њихове

морфологије и порекла. Студија показује да дробљени песак може да буде одржива алтернатива природном песку, а да се гумени отпад може користити као материјал за ојачавање малтера, мада треба пажљиво контролисати његов удео како би се избегао негативан утицај на механичка својства.

Кључне речи: малтер, седимент, дробљени песак, гумени гранулат, чврстоћа на притисак, чврстоћа на истезање.

Paper received on: 30.03.2024.
Manuscript corrections submitted on: 30.01.2025.
Paper accepted for publishing on: 31.01.2025.

Stability and neurotoxic impact of organophosphate pesticides in aqueous environments

Vladan J. Anićijević[a], *Tamara* Tasić[b], *Vedran* Milanković[c], *Radovan* M. Karkalić[d], *Tamara* D. Lazarević Pašti[e]

[a] University of Defence in Belgrade, Military Academy, Belgrade, Republic of Serbia, e-mail: anicijevicj.v@gmail.com, **corresponding author**, ORCID iD: https://orcid.org/0000-0001-8731-1378

[b] University of Belgrade, VINČA Institute of Nuclear Sciences - National Institute of the Republic of Serbia, Belgrade, Republic of Serbia, e-mail: tamara.tasic@vin.bg.ac.rs, ORCID iD: https://orcid.org/0000-0003-1988-4064

[c] University of Belgrade, VINČA Institute of Nuclear Sciences - National Institute of the Republic of Serbia, Belgrade, Republic of Serbia, e-mail: vedran.milankovic@vin.bg.ac.rs, ORCID iD: https://orcid.org/0000-0002-7706-9036

[d] University of Defence in Belgrade, Military Academy, Belgrade, Republic of Serbia, e-mail: rkarkalic@yahoo.com, ORCID iD: https://orcid.org/0000-0002-8074-7264

[e] University of Belgrade, VINČA Institute of Nuclear Sciences - National Institute of the Republic of Serbia, Belgrade, Republic of Serbia, e-mail: lazarevictlj@yahoo.com, ORCID iD: https://orcid.org/0000-0001-6220-2079

https://doi.org/10.5937/vojtehg73-53901

FIELD: environmental science, physical chemistry
ARTICLE TYPE: original scientific paper

ACKNOWLEDGMENT: Ministry for Science, Technological Development and Innovation of the Republic of Serbia (project name: A chemical-biological approach to the characterization of bioactive compounds-strategies for improving health and the environment, and Development of sustainable integrated processes for the isolation of diverse compounds using innovative solutions in accordance with the principles of green chemistry, project code: 451-03-66/2024-03/200017, and 451-03-65/2024-03/200146), and the Ministry of Defence of the Republic of Serbia (project name: Research on influence of characteristics of explosive ordnance on safety in Ministry of Defense and Army of Serbia, project code: VA-TT/1/22-24).

NOTE: A preliminary version of the article titled Dimethoate and omethoate hydrolysis in aqueous solutions and the assessment of their neurotoxic effects was presented as an oral presentation at the 10th OTEH 2022 Conference, Belgrade, Serbia.

Abstract:

Introduction/purpose: Organophosphates are widely used nowadays. They have applications as pesticides, drugs, plasticizers, flame retardants, or chemical warfare agents. Their acute toxicity is ascribed to inhibiting acetylcholinesterase (AChE), a key enzyme in the transmission of nerve impulses in animals. Their toxic effects manifest by acetylcholine accumulation in the nerve synapses and can lead to paralysis or death. Organo-thiophosphate pesticides (OPs) are used in large quantities. Their oxo-analogs can also be found in the environment due to oxidation. Once accumulated in the environment, they exhibit toxic effects on non-target organisms.

Methods: The hydrolysis of OPs in different pH was systematically analyzed, and their neurotoxic effects were evaluated. The concentration of the investigated pesticides during decomposition was monitored by ultra-performance liquid chromatography (UPLC). At the same time, a decrease in the toxicity of the treated samples was observed by measuring the activity of the enzyme AChE.

Results: OPs decompose rapidly in alkaline aqueous solutions but are highly stable in acidic solutions. Chlorpyrifos hydrolyzes the fastest and dimethoate the slowest. The toxicity of these OP solutions decreases over time, indicating that more toxic products were not formed.

Conclusion: The presented results can provide a sound basis for further efforts to find simple and efficient decomposition methods of OPs.

Keywords: organophosphate, pesticide, pH stability, toxicity.

Introduction

Water pollution is one of the biggest problems in modern society because it affects many different aspects; however, its most significant impact is on human health. Because of its vital importance, its quality must be within strictly defined limits. That is why it is necessary to continuously monitor the concentrations of toxic pollutants, including organophosphate pesticides (OPs), and reduce their presence as much as possible. Effective removal from water is also necessary to control the level of these compounds in food and the environment (Bootharaju & Pradeep, 2012; He et al, 2015; Rasmussen et al, 2015; Wang et al, 2013).

Extensive use of OPs leads to soil and water contamination (Peshin et al, 2020; Silva et al, 2019), OP residues in food (Baker et al, 2002), and public health impacts (Kunstadter et al, 2001; London et al, 2002). In addition to the inevitable acute and chronic impact on humans, overreliance on OPs for pest control has led to many problems for other

species (Greaves & Letcher, 2017). Severe contamination of aquatic ecosystems by OPs can lead to mass mortality of aquatic organisms. That is why it is necessary to purify wastewater containing OPs before mixing it with other waters.

Depending on the persistence of particular OPs, they remain in the environment for a long time or are transformed into a more toxic form. Due to the high solubility of organophosphates (OPs) in water and their low persistence in soil, they have a strong potential to run off into surface water and leach into groundwater (Van Scoy et al, 2016). The most important degradation pathways of OPs in the environment are microbial degradation, hydrolysis, oxidation and photolysis (Van Scoy et al, 2016; Aćimović & Vasić Anićijević, 2022). These processes often produce oxo-forms as end products through photocatalytic oxidation and microbial metabolism, which is problematic due to the extreme toxicity of these compounds. On the other hand, hydrolytic degradation is the main inactivating route of OPs in the environment and usually does not yield oxo-forms as end products. The hydrolysis of OPs mainly depends on pH and temperature (Anićijević et al, 2022).

Dimethoate (DMT), malathion (MLT), and chlorpyrifos (CPF) are well-known contact and systemic OPs that have been in use for years. They are used against many insects in agriculture (Anićijević & Lazarević-Pašti, 2020). The acute toxicity of OPs is primarily due to their inhibition of acetylcholinesterase (AChE), an enzyme critical for proper nerve function (Anićijević & Karkalić, 2022). The oxidation of organo-thiophosphates results in the formation of oxo-analogs, which are even more toxic to AChE than the parent compounds. These oxo-analogs can also form in the environment due to various oxidizing agents in water and soil (Lazarević-Pašti et al, 2016; Vasić Anićijević, 2020).

This work aims to investigate the half-life of OP hydrolysis in aquatic environments across a pH range of 3.00 to 9.00 and to track the toxicity of OP solutions over time. Understanding these factors is essential for developing effective strategies to remove OPs from water. Toxicity is assessed by measuring AChE inhibition through an enzyme assay, as AChE inhibition is widely used as a biomarker in environmental monitoring (Grue et al, 1991; Legradi et al, 2018), indicating the eco-neurotoxicity of cholinesterase-inhibiting compounds.

Materials and methods

Stability of organophosphate in the aqueous buffer solution

The stability of OPs in media with different pH values was investigated in a phosphate buffer solution with a concentration of 50 mmol dm^{-3} (made with deionized water) with a pH value ranging from 3.00 to 9.00, in according with the pH range supported by the UPLC system. The 1×10^{-4} mol dm^{-3} OP solutions were incubated at 25 °C in an orbital shaker-incubator (Orbital Shaker-Incubator ES-20, Grant-bio) for 10 days. Aliquots were taken at relevant time points to measure the concentrations of the OPs, as described in the following section. Additionally, the decomposition of OPs at the same concentration was analyzed in tap water samples to simulate real-world conditions. All measurements were performed in triplicate, and uncertainties were calculated using the least significant differences (LSDs) test at a 95% significance level.

Ultra performance liquid chromatography analysis

A Waters ACQUITY Ultra Performance Liquid Chromatography (UPLC) system was used to measure the concentration of DMT, MLT, and CPF, together with an adjustable UV photodiode array (PDA) detector controlled by the Empower software. Chromatographic separations were on 1.7 μm, 100 mm × 2.1 mm ACQUITY UPLC™ BEH C_{18} column (Waters).

The solutions of OP concentrations of 1×10^{-5} mol dm^{-3} were analyzed under isocratic conditions with a mobile phase consisting of 10% acetonitrile and 90% water (v/v). The eluent flow rate was 0.25 cm^3 min^{-1}, and the injection volume was 5 mm^3. Under the described conditions, the retention times of DMT, MLT, and CPF were (2.37 ± 0.05) min, (2.48 ± 0.05) min, and (2.62 ± 0.05) min, respectively. The spectra for DMT, MLT, and CPF are shown in Figures 1 (c), 2 (c), and 3 (c) as well as their absorption maxima. Optical detection was performed at 205 and 200 nm for aliphatic MLT and DMT, respectively. For aromatic CPF, 230 nm was chosen from three characteristic absorption maxima at 200, 230, and 290 nm. The spectra for DMT, MLT, and CPF are shown in Figures 1 (c), 2 (c), and 3 (c).

The concentrations of OPs were determined using linear calibration curves which were constructed from standard pesticide solutions across a broad concentration range.

Neurotoxic measurements

AChE inhibition measurements were performed to track and quantify changes in the toxicity of OPs and to investigate whether hydrolysis under different pH conditions leads to the formation of more toxic compounds. These transformation products could have harmful effects at concentrations below the detection limits of Ultra Performance Liquid Chromatography (UPLC). AChE activity was measured using a modified version of Ellman's procedure (Ellman et al, 1961). The in vitro experiments were performed by the exposure of 0.5 IU commercially purified AChE from electric eel to the OP solutions obtained in adsorption experiments at 37 °C in 50 mmol dm^{-3} phosphate buffer (PB) pH 8.00 (final volume 0.650 cm^3). The enzymatic reaction was initiated by adding acetyltiocholine-iodide (ASChI) and 5.5'-dithiobis-2-nitrobenzoic acid (DTNB) as a chromogenic reagent. The reaction was allowed for 8 minutes before being stopped with 10% sodium dodecyl sulfate (SDS). The reaction product, thiocholine, reacts with DTNB to form 5-thio-2-nitrobenzoate, measured by its optical absorbance at 412 nm. It should be noted that in these measurements, the enzyme concentration was constant and set to give an optimal spectrophotometric signal.

The following reaction shows the principle of determining AChE activity using the Ellman test:

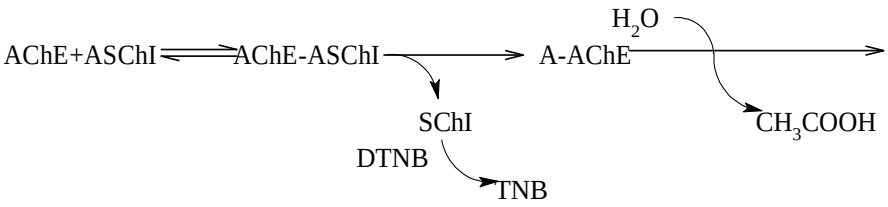

The physiological effects were quantified as AChE inhibition given as:

$$I\% = \frac{A_0 - A}{A_0} \times 100 \qquad (1)$$

where A_0 represents the AChE activity in the absence of OP, A is the AChE activity measured after exposure to a given OP. OP solutions with an initial concentration of 1×10^{-4} mol dm^{-3} were incubated in phosphate buffers (pH 3.00 to 9.00, 25 °C) and in tap water for 10 days to monitor the toxicity of the hydrolysis products formed spontaneously.

Results

Kinetics studies of organophosphate decomposition

The concentration of OPs was monitored in tap water and phosphate buffers with pH ranging from 3.00 to 9.00 for 10 days using UPLC analysis. Figures 1, 2, and 3 show the time dependence of the OP concentration. The spontaneous decay of DMT (Figure 1), MLT (Figure 2), and CPF (Figure 3) concentrations over time was relatively fast in neutral and alkaline buffers, as well as in tap water (pH 6.50). A decrease in OP concentrations was also observed in buffers with acidic pH, though it was slower. The decay followed exponential trends in all cases, consistent with pseudo-first-order kinetics. This outcome was expected, as the buffer solutions maintain constant H^+/OH^- concentrations over time, in alignment with previous literature (Wolfe et al, 1977). Consequently, the hydrolysis rate constants (k_h) were obtained by fitting the experimental data to the following equation:

$$C_t = C_0 e^{-k_h t} \quad (2)$$

where C_t and C_0 are the remaining OP concentrations at a given time (t) and the initial OP concentration.

Dimethoate

The dependence of the degradation of DMT (Richendrfer & Creton, 2015, Elmorsy et al, 2022, Sparling & Fellers, 2007) with an initial concentration of 1×10^{-4} mol dm^{-3} on the pH value of the solution at 25 ºC and 35 ºC is shown in Figure 1 (a) and (b). The results show that an increase in the pH value increases degradation efficiency. The half-life of DMT at pH 9.00 and 25 °C is 8 days, and at 35 °C, it is 2 days.

The results also show that an increase in temperature of 10 °C accelerates the degradation about tenfold at pH 9.00. The less efficient degradation at pH 8.00 and 35 °C resulted in a half-life of 9 days. It practically means that a decrease in pH by 1 unit increases the length of degradation 4.5 times. This applies to the pH reduction from 9.00 to 8.00. For other changes, the pH degradation is several times longer.

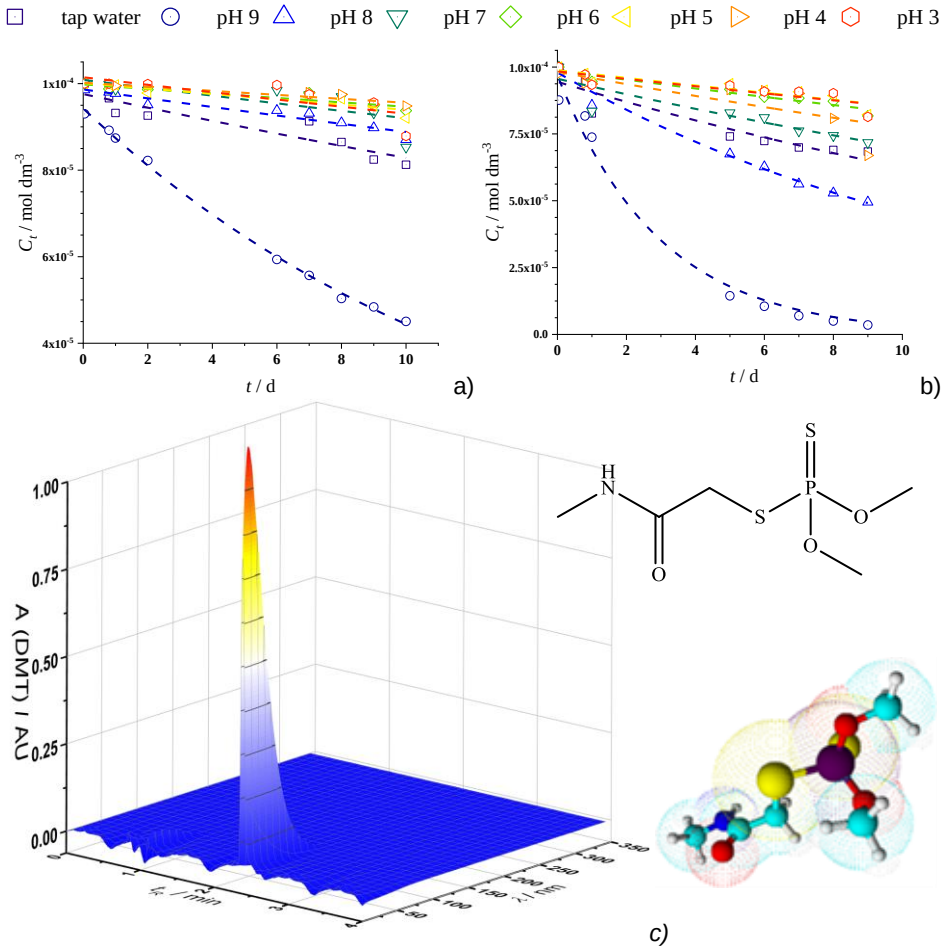

Figure 1 – Dependence of DMT degradation at pH from 3.00 to 9.00 and in tap water (pH 6.5) at 25 °C (a), 35 °C (b), and PDA spectra of concentration 1×10^{-4} mol dm^{-3} (c)

Malathion

The dependence of the degradation of MLT (Richendrfer & Creton, 2015, Elmorsy et al, 2022, Sparling & Fellers, 2007) with an initial concentration of 1×10^{-4} mol dm^{-3} on the pH value of the solution at 25 ºC and 35 ºC is shown in Figure 2 (a) and (b).

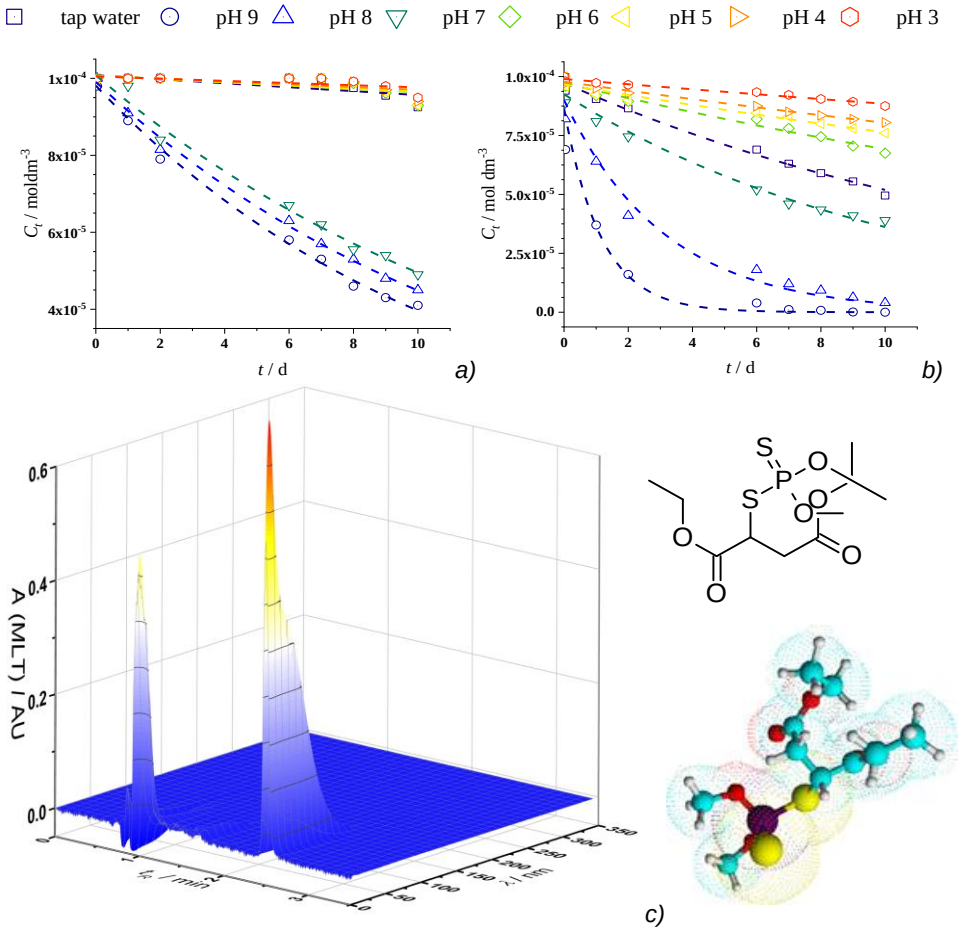

Figure 2 – Dependence of MLT degradation at pH from 3.00 to 9.00 and in tap water (pH 6.5) at 25 °C (a) and 35 °C (b), *and PDA spectra of concentration 1×10^{-4} mol dm^{-3} (c)*

As for DMT, the results show that an increase in the pH value leads to an increase in degradation efficiency. The half-life of MLT at a concentration of 1×10^{-4} mol dm^{-3} at pH 9.00 at 25 °C is 7.5 days, and at 35 °C it is 1 day, while it completely decomposes in 10 days at 35 °C. The presented results also show that an increase in temperature of 10 °C accelerates the degradation of MLT several times under the given experimental conditions (pH 9.00). This means that a decrease in pH by 1 increases the length of degradation by 2 times. As in the case of DMT, this applies to the reduction of pH from 9.00 to 8.00; for other changes in pH, the degradation is several times longer.

Chlorpyrifos

The dependence of the degradation of CPF (Ubaid ur Rahman et al, 2021) with an initial concentration of 1×10^{-4} mol dm^{-3} on the pH value of the solution at 25 ºC and 35 ºC is shown in Figure 3 (a) and (b).

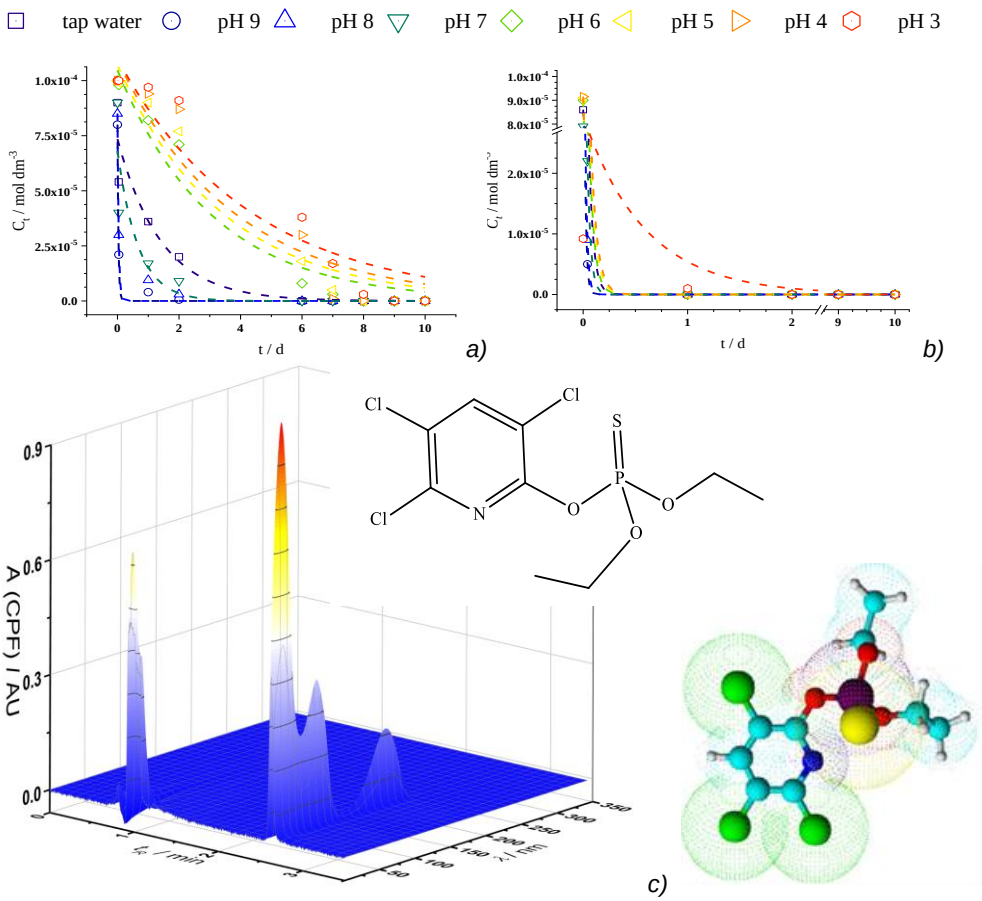

Figure 3 – Dependence of CPF degradation at pH from 3.00 to 9.00 and in tap water (pH 6.5) at 25 °C (a) and 35 °C (b), *and PDA spectra of concentration 1×10^{-4} mol dm^{-3} (c)*

As in the previous cases, the results show that, with an increase in the pH value, the degradation efficiency increases. The half-life of CPF at a concentration of 1×10^{-4} mol dm^{-3} at pH 9.00 and 25 °C is 29 min, while at 35 °C, the value is only 4 min. The degradation of aromatic CPF at pH 9.00 is much faster than in the case of both tested aliphatic OPs. At 25 °C, the

time required for a complete degradation of CPF is significantly shorter than 1 d (measured in minutes) for all pH values higher than 6.00 and in tap water.

On the other hand, at 35 °C, complete degradation is very fast for all tested pH values and almost immediate for the basic ones. The presented results also show that an increase in temperature of 10 °C accelerates the degradation of CPF by 7.5 times at pH 9.00, 8.00, and 7.00. At pH values lower than 7.00, the degradation of CPF is slowed down from 1 000 to 2 000 times when the temperature increases by 10 °C.

Toxicity assessment of organophosphate solutions

OP solutions of the initial concentration of 1×10^{-4} mol dm^{-3} were left in phosphate buffers (pH ranging from 3.00 to 9.00, 25 °C) and in tap water for 10 days to monitor the toxicity of the spontaneous hydrolysis products. The toxicity of the OP solution was evaluated using the AChE inhibition assay, as already described above. Aliquots for AChE inhibition assays were taken at the beginning of the experiment and then after 1, 2, 6, and 10 days.

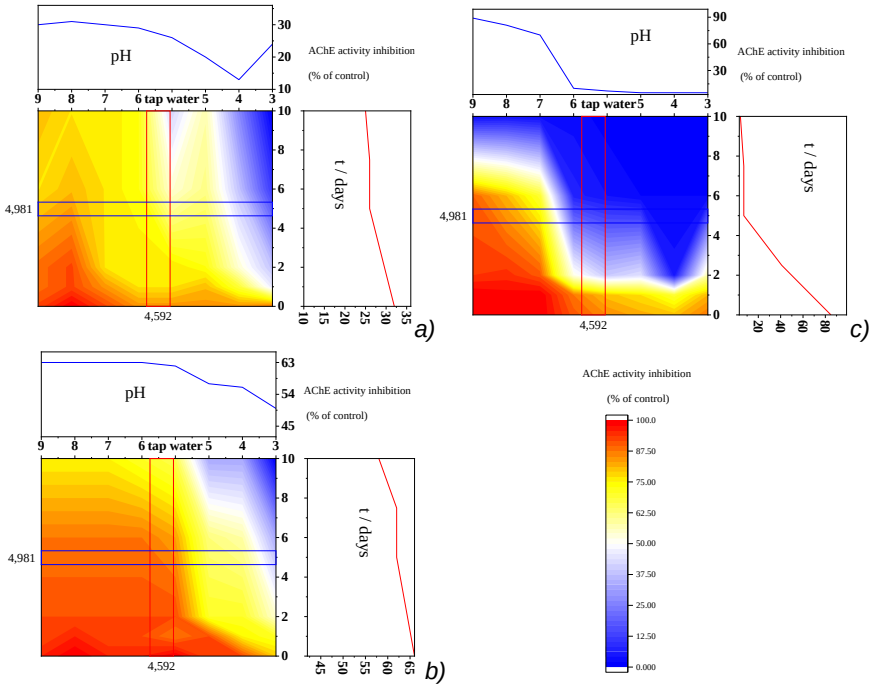

Figure 4 – Toxicity of the solutions of DMT (a), MLT (b), and CPF (c) measured during 10 days at pH from 3.00 to 9.00 for the initial concentration of Ops 1×10^{-4} mol dm^{-3}

In addition to measuring AChE activity inhibition over 10 days, we also tracked changes in inhibition using the measured concentrations of DMT, MLT, and CPF over time (C_t) and the OP inhibition curves. The results in Figure 4 show a rapid decrease in the acute toxicity of water contaminated with OPs at pH levels above 7.00.

Discussion

A fundamental understanding of the OP hydrolysis mechanisms is paramount for properly planning OP disposal and removal (Tomasi et al, 2005; Anićijević et al, 2022). For example, understanding OP hydrolysis could help optimize chemical treatments of contaminated samples to maximize OP decomposition into non-toxic products without the need for aggressive chemicals or excessive use of alkalis. The results in Figures 1, 2, and 3 show that the estimated half-lives of OPs in aqueous solution decrease with increasing pH, though the relationship is not strictly linear. Additionally, the stability of these molecules shows varied pH dependence. Further research is needed to fully resolve the link between the OP structure and stability at different pH levels in aqueous media.

Importantly, matrix effects in spiked tap water appear to have only a minor impact on the rate of hydrolysis (Figure 4). Therefore, these results can be reliably used to estimate OP half-lives in aqueous media based primarily on pH values. However, other factors, such as microbial activity or oxygen saturation levels, could also affect OP decomposition. (Lockridge et al, 2019).

Finally, the data presented in Figure 4 suggest that the inhibition of AChE activity decreased monotonically over time in all samples tested. Therefore, by combining the results of the pH stability of OPs with their AChE inhibition curve, the inhibition of AChE activity in the contaminated water samples can be reliably predicted for up to 10 days (Figure 4).

Conclusion

The investigated OPs have varying half-lives, and since their half-lives decrease rapidly with increasing pH in alkaline media, this suggests that alkaline hydrolysis is an effective method for removing DMT, MLT, and CPF from water. Unlike microbial degradation or photocatalytic oxidation, alkaline hydrolysis does not result in the accumulation of more toxic byproducts during the degradation process. Therefore, if alkaline hydrolysis removes OPs, no particular care should be taken to monitor the degradation process because the risk of toxic product formation is

negligible. Matrix effects in tap water were found to have a negligible impact on the rate of OP hydrolysis, making the presented data reliable for estimating OP half-lives in contaminated water. Additionally, toxicity data, measured as AChE inhibition, can be used to assess acute toxicity following water contamination. Estimates for periods longer than ten days can be derived by combining stability data with AChE inhibition curves for OPs. However, these results should be interpreted cautiously, and further systematic studies are recommended to evaluate the hydrolytic stability of OPs fully.

References

Aćimović, D.D. & Vasić Anićijević, D.D. 2022. Electrooxidative Removal of Organophosphates - A Combined Experimental and Theoretical Approach. In: *Organophosphates: Detection, Exposure and Occurrence. Volume 1: Impact on Health and the Natural Environment,* pp.215-250 [online]. Available at: https://vinar.vin.bg.ac.rs/handle/123456789/10726?locale-attribute=en [Accessed: 03 October 2024]. ISBN: 1-68507-724-2.

Anićijević, V.J. & Karkalić, R.M. 2022. Organophosphates as Chemical Warfare Agents. *In:* Lazarević-Pašti, T. (Ed.) *Organophosphates: Detection, Exposure and Occurrence. Volume 2: Acute Exposure and Treatments.* Hauppauge, NY: Nova Science Publishers, Inc. ISBN: 978-1-68507-734-1.

Anićijević, V.J. & Lazarević-Pašti, T.D. 2020. Chapter 1. Organophosphates: Application, Effects on Human Health and Removal. *In:* Marquis, F. (Ed.) *Organophosphate Pesticides.* Hauppauge, NY: Nova Science Publishers, Inc. ISBN: 978-1-53618-307-8.

Anićijević, V.J., Petković, M., Pašti, I.A. & Lazarević-Pašti, T.D. 2022. Decomposition of Dimethoate and Omethoate in Aqueous Solutions — Half-Life, Eco-Neurotoxicity Benchmarking, and Mechanism of Hydrolysis. *Water, Air, & Soil Pollution,* 233**,** art.number:390. Available at: https://doi.org/10.1007/s11270-022-05861-w.

Baker, B.P., Benbrook, C.M., Groth III, E. & Lutz Benbrook, K. 2002. Pesticide residues in conventional, integrated pest management (IPM)-grown and organic foods: insights from three US data sets. *Food Additives & Contaminants*, 19(5)**,** pp.427-446. Available at: https://doi.org/10.1080/02652030110113799.

Bootharaju, M.S. & Pradeep, T. 2012. Understanding the Degradation Pathway of the Pesticide, Chlorpyrifos by Noble Metal Nanoparticles. *Langmuir,* 28(5)**,** pp.2671-2679. Available at: https://doi.org/10.1021/la2050515.

Ellman, G.L., Courtney, K.D., Andres, V., Jr. & Featherstone, R.M. 1961. A new and rapid colorimetric determination of acetylcholinesterase activity. *Biochemical Pharmacology,* 7(2)**,** pp.88-95. Available at: https://doi.org/10.1016/0006-2952(61)90145-9.

Elmorsy, E., Al-Ghafari, A., Al Doghaither, H., Salama, M. & Carter, W.G. 2022. An Investigation of the Neurotoxic Effects of Malathion, Chlorpyrifos, and Paraquat to Different Brain Regions. *Brain Sciences,* 12(8)**,** art.number:975. Available at: https://doi.org/10.3390/brainsci12080975.

Greaves, A.K. & Letcher, R.J. 2017. A Review of Organophosphate Esters in the Environment from Biological Effects to Distribution and Fate. *Bulletin of Environmental Contamination and Toxicology,* 98**,** pp.2-7. Available at: https://doi.org/10.1007/s00128-016-1898-0.

Grue, C.E., Hart, A.D.M. & Mineau, P. 1991. Biological consequences of depressed brain cholinesterase activity in wildlife. In: Mineau, P. (Ed.) *Cholinesterase-inhibiting insecticides. Their impact on wildlife and the environment.*, pp.151-209. Elsevier Science Publishers B.V. ISBN: 0-444-88707-5.

He, J., Song, L., Chen, S., Li, Y., Wei, H., Zhao, D., Gu, K. & Zhang, S. 2015. Novel restricted access materials combined to molecularly imprinted polymers for selective solid-phase extraction of organophosphorus pesticides from honey. *Food Chemistry,* 187**,** pp.331-7. Available at: https://doi.org/10.1016/j.foodchem.2015.04.069.

Kunstadter, P., Prapamontol, T., Sirirojn, B.-O., Sontirat, A., Tansuhaj, A. & Khamboonruang, C. 2001. Pesticide Exposures among Hmong Farmers in Thailand. *International Journal of Occupational and Environmental Health,* 7(4)**,** pp.313-325. Available at: https://doi.org/10.1179/107735201800339227

Lazarević-Pašti, T.D., Pašti, I.A., Jokić, B., Babić, B.M. & Vasić, V.M. 2016. Heteroatom-doped mesoporous carbons as efficient adsorbents for removal of dimethoate and omethoate from water. *RSC Advances,* 6**,** pp.62128-62139. Available at: https://doi.org/10.1039/C6RA06736K.

Legradi, J.B., Di Paolo, C., Kraak, M.H.S., van Der Geest, H.G., Schymanski, E.L., Williams, A.J., Dingemans, M.M.L., Massei, R., Brack, W., Cousin, X., Begout, M.-L., van der Oost, R., Carion, A., Suarez-Ulloa, V., Silvestre, F., Escher, B. I., Engwall, M., Nilén, G., Keiter, S.H., Pollet, D., Waldmann, P., Kienle, C., Werner, I., Haigis, A.-C., Knapen, D., Vergauwen, L., Spehr, M., Schulz, W., Busch, W., Leuthold, D., Scholz, S., vom Berg, C.M., Basu, N., Murphy, C.A., Lampert, A., Kuckelkorn, J., Grummt, T. & Hollert, H. 2018. An ecotoxicological view on neurotoxicity assessment. *Environmental Sciences Europe,* 30**,** art.number:46. Available at: https://doi.org/10.1186/s12302-018-0173-x.

Lockridge, O., Verdier, L. & Schopfer, L.M. 2019. Half-life of chlorpyrifos oxon and other organophosphorus esters in aqueous solution. *Chemico-Biological Interactions,* 311**,** art.number:108788. Available at: https://doi.org/10.1016/j.cbi.2019.108788.

London, L., De Grosbois, S., Wesseling, C., Kisting, S., Rother, H.A. & Mergler, D. 2002. Pesticide Usage and Health Consequences for Women in Developing Countries: Out of Sight Out of Mind? *International Journal of Occupational and Environmental Health,* 8(1)**,** pp.46-59. Available at: https://doi.org/10.1179/oeh.2002.8.1.46.

Peshin, R., Hansra, B.S., Nanda, R., Singh, K., Sharma, R., Garg, L., Bajiya, M.R., Showkat, A., Kumar, R. & Yangsdon, S. 2020. Pesticides Hazardous Hotspots: Empirical Evidences from North India. *Environmental Management,* 66**,** pp.899-915. Available at: https://doi.org/10.1007/s00267-020-01317-1.

Rasmussen, J.J., Wiberg-Larsen, P., Baattrup-Pedersen, A., Cedergreen, N., Mcknight, U.S., Kreuger, J., Jacobsen, D., Kristensen, E.A. & Friberg, N. 2015. The legacy of pesticide pollution: An overlooked factor in current risk assessments of freshwater systems. *Water Research,* 84**,** pp.25-32. Available at: https://doi.org/10.1016/j.watres.2015.07.021.

Richendrfer, H. & Creton, R. 2015. Chlorpyrifos and malathion have opposite effects on behaviors and brain size that are not correlated to changes in AChE activity. *Neurotoxicology,* 49**,** pp.50-58. Available at: https://doi.org/10.1016/j.neuro.2015.05.002.

Silva, V., Mol, H.G.J., Zomer, P., Tienstra, M., Ritsema, C.J. & Geissen, V. 2019. Pesticide residues in European agricultural soils–A hidden reality unfolded. *Science of The Total Environment,* 653**,** pp.1532-1545. Available at: https://doi.org/10.1016/j.scitotenv.2018.10.441.

Sparling, D.W. & Fellers, G. 2007. Comparative toxicity of chlorpyrifos, diazinon, malathion and their oxon derivatives to larval Rana boylii. *Environmental Pollution,* 147(3)**,** pp.535-539. Available at: https://doi.org/10.1016/j.envpol.2006.10.036.

Ubaid Ur Rahman, H., Asghar, W., Nazir, W., Sandhu, M. A., Ahmed, A. & Khalid, N. 2021. A comprehensive review on chlorpyrifos toxicity with special reference to endocrine disruption: Evidence of mechanisms, exposures and mitigation strategies. *Science of The Total Environment,* 755(2)**,** art.number:142649. Available at: https://doi.org/10.1016/j.scitotenv.2020.142649.

Van Scoy, A., Pennell, A. & Zhang, X. 2016. Environmental Fate and Toxicology of Dimethoate. In: de Voogt, W. (Ed.) *Reviews of Environmental Contamination and Toxicology Volume 237,* pp.53-70. Cham: Springer. Available at: https://doi.org/10.1007/978-3-319-23573-8_3.

Vasić Anićijević, D.D. 2020. Chapter 3. Computational modelling of organophosphorous pesticides–density functional theory calculations. *In:* Marquis, F. (Ed.) *Organophosphate Pesticides.* Hauppauge, NY: Nova Science Publishers, Inc. ISBN: 978-1-53618-307-8.

Wang, X., Xing, H., Jiang, Y., Wu, H., Sun, G., Xu, Q. & Xu, S. 2013. Accumulation, histopathological effects and response of biochemical markers in the spleens and head kidneys of common carp exposed to atrazine and chlorpyrifos. *Food and Chemical Toxicology,* 62**,** pp.148-58. Available at: https://doi.org/10.1016/j.fct.2013.08.044.

Wolfe, N.L., Zepp, R.G., Gordon, J.A., Baughman, G.L. & Cline, D.M. 1977. Kinetics of chemical degradation of malathion in water. *Environmental Science & Technology,* 11(1)**,** pp.88-93. Available at: https://doi.org/10.1021/es60124a001.

Estabilidad e impacto neurotóxico de pesticidas organofosforados en ambientes acuosos

Vladan J. Anićijević[a], **autor de correspondencia**, *Tamara* Tasić[b], *Vedran* Milanković[b], *Radovan* M. Karkalić[a], *Tamara* D. Lazarević Pašti[b]

[a] Universidad de Defensa de Belgrado, Academia Militar, Belgrado, República de Serbia

[b] Universidad de Belgrado, Instituto de Ciencias Nucleares VINČA - Instituto Nacional de la República de Serbia, Belgrado, República de Serbia

CAMPO: ciencias ambientales, química física
TIPO DE ARTÍCULO: artículo científico original

Resumen:

Introducción/objetivo: Los organofosforados se utilizan ampliamente en la actualidad. Tienen aplicaciones como pesticidas, fármacos, plastificantes, retardantes de llama o agentes de guerra química. Su toxicidad aguda se atribuye a la inhibición de la acetilcolinesterasa (AChE), una enzima clave en la transmisión de impulsos nerviosos en animales. Sus efectos tóxicos se manifiestan por la acumulación de acetilcolina en las sinapsis nerviosas y pueden provocar parálisis o muerte. Los pesticidas organotiofosforados (OP) se utilizan en grandes cantidades. Sus oxoanálogos también se pueden encontrar en el medio ambiente debido a la oxidación. Una vez acumulados en el medio ambiente, presentan efectos tóxicos en organismos no objetivo.

Métodos: Se analizó sistemáticamente la hidrólisis de los OP a diferentes pH y se evaluaron sus efectos neurotóxicos. La concentración de los pesticidas investigados durante la descomposición se controló mediante cromatografía líquida de ultra alta resolución (UPLC). Al mismo tiempo, se observó una disminución de la toxicidad de las muestras tratadas midiendo la actividad de la enzima AChE.

Resultados: Los OP se descomponen rápidamente en soluciones alcalinas acuosas, pero son muy estables en soluciones ácidas. El clorpirifos se hidroliza más rápido y el dimetoato, más lentamente. La toxicidad de estas soluciones de OP disminuye con el tiempo, lo que indica que no se formaron productos más tóxicos.

Conclusión: . Los resultados presentados pueden proporcionar una base sólida para futuros esfuerzos encaminados a encontrar métodos de descomposición de OP simples y eficientes.

Palabras claves: organofosforado, pesticida, estabilidad del pH, toxicidad.

Стабильность и нейротоксическое действие фосфорорганических пестицидов в водной среде

Владан Й. Аничиевич[а], **корреспондент**, *Тамара* Тасич[б], *Ведран* Миланкович[б], *Радован* М. Каркалич[а], *Тамара* Д. Лазаревич-Пашти[б]

[а] Университет обороны в г. Белград, Военная академия, г. Белград, Республика Сербия

[б] Белградский университет, Институт ядерных наук «Винча» – Институт национального значения для Республики Сербия, г. Белград, Республика Сербия

РУБРИКА ГРНТИ: 87.15.00: Загрязнение окружающей среды. Контроль загрязнения

ВИД СТАТЬИ: оригинальная научная статья

Резюме:

Введение/цель: Органофосфаты широко используются в современном мире. Они используются в качестве пестицидов, лекарств, пластификаторов, антипиренов или боевых отравляющих веществ. Их острая токсичность объясняется ингибированием ацетилхолинэстеразы (АХЭ), ключевого фермента передачи нервных импульсов у животных. Их токсическое действие проявляется накоплением ацетилхолина в нервных синапсах и может привести к параличу или смерти. Тиофосфаторганические (ОФ) пестициды используются в больших количествах. Их оксоаналоги могут попасть в окружающую среду вследствие окисления. Накапливаясь в окружающей среде, они оказывают токсическое воздействие на нецелевые организмы.

Методы: В ходе исследования систематически проводились анализ гидролиза пестицидов ОФ в различных условиях pH и оценка их нейротоксического воздействия. Концентрацию исследуемых пестицидов ОФ в процессе разложения контролировались методом сверхэффективной жидкостной хроматографии (СЭЖХ). Одновременно при измерении активности фермента АХЭ наблюдалось снижение токсичности обработанных образцов.

Результаты: Пестициды ОФ быстро разлагаются в щелочных водных растворах, но они чрезвычайно стабильны в кислых растворах. Хлорпирифос гидролизуется быстрее, а диметоат − медленнее. Токсичность этих растворов со временем снижается, что указывает на то, что более токсичные продукты не образуются.

Выводы: Помимо того, представленные результаты могут стать хорошей основой в дальнейшем поиске простых и эффективных методов разложения ОФ пестицидов.

Ключевые слова: органофосфат, пестицид, ph стабильность, токсичность.

Стабилност и неуротоксични утицај органофосфатних пестицида у воденим срединама

Владан Ј. Анићијевић[а], **аутор за преписку,** *Тамара* Тасић[б], *Ведран* Миланковић[б], *Радован* М. Каркалић[а], *Тамара* Д. Лазаревић Пашти[б]

[а] Универзитет одбране у Београду, Војна академија, Београд, Република Србија

[б] Универзитет у Београду, Институт за нуклеарне науке „Винча" - Институт од националног значаја за Републику Србију, Београд, Република Србија

ОБЛАСТ: наука о животној средини, физичка хемија
КАТЕГОРИЈА (ТИП) ЧЛАНКА: оригинални научни рад

Сажетак:

Увод/циљ: Органофосфати данас имају широку примену. Користе се као пестициди, лекови, пластификатори, успоривачи пламена или хемијски бојни агенси. Њихова акутна токсичност се приписује инхибицији ацетилхолинестеразе (AChE), кључног ензима у преносу нервних импулса код животиња. Токсични ефекти се манифестују акумулацијом ацетилхолина у нервним синапсама и могу довести до парализе или смрти. Органотиофосфатни (ОФ) пестициди се користе у великим количинама. Њихови оксоаналози се такође могу наћи у животној средини услед оксидације. Када се акумулирају у животној средини, испољавају токсичне ефекте на нециљане организме.

Методе: Систематски је анализирана хидролиза ОФ пестицида у различитим pH условима, при чему су процењена њихова неуротоксична дејства. Концентрација испитиваних ОФ пестицида током разлагања праћена је течном хроматографијом ултра-перформансе (UPLC). Истовремено, примећено је смањење токсичности третираних узорака мерењем активности ензима AChE.

Резултати: Органотиофосфатни пестициди се брзо разлажу у алкалним воденим растворима, али су веома стабилни у киселим растворима. Хлорпирифос се хидролизује најбрже, а диметоат најспорије. Токсичност раствора ових ОФ пестицида се временом

смањује, што указује на то да се токсичнији производи нису формирали.

Закључак: Приказани резултати могу пружити добру основу за даље напоре у проналажењу једноставних и ефикасних метода за разградњу ОФ пестицида.

Кључне речи: органофосфати, пестициди, pH стабилност, токсичност.

Paper received on: 10.03.2024.
Manuscript corrections submitted on: 30.01.2025.
Paper accepted for publishing on: 31.01.2025.

Numerical study on the influence of the initiation point position on the fragmentation effect of a high-explosive rocket warhead

Jovica Đ. Bogdanov[a], *Mihailo* M. Marinković[b], *Branislav* M. Jovanović[c], *Zoran* J. Bajić[d]

University of Defence in Belgrade, Belgrade, Republic of Serbia

[a] e-mail: jovica.bogdanov@va.mod.gov.rs, **corresponding author**, ORCID iD: https://orcid.org/0000-0001-7995-3004

[b] Military Academy, e-mail: mihailo.marinkovic@yahoo.com, ORCID iD: https://orcid.org/0009-0000-3752-8093

[c] Military Academy, e-mail: branislav.jovanovic@eodworld.org, ORCID iD: https://orcid.org/0009-0001-7998-8415

[d] Military Academy, Department of Military Chemical Engineering, e-mail: zoran.bajic@va.mod.gov.rs, ORCID iD: https://orcid.org/0000-0002-8492-3333

https://doi.org/10.5937/vojtehg73-55292

FIELD: chemical technology, mechanical engineering
ARTICLE TYPE: original scientific paper

Abstract:

Introduction/purpose: Rockets with high-explosive (HE) warheads are the most numerous type used for multiple launch rocket systems (MLRS). They are used for a wide range of combat tasks. Besides other design characteristics, the effect on the target depends on the position where detonation is initiated in their explosive charge. The study analyses the fragmentation effects of steel balls from the 128 mm M77 HE warhead with the standard point-detonating (PD) fuze and with a differently positioned detonating assembly.

Methods: The study uses a simple numerical model for the assessment of the fragmentation effect, which requires modest resources. A numerical model of the fragmentation effect was used with Gurney's model of explosive propulsion and Taylor's and Shapiro's method for the direction of the fragment velocity vector. The penetration ability of projected steel balls through hard homogenous steel was analysed using the Project Thor analytical model of kinetic energy projectile penetration.

ACKNOWLEDGMENT: The authors are grateful for the financial support from the University of Defence in Belgrade (project: VA-TT/1/22-24).

Results: The results indicate that a change in the position of the initiation point can improve the fragmentation effect of steel balls. The most significant improvement is increased fragment dispersion, causing much larger fragment impact zones. A modest increase in the fragment velocity is observed as well, mainly because the direction of the fragment velocity vector is changed. Also, the penetration ability of both types of steel balls at distances up to 50 m is sufficient for the anti-personnel role, while larger steel balls have anti-material capabilities as well.

Conclusion: Changing the fuze on high-explosive warheads in order to change the position of the initiation point can be used to improve the fragmentation effect.

Key words: warhead, detonation, fragmentation, explosive propulsion.

Introduction

Rockets with high-explosive (HE) warheads are the most often used for weapon systems that are used for combat support, such as multiple launch rocket systems (MLRS) on land or air platforms. Their effectiveness is based on a detonation of their explosive charge, where fragmentation and blast effects are produced in accordance with specific design features of a warhead. Such designs are considered to have characteristics that provide nearly universal purposes. Thus, rockets with HE warheads can be used in different combat situations and against different targets, usually with appropriate fuze settings.

The fragmentation effect has been of interest in military research and development activities, since it has proven to be very effective against soft targets, like manpower and combat systems without or with light armour protection, especially when concentrated in bases, on landing zones, etc. Such targets require a small amount of kinetic energy or a large number of small perforations (Carlucci & Jacobson, 2018, p.429). There are many numerical models developed for reliable predictions of explosive propulsion and fragmentation effects (Zukas & Walters, 1998; Orlenko, 2004; Gold, 2017). It depends on design features of an explosive ordnance, whether during the fragmentation process, explosive propulsion or fragment flight. Preformed fragments are used in many modern designs, due to a complex nature of naturally fragmented parts of a warhead, where a wide range of fragment dimensions is expected. The main advantage of preformed fragments is a reliable prediction of fragmentation effects, since shape and dimensions can be considered constant during the effect.

Most HE projectiles have a point-detonating (PD) fuze, so that a detonation wave is traveling towards the base of a projectile. Such design is often used mainly because that the position of a fuze offers the earliest

possible and reliable interaction with a target. Additionally, that position is easily accessible for preparation, removal or replacement of a fuze. However, it is possible to use fuzes that are point-initiated and have the detonating assembly positioned elsewhere in the projectile, providing different detonation processes.

Numerical modelling of the fragmentation effect

A simple numerical model will be used to calculate the parameters that are necessary to access the fragmentation effect of the 128 mm HE M77 warhead, used on rockets for domestic multiple launch rocket systems (MLRS), such as Oganj and Morava. The same numerical model will be used to analyse the fragmentation effects of modified designs of the warhead with different positions of the buster: at the base and in the central part of the warhead. The model is not resource demanding and is applicable for engineering purposes, especially in the preliminary analysis of the HE explosive ordnance design.

Design characteristics of the 128 mm M77 HE warhead

The rockets with the 128 mm M77 HE warhead are primarily used against manpower and materiel in open and in field fortifications. They are used for intense and quick fire missions against important targets, such as command posts, telecommunication centres, military bases, depots, airfields, ports, etc.

The main parts of the warhead without a fuze are presented in Figure 1. The warhead is primarily used with the point-detonating fuze UTU M77 that is threaded to the fuze well after the closing plug (1) is removed. The UTU M77 is an impact fuze that can be pre-set for super-quick or delay action. The rocket motor is, during the production, permanently attached to the base parts of the warhead.

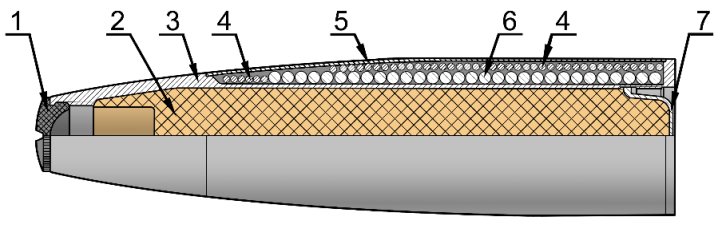

Figure 1 – Main parts of the 128 mm M77 HE warhead:
(1) fuze well closing plug, (2) explosive charge, (3) warhead body, (4) smaller steel balls, (5) liner, (6) larger steel balls and (7) warhead base

The hollow steel warhead case (3) is filled with explosive charge (2) made of 4.050 kg of explosive composition (45 % RDX, 40 % TNT and 15 % aluminium powder). Upon detonation of the explosive charge, the main fragmentation effect is provided by the matrix of steel balls (4) and (6), arranged between the warhead case (3) and the liner (5). Two types of steel balls are used: 930 larger (diameter 10.32 mm, 30 rows with 31 balls each) and 2562 smaller steel balls (diameter 6.35 mm), which are arranged in two layers (6 rows with 47 balls each, and 40 rows with 57 balls each). It should be mentioned that additional fragments are expected to be formed from other metal parts of the warhead (case, liner, base and fuze) and the rocket motor, which will be naturally fragmented.

Numerical model of the warhead fragmentation effect

The Gurney model of explosive propulsion was chosen due to its simplicity. This model has some limitations, but in many similar research studies (Carlucci & Jacobson, 2018; Catovic & Kljuno, 2021) the results have shown an acceptable correlation with experimental results. The following assumptions and approximations have been included in the model:

- detonation process is stationary and in accordance with the model of ideal detonation, so a detonation wave has a spherical shape and all detonation parameters are constant;
- position of a fragments is equal to the position of its centre of mass;
- points of initiation are considered to be on the central longitudinal axis of the warhead; and
- gravitational force is neglected.

Meanwhile, significantly more complex numerical models have been developed, based on the finite element method and hydrocodes (Tanapornraweekit & Kulsirikasem, 2012; Ugrčić & Ivanišević, 2015), which require more resources.

Considering that the warhead is a cylindrical explosive propulsion system with axial symmetry, the velocity of a fragment $v_{f,e}$ caused by the explosive propulsion can be calculated using the following equation (Gurney, 1943):

$$v_{\mathrm{f,e}} = \frac{v_G}{\sqrt{\frac{m_f}{m_e} + \frac{1}{2}}} \qquad (1)$$

where m_f is the mass of metal fragments, m_e is the mass of the explosive charge and v_G is the Gurney velocity in m/s, which is a function of the Gurney energy E_G:

$$v_G = \sqrt{2E_G} \tag{2}$$

The Gurney velocity and energy are expressing the propelling ability of an explosive charge and have constant values for an explosive composition. It can be determined experimentally or using an appropriate numerical model. The Koch's model (Koch, 2002) was used in this research:

$$v_G = \frac{D}{0.308} \tag{3}$$

where D is the detonation velocity in m/s.

Since D = 7495 m/s (Kaye & Herman, 1980, p.328) for a very similar explosive composition (a charge diameter of 51.8 mm and an initial density of 1.81 kg/dm^3) as the warhead explosive charge, so v_G = 2433 m/s for all further calculations. Equation 1 and the data for the 128 mm M77 HE warhead (m_e = 4.050 kg and m_f = 15.480 kg) yield the velocity of fragments of $v_{f,e}$ = 1170 m/s.

The initial velocity of a fragment depends on the movement of a projectile in the moment of explosion as well. Thus, the initial fragment velocity is a sum of the velocity vectors:

$$\overrightarrow{v_{f,0}} = \overrightarrow{v_{f,e}} + \overrightarrow{v_p} + \overrightarrow{v_\omega} \tag{4}$$

where v_p is the projectile flight velocity and v_ω is the tangential velocity as a consequence of projectile rotation. Accordingly, the intensity and direction of the initial fragment velocity during a flight are significantly different from those involving static explosive ordnance. It must be noted that static conditions are very usual in most of experimental warhead effectiveness methods, i.e., "arena" tests. The rocket rotates very slowly after leaving the launcher tube (380 rotations per minute), so the tangential velocity v_ω is approximately 2.4 m/s and was neglected in this study.

The Gurney model assumes that fragments move in the direction perpendicular to the layer of fragments. However, the fragment velocity vector is deflected in the direction of the detonation velocity vector by an angle Θ, that can be predicted using Taylor's method and Shapiro's formula (Lloyd, 1998, p.374):

$$\Theta = \tan^{-1}\left(\frac{v_{f,0}}{2 \cdot D}\cos\left(\frac{\pi}{2} + \alpha - \beta\right)\right) \tag{5}$$

where α is the angle between the detonation wave front and the free surface of fragments and β is the angle between the warhead axis and the line perpendicular to the free surface of fragments (Figure 2).

For known coordinates of characteristic points, all angles can be calculated using trigonometric functions, for example:

$$\alpha = \tan^{-1}\left(\frac{y_i - y_I}{x_i - x_I}\right) \tag{6}$$

where x_i and x_I are the axial coordinates and y_i and y_I are the radial coordinates of the i^{th} steel ball and the initiation point I, respectively.

During the flight, air drag constantly decreases the velocity of a fragment. Since steel balls in the warhead are symmetrical and have known dimensions, the velocity at the distance x can be written as (Carlucci & Jacobson, 2018, pp.202-210):

$$v_{f,x} = v_{f,0} \cdot e^{-\frac{\rho_a \cdot A_f \cdot C_d \cdot x}{2 \cdot m_f}} \tag{7}$$

where ρ_a is the density of air, A_f is the surface area of the fragment silhouette in a plane that is perpendicular to the velocity vector $v_{f,x}$, m_f is the mass of the fragment and C_D is the drag coefficient. The following values were adopted for further calculations: $\rho_a = 1.225 \cdot 10^{-3}$ kg/dm^3 and $C_D = 0.95$. In order to simplify the model, the constant value C_D was adopted. This can be acceptable because its value does not change significantly for short flight distances of spherical fragments at supersonic velocities (Mach number M between 2 and 4) (Moxnes et al, 2017).

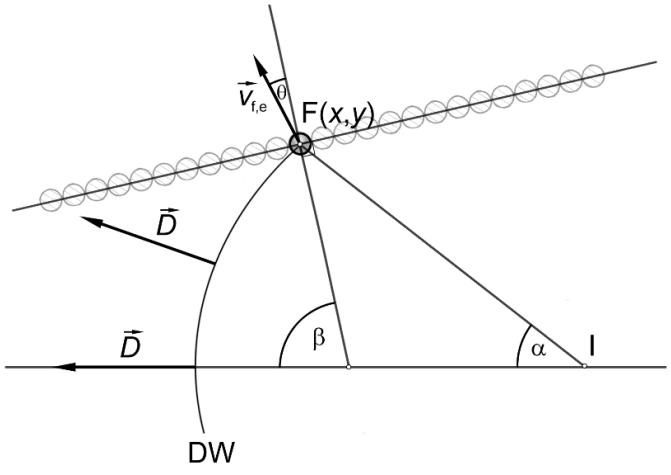

Figure 2 – Direction of the fragment velocity vector:
DW: detonation wave; F: position of a fragment; I: initiation point

Penetration ability of the fragment depends on target and fragment characteristics at impact conditions (mass and dimensions, velocity and angle). It can be evaluated using the numerical model developed in the Project Thor (Zook, 1977), which was used in similar studies (Wang et al, 2014; Rotariu & Trana, 2016). Evaluation can be done using the empirical equation for the residual fragment velocity $v_{f,res}$ (Zook, 1977, p.9):

$$v_{f,res} = v_{f,x} - 10^{C_1}\left(h_t \cdot A_f\right)^{C_2} m_f^{C_3} (\sec\varphi)^{C_4} v_{f,x}^{C_5} \qquad (8)$$

where h_t is the thickness of the target, φ is the angle of incidence at impact, while C_1, C_2, C_3, C_4 and C_5 are the empirical coefficients. The empirical coefficients are derived for parameters in the imperial units (dimensions in inches, mass in grains and velocity in feet per second). The following values for hard homogenous steel were used for further calculations: C_1 = 6.475, C_2 = 0.889, C_3 = -0.945, C_4 = .1.262 and C_5 = 0.019. The maximum penetration $h_{t,max}$ is when the fragment impact is perpendicular to the target surface (φ = 0) and $v_{f,res}$ = 0 criterion is met.

Results and discussion

Numerical modelling of the fragmentation effect for the 128 mm M77 HE warhead

The axial coordinates x_i and the radial coordinates y_i of all steel balls were measured from the central point in the mouth of the fuze well, and are listed in Tables 1 and 2.

Table 1 – Positions of larger steel balls

Number of a fragment, *i*	Coordinates of a fragment		Number of a fragment, *i*	Coordinates of a fragment	
	x_i (mm)	y_i (mm)		x_i (mm)	y_i (mm)
1	190.0	51.5	16	354.3	51.5
2	201.0	51.5	17	365.2	51.5
3	211.9	51.5	18	376.2	51.5
4	222.9	51.5	19	387.1	51.5
5	233.8	51.5	20	398.1	51.5
6	244.8	51.5	21	409.0	51.5
7	255.7	51.5	22	420.0	51.5
8	266.7	51.5	23	430.9	51.5
9	277.6	51.5	24	441.9	51.5
10	288.6	51.5	25	452.8	51.5

Number of a fragment, *i*	Coordinates of a fragment		Number of a fragment, *i*	Coordinates of a fragment	
	x_i (mm)	y_i (mm)		x_i (mm)	y_i (mm)
11	299.5	51.5	26	463.8	51.5
12	310.5	51.5	27	474.7	51.5
13	321.4	51.5	28	485.7	51.5
14	332.4	51.5	29	496.6	51.5
15	343.3	51.5	30	507.6	51.5

Table 2 – Positions of smaller steel balls

Number of a fragment, *i*	Coordinates of a fragment		Number of a fragment, *i*	Coordinates of a fragment	
	x_i (mm)	y_i (mm)		x_i (mm)	y_i (mm)
1	151.5	48.1	24	354.2	58.3
2	158.4	48.1	25	361.1	58.3
3	165.2	48.1	26	368.1	58.3
4	172.1	48.1	27	375.0	58.3
5	178.9	48.1	28	382.0	58.3
6	185.8	48.1	29	388.9	58.3
7	236.0	58.3	30	395.9	58.3
8	243.0	58.3	31	402.8	58.3
9	249.9	58.3	32	409.8	58.3
10	256.9	58.3	33	416.7	58.3
11	263.8	58.3	34	423.7	58.3
12	270.8	58.3	35	430.6	58.3
13	277.7	58.3	36	437.6	58.3
14	284.7	58.3	37	444.5	58.3
15	291.6	58.3	38	451.5	58.3
16	298.6	58.3	39	458.4	58.3
17	305.5	58.3	40	465.4	58.3
18	312.5	58.3	41	472.3	58.3
19	319.4	58.3	42	479.3	58.3
20	326.4	58.3	43	486.2	58.3
21	333.3	58.3	44	493.2	58.3
22	340.3	58.3	45	500.1	58.3
23	347.2	58.3	46	507.1	58.3

Since all steel balls are embedded in the matrix that is parallel to the longitudinal axis of the warhead, then $\beta = \pi/2$ and Equation 5 can be written as:

$$\Theta = \tan^{-1}\left(\frac{v_{f,0}}{2 \cdot D}\cos\alpha\right) \quad (9)$$

The fuze well in the 128 mm M77 HE warhead is 43.2 mm deep, so it is considered that the initiation point is positioned at the same axial distance on the longitudinal axis ($y_l = 0$). According to that and the data in Tables 1 and 2, projection angles of steel balls Θ_i were calculated using Equation 9 for the static warhead. Negative values indicate that a fragment is projected "backwards", i.e., towards the base of the warhead.

After that, projection angles of steel balls were calculated for flight conditions according to Equation 4, where the value for the rocket velocity after the end of rocket motor propulsion v_p = 647 m/s was adopted.

The average fragment velocity and the maximum penetration of steel balls $h_{t,max}$ at distances between 5 and 50 m from the point of warhead explosion for both conditions were calculated using Equation 8 and $v_{f,res} = 0$ criterion.

The results are listed in Table 3.

Table 3 – Results of the fragmentation effect for the 128 mm M77 HE warhead

Parameter	Fragment type	Conditions	
		static	flight
Angle of fragment projection (°)	smaller steel balls	-4.1 – -4.4	25.7 – 25.5
	larger steel balls	-4.2 – -4.5	25.8 – 25.5
Average fragment velocity at distances 5–50 m, $v_{f,x}$ (m/s)	smaller steel balls	1072 – 487	1186 – 539
	larger steel balls	1109 – 683	1226 –755
Maximal penetration at distances 5–50 m, $h_{t,max}$ (mm)	smaller steel balls	4.3 – 1.8	4.8 – 2.0
	larger steel balls	7.9 – 4.6	8.8 – 5.1
Surface area of the fragment impact zone at distances 5–50 m (m^2)		16.3 – 217.3	16.3 – 214.8
Areal density of fragments at distances 5–50 m (fragment/m^2)		214.1 – 16.1	214.4 – 12.9

Numerical modelling of the fragmentation effect for the modified 128 mm HE warhead with a base detonating assembly

The direction of a detonation wave in an explosive charge directly depends on a position where the detonation is initiated. Change in the position can significantly affect the fragmentation effect of a warhead.

A possible modification of the 128 mm M77 HE warhead is to position the detonating assembly in the base of the explosive charge while the

space in the fuze well for the detonation booster is filled with explosive. Such a warhead can have a fuze that has two separate assemblies, like modern electric point-initiated base-detonating (PIBD) fuzes. The main parts of such a modified warhead without a fuze are presented in Figure 3.

The coordinates of the initiation point are: x_I = 464 mm and y_I = 0 mm. Since no other design changes were made, the parameters of the fragmentation effect were calculated using the coordinates x_i and y_i of all steel balls in Tables 1 and 2, and the results are listed in Table 4.

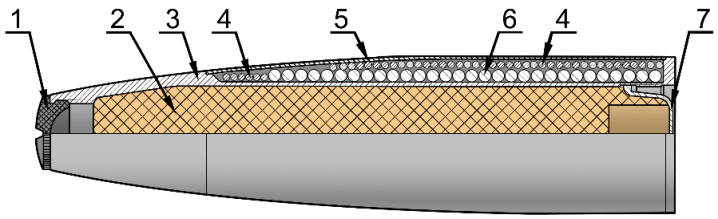

Figure 3 – Main parts of the 128 mm HE warhead with a base detonating assembly: (1) fuze well closing plug, (2) explosive charge, (3) warhead body, (4) smaller steel balls, (5) liner, (6) larger steel balls and (7) warhead base

Table 4 – Results of the fragmentation effect for the 128 mm HE warhead with a base detonating fuze assembly

Parameter	Fragment type	Conditions	
		static	flight
Angle of fragment projection (°)	smaller steel balls	4.4 – -2.7	32.3 – 26.7
	larger steel balls	4.4 – -2.9	32.3 – 26.9
Average fragment velocity at distances 5–50 m, $v_{f,x}$ (m/s)	smaller steel balls	1072 – 487	1251 – 569
	larger steel balls	1109 – 683	1294 – 797
Maximal penetration at distances 5–50 m, $h_{t,max}$ (mm)	smaller steel balls	4.3 – 1.8	5.1 – 2.1
	larger steel balls	7.9 – 4.6	9.4 – 5.5
Surface area of the fragment impact zone at distances 5–50 m (m^2)		35.1 – 2095.6	35.3 – 2111.9
Areal density of fragments at distances 5–50 m (fragment/m^2)		99.5 – 1.7	99.0 – 1.7

Numerical modelling of the fragmentation effect for the modified 128 mm HE warhead with a central detonating assembly

Another possible modification of the 128 mm M77 HE warhead is to position the detonating assembly in the central part of the explosive charge. As with the previous warhead, the fuze with two separate assemblies can be used, so that the coordinates of the initiation point are: x_I = 350 mm and y_I = 0 mm. The main parts of such a modified warhead without a fuze are presented in Figure 4.

The results of the numerical modelling are listed in Table 5.

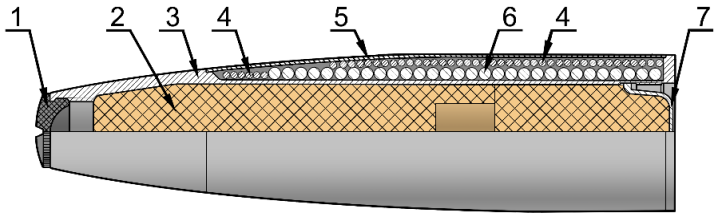

Figure 4 – Main parts of the 128 mm HE warhead with a central detonating assembly: (1) fuze well closing plug, (2) explosive charge, (3) warhead body, (4) smaller steel balls, (5) liner, (6) larger steel balls and (7) warhead base

Table 5 – Results of the fragmentation effect for the 128 mm HE warhead with a central detonating fuze assembly

Parameter	Fragment type	Conditions	
		static	flight
Angle of fragment projection (°)	smaller steel balls	4.4 – -4.2	32.2 – 25.6
	larger steel balls	4.3 – -4.3	32.2 – 25.7
Average fragment velocity at distances 5–50 m, $v_{f,x}$ (m/s)	smaller steel balls	1072 – 487	1225 – 557
	larger steel balls	1109 – 683	1267 – 780
Maximal penetration at distances 5–50 m, $h_{t,max}$ (mm)	smaller steel balls	4.3 – 1.8	4.9 – 2.1
	larger steel balls	7.9 – 4.6	9.2 – 5.3
Surface area of the fragment impact zone at distances 5–50 m (m^2)		39.0 – 2480.8	39.0 – 2481.5
Areal density of fragments at distances 5–50 m (fragment/m^2)		89.7 – 1.4	89.6 – 1.4

Analysis of the results

The results in Tables 3, 4 and 5 show that, for all warheads in static conditions, fragment sprays are directed nearly perpendicular to the warhead longitudinal axis. Fragment sprays from warheads detonated during flight are directed approximately 25-32 °towards the frontal part and have greater velocities. Also, a warhead flight velocity has the most significant influence on the direction of the fragment velocity vector. Thus, the effect of fragments on the target is significantly better than in static conditions. That fact must be taken into consideration when experimental data on the fragmentation effect are analysed.

The fragment sprays for all considered warheads are graphically represented in Figure 5.

The results of the numerical modelling also show that change in the position of the initiation point can improve the fragmentation effect of steel balls. A fragment spray from a warhead with a PD fuze is very narrow because all the fragments have nearly parallel trajectories, resulting in a small impact zone with an extremely large areal density of fragments. Practically, steel balls will achieve 100 % hit probability in such an impact zone, but 0 % outside of that zone.

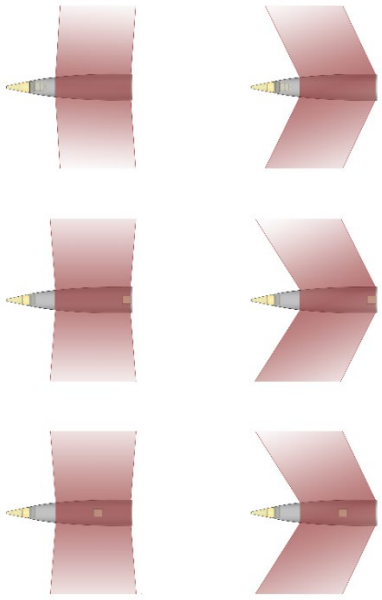

Figure 5 – Graphical representation of fragment spray directions in static (left) and flight conditions (right) for the 128 mm HE warhead with the point-detonating fuze (top), the base (middle) and the central detonating assembly (bottom)

If an explosive charge is detonated from the base or centrally, steel balls will be projected with a slightly higher velocity and in significantly wider sprays due to divergent trajectories of fragments. Both effects will increase the efficiency of a fragmentation warhead. Fragment impact zones are many times larger than those from a warhead with a PD fuze. For both types, at distances up to 50 m, the areal density of fragments is larger than 1 fragment per m^2 (1.7 and 1.4 fragments per m^2, respectively), which is a threshold for the lethal zone in many methods and standards.

Both types of steel balls show penetration abilities at distances up to 50 m which are much better than needed for the anti-personnel role. Penetration abilities of larger steel balls are significantly better compared to smaller ones. According to the results, it can be expected that larger steel balls are effective in the anti-materiel role as well, even against lightly armoured targets.

Conclusion

Changing the position of the initiation point can be used to improve the fragmentation effect of high-explosive warheads. That can be done using an appropriate fuze system which has the most appropriate position of a detonating assembly for required capabilities. Such designs can achieve a better fragment dispersion, so that fragment impact zones are larger, and a slightly larger fragment velocity.

References

Carlucci, D.E. & Jacobson, S.S. 2018. *Ballistics: Theory and Design of Guns and Ammunition, 3rd Edition*. Boca Raton, FL, USA: CRC Press. Available at: https://doi.org/10.1201/b22201.

Catovic, A. & Kljuno, E. 2021. A novel method for determination of lethal radius for high-explosive artillery projectiles. *Defence Technology*, 17(4), pp.1217-1233. Available at: https://doi.org/10.1016/j.dt.2020.06.015.

Gold, V.M. 2017. Fragmentation model for large L/D (Length over Diameter) explosive fragmentation warheads. *Defence Technology*, 13(4), pp.300-309. Available at: https://doi.org/10.1016/j.dt.2017.05.007.

Gurney, R.W. 1943. *The Initial Velocities of Fragments from Bombs, Shell and Grenades*. Fort Belvoir, VA, USA: Defense Technical Information Center [online]. Available at: https://apps.dtic.mil/sti/citations/ADA800105 [Accessed: 9 June 2024].

Kaye, S.M. & Herman, H.L. 1980. *Encyclopedia of Explosives and Related Items. Volume 9*. Fort Belvoir, VA, USA: Defense Technical Information Center [online]. Available at: https://apps.dtic.mil/sti/citations/ADA097595 [Accessed: 9 June 2024].

Lloyd, R.M. 1998. *Conventional Warhead Systems Physics and Engineering Design*. Reston, VA, USA: American Institute of Aeronautics and Astronautics. Available at: https://doi.org/10.2514/4.472558.

Moxnes, J.F., Frøyland, Ø., Øye, I.J., Brate, T.I., Friis, E., Ødegårdstuen, G. & Risdal, T.H. 2017. Projected area and drag coefficient of high velocity irregular fragments that rotate or tumble. *Defence Technology*, 13(4), pp.269-280. Available at: https://doi.org/10.1016/j.dt.2017.03.008.

Orlenko, L.P. 2004. *Fizika Vzryva*. Moscow: Fizmatlit. (In the original: Орленко, Л.П. 2004. *Физика взрыва.* Москва: Физматлит). ISBN: 5-9221-0219-2.

Rotariu, A. & Trana, E. 2016. Modelling and simulation for ballistic protection. In: *GSEBS-2016: Greener and Safer Energetic and Ballistic Systems*, Bucharest, Romania, May 16-28.

Tanapornraweekit, G. & Kulsirikasem, W. 2012. FEM Simulation of HE blast-fragmentation warhead and the calculation of lethal range. *International Journal of Mechanical and Mechatronics Engineering*, 6(6), pp.1070-1074 [online]. Available at: https://publications.waset.org/6890.pdf [Accessed: 9 June 2024].

Ugrčić, M. & Ivanišević, M. 2015. Characterization of the Natural Fragmentation of Explosive Ordnance Using the Numerical Techniques Based on the FEM. *Scientific Technical Review*, 65(4), pp.14-27 [online]. Available at: http://www.vti.mod.gov.rs/ntp/rad2015/4-2015/2/2.pdf [Accessed: 9 June 2024].

Wang, J., Wang, Y.-c., Zhu, S.-q., Ren, W.-h. & Niu, T.-l. 2014. Improvement and Simulation of THOR Formula with Yaw Angle. *Journal of Engineering Science and Technology Review*, 7(2), pp.106-112 [online]. Available at: http://www.jestr.org/downloads/Volume7Issue2/fulltext167214.pdf [Accessed: 9 June 2024].

Zook, J. 1977. *An Analytical Model of Kinetic Energy Projectile/Fragment Penetration.* Fort Belvoir, VA, USA: Defense Technical Information Center [online]. Available at: https://apps.dtic.mil/sti/citations/ADA086546 [Accessed: 9 June 2024].

Zukas, J.A. & Walters, W.P. 1998. *Explosive Effects and Applications.* New York, NY: Springer. Available at: https://doi.org/10.1007/978-1-4612-0589-0.

Estudio numérico sobre la influencia de la posición del punto de iniciación en el efecto de fragmentación de una ojiva de cohete de alto poder explosivo

Jovica Đ. Bogdanov[a], **autor de correspondencia**, *Mihailo* M. Marinković[ab], *Branislav* M. Jovanović[ab], *Zoran* J. Bajić[abc]

[a] Universidad de Defensa de Belgrado, Belgrado, República de Serbia

[b] Academia Militar

[c] Departamento de Ingeniería Química Militar

CAMPO: tecnología química, ingeniería mecánica
TIPO DE ARTÍCULO: artículo científico original

Resumen:

Introducción/objetivo: Los cohetes con ojivas de alto poder explosivo (HE) son el tipo más numeroso que se utiliza en los sistemas de lanzamiento múltiple de cohetes (MLRS). Se emplean para una amplia gama de tareas de combate. Además de otras características de diseño, el efecto sobre el objetivo depende de la posición en la que se inicia la detonación en su carga explosiva. El estudio analiza los efectos de fragmentación de las bolas de acero de la ojiva HE M77 de 128 mm con la espoleta de detonación puntual (PD) estándar y con un conjunto detonador ubicado en una posición diferente.

Métodos: El estudio utiliza un modelo numérico simple para la evaluación del efecto de fragmentación, que requiere recursos modestos. Se utilizó un modelo numérico del efecto de fragmentación con el modelo de Gurney de propulsión explosiva y el método de Taylor y Shapiro para la dirección del vector de velocidad de los fragmentos. La capacidad de penetración de las bolas de acero proyectadas a través de acero duro homogéneo se analizó utilizando el modelo analítico de penetración de proyectiles de energía cinética del Proyecto Thor.

Resultados: Los resultados indican que un cambio en la posición del punto de inicio puede mejorar el efecto de fragmentación de las bolas de acero. La mejora más significativa es el aumento de la dispersión de los fragmentos, lo que provoca zonas de impacto de fragmentos mucho más grandes. También se observa un aumento modesto en la velocidad de los fragmentos, principalmente porque se cambia la dirección del vector de velocidad de los fragmentos. Además, la capacidad de penetración de ambos tipos de bolas de acero a distancias de hasta 50 m es suficiente para el papel antipersonal, mientras que las bolas de acero más grandes también tienen capacidades antimateriales.

Conclusión: Cambiar la espoleta de las ojivas de alto poder explosivo para cambiar la posición del punto de iniciación puede servir para mejorar el efecto de fragmentación.

Palabras claves: ojiva, detonación, fragmentación, propulsión explosiva.

Исследование влияния положения точки инициирования на осколочное действие головной части реактивного снаряда с использованием численной модели

Йовица Дж. Богданов[а], **корреспондент**, *Михаило* М. Маринкович[аб], *Бранислав* М. Йованович[аб], *Зоран* Й. Байич[абв]

[а] Университет обороны в г. Белград, г. Белград, Республика Сербия

[б] Военная академия

[в] Департамент военного химического инжиниринга

РУБРИКА ГРНТИ: 61.43.29 Взрывчатые вещества,
78.25.16 Вооружение и техника ракетных войск
ВИД СТАТЬИ: оригинальная научная статья

Резюме:

Введение/цель: Реактивные снаряды с осколочно-фугасной головной частью являются наиболее распространенным типом боеприпасов для реактивных систем залпового огня. Они используются для выполнения широкого спектра боевых задач. Действие на цель, помимо других конструктивных особенностей, зависит от положения, в котором инициируется детонация разрывного заряда. В исследовании анализируется осколочное действие стальных шариков в 128-мм осколочно-фугасних головных частей M77 со стандартным контактным взрывателем и с другим расположением детонирующего узла.

Методы: В данном исследовании используется простая численная модель для определения осколочного действия, не требующая больших ресурсов. Численная модель содержит модель метательной способности Герни и метод Тейлора-Шапиро для определения направления вектора скорости осколка. Пробивная способность стальных шариков сквозь твердую гомогенную сталь анализировалась с помощью аналитической модели кинетического пробития осколков, разработанной в рамках «Проекта Тор».

Результаты: Результаты показывают, что изменение положения точки инициирования может улучшить осколочное действие стальных шариков. Наиболее значительным улучшением является увеличение рассеивания осколков, что приводит к увеличению зон поражения. Также наблюдается незначительное увеличение скорости движения осколков, главным образом из-за изменения направления вектора скорости движения осколков. Помимо того, пробивная способность обоих типов стальных шариков на расстоянии до 50 м достаточна для борьбы с пехотой, в то время как более крупные стальные шарики также обладают антиматериальными свойствами.

Вывод: Изменение взрывателя на осколочно-фугасных головных частях реактивного снаряда с целью изменения положения точки инициирования может быть использовано для улучшения осколочного действия.

Ключевые слова: головная часть реактивного снаряда, детонация, осколочное действие, метательная способность взрыва.

Истраживање утицаја положаја места иницирања на парчадно дејство разорне бојне главе ракете помоћу нумеричког модела

Јовица Ђ. Богданов[а], **аутор за преписку**, *Михаило* М. Маринковић[аб], *Бранислав* М. Јовановић[аб], *Зоран* Ј. Бајић[абв]

[а] Универзитет одбране у Београду, Београд, Република Србија

[б] Војна академија

[в] Катедра војнохемијског инжењерства

ОБЛАСТ: хемијске технологије, машинство
КАТЕГОРИЈА (ТИП) ЧЛАНКА: оригинални научни рад

Сажетак:

Увод/циљ: Ракете са разорном бојном главом најзаступљенија су врста убојних средстава за вишецевне лансере ракета. Намењене су за извршење највећег дела борбених задатака. Њихово дејство на циљу зависи, поред одређених карактеристика конструкције, и од положаја иницирања процеса детонације у експлозивном пуњењу. Анализирано је парчадно дејство челичних куглица лаборисаних у тренутно-фугасне бојне главе 128 mm M77 са стандардним горњим упаљачем и са упаљачима чији се осигурани детонатор налази у другим положајима.

Методе: У истраживању је коришћен једноставан нумерички модел за одређивање парчадног дејства, који захтева скромне ресурсе. Нумерички модел садржи Гурнијев модел експлозивне пропулзије и Тејлор-Шапирову методу за одређивање смера вектора брзине парчади. Способност продирања челичних куглица кроз тврди хомогени челик анализирана је помоћу аналитичког модела продирања кинетичких пројектила, који је развијен у оквиру „Пројекта Тор".

Резултати: Указано је да промена положаја тачке иницирања експлозивног пуњења може да побољша парчадно дејство челичних куглица. Најзначајније побољшање уочено је у повећању дисперзије парчади, чиме се остварују много веће зоне парчадног дејства. Такође, запажено је и мало повећање брзине парчади, што је, пре свега, последица промене смера вектора брзине парчади. Поред тога, пробојност обе врсте челичних куглица на даљинама до 50 m омогућава противпешадијску намену, док веће челичне куглице имају и способност дејства против материјалних средстава.

Закључак: Промена упаљача на разорним бојним главама, ради промене положаја места иницирања експлозивног пуњења, може се користити за побољшање парчадног дејства.

Кључне речи: бојна глава, детонација, парчадно дејство, експлозивна пропулзија.

Paper received on: 21.06.2024.
Manuscript corrections submitted on: 30.01.2025.
Paper accepted for publishing on: 31.01.2025.

Static and dynamic study of composite beams with a new interlaminar sliding field using different beam theories

Rachida Mohamed Krachaï[a], *Noureddine* Elmeiche[b], *Ismail* Mechab[c], *Fabrice* Bernard[d], *Hichem* Abbad[e]

[a] Djilali Liabes University, Faculty of Technology,
Department of Civil Engineering and Public Works,
Civil and Environmental Engineering Laboratory (LGCE),
Sidi Bel-Abbes, People's Democratic Republic of Algeria +
Mustapha Stambouli University, Faculty of Science and Technology,
Department of Civil Engineering,
Mascara, People's Democratic Republic of Algeria,
e-mail: rm.kirachai@univ-mascara.dz,
ORCID iD: https://orcid.org/0009-0004-7530-433X

[b] Djilali Liabes University, Faculty of Technology,
Department of Civil Engineering and Public Works,
Civil and Environmental Engineering Laboratory (LGCE),
Sidi Bel-Abbes, People's Democratic Republic of Algeria,
e-mail: noureddine.elmeiche@univ-sba.dz, **corresponding author**,
ORCID iD: https://orcid.org/0000-0002-6412-0840

[c] Djilali Liabes University, Faculty of Technology,
Department of Mechanical Engineering,
Laboratory of Mechanics and Physics of Materials (LMPM),
Sidi Bel-Abbes, People's Democratic Republic of Algeria,
e-mail: ismail.mechab@gmail.com,
ORCID iD: https://orcid.org/0009-0004-4922-6980

[d] University of Rennes, INSA Rennes,
Civil and Mechanical Engineering Laboratory (LGCGM),
Rennes, French Republic,
e-mail: fabrice.bernard@insa-rennes.fr,
ORCID iD: https://orcid.org/0000-0001-7495-936X

[e] Djilali Liabes University, Faculty of Technology,
Department of Civil Engineering and Public Works,
Civil and Environmental Engineering Laboratory (LGCE),
Sidi Bel-Abbes, People's Democratic Republic of Algeria,
e-mail: hi_abbad@yahoo.fr,
ORCID iD: https://orcid.org/0000-0001-9896-5369

https://doi.org/10.5937/vojtehg73-52773

FIELD: civil engineering
ARTICLE TYPE: original scientific paper

Abstract:

Introduction/purpose: The present work aims to carry out a static and dynamic investigation of composite beams composed of two elements

connected together, with a partial interaction between the beam layers, while taking into account the interlaminar sliding effect.

Methods: A new interlaminar slip field which takes into account, for each layer, the axial displacement, the rotation due to bending, and the high-order transverse shear with a new warping shape function, has been introduced in this study. The equilibrium equations were solved analytically based on the principle of Hamilton. In addition, the numerical resolution of these equations was based on the principle of minimizing all energies using the Ritz method, while taking into account different beam theories. Afterwards, a comparative study was carried out in order to calculate the natural vibration frequencies of two composite beams made of steel and wood materials.

Results: It was found that the results obtained for the ten natural vibration frequencies are in perfect agreement with those reported in previous works found in the literature.

Conclusion: Further, a detailed study was conducted, depending on the geometric and material parameters, for the two mixed materials, i.e., concrete-wood and steel-concrete, with two interlaminar sliding fields, namely the classical sliding field based on the Timoshenko beam theory and a new interlaminar sliding field that is based on the high order theory. Furthermore, bending was studied in the static case in order to examine the effect of the interlaminar shear force on short and long beams.

Keywords: static and dynamic study, composite beams, partial interaction, new interlaminar slip field, high order transverse shear, new warping shape function, Ritz method.

Introduction

Sliding in mixed structures is a complex phenomenon that often occurs at the interface between two or more different materials, under the effect of variable static, dynamic or thermal stresses which may engender some deformation or critical damage. It should be noted that the connection between a concrete slab and a steel or wooden beam, for example, is generally ensured by shear connectors placed in the composite beams. The role of these connectors is to prevent the occurrence of shear at the interface, along the composite beam, which is subjected to a bending load. The interface is an essential element that plays an indispensable role in the behavior of the composite beam. Indeed, if the concrete slab and the beam are freely superimposed, then the two elements flex independently and considerable sliding occurs at their interface. Therefore, in order to reduce or eliminate this sliding, it is deemed appropriate to have a sufficient number of shear connectors at the interface between the slab and the beam. This technique allows

transferring the forces between the two materials, and therefore producing a mixed bending of one single element that is more resistant and has higher rigidity. It was revealed that numerous works have been carried out on the topic under study. Regarding Xu & Wu (2008), they examined the free vibration and buckling of composite beams with interlayer sliding based on a two-dimensional theory, and using semi-analytical solutions, under boundary conditions that were determined with a coupling between the Differential Quadrature method and the State Space method. As for Nguyen (2009), he developed numerical models that are capable of predicting the instantaneous and delayed behavior of composite steel-concrete beams. Similarly, Le Grognec et al. (2012) proposed an exact buckling solution for two-layer Timoshenko beams with interlayer slip. Likewise, Lenci & Clementi (2012) examined the effects of shear stiffness, rotary and axial inertia, and interface stiffness, on the free vibrations of a two-layer beam. With regard to Castel (2013), he presented a model that can be employed to describe the vibrational behavior of composite structures, i.e., plates that are partially covered with passive constrained layer damping (PCLD) patches that play the role of damping elements. He investigated the energy of the system under study using three different methods, namely the Rayleigh-Ritz method, the Navier method, and the finite element method. On the other hand, Galuppi & Royer-Carfagni (2014) investigated the buckling of three-layer composite beams with viscoelastic interaction. Furthermore, Čas et al. (2018) proposed an analytical solution to the two-layer three-dimensional composite beam with interlayer slips. Likewise, Perkowski & Czabak (2019) described the behavior of composite wood-concrete beams under hygrothermal loading. The two materials, i.e., wood and concrete, are linked by a joint. In this case, the eventual interlayer sliding and the joint uplift were taken into account in order to determine the rigidity of the composite beam and also to estimate the shrinkage/swelling that is due to humidity of wood and concrete in the long term. This allowed them to propose a model and formulate an inverse problem. As for Adam & Furtmüller (2020), they studied the bending vibrations of composite beams presenting geometric nonlinearities, and subjected to interlayer sliding. In addition, Santos (2020) analyzed the buckling of two-layer laminated composite beams, with interlayer sliding, using the finite element method. It should be noted that the geometrically nonlinear beam elements have a single flexible shear interface and each layer is modeled using the Timoshenko theory. Subsequently, the inter-element equilibrium as well as the Neumann boundary conditions was applied while using the Lagrangian multiplier method. On the other hand, Lemes et al. (2021) carried out a numerical

analysis of composite steel-concrete beams, with partial shear interaction, in order to theoretically determine two-dimensional displacement using the plastic-hinge approach. Moreover, Lemes et al. developed an effective numerical method for the purpose of analyzing mixed steel-concrete structures while taking into account the nonlinear geometric and material effects. Afterwards, a methodology based on the Refined Plastic Hinge Method (RPHM) was developed and the stiffness parameters were obtained by considering a homogeneous cross section of the structure. The strain compatibility method (SCM) was applied to evaluate the strength of structural elements. Likewise, the Newton-Raphson method was adopted to solve nonlinear global and local equations, at the cross section level. The results obtained were then compared with the others found in the experimental and numerical databases available in the literature (Lemes et al, 2017). With regard to Barbosa et al. (2019) they presented an experimental study with a view to developing a Truss connector in a mixed concrete-steel beam and also to analyzing the behavior of failure loads, the transverse displacements between concrete slabs, and the relative vertical sliding between the reinforced concrete slabs and the metal profiles of the developed models. Further, Yoo et al. (2021) presented a nonlinear analysis method to evaluate the bending behavior of a composite beam while taking into account partial interaction. They applied the Fourier series for the purpose of determining the shear interface forces in the composite beam while taking into consideration the sliding effect between steel and concrete, and by considering the inelastic behavior of the steel beam and the nonlinear behavior of the ultra-high performance fiber-reinforced concrete (UHPC). As for Honarvar et al. (2020), they examined the steel-concrete composite beam with bolt shear connectors. The composite beam was subjected to three different loading conditions, including pure bending loading and simultaneous bending loading, with two alternative torsional loading modes. The results obtained were analyzed using a 3D nonlinear finite element model. This study was aimed to carry out the analysis of the mid-span deflection, rotation and sliding of composite beams, under different loading conditions. In addition, the effect of the type and number of shear connectors on the sliding of the composite beam was also investigated.

The findings indicated that the slip between the steel beam and concrete slab, along the composite beam, increased in the direction of increasing bending load, while torsion load had a slight effect on sliding. In this context, Carvalho et al. (2021) developed two methods which are based on plane displacement with concentrated nonlinear effects for the numerical analysis of composite beams. It should be noted that the effects

of geometric nonlinearity, plasticity, and partial shear connection are taken into account. In the two approaches used, the co-rotational system is defined in such a way as to allow large displacements and rotations in the numerical model. The first method is based on the strain compatibility method. In this case, the deformations of the sections and the sliding at the steel-concrete interface are analyzed as well as the axial and bending rigidity of the cross section. The second approach is based on the finite element method in order to simulate plasticity. All the numerical results obtained by these two approaches turned out to be quite accurate. They are close to the experimental data reported in the literature (Carvalho et al, 2021). In this regard, Oliveira et al. (2021) carried out a study on the serviceability limit state of excessive deflections by adopting two simplified approaches, namely Eurocode 4:2004 (European code) and AS/NZS 2327:2017 (Australian code). The results obtained were compared with the experimental ones that have previously been reported by other authors in the literature. The occurrence of non-uniform shrinkage becomes a relevant aspect due to the impermeability of the face that is favored by the steel decking. Based on the above, it was deemed appropriate to neglect the deflections when Eurocode 4 was adopted. At the same time, the simplified AS/NZS 2327 approach, which explicitly takes into account non-uniform shrinkage, gave results that are more precise than those obtained by the experimental method. In addition, several studies were carried out using the First-order Shear Deformation Theory (FSDT) which applies in the case of short beams. This theory is based on the principle which states that after deformation the plane section remains plane but loses its perpendicularity with respect to the mean line of the beam. This is due to the transverse shear occurring through the thickness of the beam that was initially discovered by Timoshenko. The First-order Shear Deformation Theory (FSDT) is attributed to Reissner (1945) and Mindlin (1951) who developed the Reissner-Mindlin plate model. Other similar works, such as those carried out by Timoshenko & Woinowsky-Krieger (1959), Whitney (1969), Reddy (1984), Kant & Swaminathan (2001), Della Croce & Venini (2004), Wang et al. (2000), Valizadeh et al. (2013), Mechab (2005), also deserve to be mentioned.

The primary purpose of this investigation is to conduct an analytical and numerical study on free vibrations and the interlaminar bending shear force. For this, a new interlaminar sliding field of a composite beam was introduced. This field takes into account the axial displacements, rotations, as well as the warping effect of the section of the two composite beams. Furthermore, a new transverse shear strain shape function was introduced in order to see the transverse shear influence of short beams. For this, two

types of composite beams were studied, i.e., one composite steel-wood beam and one steel-concrete beam. The numerical results were compared with the ones found in the literature and in other deformation theories.

Equation of interlaminar slip between layers

Balance of forces

Consider a composite beam composed of two different materials in partial connection (Figure 1). This beam is subjected to bending under uniformly distributed loading. Figure 2 shows the free-body diagram of an infinitesimal element of length dx of the composite beam subjected to an external force distributed along the element. The bending moment, the shear force, and the normal force are denoted by M, Q, and N, respectively.

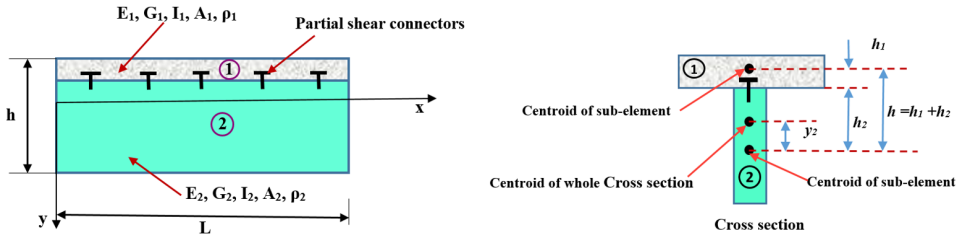

Figure1 – Composite member and the coordinate system; (a) elevation; (b) cross-section

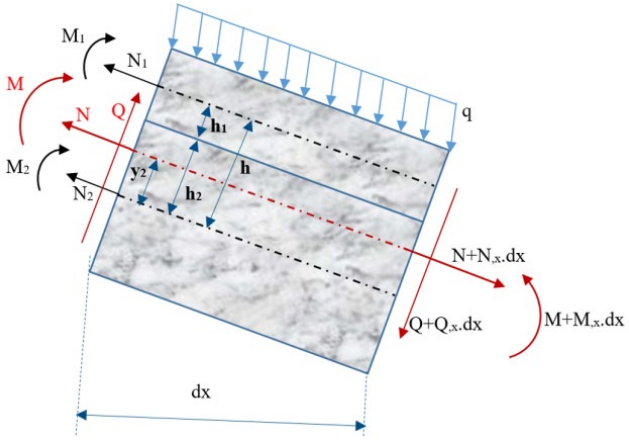

Figure 2 – Internal forces acting on an infinitesimal element of the composite beam under bending

According to the small deformation hypothesis, the dynamic equilibrium equations of the force applied along the x and y directions and the bending moment can be expressed using the three equations given below:

$N=F$

Here, F is the applied axial force

$$\frac{dQ}{dx}=q+\overline{\rho A}\frac{d^2v}{dt^2}-N\frac{d^2v}{dx^2},\ \frac{dM}{dx}=Q-\overline{\rho}I\frac{d^2\theta}{dt^2} \tag{1}$$

with

$$\overline{\rho A}=\rho_1A_1+\rho_2A_2,\ \overline{\rho}I=\rho_1I_1+\rho_2I_2\quad . \tag{2}$$

It should be noted that the small deformation hypothesis is part of the small disturbance hypothesis which is the combination of two hypotheses, namely the small deformation hypothesis and the small displacement hypothesis.

It is to be noted that N_1, N_2, M_1 and M_2 represent the axial forces and the bending moments for the two elements 1 and 2, respectively. In addition, the axial force *N* and the bending moment *M* of the entire section are assumed to be applied at the center of gravity of the solid composite section. Then, using the static equilibrium equations allows writing:

$$\begin{gathered} N=N_1+N_2=F \\ N_2=F-N_1 \\ M=M_1+M_2-N_1h+Ny_2 \end{gathered} \tag{3}$$

Furhermore, the sliding at the interface between the two elements 1 and 2 is taken into account. Figure 3 clearly depicts the normal force applied on each element, including the shear force produced by the shear connectors, as well as the two normal forces N_1 and N_2.

Hence, considering the equilibrium of forces in the axial direction helps to determine the shear force at the interface between the two elements as follows:

$$\frac{dN_1}{dx}=-\frac{dN_2}{dx}=-Q_s \tag{4}$$

The shear force Q_s between the two elements is then determined as:

$$Q_s=k_su_s \tag{5}$$

where u_s denotes the slip filed between the two elements, and k_s is stiffness of the shear connector.

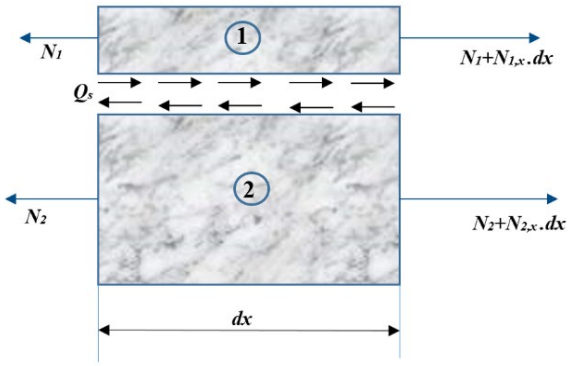

Figure 3 – Forces applied along the axial direction of the composite beam

Kinematics of the interlaminar slip field

Considering Figure 4, and according to Timoshenko's hypothesis, the interlaminar sliding field u_s between the materials of the composite beam is a function of the longitudinal displacements of each element and the overall rotation of the beam. It can be expressed in the following form:

$$u_s = u_2(x,y) - u_1(x,y) + h_1 \cdot \theta(x) + h_2 \cdot \theta(x)$$
$$u_s = u_2(x,y) - u_1(x,y) + h \cdot \theta(x) \quad (6)$$

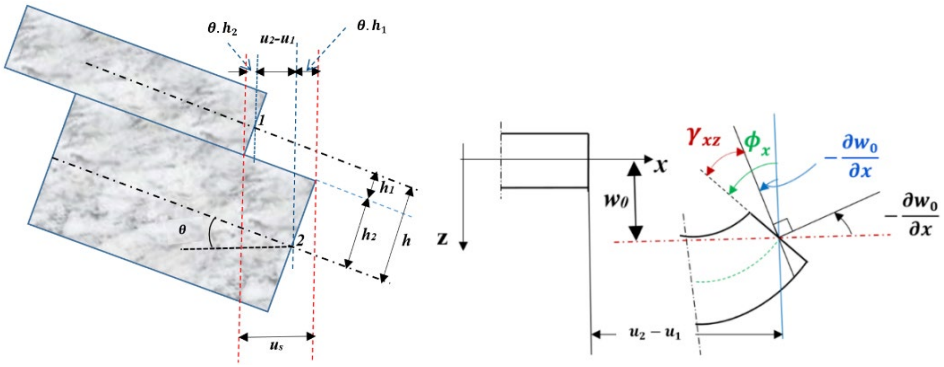

Figure 4 – Sliding diagram of the two elements, considering the Timoshenko beam theory

The interlayer shear strain may be determined by deriving equation 6 with respect to x, which gives:

$$\frac{du_s}{dx} = \frac{du_2(x,y)}{dx} - \frac{du_1(x,y)}{dx} + h \cdot \frac{d\theta(x)}{dx}$$
$$\frac{du_s}{dx} = \varepsilon_2 - \varepsilon_1 + h \cdot \frac{d\theta(x)}{dx} \quad (7)$$

where ε_1, and ε_2 are the normal deformations, in the x direction, with respect to the centers of gravity of elements 1 and 2, respectively. They can be determined as:

$$u_{1,x}=\varepsilon_1=\frac{N_1}{E_1A_1}, u_{2,x}=\varepsilon_2=\frac{N_2}{E_2A_2} \tag{8}$$

Furthermore, the Timoshenko beam theory may be used to express the bending moment as follows:

$$M_1=E_1I_1\frac{d\theta}{dx}, M_2=E_2I_2\frac{d\theta}{dx}, \overline{kGA}=k_1G_1A_1+k_2G_2A_2 \tag{9}$$

Here k_1 and k_2 are the coefficients of the shear connectors used in the beam under study. They depend on the shape of the cross section of the elements of the composite beam.

Then, deriving equation (6) with respect to x gives:

$$u_{s,x}=u_{2,x}-u_{1,x}+h\cdot\theta(x),_x \tag{10}$$

Likewise, deriving equation (5) with respect to x leads to:

$$Q_{s,x}=k_s\cdot u_{s,x} \tag{11}$$

Next, equation (8) is substituted into equation (11) to get:

$$Q_{s,x}=k_s\cdot\left(\frac{N_2}{E_2A_2}-\frac{N_1}{E_1A_1}+h\cdot\theta(x),_x\right) \tag{12}$$

After derivation and some substitutions, the following differential equation is then obtained:

$$\begin{aligned}
&N_{1,xx}=-N_{2,xx}=-Q_{s,x}\\
&N_{1,xx}=-k_s\cdot\left(\frac{F-N_1}{E_2A_2}-\frac{N_1}{E_1A_1}+h\cdot\theta(x),_x\right)\\
&N_{1,xx}-k_sN_1\left[\frac{1}{E_2A_2}+\frac{1}{E_1A_1}\right]=-k_s\cdot\left(\frac{F}{E_2A_2}+h\cdot\theta(x),_x\right)\\
&N_{1,xx}-k_sN_1\left[\frac{1}{E_2A_2}+\frac{1}{E_1A_1}\right]=-k_s\cdot\left(\frac{F}{E_2A_2}-h\cdot\frac{M+N_1h-Fy_2}{E_1I_1+E_2I_2}\right)\\
&N_{1,xx}-k_sN_1\left[\frac{1}{E_2A_2}+\frac{1}{E_1A_1}+\frac{h^2}{E_1I_1+E_2I_2}\right]=-k_s\cdot\left(\left(\frac{1}{E_2A_2}+\frac{hy_2}{E_1I_1+E_2I_2}\right)F-\frac{Mh}{E_1I_1+E_2I_2}\right)\\
&N_{1,xx}-\alpha^2N_1=\frac{k_sh}{E_1I_1+E_2I_2}\cdot M-k_s\left(\frac{1}{E_2A_2}+\frac{hy_2}{E_1I_1+E_2I_2}\right)F\\
&\frac{d^2N_1}{dx^2}-\alpha^2N_1=\frac{k_sh}{\sum E_iI_i}M-k_s\left(\frac{1}{E_2A_2}+\frac{hy_2}{\sum E_iI_i}\right)F
\end{aligned} \tag{13}$$

with

$$\theta(x),_x = -\frac{M_1}{E_1 I_1} = -\frac{M_2}{E_2 I_2} = -\frac{M + N_1 h - F y_2}{E_1 I_1 + E_2 I_2}$$

$$M_1 = -E_1 I_1 \cdot \theta(x),_x$$

$$M_2 = -E_2 I_2 \cdot \theta(x),_x$$

$$M = M_1 + M_2 - N_1 h + F y_2 = -(E_1 I_1 + E_2 I_2)\theta(x)_{,x} - N_1 h + F$$

$$\sum E_i I_i = E_1 I_1 + E_2 I_2 \tag{14}$$

where α is the connector shear parameter.

$$\alpha^2 = k_s \left[\frac{1}{E_2 A_2} + \frac{1}{E_1 A_1} + \frac{h^2}{E_1 I_1 + E_2 I_2} \right] = k_s \left(\frac{1}{E_2 A_2} + \frac{1}{E_2 A_2} + \frac{h^2}{\sum E_i I_i} \right) \tag{15}$$

Dynamic analysis using shear deformation theories

Timoshenko's first-order shear deformation theory

Consider a mixed beam that is composed of two elements. According to the Timoshenko hypothesis, there is a uniform shear and deformations due to transverse shear should not be neglected, which requires the introduction of a shear correction factor. In this case, the displacement field may be written in the following form:

$$\begin{cases} u_1(x,z) = u_{01} + z\theta(x) \\ u_2(x,z) = u_{02} + z\theta(x) \\ w(x,z) = w_0 \end{cases} \tag{16}$$

where u_{01}, u_{02} and w_0 are unknown displacements of the midplane of each element of the beam, and f(z) represents a shape function that describes the variation of transverse shear stresses and that of stresses through the beam thickness. The deformation relations are given by:

$$\begin{cases} \varepsilon_{xx1} = \dfrac{\partial u_1(x,z)}{\partial x} = u_{01,x} + z\theta_{,x} \\ \varepsilon_{xx2} = \dfrac{\partial u_2(x,z)}{\partial x} = u_{02,x} + z\theta_{,x} \\ \gamma_{xz1} = \gamma_{xz2} = \dfrac{\partial u_1(x,z)}{\partial z} + \dfrac{\partial w(x,z)}{\partial x} = \theta + w_{,x} \end{cases} \tag{17}$$

Equations of motion

The equations of motion are obtained using Hamilton's principle which is expressed as follows:

$$\int_{t_1}^{t_2} \left((\boldsymbol{\delta} T - \boldsymbol{\delta} U - \boldsymbol{\delta} U_s) \right) dt = 0 \tag{18}$$

Here δU is the variation of the virtual strain energy, δU_s is the variation of the strain energy of the connectors, and δT is the variation of the total kinetic energy.

The deformation energy of the beam is given by the following relation:

$$U = \frac{1}{2} \iiint \left(\sigma_{1xx}.\varepsilon_{1xx} + \sigma_{2xx}.\varepsilon_{2xx} + \tau_{1xz}.\gamma_{1xz} + \tau_{2xz}.\gamma_{2xz} \right) dxdydz = 0 \tag{19}$$

$$U = \frac{1}{2} \iiint \left(E_1 (\varepsilon_{1xx})^2 + E_2.(\varepsilon_{2xx})^2 + G_1.\left(\gamma_{1xz}\right)^2 + G_2.\left(\gamma_{2xz}\right)^2 \right) dxdydz = 0 \tag{20}$$

with

$$\sigma_{xx} = E.\varepsilon_{xx} \quad et \quad \tau_{xz} = G\gamma_{xz}$$

$$\begin{aligned} U = \frac{1}{2} \iiint \Big(\Big(& E_1 \left(u_{01,x} + z\theta_{,x}\right)^2 + E_2.\left(u_{02,x} + z\theta_{,x}\right)^2 \\ & + G_1.\left(w_{,x} + \theta\right)^2 + G_2.\left(w_{,x} + \theta\ \right)^2 \Big) \Big) dxdydz \end{aligned} \tag{21}$$

Hence, minimization of the strain energy allows writing:

$$\begin{aligned} \delta U = & -\int \left(E_1 A_1 \delta u_{01,x}.u_{01,x} + E_1 I_1.\theta_{,x}.\delta\theta_{,x} \right) dx \\ & - \int \left(E_2 A_2.u_{02,x} \delta u_{02,x} + E_2 I_2.\theta_{,x}.\delta\theta_{,x} \right) dx \\ & + \int KGA^1 \left(\theta + w_{,x}\right)\left(\delta\theta + \delta w_{,x}\right) dx \\ & + \int KGA^2 \left(\theta + w_{,x}\right)\left(\delta\theta + \delta w_{,x}\right) dx \end{aligned} \tag{22}$$

with

$$\iint E_1 dydz = E_1 A_1,\ \iint E_2 dydz = E_2 A_2,\ \iint E_1 z^2 dydz = E_1 I_1,\ \iint E_2 z^2 dydz = E_2 I_2 \tag{23}$$

where *K* is a shear correction factor used for transverse shear stress correction. The deformation energy due to the interlaminar sliding of the layers of the composite beam is given by the following relation (Type I slip field):

$$U_s=\frac{1}{2}\int K_s(u_{02}\text{-}u_{01}\text{-}h\theta)^2 dx \tag{24}$$

After minimization, the following expression is then obtained:

$$\delta U_s = \int K_S(u_{02}\text{-}u_{01}\text{-}h\theta)(\delta u_{02}\text{-}\delta u_{01}\text{-}h\delta\theta)dx \tag{25}$$

The kinetic energy of the composite beam under study is then given as:

$$T = \frac{1}{2}\int m\dot{w}^2 dx=\frac{1}{2}\int (m_1+m_2)\dot{w}^2 dx \tag{26}$$

After minimization, the kinetic energy then becomes:

$$\boldsymbol{\delta} T=\int (m_1+m_2)\dot{w}\,\delta\dot{w}dx \tag{27}$$

Subsequently, substituting equations 22, 25 and 27 into equation (18) gives the following equilibrium equations:

$$\begin{aligned}\iiint (\boldsymbol{\delta}T\text{-}\boldsymbol{\delta}U\text{-}\boldsymbol{\delta}U_s)\,dt=&\iint (m_1+m_2)w\,\delta\dot{w}dxdt\\ -\int &\left(E_1A_1\delta u_{01,x}.u_{01,x}+E_1I_1.\theta_{,x}.\delta\theta_{,x}\right)dxdy\\ -\int &\left(E_2A_2.u_{02,x}\delta u_{02,x}+E_2I_2.\theta_{,x}.\delta\theta_{,x}\right)dxdy\\ +\int &KGA^1\left(\theta+w_{,x}\right)\left(\delta\theta+\delta w_{,x}\right)dxdt\\ +\int &KGA^2\left(\theta+w_{,x}\right)\left(\delta\theta+\delta w_{,x}\right)dxdt\\ -\int &K_S(u_{02}\text{-}u_{01}\text{-}h\theta)\,(\delta u_{02}\text{-}\delta u_{01}\text{-}h\delta\theta)dxdt\end{aligned} \tag{28}$$

Afterwards, integration by part allows obtaining the system of differential equations describing the free vibration motion of a mixed Timoshenko beam:

$$\begin{aligned}eq1=&\ E_2A_2\left(\frac{\partial^2}{\partial x^2}u_{02}(x)\right)\text{-}K_S\left(u_{02}(x)\text{-}u_{01}(x)+h\theta(x)\right)\\ eq2=&E_1A_1\left(\frac{\partial^2}{\partial x^2}u_{01}(x)\right)+K_S\left(u_{02}(x)\text{-}u_{01}(x)+h\theta(x)\right)\\ eq3=&\ (E_1I_1+E_2I_2)\left(\frac{\partial^2}{\partial x^2}\theta(x)\right)\text{-}(K_1G_1A_1+K_2G_2A_2)\left(\frac{\partial}{\partial x}w(x,t)+\theta(x)\right)\end{aligned} \tag{29}$$

$$+K_S h\left(u_{02}(x)\text{-}u_{01}(x)+h\theta(x)\right)$$

$$eq4 = (K_1G_1A_1+K_2G_2A_2)\left(\frac{\partial^2}{\partial x^2}w(x,t)+\frac{\partial}{\partial x}\theta(x)\right)\text{-}m\omega^2 w(x,t)$$

High order shear deformation theory

Unlike the classical theory and the Timoshenko theory, which are both based on the linear distribution of displacement through the beam thickness, the high order theory is based on a nonlinear distribution of fields through the thickness. For this reason, it was deemed necessary to take into account the effects of the transverse shear strain and the transverse normal strain. It should be noted that the models considered do not require a correction factor. This theory is more precise than the first order theory as it introduces a function that takes into account the warping phenomenon. The present study takes into account the warping effect which uses a new transverse deformation function and can be written in the following form:

$$\begin{cases} U_1(x,z,t)=u_1(x,t)\text{-}z\dfrac{\partial}{\partial x}w(x,t)+f(z).\theta_1(x,t) \\ U_2(x,z,t)=u_2(x,t)\text{-}z\dfrac{\partial}{\partial x}w(x,t)+f(z).\theta_2(x,t) \\ W(x,z,t)=w(x,t) \end{cases} \tag{30}$$

Substituting the strain energy into equation (19) gives:

$$U=\frac{1}{2}\left(\int_{-\frac{h_1}{2}}^{\frac{h_1}{2}}E_1b_1\left(\frac{\partial U_1(x,z,t)}{\partial x}\right)^2dz+\int_{-\frac{h_2}{2}}^{\frac{h_2}{2}}E_2b_2\left(\frac{\partial U_2x,z,t)}{\partial x}\right)^2dz\right.$$
$$\left.+\int_{-\frac{h_1}{2}}^{\frac{h_1}{2}}K_1G_1b_1\left(\frac{\partial U_1(x,z,t)}{\partial z}\right)^2dz+\int_{-\frac{h_2}{2}}^{\frac{h_2}{2}}K_2G_2b_2\left(\frac{\partial U_2(x,z,t)}{\partial z}\right)^2dz\right)dx \tag{31}$$

$$U=\frac{1}{2}\left(\int_{-\frac{h1}{2}}^{\frac{h1}{2}}E_1b_1\left(\frac{\partial}{\partial x}u_1(x,t)\text{-}z\frac{\partial^2}{\partial x^2}w(x,t)+f(z)\frac{\partial}{\partial x}\theta_1(x,t)\right)^2dz\right.$$
$$\left.+\int_{-\frac{h2}{2}}^{\frac{h2}{2}}E_2b_2\left(\frac{\partial}{\partial x}u_2(x,t)\text{-}z\frac{\partial^2}{\partial x^2}w(x,t)+f(z)\frac{\partial}{\partial x}\theta_2(x,t)\right)^2dz\right) \tag{32}$$

$$+\int_{-\frac{h1}{2}}^{\frac{h1}{2}} k_1 b_1 G_1 \left(-\frac{\partial}{\partial x} w(x,t) + \left(\frac{d}{dz} f(z) \right) \theta_1(x,t) \right)^2 dz$$

$$+\int_{-\frac{h2}{2}}^{\frac{h2}{2}} k_2 b_2 G_2 \left(-\frac{\partial}{\partial x} w(x,t) + \left(\frac{d}{dz} f(z) \right) \theta_2(x,t) \right)^2 dz \Bigg) dx$$

The present theory is based on a new interlaminar slip field that was initially developed by N. Elmeiche, I. Mechab, and F. Bernard. This field takes into account the longitudinal sliding of the two elements of the composite beam, the rotating sliding, and the sliding that is due to the transverse warping of the beam (new type II slip field):

$$U_s = \int \frac{1}{2} k_s \Bigg(u_2(x) - u_1(x) - \frac{h_1}{2}.\theta_1(x) - \frac{h_2}{2}.\theta_2(x) - \left(f(z)|_{z=\frac{h_1}{2}} \right) . \left(\frac{\partial W(x,z,t)}{\partial x} + \theta_1(x) \right) - \left(f(z)|_{z=\frac{h_2}{2}} \right) \cdot \left(\frac{\partial W(x,z,t)}{\partial x} + \theta_2(x) \right) \Bigg)^2 dx \tag{33}$$

In addition, the kinetic energy along the three directions, with the rotational inertia (RT), can be expressed in the form:

$$T = \frac{1}{2} \int \left(\omega^2 . \left(b_1.\rho_1.\left(U_1(x,z,t) \right)^2 + \left(b_2.\rho_2.\left(U_2(x,z,t) \right)^2 + \left(b_1.\rho_1 + b_2.\rho_2 \right).(W(x,z,t))^2 \right) dz \right) dx \tag{34}$$

$$T = \frac{1}{2} \int \Bigg(\omega^2 b_1 u_1(x,t)^2 \left(\int \rho_1 dz \right) - \omega^2 b_1 u_1(x,t) \left(\frac{\partial}{\partial x} w(x,t) \right) \left(\int \rho_1 z dz \right) + \omega^2 b_1 u_1(x,t) \theta_1(x,t) \int \rho_1 f(z)\, dz + \frac{1}{2} \omega^2 b_1 \left(\frac{\partial}{\partial x} w(x,t) \right)^2 \left(\int \rho_1 z^2 dz \right) b_1 \left(\frac{\partial}{\partial x} w(x,t) \right) \theta_1(x,t) \left(\int \rho_1 z f(z) dz \right) + \frac{1}{2} \omega^2 b_1\, \theta_1(x,t)^2 \left(\int \rho_1 f(z)^2 dz \right) + \frac{1}{2} b_2 u_2(x,t)^2 \left(\int \rho_2 dz \right) - \omega^2 b_2\, u_2(x,t) \left(\frac{\partial}{\partial x} w(x,t) \right) \left(\int \rho_2 z dz \right) + b_2 u_2(x,t) \theta_2(x,y) \left(\int \rho_2 f(z) dz \right) + \frac{1}{2} \omega^2 b_2 \left(\frac{\partial}{\partial x} w(x,t) \right)^2 \left(\int \rho_2 z^2 dz \right) \tag{35}$$

$$-b_2\left(\frac{\partial}{\partial x}w(x,t)\right)\theta_2(x,t)\left(\int\rho_2 zf(z)dz\right)+\frac{1}{2}\omega^2 b_2\theta_2(x,t)^2\left(\int\rho_2 f(z)^2dz\right)$$
$$+\frac{1}{2}b_1\, w(x,t)^2\left(\int\rho_1 dz\right)+\frac{1}{2}\omega^2 b_2 w(x,t)^2\left(\int\rho_2 dz\right)\Bigg)dx$$

with

$$\begin{cases} I_{11}, I_{21}, I_{31} = \int_{-\frac{h1}{2}}^{\frac{h1}{2}}\{1, z, z^2\}\rho_1\, dz \\ I_{12}, I_{22}, I_{32} = \int_{-\frac{h2}{2}}^{\frac{h2}{2}}\{1, z, z^2\}\rho_2\, dz \\ I_{41}, I_{51}, I_{61} = \int_{-\frac{h1}{2}}^{\frac{h1}{2}}\{1, z, z^2\}\rho_1 \cdot f(z)dz \\ I_{42}, I_{52}, I_{62} = \int_{-\frac{h2}{2}}^{\frac{h2}{2}}\{1, z, f(z)\}\rho_2 \cdot f(z)dz \end{cases} \tag{36}$$

The new warping shape function, previously developed by N. Elmeiche and I. Mechab, gives:

$$f(z) = z+\frac{1}{6}\frac{z^3}{\left(cos\left(\frac{1}{2}\right)-1\right)H^2} \tag{37}$$

Static analysis using shear deformation theories

The composite beam is subjected to a uniformly distributed bending load. The work of the external force is then given as:

$$E_{we}=\frac{1}{2}\int q\cdot\left(W(x,z,t)\right)^2 dx \tag{38}$$

Using the displacement field expressed in equation 30 allows writing the total energy of the composite beam as:

$$Eq=E_{we}-U-U_s =$$
$$\frac{1}{2}\left(\int_{-\frac{h1}{2}}^{\frac{h1}{2}} E_1 b_1\left(\frac{\partial}{\partial x}u_1(x,t)-z\frac{\partial^2}{\partial x^2}w(x,t)+f(z)\frac{\partial}{\partial x}\theta_1(x,t)\right)^2 dz\right. \tag{39}$$

$$+\int_{-\frac{h2}{2}}^{\frac{h2}{2}} E_2 b_2 \left(\frac{\partial}{\partial x}u_2(x,t)-z\frac{\partial^2}{\partial x^2}w(x,t)+f(z)\frac{\partial}{\partial x}\theta_2(x,t)\right)^2 dz$$

$$+\int_{-\frac{h1}{2}}^{\frac{h1}{2}} k_1 b_1 G_1 \left(-\frac{\partial}{\partial x}w(x,t)+(\frac{d}{dz}f(z))\theta_1(x,t)\right)^2 dz$$

$$+\int_{-\frac{h2}{2}}^{\frac{h2}{2}} k_2 b_2 G_2 \left(-\frac{\partial}{\partial x}w(x,t)+(\frac{d}{dz}f(z))\theta_2(x,t)\right)^2 dz\Bigg)dx$$

$$+\frac{1}{2}\int k_s \left(u_2(x)-u_1(x)-\frac{h_1}{2}.\theta_1(x)-\frac{h_2}{2}.\theta_2(x)-\left(f(z)|_{z=\frac{h_1}{2}}\right)\right.$$

$$\left.\cdot\left(\frac{\partial W(x,z,t)}{\partial x}+\theta_1(x)\right)-\left(f(z)|_{z=\frac{h_2}{2}}\right)\cdot\left(\frac{\partial W(x,z,t)}{\partial x}+\theta_2(x)\right)\right)^2 dx$$

$$+\frac{1}{2}\int q\big(W(x,z,t)\big)^2 dx$$

Numerical solution by the Ritz method

Consider a simply supported composite beam of the length L. The numerical resolution of the problem, using the Ritz method, consists of minimizing the total energy related to the amplitudes of the displacement and rotation fields:

$$\begin{cases} u_1(x)=\sum_{i=0}^{n}\left[U_{1i}.\left(\frac{x}{L}\right)^i.\left(\frac{x}{L}-1\right)\right] \\ u_2(x)=\sum_{i=0}^{n}\left[U_{2i}.\left(\frac{x}{L}\right)^i.\left(\frac{x}{L}-1\right)\right] \\ \theta_1(x)=\sum_{i=0}^{n}\left[\theta_{1i}.\left(\frac{x}{L}\right)^i.\left(\frac{x}{L}-1\right)\right] \\ \theta_2(x)=\sum_{i=0}^{n}\left[\theta_{2i}.\left(\frac{x}{L}\right)^i.\left(\frac{x}{L}-1\right)\right] \\ w(x)=\sum_{i=0}^{n}\left[W_i.\left(\frac{x}{L}\right)^i.\left(\frac{x}{L}-1\right)\right] \end{cases} \quad (40)$$

After the substitution and the minimization of the Ritz solutions in equations 32 - 36, a square matrix of the dimension 5.(n+1).5.(n+1) may then be obtained in the following form (see Appendix):

$$\begin{pmatrix} [A_{11}][A_{12}][A_{13}][A_{14}][A_{15}]_i \\ [A_{21}][A_{22}][A_{23}][A_{24}][A_{25}]_i \\ [A_{31}][A_{32}][A_{33}][A_{34}][A_{35}]_i \\ [A_{41}][A_{42}][A_{43}][A_{44}][A_{45}]_i \\ [A_{51}][A_{52}][A_{53}][A_{54}][A_{55}]_i \end{pmatrix}_{i=0..n} \cdot \begin{Bmatrix} \{U_{1i}\} \\ \{U_{2i}\} \\ \{\theta_{1i}\} \\ \{\theta_{2i}\} \\ \{W_i\} \end{Bmatrix}_{i=0..n} = \begin{Bmatrix} \{0_i\} \\ \{0_i\} \\ \{0_i\} \\ \{0_i\} \\ \{0_i\} \end{Bmatrix}_{i=0..n} \tag{41}$$

In dynamics, the determinant of the system of equations gives the natural vibration frequencies:

$$\omega^2 = det[A] \tag{42}$$

Digital application

The numerical calculation of the natural frequency of vibration and the interlaminar shear force of two types of simply supported composite beams with a partial connection between the materials was carried out. The first composite beam is made of concrete-wood materials, with a T-shaped cross section. It is composed of a concrete slab, rectangular in shape in its upper part, while the lower part is made of wood.

The other composite beam has an I-shaped cross section. It is made of a concrete slab, rectangular in shape in its upper part, while the lower part has a HEA steel profile in the form of the capital letter I. The properties of each composite beam are presented in Figure 5.

Furthermore, a validation study of the ten free vibration frequencies was carried out using the first order shear deformation theory of the composite beam made of concrete-wood materials. The results, depicted in Table 1, were verified and then compared with those reported in the work of Xu & Wu (2008). In this study, a shear correction factor equal to 5/6 was used. The relative frequency error, for all modes, did not exceed 0.37%, which means that the frequency values found in the present work are in good agreement with those reported in the literature.

E_1=12GPa, E_2 =8GPa, G_1=5GPa, G_2 =3GPa, m_1 =34.5kg, m_2 = 5.25kg, Ksc= 50MPa

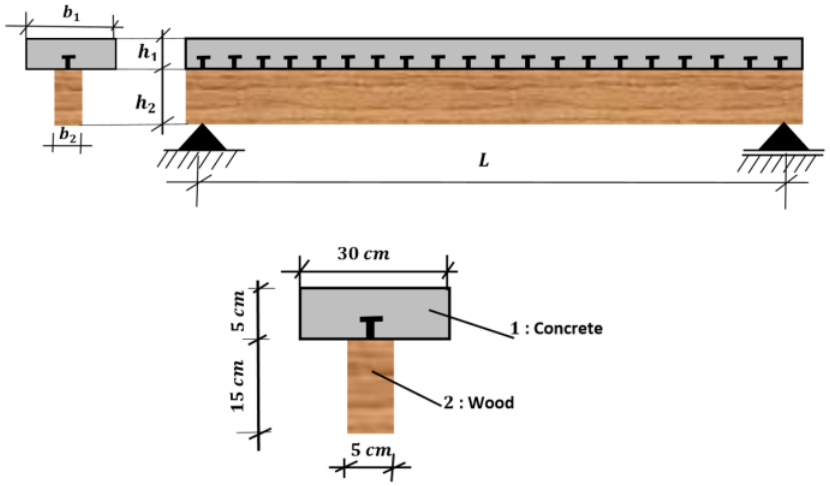

(a)

HEA 200 SIS 1312	b_1=1.5 m	r =0.145 m	K= 0.20	E_1I_1 =1.06	α = 0.901 m^{-1}
A_2 =5.383 x 10^{-3} m^2	b_2 =0.2 m	r_1 = 0.050 m	E_1 =8.5 [a]	E_2I_2 =7.75	EI_0/EI_∞=0.412
I_2= 3.692x10^{-5} m^2	h_1 =0.10 m	r_2 = 0.095 m	E_2 =210	EI_0=8.81	αL =5.40 for L =6m
t_{flange}=0.010 m	h_2 =0.19 m	$z_{cg,\infty}$= 0.0681m	E_1A_1 =1275	EI_∞=21.4	
t_{web} = 0.0065 m			E_2A_2 =1130	EI_{eff}=15.7 for L = 6m	
			EA_0=2405	And μ= 1	

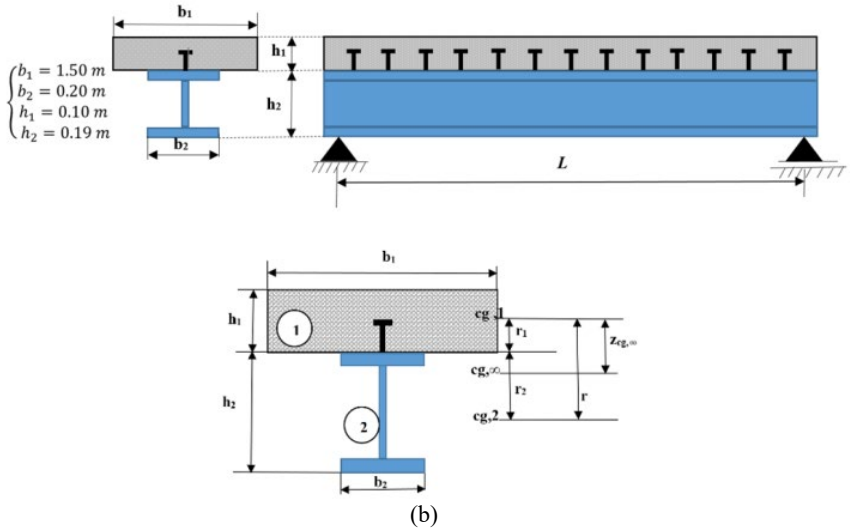

(b)

Figure 5 – Types of the beams under study:(a) Mixed beam in concrete-wood materials (materials I);(b) composite beam in steel-concrete materials (materials II)

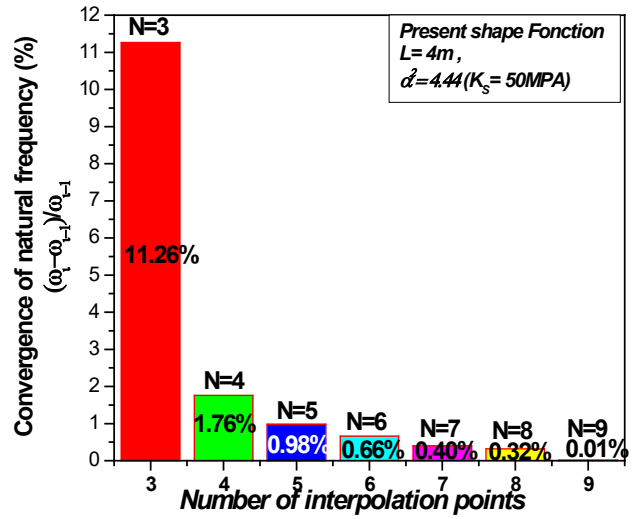

Figure 6 – Convergence test of the vibration frequency for the composite beam I

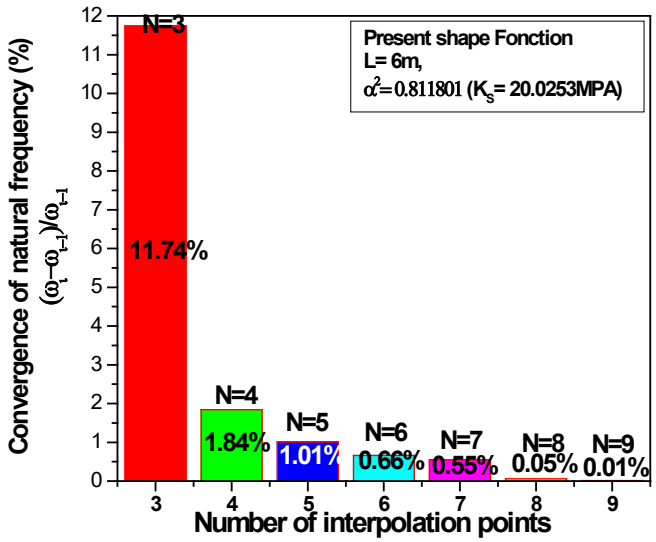

Figure 7 – Convergence test of the vibration frequency for the composite beam II

Table 1 – First ten vibration frequencies (Hz) of the composite beam made of material I with a sliding field of type I

L/H	Mode	Present	Xu & Wu (2008)		Relative error %
			Exact	DQM	
20	1	10.2787	10.2768	10.3023	0.02
	2	33.1627	33.1771	33.3569	0.04
	3	65.2411	65.3343	65.8811	0.14
	4	107.0528	107.3095	108.6140	0.24
	5	158.6972	159.2021	161.9071	0.32
	6	219.8142	220.6233	225.6710	0.37
	7	289.8239	290.9092	299.5853	0.37
	8	368.0599	369.2557	383.2073	0.32
	9	453.8387	454.7913	476.0263	0.21
	10	546.5014	546.6124	577.4941	0.02

Table 2 – Natural frequency of the composite beam made of concrete and wood materials as a function of the shear parameter α2 of the connectors, with shear deformation (SD) and rotary inertia (RI), for a type II slip field

Number of interpolation N=9,Present with (SD and RI)								
L/H=5					L/H=10			
Theories	**PSDBT**	**HSDBT**	**Present**	**Error**	**PSDBT**	**HSDBT**	**Present**	**Error**
α^2								
10^{-3}	79.159	80.461	81.070	0.76%	39.330	39.939	40.248	0.77%
10^{-2}	79.186	80.489	81.097	0.76%	39.344	39.953	40.261	0.77%
10^{-1}	79.462	80.760	81.363	0.75%	39.484	40.090	40.395	0.76%
1	82.095	83.390	83.906	0.62%	40.752	41.336	41.607	0.66%
10	101.394	102.504	102.664	0.16%	48.564	49.025	48.885	0.29%
50	140.572	141.081	141.127	0.03%	58.094	58.404	58.656	0.43%
10^2	160.831	160.992	161.128	0.08%	61.399	61.667	61.877	0.34%
$5.5.10^2$	194.117	194.142	194.099	0.02%	65.130	65.349	65.549	0.31%
10^3	199.265	199.229	199.203	0.01%	65.575	65.790	65.989	0.30%
$5.5.10^3$	205.015	204.911	204.193	0.35%	66.041	66.253	66.455	0.30%
10^4	205.676	205.559	205.57	0.01%	66.094	66.304	66.506	0.30%

Number of interpolation N=9, Present with (SD and RI)	
L/H=15	L/H=20

Theories	PSDBT	HSDBT	Present	Error	PSDBT	HSDBT	Present	Error
α^2								
10^{-3}	25.887	26.516	26.757	0.91%	19.499	19.884	20.010	0.63%
10^{-2}	25.897	26.526	26.766	0.90%	19.506	19.890	20.016	0.63%
10^{-1}	25.994	26.615	26.854	0.90%	19.574	19.957	20.082	0.63%
1	26.811	27.377	27.603	0.83%	20.109	20.483	20.597	0.56%
10	30.670	31.056	31.240	0.59%	22.227	22.539	22.641	0.45%
50	34.142	34.410	34.595	0.54%	23.707	23.948	24.089	0.59%
10^2	35.002	35.248	35.440	0.54%	24.029	24.254	24.410	0.64%
$5.5.10^2$	35.867	36.091	36.291	0.55%	24.341	24.549	24.718	0.69%
10^3	35.961	36.185	36.385	0.55%	24.374	24.582	24.751	0.69%
10^{-3}	36.060	36.292	36.482	0.52%	24.408	24.616	24.785	0.69%

Table 3 – Natural frequency of the composite beam made of concrete and steel materials as a function of the shear parameter α2 of the connectors, with shear deformation (SD) and rotary inertia (RI), for a type II slip field

Number of interpolation N=9, Present with (SD and RI)								
L/H=5					L/H=10			
Theories	**PSDBT**	**HSDBT**	**Present**	**Error**	**PSDBT**	**HSDBT**	**Present**	**Error**
α^2								
10^{-3}	29.468	29.956	30.153	0.66%	13.804	14.103	14.124	0.15%
10^{-2}	29.589	30.075	30.271	0.65%	13.868	14.167	14.186	0.13%
10^{-1}	30.772	31.234	31.420	0.60%	14.484	14.786	14.784	0.01%
1	40.241	40.566	40.686	0.30%	19.982	19.304	19.182	0.63%
10	79.833	80.132	79.876	0.32%	33.475	33.485	33.305	0.54%
50	122.680	123.310	122.502	0.66%	42.668	42.665	42.644	0.05%
10^2	136.870	136.326	136.530	0.15%	44.629	44.616	44.596	0.04%
$5.5.10^2$	153.651	153.362	153.268	0.06%	46.496	46.478	46.454	0.05%
10^3	155.769	155.467	155.370	0.06%	46.706	46.691	46.661	0.06%
$5.5.10^3$	158.435	157.983	158.739	0.48%	46.989	46.962	46.895	0.14%
10^4	159.121	158.748	159.133	0.24%	47.065	47.029	47.027	0.00%

Number of interpolation N=9, Present with (SD and RI)	
L/H=15	L/H=20

Theories	PSDBT	HSDBT	Present	Error	PSDBT	HSDBT	Present	Error
α^2								
10^{-3}	9.029	9.179	9.235	0.61%	6.715	6.839	6.870	0.45%
10^{-2}	9.073	9.222	9.277	0.60%	6.748	6.871	6.902	0.45%
10^{-1}	9.481	9.623	9.675	0.54%	7.048	7.167	7.195	0.39%
1	12.214	12.324	12.348	0.19%	8.889	8.990	9.000	0.11%
10	19.039	19.110	19.083	0.14%	12.469	12.582	12.557	0.20%
50	21.898	21.921	21.919	0.01%	13.587	13.620	13.645	0.18%
10^2	22.391	22.417	22.408	0.04%	13.756	13.791	13.809	0.13%
$5.5.10^2$	22.829	22.851	22.881	0.13%	13.903	13.939	13.951	0.09%
10^3	22.867	22.887	22.914	0.12%	13.919	13.955	13.967	0.09%
$5.5.10^3$	22.936	22.959	22.968	0.04%	13.939	13.977	13.987	0.07%
10^{-3}	22.952	23.010	22.984	0.11%	13.944	13.956	13.992	0.26%

Tables 2 and 3 present the variation of the natural vibration frequencies of the composite beam in concrete-wood and concrete-steel materials as a function of the shear parameter of the connectors with transverse shear deformation (SD) and rotational inertia (RI). The results of the present theory with a new warping shape function (equation 37) were then recorded and compared with those given by the parabolic shear strain beam theory (PSDBT) and the hyperbolic shear strain beam theory (HSDBT). For the different slenderness values of the two types of beams, the relative error did not exceed 0.91% for the beam in material I and 0.66% for the beam in material II. The results obtained for the two types of beams are in good agreement. This is certainly due to the perfect convergence of the Ritz method and the new shear strain function.

The dynamic analysis of the natural frequency of vibrations with transverse shear deformation (SD) and rotational inertia (RI) of the composite beam made of concrete-wood materials and concrete-steel materials is presented in Figures 8 and 9. The values of the connector shear parameter α^2 are given by a logarithmic scale with the new interlaminar slip field (type II slip field). The frequency is stationary for low connector parameter values, i.e., α^2 between 10^{-3} and 10^{-1}. This frequency gradually increases while exhibiting a non-linear behavior, and the deviation point of the curves is observed at $\alpha^2 = 10$. In addition, the difference between the maximum frequency, which corresponds to $\alpha^2 = 10^4$, and the frequency that corresponds to $\alpha^2 = 10$ and which is considered

as the point of deviation of the curves, varies from 55.33% to 1.42% for type I material and from 52.46% to 8.24% for type II material. The maximum deviation is obtained with the short composite beam (L/H = 5) and the minimum deviation is observed with the slender composite beam (L/H = 20). The nonlinear behavior of the beam is due to the fact that the significant effects of transverse shear and warping of the short composite beam, for type I and II materials, are taken into account.

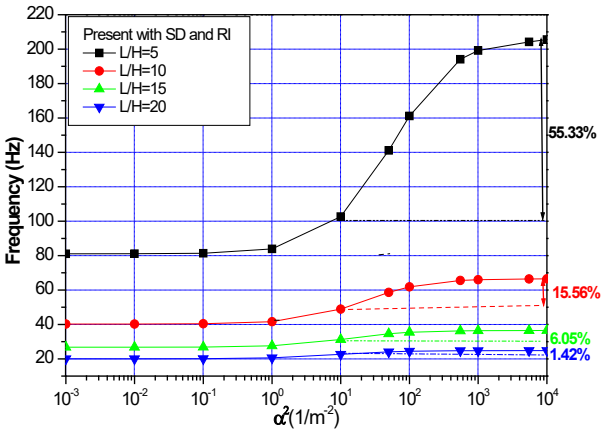

Figure 8 – Variation of the natural frequency of the composite beam made of concrete and wood materials as a function of the shear parameter α^2 of the connectors, for a type II slip field

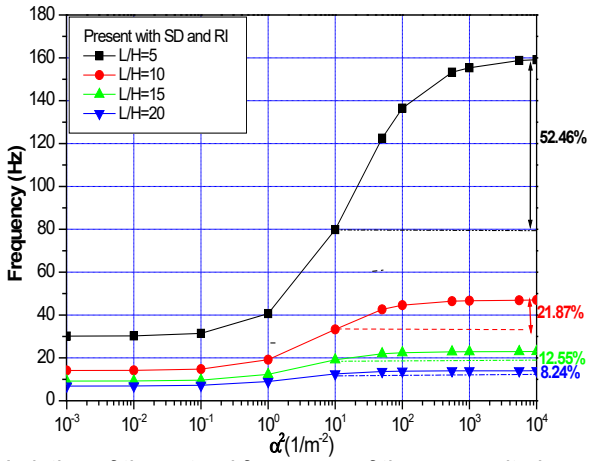

Figure 9 – Variation of the natural frequency of the composite beam made of concrete and steel materials as a function of the shear parameter α^2 of the connectors, for a type II slip field

Analysis of bending

The static analysis is based on the numerical calculation of the bending of the two composite beams made with materials I and II. The two beams are simply supported and are subjected to a uniformly distributed load, with q = 15 KN/m and q = 4 KN/m, respectively. Figures 9 and 10 illustrate the variation of the interlaminar shear force as a function of the shear coefficient of the connectors.

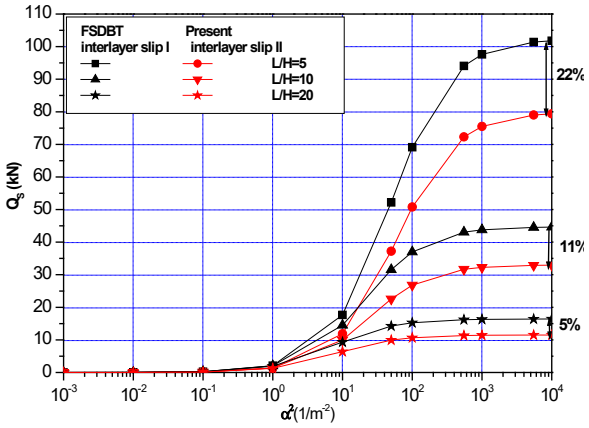

Figure 10 – Variation of the interlaminar shear force Q_s for the composite beam made of steel-concrete materials

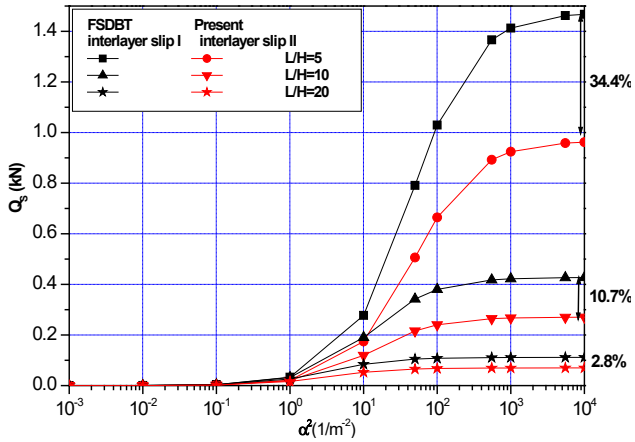

Figure 11 – Variation of the interlaminar shear force Q_s for the composite beam made of concrete-wood materials

Figures 10 and 11 show the variation of the interlaminar shear force for the two materials I and II, with two interlaminar slip fields, i.e., a classic sliding field of the Timoshenko beam, and a new sliding field proposed using the higher order theory. The deviation of the interlaminar shear force, for the two slip fields, varies from 22% to 11%, and to 5%, respectively, for the beams of material I with the slenderness (L/H) equal to 5, 10 and 20. The deviation of the interlaminar shear force for the two slip fields varies from 34% to 10.7% and to 2.8%, respectively, for the beams of material II with the slenderness (L/H) equal to 5, 10 and 20. These findings suggest that the introduction of the warping effect into the new interlaminar slip field of a composite beam is significantly important, which is not the case for the slender beam because in this case the transverse shear and the warping effects are negligible. Based on the above, it can be said that the composite beam behaves like an Euler-Bernoulli beam.

Conclusion

The present study primarily focused on the detailed investigation of the dynamic part and the static part of a composite beam that was analyzed using different theories. A new interlaminar slip field of a composite beam was then introduced in the method used. This field accounts for the warping effect with a new transverse shear strain shape function. The equations of motion were deduced and solved using the Ritz numerical method, while considering two different types of composite beams, i.e., a composite beam made of steel and wood materials and another made of steel and concrete materials. The numerical results obtained were compared with those found in the literature. These results were also compared with others obtained from deformation theories. It was found that the free frequency of vibration with transverse deformation shear and rotational inertia of the two composite beams in steel-wood and steel-concrete materials with a new interlaminar slip field was quite significant for the short beam but not very important for the long beam.

A similar remark was made for the static case of the interlaminar shear force. This was primarily due to the introduction of the new shear strain shape function in the equilibrium equations and in the new interlaminar slip field. These findings describe quite well the behavior of composite beams with cross-sectional warping. Furthermore, it turned out that the proposed sliding model can be employed in characterizing the real behavior of short composite beams undergoing small and large deformations.

Appendix

$$[A] = \begin{pmatrix} [A_{11}][A_{12}][A_{13}][A_{14}][A_{15}]_i \\ [A_{21}][A_{22}][A_{23}][A_{24}][A_{25}]_i \\ [A_{31}][A_{32}][A_{33}][A_{34}][A_{35}]_i \\ [A_{41}][A_{42}][A_{43}][A_{44}][A_{45}]_i \\ [A_{51}][A_{52}][A_{53}][A_{54}][A_{55}]_i \end{pmatrix} \tag{43}$$

$$[A_{11}]=[A_{12}]=[A_{21}]=[A_{13}]=[A_{31}]=[A_{14}]=[A_{41}]=[A_{15}]=[A_{51}]=\begin{bmatrix} \frac{d}{dU1_0}E_q & \cdots & \frac{d}{dU1_0}E_q \\ \vdots & \ddots & \vdots \\ \frac{d}{dU1_i}E_q & \cdots & \frac{d}{dU1_i}E_q \end{bmatrix}_{i=0..9}$$

$$[A_{22}]=[A_{23}]=[A_{32}]=[A_{24}]=[A_{42}]=[A_{25}]=[A_{52}]=\begin{bmatrix} \frac{d}{dU2_0}E_q & \cdots & \frac{d}{dU2_0}E_q \\ \vdots & \ddots & \vdots \\ \frac{d}{dU2_i}E_q & \cdots & \frac{d}{dU2_i}E_q \end{bmatrix}_{i=0..9}$$

$$[A_{33}]=[A_{34}]=[A_{43}]=[A_{35}]=[A_{53}]=\begin{bmatrix} \frac{d}{d\theta 1_0}E_q & \cdots & \frac{d}{d\theta 1_0}E_q \\ \vdots & \ddots & \vdots \\ \frac{d}{d\theta 1_i}E_q & \cdots & \frac{d}{d\theta 1_i}E_q \end{bmatrix}_{i=0..9}$$

$$[A_{44}]=[A_{45}]=[A_{54}]=\begin{bmatrix} \frac{d}{d\theta 2_0}E_q & \cdots & \frac{d}{d\theta 2_0}E_q \\ \vdots & \ddots & \vdots \\ \frac{d}{d\theta 2_i}E_q & \cdots & \frac{d}{d\theta 2_i}E_q \end{bmatrix}_{i=0..9}$$

$$[A_{55}]=\begin{bmatrix} \frac{d}{dW_0}E_q & \cdots & \frac{d}{dW_0}E_q \\ \vdots & \ddots & \vdots \\ \frac{d}{dW_i}E_q & \cdots & \frac{d}{dW_i}E_q \end{bmatrix}_{i=0..9} \tag{44}$$

References

Adam, C. & Furtmüller, T. 2020. Flexural vibrations of geometrically nonlinear composite beams with interlayer slip. *Acta Mechanica,* 231, pp.251-271. Available at: https://doi.org/10.1007/s00707-019-02528-2.

Barbosa, W.C.S., Bezerra, L.M., Chater, L. & Cavalcante, O.R.O. 2019. Experimental evaluation on the structural behavior of truss shear connectors in composite steel-concrete beams. *Revista IBRACON de Estruturas e Materiais,* 12(5), pp.1157-1182. Available at: https://doi.org/10.1590/S1983-41952019000500010.

Carvalho, T.A., Lemes, Í.J.M., Silveira, R.A.M., Dias, L.E.S. & Barros, R.C. 2021. Concentrated Approaches for Nonlinear Analysis of Composite Beams with Partial Interaction. *ce/papers,* 4(2-4), pp.715-722. Available at: https://doi.org/10.1002/cepa.1353.

Castel, A. 2013. *Comportement vibratoire de structures composites intégrant des éléments amortissants.* PhD thesis. Nevers, France: Université de Bourgogne, École doctorale Sciences pour l'ingénieur et microtechniques, Département de Recherche en Ingénierie des Véhicules pour l'Environnement (DRIVE) [online]. Available at: https://www.sudoc.fr/177960620 [Accessed: 06 December 2024].

Čas, B., Planinc, I. & Schnabl, S. 2018. Analytical solution of three-dimensional two-layer composite beam with interlayer slips. *Engineering Structures,* 173, pp.269-282. Available at: https://doi.org/10.1016/j.engstruct.2018.06.108.

Della Croce, L. & Venini, P. 2004. Finite elements for functionally graded Reissner–Mindlin plates. *Computer Methods in Applied Mechanics and Engineering,* 193(9-11), pp.705-725. Available at: https://doi.org/10.1016/j.cma.2003.09.014.

Galuppi, L. & Royer-Carfagni, G. 2014. Buckling of three-layered composite beams with viscoelastic interaction. *Composite Structures,* 107, pp.512-521. Available at: https://doi.org/10.1016/j.compstruct.2013.08.006.

Honarvar, H., Shayanfar, M., Babakhani, B. & Zabihi-Samani, M. 2020. Numerical Analysis of Steel-Concrete Composite Beam with Blind Bolt under Simultaneous Flexural and Torsional Loading. *Civil Engineering Infrastructures Journal (CEIJ),* 53(2), pp.379-393. Available at: https://doi.org/10.22059/ceij.2020.287376.1606.

Kant, T. & Swaminathan, K. 2001. Free vibration of isotropic, orthotropic, and multilayer plates based on higher order refined theories. *Journal of Sound and Vibration,* 241(2), pp.319-327. Available at: https://doi.org/10.1006/jsvi.2000.3232.

Le Grognec, P., Nguyen, Q.-H. & Hjiaj, M. 2012. Exact buckling solution for two-layer Timoshenko beams with interlayer slip. *International Journal of Solids and Structures,* 49(1), pp.143-150. Available at: https://doi.org/10.1016/j.ijsolstr.2011.09.020.

Lemes, Í.J.M., Dias, L.E.S., Silveira, R.A.M., Silva, A.R. & Carvalho, T.A. 2021. Numerical analysis of steel–concrete composite beams with partial

interaction: A plastic-hinge approach. *Engineering Structures,* 248, art.number:113256. Available at: https://doi.org/10.1016/j.engstruct.2021.113256.

Lemes, Í.J.M., Silva, A.R.D., Silveira, R.A.M. & Rocha, P.A.S. 2017. Numerical analysis of nonlinear behavior of steel concrete composite structures. *Revista IBRACON de Estruturas e Materiais,* 10(1), pp.53-83. Available at: https://doi.org/10.1590/S1983-41952017000100004.

Lenci, S. & Clementi, F. 2012. Effects of shear stiffness, rotatory and axial inertia, and interface stiffness on free vibrations of a two-layer beam. *Journal of Sound and Vibration,* 331(24), pp.5247-5267. Available at: https://doi.org/10.1016/j.jsv.2012.07.004.

Mechab, I. 2005. *Contribution à l'analyse des plaques stratifiées et sanduricly en utilisant les théories à ordre élevés.* PhD thesis. Oran, Algeria : Université d'Oran1 - Ahmed Ben Bella, Département de Génie Civil [online]. Available at: https://www.pnst.cerist.dz/detail.php?id=16616 [Accessed: 06 December 2024].

Mindlin, R.D. 1951. Influence of Rotary Inertia and Shear on Flexural Motions of Isotropic Elastic Plates. *Journal of Applied Mechanics,* 18(1), pp.31-38. Available at: https://doi.org/10.1115/1.4010217.

Nguyen, Q.H. 2009. *Modelling of the nonlinear behaviour of composite beams taking into account time effects.* PhD Thesis. Rennes, France: INSA Institut national des sciences appliquées de Rennes. Available at: https://doi.org/10.13140/RG.2.1.1706.9923.

Oliveira, L.A.M., Borghi, T.M., Rodrigues, Y.O. & El Debs, A.L.H.C. 2021. Assessment of design codes for the in-service behaviour of steel-concrete composite slabs. *Revista IBRACON de Estruturas e Materiais,* 14(5), e14501. Available at: https://doi.org/10.1590/S1983-41952021000500001.

Perkowski, Z. & Czabak, M. 2019. Description of behaviour of timber-concrete composite beams including interlayer slip, uplift, and long-term effects: Formulation of the model and coefficient inverse problem. *Engineering Structures,* 194, pp.230-250. Available at: https://doi.org/10.1016/j.engstruct.2019.05.058.

Reddy, J.N. 1984. A Simple Higher-Order Theory for Laminated Composite Plates. *Journal Applied Mechanics,* 51(4), pp.745-752. Available at: https://doi.org/10.1115/1.3167719.

Reissner, E. 1945. The Effect of Transverse Shear Deformation on the Bending of Elastic Plates. *Journal of Applied Mechanics,* 12(2), pp.A69-A77. Available at: https://doi.org/10.1115/1.4009435.

Santos, H.A.F.A. 2020. Buckling analysis of layered composite beams with interlayer slip: A force based finite element formulation. *Structures,* 25, pp.542-553. Available at: https://doi.org/10.1016/j.istruc.2020.03.002.

Timoshenko, S. & Woinowsky-Krieger, S. 1959. *Theory of Plates and Shells.* McGraw-Hill Book Company. ISBN: 0-07-064779-8.

Valizadeh, N., Natarajan, S., Gonzalez-Estrada, O.A., Rabczuk, T., Bui, T.Q. & Bordas, S.P.A. 2013. NURBS-based finite element analysis of functionally graded plates: Static bending, vibration, buckling and flutter. *Composite*

Structures, 99, pp.309-326. Available at: https://doi.org/10.1016/j.compstruct.2012.11.008.

Wang, C.M., Reddy, J.N. & Lee, K. H. 2000. *Shear Deformable Beams and Plates: Relationships with Classical Solutions*. Elsevier Science. Available at: https://doi.org/10.1016/B978-0-08-043784-2.X5000-X

Whitney, J.M. 1969. The Effect of Transverse Shear Deformation on the Bending of Laminated Plates. *Journal of Composite Materials,* 3(3), pp.534-547. Available at: https://doi.org/10.1177/002199836900300316.

Xu, R. & Wu, Y.-F. 2008. Free vibration and buckling of composite beams with interlayer slip by two-dimensional theory. *Journal of Sound and Vibration,* 313(3-5), pp.875-890. Available at: https://doi.org/10.1016/j.jsv.2007.12.029.

Yoo, S.-W., Choi, Y.-C., Choi, J.-H. & Choo, J.F. 2021. Nonlinear flexural analysis of composite beam with Inverted-T steel girder and UHPC slab considering partial interaction. *Journal of Building Engineering,* 34, art.number:101887. Available at: https://doi.org/10.1016/j.jobe.2020.101887.

Estudio estático y dinámico de vigas compuestas con un nuevo campo deslizante interlaminar utilizando diferentes teorías de vigas

Rachida Mohamed Krachaï[ab], *Noureddine* Elmeiche[a], **autor de correspondencia**, *Ismail* Mechab[c], *Fabrice* Bernard[d], *Hichem* Abbad[a]

[a] Universidad Djilali Liabes, Facultad de Tecnología,
Departamento de Ingeniería Civil y Obras Públicas,
Laboratorio de Ingeniería Civil y Ambiental (LGCE),
Sidi Bel-Abbes, República Argelina Democrática y Popular

[b] Universidad Mustapha Stambouli, Facultad de Ciencia y Tecnología,
Departamento de Ingeniería Civil,
Mascara, República Argelina Democrática y Popular

[c] Universidad Djilali Liabes, Facultad de Tecnología,
Departamento de Ingeniería Mecánica,
Laboratorio de Mecánica y Física de Materiales (LMPM),
Sidi Bel-Abbes, República Argelina Democrática y Popular

[d] Universidad de Rennes, INSA Rennes,
Laboratorio de Ingeniería Civil y Mecánica (LGCGM),
Rennes, República Francesa

CAMPO: ingeniería civil
TIPO DE ARTÍCULO: artículo científico original

Resumen:

Introducción/objetivo: El presente trabajo tiene como objetivo realizar una investigación estática y dinámica de vigas compuestas por dos elementos conectados entre sí, con una interacción parcial entre las capas de la viga, teniendo en cuenta el efecto de deslizamiento interlaminar.

Métodos: En este estudio se ha introducido un nuevo campo de deslizamiento interlaminar que tiene en cuenta, para cada capa, el

desplazamiento axial, la rotación debida a la flexión y el corte transversal de alto orden con una nueva función de forma de alabeo. Las ecuaciones de equilibrio se resolvieron analíticamente basándose en el principio de Hamilton. Además, la resolución numérica de estas ecuaciones se basó en el principio de minimizar todas las energías utilizando el método de Ritz, teniendo en cuenta diferentes teorías de vigas. Posteriormente se llevó a cabo un estudio comparativo para calcular las frecuencias de vibración naturales de dos vigas compuestas de acero y madera.

Resultados: Se encontró que los resultados obtenidos para las diez frecuencias de vibración naturales concuerdan perfectamente con los reportados en trabajos previos encontrados en la bibliografia.

Conclusión: Además, se realizó un estudio detallado, dependiendo de los parámetros geométricos y materiales, para los dos materiales mixtos, es decir, hormigón-madera y acero-hormigón, con dos campos de deslizamiento interlaminares, concretamente el campo de deslizamiento clásico basado en la teoria de la viga de Timoshenko y un nuevo campo de deslizamiento interlaminar que se basa en la teoría de orden superior. Además, se estudió la flexión en el caso estático para examinar el efecto de la fuerza cortante interlaminar en vigas cortas y largas.

Palabras claves: estudio estático y dinámico, vigas compuestas, interacción parcial, nuevo campo de deslizamiento interlaminar, cortante transversal de alto orden, nueva función de forma de alabeo, método de Ritz.

Статическое и динамическое исследование композитных балок с новым полем межслойного скольжения с использованием различных теорий изгиба балок

Рашида Мохаммед Крачаи[аб], *Нуреддин* Эль Михельс[а], **корреспондент**, *Исмаил* Мечаб[в], *Фабрис* Бернар[г], *Хишам* Аббас[а]

[а] Университет Джиллали Лиабес - Сиди-Бель-Аббес, технологический факультет, Департамент гражданского строительства и общественных работ, Лаборатория гражданского строительства и охраны окружающей среды (ЛГСОС), г. Сиди-Бель-Аббес, Алжирская Народная Демократическая Республика

[б] Университет Туши Мустафы Стамбули, факультет науки и технологий, г. Маскара, Алжирская Народная Демократическая Республика

[в] Университет Джиллали Лиабес - Сиди-Бель-Аббес, технологический факультет, кафедра гражданского строительства, Лаборатория механики и физики материалов (МФМ), г. Сиди-Бель-Аббес, Алжирская Народная Демократическая Республика

[г] Реннский университет, INSA Rennes, лаборатория гражданского строительства и машиностроения (LGCGM), г. Ренн, Французская Республика

РУБРИКА ГРНТИ: 67.11.00 Строительные конструкции
ВИД СТАТЬИ: оригинальная научная статья

Резюме:

Введение/цель: Целью настоящей статьи является проведение статического и динамического исследования композитных балок, состоящих из двух соединенных элементов с частичным взаимодействием между слоями балки и с учетом эффекта межслойного скольжения.

Методы: В данном исследовании было введено новое поле межслойного скольжения, которое учитывает осевое смещение по каждому слою, поворот изгиба и поперечный сдвиг высшего порядка с новой функцией формы изгиба. Уравнения равновесия были решены аналитически, основываясь на принцип Гамильтона. Помимо того, численное решение этих уравнений было основано на принципе минимизации всех энергий с использованием метода Ритца с учетом различных теорий пучков. Затем проведен сравнительный анализ с целью расчета собственных частот колебаний двух композитных балок, изготовленных из стали и дерева.

Результаты: Было обнаружено, что результаты, полученные по десяти собственным частотам колебаний, полностью согласуются с результатами, представленными в ранее опубликованных работах.

Вывод: Далее было проведено детальное исследование зависимости от геометрических параметров и параметров материалов двух композитных материалов, то есть бетона, дерева и сталебетона с двумя межслойными полями скольжения, а именно, классическим полем скольжения, основанным на теории балок Тимошенко, и новым межслойным полем скольжения, основанным на теории высшего порядка. Помимо того, изгиб был изучен в статическом режиме с целью изучения влияния межслойной силы сдвига на короткие и длинные балки.

Ключевые слова: статические и динамические исследования, композитные балки, частичное взаимодействие, новое поле межслойного скольжения, поперечный сдвиг высокого порядка, новая функция формы изгиба, метод Ритца.

Статичко и динамичко проучавање спрегнутих носача са новим интерламинарним смичућим пољем коришћењем различитих теорија носача

Рашида Мухамед Крачаи[аб], *Нуредин* Елмиш[а], **аутор за преписку**, *Исмаил* Метаб[в], *Фабрис* Бернар[г], *Етшам* Абад[а]

[а] Универзитет „Ђилали Лиабес”, Технолошки факултет,
Департман за грађевинарство и јавне радове,
Лабораторија за грађевинско и еколошко инжењерство (LGCE),
Сиди Бел Абес, Народна Демократска Република Алжир

[б] Универзитет „Мустафа Стамболи”,
Факултет науке и технологије, Одсек за грађевинарство,
Маскара, Народна Демократска Република Алжир

[в] Универзитет „Ђилали Лиабес”, Технолошки факултет,
Департман за машинство,
Лабораторија за механику и физику материјала (LMPM),
Сиди Бел Абес, Народна Демократска Република Алжир

[г] Универзитет у Рену, ИНСА Рен,
Лабораторија за грађевинарство и машинство (LGCGM),
Рен, Француска Република

ОБЛАСТ: грађевинарство
КАТЕГОРИЈА (ТИП) ЧЛАНКА: оригинални научни рад

Сажетак:

Увод/циљ: У овом раду су статички и динамички проучавани спрегнути носачи састављени од два спојена дела са парцијалном интеракцијом између слојева носача, при чему је узет у обзир ефекат интерламинарног смицања.

Методе: Уводи се ново интерламинарно поље смицања које за сваки слој узима у обзир аксијални померај, ротацију услед савијања и попречно смицање високог реда са новом функцијом облика савијања. Једначине равнотеже су решене аналитички на основу Хамилтоновог принципа. При томе је нумеричко решавање ових једначина било засновано на принципу минимизирања свих енергија коришћењем Рицовог метода и различитих теорија носећих греда. Затим је урађена компаративна студија ради израчунавања фреквенција природних вибрација два спрегнута носача од челика и дрвета.

Резултати: Утврђено је да су резултати добијени за десет фреквенција природних вибрација у савршеном складу са онима из претходно објављених радова.

Закључак: Урађена је детаљна студија на основу параметара геометрије и материјала за два композита (бетон-дрво и челик-бетон) са два интерламинарна поља смицања, односно са класичним пољем смицања на основу теорије греде Тимошенка и са новим интерламинарним пољем смицања на основу теорије високог реда. Савијање је анализирано и статички ради испитивања утицаја интерламинарне силе смицања на кратке као и на дугачке греде.

Кључне речи: статичко и динамичко испитивање, спрегнути носачи, парцијална интеракција, ново поље интерламинарног смицања, попречно смицање високог реда, нова функција облика савијања, Рицов метод.

Paper received on: 14.08.2024.
Manuscript corrections submitted on: 30.01.2025.
Paper accepted for publishing on: 31.01.2025.

REVIEW PAPERS

Standardization for 5G technology and beyond: impact on military communications

Zoran M. Miličević[a], *Zoran* S. Bojković[b], *Nataša* Z. Bojković[c] *Tanja* M. Živojinović[d]

[a] Serbian Armed Forces, General Staff, Telecommunications and Information Technology Directorate (J-6), Belgrade, Republic of Serbia, e-mail: zoran.milicevic@vs.rs, **corresponding author**, ORCID iD: https://orcid.org/0000-0003-3512-4188

[b] University of Belgrade, Belgrade, Republic of Serbia, e-mail: z.bojkovic@yahoo.com, ORCID iD: https://orcid.org/0000-0003-1323-0115

[c] University of Belgrade, Faculty of Transport and Traffic Engineering, Belgrade, Republic of Serbia, e-mail: n.bojkovic@sf.bg.ac.rs, ORCID iD: https://orcid.org/0000-0002-9291-8999

[d] University of Belgrade, Faculty of Transport and Traffic Engineering, Belgrade, Republic of Serbia, e-mail: t.zivojinovic@sf.bg.ac.rs, ORCID iD: https://orcid.org/0000-0003-0015-1637

https://doi.org/10.5937/vojtehg73-52585

FIELD: telecommunications
ARTICLE TYPE: review paper

Abstract:

Introduction/purpose: The presented review paper deals with the standardization proces for 5G technology and beyond and its impact on military communications.

Methods: Dominant methods such as analyzes and syntheses were provided for considering the key aspects of the 5G standardization evolution process through presentations of the roles of different Third Generation Partnership Project (3GPP) standard releases and its implementation and usage in military communication networks environment.

Results: The background and key areas in 5G evolution and beyond are presented. Also, 5G standardization and military issues and challenges are discussed.

Conclusion: Standardization for 5G and the emerging 6G landscape is extremely complex and highly innovative with many rapidly evolving industry-driven and societal requirements. Standard development organizations, industry, and academia need to collaborate on standardization to facilitate worldwide interoperability. The paper gives an overview of standardization functionalities and efforts to improve 5G system performance as well as its impact on military communications and services. It analyzes the areas of major enhancements for the existing features and expansion to new use cases and industries as well as to military usage through the 3GPP Releases, starting from Release 15 as 5G Basic, over 16 and 17 as 5G Evolution, up to 18 and 19 as 5G Advanced which precede the upcoming Release 20 and the initial 6G network whose launch is expected by the end of this decade.

Key words: the fifth generation (5G) technology, 5G standardization process releases, 5G functionalities, 5G interoperability.

Introduction

Standardization on a global level is of fundamental importance and even more for wireless networks because of the need for worldwide interoperability (Shafi et al, 2017). First of all, the data rate supported by each generation of mobile networks has significantly increased over time. The advantages of 1G technology included service areas. There was neither roaming between operators of various networks nor a capability of networks to use different frequency bands. The widespread adaption of 1G enabled the introduction of 2G mobile networks, in spite of these shortcomings. 2G networks have a throughput of 9.6 – 236 Kbps. 3G increased this range to 42 Mbps, while 4G further improved it from 100 Mbps to 1 Gbps. 5G has made a leap with of 10 Gbps to 20 Gbps. As for 6G, it is expected to reach 100 Gbps to 1 Tbps. Latency has decreased significantly with each generation. For example, 2G had a latency of 300-1000 ms, 3G reduced it to 100-500 ms, while 4G further decreased this to 30-100 ms. As for 5G, it has lowered latency to 1-10ms. 6G is expected to achieve submilisecond latency. 2G had low spectrum efficiency, while 3G and 4G made significant improvements. 5G has very high spectrum efficiency thanks to Multiple-Input-Multiple-Output (MIMO) and beamforming technologies. For 6G, it is expected to push the limits of spectrum efficiency further using THz frequencies as well as advanced network architectures (Fowdur et al, 2024). Nowadays, there is a focus on wireless regional network standards. Scientific efforts for the fifth generation (5G) specification are going to be finished with the full phase, soon. Also, today there are different studies towards the sixth generation

(6G) standardization. The 3GPP and its first full Release for 5G started with Release 15. Release 15 consists of the Non-Stand Alone and the Stand Alone specifications. Also, Release 15 is recognized as the foundation for network implementation and devices. Release 15 becomes an excellent performance for mobile communication broadband service, that is, data rate, spectral efficiency and latency. The Release 15 performance is recognized as excellent in the Key Performance Indicators. Therefore, Standard Development Organizations and academic society are necessary to cooperate in the standardization process to facilitate interoperability (Abdelkafi et al, 2021).

The evoluton of 5G standard started from Release 15 as 5G Basic, continues with Releases 16, and 17 as 5G Evolution, and achieves Releases from 18 to 21 as 5G Advanced. Next, Release 21 will establish a road map for the 6G standard. Currently, Releases 18 and 19 are open while Releases 20 and 21 are planed.

Key areas in 5G evolution and beyond

It is projected that 5G networks will be widely available all over the world because of some key features such as:

- Data transfer rates on 5G networks are expected to be significiantly higher than those of previous mobile network generations (10 Gbps or more),
- Latency reaching levels are as low as a few miliseconds,
- 5G networks are designed to support a larger number of devices and connections, enabling new applications and services, and
- 5G networks offer improved coverage and reliability.

The first official specification to outline a complete 5G network was Release 15 available in 2018. It includes the specifications for 5G New Radio (NR) (Kim et al, 2019). Representing the current state-of-the-art in cellular network technology, Release 15 forms the basis for the deployment of 5G network all over the world (Bertenyi, 2021).

Releases 16 and 17 respectively belong to the key standardization of the 5G evolution system (Bertenyi, 2021). The specifications for Release 16 were frozen up in the first half of 2020. Next, the Release 17 specification process was underway towards its completion at the end of 2021. The main focus of both Releases 16 and 17 is to expand the ecosystem in order to provide possibilities of different industries to use 5G advantages (Wang et al, 2014). Both releases contain many features in all the key areas of 5G environment, i.e., Industrial Internet of Things, vertical

industries (Ghosh et al, 2019), network deployment and automation, and device evolution.

Releases 15, 16 and 17 unified platforms for innovations in technological advancement of the 5G 3GPP (Lin & Lee, 2021).

The most recent Release 18 named 5G Advanced brings a new wave of innovations especially in the area of Artificial Intelligence and Machine Learning (AI/ML). Further enhancements in AI/ML are expected in the forthcoming Release 19. The first 3GPP standards release for 6G is still several years away, while the work being done today gives the foundation.

Role of Release 16

Additional improvements to the 5G NR air interface brings Release 16 in 2020. In that way, Release 16 complements the full 5G specification which allows for the advanced use cases and applications such as network slicing (NS) and enterprise services (Wijethilaka & Liyanage, 2021). Release 16 expanded on the success of Release 15 conserving consumer and enterprise service field. Two examples of new services and applications it supports are: mission-critical communication as well as the Internet of Things (IoT). Release 16 includes the next main areas such as: massive machine – type communication, ultra – reliable low-latency communication and improved mobile broadband. In order to help cellular networks to continue with progress, additional technical improvements and support for new frequency bands are included in Release 16 (Chen et al, 2021).

The Ultra Reliable Low Latency Communications (URLLC) functionality, critical for Industrial IoT (IIoT) scenarios is completed in Release 16.

Release 16 introduces support for Time Sensitive Communication including integration with Time Sensitive Networking.

Also, Release 16 introduces some significant features which allow NR to use the unlicensed radio spectrum.

Access to the NR-Unlicensed Spectrum (NR-U) provides an important tool to increase capacity for both service providers and private networks. Release 16 NR-U uses the same flexible frame and slot structure, physical layer design, and protocol as NR Release 15 (Milovanovic et al, 2020). In that way, the magnitude of changes to the user equipment compared to the licensed-band operator is limited. The fact that Release 15 provides the basic positioning protocol support is extended in Release 16 to include the capability of locating devices using 5G radio signals themselves leading to an expected accuracy in the order of metrics for a vast majority of users.

The means to reduce operating expenses of running 5G systems enables new application capability for communication service providers. In order to improve the overall separability and automation of network slice deployments, Release 16 is applied. It allows the operator to outsource network slice subscription management to third parties who are using the operator's networks to provide services to their customers. Release 16 introduces network slice-specific authentication and authorization which allows a third party to manage a user's subscription to a particular slice without requiring the operator to be involved in managing transportation. Integrated access and backhaul (IAB) has been introduced in Release 16 as a key enabler for fast and cost-efficient applications, mainly targeting dense mmWave deployments outdoor when using the same spectrum and air interface for access and backhaul, creating a hierarchical wireless multi-hop network between sites. The main purposes for deploying IAB nodes are: to have isolated coverage gaps, to provide backhaul with filter deployment sparse, to enhance system capacity, and to bridge coverage from outdoor to indoor. There are some aspects of 5G standards that directly impact the energy efficiency of devices. Release 16 introduces signaling from the network to the devices enabling the device power consumption to be well optimized during the period of additive transmission and reception.

In Release 16, the 3GPP further expanded the 5G NR frequency spectrum in order to support operation with bands starting from under 1 GHz up to 52.6 GHz with 5 MHz and more channel bandwidth.

Also, Release 16 further enhances the NR support for URLLC services by enabling latency in the range of 0.5 to 1 ms and improved reliability with a target error rate of 10^{-6} in order to provide new use cases, such as factory automation and transport industry as well as to improve use cases such as Augmented Reality (AR)/Virtual Reality (VR) and gaming.

Also, NR Release 16 introduces native positioning support not only for regulatory but also for commercial and other use cases with positioning accuracy down to at least 3 meters and end-to-end latency less than 1 second for commercial use cases.

The improvements due to Release 16 are described in Table 1 (3GPP, 2021).

Table 1 – Areas with the improvements due to Release 16

IMPROVEMENTS	DESCRIPTIONS
Massive MIMO	• Strong management to increase connection stability
	• Enhance coverage at the cell edge
	• Full power uplink for MIMO-capable devices
Enhanced Ultra-Reliable, Low-latency Communication (eURLLC)	• Vertical user cases (industrial automation)
	• High connection dependability provided by improving the 5G URLLC architecture
	• Strict latency restriction
	• Continues communication even if one link is temporally blocked
Power saving	• Low power optimization
	• Overhead reduction
	• Better power control techniques
Integrated Access and Backhaul (IAB)	• Combine access and backhaul to reduce the cost of mm Wave densification
	• Allows a single base station to serve as a wireless access point for end devices and a backhaul node
	• Operators may add more base stations on the fly without having to deploy extra fibers for more backhaul capacity
	• More adaptable densification plan
Unlicensed spectrum (NR-U)	• Enabling 5G service in unlicensed bands
	• Cellular technology can operate "standalone" in unlicensed spectrum
Time-Sensitive Networking (TSN)	• Introduced support for TSN which can guarantee time-deterministic delivery of data pockets
Cellular-Vehicle-to Everything (CV2X)	• Prioritizes the use of 5G to improve automotive safety

Role of Release 17

Release 17 was published in March 2022. It refers to further enhancements and improvements to the 5G NR air interface. The Release 17 development is the result of evolving needs and requirements of the mobile industry. The first stage decade's technological evolution area concluded with Release 17. The 3GPP is part of the Release 16 and Release 17 specifications. These enable 5G media streaming and enhancements edge processing, analytics and event presentation as well as extended reality (XR) experiences.

Enhancements to IAB in Release 17 will improve the options for multiplexing concerning links of an IAB node. Also, increased flexibility and robustness in the network topology will be improved.

In both Releases 15 and 16, the design of 5G NR allows the network to operate in the conventional cellular radio spectrum and the mmWave spectrum up to 52.2 GHz.

The 3GPP makes effort to provide new bands together with band communications for 5G implementation (Zong et al, 2019).

The main goal was to recognize demands of network operators worldwide.

The major step in Release 17 in this domain is the introduction of support for 5G NR in the 52-71 GHz frequency range.

Release 17 scales the existing 5G NR design to expand the mmWave spectrum range from 24.25—52.6 GHz to up to 71 GHz in order to cover the original 60 GHz band (57-66 GHz) as well as the 66-71 GHz frequency band together with 5 MHz and more channel bandwidth.

Also, Release 17 scales down the wideband 5G NR design (i.e., 100 MHz bandwidth) to 20 MHz/100 MHz in the sub-7/mmWave to efficiently support lower complexity IoT devices.

In the focus of Release 17 is power saving for devices in order to improve the battery life (Milovanovic & Bojkovic, 2020).

Release 17 seeks to provide time-sensitive communication (TSC), offering in that way enhanced specific tools for the 5G system in order to support TSC in the application domain.

In that way it is possible to allow the implementation of private wider area networks (WANs).

Release 17 private network support is being further extended in order to support neural host models where the network owner and the service provider need not to belong to the same entity. This provides accessing private networks together with public network operators.

Release 17 offers support of the IoT by NR, in order to support optimal operational device type's characteristic for the IIoT network services.

Next, Release 17 has potential to enhance NR to address the following use cases in the Industrial IoT and other verticals:

- Industrial wireless sensors with 99.99% availability, latency less than 100ms in general and 5-10ms for safety-related sensors, and a medium data rate (<2 Mbps), and a battery life of a few years,
- Video transmission with 99%-99.9% reliability, latency less than 500ms, and a medium to high data rate (2-25 Mbps), and
- Wearables with a high data rate (up to 150 Mbps for downlink and up to 50 Mbps for uplink) with a long battery life (up to 1-2 weeks).

In order to support enhanced positioning in Release 17, the study item focuses on more high-accuracy positioning targeting commercial IoT use cases such as location of assets and moving objects within factories, with sub-meter-lever accuracy and end-to-end latency less than 100 ms.

Release 17 supports a wide but key range of military services, Enhanced Mobile Broadband (eMBB), URLLC, and Massive Machine-Type Communications (mMTC). The description of the improvements due to Release 17 are presented in Table 2 (3GPP, 2022).

Table 2 – Capabilities for primary use cases in Release 17

CAPABILITIES	DESCRIPTION
eMBB	• Support for 5G NR from 52.6 MHz to 71GHz frequency range
	• Thanks to the expansion of the NR frequency range, more spectrum up to and including the unlicensed 60 GHz is available
	• Multicast and broadcast services such as vehicle-to-vehicle (V2X) public safety, IP multicast, software delivery, and IoT are the primary targets
	• Allows the network notification and the avoidance of paging collisions when the user equipment changes networks
	• Support for non-terrestrial networks
	• Through the use of high-altitude platforms, better coverage can be achieved in remote places
	• Sidelink relaying including single hop, User Equipment (UE) to UE and UE to network relaying
URLLC	• Enhanced physical layer feedback for manufacturing automation
	• Positioning, reduced latency, especially for IoT applications
	• Sidelink, V2X, public safety, resource allocation enhancement
	• Continuity mechanisms for ultra-radio access technology
	• UE can quickly read the cell that provides the desired slice
	• Anything reality (XR) evaluations
	• Help for a wide variety of XR applications
mMTC	• Small data transmission in the inactive state
	• Sensors benefit from lower connection establishment overhead
	• Support of reduced-capabilities NR devices
	• Useful for transmitting data over machines

Role of Release 18

Release 18 refers more to 5G Advanced, which is represented in industry and technology that comes between 5G and 6G (Lin & Lee, 2021). It has started in the second quarter of 2022 as the first standard which will witness a greater emphasis on AI, ML and extended reality (XR). Also, it should be noted that there will be a greater focus on sustainability initiatives. The initial freeze data for this standard package was planned in December 2023. After that time, vendors will start integrating the approved changes into commercial equipment. 5G Advanced with XR applications such as video streaming, remote sensing, etc. will create financial improvement in the consumer enterprise market. In order to encourage mass market adoption, 3GPP working groups are going to enhance XR-specifies traffic performance and power consumption. AI/ML is also becoming of great interest for future networks. As for generators, they need to save system-level energy in order to reduce deployment costs and maintain network performance for a range of use cases (Lin, 2022).

The key features in Release 18 involve the 20-MHz or 5-MHz bandwidth (in Frequency Range 1), full duplex/half duplex and time division signal duplication, 64-level QAM (256 optional), and 10 Mbits/sec maximum data speeds (Downlink and Uplink).

Also, Release 18 includes enhancements to the 5G NR technology that enables lower latency, down to less than 0.5 ms in some cases. These enhancements include improvements to the scheduling algorithms and support for low-latency services such as URLLC.

Next, Release 18 has included advancements in spectrum operation utilization for 5G NR, important for networks which require mission critical communications. In order to achieve this, the 3GPP has introduced operation in a narrowband spectrum with channels smaller than 5 MHz, i.e., it specified a new channel bandwidth of 3 MHz, as well as a new synchronization raster (600 KHz) and the technique of SSB (Synchronization Signal Block) puncturing.

The 3GPP radio access network (RAN) approved a work package for its Release 18. It represents a major emulation in the first release of 5G-Advanced. The work package includes diverse study and work items which will significantly contribute to a variety of new use cases. The works conducted in 5G Advanced will shape the evaluation of wireless networks on the path to 6G. In Release 18, the standardization sidelink (SL) communication was extended to the unlicensed spectrum, while the SL positioning is standardized with the licensed spectrum (Lin, 2022). The notable changes and description of the capabilities from Release 18 as well as future research are given in Table 3 (3GPP, 2023).

Table 3 – Description of the capabilities offered by Release 18 and further research

CAPABIITIES	DESCRIPTION AND FURTHER RESEARCH
Network energy saving	• A slicing on network energy has to be correctly done for NR. Also, new methods for maximizing network energy efficiency are welcome
Mobility support	• Mobility focuses on improving conditional handover support
	• UE gets a handover command with a condition from the network
MIMO evaluation	• Support for antenna ports in the uplink and simultaneous multipanel uplink
	• Better support advanced UEs such us customer premise equipment
	• Fixed wireless access devices and vehicular UEs
Multicast and broadcast	• Increase resources efficiency in RAN sharing scenarios and extend multicast support to UEs
	• Make enhancements to allow UEs in connected state to receive broadcast service and unicast services simultaneously
Improved positioning	• Accuracy, integrity, and power efficiency along with positioning

Role of Release 19

Release 19 is the second release of 5G Advanced. Not only is it a continuation of Release 18, but it also represents a bridge towards 6G technology of new capabilities and efficiency. As for the specifications, they are expected to be finalized and frozen in March 2025. What has emerged, for example, is a set of features which will offer services such as extended reality.

In Release 19, at least for the 7-24 GHz spectrum, the 3GPP will validate its existing channel models and if necessary, adopt them to take into account spatial non-stationarity. As the second Release of 5G Advanced, Release 19 will focus primarily on the commercial deployment needs by further enhancing performance, evolving network topology, improving energy efficiency and utilizing AI/ML. Here the innovation work carried out will provide the baseline for 6G standardization.

The 3GPP 5G Work Plan for Release 19 deals with the problems such as: support frequencies up to THz, advanced radio interface including full duplex, joint sensing and communication, energy harvesting and passive IoT, and cognitive access to wireless technologies cellular satellite WiFi (Chen et al, 2023).

Current expectations

Release 20 workshop in July 2024 defined the scope of technology foundation for the next generation innovation platform going towards its finalization in September 2026. The current expectations are that the official specification work on 6G standards will start around 2025. Anticipating supporting use cases requirements in 2030 and beyond, the first 6G standard Release 21 will need to be completed and redefined by early 2028.

5G standardization - military issues and challenges

5G technologies are important in the military environment because it supports various applications. 5G can be implemented for different purposes from the traditional ones such as Intelligence, Surveillance, and Reconnaissance (ISR) systems capabilities for decision making in command and control (*C2*), over training, maintenance, logistics, up to autonomous vehicles, AI, augmented and virtual reality (Miličević & Bojković, 2024).

Also, 5G wireless technology brings significant benefits for military forces. Some of them are (Maris, 2024):

1. Enhanced Communication, Control and Operational Efficiency: The high data rate, ultra-reliable and low latency of 5G enable more efficient communication and information exchange technology in the battlefield, improving command and control capabilities.

Command and Control (C2) which is now expanding to incorporate computers, intelligence, surveillance, target acquisition, reconnaissance and cyber (C5ISTAR) technologies is incorporating all domains of traditional warfare theatre which involve air, land, sea and space for combat operations. To be important in the military domain, C2 has necessity to follow modern technology advancements in order to respond to the challenges and requests of modern warfare in combat fields. In line with this, 5G plays an important role in the optimization and transmission of leading military C2 applications.

From the military perspective, 5G with its main characteristics has huge potential to be vital for effective C2 communication systems in order to provide secure and resilient information exchange between units and commands as well as for intelligence collaboration in the battlefield, coupled with real-time data that are processed in different combat networks.

5G provides enhanced C2 by real-time data transmission with ultra-reliability and low latency and in that way it allows Real-time situational

awareness and Distributed Command and Control for military purposes. In Real-time situational awareness, combat staff have possibility of faster decision making upon receiving critical information from the battlefield (video stream, sensor data, and etc.) On the other hand, by Distributed Command and Control, units operate independently while staying connected to the central command and can use for this purpose a 5G robust, high-speed network.

The ability to run secure C2 applications on 5G ensures that both superiors and subordinates in chain of command can see, monitor and track the same combat or non-combat activities at the same time as well as use C2 services which must be able to share and access data at any time from any location.

2. Real-time Data Processing and Support for ISR systems: 5G allows for the ultra-rapid processing and sharing of large volumes of data, crucial and critical for ISR operations.

5G can enhance Intelligence, Surveillance, and Reconnaissance (ISR) capabilities for military matters by high-bandwidth data rate transmission and edge computing. High-bandwidth data rate transmission has potential to provide transmission of HD (high-definition) and beyond for imagery and video formats from different surveillance platforms (drones and others). Also, implemented support for 5G edge computing has purpose to process data closer to the source and in that way reduces latency and allows for faster analysis and response.

3. Autonomous and Remote Operations Capabilities: The reliable and fast connectivity of 5G supports the deployment of different kinds of modern autonomous systems which are increasingly becoming integral and important to modern warfare.

5G is a technology platform which provides reliable communication links important to ensuring uninterrupted connectivity for remote control and autonomous operations as well as high-speed data transfer which enables real-time video streaming and sensor data transmission for navigation and mission implementation. Both mentioned characteristics provided by 5G are important for the operation of autonomous vehicles and drones.

Autonomous transportation and Remotely Operated Vehicles (ROVs) enabled by high capacity, low latency wireless 5G technology are developed to execute high-risk combat missions without endangering soldier lives, different navigation tasks in hazardous environments, as well as special tasks like reconnaissance and explosive disposal.

Also, they can be used to ensure timely delivery of supplies, provide real-time intelligence, and support decision making.

Generally, in 5G, anything can be user equipment, not only traditional cell phones, but also different types of assets like aircraft, ships, as well as combat and non–combat vehicles.

Equipped with 5G for long-haul communication systems, these vehicles can use the 5G network to enable communications, high-data-rate video conferencing, and Internet of Things sensors to become self-driving or autonomous vehicles in order to remove, for example, soldiers from some missions, regadless of the fact that someone is required on board to oversee the vehicle performance.

Also, different vehicles, from base-contained vehicles to field and combat vehicles equipped with radar, lidar, and sensing techniques to identify and understand their surroundings, which use artificial intelligence and machine learning to sort through, process, and act on this information, can use the potential of 5G to connect all this information.

4. Augmented Reality (AR)/Virtual Reality (VR)/Extended Reality (XR)/Artificial Intelligence (AI) enabled simulations and training.

Simulations and training are essential for military units combat readiness and exactly 5G networks are improving military training capabilities by implementing advanced AR, VR, XR, and AI technologies. In the process of implementing military training, simulations are increasingly used so that accurately reflect real combat scenarios. Precisely speaking, 5G networks, thanks to their high bandwidth and ultra-low latency in real time, can provide support for the modern training process.

The 5G communications capabilities, together with AR for military training, provide a multi-participant training process by an experienced trainer in order to provide military personnel with remote access to the best possible training staff for different specialist jobs as well as to simplify access to cutting-edge programs and platforms for training, regardless of where they are stationed, installed or deployed.

5G enables training and simulation in such a way that military staff can engage in realistic training scenarios using AR/VR as well as in mission operation planning by AR/VR in order to visualize mission conditions and plan operations in a virtual environment.

Also, the high bandwidth and ultra-low latency of 5G ensure real-time, immersive simulations that mirror actual combat scenarios with precision. Soldiers benefit from interactive environments where AR

overlays critical information, and VR and XR offer dynamic, scenario-based exercises.

5. Improved Network-Centric Warfare and Interoperability Concept: 5G's ability to connect numerous devices and systems in such a manner to support the concept of network-centric warfare, enhancing interoperability among different military forces in operations.

For example, 5G has capacity and flexibility to provide military tactical networks well known as Mobile Ad Hoc Networks (MANets). MANets represent some kind of a nomad type of networks that has possibility of self-configuring (reconfiguring) in order to provide connectivity between deployed military commands/units without necessity to build fixed infrastructure in the area of operation, for enabling for users real-time data sharing, coordination and security in dynamic military operational environment. Above all, 5G MANets could enhance situational awareness and have huge impact on a quicker decision-making process in order to improving operational efficiency by providing rapid deployment and reconfiguration in response to changing battlefield conditions.

5G for tactical communications increased flexibility for use cases from enhanced mobile broadband to ultra-reliable low-latency and massive machine-type communications, as well as increased security. Also, 5G tactical networks can provide augmented/virtual reality in combat situations and training, telesurgery on the battlefield, tactical self-driving vehicles, ad hoc secure communications, and the interconnection of different battlefield assets.

Also, the 5G tactical network can be used in different combat/exercise scenarios, for example, to transfer high-speed, secure and reliable data from different sensor platforms over the C2 system or Command Information Systems (CIS) to the command post, for example to choose targets, and from the command post over the C2 system or CIS to artillery units that use this data for calculations and after that for acting on targets in a short period of time in order to eliminate threats on the field. The positive characteristic of the previous scenario is a possiblity to fast deploy eMBB, URLLC and mMTC 5G tactical networks with a smaller propagation footprint for a reliable and resilient communication data flow in order to plan and solve military tasks. On the other hand, the negative characteristic will be a possbility of jamming, intercepting and interupting 5G tactical network communication by enemy electonic warfare systems.

6. Cybersecurity Challenges and Resilient Communications: With rapidly increasing cyber threats, 5G's advanced security features are essential

to answer to them by protecting sensitive military communications and ensuring resilient networks.

The advanced key security features that are implemented in 5G networks for protection against cyber threats are: network slicing and AI-driven security. Network slicing can enhance security and performance by creation of separate network segments for different applications. On the other hand, AI algorithms have a possibility to detect and respond to threats in real time, promising the integrity of military communications.

7. Improving military logistics and supply chain management.

5G supports automated inventory management by applied IoT devices connected via 5G to monitor and manage inventory in real-time enabling. Also, 5G supports enhanced tracking and delivery in order to track in real time supplies, assets, and equipment thus ensuring timely delivery on the location of interest and reducing the risk of shortages, especially those of critical supplies.

5G can enhance logistics military operations through:

- Enhanced communication with 5G - integrating 5G in logistics enables providing a high bandwidth that offers speedy data movement to multiple systems in real time and allows in that way devices and systems to interact and share critical information for logistic operations.
- 5G IoT application in logistics - is suitable for real-time tracking that helps transmit real-time data across long/short distances in order to improve supply chain visibility for command staff with possibility to track and monitor assets shipment status.
- 5G network for smart warehouses – through effective, reliable and faster data transmission for devices in smart warehouses via 5G technology, it can be possible to establish smart inventory tracking and a smart shelves system, because IoT sensors can detect and alert if any product in the inventory is getting out of stock and needs to be restocked.
- Autonomous vehicles for logistics – applying 5G technology allows autonomous vehicles to self-regulate themselves reliably, accurately and safely with its high-speed data transmission, bandwidth and granular data. These self-driven autonomous vehicles are confined to warehouses but can also move onto public roads or off-roads.
- Optimizing transport routes – optimized routes are important to save expenses, fuel usage, and environmental damage. Still, in emergencies situation, it is necessary to change routes immediately to avoid any disruptions and delays. 5G technology has potential to take action and optimize new and better routes.

- Augmented Reality and Virtual Reality training in logistics – 5G, with its robust technology, higher bandwidth, and fast speed, can help boost applying augmented reality and virtual reality as technologies that can be used to train logistic staff to make them more skilled in their jobs by offering a virtually simulated environment for education in logistics.

8. 5G transforms medical care for military personnel.

The 5G-enabled AR training platform which could provide warfighters with more quality military care by enabling 5G AR telemonitoring for medical procedures, which would allow streamlined communication between centrally located medical specialists and their patients in remote locations.

It means that 5G enables a new application that promises to transform medical care for military personnel: robotic surgery. With robotic surgery, military doctors could quickly perform operations from a distance using robotic arms and cameras. Housing such equipment on medical vehicles would eliminate the need to transport patients elsewhere to begin treatment.

From the military point of view, Spectrum, 5G New Radio, 5G Core Network, Proximity Services, and Non-Terrestrial Networks (NTNs) (Bastos et al, 2021) are recognized as 5G technology enablers which have interesting potential and opportunities to be in connection with 5G Releases 15, 16 and 17, respectively.

One of important 5G technology enablers for military applications is the available radio-frequency spectrum. A significant amount of the spectrum for military usage which is arranged in multiple bands from high or mmWaves bands (above 6 GHz), over medium bands (between 1.5 and 6 GHz) to low bands (below 1 GHz) will be targeting bands for implementing 5G military technology in order to provide trade-off between capacity and coverage as well as mobility. The implementation of 5G in different sub-bands of the spectrum assigned to the military can provide cost-effective capabilities for 5G military systems.

Next, an important enabler for the military ecosystem is the 5G New Radio (NR) concept because it offers most prominent features from supporting several significant frequency ranges (from 410 MHz up to 7 GHz and from 24 GHz up to 52 GHz), over psychical layer design (using Orthogonal Frequency Multiplexing modulation (OFDM), providing Frequency Division Duplexing (FDD) and Time Division Duplexing (TDD) modes, as well as using a massive Multiple Input Multiple Output (MIMO) concept of active antennas which allow beam forming and steering in order

to reduce self and external interference and contribute the lower probability of interception as well as improve the link budget) to Integrated Access Backhaul (allowing 5G NR base stations to communicate mutually over the 5G NR air interface without the need to be connected on the backbone network and offer various opportunities to rapid deployment of sustainable 5G networks in the battlefield).

Also, 5G Core Network can play a significant role to support military usage requirements through network slicing (possibility to define the subsets of the main network (slices) which can be optimized for particular military service and performances required of the available network). Also, together with virtualization, it offers new opportunities to the military. On the other hand, Mobile Edge Computing (cloud computing can be distributed to the edge of the network (close to the Radio Access Network (RAN)) in order to provide low latency and independent operation of 5G clusters).

5G Proximity services (i.e. D2D technology as 5G Sidelink) have significant potential to provide reliable and secure communication between 5G military user equipment, especially in some military critical scenarios without necessity to use 5G RAN and core network infrastructure.

Finally, Non-Terrestrial Networks (provided by 5G satellites, aircraft or any other airborne vehicles) can extend 5G NR technology in order to provide military services with a lower propagation delay in the locations where terrestrial networks are not available. In that way, Non-Terrestrial Networks (NTNs) create opportunities to extend tactical communications and application services. Non-terrestrial networking is shown in Figure 1.

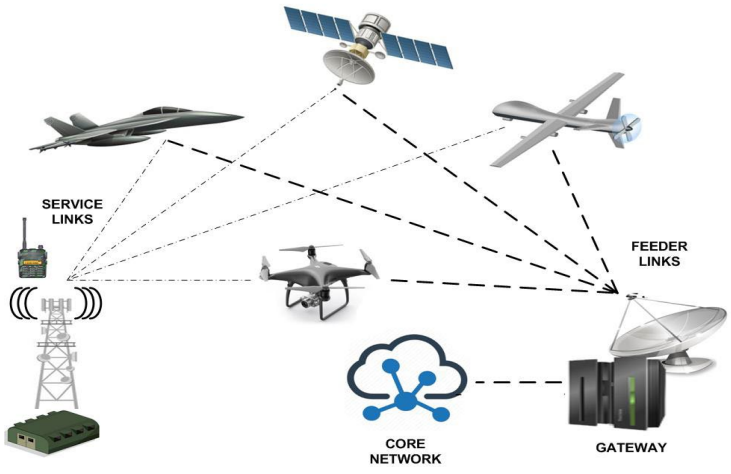

Figure 1 – Non-terrestrial networking presentation

Also, some of interesting 5G device-to-device use cases for the military are vehicle-to-everything communication (V2X) and soldier safety. The block scheme of the V2X communication modes is presented in Figure 2.

Figure 2 shows the basic concept of V2X communication modes where in some combat scenarios the combat and command vehicle as the main 5G station is interconnected with other combat vehicles by the Vehicle-to-Vehicle (V2V) mode, with soldiers by the Vehicle-to-Soldier (V2S) mode, with field command posts by the Vehicle-to-Network (V2N) mode, and with stationary command posts by the Vehicle-to-Infrastructure (V2I) mode using 5G communication infrastructure.

Wherever the network coverage is available, V2X (Vehicle-to-Vehicle, Vehicle-to-Infrastructure, Vehicle-to-Soldier and Vehicle-to-Network) can be supported via the stations using the URLLC functionality of NR together with edge computing to deliver low latencies. To support military safety applications, enhancement to the side link and proximity services are introduced. An example of the usage is when sidebank power saving features are introduced for handheld or manpack devices which are also used as position devices designed to communicate directly with combat vehicles in order to provide soldier safety.

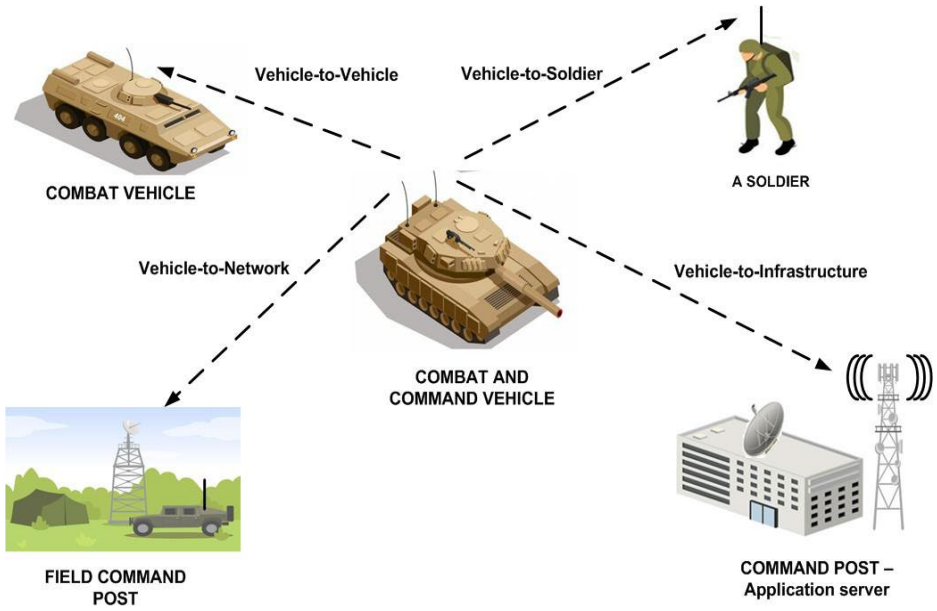

Figure 2 – V2X communication modes

Next, in the available literature, there are elaborated examples of different scenarios in several 5G military application domains which refer to deployable Communication and Information Systems (CISs), land tactical operations, maritime operations, and static communications (Bastos et al, 2021).

From the military point of view, Releases 18 and 19 are interesting because of their focus on AI/ML. Different forms of artificial intelligence incorporated in 5G communications can support military operations in order to provide operational success in various situations and scenarios as well as asset survivability through, first of all, faster situational awareness based on efficient data sharing together with effective collaborative decision making. Also, in 5G, the military's network AI will apply different techniques to provide an appropriate level of intelligence to connect different domain architectures and perform dynamic reconfigurations of the network topology at the edge in order to increase node and data security and to be more resilient to attack. The ML and heuristics as forms of AI will enable automation in the process of tracking and predicting the position of military units and resources, using the weather forecast systems, detecting different obstacles, rapidly rebuilding parts of the infrastructure, and expanding or contracting the network as needed. AI can support deploying swarms of drones in order to form autonomous, adaptive 5G cellular relays stations, which can continually adjust their positions to optimize network communications for mobile combatants and military equipment. For AI, data collection and processing is necessary to be performed between network edge devices and clouds or data centers. 5G and AI together can better support combatants, improve equipment survivability, and contribute to mission operational success in the battlefield.

Finally, different international organizations including NATO bodies and the European Defense Agency (EDA) have considered models of usage of 5G technology for military operations. Generally, they recognized 5G usage potential and benefits for defense reasons especially in the areas of deployed facilities, support, and battle zones (Zmysłowski et al, 2023).

Conclusion

One of the main ways to represent slicing as a powerful tool is to apply this technology in 5G and beyond to mobile communication systems. On the other hand, an important feature of the 3GPP Releases 15 and 16 is

that they pave the way for the introduction of 5G and 5G Advanced as well as for further development.

In the next period, it will be enabled for use cases to increase mobile broadbands. This is the time of industrial productivity resulting from the introduction of Release 16 and Release 17. The initial 6G networks will start with basic research. Network slicing is one of the types in 3GPP Release 16 and further addressed in Release 17 which were in progress in 2021 and 2022, respectively. This motivates an integration of security aspects in network slicing. Also, Release 18 which represents the first release named 5G Advanced puts the main focus on AI, ML and XR. Release 19 as the second release of 5G Advanced with its new capabilities and efficiency such as a set of features which will offer services based on extended reality as well as enhancements in AI/ML will be the next step towards 6G technology.

Next, Release 20 as one more step closer to 6G is expected in the near future.

It is evident that the 5G and emerging 6G landscapes are extremely complex with many complementary technologies and standardization effects, spectrum usage models, and industry-driven consortium developments. In the next period, in no more than five years, it will be evident that 5G and beyond networks will enable different use cases and mobile broadbands to increase. This relates, first of all, to the 3GPP features to be provided with Release 16 and 17. The end of the decade will witness the appearance of the initial 6G networks, already in development.

The standardization process for 5G different functionalities and capabilities contained in 5G Releases up to now as well as in the near future are recognized as the key enablers suitable for implementations in the military environment in modern warfare in order to provide: support for enhanced communication; control and operational efficiency; real-time data processing and support for ISR; autonomous and remote operations capabilities; improved network-centric warfare as well as the interoperability concept and cybersecurity challenges and resilient communications.

References

-3GPP. 2021. *Release 16 Description; Summary of Release-16 Work Items (TR 21.916)* 21 June [online]. Available at: https://portal.3gpp.org/desktopmodules/Specifications/SpecificationDetails.aspx?specificationId=3493 [Accessed: 04 August 2024].

-3GPP. 2022. *Release 17 Description; Summary of Release-17 Work Items (TR 21.917),* 20 December [online]. Available at: https://portal.3gpp.org/desktopmodules/Specifications/SpecificationDetails.aspx?specificationId=3937 [Accessed: 04 August 2024].

-3GPP. 2023. *Release 18 Description; Summary of Release-18 Work Items (TR 21.918),* 01 December [online]. Available at: https://portal.3gpp.org/desktopmodules/Specifications/SpecificationDetails.aspx?specificationId=4229 [Accessed: 04 August 2024].

Abdelkafi, N., Bekkers, R., Bolla, R., Rodriguez-Ascaso, A. & Wetterwald, M. 2021. *Understanding ICT Standardization-Principles and Practice*, *2nd Edition.* Sophia Antipolis Cedex, France: ETSI (European Telecommunications Standards Institute) [online]. Available at: https://research.tue.nl/en/publications/understanding-ict-standardization-principles-and-practice [Accessed: 04 August 2024]. ISBN: 979-10-92620-50-1.

Bertenyi, B. 2021. 5G evolution: What's next?, *IEEE Wireless Communications*, 28(1), pp.4-8. Available at: https://doi.org/10.1109/MWC.2021.9363048.

Bastos, L., Capela, G., Koprulu, A. & Elzinga, G. 2021. Potential of 5G technologies for military applications, In: *2021 International Conference on Military Communication and Information Systems (ICMCIS)*, The Hague, Netherlands, pp.1-8, May 04-05. Available at: https://doi.org/10.1109/ICMCIS52405.2021.9486402.

Chen, W., Goal, P., Montojo, J. & Zisimopoulos, H. 2021. *Fundamentals of 5G Communications: Connectivity for Enhanced Mobile Broadband and Beyond, 1st Edition*. New York: McGraw Hill [online]. Available at: https://www.accessengineeringlibrary.com/content/book/9781260459999 [Accessed: 04 August 2024]. ISBN: 9781260459999.

Chen, W., Lin, X., Lee, J., Toskala, A., Sun, S. & Chiasserin, C.F. 2023. 5G-Advanced Toward 6G: Past, Present and Future. *IEEE Journal on Selected Areas in Communications*, 41(6), pp.1592-1619. Available at: https://doi.org/10.1109/JSAC.2023.3274037.

Fowdur, T.P., Indoonundor, M., Milovanovic, D.A. & Bojkovic, Z.S. 2024. *5G NR Modeling in MATLAB: Network Architecture, Protocols and Physical Layer*, *1st Edition*. Boca Raton, FL, USA: CRC Press. Available at: https://doi.org/10.1201/9781003465393.

Ghosh, A., Maeder, A., Baker, M. & Chandramouli, D. 2019. 5G evolution: A view on 5G cellular technology beyond 3GPP release 15. *IEEE Access*, 7, pp.127639-127651. Available at: https://doi.org/10.1109/ACCESS.2019.2939938.

Kim, Y., Kim, Y., Oh, J., Ji, H, Yeo, J., Choi, S., Ryu, H., Noh, H., Kim, T., Sun, F., Wang, Y., Qi, Y. & Lee, J., 2019. New Radio (NR) and its Evolution toward 5G-Advanced. *IEEE Wireless Communications,* 26(3), pp.2-7. Available at: https://doi.org/10.1109/MWC.2019.8752473.

Lin, X. 2022. An Overview of 5G Advanced Evolution in 3GPP Release 18. *IEEE Communications Standards Magazine*, 6(3), pp.77-83. Available at: https://doi.org/10.1109/MCOMSTD.0001.2200001.

Lin, X. & Lee, N. (Eds). 2021. *5G and Beyond: Fundamentals and Standards*. Cham: Springer. Available at: https://doi.org/10.1007/978-3-030-58197-8.

-Maris. 2024. The Future of Connectivity: 5G Technology in The Defense Industry. *Maris*, 28 February [online]. Available at: https://www.maris-tech.com/blog/5g-in-defense-revolutionizing-military-connectivity-and-operations/ [Accessed: 04 August 2024].

Miličević, Z.M. & Bojković, Z.S. 2024. Review of 5G and 6G applications for mobile wireless communication in the military environment. *Vojnotehnički glasnik/Military Technical Courier*, 72(1), pp.435-451. Available at: https://doi.org/10.5937/vojtehg72-47037.

Milovanovic, D.A. & Bojkovic, Z.S. 2020. An Evolution of 5G Multimedia Communication: New Ecosystem. In: Bojkovic, Z.S., Milovanovic, D.A. & Fowdur, T.P. (Eds.) *5G Multimedia Communication: Technology, Multiservices, and Deployment*, *1st Edition*, *Chapter VII,* pp.129-156*.* Boca Raton, FL, USA: CRC Press. Available at: https://www.taylorfrancis.com/chapters/edit/10.1201/9781003096450-7/evolution-5g-multimedia-communication-dragorad-milovanovic-zoran-bojkovic [Accessed: 04 August 2024]. ISBN: 9781003096450.

Milovanovic, D.A., Bojkovic, Z.S., & Kukolj, D.D. 2020. 5G ML-Based Networks toward 6G: Convergence and Key Technology Drivers. In: Bojkovic, Z.S., Milovanovic, D.A. & Fowdur, T.P. (Eds.) *5G Multimedia Communication: Technology, Multiservices, and Deployment*, *1st Edition, Chapter VI,* pp.115-125*.* Boca Raton, FL, USA: CRC Press [online]. Available at: https://www.taylorfrancis.com/chapters/edit/10.1201/9781003096450-6/5g-ml-based-networks-toward-6g-dragorad-milovanovic-zoran-bojkovic-dragan-kukolj [Accessed: 04 August 2024] ISBN: 9781003096450.

Shafi, M., Molisch, A.F., Smith, P.J., Haustein, T., Zhu P., De Silva, P., Tufvesson, F., Benjebbour, A. & Wunder, G. 2017. 5G: A Tutorial Overview of Standards, Trials, Challenges, Deployment, and Practice. *IEEE Journal on Selected Areas in Communications*, 35(6), pp.1201-1221. Available at: https://doi.org/10.1109/JSAC.2017.2692307.

Wang, C-X., Haider, F., Gao, X., You X-H., Yang Y., Yuan, D., Aggou, H. M., Harald, H., Fletcher, S. & Hepsaydir, E. 2014. Cellular architecture and key technologies for 5G wireless communication networks. *IEEE Communications Magazine*, 52(2), pp.122-130. Available at: https://doi.org/10.1109/MCOM.2014.6736752.

Wijethilaka, S. & Liyanage, M. 2021. Survey on network slicing for Internet of Things realization in 5G networks. *IEEE Communications Surveys & Tutorials*, 23(2), pp.957-994. Available at: https://doi.org/10.1109/COMST.2021.3067807.

Zmysłowski, D., Skokowski, P., Malon, K., Maślanka, K. & Kelner, J.M. 2023. Naval Use Cases of 5G Technology. *International Journal on Marine Navigation*

and Safety of Sea Transportation, 17(3), pp.595-603. Available at: https://doi.org/10.12716/1001.17.03.11.

Zong, B., Fan, C., Wang, X., Duan, X., Wang, B. & Wang, J. 2019. 6G technologies: Key drivers, core requirements, system architectures, and enabling technologies. *IEEE Vehicular Technology Magazine*, 14(3), pp.18-27. Available at: https://doi.org/10.1109/MVT.2019.2921398.

Estandarización para la tecnología 5G y más allá: impacto en las comunicaciones militares

Zoran M. Miličević[a], *Zoran* S. Bojković[b],
Nataša Z. Bojković[c], *Tanja* M. Živojinović[c]

[a] Fuerzas Armadas de Serbia, Estado Mayor, Telecomunicaciones y Dirección de Tecnología de la Información (J-6), Belgrado, República de Serbia, **autor de correspondencia**

[b] Universidad de Belgrado, Belgrado, República de Serbia

[c] Universidad de Belgrado, Facultad de Ingeniería de Transporte y Tráfico, Belgrado, República de Serbia

CAMPO: telecomunicaciones
TIPO DE ARTÍCULO: artículo de revisión

Resumen:

Introducción/objetivo: El presente artículo de revisión trata sobre el proceso de estandarización de la tecnología 5G y más allá y su impacto en las comunicaciones militares.

Métodos: Se proporcionaron métodos dominantes como análisis y síntesis para considerar los aspectos clave del proceso de evolución de la estandarización 5G a través de presentaciones de los roles de diferentes lanzamientos de estándares del Proyecto de Asociación de Tercera Generación (3GPP) y su implementación y uso en el entorno de redes de comunicación militar.

Resultados: Se presentan los antecedentes y las áreas clave en la evolución de 5G y más allá. Además, se discuten la estandarización de 5G y los problemas y desafíos militares.

Conclusión: La estandarización para 5G y el panorama emergente 6G es extremadamente compleja y altamente innovadora con muchos requisitos impulsados por la industria y la sociedad en rápida evolución. Las organizaciones de desarrollo de estándares, la industria y el mundo académico necesitan colaborar en la estandarización para facilitar la interoperabilidad mundial. El documento ofrece una descripción general de las funcionalidades de estandarización y los esfuerzos para mejorar el rendimiento del sistema 5G, así como su impacto en las comunicaciones y servicios militares. Analiza las áreas de mejoras principales para las

características existentes y la expansión a nuevos casos de uso e industrias, así como al uso militar a través de las versiones 3GPP, comenzando con la versión 15 como 5G Basic, pasando por la 16 y 17 como 5G Evolution, hasta la 18 y 19 como 5G Advanced que preceden a la próxima versión 20 y la red 6G inicial cuyo lanzamiento se espera para fines de esta década.

Palabras claves: la tecnología de quinta generación (5G), lanzamientos del proceso de estandarización 5G, funcionalidades 5G, interoperabilidad 5G.

Стандартизация технологии 5G и не только: влияние на военные коммуникации

Зоран М. Миличевич[а], *Зоран* С. Бойкович[б],
Наташа З. Бойкович[в], *Таня* М. Живойинович[в]

[а] Вооруженные силы Республики Сербия, Генеральный штаб, Управление телекоммуникаций и информационных технологий (J-6), г. Белград, Республика Сербия, **корреспондент**

[б] Белградский университет, г. Белград, Республика Сербия

[в] Белградский университет, факультет дорожного движения, г. Белград, Республика Сербия

РУБРИКА ГРНТИ: 49.33.29 Сети связи
ВИД СТАТЬИ: обзорная статья

Резюме:

Введение/цель: Представленная обзорная статья посвящена процессам стандартизации технологии 5G и последующих технологий, а также ее влиянию на военные коммуникации.

Методы: На рассмотрение были вынесены доминирующие методы, такие как анализ и синтез ключевых аспектов процесса развития стандартизации 5G посредством презентации ролей различных выпусков стандартов Проекта партнерства третьего поколения (3GPP), а также его внедрения и использования в среде военных сетей связи.

Результаты: В статье представлены предыстория, ключевые и прочие области развития 5G. Также обсуждаются проблемы стандартизации 5G, военные вопросы и вызовы.

Выводы: Стандартизация 5G и формирующегося рынка 6G является чрезвычайно сложной и инновационной деятельностью, поскольку многие требования, предъявляемые промышленностью и социумом в целом, скоротечно меняются. В данной связи организациям, занимающимся разработкой стандартов, промышленным предприятиям и научному сообществу необходимо сотрудничать в области стандартизации для того, чтобы

обеспечить совместимость во всем мире. В статье представлен обзор функциональных возможностей стандартизации и усилий по повышению производительности системы 5G, а также ее влияния на военную связь и услуги. Также в статье анализируются области главных улучшений существующих функций и их распространения на новые варианты использованияв разных отраслях промышленности, в том числе в военном применении с помощью выпусков 3GPP, начиная с 15-го выпуска под названием 5G Basic, продолжая 16-м и 17-м под названием 5G Evolution и заканчивая выпуском 18-м и 19-м под названием 5G Advanced, которые предшествуют предстоящему 20-му выпуску и первой 6G сети, запуск которой ожидается в конце этого десятилетия.

Ключевые слова: технология пятого поколения (5Г), выпуски процесса стандартизации 5Г, функциональные возможности 5Г, совместимость 5Г.

Стандардизација за 5Г технологију: утицај на војне комуникације и остале области

Зоран М. Миличевић[а], *Зоран* С. Бојковић[б], *Наташа* С. Бојковић[в], *Тања* М. Живојиновић[в]

[а] Војска Србије, Генералштаб, Управа за телекомуникације и информатику (J-6), Београд, Република Србија, **аутор за преписку**

[б] Универзитет у Београду, Београд, Република Србија

[в] Универзитет у Београду, Саобраћајни факултет, Београд, Република Србија

ОБЛАСТ: телекомуникације
ВРСТА ЧЛАНКА: прегледни рад

Сажетак:

Увод/циљ: Овај прегледни рад бави се процесом стандардизације за технологију пете генерације (5Г) и њеним утицајем на војне комуникације и остале области.

Методе: Доминантне методе као што су анализа и синтеза коришћене су за разматрање кључних аспеката процеса еволуције стандардизације 5Г кроз презентације улога различитих стандардних издања Пројекта партнерства треће генерације (3ГПП) и његове имплементације и употребе у окружењу војних комуникационих мрежа.

Резултати: Представљене су позадина и кључне области у еволуцији 5Г. Такође, дискутује се о стандардизацији 5Г и војним питањима и изазовима.

Закључак: Стандардизација за 5Г и 6Г окружење у настајању изузетно је сложена и веома иновативна и мора задовољити многе

захтеве индустрије и друштва који се брзо развијају. Организације за развој стандарда, индустрија и академска заједница морају да сарађују на стандардизацији како би се олакшала интероперабилност широм света. У раду су наведене функционалности стандардизације и настојања да се побољшају перформансе 5Г система, као и његов утицај на војне комуникације и услуге. Анализиране су области великих побољшања за постојеће функције и проширења на нове случајеве употребе у индустрији, као и за војну употребу кроз издања 3ГПП, почевши од издања 15 као 5Г Основа, преко 16 и 17 као 5Г Развој, па навише до 18 и 19 као 5Г Напредни који претходе предстојећем издању 20 и почетној 6Г мрежи чије се лансирање очекује до краја ове деценије.

Кључне речи: технологија пете генерације (5Г), издања процеса стандардизације 5Г, 5Г функционалности, 5Г интероперабилност.

Paper received on: 05.08.2024.
Manuscript corrections submitted on: 30.01.2025.
Paper accepted for publishing on: 31.01.2025.

Нови високоенергетски лаки ласерски системи[1]

LITE BEAM

Израелска одбрамбена компанија *Rafael Advanced Defense Systems* најавила је увођење најновије верзије свог високоенергетског ласерског система оружја *LITE BEAM* на изложби одбрамбених система (*AUSA*) 2024. године. Систем је пројектован за брзо и прецизно неутралисање претњи из ваздушног простора, укључујући ројеве дронова, *и* представља значајан напредак у прецизној одбрани. Овај ласерски систем од 10 kW намењен је побољшању заштите снага у мобилним копненим операцијама, комбинујући ефикасност са исплативом употребом.

Погодан за лака возила, LITE BEAM се може распоредити у различитим оперативним зонама, што му омогућава да се супротстави широком спектру претњи, од дронова и ракета до минобацачких граната. (Извор фотографије: компанија Rafael Advanced Defense Systems)

[1] Defense News Army 2024 (7 October, 15 October, 8 October)

Vučković, D., SAVREMENO NAORUŽANJE I VOJNA OPREMA / MODERN WEAPONS AND MILITARY EQUIPMENT, pp.359-371

LITE BEAM представља део стратегије компаније *Rafael* за проширење примене оружја усмерене енергије за сузбијање разних претњи из ваздушног простора и са земље. Овај мобилни модел представља адаптацију Рафаеловог система *Iron Beam*, фиксног ласера од 100 kW који може да уништи мете на удаљености од неколико километара.

Погодан за лака возила, *LITE BEAM* се може распоредити у различитим оперативним зонама, што му омогућава да се супротстави широком спектру претњи, од дронова и ракета до минобацачких граната. Поред тога, овај систем може да неутралише идентификоване импровизоване експлозивне направе (IED) и друге претње са земље, што га чини свестраним на бојном пољу.

Нова верзија система *LITE BEAM*, представљена на сајму *AUSA* 2024, има повећани капацитет од 10 kW, у односу на претходних 7,5 kW, па се може поредити са системима као што су *Jupiter* компаније *MBDA* и *Rheinmetall*. Са ефективним дометом од неколико стотина метара до око 2.000 м, *LITE BEAM* се одликује способношћу да прецизно прати циљеве путем напредног система праћења, који се такође може интегрисати у друге системе против беспилотних летелица (C-UAV).

Његова модуларност омогућава инсталацију на различите платформе, укључујући оклопна возила, бродове и фиксне земаљске платформе. *LITE BEAM* је флексибилан, јер се може напајати или дизел генераторима или батеријама, у зависности од оперативних потреба.

Технологија високоенергетских ласерских система брзо напредује и код других међународних конкурената, као што су компаније *MBDA, Rheinmetall, Lockheed Martin* и *Raytheon* које такође развијају решења од 10 kW. Међу њима, систем *ATHENA* компаније *Lockheed Martin* омогућава комбиновање више ласера како би се постигла излазна снага од 30 кW, док је систем компаније *Raytheon HELWS* пројектован за екстремну мобилност и може се инсталирати на обично теренско возило.

*И*ако је још увек у раној фази развоја са многим системима, у истраживању или тестирању, ова технологија представља потенцијал за будуће одбрамбене апликације. Способност система *LITE BEAM* да обезбеди брзу и прецизну ласерску одбрану у мобилном спектру напредак је компаније *Rafael* у овој области, јер га позиционира као потенцијално стратешко средство за сузбијање нових претњи.

Stryker C-UAS DE

Компаније *Leonardo DRS* и *BlueHalo* произвеле су нову варијанту борбеног возила пешадије *Stryker,* класификације 8x8, која представља систем за одбрану од беспилотних летелица усмереном енергијом или *Counter-Unmanned Aircraft System (C-UAS) Directed Energy (DE) Stryker*. Ова верзија борбеног возила, која је представљена на изложби наоружања *AUSA* 2024, опремљена је ласерски усмереним енергетским оружјем, ласерски вођеним ракетама 70 мм, аутоматским топом 30 мм и разним

радарима и сензорима. Компаније су недавно извеле бојеву демонстрацију у којој су успешно неутралисане мете беспилотне летелице групе 1-3.

Counter-Unmanned Aircraft System (C-UAS) Directed Energy (DE) Stryker опремљен је ласерски усмереним енергетским оружјем, ласерски вођеним ракетама 70 мм, аутоматским топом 30 мм и разним радарима и сензорима. (Извор фотографије: Army Recognition)

Током демонстрације, која је одржана 2024. пред званичницима америчке војске у Сокору, у Новом Мексику, мобилни систем *C-UAS* користио је ласерски оружани систем (*Locust Laser Weapon System*) *BlueHalo* 26kW током два дана. Показано је да оклопно возило *C-UAS Directed Energy (DE) Stryker* може бити платформа за ласерско и друго оружје за борбу против ваздухоплова и копнених циљева, укључујући ласерско оружје и даљинску оружну станицу (RWS) калибра30 мм за гађање циљева.

Према наводима компаније *Leonardo DRS*, ово усмерено енергетско оружје, постављено на мобилној платформи у задњем делу оклопног возила Stryker 8x8, може да се бори против беспилотних летелица групе 1, 2 и 3 (UAS). Такође, може се супротставити беспилотним летелицама масе до 600 кг које достижу висине од 5.486 м и брзине до 463 км/х. *Locust Laser Weapon System* је ласер од 26 kW, врло је мобилан и омогућава брзо распоређивање. Поред тога, интегрише елементе за контролу снопа, поравнање, снагу и термичку регулацију унутар компактног дизајна који се

монтира на клизаче, што омогућава да га померају стандардна возила као што су виљушкари и камиони.

Систем је оперативан у року од 15 мин од постављања, а контролише га један оператер преко мрежног интерфејса. Његов модуларни дизајн омогућава брзу замену појединачних подсклопова, подржавајући минимално време застоја. Са скалабилним опсегом излазне снаге од 2 до 20 kW, систем се брани од вишеструких претњи из ваздушног простора помоћу пулсног доплера, електронски скенираног радара за покривеност од 360 степени. Такође, подржава операције против беспилотних летелица, противваздухопловну одбрану и детектује непријатељску ватру.

Са скалабилним опсегом излазне снаге од 2 до 20 kW, систем се брани од вишеструких претњи из ваздушног простора помоћу пулсног доплера, електронски скенираног радара за покривеност од 360 степени. (Извор фотографије: BlueHalo)

Краткоталасна инфрацрвена камера *SWIR* обезбеђује велики број фрејмова, између 500 и 2.500 Hz, са троструким увећањем и укључује безбедан ласерски даљиномер за прецизно праћење. Осветљивач са подесивом величином тачке побољшава слику у различитим условима. Сензори за аквизицију раде на 120 Hz са резолуцијом од 1280 x 720, покривајући и видљиви и средњеталасни инфрацрвени *MWIR* спектар, омогућавајући широко поље праћења малих циљева.

Прилагодљиви систем напајања може да користи конфигурације батерије, генератора или копнене енергије и укључује интегрисани систем хлађења који омогућава преко 100 с непрекидног ласерског рада са циклусом од 25%. Кардан обезбеђује ротацију азимута за 360 степени и распон елевације од -30 до +90 степени, што гарантује широке могућности праћења.

Ирански (кинески) ласерски систем

Чини се да је Иран опремљен новим напредним ласерским одбрамбеним системом, судећи према фотографији објављеној на X налогу *Mehdi H 4*, октобра 2024. године. Прве анализе сугеришу да би овај ласерски систем могао бити кинески *Shen Nung* (Божански фармер) – ласерски одбрамбени систем *Shield 3000/5000*, такође познат као „Тихи ловац". Могло би се закључити да је Иран можда набавио ову најсавременију технологију како би побољшао своје одбрамбене способности против претњи на малим висинама.

Ирански ласерски одбрамбени систем Shield 3000/5000

*Shield 3000/5000*је одбрамбени систем за напад на циљеве на малим висинама (*LASS*), којег карактерише способност да циља и неутралише беспилотне летелице (*UAV*) и друге нисколетеће објекте. Варијанта „Тихи ловац" је систем ласерског оружја на електрични погон развијен у Кини. Велика излазна снага у распону од 30 до 100 kW омогућава му да ефикасно гађа циљеве на различитим дометима и висинама.

Једна од изузетних карактеристика „Тихог ловца" је његов максимални оперативни домет од 4 км. На удаљености од 800 мможе да пробије челик дебљине10 мм, што указује на његову ефикасност против оклопних циљева. Ова способност чини га значајним средством за сузбијање ројева дронова и заштиту критичне инфраструктуре од претњи из ваздушног простора.

Недавне одбрамбене везе између Ирана и Кине одражавају продубљивање стратешког партнерства, што је потврђено свеобухватним 25-годишњим споразумом о сарадњи, потписаним 2021. године. Споразум је намењен јачању иранских војних и технолошких капацитета, укључује заједничку војну обуку, размену обавештајних података и потенцијалне трансфере наоружања. Такође, омогућава Кини да користи иранске ваздухопловне и поморске објекте, посебно у Персијском заливу, што јача позиције обе државе у региону услед промена геополитичких савеза. Кинеска одбрамбена сарадња укључивала је трансфер технологије и обуку ради јачања иранских способности против приступа и ускраћивања подручја, посебно против претњи из ваздушног простора и са мора.

Као део овог партнерства, Иран би могао да добије приступ напредном кинеском наоружању, укључујући системе за борбу против беспилотних летелица, као и ракетну технологију. Овај одбрамбени савез позиционира обе земље као стратешку противтежу утицају САД на Блиском истоку. Кинески ласерски одбрамбени систем „Тихи ловац", недавно примећен у Техерану, представља пример могућег трансфера наоружања који штити иранску одбрамбену инфраструктуру од претњи из ваздушног простора са малих висина, означавајући значајан корак напред у билатералној војној сарадњи.

Оружане снаге сматрају да су ласерски системи веома ефикасни у борби против дронова због њихове прецизности, брзине и ниских оперативних трошкова. Ласери могу да онеспособе или униште беспилотне летелице скоро тренутно, циљајући њихове сензоре или структурне компоненте, што их чини идеалним за супротстављање ројевима малих, нисколетећих беспилотних летелица. Ови системи, такође, обезбеђују скалабилност у излазној снази, омогућавајући одбрамбеним снагама да прилагоде утрошак енергије на основу типа мете, што је исплативо у поређењу са традиционалном муницијом за пресретање. Поред тога, ласерски системи стварају минималну колатералну штету и могу да раде непрекидно све док има довољно снаге, што их чини поузданим средствима у одбрани осетљивих локација.

Неколико оружаних снага широм света унапређује ласерске системе оружја како би се супротставило растућој претњи од дронова и других циљева у ваздушном простору. Америчка војска, на пример, развија систем ласерског оружја високе енергије (*HELWS*) за неутрализацију беспилотних летелица и ракета, са тестовима који показују обећавајуће резултате и у покретним и у стационарним одбрамбеним поставкама. Слично томе, израелски „Гвоздени сноп" (*Iron Beam*) представља ласерски систем велике снаге дизајниран да пресреће беспилотне летелице, минобацаче и пројектиле из непосредне близине, допуњујући одбрамбени систем ракетама „Гвоздена купола" (*Iron Dome*). У Европи, Немачка је тестирала сопствене ласерске системе у оквиру Бундесвера за сличне одбрамбене задатке против беспилотних летелица. Ови развоји имају за циљ да

обезбеде исплативо, прецизно и одговорно одбрамбено решење за претње дроном које еволуирају у сложености и обиму.

Увођење таквог система у ирански арсенал могло би имати значајне импликације на динамику регионалне безбедности. То указује на потенцијално продубљивање војне сарадње између Ирана и Кине, у складу са стратешким интересима обе државе. Штавише, побољшава способност Ирана да брани свој ваздушни простор од све софистицираних упада беспилотних летелица, који су постали карактеристика модерног асиметричног ратовања.

Драган М. Вучковић (*Dragan* M. Vučković),
e-mail: draganvuckovic64@gmail.com,
ORCID iD: https://orcid.org/0000-0003-1620-5601

Тенк К3 следеће генерације са погоном на водоник[2]

Компанија *Hyundai Rotem*, подружница *Hyundai Motor Group,* најавила је развој К3 – првог борбеног тенка на водоник на свету, у партнерству са Агенцијом за развој одбране и Корејским истраживачким институтом за планирање и унапређење одбрамбене технологије. Пројектован је тако да унапреди војне способности Републике Јужне Кореје, док истовремено испуњава глобалне циљеве енергетске одрживости. Опремљен је водоничним горивним ћелијама, па се очекује да ће заменити дизел моторе у постојећим тенковима, као што је К2, обезбеђујући тише и скривеније оперативне могућности.

Сарадња између компаније *Hyundai Rotem*, Агенције за развој одбране и Корејског истраживачког института за планирање и унапређење одбрамбених технологија представља значајан технолошки напредак. Очекује се да ће тенк К3 бити опремљен водоничним горивним ћелијама, напредним електричним моторима и пуњивим батеријама, што ће бити еколошки прихватљива алтернатива дизел моторима. Овај иновативни систем не само да смањује емисије штетних гасова, већ и омогућава оклопном возилу да ради у готово потпуној тишини, увелико побољшавајући могућности прикривености – суштинску стратешку предност у модерном ратовању.

Пројекат тенка К3 нуди значајне оперативне предности, укључујући могућност навигације по тешким теренима и стрмим нагибима. Поред водоничних горивних ћелија, тенк ће имати топ са глатком цеви 130 мм, значајну надоградњу у односу на топ 120 мм са тенка К2, чиме се повећава његова ватрена моћ. Такође, компанија *Hyundai Rotem* је открила планове за интеграцију вештачке интелигенције (AI) у систем за контролу ватре тенка. Ова функција, вођена вештачком интелигенцијом, има за циљ да

[2] Defence & Security Industry Technology 2024, 31 October

побољша способности гађања и прецизности К3, дајући му предност у превентивним ударима и брзој процени претње на бојном пољу.

К3 – први борбени тенк на водоник на свету

Производња тенка К3 са пуним погоном на водоник планирана је за 2040. годину. Као прелазно решење, Компанија *Hyundai Rotem* ће прво представити хибридни модел, комбинујући системе дизела и водоника. Ова прелазна фаза омогућиће војсци Јужне Кореје да искористи неке од предности технологије водоника док се припрема за потпуни прелазак на овај извор енергије. Званичници компаније *Hyundai Rotem* потврдили су да ће ова хибридна верзија ускоро бити оперативна, подржавајући стратешке циљеве Јужне Кореје са смањеним емисијама на бојишту, уз одржавање снажне војне ефикасности.

Развој тенка К3 је у складу са ширим трендом примене водоничног горива у глобалном сектору одбране и транспорта. Компанија *Hyundai* већ је позната по свом пионирском раду на горивним ћелијама и проширује своју експертизу на војну технологију, доприносећи еволуцији решења за мобилност на бази водоника. На пример, компанија је раније сарађивала са кинеском компанијом *WeRide* на аутономним возилима на водоник. Слично томе, у Сједињеним Државама напредак у технологији водоника изазива таласе у комерцијалном и војном поморском транспорту, са пројектима као што је „*Sea Change*”, први трајект на водоник који је одобрила америчка обалска стража, који ће ускоро бити поринут у заливу у Сан Франциску.

Водонична горивна ћелија ради тако што претвара водоник и кисеоник у електричну енергију, воду и топлоту путем електрохемијске реакције. Састоји се од три главне компоненте: аноде, катоде и електролита. Водоник, ускладиштен у резервоару, убризгава се у аноду, где се катализом дели на протоне и електроне. Протони пролазе кроз електролит да би стигли до катоде, док електрони, неспособни да пређу електролит, пролазе кроз спољашње коло, стварајући употребљиву електричну струју. С друге стране, кисеоник, који се обично црпи из ваздуха, уводи се на катоду, где се комбинује са протонима и електронима и формира воду, чисти нуспроизвод ове реакције. Ова технологија, која емитује само воду и топлоту, обезбеђује одржив извор енергије без загађења; идеална је за апликације које захтевају ниске акустичне и термичке карактеристике, као што су стелт војне операције.

У сукобу попут оног у Украјини, тенк на водоник би имао значајне стратешке предности, посебно у смислу прикривености, аутономије и оперативности у непријатељским окружењима. Због ниског термалног одраза, тенк на водонични погон би било теже открити инфрацрвеним системима за надзор, што би омогућило дискретне маневре, ноћне патроле и инфилтрацију иза непријатељских линија. Његова повећана аутономија би, такође, омогућила оклопним јединицама да продру дубље у непријатељску територију без честог допуњавања горива, што је драгоцена способност у областима са сложеним логистичким ланцима снабдевања. Поред тога, производња само водене паре без загађујућих емисија учинило би резервоар отпорним на деградирано или контаминирано окружење, типично за урбана и индустријска подручја погођена ратом. Смањењем ослањања на фосилна горива, ова врста возила би олакшала логистичке захтеве и заштитила линије снабдевања, који су често рањиви на циљане нападе. Коначно, тихи рад водоничне технологије понудио би кључну предност за заседне активности или одбрану у шумовитим или урбаним подручјима, омогућавајући тенку да остане неоткривен до почетка борбеног дејства. Дакле, тенк на водонични погон могао би да одговори на јединствене изазове савременог сукоба, попут оног у Украјини, нудећи комбинацију дискреције, аутономије и отпорности на животну средину, што би значајно ојачало оперативне способности на терену.

Пројекти развоја војних возила на водоник добијају на глобалном замаху, иако је Јужна Кореја, са својим тенком К3, у првом плану. Друге земље и одбрамбене компаније такође истражују потенцијал водоника за војну примену, иако су у томе мање напредовале од компаније *Hyundai Rotem* .

У Сједињеним Државама војска процењује одрживост водоника као део свог програма *Next Generation Combat Vehicle (NGCV).* Компанија *General Motors Defense* је, на пример, развила прототип ZH2, теренско возило на водоник пројектовано за америчку војску. Овај модел има за циљ да тестира могућности прикривености и аутономије водоничне технологије за мисије. Поред тога, компаније *BAE Systems u Oshkosh Defense*, два

главна одбрамбена извођача, такође истражују хибридне и водоничне технологије за будуће примене, иако је њихов фокус за сада првенствено на хибридним возилима.

У Европи, програм *MGCS (Main Ground Combat System*), заједно воде компаније *Krauss-Maffei Wegmann (KMW)* и *Nexter.* Ради се о водећем пројекту за развој будућег европског борбеног тенка. Док су још у фази спецификације, разматрају се хибридне и водоничне опције како би се смањиле емисије и побољшала прикривеност. Компанија *Rheinmetall*, која је такође укључена у пројекат, истражује алтернативна решења за погон, али није донела коначну одлуку у вези са усвајањем технологије водоника.

Јапан је такође заинтересован за водоничне горивне ћелије за оклопна возила преко компаније *Mitsubishi Heavy Industries.* Овај индустријски конгломерат истражује употребу технологије водоника за своје будуће борбене тенкове, реагујући на захтеве јапанског Министарства одбране за решењима која повећавају аутономију уз смањење угљеничнког отиска. Компанија *Mitsubishi Heavy Industries* се првенствено фокусира на прототипове и тестирање перформанси на тешким теренима како би проценила применљивост водоника у својим борбеним возилима.

Израел је такође заинтересован за предности водоника за мисије које захтевају ниске акустичне и термичке карактеристике. Израелске компаније, као што *су Elbit Systems u Israel Aerospace Industries* (IAI), спроводе истраживања о стелт одбрамбеним возилима и разматрају алтернативна решења будућег погона како би задовољиле специфичне потребе Израелских одбрамбених снага (ИДФ), иако до данас не постоји званични програм посвећен водонику.

Иако је неколико земаља и одбрамбених компанија активно ангажовано у истраживању нових погонских технологија како би се смањио утицај војних возила на животну средину, мало њих је поставило водоник као непосредан приоритет. Захваљујући пројекту тенка К3 компаније *Hyundai Rotem,* Јужна Кореја сврстала се на чело развоја борбених тенкова на водоник, нудећи мапу пута за друге државе. Ова иновација могла би да подстакне европске, америчке и азијске компаније, као што су *BAE Systems, General Motors Defense, KMW, Nexter* и *Mitsubishi Heavy Industries,* да убрзају сопствене програме водоника, истражујући потенцијал ове технологије за војну примену.

Драган М. Вучковић (*Dragan* M. Vučković),
e-mail: draganvuckovic64@gmail.com,
ORCID iD: https://orcid.org/0000-0003-1620-5601

Нови кинески ракетни систем земља-ваздух HQ-19[3]

Ракетни систем земља-ваздух *HQ-19*, познат као *Hongqi-19*, први пут је представљен јавности на сајму авијације u Џухају 2024. године. Овај пресретач против балистичких пројектила (АВМ), који је развијен у Кини и пројектован за сузбијање претњи од балистичких пројектила унутар и изван атмосфере, упоредив је по концепту са америчким системом *THAAD-ER*. Иначе, *HQ-19* је већ у оперативној употреби Ваздухопловства Народне ослободилачке војске (*PLAAF*).

Посматрачи су приметили да би HQ-19 могао да се употреби против балистичких пројектила у јужноазијском региону, посебно против система као што су индијски Agni-4 и Agni-5.

Систем *HQ-19* је смештен на камиону високе покретљивости 8x8, који има конфигурацију лансера са шест пројектила. Користи механизам хладног лансирања под стрмим углом, што му омогућава да ефикасно пресреће долазеће балистичке ракете. Радарска технологија система, укључујући информациони радар *610A*, открива циљеве на дометима до приближно 4.000 км, покривајући подручја од северног дела јужне Азије до унутрашњих региона Кине, као што је Тибетанска висораван. Систем командовања и контроле *HQ-19* интегрише ове радарске податке како би побољшао праћење и пресретање циљева.

Развој система *HQ-19* датира из касних 90-их година, као део кинеског програма 863, чији је приоритет био напредак у високотехнолошким одбрамбеним способностима. Систем за навођење *HQ-19* поседује инфрацрвени трагач са бочним прозорима, дизајниран да смањи атмосферске сметње и обезбеди прецизно гађање на великим висинама.

[3] Defense News Army 2024, 5 November

Пројектил покреће двостепени ракетни мотор на чврсто гориво, који укључује конструкцију од угљеничних влакана и чврсто гориво *N-15B.* Ова конфигурација даје специфичан импулс од 260 с, подржавајући високу маневарску способност за пресретање бојевих глава у покрету. Мотор ракете има могућност двоструког импулса, што побољшава терминалну кинетичку ефикасност и проширује њен оперативни домет. Побољшана иновацијама у композитним материјалима, ова конфигурација омогућава ракети да маневрише силама до 60 г током пресретања.

Домет пресретања *HQ-19* наводно се протеже до 3.000 км, што му омогућава гађање балистичке ракете у том домету, укључујући њихове бојеве главе за поновни улазак. Због кинетичке бојеве главе система спада међу неколико система који су опремљени таквим механизмом, поред америчких кинетичких пројектила за уништавање (*KKV*). Кина је овладала технологијом кинетичког погађања и наводно је завршила успешан пробни лет 1999. године, што је чини другом државом која је развила овај приступ након што су вишеструки тестови у САД потврдили функционалност *HQ-19,* укључујући пресретање на висини од преко 200 км са релативним брзинама до 10.000 м/с. У фебруару 2021. кинеско министарство националне одбране известило је о тесту који је потврдио да је *HQ-19* испунио сва очекивања. Кина је спровела неколико таквих тестова од 2010. до 2021. године, наглашавајући одбрамбену природу свог система и наводећи да он није усмерен ни на једну конкретну земљу.

Представљање система *HQ-19* на сајму може да указује да је доступан за потенцијални извоз на тржиштима у регионима као што је Блиски исток. Кинеска одбрамбена индустрија заинтересована је за проширење базе клијената, поред кључних као што су Пакистан, Саудијска Арабија и Египат, како би успоставила већи фокус на тржиштима у развоју. Могућности система *HQ-19* у пресретању пројектила могу представљати опцију за земље које траже сличне одбрамбене системе. Овај приступ одражава шири интерес Кине за јачање свог војног извозног сектора упоредо са глобалним економским дометом, при чему се одбрамбена сарадња посматра као пут за изградњу ближих билатералних веза.

Поред система *HQ-19*, кинески оквир одбране од балистичких ракета укључује комплементарне системе као што су *HQ-9* и *HQ-26.* Систем *HQ-26*, са својим вишепулсним мотором на чврсто ракетно гориво, који је пројектован да побољша терминалне кинетичке перформансе, проширује свој домет и омогућава гађање различитих ракетних циљева. Радар са фазном решетком система *HQ-19,* намењен да ради у складу са овим системима, пружа могућности раног упозорења које подржавају вишеслојну противракетну одбрану. Радарска покривеност система и могућности пресретања такође га позиционирају као контрамеру против потенцијалних регионалних претњи, укључујући системе балистичких ракета из суседних земаља.

Може се закључити да *HQ-19* представља пример наставка кинеских напора да унапреде своје способности противракетне одбране. Поређење

овог система са америчким системима *THAAD* и *SM-3* изазвало је интересовање, а његове пријављене способности могу утицати на регионалну безбедносну динамику. Посматрачи су приметили да *HQ-19* може послужити као контрамера против балистичких пројектила у јужноазијском региону, посебно против система као што су индијске балистичке ракете *Agni-4* и *Agni-5*. Представљањем *HQ-19*, Кина наглашава свој стратешки циљ – проширење одбрамбених способности, као одговор на промену глобалних структура моћи и због забринутости за регионалну безбедност.

Драган М. Вучковић (*Dragan* M. Vučković),
e-mail: draganvuckovic64@gmail.com,
ORCID iD: https://orcid.org/0000-0003-1620-5601

ПОЗИВ И УПУТСТВО АУТОРИМА
ПРИГЛАШЕНИЕ И ИНСТРУКЦИЯ ДЛЯ АВТОРОВ РАБОТ
CALL FOR PAPERS AND INSTRUCTIONS FOR AUTHORS

ПОЗИВ И УПУТСТВО АУТОРИМА О НАЧИНУ ПРИПРЕМЕ ЧЛАНКА

Упутство ауторима о начину припреме чланка за објављивање у *Војнотехничком гласнику* урађено је на основу Правилника о категоризацији и рангирању научних часописа Министарства просвете, науке и технолошког развоја Републике Србије ("Службени гласник РС", број 159/20). Примена овог Правилника првенствено служи унапређењу квалитета домаћих часописа и њиховог потпунијег укључивања у међународни систем размене научних информација.

Војнотехнички гласник / Vojnotehnički glasnik / Military Technical Courier (втг.мо.упр.срб, www.vtg.mod.gov.rs, ISSN 0042-8469 – штампано издање, e-ISSN 2217-4753 – online, UDC 623+355/359, DOI: 10.5937/VojnotehnickiGlasnik; https://doi.org/10.5937/VojnotehnickiGlasnik), јесте рецензирани научни часопис.

Власници часописа су Министарство одбране Републике Србије и Војска Србије. Издавач и финансијер часописа је Универзитет одбране у Београду (Војна академија).

Програмска оријентација часописа заснива се на годишњој категоризацији часописа, коју врши надлежно државно министарство у одређеним областима, као и на његовом индексирању у међународним индексним базама.

Часопис обухвата научне, односно стручне области у оквиру образовно-научног поља **природно-математичких наука**, као и у оквиру образовно-научног поља **техничко-технолошких наука**, а нарочито области **одбрамбених наука и технологија**. Објављује теоријска и практична достигнућа која доприносе усавршавању свих припадника српске, регионалне и међународне академске заједнице, а посебно припадника војски и министарстава одбране. Публикује радове са уравнотеженим извештавањем о аналитичким, експерименталним и примењеним истраживањима, као и нумеричким симулацијама, обухватајући различите дисциплине. Објављени материјали су високог квалитета и релевантности, написани на начин који их чини доступним широкој читалачкој публици. Сви радови који извештавају о оригиналним теоријским и/или практично оријентисаним истраживањима или проширеним верзијама већ објављених радова са конференција су добродошли. Радови за објављивање одабиру се двоструко слепим поступком рецензије како би се осигурала оригиналност, релевантност и читљивост. Притом циљ није само да се квалитет објављених радова одржи високим већ и да се обезбеди правовремени, темељни и уравнотежени поступак рецензије.

Уређивачка политика *Војнотехничког гласника* заснива се на препорукама Одбора за етичност у издаваштву (COPE Core Practices) и заједничким принципима транспарентности и најбоље праксе у издаваштву COPE, DOAJ, OASPA и WAME, као и на најбољим прихваћеним праксама у научном издаваштву. *Војнотехнички гласник* је члан COPE (Committee on Publication Ethics) од 2. маја 2018. године и члан OASPA (Open Access Scholarly Publishers Association) од од 27. новембра 2015. године.

Министарство науке, технолошког развоја и иновација Републике Србије утврдило је дана 13. 12. 2024. године категоризацију *Војнотехничког гласника*, за 2024. годину:

– на листи часописа за рачунарске науке:
категорија врхунски часопис националног значаја **(M51)**,

– **на листи часописа за електронику, телекомуникације и информационе технологије:**
категорија врхунски часопис националног значаја **(M51)**,

– **на листи часописа за машинство:**
категорија врхунски часопис националног значаја **(M51)**,

– **на листи часописа за материјале и хемијске технологије:**
категорија национални часопис међународног значаја **(M24)**.

Усвојене листе домаћих часописа за 2024. годину могу се видети на сајту *Војнотехничког гласника*, страница *Категоризација часописа*.

Детаљније информације могу се пронаћи и на сајту Министарства просвете, науке и технолошког развоја Републике Србије.

Подаци о категоризацији могу се пратити и на сајту КОБСОН-а (Конзорцијум библиотека Србије за обједињену набавку).

Категоризација часописа извршена је према Правилнику о категоризацији и рангирању научних часописа Министарства просвете, науке и технолошког развоја Републике Србије ("Службени гласник РС", број 159/20).

Часопис се прати у контексту Српског цитатног индекса – СЦиндекс (база података домаћих научних часописа), Научно-информационог система Redalyc и Руског индекса научног цитирања (РИНЦ). Подвргнут је сталном вредновању (мониторингу) у зависности од утицајности (импакта) у самим базама. Детаљи о индексирању могу се видети на сајту *Војнотехничког гласника*, страница *Индексирање часописа*.

Војнотехнички гласник, у погледу свог садржаја, пружа могућност отвореног приступа (DIAMOND OPEN ACCESS) и примењује Creative Commons (CC BY) одредбе о ауторским правима. Детаљи о ауторским правима могу се видети на сајту часописа, страница *Ауторска права и политика самоархивирања*.

Радови се предају путем онлајн система за електронско уређивање АСИСТЕНТ, који је развио Центар за евалуацију у образовању и науци (ЦЕОН).

Приступ и регистрација за сервис врше се на сајту www.vtg.mod.gov.rs, преко странице *АСИСТЕНТ* или *СЦИНДЕКС*, односно директно на линку aseestant.ceon.rs/index.php/vtg.

Детаљно упутство о регистрацији и пријави за сервис налази се на сајту www.vtg.mod.gov.rs, страница *Упутство за АСИСТЕНТ*.

Потребно је да се сви аутори који подносе рукопис за објављивање у *Војнотехничком гласнику* региструју у регистар ORCID (Open Researcher and Contributor ID), према упутству на страници сајта *Регистрација за добијање ORCID идентификационе шифре*.

Војнотехнички гласник објављује чланке на енглеском језику (arial, величина слова 11 pt, проред Single).

Поступак припреме, писања и уређивања чланка треба да буде у сагласности са *Изјавом о етичком поступању* (http://www.vtg.mod.gov.rs/izjava-o-etickom-postupanju.html).

Чланак треба да садржи сажетак са кључним речима, увод (мотивацију за рад), разраду (адекватан преглед репрезентативности рада у његовој области, јасну изјаву о новини у представљеном истраживању, одговарајућу теоријску позадину, један или више примера за демонстрирање и дискусију о представљеним идејама), закључак и литературу (без нумерације наслова и поднаслова). Обим чланка треба да буде до

једног ауторског табака (16 страница формата А4 са проредом Single), а највише 24 странице.

Чланак треба да буде написан на обрасцу за писање чланка, који се у електронској форми може преузети са сајта на страници *Образац за писање чланка*.

Наслов

Наслов треба да одражава тему чланка. У интересу је часописа и аутора да се користе речи прикладне за индексирање и претраживање. Ако таквих речи нема у наслову, пожељно је да се придода и поднаслов.

Текући наслов

Текући наслов се исписује са стране сваке странице чланка ради лакше идентификације, посебно копија чланака у електронском облику. Садржи презиме и иницијал имена аутора (ако аутора има више, преостали се означавају са „et al.“ или „и др.“), наслове рада и часописа и колацију (година, волумен, свеска, почетна и завршна страница). Наслови часописа и чланка могу се дати у скраћеном облику.

Име аутора

Наводи се пуно име и презиме (свих) аутора. Веома је пожељно да се наведу и средња слова аутора. Имена и презимена домаћих аутора увек се исписују у оригиналном облику (са српским дијакритичким знаковима), независно од језика на којем је написан рад.

Назив установе аутора (афилијација)

Наводи се пун (званични) назив и седиште установе у којој је аутор запослен, а евентуално и назив установе у којој је аутор обавио истраживање. У сложеним организацијама наводи се укупна хијерархија (нпр. Универзитет одбране у Београду, Војна академија, Катедра природно-математичких наука). Бар једна организација у хијерархији мора бити правно лице. Ако аутора има више, а неки потичу из исте установе, мора се, посебним ознакама или на други начин, назначити из које од наведених установа потиче сваки од наведених аутора. Афилијација се исписује непосредно након имена аутора. Функција и звање аутора се не наводе.

Контакт подаци

Адреса или е-адреса свих аутора даје се поред имена и презимена аутора.

Категорија (тип) чланка

Категоризација чланака обавеза је уредништва и од посебне је важности. Категорију чланка могу предлагати рецензенти и чланови уредништва, односно уредници рубрика, али одговорност за категоризацију сноси искључиво главни уредник.

Војнотехнички гласник објављује научне чланке.

Научни чланак је:

– оригиналан научни рад (рад у којем се износе претходно необјављени резултати сопствених истраживања научним методом);

– прегледни рад (рад који садржи оригиналан, детаљан и критички приказ истраживачког проблема или подручја у којем је аутор остварио одређени допринос, видљив на основу аутоцитата);

– кратко или претходно саопштење (оригинални научни рад пуног формата, али мањег обима или прелиминарног карактера);

– научна критика, односно полемика (расправа на одређену научну тему, заснована искључиво на научној аргументацији) и осврти.

Изузетно, у неким областима, научни рад у часопису може имати облик монографске студије, као и критичког издања научне грађе (историјско-архивске, лексикографске, библиографске, прегледа података и сл.), дотад непознате или недовољно приступачне за научна истраживања.

Радови класификовани као научни морају имати бар две позитивне рецензије.

Ако се у часопису објављују и прилози ваннаучног карактера, научни чланци треба да буду груписани и јасно издвојени у првом делу свеске.

Пожељно је да обим кратких саопштења буде 4 до 7 страница, научних чланака и студија случаја 10 до 14 страница, док прегледни радови могу бити и дужи. Број страница није строго ограничен и, уз одговарајуће образложење, пријављени чланци такође могу бити дужи или краћи.

Ако су радови који су претходно објављени на конференцији проширени, уредници ће проверити да ли је додато довољно новог материјала који испуњава стандарде часописа и квалификује поднесак за поступак рецензије. Додати материјал не сме бити претходно објављен. Нови резултати нису нужно потребни, али су пожељни. Међутим, поднесак треба да садржи проширене кључне идеје, примере, разраде, итд., који су претходно били садржани у поднеску са конференције.

Језик рада

Језик рада треба да буде енглески.

Текст мора бити језички и стилски дотеран, систематизован, без скраћеница (осим стандардних). Све физичке величине морају бити изражене у Међународном систему мерних јединица – SI. Редослед образаца (формула) означава се редним бројевима, са десне стране у округлим заградама.

Сажетак

Сажетак јесте кратак информативан приказ садржаја чланка који читаоцу омогућава да брзо и тачно оцени његову релевантност. У интересу је уредништава и аутора да сажетак садржи термине који се често користе за индексирање и претрагу чланака. Саставни делови сажетка су увод/циљ истраживања, методи, резултати и закључак. Сажетак треба да има од 100 до 250 речи и треба да се налази између заглавља (наслов, имена аутора и др.) и кључних речи, након којих следи текст чланка.

Кључне речи

Кључне речи су термини или фразе које адекватно представљају садржај чланка за потребе индексирања и претраживања. Треба их додељивати ослањајући се на неки међународни извор (попис, речник или тезаурус) који је најшире прихваћен или унутар дате научне области. За нпр. науку уопште, то је листа кључних речи Web of Science. Број кључних речи не може бити већи од 10, а у интересу је уредништва и аутора да учесталост њихове употребе буде што већа. У чланку се пишу непосредно након сажетка.

Систем АСИСТЕНТ у ту сврху користи специјалну алатку KWASS: аутоматско екстраховање кључних речи из дисциплинарних тезауруса/речника по избору и рутине за њихов одабир, тј. прихватање односно одбацивање од стране аутора и/или уредника.

Датум прихватања чланка

Датум када је уредништво примило чланак, датум када је уредништво коначно прихватило чланак за објављивање, као и датуми када су у међувремену достављене евентуалне исправке рукописа наводе се хронолошким редоследом, на сталном месту, по правилу на крају чланка.

Захвалница

Назив и број пројекта, односно назив програма у оквиру којег је чланак настао, као и назив институције која је финансирала пројекат или програм, наводи се у посебној напомени на сталном месту, по правилу при дну прве стране чланка.

Претходне верзије рада

Ако је чланак у претходној верзији био изложен на скупу у виду усменог саопштења (под истим или сличним насловом), податак о томе треба да буде наведен у посебној напомени, по правилу при дну прве стране чланка. Рад који је већ објављен у неком часопису не може се објавити у *Војнотехничком гласнику* (прештампати), ни под сличним насловом и измењеном облику.

Табеларни и графички прикази

Пожељно је да наслови свих приказа, а по могућству и текстуални садржај, буду дати двојезично, на језику рада и на енглеском језику.

Табеле се пишу на исти начин као и текст, а означавају се редним бројевима са горње стране. Фотографије и цртежи треба да буду јасни, прегледни и погодни за репродукцију. Цртеже треба радити у програму word или corel. Фотографије и цртеже треба поставити на жељено место у тексту.

За слике и графиконе не сме се користити снимак са екрана рачунара програма за прикупљање података. У самом тексту чланка препоручује се употреба слика и графикона непосредно из програма за анализу података (као што су Excel, Matlab, Origin, SigmaPlot и други).

Навођење (цитирање) у тексту

Начин позивања на изворе у оквиру чланка мора бити једнообразан.

Војнотехнички гласник за референцирање (цитирање и навођење литературе) примењује Харвардски систем референци, односно Харвардски приручник за стил (Harvard Referencing System, Harvard Style Manual). У самом тексту, у обичним заградама, на месту на којем се врши позивање, односно цитирање литературе набројане на крају чланка, обавезно у обичној загради написати презиме цитираног аутора, годину издања публикације из које цитирате и, евентуално, број страница. Нпр. (Petrović, 2012, pp.10–12).

Детаљно упутство о начину цитирања, са примерима, дато је на страници сајта *Упутство за Харвардски приручник за стил*. Потребно је да се позивање на литературу у тексту уради у складу са поменутим упутством.

Систем АСИСТЕНТ у сврху контроле навођења (цитирања) у тексту користи специјалну алатку CiteMatcher: откривање изостављених цитата у тексту рада и у попису референци.

Напомене (фусноте)

Напомене се дају при дну стране на којој се налази текст на који се односе. Могу садржати мање важне детаље, допунска објашњења, назнаке о коришћеним

изворима (на пример, научној грађи, приручницима), али не могу бити замена за цитирану литературу.

Листа референци (литература)

Цитирана литература обухвата, по правилу, библиографске изворе (чланке, монографије и сл.) и даје се искључиво у засебном одељку чланка, у виду листе референци. Референце се не преводе на језик рада и набрајају се у посебном одељку на крају чланка.

Војнотехнички гласник, као начин исписа литературе, примењује Харвардски систем референци, односно Харвардски приручник за стил (Harvard Referencing System, Harvard Style Manual).

Литература се обавезно пише на латиничном писму и набраја по абецедном редоследу, наводећи најпре презимена аутора, без нумерације.

Детаљно упутство о начину пописа референци, са примерима, дато је на страници сајта *Упутство за Харвардски приручник за стил*. Потребно је да се попис литературе на крају чланка уради у складу са поменутим упутством.

Нестандардно, непотпуно или недоследно навођење литературе у системима вредновања часописа сматра се довољним разлогом за оспоравање научног статуса часописа.

Систем АСИСТЕНТ у сврху контроле правилног исписа листе референци користи специјалну алатку RefFormatter: контрола обликовања референци у складу са Харвардским приручником за стил.

Изјава о ауторству

Поред чланка доставља се *Изјава о ауторству* у којој аутори наводе свој појединачни допринос у изради чланка. Такође, у тој изјави потврђују да су чланак урадили у складу са *Позивом и упутством ауторима* и *Изјавом о етичком поступању часописа*.

Сви радови подлежу стручној рецензији.

Списак рецензената *Војнотехничког гласника* може се видети на страници сајта *Списак рецензената*. Процес рецензирања објашњен је на страници сајта *Рецензентски поступак*.

Уредништво

Адреса редакције:
Војнотехнички гласник
Вељка Лукића Курјака 33
11042 Београд
e-mail: vojnotehnicki.glasnik@mod.gov.rs.
тел: војни 40-260 (011/3603-260), 066/8700-123

ПРИГЛАШЕНИЕ И ИНСТРУКЦИЯ ДЛЯ АВТОРОВ О ПОРЯДКЕ ПОДГОТОВКИ СТАТЬИ

Инструкция для авторов о порядке подготовки статьи к опубликованию в журнале *«Военно-технический вестник»* разработана согласно Регламенту о категоризации и ранжировании научных журналов Министерства образования, науки и технологического развития Республики Сербия («Службени гласник РС», № 159/20). Применение этого Регламента способствует повышению качества отечественных журналов и их более полному вовлечению в международную систему обмена научной информацией.

Военно-технический вестник (**Vojnotehnički glasnik / Military Technical Courier**), втг.мо.упр.срб, www.vtg.mod.gov.rs/index-ru.html, ISSN 0042-8469 – печатное издание, e-ISSN 2217-4753 – online, UDK 623+355/359, DOI: 10.5937/VojnotehnickiGlasnik; https://doi.org/10.5937/VojnotehnickiGlasnik, является рецензируемым научным журналом.

Собственники журнала: Министерство обороны и Вооруженые силы Республики Србия.

Издатель журнала: Университет обороны в г. Белград (Военная академия).

Программная ориентация журнала основана на ежегодной категоризации журнала, которая производится соответствующим отраслевым министерством, в зависимости от области исследований, а также на его индексировании в международных наукометрических базах данных.

Журнал охватывает научные и профессиональные сферы в рамках учебно-научной области **естественно-математических наук**, а также в рамках учебно-научной области **технико-технологических наук**, особенно в области **оборонных наук и технологии**. В журнале публикуются теоретические и практические достижения, которые способствуют повышению квалификации представителей сербского, регионального и международного академического сообщества, особенно служащих Министерств Обороны и Вооружённых сил. В журнале публикуются статьи со соответствующими обзорами об аналитических, экспериментальных и прикладных исследованиях, а также о численном моделировании, охватывая различные дисциплины. Публикуемые материалы отличаются высоким качеством и актуальностью. Они написаны научным, но понятным и доступным для широкого круга читателей языком. Приветствуются все статьи, сообщающие об оригинальных теоретических и/или практических исследованиях и/или расширенные версии ранее опубликованных статей, представленных на конференциях. Статьи для публикации отбираются путем двойного слепого рецензирования, которое гарантирует оригинальность, актуальность и удобочитаемость. Цель состоит не только в поддержании высокого качества публикуемых статей, но и в обеспечении своевременного, тщательного и соответствующего процесса рецензирования.

Редакционная политика журнала *«Военно-технический вестник»* основана на рекомендациях Комитета по этике научных публикаций (COPE Core Practices), общих принципах прозрачности и лучшей практике издательской деятельности COPE, DOAJ, OASPA и WAME, а также на лучшей практике научно-издательской деятельности. Журнал *«Военно-технический вестник»* является членом COPE (Комитет по этике научных публикаций) со 2 мая 2018 года и членом OASPA (Ассоциация научных издателей открытого доступа) с 27 ноября 2015 года.

Министерством науки, технологического развития и инноваций Республики Сербия утверждена 13 декабря 2024 г. категоризация журнала *«Военно-технический вестник»* за 2024 год:

- **Область компьютерные науки:**
  ведущий журнал государственного значения **(M51)**,
- **Область электроники, телекоммуникаций и информационных технологий:**
  ведущий журнал государственного значения **(M51)**,
- **Область машиностроения:**
  ведущий журнал государственного значения **(M51)**,
- **Область материалов и химической технологии:**
  национальный журнал международного значения **(M24)**.

С информацией относительно категоризации за 2024 год можно ознакомиться на странице сайта *«Военно-технического вестника» Категоризация Вестника*.

Более подробную информацию можно найти на сайте Министерства образования, науки и технологического развития Республики Сербия.

С информацией о категоризации можно ознакомиться и на сайте КОБСОН (Консорциум библиотек Республики Сербия по вопросам объединения закупок).

Категоризация Вестника проведена согласно Регламенту о категоризации и ранжировании научных журналов Министерства образования, науки и технологического развития Республики Сербия («Службени гласник РС», № 159/20)

Журнал соответствует стандартам Сербского индекса научного цитирования (СЦИндекс/SCIndeks) - наукометрической базы данных научных журналов Республики Сербия, Научно-информационного система Redalyc, а также Российского индекса научного цитирования (РИНЦ). Журнал постоянно подвергается мониторингу и оценивается количественными наукометрическими показателями отражающими его научную ценность.

С информацией об индексировании можно ознакомиться на странице сайта журнала *Индексирование Вестника*.

«Военно-технический вестник» относительно своего содержания предоставляет пользователям возможность открытого доступа (DIAMOND OPEN ACCESS) и положениями об авторских правах, утвержденными Creative Commons (CC BY). С инструкцией об авторских правах можно ознакомиться на странице сайта журнала *Авторские права и политика самоархивирования*.

Рукописи статей направляются в редакцию журнала с использованием online системы ASSISTANT, запущенной Центром поддержи развития образования и науки (ЦПРОН). Регистрация в системе и оформление прав доступа выполняется по адресу http://www.vtg.mod.gov.rs/index-ru.html, через страницу *ASSISTANT* или *СЦИНДЕКС* (aseestant.ceon.rs/index.php/vtg). С инструкцией по регистрации и правам доступа можно ознакомиться по адресу http://www.vtg.mod.gov.rs/index-ru.html, на странице *Инструкция по ASSISTANT*.

Все авторы, предоставляющие свои рукописи для публикации в редакцию журнала *«Военно-технический вестник»* должны пройти предварительную регистрацию в реестре ORCID (Open Researcher and Contributor ID). Эта процедура осуществляется в соответствии с инструкцией, размещенной на странице сайта *Регистрация в реестре ORCID для присвоения идентификационного кода*.

«Военно-технический вестник» публикует статьи на английском языке (Arial, шрифт 11 pt, пробел Single). Процесс подготовки, написания и редактирования статьи должен осуществляться в соответствии с принципами *Этического кодекса*

(http://www.vtg.mod.gov.rs/etichyeskiy-kodyeks.html). Статья должна содержать резюме с ключевыми словами, введение (цель исследования), основную часть (соответствующий обзор представительного исследования в данной области, четкое изложение научной новизны в представленном исследовании, соответствующую теоретическую основу, один или несколько примеров для демонстрирования и обсуждения представленных тезисов), заключение и список литературы (без нумерации заголовков и подзаголовков). Объем статьи не должен превышать один авторский лист (16 страниц формата А4 с одинарным интервалом, максимум до 24 страниц, включая ссылки и приложения). Статья должна быть набрана на компьютере с использованием специально подготовленного редакцией макета, который можно скачать на странице сайта *Правила и образец составления статьи*.

Заголовок

Заголовок должен отражать тему статьи. В интересах журнала и автора необходимо использовать слова и словосочетания, удобные для индексации и поиска. Если такие слова не содержатся в заголовке, то желательно их добавить в подзаголовок.

Текущий заголовок

Текущий заголовок пишется в титуле каждой страницы статьи с целью упрощения процесса идентификации, в первую очередь копий статьей в электронном виде. Заголовок содержит в себе фамилию и инициал имени автора (в случае если авторов несколько, остальные обозначаются с «et al.» или «и др.»), название работы и журнала (год, том, выпуск, начальная и заключительная страница). Заголовок статьи и название журнала могут быть приведены в сокращенном виде.

ФИО автора

Приводятся полная фамилия и полное имя (всех) авторов. Желательно, чтобы были указаны инициалы отчеств авторов. Фамилия и имя авторов из Республики Сербия всегда пишутся в оригинальном виде (с сербскими диакритическими знаками), независимо от языка, на котором написана работа.

Наименование учреждения автора (аффилиация)

Приводится полное (официальное) наименование и местонахождение учреждения, в котором работает автор, а также наименование учреждения, в котором автор провёл исследование. В случае организаций со сложной структурой приводится их иерархическая соподчинённость (напр. Военная академия, кафедра военных электронных систем, г. Белград). По крайней мере, одна из организаций в иерархии должна иметь статус юридического лица. В случае если указано несколько авторов, и если некоторые из них работают в одном учреждении, нужно отдельными обозначениями или каким-либо другим способом указать в каком из приведённых учреждений работает каждый из авторов. Аффилиация пишется непосредственно после ФИО автора. Должность и специальность по диплому не указываются.

Контактные данные

Электронный адрес автора указываются рядом с его именем на первой страницы статьи.

Категория (тип) статьи

Категоризация статьей является обязанностью редакции и имеет особое значение. Категорию статьи могут предлагать рецензенты и члены редакции, т.е. редакторы рубрик, но ответственность за категоризацию несет исключительно главный редактор.

Журнал *«Военно-технический вестник»* публикует научные статьи.

Научные статьи:

– оригинальная научная статья (работа, в которой приводятся ранее неопубликованные результаты собственных исследований, полученных научным методом);

– обзорная статья (работа, содержащая оригинальный, детальный и критический обзор исследуемой проблемы или области, в который автор внёс определённый вклад, видимый на основе автоцитат);

– краткое сообщение (оригинальная научная работа полного формата, но меньшего объёма или имеющая предварительный характер);

– научная критическая статья (дискуссия-полемика на определённую научную тему, основанная исключительно на научной аргументации) и научный комментарий.

Однако, в некоторых областях знаний научная работа в журнале может иметь форму монографического исследования, а также критического обсуждения научного материала (историко-архивного, лексикографического, библиографического, обзора данных и т.п.) – до сих пор неизвестного или недостаточно доступного для научных исследований. Работы, классифицированные в качестве научных, должны иметь, по меньшей мере, две положительные рецензии. В случае если в журнале объявляются и приложения, не имеющие научный характер, научные статьи должны быть сгруппированы и четко выделены в первой части номера.

Объем кратких сообщений составляет 4-7 страниц, исследовательские статьи и тематические исследования с проблемно-ситуационным анализом − 10-14 страниц, однако объем обзорных статей может быть больше. Ограничения по количеству страниц не являются строгими, следовательно при соответствующем обосновании предоставленные работы могут быть длиннее или короче. В случае подачи расширенных версий ранее опубликованных докладов, представленных на конференции, редакция проверит было ли добавлено достаточно новых материалов для того, чтобы статья соответствовала стандартам журнала и условиям рецензирования. Добавленный материал должен быть новым, неопубликованным ранее. Новые результаты приветствуются, но не являются обязательным условием; однако ключевые тезисы, примеры, разработки и пр. должны быть более подробно представлены в статье по сравнению с первичным докладом на конфереции.

Язык работы

Статья должна быть написана на английском языке. Текст должен быть в лингвистическом и стилистическом смысле упорядочен, систематизирован, без сокращений (за исключением стандартных). Все физические величины должны соответствовать Международной системе единиц измерения – СИ. Очередность формул обозначается порядковыми номерами, проставляемыми с правой стороны в круглых скобках.

Резюме

Резюме является кратким информативным обзором содержания статьи, обеспечивающим читателю быстроту и точность оценки её релевантности. В интересах редакции и авторов, чтобы резюме содержало термины, часто используемые для индексирования и поиска статьей. Составными частями резюме являются введение/цель исследования, методы, результаты и выводы. В резюме должно быть от 100 до 250 слов, и оно должно находится между титулами (заголовок, ФИО авторов и др.) и ключевыми словами, за которыми следует текст статьи.

Ключевые слова

Ключевыми словами являются термины или фразы, адекватно представляющие содержание статьи, необходимые для индексирования и поиска. Ключевые слова необходимо выбирать, опираясь при этом на какой-либо международный источник (регистр, словарь, тезаурус), наиболее используемый внутри данной научной области. Число ключевых слов не может превышать 10. В интересах редакции и авторов, чтобы частота их встречи в статье была как можно большей. В статье они пишутся непосредственно после резюме.

Программа ASSISTANT предоставляет возможность использования сервиса KWASS, автоматически фиксирующего ключевые слова из источников/словарей по выбору автора/редактора.

Дата получения статьи

Дата, когда редакция получила статью; дата, когда редакция окончательно приняла статью к публикации; а также дата, когда были предоставлены необходимые исправления рукописи, приводятся в хронологическом порядке, как правило, в конце статьи.

Выражение благодарности

Наименование и номер проекта, т.е. название программы благодаря которой статья возникла, совместно с наименованием учреждения, которое финансировало проект или программу, приводятся в отдельном примечании, как правило, внизу первой страницы статьи.

Предыдущие версии работы

В случае если статья в предыдущей версии была изложена устно (под одинаковым или похожим названием, например, в виде доклада на научной конференции), сведения об этом должны быть указаны в отдельном примечании, как правило, внизу первой страницы статьи. Работа, которая уже была опубликована в каком-либо из журналов, не может быть напечатана в *«Военно-техническом вестнике»* ни под похожим названием, ни в изменённом виде.

Нумерация и название таблиц и графиков

Желательно, чтобы нумерация и название таблиц и графиков были исполнены на двух языках (на языке оригинала и на английском). Таблицы подписываются таким же способом как и текст и обозначаются порядковым номером с верхней стороны. Фотографии и рисунки должны быть понятны, наглядны и удобны для репродукции. Рисунки необходимо делать в программах Word или Corel. Фотографии и рисунки надо поставить на желаемое место в тексте. Для создания изображений и графиков использование функции снимка с экрана (скриншота) не допускается. В самом тексте статьи рекомендуется применение изображений и графиков, обработанных такими компьютерными программами, как: Excel, Matlab, Origin, SigmaPlot и др.

Ссылки (цитирование) в тексте

Оформление ссылок на источники в рамках статьи должно быть однообразным. *«Военно-технический вестник»* для оформления ссылок, цитат и списка использованной литературы применяет Гарвардскую систему (Harvard Referencing System, Harvard Style Manual). В тексте в скобках приводится фамилия цитируемого автора (или фамилия первого автора, если авторов несколько), год издания и по необходимости номер страницы. Например: (Petrović, 2010, pp.10-20). Рекомендации о способе цитирования размещены на странице сайта *Инструкция по использованию Гарвардского стиля*. При оформлении ссылок, цитат и списка использованной литературы необходимо придерживаться установленных норм. Программа

ASSISTANT предоставляет при цитировании возможность использования сервиса CiteMatcher, фиксирующего пропущенные цитаты в работе и в списке литературы.

Примечания (сноски)

Примечания (сноски) к тексту указываются внизу страницы, к которой они относятся. Примечания могут содержать менее важные детали, дополнительные объяснения, указания об использованных источниках (напр. научном материале, справочниках), но не могут быть заменой процедуры цитирования литературы.

Литература (референции)

Цитированной литературой охватываются, как правило, такие библиографические источники как статьи, монографии и т.п. Вся используемая литература в виде референций размещается в отдельном разделе статьи. Названия литературных источников не переводятся на язык работы. *«Военно-технический вестник»* для оформления списка использованной литературы применяет Гарвардскую систему (Harvard Style Manual). В списке литературы источники указываются в алфавитном порядке фамилий авторов или редакторов. Рекомендации о способе цитирования размещены на странице сайта *Инструкция по использованию Гарвардского стиля*. При оформлении списка использованной литературы необходимо придерживаться установленных норм. При оформлении списка литературы программа ASSISTANT предоставляет возможность использования сервиса RefFormatter, осуществляющего контроль оформления списка литературы в соответствии со стандартами Гарвардского стиля. Нестандартное, неполное и непоследовательное приведение литературы в системах оценки журнала считается достаточной причиной для оспаривания научного статуса журнала.

Авторское заявление

Авторское заявление предоставляется вместе со статьей, в нем авторы заявляют о своем личном вкладе в написание статьи. В заявлении авторы подтверждают, что статья написана в соответствии с *Приглашением и инструкциями для авторов*, а также с *Кодексом профессиональной этики журнала*.

Все рукописи статей подлежат профессиональному рецензированию.

Список рецензентов журнала *«Военно-технический вестник»* размещён на странице сайта *Список рецензентов*. Процесс рецензирования описан в разделе *Правила рецензирования*.

Редакция

Почтовый адрес редакции:

«Војнотехнички гласник»
ул. Велька Лукича Куряка 33, 11042 Белград, Республика Сербия
e-mail: vojnotehnicki.glasnik@mod.gov.rs,
тел: +381 11 3603 260, +381 66 8700 123

CALL FOR PAPERS AND ARTICLE FORMATTING INSTRUCTIONS

The instructions to authors about the article preparation for publication in the *Military Technical Courier* are based on the Regulations on categorization and ranking of scientific journals of the Ministry of Education, Science and Technological Development of the Republic of Serbia (Official Gazette of the Republic of Serbia, No 159/20). This Regulations aims at improving the quality of national journals and raising the level of their compliance with the international system of scientific information exchange.

The Military Technical Courier / Vojnotehnički glasnik (www.vtg.mod.gov.rs/index-e.html, втг.мо.упр.срб, ISSN 0042-8469 – print issue, e-ISSN 2217-4753 – online, UDC 623+355/359, DOI: 10.5937/VojnotehnickiGlasnik; https://doi.org/10.5937/VojnotehnickiGlasnik), is an peer-reviewed scientific journal.

The owners of the journal are the Ministry of Defence of the Republic of Serbia and the Serbian Armed Forces. The publisher and financier of the *Military Technical Courier* is the University of Defence in Belgrade (Military Academy).

The program of the journal is based on the annual classification of journals performed by a relevant Ministry as well as on its indexing in international indexing databases.

The journal covers scientific and professional fields within the educational-scientific field of **Natural-Mathematical Sciences**, as well as within the educational-scientific field of **Technical-Technological Sciences**, and especially the field of **defense sciences and technologies**. It publishes theoretical and practical achievements leading to professional development of all members of Serbian, regional and international academic communities as well as members of the military and ministries of defence in particular. It publishes papers with balanced coverage of analytical, experimental, and applied research as well as numerical simulations from various disciplines. The material published is of high quality and relevance, written in a manner that makes it accessible to a wider readership. The journal welcomes papers reporting original theoretical and/or practice-oriented research as well as extended versions of already published conference papers. Manuscripts for publication are selected through a double-blind peer-review process to validate their originality, relevance, and readability. This being so, the objective is not only to keep the quality of published papers high but also to provide a timely, thorough, and balanced review process.

The editorial policy of the *Military Technical Courier* is based on the COPE Core Practices, common COPE, DOAJ, OASPA and WAME Principles of Transparency and Best Practice in Scholarly Publishing as well as on the best accepted practices in scientific publishing. The Military Technical Courier has been a COPE (Committee on Publication Ethics) member since 2nd May 2018 and a member of OASPA (Open Access Scholarly Publishers Association) since 27th November 2015.

The Ministry of Science, Technological Development and Innovation of the Republic of Serbia classified the *Military Technical Courier* for the year 2024, on December 13, 2024

- **on the list of periodicals for computer sciences,**
  category: reputed national journal **(M51)**,
- **on the list of periodicals for electronics, telecommunications and IT,**
  category: reputed national journal **(M51)**,
- **on the list of periodicals for mechanical engineering,**
  category: reputed national journal **(M51)**,
- **on the list of periodicals for materials and chemical technology,**
  category: national journal of international importance **(M24)**.

The approved lists of national periodicals for the year 2024 can be viewed on the website of the *Military Technical Courier*, page *Journal categorization*.

More detailed information can be found on the website of the Ministry of Education, Science and Technological Development of the Republic of Serbia.

The information on the categorization can be also found on the website of KOBSON (Consortium of Libraries of Serbia for Unified Acquisition).

The periodical is categorized in compliance with the Regulations on categorization and ranking of scientific journals of the Ministry of Education, Science and Technological Development of the Republic of Serbia (Official Gazette of the Republic of Serbia, No 159/20). More detailed information can be found on the website of the Ministry of Education, Science and Technological Development.

The journal is in the Serbian Citation Index – SCIndex (data base of national scientific journals), in the Scientific Information System Redalyc, and in the Russian Index of Science Citation/Российский индекс научного цитирования (RINC/РИНЦ) and is constantly monitored depending on the impact within the bases themselves. More detailed information can be viewed on the website of the *Military Technical Courier*, page *Journal indexing*.

The *Military Technical Courier*, in terms of its content, offers the possibility of open access (DIAMOND OPEN ACCESS) and applies the Creative Commons Attribution (CC BY) licence on copyright. The copyright details can be found on the *Copyright notice and Self-archiving policy* page of the journal's website.

Manuscripts are submitted online, through the electronic editing system ASSISTANT, developed by the Center for Evaluation in Education and Science – CEON.

The access and the registration are through the *Military Technical Courier* site http://www.vtg.mod.gov.rs/index-e.html, on the page *ASSISTANT* or the page *SCINDEKS* or directly through the link (aseestant.ceon.rs/index.php/vtg).

The detailed instructions about the registration for the service are on the website http://www.vtg.mod.gov.rs/index-e.html, on the page *Instructions for ASSISTANT*.

All authors submitting a manuscript for publishing in the *Military Technical Courier* should register for an ORCID ID following the instructions on the web page *Registration for an ORCID identifier*.

The *Military Technical Courier* publishes articles in English, using Arial and a font size of 11pt with Single Spacing.

The procedures of article preparation, writing and editing should be in accordance with the *Publication ethics statement* (http://www.vtg.mod.gov.rs/publication-ethics-statement.html).

The article should contain an abstract with keywords, introduction (motivation for the work), body (adequate overview of the representative work in the field, a clear statement of the novelty in the presented research, suitable theoretical background, one or more examples to demonstrate and discuss the presented ideas), conclusion, and references (without heading and subheading enumeration). The article length should not normally exceed 16 pages of the A4 paper format with single spacing, up to a maximum of 24 pages with references and supplementary material included.

The article should be formatted following the instructions in the Article Form which can be downloaded from website page *Article form*.

Title

The title should be informative. It is in both Journal's and author's best interest to use terms suitable for indexing and word search. If there are no such terms in the title, the author is strongly advised to add a subtitle.

Letterhead title

The letterhead title is given at a top of each page for easier identification of article copies in an electronic form in particular. It contains the author's surname and first name initial (for multiple authors add "et al"), article title, journal title and collation (year, volume, issue, first and last page). The journal and article titles can be given in a shortened form.

Author's name

Full name(s) of author(s) should be used. It is advisable to give the middle initial. Names are given in their original form (with diacritic signs if in Serbian).

Author's affiliation

The full official name and seat of the author's affiliation is given, possibly with the name of the institution where the research was carried out. For organizations with complex structures, give the whole hierarchy (for example, University of Defence in Belgrade, Military Academy, Department for Military Electronic Systems). At least one organization in the hierarchy must be a legal entity. When some of multiple authors have the same affiliation, it must be clearly stated, by special signs or in other way, which department exactly they are affiliated with. The affiliation follows the author's name. The function and title are not given.

Contact details

The postal addresses or the e-mail addresses of the authors are given in the first page.

Type of articles

Classification of articles is a duty of the editorial staff and is of special importance. Referees and the members of the editorial staff, or section editors, can propose a category, but the editor-in-chief has the sole responsibility for their classification.

The *Military Technical Courier* publishes scientific articles.

Scientific articles:

– Original scientific papers (giving the previously unpublished results of the author's own research based on scientific methods);

– Review papers (giving an original, detailed and critical view of a research problem or an area to which the author has made a contribution demonstrated by self-citation);

– Short communications or Preliminary communications (original scientific full papers but shorter or of a preliminary character);

– Scientific commentaries or discussions (discussions on a particular scientific topic, based exclusively on scientific argumentation) and opinion pieces.

Exceptionally, in particular areas, a scientific paper in the Journal can be in a form of a monograph or a critical edition of scientific data (historical, archival, lexicographic, bibliographic, data survey, etc.) which were unknown or hardly accessible for scientific research.

Papers classified as scientific must have at least two positive reviews.

If the journal contains non-scientific contributions as well, the section with scientific papers should be clearly denoted in the first part of the Journal.

Short communications are usually 4-7 pages long, research articles and case studies 10-14 pages, while reviews can be longer. Page number limits are not strict and, with

appropriate reasoning, submitted manuscripts can also be longer or shorter. If extended versions of previously published conference papers are submitted, Editors will check if sufficient new material has been added to meet the journal standards and to qualify such manuscripts for the review process. The added material must not have been previously published. New results are desired but not necessarily required; however, submissions should contain expansions of key ideas, examples, elaborations, etc. of conference papers.

Language

The language of the article should be in English. The grammar and style of the article should be of good quality. The systematized text should be without abbreviations (except standard ones). All measurements must be in SI units. The sequence of formulae is denoted in Arabic numerals in parentheses on the right-hand side.

Abstract and summary

An abstract is a concise informative presentation of the article content for fast and accurate evaluation of its relevance. It contains the terms often used for indexing and article search. A 100- to 250-word abstract has the following parts: introduction/purpose of the research, methods, results and conclusion.

Keywords

Keywords are terms or phrases showing adequately the article content for indexing and search purposes. They should be allocated heaving in mind widely accepted international sources (index, dictionary or thesaurus), such as the Web of Science keyword list for science in general. The higher their usage frequency is, the better. Up to 10 keywords immediately follow the abstract and the summary, in respective languages. For this purpose, the ASSISTANT system uses a special tool KWASS for the automatic extraction of key words from disciplinary thesauruses/dictionaries by choice and the routine for their selection, i.e. acceptance or rejection by author and/or editor.

Article acceptance date

The date of the reception of the article, the dates of submitted corrections in the manuscript (optional) and the date when the Editorial Board accepted the article for publication are all given in a chronological order at the end of the article.

Acknowledgements

The name and the number of the project or programme within which the article was realised is given in a separate note at the bottom of the first page together with the name of the institution which financially supported the project or programme.

Article preliminary version

If an article preliminary version has appeared previously at a meeting in a form of an oral presentation (under the same or similar title), this should be stated in a separate note at the bottom of the first page. An article published previously cannot be published in the *Military Technical Courier* even under a similar title or in a changed form.

Tables and illustrations

All the captions should be in the original language as well as in English, together with the texts in illustrations if possible. Tables are typed in the same style as the text and are denoted by Arabic numerals at the top. Photographs and drawings, placed appropriately in the text, should be clear, precise and suitable for reproduction. Drawings should be created in Word or Corel.

For figures and graphs, proper data plot is recommended i.e. using a data analysis program such as Excel, Matlab, Origin, SigmaPlot, etc. It is not recommended to use a screen capture of a data acquisition program as a figure or a graph.

Citation in the text

Citation in the text must be uniform. The *Military Technical Courier* applies the Harvard Referencing System given in the Harvard Style Manual. When citing sources within your paper, i.e. for in-text references of the works listed at the end of the paper, place the year of publication of the work in parentheses and optionally the number of the page(s) after the author's name, e.g. (Petrovic, 2012, pp.10-12). A detailed guide on citing, with examples, can be found on *Military Technical Courier* website on the page *Instructions for Harvard Style Manual*. In-text citations should follow its guidelines. For checking in-text citations, the ASSISTANT system uses a special tool CiteMatcher to find out quotes left out within papers and in reference lists.

Footnotes

Footnotes are given at the bottom of the page with the text they refer to. They can contain less relevant details, additional explanations or used sources (e.g. scientific material, manuals). They cannot replace the cited literature.

Reference list (Literature)

The cited literature encompasses bibliographic sources such as articles and monographs and is given in a separate section in a form of a reference list. References are not translated to the language of the article.

In compiling the reference list and bibliography, the *Military Technical Courier* applies the Harvard System – Harvard Style Manual. All bibliography items should be listed alphabetically by author's name, without numeration. A detailed guide for listing references, with examples, can be found on *Military Technical Courier* website on the page *Instructions for Harvard Style Manual*. Reference lists at the end of papers should follow its guidelines. In journal evaluation systems, non-standard, insufficient or inconsequent citation is considered to be a sufficient cause for denying the scientific status to a journal.

Authorship Statement

The Authorship statement, submitted together with the paper, states authors' individual contributions to the creation of the paper. In this statement, the authors also confirm that they followed the guidelines given in *the Call for papers* and the *Publication ethics and malpractice statement of the journal*.

All articles are peer reviewed.

The list of referees of the *Military Technical Courier* can be viewed at website page *List of referees*. The article review process is described on the *Peer Review Process* page of the website.

Editorial Team

Address of the Editorial Office:
Vojnotehnički glasnik / Military Technical Courier
Veljka Lukića Kurjaka 33
11042 Belgrade, Republic of Serbia
e-mail: vojnotehnicki.glasnik@mod.gov.rs, tel.: +381 11 3603 260, +381 66 8700 123

СПИСАК РЕЦЕНЗЕНАТА ВОЈНОТЕХНИЧКОГ ГЛАСНИКА
СПИСОК РЕЦЕНЗЕНТОВ ЖУРНАЛА «ВОЕННО-ТЕХНИЧЕСКИЙ ВЕСТНИК»
LIST OF REFEREES OF THE MILITARY TECHNICAL COURIER

Списак рецензената *Војнотехничког гласника* **који су ангажовани током 2024. године** доступан је на страници сајта часописа
http://www.vtg.mod.gov.rs/spisak-recenzenata.html
као и на страници *Војнотехничког гласника* у Српском цитатном индексу
https://scindeks.ceon.rs/EditorialBoard.aspx?issn=0042-8469

Список рецензентов журнала *«Военно-технический вестник»*, **привлеченных в 2024 году**, доступен на сайте журнала
http://www.vtg.mod.gov.rs/spisok-recenzetov.html
а также на странице журнала *«Военно-технический вестник»* в Сербском индексе цитирования
https://scindeks.ceon.rs/EditorialBoard.aspx?issn=0042-8469&lang=en

The list of the referees of the *Military Technical Courier* **engaged during 2024** is available on the journal's website
http://www.vtg.mod.gov.rs/list-of-referees.html
as well as on the *Military Technical Courier* page in the Serbian Citation Index
https://scindeks.ceon.rs/EditorialBoard.aspx?issn=0042-8469&lang=en

ИЗЈАВА О ЕТИЧКОМ ПОСТУПАЊУ
ЭТИЧЕСКИЙ КОДЕКС
PUBLICATION ETHICS STATEMENT

ИЗЈАВА *ВОЈНОТЕХНИЧКОГ ГЛАСНИКА* О ЕТИЧКОМ ПОСТУПАЊУ

НАПОМЕНА: Уређивачка политика Војнотехничког гласника заснива се на препорукама Одбора за етичност у издаваштву (COPE Core Practices) и заједничким принципима транспарентности и најбоље праксе у издаваштву COPE, DOAJ, OASPA и WAME, као и на најбољим прихваћеним праксама у научном издаваштву. Војнотехнички гласник је члан COPE (Committee on Publication Ethics) од 2. маја 2018. године и члан OASPA (Open Access Scholarly Publishers Association) од од 27. новембра 2015. године. Уредништво примењује Контролну листу за издаваче отвореног приступа о спровођењу Препоруке УНЕСКО-а о отвореној науци. Овај документ је део Унесковог комплета алата за отворену науку, осмишљеног да подржи имплементацију Препоруке Унеска о отвореној науци. Произведен је у партнерству са OASPA.

Основна делатност научног часописа *Војнотехнички гласник* је објављивање чланака након стручне рецензије. У процесу уређивања, који има за циљ објављивање научних чланака, неопходно је постићи сагласност о етичким начелима у поступцима свих учесника (редакције, тј. уредника, чланова Уређивачког одбора и рецензената часописа, као и самих аутора). Поменута начела и поступци дефинисани су овом Изјавом Војнотехничког гласника о етичком поступању.

Мере, радње, одговорности и обавезе Редакције Војнотехничког гласника

Уредништво Војнотехничког гласника не тражи од аутора, нити од трећих страна, плаћање накнаде за аплицирање чланка за објављивање. Читав поступак уређивања и објављивања чланка за ауторе је потпуно бесплатан, како услуге пријављивања рукописа и њихове обраде, тако и услуге публиковања чланака. Не постоје било какви скривени трошкови.

Уредништво Војнотехничког гласника доноси коначну одлуку о томе који ће се рукописи објавити. Одлуке се доносе искључиво на основу вредности рукописа. Морају бити ослобођене расних, полних/родних, верских, етничких или политичких предрасуда. Приликом доношења одлуке о објављивању уредништво се руководи уређивачком политиком, водећи рачуна о законским прописима који се односе на клевету, кршења ауторских права и плагирање.

Рукописи се чувају као поверљив материјал. Информације и идеје садржане у рукописима не смеју се користити у личне сврхе без изричите писане дозволе аутора.

У свом раду, према препоруци Центра за евалуацију у образовању и науци (ЦЕОН), Редакција користи електронски систем уређивања часописа СЦИндекс (Српски цитатни индекс) АСИСТЕНТ (развијен на бази платформе OJS), који омогућава транспарентност и јавност рада, подразумевајући пуну одговорност за прихватање и објављивање чланка.

Процес уређивања чланка у Војнотехничком гласнику подразумева следеће обавезе Редакције:

1. Након пријема чланка, Редакција од аутора прибавља Изјаву о ауторству у којој аутори: наводе свој појединачни допринос у изради чланка; потврђују да су упознати са политком часописа у вези са повлачењем већ објављених радова; потврђују да послати рукопис представља оригиналан рад који су написали и потписали наведени аутори и који није објављен раније на неком другом месту, те да

се рукопис не разматра за објављивање на другом месту и није истовремено послат на рецензију у друге часописе; потврђују да чланак и додатни материјали не садрже тврдње које би се могле сматрати клеветом или било какве незаконите тврдње и не садрже материјал који на било који начин угрожава лична или власничка права физичких или правних лица; потврђују да немају сукоб интереса који би могао да доведе у питање интегритет и веродостојност резултата који су објављени у чланку, као и да су добили сагласност од носилаца ауторских права за коришћење свих извода из дела заштићених ауторским правима и других материјала заштићених ауторским правима који су коришћени у рукопису и да су навели изворе у рукопису и додатним материјалима.

2. Пре доделе рукописа уреднику Редакција проверава да ли је садржај рукописа плагијат, ради провере оригиналности приспелих радова и спречавања публиковања плагијата и дупликата. Војнотехнички гласник не објављује плагиране радове. Уредништво полази од става да је плагирање, односно преузимање туђих идеја, речи или других облика креативног доприноса и њихово представљање као сопствених, грубо кршење научне и издавачке етике. Плагирање може да укључује и кршење ауторских права, што је законом кажњиво.

Плагирање обухвата:

– дословно (реч по реч) или готово дословно преузимање или смишљено, ради прикривања извора, парафразирање делова текстова других аутора без јасног назначавања извора;

– копирање једначина, података или табела из других докумената без правилног назначавања извора и/или без дозволе изворног аутора или носиоца ауторског права.

Рукопис у којем се утврде јасне индиције да је плагиран биће аутоматски одбијен. У случају да се плагијаризам открије у већ објављеном раду, чланак ће бити опозван (повучен) у складу са процедуром описаном у тачки 6.

Ради спречавања плагијата у часопису рукописи се подвргавају провери уз помоћ система iThenticate/CrossRef у оквиру сервиса СЦИндекс АСИСТЕНТ. Резултате добијене провером верификује уредништво часописа у складу са смерницама и препорукама Комитета за етику публиковања (COPE).

Војнотехнички гласник не дозвољава употребу генеративне вештачке интелигенције (енгл. generative AI), као ни технологија подржаних вештачком интелигенцијом (енгл. AI-assisted), као што су велики језички модели (енгл. Large Language Models), за писање рада. Употреба ових технологија дозвољена је једино за унапређење језика и читљивости рада, али уз строгу контролу аутора. Редакција Војнотехничког гласника може користити форензичке алате и специјалне софтвере за идентификацију нерегуларног писања рада помоћу генеративне вештачке интелигенције и технологија подржаних вештачком интелигенцијом. Радови код којих се утврди нерегуларно коришћење ових технологија биће одбијени у процесу уређивања и рецензије или накнадно опозвани ако се ови недостаци утврде у већ објављеним чланцима.

3. Након провере на плагијаризам Редакција додељује приспели рукопис уреднику који ће надаље водити уређивачки процес и одабрати рецензенте. Уредништво и уредник којем је додељен приспели чланак не смеју бити у сукобу интереса у вези са рукописом који разматрају.

Ако такав сукоб интереса постоји, о избору рецензената и судбини рукописа одлучује Уређивачки одбор. Чланови Уређивачког одбора за које се претпостави да би могли бити у сукобу интереса такође не учествују у поступку одлучивања о одређеном рукопису.

4. Рукописи се упућују на рецензију тек након иницијалне оцене да ли су, с обзиром на форму и тематски делокруг, подобни за објављивање у Војнотехничком гласнику. Посебна се води рачуна да иницијална оцена не траје дуже него што је неопходно.

Војнотехнички гласник примењује поступак „двоструког анонимног рецензирања свих радова".

Главни уредник и чланови уредништва дужни су да предузму одговарајуће мере да аутори и рецензенти остану међусобно анонимни током и након процеса рецензије, у складу са двоструким слепим процесом рецензије. Поред тога, уредништво Војнотехничког гласника може пружити информацију о пристиглом рукопису само аутору, рецензентима или потенцијалним рецензентима, уколико је то потребно.

Сваки рукопис рецензирају бар два рецензента, независно један од другог, а њихов идентитет је међусобно непознат. Рецензенти се бирају искључиво према томе да ли располажу релевантним знањима за оцену рукописа. Не смеју бити из исте институције као аутори рукописа, нити бити њихови коаутори у скоријој прошлости. Евентуални предлози аутора рукописа да се ангажују одређени рецензенти не уважавају се.

Циљ рецензије јесте да уредништву помогне у доношењу одлуке да ли рад треба прихватити или одбити, као и да се у процесу комуникације с уредником, ауторима и другим рецензентима побољша квалитет рукописа.

Током поступка рецензије главни уредник може да захтева од аутора да доставе додатне информације, укључујући и примарне податке, ако су оне неопходне за доношење суда о рукопису. Уредник и рецензенти морају да чувају такве информације као поверљиве и не смеју их употребити у друге сврхе.

У редовним околностима поступак рецензирања траје највише четири недеље, а само изузетно до три месеца. Период од пријема рада до његовог објављивања траје, у просеку, 90 дана.

У случају да аутори имају озбиљне и основане замерке на рецензију, уредништво проверава да ли је она објективна и да ли задовољава академске стандарде. Ако се посумња у објективност или квалитет рецензије, уредник ангажује додатне рецензенте.

Додатни рецензенти се ангажују и у случају када су одлуке постојећа два рецензента међусобно опречне (одбити/прихватити) или на други начин непомирљиве.

Коначну одлуку о прихватању рукописа за објављивање доноси искључиво уредништво.

5. У изузетним случајевима, а посебно у оним околностима када је избор часописа ограничен због специфичне тематике чланка, чланови уредништва часописа Војнотехнички гласник могу бити и аутори његових научних радова. Ипак, у овом случају уредништво спроводи додатно транспарентнији и ригорознији двоструко слепи процес рецензије. То подразумева да ће Редакција часописа уложити напор да одржи интегритет рецензије и необјективност сведе на најмању могућу меру, тако што ће други уредник сарадник водити процедуру рецензије независно од уредника аутора, при чему ће тај процес бити апсолутно транспарентан. Уредништво ће посебно водити рачуна да рецензент не препозна ко је написао рад. Као додатну меру предострожности, ако и када се такав чланак објави, уредништво може објавити пропратни коментар који показује колико је процес уређивања и рецензије био транспарентан.

6. У случају кршења права Војнотехничког гласника, носилаца ауторских права или самих аутора, објављивања истог рукописа у више часописа, лажног ауторства, плагијата, манипулације подацима ради преваре или било које друге злоупотребе, објављени рад се мора опозвати.

Чланак се може опозвати и зато да би се исправиле озбиљне и бројне омашке које није могуће обухватити објављивањем исправке. Опозив објављује уредништво, аутор(и) или обе стране споразумно.

Опозив има облик засебног рада који се приказује у садржају свеске и уреднички класификује као Опозив или Ретракција.

Опозиви се публикују према захтевима COPE које је разрадио CEON, као издавач базе у којој се Војнотехнички гласник примарно индексира, односно издавач националног цитатног индекса где се метаподаци опозива и опозваних радова морају означити одговарајућим упозорењима и међусобно повезати унакрсним линковима:

У електронској верзији изворног чланка (оног који се повлачи) успоставља се веза (HTML линк) са обавештењем о повлачењу. Повучени чланак се чува у изворној форми, али са воденим жигом на PDF документу, на свакој страници, који указује да је чланак повучен (RETRACTED).

7. Редакција је отворена за академску, научно засновану, колегијалну и подстицајну размену мишљења и критику, односно за изношење евентуалних неслагања у вези са резултатима објављеним у чланцима Војнотехничког гласника, тиме што ће пружити могућност учесницима да њихови предметни дописи или полемике буду објављени у рубрици часописа „Писма уреднику".

Мере, радње, одговорности и обавезе рецензената Војнотехничког гласника

Рецензенти су дужни да квалификовано и у задатим роковима доставе уреднику оцену научне, односно стручне вредности рукописа. Рецензент води посебну бригу о стварном доприносу и оригиналности рукописа. Рецензија мора бити сасвим објективна, а суд рецензента јасан и поткрепљен аргументима.

Рецензенти оцењују рукописе у односу на усклађеност садржаја с профилом Војнотехничког гласника, значај и корисност садржаја, адекватност примењених метода, научну вредност садржаних информација, стил излагања и опремљеност текста. Рецензија има стандардни формат који обухвата оцене појединих димензија рада, општу оцену и закључну препоруку. Неприхватљива је лична критика аутора.

Рецензент не сме бити у сукобу интереса са ауторима или финансијером истраживања. Уколико такав сукоб постоји, рецензент је дужан да о томе правовремено обавести уредника. Рецензент не прихвата на рецензију радове изван области за коју се сматра потпуно компетентним.

Рецензенти треба да упозоре главног уредника ако основано сумњају или имају сазнање о повредама етичких стандарда од стране аутора рукописа. Дужност рецензента јесте да скрене пажњу уреднику на значајна подударања или сличност рукописа са већ објављеним радом, уколико о томе има лична сазнања. Такође, треба да препозна релевантне изворе који у раду нису узети у обзир. Може да препоручи цитирање одређених референци, али не сме да захтева цитирање радова објављених у часопису Војнотехнички гласник или својих радова, ако за то не постоји оправдање.

Од рецензената се очекује да својим сугестијама унапреде квалитет рукописа. Ако оцене да рад заслужује објављивање уз корекције, дужни су да прецизирају начин на који то може да се оствари.

Рукописи који су послати рецензенту морају се сматрати поверљивим документима. Рецензенти не смеју да користе материјал из рукописа за своја истраживања без изричите писане дозволе аутора.

Редакција Војнотехничког гласника подстиче рецензенте да рецензије верификују на својим персонализованим страницама на платформи Web of Science (WoS). Када рецензент уради рецензију чланка за Војнотехнички гласник биће питан да ли жели да прати, потврди и добије признање за свој рад на платформи WoS. Рецензент затим може користити своју верификовану рецензију као доказ о својим доприносима научној заједници у апликацијама за промоцију, финансирање и сл.

Рецензентска политика часописа:

– омогућава јавно приказивање рецензије (**искључиво након објављивања чланка**),

– рецензентима приказује наслове рецензираног чланка (**искључиво након објављивања чланка**).

Мере, радње, одговорности и обавезе аутора који пишу чланке за Војнотехнички гласник

Аутори гарантују да рукопис представља њихов оригиналан допринос, да није објављен раније и да се не разматра за објављивање на другом месту. Истовремено предавање истог рукописа у више часописа представља кршење етичких стандарда, што га искључује из даљег разматрања за објављивање у Војнотехничком гласнику. Рад који је већ објављен на неком другом месту не може бити прештампан у часопису Војнотехнички гласник.

Аутори сносе сву одговорност за целокупни садржај рукописа. Рукопис не сме да садржи неосноване или незаконите тврдње, нити да крши права других лица.

Приликом писања рада, аутори не смеју користити генеративне вештачке интелигенције (енгл. generative AI), као ни технологије подржане вештачком интелигенцијом (енгл. AI-assisted), као што су велики језички модели (енгл. Large Language Models). Ове технологије се не могу користити за реализацију кључног задатка аутора, а то је извођење закључака и препорука који су научно засновани. Алати вештачке интелигенције се могу користити у процесу истраживања за анализу и извођење закључака из података.

Аутори су дужни да обезбеде да њихов ауторски тим наведен у рукопису обухвати само она лица која су значајно допринела садржају рукописа. Ако су у битним аспектима истраживачког пројекта и припреме рада учествовала и друга лица, њихов допринос треба навести у фусноти или посебној напомени (Захвалница, Acknowledgements).

Обавеза је аутора да у напомени наведу назив и кодну ознаку научноистраживачког пројекта у оквиру којег је рад настао, као и пун назив финансирајуће институције. У случају да је рад под истим или сличним насловом био изложен на неком скупу у виду усменог саопштења, детаљи о томе треба да буду наведени на истом месту.

Аутори су дужни да потпуно и правилно цитирају изворе који су значајно утицали на садржај истраживања и рукописа. Делови рукописа, укључујући текст, једначине, слике или табеле, који су дословно преузети из других радова, морају бити јасно означени посебном напоменом, нпр. знацима навода са прецизном ознаком места преузимања (броја странице) или, ако су обимнији, наведени у засебном параграфу.

Пуне референце свих навода у тексту (цитата) морају бити наведене у засебном одељку (Литература) и то на једнообразан начин, у складу са цитатним

стилом који Војнотехнички гласник користи (Harvard Style Manuel). У одељку Литература наводе се само цитирани, а не и остали извори коришћени приликом припреме рукописа.

У случају да аутори открију важну грешку у свом раду након његовог објављивања, дужни су да одмах о томе обавесте главног уредника (или Редакцију Војнотехничког гласника) и да сарађују у процесу повлачења или исправљања рада.

Обавеза је аутора да у рукопису наведу да ли су у финансијском или било ком другом битном сукобу интереса који би могао да утиче на њихове резултате или интерпретацију резултата.

Ако се у ауторовом истраживању појављују хемијска једињења, поступци или опрема који су опасни по здравље људи или животиња, то мора бити јасно назначено у рукопису.

Предавањем рукописа аутори се обавезују на поштовање уређивачке политике часописа Војнотехнички гласник, што потврђују достављањем Изјаве о ауторству.

Разрешавање спорних ситуација

Сваки појединац или институција могу уреднику и/или уредништву пријавити сазнања о кршењу етичких стандарда и другим неправилностима и о томе доставити веродостојне информације/доказе ради покретања истраге. Поступак провере изнетих доказа одвија се на следећи начин:

– главни уредник доноси одлуку о покретању истраге;

– током тог поступка сви докази се сматрају поверљивим материјалом и предочавају само оним лицима која су директно обухваћена случајем;

– осумњиченим лицима пружа се прилика да одговоре на изнете оптужбе;

– ако се утврди да је заиста дошло до неправилности, оцењује се да ли је реч о мањем прекршају или грубом кршењу етичких стандарда.

Мањи прекршаји, без последица по интегритет рада и Војнотехничког гласника, на пример када је реч о неразумевању или погрешној примени публицистичких стандарда, разрешавају се у директној комуникацији с ауторима и рецензентима, без укључивања трећих лица, на неки од следећих начина:

– ауторима и/или рецензентима упућује се писмо упозорења;

– објављује се исправка рада, на пример у случају када се са списка референци изоставе извори који су у самом тексту цитирани на прописан начин;

– објављује се ератум, на примеруколико се испостави да је грешка настала омашком уредништва.

У случају грубог кршења етичких стандарда, уредништво може да предузме различите мере:

– објављује саопштење или уводник у којем се случај описује;

– службено обавештава афилијативну организацију аутора/рецензента;

– повлачи објављени рада;

– изриче забрану објављивања у часопису на одређени период;

– предочава случај надлежним организацијама и регулаторним телима ради предузимања мера из њихове надлежности.

Ове мере могу се примењивати појединачно или истовремено. У процесу разрешавања случаја по потреби се консултују релевантне експертске организације, тела или појединци.

Приликом разрешавања етички спорних поступака уредништво се руководи смерницама Комитета за етику публиковања (COPE).

Одрицање одговорности

Изнесени ставови у објављеним радовима не изражавају ставове уредника, чланова Редакције и Уређивачког одбора часописа Војнотехнички гласник. Аутори преузимају правну и моралну одговорност за идеје изнесене у својим радовима.

Изнесени ставови у објављеним радовима не изражавају ставове уредника, чланова Редакције и Уређивачког одбора часописа Војнотехнички гласник. Аутори преузимају правну и моралну одговорност за идеје изнесене у својим радовима. Издавач неће сносити никакву одговорност у случају испостављања било каквих захтева за накнаду штете.

Сукоб интереса

Војнотехнички гласник се придржава политике сукоба интереса коју препоручују COPE и/или друга међународна регулаторна тела (ICMJE, EASE). Од аутора се тражи да се изјасне о свом сукобу интереса у Изјави о сукобу интереса. У Изјави су аутори дужни да наведу: 1) изјаву о свим потенцијалним сукобима интереса за сваког именованог аутора релевантну за садржај чланка или изјаву да немају такве сукобе; 2) тврдња о начину на који је чланак финансиран, конкретно о финансирању, делимично или потпуно, од стране неке компаније или, алтернативно, тврдња да није било тог учешћа и 3) свеобухватно објашњење улоге спонзора у припреми чланка ако је чланак спонзорисан, било у целини или делимично.

Рекламирање

Није дозвољено рекламирање у Војнотехничком гласнику.

Детаљи о етичком поступању Војнотехничког гласника доступни су и на страницама часописа: ***Уређивачка политика, Управљање квалитетом часописа, Подршка квалитету радова*** *у Српском цитатном индексу – издавачу базе у којој се Војнотехнички гласник примарно индексира, односно издавачу националног цитатног индекса.*

КОДЕКС ПРОФЕССИОНАЛЬНОЙ ЭТИКИ ЖУРНАЛА «*ВОЕННО-ТЕХНИЧЕСКИЙ ВЕСТНИК*» ЗАЯВЛЕНИЕ

ПРИМЕЧАНИЕ: Редакционная политика журнала «Военно-технический вестник» основана на рекомендациях Комитета по этике научных публикаций (COPE Core Practices), общих принципах прозрачности и лучшей практике издательской деятельности COPE, DOAJ, OASPA и WAME, а также на лучшей практике научно-издательской деятельности. Журнал «Военно-технический вестник» является членом COPE (Комитет по этике научных публикаций) со 2 мая 2018 года и членом OASPA (Ассоциация научных издателей открытого доступа) с 27 ноября 2015 года. Редакция применяет Контрольный перечень по выполнению Рекомендации ЮНЕСКО об открытой науке для издателей с открытым доступом. Данный документ является частью инструментария ЮНЕСКО по открытой науке, разработанного с целью поддержки внедрения Рекомендации ЮНЕСКО по открытой науке. Документ составлен при содействии с OASPA.

Публикация статей после их профессиональной рецензии является основной деятельностью научного журнала «Военно-технический вестник». В редакционно-издательском процессе в первую очередь необходимо достичь договоренности об этических нормах и принципах, применяемых ко всем участникам, начиная с автора, редакционной коллегии, профессиональных рецензентов до самого издателя. Вышеперечисленные принципы и процедуры утверждены настоящим Заявлением и Кодексом профессиональной этики журнала «Военно-технический вестник».

Меры, деятельность, права и обязанности редакции журнала «Военно-технический вестник»

Редакция журнала «Военно-технический вестник» не взимает плату за подачу и публикацию статей ни с их авторов, ни с третьих лиц. Все процедуры редактирования и публикации абсолютно бесплатны для авторов, включая подачу, прием, редактуру, корректуру, обработку и публикацию статьи. Нет никаких скрытых затрат.

Окончательное решение по выбору статей к публикации принимается редколлегией журнала «Военно-технический вестник». Решение принимается исключительно на основании научной ценности статьи. Не допускается дискриминация по признаку расы, пола, религии, этнического происхождения или политических убеждений. При принятии решений редакция руководствуется редакционной политикой, соблюдая положения законодательства, касающихся клеветы, нарушения авторских прав или плагиата.

Рукописи являются конфиденциальным материалом и хранятся соответствующим образом. Пользоваться информацией и идеями из рукописей в личных целях без письменного согласия авторов недопустимо.

По рекомендациям Центра поддержки оценки в образовании и науке (ЦЕОН) редакция журнала в своей работе пользуется электронной системой редактирования SCIndex (Сербский индекс цитирования) ASSISTANT (разработанной на основе платформы OJS), обеспечивающей прозрачность и доступность информации о текущем состоянии рукописи. Редакция несет полную ответственность за принятие решения о её публикации.

Процедура редактирования статьи в журнале «Военно-технический вестник» включает следующие обязанности редакции:

1. После приема статьи редакции необходимо получить от автора Авторское заявление, в котором авторы: должны указать свой индивидуальный вклад в создание статьи; подтвердить, что ознакомлены с политикой журнала в отношении отзыва уже опубликованных статей; подтвердить, что представленная рукопись является оригинальной работой, написанной и подписанной указанными авторами, что ранее она не публиковалась, а также, что рукопись не рассматривается другими изданиями для публикации и не проходит рецензирование в других журналах; подтвердить, что статья и дополнительные материалы не содержат никаких ложных высказываний, которые могли бы рассматриваться как клевета, не содержат никаких противоречащих закону утверждений или материалов, которые каким-либо образом могут поставить под угрозу личные или имущественные права физических или юридических лиц; подтвердить, что у них нет конфликта интересов, который мог бы поставить под сомнение целостность и достоверность результатов, представленных в статье, и что авторы получили согласие от правообладателей на использование всех выдержек из трудов и других материалов, защищенных авторским правом, которые использовались в рукописи, а также подтвердить, что они указали цитируемые источники в рукописи и дополнительных материалах.

2. Прежде чем редактор ознакомится с рукописью, редколлегия проверяет содержание рукописи на предмет плагиата, для того чтобы удостовериться в оригинальности представленных статей и предотвратить публикацию плагиата и дублирования. Журнал «Военно-технический вестник» не публикует статьи, содержащие плагиат. Редакция придерживается мнения, что плагиат, то есть использование чужих идей, слов или других творческих способов внесения вклада в науку без намеренного указания источника и их представление как своих собственных, является серьезным нарушением исследовательской и публикационной этики. Плагиат является нарушением авторских прав, и он уголовно наказуем.

Под плагиатом понимается:

- Дословное или приблизительное заимствование, а также намеренное перефразирование частей текстов других авторов без четкого указания источника, с целью скрыть источник;
- Копирование уравнений, данных или таблиц из чужих документов без четкого указания источника и/или без согласия автора или правообладателя;

Рукописи с явными признаками плагиата будут автоматически отклонены. Если плагиат выявлен в уже опубликованной статье, то она будет отозвана в порядке, описанном в пункте 6.

В целях предотвращения публикации плагиата в журнале рукописи проверяются с помощью системы iThenticate/CrossRef в рамках платформы SCIndex ASSISTANT. Результаты проверки перепроверяются редакционной коллегией журнала в соответствии с принципами и рекомендациями Комитета по этике научных публикаций (COPE).

Журнал «Военно-технический вестник» запрещает использование генеративных инструментов искусственного интеллекта (ИИ) (engl. AI-assisted), таких как большие языковые модели (engl. Large Language Models) при написании статьи. Использование этих технологий разрешено исключительно для улучшения языка и удобочитаемости статей, но только под строгим наблюдением авторов. Редакция журнала «Военно-технический вестник» может использовать форензические инструменты и специальное программное обеспечение для выявления неэтичного написания статей с помощью генеративного искусственного интеллекта и технологий, поддерживаемых ИИ. Статьи, в которых было обнаружено неэтичное

использование этих технологий, будут отклонены в процессе редактирования и рецензирования. Если такого рода нарушения будут выявлены в ранее опубликованных статьях, то они будут отозваны.

3. После проверки на плагиат редколлегия передает рукопись редактору, который в дальнейшем будет вести редакционный процесс и выбирать рецензентов. Редколлегия и редактор, которым направлена представленная статья, не должны иметь конфликта интересов в отношении рассматриваемой ими рукописи.

При наличии такого конфликта интересов о выборе рецензентов и судьбе рукописи решение принимает редакционный совет. Члены редакционного совета, у которых тоже может быть конфликт интересов, также не участвуют в процессе принятия решения по конкретной рукописи.

4. Рукописи представляются на рецензирование только после первичной оценки с учетом соответствия оформления и тематики статьи для публикации в журнале «Военно-технический вестник». Особое внимание уделяется продолжительности оценки, которая длится ровно столько, сколько это необходимо.

Редакция журнала «Военно-технический вестник» проводит конфиденциальное рецензирование всех статей, применяя «двойной слепой метод».

Главный редактор и члены редколлегии обязаны принять соответствующие меры для того, чтобы авторы и рецензенты оставались анонимными друг для друга во время и после процесса рецензирования, проведенного методом двойного слепого рецензирования. Редакция журнала «Военно-технический вестник» при необходимости может предоставить информацию о представленной рукописи только автору, рецензентам или потенциальным рецензентам.

Все рукописи рецензируются как минимум двумя анонимными рецензентами, которые рецензируют рукопись независимо друг от друга. Рецензенты выбираются исключительно на основании их компетенции в области исследования рукописи. Рецензенты не могут быть коллегами авторов, то есть работать в том же учреждении, где работает автор, и они не должны иметь с авторами совместных работ, опубликованных в ближайшем прошлом. Возможные пожелания и предложения авторов о привлечении конкретных рецензентов не принимаются.

Рецензирование проводится с целью оказания помощи редколлегии при принятии решений о публикации статей или отказе авторам, а также улучшения качества статьи путем коммуникации рецензента с редактором, авторами и другими рецензентами.

В процессе рецензирования главный редактор вправе потребовать от автора дополнительную информацию, включая исходные данные, если это необходимо для оценки рукописи. Редактор и рецензенты должны хранить данную информацию в конфиденциальности и не вправе использовать ее в иных целях.

Процесс рецензирования обычно занимает максимум четыре недели и только в исключительных случаях он может длиться до трех месяцев. Период времени от подачи рукописи до ее публикации составляет примерно 90 дней.

Если авторы предъявляют серьезные и обоснованные претензии на рецензию, редколлегия должна проверить являются ли рассматриваемые рецензии объективными и соответствуют ли они академическим стандартам. Если объективность или качество этих рецензий вызывает сомнения, редактор привлекает дополнительных рецензентов.

Дополнительные рецензенты также привлекаются, в случае если решения выбранных рецензентов полностью расходятся (принять/отклонить) или противоречат друг другу по другим признакам.

Окончательное решение о принятии рукописи к публикации принимается исключительно редакционной коллегией.

5. В исключительных случаях, особенно когда выбор журнала ограничен из-за специфической темы статьи, членам редколлегии журнала «Военно-технический вестник» допускается публиковаться в нем. В таком случае редколлегия гарантирует, что процесс двойного слепого рецензирования будет еще более прозрачным и строгим. Это означает, что редакция приложит все усилия для того, чтобы сохранить целостность рецензии и свести к минимуму любую предвзятость. Заместитель редактора проведет абсолютно прозрачную процедуру рецензирования независимо от редактора-автора. Редакционная коллегия позаботится о том, чтобы рецензент не узнал кто является автором статьи. В качестве дополнительной меры предосторожности, если и когда такая статья будет опубликована, редколлегия к статье добавит примечание, содержащее информацию о высоком уровне прозрачности, проведенных процессов редактирования и рецензирования.

6. В случае нарушения прав журнала «Военно-технический вестник», авторских прав или самих авторов, а также в случае повторной публикации одной и той же статьи в различных изданиях, присвоения авторства, плагиата, манипулирования данными или другого вида нарушения этических норм, опубликованная статья будет отозвана.

Статья также может быть отозваны с целью исправления многочисленных и/или фундаментальных недостатков, которые не могут быть устранены исправлениями после публикации. Отзыв статьи производится редакцией, автором (авторами) или обеими сторонами по взаимному согласию.

Уведомление об отзыве имеет форму отдельного документа, указанного в содержании выпуска под названием «Отзыв» или «Ретракция».

Отзывы публикуются в соответствии с требованиями COPE, разработанными CEON в его базе данных, где «Военно-технический вестник» индексируется в первую очередь, при этом метаданные отозванных и снятых с публикации статей должны быть обозначены соответствующим предупреждением и связаны между собой ссылками.

За статьей (утвержденной к отзыву) в электронном формате закрепляют HTML ссылку с уведомлением о её снятии с публикации. Изъятая статья хранится в исходном виде, но каждая страница ПДФ формата визируется водяным знаком, свидетельствующим об изъятии статьи с публикации (RETRACTED).

7. Редакция открыта для академического, научно обоснованного, коллегиального и продуктивного обмена мнениями и критикой, а также для выражения возможных разногласий относительно результатов в статьях, опубликованных в журнале «Военно-технический вестник», предоставляя возможность участникам дискуссии публиковать свои письма по предмету полемики в рубрике: «Письма редактору».

Меры, деятельность, права и обязанности рецензентов журнала «Военно-технический вестник»

Рецензенты должны профессионально и объективно аргументировать свою позицию и в указанный срок предоставлять редактору оценку научной ценности и оригинальности рукописи.

Рецензенты, рассматривая работы оценивают соответствие содержания статьи с профилем журнала «Военно-технический вестник», релевантность исследуемой области и примененных методов, оригинальность и научную значимость результатов, представленных в рукописи, стиль научного изложения, а также

использование в тексте научного аппарата. Рецензия должна быть выполнена в стандартном формате, включающем оценки отдельных аспектов работы, общую оценку и заключительную рекомендацию. Личная критика автора недопустима.

У рецензента не должно быть конфликта интересов с авторами или организацией, финансирующей исследование. При наличии такого конфликта рецензент обязан своевременно сообщить об этом редактору. Рецензент может выполнять оценку только тех рукописей, которые соответствуют его области научных и профессиональных интересов, в которой он считается экспертом.

Рецензенты обязаны уведомлять главного редактора в случае, если они обоснованно подозревают или, если они выявили нарушения этических норм в рукописи.

Рецензенты обязаны идентифицировать релевантные существующие работы, которые автор не цитировал. По любому общему сведению или аргументу приведенным в работе должны быть указаны соответствующие источники цитирования. Рецензент обязан обратить внимание редактора на значимые сходства работы с другими опубликованными работами, в случае если такое будет обнаружено. Также рецензенты должны рекомендовать релевантные источники для цитирования, которые не были учтены в работе. Однако они не вправе необоснованно требовать от авторов цитирования работ, опубликованных в журнале «Военно-технический вестник» или своих собственных работ.

Рецензенты оказывают содействие в улучшении качества рукописи своими предложениями и рекомендациями. Если они считают, что работу можно публиковать только после внесения определенных исправлений, то они обязаны указать каким именно образом это лучше сделать.

Рукописи, представленные рецензенту, считаются конфиденциальным документом. Рецензенты не вправе использовать материалы рукописей в своих собственных исследованиях без письменного согласия автора.

Редакция журнала «Военно-технический вестник» призывает рецензентов подтверждать свои рецензии на своей личной странице на платформе Web of Science (WoS). По завершении рецензии статьи, предложенной к публикации в журнале «Военно-технический вестник» рецензенты получат вопрос о том, желают ли они чтобы их рецензия была оценена и признана системой WoS. Таким образом, подтверждённую рецензию рецензент сможете использовать в качестве подтверждения научной деятельности, что поможет при подаче заявок на получение научных грантов, их финансирование и т.д.

Политика журнала относительно рецензий:

- обеспечивает публичный доступ к рецензии (**но только после публикации статьи**),
- позволяет рецензентам отображать заголовок рецензируемой статьи (**но только после публикации статьи**).

Меры, деятельность, права и обязанности авторов, публикующихся в журнале «Военно-технический вестник»

При подаче рукописи в журнал «Военно-технический вестник» автор гарантирует, что рукопись является оригинальной работой, которая не была опубликована ранее и не рассматривается к публикации в других издательствах. Дублирование одной и той же статьи является нарушением этического кодекса, соответственно при обнаружении дублирования автору будет отказано в ее публикации.

Авторы несут ответственность за полное содержание своей рукописи. Рукопись не должна содержать необоснованных или противоречащих закону высказываний, а также не должна нарушать права других лиц.

При написании статьи авторам запрещено пользоваться генеративным искусственным интеллектом (engl. generative AI), а также технологиями, поддерживаемыми искусственным интеллектом (engl. AI-assisted), такими как большие языковые модели (engl. Large Language Models). Этими технологиями нельзя пользоваться в осуществлении ключевой авторской задачи, которая заключается в научных выводах и рекомендациях автора. Инструменты искусственного интеллекта могут использоваться в процессе исследования для анализа и выводов на основании данных.

Авторы должны указать имена, отчества, фамилии всех соавторов, действительно участвующих в процессе исследования и внесших вклад в содержание рукописи. Если в важных аспектах исследовательского проекта и подготовке работы участвовали и другие лица необходимо описать их вклад в сноске или в отдельном примечании (Благодарность, Acknowledgements).

В примечании также должны быть указаны название и кодовый номер научно-исследовательского проекта, в рамках которого была написана статья, а также полное название учреждения/организации, оказавшей финансовую поддержку в осуществлении исследования. В случае, если данное исследование ранее уже было представлено в устной форме, например, на конференции, в примечании необходимо указать название конференции и прочие данные.

Авторы обязаны правильно и полностью цитировать источники, которые оказали значительное влияние на содержание исследования и рукописи. Фрагменты рукописи, включая текст, уравнения, рисунки, графики и таблицы, непосредственно взятые из работ других авторов, должны быть наглядно выделены, например, кавычками с точной ссылкой на первоисточник (номер страницы). Если предмет цитирования длинный, то его следует оформить отдельным абзацем.

Подробная информация о ссылках в тексте (цитирование) должна быть указана в отдельном разделе (Литература) в соответствии со стилем цитирования, используемым журналом «Военно-технический вестник» (Harvard Style Manuel). В разделе «Литература» следует указывать не все источники, использованные при подготовке рукописи, а только цитируемые.

Авторы обязаны незамедлительно уведомить главного редактора (или редакцию журнала «Военно-технический вестник») и содействовать редакции в процессе отзыва или исправления ошибок, в случае если после публикации статьи ими была обнаружена грубая ошибка в ее содержании.

Авторы обязаны указать в рукописи, если существует финансовый или любой другой конфликт интересов, который может повлиять на результаты или интерпретацию результатов исследования.

Если исследование связано с химическими веществами, видами деятельности или оборудованием, представляющими угрозу здоровью людей или животных, это должно быть четко указано в рукописи.

При подаче рукописи авторы соглашаются соблюдать редакционную политику журнала «Военно-технический вестник», подтвердив свое согласие с условиями редакционной политики журнала предоставлением Авторского заявления.

Разрешение спорных ситуаций

Любое лицо либо учреждение вправе в любой момент предъявить претензию редактору или редколлегии в связи с нарушением этических стандартов, подкрепив

ее достоверными доказательствами. По получении претензии, подкрепленной доказательствами, редакционная комиссия проведет расследование в соответствии со следующими принципами:

- главный редактор принимает решение о проведении расследования;
- в процессе проверки доказательств все материалы считаются конфиденциальными и будут предоставлены только тем лицам, которые непосредственно причастны к процессу проверки;
- подозреваемым лицам в нарушении этических норм будет предоставлена возможность ответить на выдвинутое против них обвинение;
- если установлено, что нарушение действительно произошло, оценивается степень тяжести нарушения этических норм.

В случае негрубого нарушения (без угрозы репутации журнала „Военно-технический вестник“), например, в случае неправильного толкования или применения публикационных стандартов, редакция напрямую без содействия третьих лиц, обращается к нарушителю следующим образом:

- автору/рецензенту, допустившему ошибку/нарушение направляется письменное предупреждение;
- публикуется уведомление об исправлении, например, если источник, цитируемый в тексте статьи не внесен в список литературы;
- публикуется исправление ошибки, в случае если ошибка произошла по вине редакции.

В случае грубого нарушения этических норм редакция принимает решение о дальнейших мерах:

- публикуется отдельная заметка или статья редактора с описанием случая нарушения этических стандартов;
- направляет официальное уведомление руководителям учреждения, в котором работает автор/рецензент;
- редакция производит отзыв опубликованной статьи;
- редакция объявляет запрет к публикации автора/рецензента на определенный срок;
- информирует соответствующие профессиональные организации и компетентные учреждения о случае, в целях привлечения нарушителя к ответственности.

Редакция вправе предпринимать меры одновременно или поочередно по отдельности. В процессе разрешения дела по мере необходимости проводятся консультации с соответствующими экспертными организациями, органами или лицами.

При разрешении спорных ситуаций редакция журнала руководствуется предписаниями и инструкциями Комитета по этике научных публикаций (COPE).

Отказ от ответственности

Выносимые положения в опубликованных статьях не отражают точку зрения редактора, редколлегии и редакционного совета журнала «Военно-технический вестник». Авторы несут юридическую и моральную ответственность за представленные в своих работах идеи. Редакция не несет никакой ответственности в случае возникновения требований по возмещению материального ущерба и взысканию компенсации морального вреда.

Конфликт интересов

Журнал «Военно-технический вестник» придерживается политики конфликта интересов, рекомендованной COPE и/или другими международными органами, регулирующими публикации научных исследований (ICMJE, EASE). Авторы должны заявить о своем конфликте интересов в Заявлении о конфликте интересов (CoIS). В CoIS каждый названный автор статьи обязан предоставить: (1) Заявление о любых потенциальных конфликтах интересов, имеющих отношение к содержанию, или заявление об отсутствии таких конфликтов. (2) Раскрытие информации о том, как финансируется статья, включая конкретное раскрытие любого и всего финансирования компании (частичного или полного) или заявление об отсутствии такого участия (если применимо). (3) Подробное объяснение роли спонсоров в подготовке статьи, если статья спонсируется частично или полностью.

Реклама

Реклама в журнале «Военно-технический вестник» не допускается.

Более подробно с информацией об Этическом кодексе журнала «Военно-технический вестник» можно ознакомиться на интернет-страницах журнала: ***Редакционная политика, Управление качеством журнала, Поддержка качеству работ*** *на сайте Сербского индекса научного цитирования, в базе которой журнал «Военно-технический вестник» первично индексируется.*

STATEMENT OF THE *MILITARY TECHNICAL COURIER* ON ETHICAL CONDUCT

NOTE: The editorial policy of the Military Technical Courier is based on the COPE Core Practices, common COPE, DOAJ, OASPA and WAME Principles of Transparency and Best Practice in Scholarly Publishing as well as on the best accepted practices in scientific publishing. The Military Technical Courier has been a COPE (Committee on Publication Ethics) member since 2nd May 2018 and a member of OASPA (Open Access Scholarly Publishers Association) since 27th November 2015. The editorial office applies Checklist for open access publishers on implementing the UNESCO Recommendation on Open Science. This document is part of the UNESCO Open Science Toolkit, designed to support implementation of the UNESCO Recommendation on Open Science. It has been produced in partnership with OASPA.

The main scope of the Military Technical Courier scientific journal is publishing scientific articles after peer reviewing. In the editing process leading to publishing scientific articles, it is necessary to reach an agreement on ethical principles in the behavior of all parties involved (Editorial Office i.e. Editor, members of the Editorial Board, reviewers, and authors alike). The aforementioned principles and practices are defined by this Statement of the Military Technical Courier on Ethical Conduct.

Measures, activities, responsibilities, and duties of the Military Technical Courier Editorial Office

The Editorial Office of the Military Technical Courier does not charge for submitting manuscripts from their authors nor from third parties. The whole process of processing and publishing is completely free of charge for authors – from the manuscript submission services through processing to the article publishing services. There are no hidden costs whatsoever.

The Editorial Office decides finally which manuscripts are to be published. Decisions are based only on manuscript values. In making decisions, there is no discrimination on the basis of race, sex/gender, religion, ethnic origin or political beliefs. In making decisions, the Editorial Office is guided by the Journal's policy, complying with legal regulations dealing with libel, copyright infringement and plagiarism.

Manuscripts are kept as confidential material. No information and/or ideas from manuscripts are to be used for private purposes without authors' explicit consent in writing.

In its work, following the recommendations of the Centre for Evaluation in Education and Science (CEON/CEES), the Editorial Office uses the Serbian Citation Index (SCIndeks) ASSISTANT electronic editing system which provides full transparency of the publishing process (developed on the basis of the OJS platform) while being fully responsible for accepting and publishing articles.

The editing process in the Military Technical Courier consists of the following steps of the Editorial Office:

1. After receiving manuscripts, the Office asks the authors to fill in the Authorship Statement in which they: specify their contribution to the manuscript; confirm that they are familiar with the Journal's policy regarding the retraction of already published articles; confirm that the submitted manuscript is an original paper written and signed by its authors, not previously published, not considered for publication elsewhere and not concurrently sent for review to other journals; confirm that the manuscript and the additional material contain neither any false statements that could be considered defamation, any false claims nor material that in any way endangers personal or property rights of natural or legal persons; confirm that they do not have a conflict of interest that could cast doubt on the

article's integrity and the credibility of the results published in it; confirm that they have obtained permission from copyright holders to use all content from copyright-protected works and other copyright-protected material used in the manuscript; and confirm that they have acknowledged the sources in the manuscript and supplementary material.

2. Before the Editor attends to the manuscript, the Editorial Office checks the manuscript content for plagiarism in order to establish the originality of submitted papers and prevent plagiarism and duplication. The Military Technical Courier does not publish plagiarized papers. The Editorial Office is of the opinion that plagiarism i.e. using another's ideas, words or other creative ways of contributing without acknowledging their source and presenting them as one's own is serious violation of research and publication ethics. Plagiarism may also involve copyright infringement which is violation of law.

Plagiarism involves:

- Verbatim or nearly verbatim copying or paraphrasing parts of other authors' texts without clear citing of the source purposefully, in order to hide the source;
- Copying equations, data or graphical presentations from documents of others without clearly acknowledging the source and/or without the authorization of the original author or copyright holder;

A manuscript showing obvious signs of plagiarism is rejected automatically. In case plagiarism is found in an already published article, the article is revoked (retracted) following the procedure given in point 6.

In order to prevent plagiarism, the Journal uses the iThenticate/CrossRef system within the SCIndeks Assistant service for checking manuscripts. The results obtained by such checking are verified by the Editorial Office in accordance with the COPE guidelines and recommendations.

The Military Technical Courier does not allow the use of generative AI nor AI-assisted technologies such as Large Language Models for writing papers. The use of these technologies is allowed exclusively for improving the language and readability of papers but only under strong supervision of authors. The Editorial Office of the Military Technical Courier may use forensic tools and special software to identify unethical writing of papers with the help of generative artificial intelligence and AI-assisted technologies. Papers found to have used these technologies unethically will be rejected during the editing and review process or they will be subsequently retracted if these malpractices are found in already published articles.

3. After being checked for plagiarism, a manuscript is dealt with by the Editor who continues the publishing process by choosing peer reviewers. Neither the Editorial Team nor the Editor in charge of the particular manuscript are allowed to be in a conflict of interest in the case of the manuscript in question.

If there is a conflict of interest, it is up to the Editorial Board to decide on peer reviewers and further actions regarding the manuscript. The Editorial Board members who might be in a conflict of interest are also excluded from the decision-making process in the case of the manuscript in question.

4. Manuscripts are sent to reviewers only after the initial assessment stating that, based on their form and content scope, they are eligible for publication in the Military Technical Courier. Special care is taken that the initial assessment does not last longer than necessary.

The Military Technical Courier makes use of double-blind peer review of all papers.

It is mandatory for the Editor-in-Chief and the Editorial Team members to take appropriate measures that authors and reviewers remain anonymous to each other during and after the reviewing process, in accordance with the double-blind peer review method.

The Editorial Team of the Military Technical Courier can give information on the submitted manuscript only to the author, reviewers or potential reviewers if necessary.

Every manuscript has to be reviewed by at least two reviewers who are not aware of each other's identity and who review the manuscript independently of each other. Reviewers are chosen solely based on whether they have relevant knowledge for the particular paper review. They must not have the same affiliation as the paper author(s) and they are not allowed to have been co-authors with them in the recent past. Possible suggestions of manuscript authors on engaging particular reviewers are not accepted.

The purpose of a review is to help the Editorial Team make a decision whether the paper should be accepted or rejected and to improve the quality of the manuscript through the process of communication with the Editor, authors and other reviewers. During the reviewing process, the Editor-in-Chief may ask the author to submit additional information, including raw data, if it is necessary for assessing the manuscript. The Editor and the reviewers should treat such information as confidential and should not use it for any other purpose.

The reviewing process usually lasts for four weeks maximum, and only exceptionally up to three months. The period of time from the manuscript submission to its publishing is approximately 90 days.

If authors have some serious and justifiable concern with reviews, the Office checks whether the reviews in question are objective and of academic standard. If the objectivity or quality of these reviews are questionable, the Editor engages additional peer reviewers.

Additional reviewers are also engaged when the decisions of the assigned reviewers are contradictory (accept/reject) or somehow incompatible.

The final decision on the acceptance of a manuscript for publication is made exclusively by the Editorial Team.

5. In extreme cases, especially when the choice of journals is limited due to the paper's narrow subject field, it is acceptable that the members of the Editorial Team of the Military Technical Courier may also be authors of scientific articles published in it. However, in this case, the Editorial Team ensures that the double-blind review process is even more transparent and more rigorous. This means that the Editorial Office will make every effort to maintain the integrity of the review and to minimize any bias by having another associate editor handle the review procedure independently of the editor – author in a completely transparent process. The Editorial Team will take special care that a reviewer does not recognize the author's identity. As an extra precaution, if and when such an article is published, the Editorial Team may accompany the article with a note about a high level of transparency of the editing and reviewing processes in question.

6. In case of the violation of the rights of the Military Technical Courier, copyright holders or authors as well as in case of multiple publication, fake authorship, plagiarism, data manipulation or any other malpractice, the published article must be retracted.

Articles can also be retracted for correcting numerous and/or fundamental flaws which cannot be dealt with by post-publication corrections. Retractions are issued by the Editorial Team, the author(s) or by both parties based on mutual agreement.

A retraction notice has a form of a separate paper listed in the Contents of an issue, classified as "Retraction".

Retractions are published in accordance with the COPE Guidelines elaborated by the CEON/CEES in its database where the Military Technical Courier is primarily indexed.

The CEON/CEES publishes the national citation index where the metadata of retraction notices and related retracted articles must be clearly and appropriately marked and mutually cross-linked. An electronic version of the original article (the one being retracted) is provided with a HTML link to the retraction notice. Retracted articles are

retained in their original form but with a watermark on each page of the PDF document indicating that the article in question is RETRACTED.

7. The Editorial Office is open to academic, scientifically based, collegial and productive exchange of opinions and critiques as well as for expressing possible disagreements regarding the results in articles published in the Military Technical Courier by enabling polemics and reactions to be published in the Journal's section "Letters to the Editor".

Measures, activities, responsibilities, and duties of the Military Technical Courier reviewers

Reviewers are required to assess the scientific and professional values of manuscripts in a qualified and timely manner. They have to focus especially on the genuine contribution and originality of manuscripts. A review should be completely unbiased and the reviewer's assessment unambiguous and backed with arguments.

Reviewers assess manuscripts with regard to the compliance of the content with the Journal's character, importance and effectiveness of the content, convenience of the methods applied, scientific value of the presented information as well as with regard to the style, tone and form of the text. A review has a standard form which comprises assessment of particular elements of a manuscript, general assessment and final recommendation. Personal criticism of the author is unacceptable.

Reviewers must not be in a conflict of interest with authors or research funders. If such a conflict exists, the reviewer is obliged to inform the Editor about it in due time. Reviewers should not accept to review papers out of the scope of their full competence.

They should notify the Editor-in-Chief if they have a reasonable doubt about the author violating ethical standards. A duty of reviewers is to call to the editor's attention any substantial similarity or overlap between the manuscript under consideration and any other published paper of which they have personal knowledge. Also, hey should recognize relevant sources which have not been taken into account in the manuscript. They may recommend citing particular references but must not insist on citing articles published in the Military Technical Courier or their own papers if there is no justification for doing so.

Their suggestions should aim at improving the manuscript's quality. If they conclude the paper deserves to be published but with corrections, they are required to provide detailed instructions.

Manuscripts sent to reviewers must be treated as confidential documents. The material from manuscripts must not be used for reviewers' own research without the author's explicit consent in writing.

The Editorial Office of The Military Technical Courier encourages reviewers to verify their reviews on their personal profile pages on the Web of Science (WoS) platform. When reviewers submit their peer reviews to The Military Technical Courier, they will be asked whether they would like to track, verify and showcase them on the WoS platform. Reviewers can further use their verified peer reviews as evidence of their contribution to the scientific community in applications for promotion, grants, etc.

The reviewing policy of the journal:

- allows visibility of the review in public (**only after the article has been published**),
- shows titles of reviewed articles to reviewers (**only after the article has been published**).

Measures, activities, responsibilities and duties of the Military Technical Courier authors

Authors undertake that the manuscripts are their original contribution, that they have not been published before, and that they are not considered for publication elsewhere.

Parallel submission represents violation of ethical codes which eliminates the manuscript in question from being further considered for publication in the Military Technical Courier. A paper already published elsewhere cannot be published in the Military Technical Courier.

Authors are fully responsible for the complete content of their manuscripts. The manuscript should not contain unfunded or illegal statements nor infringe on the rights of others.

When writing their papers, authors are not allowed to use generative AI nor AI-assisted technologies such as Large Language Models. These technologies are not to be used for the realization of the key authors' task which is to draw scientifically based conclusions and recommendations. Artificial intelligence tools can be used in the process of research to analyze and draw conclusions from data.

Authors are required to make sure that their team mentioned in the manuscript consisits only of individuals whose contribution to the content of the manuscript is significant. If there were other individuals who participated in some other important moments of the research project or in the manuscript preparation, their contribution is to be mentioned in a footnote or in a separate note (Acknowledgement).

The name and the code number of the research project from which the paper originates must be given in a note, as well as the full name of the funding institution. In case the paper has been presented orally elsewhere with the same title or a similar one, the details of such a communication have to be metioned in a note as well.

Authors' duty is to correctly and completely quote the sources which had a significant influence on the content of the research and the manuscript. Fragments of the manuscript, including the text, equations, graphical presentations, figures and tables, directly included from the works of others, must be clearly marked e.g. by quotation marks with a precise reference to the original source (page number) or in a separate paragraph if they are bigger in size.

Full references of all citations in the main text must be given in a separate section (References) in a uniform way, complying with the citation style used in the Military Technical Courier (Harvard Style Manual). The Reference Section contains only the cited sources, not all sources used in the preparation of the manuscript.

In case authors find an error in their article after its publication, they are obliged to promptly notify the Editor-in-Chief (or the Editorial Office) and cooperate in the process of retracting or correcting the article.

Authors are under the obligation to declare in their manuscript whether there is a financial or any other conflict of interest that may influence the results or interpretations of the results.

If the research involves chemicals, activities or equipment posing risk to the health of humans or animals, this must be clearly stated in the manuscript.

When submitting their manuscript, authors agree to comply with the editorial policy of the Military Technical Courier and they confirm such compliance by submitting the Authorship Statement.

Handling allegations of misconduct

Any individual or institution may notify the Editor and/or Editorial Team of ethical malpractice and other misconduct by supplying undisputed information/evidence to start an enquiry. The procedure for investigating the case raised with the supplied evidence is as follows:

- Editor-in-Chief determines to start investigation;
- all evidence is considered confidential during investigation and is available only to those directly involved in the case;
- individuals suspected of ethical breaches are given a chance to respond to the allegations;
- if a misconduct is confirmed, it is further established whether there is a minor or a major violation of publication ethics.

Minor issues not affecting either the integrity of the paper or that of the Journal, e.g. misunderstanding or misapplication of publication standards, are dealt with by directly communicating authors and reviewers, without third parties involved, in one of the following ways:

- authors and/or reviewers are sent a letter of warning;
- a correction notice is published, e.g. when a source, otherwise properly cited within the main text, has been omitted from the Reference List;
- an erratum is published, e.g. when an error is made by the Editorial staff. Serious, major violations of the ethical code may lead to different measures:
- a separate note or a leading article is published, describing the case;
- afilliate institution of the author/reviewer is officially notified;
- the published article is retracted;
- publishing in the Journal is prohibited for a defined period of time;
- relevant organisations and regulatory bodies are informed about the case for taking course of actions within their competence.

These measures may be taken separately or jointly. In the process of handling the case, relevant expert organisations, bodies or individuals are consulted when necessary.

In resolving ethically controversial issues, the Editorial Team follows the guidelines of the Committee on Publication Ethics (COPE).

Disclaimer

The views in the published articles do not represent the views of the Editor, the Editorial Office, the Editorial Team or the Editorial Board of the Military Technical Courier journal. Authors take full legal and moral responsibility for the information and opinions expressed in their articles. The publisher will not be held liable in any way for any claims or damages.

Conflict of interest

The Military Technical Courier adheres to the conflict of interest policy recommended by COPE and/or other international research publishing regulatory authorities (ICMJE, EASE). The authors must declare their conflicts of interest in the Conflict of Interest Statement (CoIS). In the CoIS, each named author of the article is required to provide: (1) A statement of any potential conflicts of interest relevant to the content or a statement that there are no such conflicts. (2) Disclosure of how the article is funded, including specific disclosure of any and all company funding (partial or total), or a statement that there was no such involvement (if applicable). (3) A comprehensive explanation of the role of sponsors in article preparation if the article is sponsored in part or whole.

Advertising

Advertising in the Military Technical Courier is not permitted.

Details on the ethical conduct of the Military Technical Courier are also available on the Journal pages: ***Publication Policy, Journal Quality Management and Article Quality Support*** *via the website of the Serbian Citation Index (SCIndex) – publisher of the national citation index, i.e. publisher of the base in which the Military Technical Courier is primarily indexed.*

Ликовно-графички уредник
Марија Марић, e-mail: marija.maric@mod.gov.rs

Лектор
Добрила Милетић, e-mail: miletic.dobrila@gmail.com

Превод на енглески
Јасна Вишњић, e-mail: jasnavisnjic@yahoo.com

Превод на шпански
Јована Јовановић, e-mail: jovana.jov92@gmail.com

Превод на руски
Др *Карина* Авагјан, e-mail: karinka2576@mail.ru

CIP – Каталогизација у публикацији
Народна библиотека Србије, Београд

623+355/359

ВОЈНОТЕХНИЧКИ гласник : научни часопис Министарства одбране и Војске Србије = Военно-технический вестник : научный журнал Министерства обороны и Вооружённых сил Республики Сербия = Military Technical Courier : scientific Journal of the Ministry of Defence and the Serbian Armed Forces / главни и одговорни уредник Драган Памучар. - Год. 1, бр. 1 (1. јан. 1953)- . - Београд : Универзитет одбране у Београду, Војна академија, 1953- (Београд : Војна штампарија). - 23 cm

Тромесечно. - Текст на срп., рус. и енгл. језику. - Друго издање на другом медијуму: Vojnotehnički glasnik (Online) = ISSN 2217-4753
ISSN 0042-8469 = Војнотехнички гласник
COBISS.SR-ID 4423938

Цена: 600,00 динара

Тираж: 100 примерака

На основу мишљења Министарства за науку, технологију и развој Републике Србије, број 413-00-1201/2001-01 од 12. 9. 2001. године, часопис „Војнотехнички гласник“ је публикација од посебног интереса за науку.

УДК: Народна библиотека Србије, Београд

Адреса редакције: Војнотехнички гласник,
Вељка Лукића Курјака 33, 11042 Београд

https://www.scopus.com/sourceid/21101207440
http://www.vtg.mod.gov.rs
http://aseestant.ceon.rs/index.php/vtg/issue/current
http://scindeks.nb.rs/journaldetails.aspx?issn=0042-8469
https://www.redalyc.org/revista.oa?id=6617
http://elibrary.ru/title_about.asp?id=53280
https://doaj.org/toc/2217-4753

Војнотехнички гласник је лиценциран код EBSCO Publishing-a.
Комплетан текст *Војнотехничког гласника* доступан је у базама података EBSCO Publishing-a.

e-mail: vojnotehnicki.glasnik@mod.gov.rs; X: @MilTechCourier

Претплата на штампано издање: e-mail: vojnotehnicki.glasnik@mod.gov.rs; тел. 066/87-00-123.

Часопис излази тромесечно.

Први штампани број *Војнотехничког гласника* објављен је 1. 1. 1953. године.

Прво електронско издање *Војнотехничког гласника* на Интернету објављено је 1. 1. 2011. г.

Штампа: Војна штампарија – Београд, Ресавска 40б, e-mail: vojna.stamparija@mod.gov.rs

Художественный редактор
Мария Марич, e-mail: marija.maric@mod.gov.rs

Корректор
Добрила Милетич, e-mail: miletic.dobrila@gmail.com

Перевод на английский язык
Ясна Вишнич, e-mail: jasnavisnjic@yahoo.com

Перевод на испанский язык
Йована Йованович, e-mail: jovana.jov92@gmail.com

Перевод на русский язык
Д.филол.н. *Карина* Кареновна Авагян, e-mail: karinka2576@mail.ru

CIP – Каталогизация в публикации
Национальная библиотека Сербии, г. Белград

623+355/359

ВОЈНОТЕХНИЧКИ гласник : научни часопис Министарства одбране и Војске Србије = Военно-технический вестник : научный журнал Министерства обороны и Вооружённых сил Республики Сербия = Military Technical Courier : scientific Journal of the Ministry of Defence and the Serbian Armed Forces / главни и одговорни уредник Драган Памучар. - Год. 1, бр. 1 (1. јан. 1953)- . - Београд : Универзитет одбране у Београду, Војна академија, 1953- (Београд : Војна штампарија). - 23 cm

Тромесечно. - Текст на срп., рус. и енгл. језику. - Друго издање на другом медијуму: Vojnotehnički glasnik (Online) = ISSN 2217-4753
ISSN 0042-8469 = Војнотехнички гласник
COBISS.SR-ID 4423938

Цена: 600,00 динаров

Тираж: 100 экземпляров

На основании решения Министерства науки и технологий Республики Сербия, № 413-00-1201/2001-01 от 12. 9. 2001 года, журнал «Военно-технический вестник» объявлен изданием, имеющим особое значение для науки.

УДК: Национальная библиотека Сербии, г. Белград

Адрес редакции: Војнотехнички гласник,
Ул. Велька Лукича Куряка 33, 11042 Белград, Республика Сербия

https://www.scopus.com/sourceid/21101207440
http://www.vtg.mod.gov.rs
http://aseestant.ceon.rs/index.php/vtg/issue/current
http://scindeks.nb.rs/journaldetails.aspx?issn=0042-8469
https://www.redalyc.org/revista.oa?id=6617
http://elibrary.ru/title_about.asp?id=53280
https://doaj.org/toc/2217-4753

«Военно-технический вестник» включен в систему EBSCO. Полный текст журнала «Военно-технический вестник» можно найти в базах данных EBSCO Publishing.

e-mail: vojnotehnicki.glasnik@mod.gov.rs, X: @MilTechCourier
Подписка на печатную версию журнала: e-mail: vojnotehnicki.glasnik@mod.gov.rs; тел. +381 66 87 00 123.

Журнал выпускается ежеквартально.

Первый номер журнала «Военно-технический вестник» выпущен 1.1.1953 года.

Первая электронная версия журнала размещена на интернет странице 1.1.2011 года.

Типография: Војна штампарија – Белград, Ресавска 40б, e-mail: vojna.stamparija@mod.gov.rs

Graphic design editor
Marija Marić, e-mail: marija.maric@mod.gov.rs

Proofreader
Dobrila Miletić, e-mail: miletic.dobrila@gmail.com

English translation and polishing
Jasna Višnjić, e-mail: jasnavisnjic@yahoo.com

Spanish translation and polishing
Jovana Jovanović, e-mail: jovana.jov92@gmail.com

Russian translation and polishing
Dr. *Karina* Avagyan, e-mail: karinka2576@mail.ru

CIP – Catalogisation in the publication
National Library of Serbia, Belgrade

623+355/359

ВОЈНОТЕХНИЧКИ гласник : научни часопис Министарства одбране и Војске Србије = Военно-технический вестник : научный журнал Министерства обороны и Вооружённых сил Республики Сербия = Military Technical Courier : scientific Journal of the Ministry of Defence and the Serbian Armed Forces / главни и одговорни уредник Драган Памучар. - Год. 1, бр. 1 (1. јан. 1953)- . - Београд : Универзитет одбране у Београду, Војна академија, 1953- (Београд : Војна штампарија). - 23 cm

Тромесечно. - Текст на срп., рус. и енгл. језику. - Друго издање на другом медијуму: Vojnotehnički glasnik (Online) = ISSN 2217-4753
ISSN 0042-8469 = Војнотехнички гласник
COBISS.SR-ID 4423938

Price: 600.00 RSD

Printed in 100 copies

According to the Opinion of the Ministry of Science and Technological Development No 413-00-1201/2001-01 of 12th September 2001, the *Military Technical Courier* is a publication of special interest for science.

UDC: National Library of Serbia, Belgrade

Address: Vojnotehnički glasnik/Military Technical Courier,
Veljka Lukića Kurjaka 33, 11042 Belgrade, Republic of Serbia

https://www.scopus.com/sourceid/21101207440
http://www.vtg.mod.gov.rs/index-e.html
http://aseestant.ceon.rs/index.php/vtg/issue/current
http://scindeks.nb.rs/journaldetails.aspx?issn=0042-8469
https://www.redalyc.org/revista.oa?id=6617
http://elibrary.ru/title_about.asp?id=53280
https://doaj.org/toc/2217-4753

Military Technical Courier has entered into an electronic licensing relationship with EBSCO Publishing. The full text of *Military Technical Courier* can be found on EBSCO Publishing's databases.

e-mail: vojnotehnicki.glasnik@mod.gov.rs, X: @MilTechCourier
Subscription to print edition: e-mail: vojnotehnicki.glasnik@mod.gov.rs; Tel. +381 66 87 00 123.

The journal is published quarterly.

The first printed issue of the *Military Technical Courier* appeared on 1st January 1953.
The first electronic edition of the *Military Technical Courier* on the Internet appeared on 1st January 2011.

Printed by Vojna štamparija – Belgrade, Resavska 40b, e-mail: vojna.stamparija@mod.gov.rs


ОД 1953.
70
ГОДИНА
ВТГ

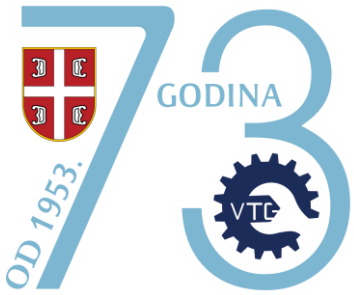
OD 1953.
70
GODINA
VTG


С 1953 г.
70
ЛЕТ
ВТБ


SINCE 1953
70
YEARS
MTG